TREM2 modulates differential deposition of post-translationally modified Aβ variants in the brain parenchyma and the vasculature

Dissertation

zur

Erlangung des Doktorgrades (Dr. rer. nat.)

der

Mathematisch-Naturwissenschaftlichen Fakultät

der

Rheinischen Friedrich-Wilhelms-Universität Bonn

vorgelegt von

Pranav Chintamani Joshi

aus

Ponda, Goa

Bonn, 2022

Angefertigt mit Genehmigung der Mathematisch-Naturwissenschaftlichen Fakultät
der Rheinischen Friedrich-Wilhelms-Universität Bonn

Gutachter: Prof. Dr. rer. nat. Jochen Walter
Gutachter: Prof. Dr. rer. nat. Thorsten Lang

Tag der Promotion: 02.06.2022
Erscheinungsjahr: 2022

Declaration

I solemnly declare that the work submitted entitled **"TREM2 modulates differential deposition of post-translationally modified Aβ variants in the brain parenchyma and the vasculature"** is a result of my investigation and the work of others that has been quoted or reproduced citing appropriate references. I further declare that this work has not been submitted, in whole or in part, for any other degree or professional qualification.

- A significant portion of Chapter 4 was published in GLIA, in an article entitled **Differential interaction with TREM2 modulates microglial uptake of modified Aβ species**. I conceived the study along with Prof. Dr Jochen Walter, Prof. Dr Paul E. Fraser, and Prof. Dr Peter St George-Hyslop and also performed most of the experiments and analyzed data.
- A significant portion of Chapter 6 was published in Acta Neuropathologica Communications, in an article entitled **TREM2 modulates differential deposition of modified and non-modified Aβ species in extracellular plaques and intraneuronal deposits**. I conceived the study along with Prof. Dr Jochen Walter and also performed most of the experiments and analyzed data.

Dedicated to my Mother and Motherland

Vande Mataram

Contents

LIST OF TABLES ..... **I**
LIST OF FIGURES ..... **II**
LIST OF ABBREVIATIONS ..... **IV**
AMINO ACIDS ABBREVIATIONS ..... **VII**
ABSTRACT ..... **VIII**
Chapter 1 | Introduction **1**
1.1 | Alzheimer's Disease (AD) 1
1.1.1 | Etiology of AD 2
1.1.1.1 | Amyloid precursor protein (APP) processing 3
1.1.1.2 | Familial Alzheimer's Disease (fAD) 4
1.1.1.3 | Sporadic Alzheimer's Disease (sAD) 5
1.1.2 | Amyloid cascade hypothesis 6
1.1.3 | Deposition and propagation of Aβ in the brain 10
1.1.4 | Heterogeneity of Aβ in the AD brain 11
1.1.4.1 | Pyroglutamation 12
1.1.4.2 | Nitration 13
1.1.4.3 | Phosphorylation (pSer8, pSer26) 13
1.2 | Mouse models of amyloid pathology 14
1.2.1 | APPPS1 transgenic models 16
1.2.1.1 | APPKM670/671NL; PS1L166P 16
1.2.1.2 | APPKM670/671NL; PS1ΔE9 18
1.2.1.3 | 5xFAD 18
1.3 | Neuroinflammation and microglia in AD 19
1.4 | TREM2 24
1.4.1 | TREM2 structure and expression 25
1.4.2 | sTREM2 27
1.4.3 | TREM2 ligands and signalling 28
1.4.4 | TREM2 in AD 30
1.4.5 | TREM2 and FTD 32
1.4.6 | TREM2/DAP12 and Nasu Hakola disease (NHD) 33
1.5 | Aim of the study 36
Chapter 2 | Materials and methods **37**
2.1 | Chemicals and materials 37
2.1.1 | Chemicals 37
2.1.2 | Laboratory instruments and equipments 37
2.1.3 | Buffers and solutions 38
2.1.4 | Solutions for Immunofluorescence/immunostainings 39
2.1.5 | Assay kits 39
2.2 | Antibodies 40
2.3 | Oligomerisation of Aβ peptides 42
2.4 | Experimental animals 43
2.5 | Animal behaviour tests 44
2.5.1 | Open-Field Test (OFT) 44
2.5.2 | Partner Recognition Test (PRT) 44
2.5.3 | Morris water maze (MWM) test 45

2.6 | Human brain samples 45
2.7 | Molecular biological methods 46
2.7.1 | Plasmids 46
2.7.2 | Site-directed mutagenesis of plasmid DNA 46
2.8 | Bacterial culture and transformation 46
2.8.1 | Bacterial strain for cloning 47
2.8.2 | Transformation of competent *E. Coli* 47
2.8.3 | Small and large scale plasmid preparation 47
2.9 | Cell culture and transfection 47
2.9.1 | Culture of HEK293 Flp-In and stable cell lines 47
2.9.2 | Transient transfection 48
2.9.3 | Generation of stable cell clones 48
2.9.4 | Passaging and cryopreservation of stable cell lines 49
2.9.5 | Culture of Expi293F^{TM} cells 49
2.9.6 | Culture of WT and TREM2^{T66M} primary microglia cells 50
2.10 | Binding and phagocytosis assays 50
2.11 | TREM2 ectodomain purification 51
2.11.1 | sTREM2 for the dot blot experiments 51
2.11.2 | sTREM2 ectodomain for BLI studies 51
2.11.3 | sTREM2-Fc and Fc for Pulldown experiments 51
2.12 | Protein biochemical techniques 52
2.12.1 | Subcellular fractionation 52
2.12.2 | Extractions of proteins from mouse brains 53
2.12.3 | Extractions of proteins from cultured cells 53
2.13 | Protein precipitation with methods 53
2.13.1 | Acetone precipitation method 53
2.13.2 | Ammonium sulphate (AS) method 53
2.13.3 | Trichloroacetic acid (TCA) 54
2.14 | Measurement of protein concentration 54
2.15 | Western blotting (WB) 54
2.15.1 | Sodium dodecyl sulfate-polyacrylamide gel electrophoresis (SDS-PAGE) 54
2.15.2 | Native-PAGE 55
2.16 | Immunochemical staining techniques 55
2.16.1 | Immunocytochemistry (ICC) 55
2.16.2 | Immunocytochemistry (ICC) of primary microglia 56
2.16.3 | Immunohistochemistry of mouse brains 56
2.16.4 | Immunohistochemistry (IHC) on human post-mortem brain tissue 57
2.16.5 | Data analysis of Aβ deposits in mouse and human brain 57
2.17 | Microscopy 62
2.17.1 | Transmission Electron Microscopy 62
2.17.2 | Confocal and bright field imaging 63
2.18 | TREM2-Aβ Interaction studies 63
2.18.1 | Dot blot assay 63
2.18.2 | Biolayer Interferometry (BLI) studies 63
2.18.3 | Immunoprecipitation (IP) of Aβ using sTREM2-Fc 67
2.19 | Thioflavin T (ThT) aggregation assay 67
2.20 | Statistics 67

Chapter 3 | Mutation specific effects of TREM2 variants on secretory transport and ER stress response 69
3.1 | Generation of TREM2 expressing HEK293 Flp-In cell lines 69
3.2 | Ectodomain mutations alter the cellular localization of sTREM2 leading to ER stress 72
3.3 | Increased expression of BiP/GRP78 in the plaque-associated microglia in transgenic mouse brains 74
3.4 | T66M mutation increases translocation of CHOP into the nucleus in plaque-associated microglia 74
Chapter 4 | Differential interaction with TREM2 modulates microglial uptake of modified Aβ species 77
4.1 | Characterisation of Aβ preparation for the BLI studies 77
4.2 | Differential binding of TREM2 to post-translationally modified Aβ species 79
4.2.1 | Interaction of Aβ monomers with TREM2 measured by BLI 79
4.2.2 | Interaction of Aβ oligomers with TREM2 by using BLI studies 81
4.3 | TREM2 inhibits the aggregation of Aβ variants 84
4.4 | TREM2 dependent binding and phagocytosis of modified Aβ species by primary microglia 85
4.5 | TREM2 deletion leads to altered deposition of phosphorylated Aβ variants 91
Chapter 5 | Amyloid phosphorylation at Ser26 causes intraneuronal and vascular Aβ deposits leading to impaired memory in the S26D pseudophosphorylated transgenic mouse model 95
5.1 | AβS26D-Tg mice showed intraneuronal accumulation of Aβ without extracellular deposits at 4,8 and 24 months of age 95
5.2 | AβS26D-Tg mice did not show a change in the exploratory behaviour as compared to non-transgenic mice in the Open field test (OFT) 103
5.3 | Social recognition was not impaired in AβS26D-Tg mice as compared to non-Tg mice 105
5.4 | AβS26D-Tg mice showed impairment in the spatial memory as compared to non-transgenic mice in the MWM test 106
Chapter 6 | TREM2 modulates differential deposition of modified and non-modified Aβ species in extracellular plaques and intraneuronal deposits 110
6.1 | Selective accumulation of Ser8-phosphorylated Aβ species upon loss of TREM2 function in brains of transgenic mice 110
6.2 | TREM2^{T66M} mutation leads to increased deposition of pSer8-Aβ in transgenic mouse brain 122
6.3 | Loss of TREM2 function increases intraneuronal and vascular deposition of Aβ species 123
6.4 | TREM2 variants are associated with quantitative and qualitative differences in the deposition of distinct Aβ species in human brains 128
6.5 | TREM2 modulates intraneuronal deposition of pSer26-Aβ in mouse and human brains 134
Chapter 7 | Discussion 139
7.1 | Effects of disease-associated TREM2 variants on their subcellular transport and cellular stress response 139
7.2 | Increased interaction with TREM2 modulates microglial uptake of phosphorylated Aβ species 141
7.3 | Intraneuronal and vascular deposition of Ser26 pseudophosphorylated Aβ is associated with impaired memory of transgenic mice 149
7.4 | TREM2 modulates differential deposition of modified and non-modified Aβ species in extracellular plaques and intraneuronal deposits 151
7.5 | Future Outlook 157
REFERENCES 160
LIST OF PUBLICATIONS 197
ACKNOWLEDGEMENT 198

List of tables

Table 1.1 | Disease-associated mutations in TREM2 35
Table 2.1 | Laboratory instruments and equipments 38
Table 2.2 | Buffers and solutions 39
Table 2.3 | Solutions for Immunofluorescence/immunostainings 39
Table 2.4 | Assay kits 39
Table 2.5 | Primary and secondary antibodies 42
Table 2.6 | Experimental mouse models 43
Table 2.7 | Primers used for site-directed mutagenesis 46
Table 2.8 | Composition of culture media in bacterial cell culture 46
Table 2.9 | Composition of culture media in eukaryotic cell culture 48
Table 4.1 | BLI kinetic assay representing values from two trials 82
Table 5.1 | Region-specific distribution of Aβ at different ages of male and female AβS26D-Tg mice 103
Table 6.1 | Details of transgenic mouse models and quantification of Aβ plaque pathology 111
Table 6.2 | Demographic and clinical characteristics of the TREM2 coding variants and control (CV) groups 129

List of figures

Figure 1.1 | Alzheimer's disease (AD) pathology in the human brain 2
Figure 1.2 | Amyloid precursor protein (APP) processing pathway 3
Figure 1.3 | Rare and common variants of AD genes and their risk 6
Figure 1.4 | The amyloid cascade hypothesis showing major pathogenic events leading to AD 8
Figure 1.5 | Post-translational modifications (PTMs) of Aβ 11
Figure 1.6 | Transgenic mouse brains with AD 15
Figure 1.7 | Microglial functions in CNS 20
Figure 1.8 | Activation of disease-associated microglia (DAM) from homeostatic microglia 23
Figure 1.9 | Structural features of human TREM2 25
Figure 1.10 | TREM2 signalling 30
Figure 1.11 | Microglial dysfunction upon TREM2 loss in a mouse model of AD 32
Figure 2.1 | Purified sTREM2 for various binding experiments 52
Figure 2.2 | Visualization and approach of analysis of area and number of Aβ plaques 58
Figure 2.3 | Analysis of area and size of Aβ plaque in the transgenic mouse brains 59
Figure 2.4 | Analysis of staining intensity of Aβ plaque stained with different antibodies 61
Figure 2.5 | Principle of Bio-layer interferometry 64
Figure 2.6 | Optimization of BLI experiments with varying concentrations of Aβ peptides 65
Figure 3.1 | Illustration of TREM2 and the cleaved sTREM2 fraction with different mutations 69
Figure 3.2 | Comparison of sTREM2 and full-length TREM2 after transient transfection 70
Figure 3.3 | sTREM2 and full-length TREM2 stable cell line with ectodomain mutations 71
Figure 3.4 | Effect of protein transport inhibitor on sTREM2-WT and mutants 72
Figure 3.5 | T66M mutation alters the cellular accumulation of sTREM2 leading to ER stress 73
Figure 3.6 | Accumulation of T66M mutant led to an increased BiP/GRP78 expression in plaque-associated microglia 75
Figure 3.7 | Accumulation of T66M mutant led to nuclear translocation of CHOP in plaque-associated microglia 76
Figure 4.1 | Characterization of synthetic Aβ preparations used for the BLI and dot blot experiments 78
Figure 4.2 | BLI studies of mAβ with TREM2 ectodomain using Aminopropylsilane (APS) biosensors 80
Figure 4.3 | Differential interaction of TREM2 with modified Aβ variants 81
Figure 4.4 | Increased interaction of TREM2 with oligomeric phosphorylated Aβ variants 83
Figure 4.5 | TREM2 inhibits aggregation of modified Aβ(x-42) variants 85
Figure 4.6 | Modified Aβ(x-42) variants showed differences in the aggregation kinetics 86
Figure 4.7 | Reduced uptake of latex beads by TREM2^{T66M} primary microglia 87
Figure 4.8 | Phosphorylated Aβ variants showed differential binding and uptake by the primary microglia with and without functional mutation of TREM2 88
Figure 4.9 | Phosphorylated Aβ variants showed differential internalization by primary microglia 90
Figure 4.10 | Decreased microglial barrier function alters deposition of pSer8-Aβ and nmAβ in the transgenic mouse brain 91
Figure 4.11 | Decreased microglial barrier function alters deposition of Aβ in the transgenic mouse brain 92
Figure 4.12 | TREM2 deletion or mutation leads to decreased microglial pSer26-Aβ deposits in TREM2 transgenic mouse brain 93
Figure 5.1 | Intraneuronal Aβ accumulation in the cortex of 4M, 8M, and 24M old AβS26D-Tg mice 96
Figure 5.2 | Intraneuronal Aβ accumulation in the hippocampus of 4M, 8M, and 24M old AβS26D-Tg mice 97
Figure 5.3 | AβS26D-Tg mice show changes in the microglial phenotype at 24M of age 99

Figure 5.4 | No change in the locomotion as well as anxiety phenotype at 24M of male and female AβS26D-Tg mice in the OFT 104
Figure 5.5 | Social recognition was not impaired at 24M of male and female AβS26D-Tg mice in partner recognition test (PRT) 105
Figure 5.6 | No change in the spatial learning at 24M of male and female AβS26D-Tg mice in the MWM training 107
Figure 5.7 | Memory impairment in the male and female AβS26D-Tg mice in MWM probe trial. 108
Figure 6.1 | TREM2 deletion leads to increased deposition of pSer8-Aβ in 15M old 5xFAD transgenic mouse brains 112
Figure 6.2 | TREM2 deletion leads to increased deposition of Aβ in 5xFAD transgenic mouse brains 113
Figure 6.3 | TREM2 deletion leads to increased deposition of pSer8-Aβ in 5M old 5xFAD transgenic mouse brains 114
Figure 6.4 | Size distribution of Aβ plaques stained with different Aβ antibodies in 5xFAD-TREM2$^{+/+}$ and 5xFAD-TREM2$^{-/-}$ mice 115
Figure 6.5 | TREM2 deletion leads to increased deposition of pSer8-Aβ in APP/PS1L166P transgenic mouse brains 117
Figure 6.6 | Size distribution of Aβ plaques stained with different Aβ antibodies in APP/PS1L166P-TREM2$^{+/+}$ and TREM2$^{-/-}$ mice 118
Figure 6.7 | TREM2 deletion leads to increased N3pE-Aβ deposits in 5xFAD transgenic mouse brains 119
Figure 6.8 | TREM2 deletion leads to increased deposition of N3pE-Aβ in APP/PS1L166P transgenic mouse brains 121
Figure 6.9 | TREM2^{T66M} causes increased deposition of pSer8-Aβ and N3pE-Aβ in APP/PS1 transgenic mouse brains 122
Figure 6.10 | Size distribution of Aβ plaques stained with different Aβ antibodies in APP/PS1ΔE9-TREM2 and APP/PS1ΔE9-TREM2^{T66M} mice 124
Figure 6.11 | Loss of microglial barrier functions upon TREM2 deletion leads to increased intraneuronal pSer8-Aβ deposits in the APP/PS1L166P transgenic mouse brains 125
Figure 6.12 | TREM2^{T66M} causes increased Aβ in the APP/PS1 transgenic mouse brains 126
Figure 6.13 | Increased pSer8-Aβ in brain extracts of APP/PS1 ΔE9-TREM2^{T66M} transgenic mouse brains 127
Figure 6.14 | Differential deposition of phosphorylated Aβ species in human brains with the common and rare variants of TREM2 132
Figure 6.15 | TREM2 ectodomain mutation leads to differential deposition of post-translationally modified Aβ species in the human brains 134
Figure 6.16 | TREM2 deletion or mutation leads to increased intraneuronal pSer26-Aβ deposits in TREM2 transgenic mouse brain 135
Figure 6.17 | TREM2 deletion leads to increased intracellular pSer26-Aβ deposits in young age transgenic mouse brains 136
Figure 6.18 | TREM2 ectodomain mutation leads to increased intracellular pSer26-Aβ deposits in the human brain 137
Figure 7.1 | Effect of dysfunctional TREM2 on the deposition of phosphorylated Aβ variants in transgenic mouse brains 147
Figure 7.2| Effect of dysfunctional TREM2 on deposition of modified and non-modified Aβ species in extracellular plaques and intraneuronal deposits 155

List of abbreviations

[^{11}C]	Radioactive isotope of carbon	**KWH**	Kruskal-Wallis H
^{18}F	Fluorodeoxyglucose	**l**	Liter
1E4E11	Antibody recognizing Aβ phosphorylated at Ser8 (pSer8Aβ)	**LANUV**	Landesamt für Natur, Umwelt und Verbraucherschutz
3NTyr10 -Aβ	N-terminal nitrated Aβ at position 10	**LAT**	Linker for activation of T-cells family member
aa	Amino acid	**LBD**	Lewy body dementia
ABC	Avidin-Biotin complex	**LCP2**	Lymphocyte cytosolic protein 2
ABCA7	ATP-binding cassette sub-family A member 7	**LDL**	Low-density lipoproteins
AD	Alzheimer's disease	**LDS**	Lithium dodecyl sulfate
ADAM	A disintegrin and metalloproteinases	**Lpl**	Lipoprotein lipase
AICD	APP intracellular domain	**LPS**	Lipopolysaccharide
AKT	A serine/threonine-specific protein kinases	**M**	Molar
ALS	Amyotrophic lateral sclerosis	**mAbs**	Monoclonal antibodies
ANOVA	Analysis of variance	**MAPK**	Mitogen-activated protein kinase
APH1 and 2	Anterior pharynx defective 1 & 2	**MBP**	Myelin basic protein
APO	Apolipoproteins	**mg**	Milligram
ApoE-ε4	Apolipoprotein E- ε4	**min**	Minutes
ApoJ	Apolipoprotein J	**ml**	Millilitre
APP	Amyloid precursor protein	**µM/µl/µm**	Micromolar / Microlitre / Micrometer
APPswe	Swedish mutation of the amyloid precursor protein	**mM**	Millimolar
APS	Aminopropylsilane	**MS4A**	Membrane-spanning 4A
Axl	Cell surface receptor tyrosine kinase	**MS4A4E**	Membrane-spanning 4A, member 4
Aβ	Amyloid-β	**MS4A6A**	Membrane-spanning 4A, member 6A
Aβ40	Amyloid β (aa1-aa40)	**MTL**	Medial temporal lobe
Aβ42	Amyloid β (aa1-aa42)	**MVB**	Multivesicular bodies
BCA	Bicinchoninic acid	**MWM**	Morris water maze
BIN1	Bridging integrator 1	**n**	Number
BiP	Binding immunoglobulin protein	**N11pE-Aβ**	N-terminal pyroglutamate-modified Aβ at position 11
BLI	Bio-layer interferometry	**N3pE-Aβ**	N-terminal pyroglutamate-modified Aβ at position 3
BMDMs	Bone marrow-derived macrophages	**NaDOC**	Sodium Deoxycholate
BSA	Bovine serum albumin	**NAG**	N-acetylglucosamine
CA1 &3	Cornu ammonis 1&3	**NaOH**	Sodium hydroxide
CAA	Cerebral amyloid angiopathy	**NB**	Neurobasal
CBF	Cerebral blood flow	**NCT**	Nicastrin
CBL	Casitas B-lineage Lymphoma	**NFAT**	Nuclear factor of activated T-cells
CD	Circular dichroism	**NFTs**	Neurofibrillary tangles
CD2AP	CD2 associated protein	**NF-κB**	Nuclear factor kappa B
CD33	Sialic acid-binding Ig-like lectin 3	**NHD**	Nasu-Hakola disease
Cdc2	Cell division cycle protein 2 homolog	**NIA-AA**	National Institute on Aging - Alzheimer's Association
Cdk1	Cyclin-dependent kinase 1	**nm**	Nanometer

CDR-2	Complementarity-determining region 2	**nmAβ**	Non-modified amyloid-β
CERAD	Consortium to establish a registry for Alzheimer's disease	**NO**	Nitric oxide
CHOP	C/EBP homologous protein	**NOS**	Nitric oxide synthase
CLU	Clusterin	**OFT**	Open field test
CNS	Central nervous system	**P2ry12**	Purinergic receptor P2Y, G-protein coupled, 12/ 13
CpG	Cytosine triphosphate deoxynucleotide linked to guanine triphosphate deoxynucleotide	**PAD**	Peptidyl arginyl deiminase
CR1	Complement Receptor 1	**PAGE**	Polyacrylamide gel electrophoresis
CSF	Cerebrospinal fluid	**PBB3**	2-((1E,3E)-4-(6-((11)C-methylamino)pyridin-3-yl)buta-1,3-dienyl) benzo[d]thiazol-6-ol
CSF1	Colony stimulating factor 1	**PBS**	Phosphate buffer saline
Cst3	Cystatin 3	**PCMT1**	Protein carboxyl methyltransferase 1
CTF	C-terminal fragment	**PEN2**	Presenilin enhancer 2
Ctsd	Gene encoding cathepsin D	**PERK**	Protein kinase R-like endoplasmic reticulum kinase
CV	Common variant	**PET**	Positron emission tomography
Cx3cr1	C-X3-C Motif Chemokine Receptor 1	**PFA**	Paraformaldehyde
DAA1106	N-(2,5-Dimethoxybenzyl)-N-(5-fluoro-2-phenoxyphenyl)acetamide	**PHFs**	Paired helical filaments
DAB	3,3'-diaminobenzidine	**PI3K**	Phosphoinositide 3-kinase
DAG	diacylglycerol	**PiB**	Pittsburgh compound B
DAM	Disease-associated microglia	**PICALM**	Phosphatidylinositol binding clathrin assembly protein
DAP12	DNAX activating protein of 12 kDa	**PIP3**	Phosphatidylinositol-3,4,5-trisphosphate
DAPI	4',6-diamidino-2-phenylindol	**PKA /C**	Protein kinase A/ C
DG	Dentate gyrus	**PKCθ**	Protein kinase C-θ
dH_2O	Distilled water	**PLCγ**	phospholipase C-γ
DMEM	Dulbecco's modified Eagle medium	**PLL**	Poly-L-lysine
DMSO	Dimethyl sulfoxide	**PRR**	Pattern recognition receptor
DNA	Deoxyribonucleic acid	**PS**	Presenilin
DS	Down's syndrome	**PSEN1 /2**	Presenilin 1/2
DTT	Dithiothreitol	**pSer8-Aβ**	Phosphorylation at serine 8 of Amyloid-β
E	Exon	**PVDF**	Polyvinylidene fluoride
e.g.	exempli gratia (Latin: for example)	**QPCT**	Gene encoded for glutaminyl-peptide cyclotransferase enzyme
ECD	Extracellular domain	**RANKL**	Receptor activator of nuclear factor kappa B ligand
ECL	Enhanced chemiluminescence	**RIPA**	Radioimmunoprecipitation assay
EDTA	Ethylenediaminetetraacetic acid	**RNA**	Ribonucleic acid
EGTA	Ethylene glycol-bis(β-aminoethyl ether)-N,N,N',N'-tetraacetic acid	**RNS**	Reactive nitrogen species
eIF2α	Eukaryotic initiation factor-2α	**ROI**	Region of interest
ELISA	Enzyme-linked immunosorbent assay	**ROS**	Reactive oxygen species
EM	Electron microscopy	**rpm**	Rotations per minute
Endo Hf	Endoglycosidase H and maltose binding protein fusion	**RSC**	Retrosplenial cortex

ENPEP	Gene encoded for glutamyl aminopeptidase enzyme	**RT**	Room temperature
EOAD	Early-onset Alzheimer's disease	**s**	Second
EPHA1	Ephrin type-A receptor 1	**sAPP**	Soluble amyloid precursor protein
EPM	Elevated plus maze	**SDC**	Sodium deoxycholate
ER	Endoplasmic reticulum	**SDS**	Sodium dodecyl sulphate
EtOH	Ethanol	**SEM**	Standard error of the mean
fAD	Familial Alzheimer's Disease	**SSC**	Somatosensory cortex
FCS	Fetal calf serum	**sTREM2**	Soluble variant of Triggering receptor expressed on myeloid cells 2
FDG	Fluorodeoxyglucose	**swe**	Swedish
FDG-PET	Fluorodeoxyglucose positron emission tomography	**SYK**	Spleen tyrosine kinase
fMRI	Functional magnetic resonance imaging	**TBI**	Traumatic brain injury
FPLC	Fast protein liquid chromatography	**TBS**	Tris-buffered saline
FTD	Frontotemporal dementia	**TC**	Temporal cortex
g	Force per unit mass	**TEM**	Transmission electron microscopy
GCL	Granule cell layer	**Thy1**	Thymocyte differentiation antigen 1
GFAP	Glial fibrillary acidic protein	**TLRs**	Toll-like receptors
GRB2	Growth factor receptor-bound protein 2	**Tmem119**	Transmembrane Protein 119
GVD	Granulovacuolar degeneration	**TNFα**	Tumour necrosis factor-alpha
GWAS	Genome-wide association studies	**TREM2**	Triggering receptor expressed on myeloid cells 2
h	Hour	**Tris**	Tris(hydroxymethyl)aminomethane
HDL	High-density lipoproteins	**TRITC**	Tetramethylrhodamine isothiocyanate
HEK	Human embryonic kidney	**TSPO**	Translocator protein
Hexβ	Hexosaminidase subunit β	**TYROBP**	TYRO protein tyrosine kinase-binding protein
HNE	4-hydroxynonenal	**UPR**	Unfolded protein response
HPLC	High-performance liquid chromatography	**VAV1**	Gene encoded for proto-oncogene vav
HRP	Horseradish peroxidase	**VD**	Vascular dementia
i.e.	id est (Latin: that is)	**WT**	Wild type
Iba1	Ionized calcium-binding adaptor molecule 1	**XBP1**	X-box binding protein 1
ICC	Immunocytochemistry	**~**	Approximately
IF	Immunofluorescence	**%**	Percent
Ig	Immunoglobulin	**ε**	Epsilon
IgG	Immunoglobulin G	**τ**	Tau
IHC	Immunohistochemistry	**&**	and
IL1β	Interleukin 1 beta	**º**	Degree
IntDen	Integrated density	**x**	Any number
IR	Infrared	**α**	Alpha
IRE1	Inositol-requiring kinase 1	**β**	Beta
ITAMs	Immunoreceptor tyrosine-based activation motifs	**γ**	Gamma
JIP-1	JNK-interacting protein 1	**Δ**	Delta
kDa	Kilodalton	**θ**	Theta
KI	Knock-In	**κ**	Kappa
kg	Kilogram	**μ**	Mu

Amino acids abbreviations

Amino acid	Abbreviation	Single-letter code
Alanine	Ala	A
Arginine	Arg	R
Asparagine	Asn	N
Aspartic acid	Asp	D
Cysteine	Cys	C
Glutamine	Gln	Q
Glutamic acid	Glu	E
Glycine	Gly	G
Histidine	His	H
Isoleucine	Ile	I
Leucine	Leu	L
Lysine	Lys	K
Methionine	Met	M
Phenylalanine	Phe	F
Proline	Pro	P
Serine	Ser	S
Threonine	Thr	T
Tryptophan	Trp	W
Tyrosine	Tyr	Y
Valine	Val	V
Any amino acid		X

Abstract

Alzheimer's disease (AD) is characterized by the combined presence of extracellular amyloid-beta (Aβ) plaques [1] and intracellular neurofibrillary tangles (NFTs) with abnormally phosphorylated tau (τ) protein in the brain. Genome-wide association studies (GWAS) and whole exome sequencing (WES) of sporadic AD cases have recently identified DNA polymorphisms that increase the risk for AD, including the Triggering Receptor Expressed on Myeloid cells 2 (TREM2). ADAM [2] proteases shed this surface TREM2, resulting in the generation of soluble ectodomain fraction of TREM2 (sTREM2). To investigate the potential role of sTREM2, to compare sTREM2 with disease-associated mutations (in particular R47H and T66M), and to characterize ligand interactions; stable cell lines were generated using the Flp-In system[3]. The cellular trafficking and processing of AD-associated variants (such as R47H) are similar to wild-type TREM2, but frontotemporal dementia (FTD) or Nasu-Hakola disease (NHD) mutations (such as T66M) impair folding, trafficking to the plasma membrane and accumulates TREM2 in the endoplasmic reticulum (ER).

The heterogeneity of proteolytic cleavages and post-translational modifications by various enzymes can lead to modified Aβ peptides with differences in the stability, toxicity, and aggregation kinetics. In particular, phosphorylation at serine 8 (pSer8-Aβ) promotes fibrillization, while phosphorylation at serine 26 (pSer26-Aβ) stabilizes oligomeric assemblies, and rather decreases the fibrillization of Aβ. While pSer8-Aβ was abundant in plaque core, the reactivity of pSer26-Aβ is limited in extracellular plaques and both of these species were detected in neurons and vessels resembling cerebral amyloid angiopathy (CAA). In parallel, a novel AβS26D-Tg transgenic mouse[4] model was generated, which demonstrated the presence of Aβ oligomers within neurons throughout life and exhibited cognitive impairment without evidence of extracellular plaques as observed in old age mice.

Further, to assess whether phosphorylation of Aβ affects the interaction with TREM2, interaction studies were performed by Biolayer interferometry, co-immunoprecipitation, and dot blot overlay assays. Phosphorylation of Aβ increases its binding to TREM2 and this increased interaction plays an important role in the uptake of Aβ in distinct aggregation states by the primary microglia. Also, TREM2 deletion or functional mutation of TREM2 in the microglia leads to the accumulation of these toxic Aβ species in transgenic mice. In addition, human brains with rare TREM2 AD risk variants showed an altered deposition of modified Aβ

[1] Plaques: The extracellular deposits of aggregated insoluble amyloid beta (Aβ);
[2] ADAM: A disintegrin and metalloproteinase are a family of cell surface proteases;
[3] Flp-In system: A system that allows integration and expression of gene of interest in mammalian cells at a specific genomic location;
[4] AβS26D-Tg transgenic mouse: A genetically modified mouse that expresses the human APP751 variant carrying the Swedish (KM→NL) and phosphomimicking (S→D) mutations at Ser26 residue of Aβ.

species in the different brain lesions as compared to AD cases with the common variant of TREM2.

Together, this work demonstrates that the differences in the aggregation of phosphorylated Aβ species led to differential deposition characteristics in the form of plaques, intraneuronal and CAA. Also, this study provides a new perspective on TREM2 function and highlights the importance of further investigating the potential of targeting phosphorylated Aβ species for AD therapy and prevention.

Chapter 1 | Introduction

1.1 | Alzheimer's Disease (AD)

Alzheimer's disease (AD) was described in 1907 by the German physiatrist Alois Alzheimer in a histopathologic study of the brain of his patient, Auguste Deter, suffering from dementia. He brought to light the presence of two types of lesions in the brain, senile plaques and neurofibrillary tangles (NFTs). He concluded that as a distinct disease of the cerebral cortex (Alzheimer et al. 1995; Alzheimers 1911).

AD is an age-related progressive neurodegenerative disease and the most common cause of dementia ('2020 Alzheimer's disease facts and figures' 2020). Alzheimer's is believed to begin before symptoms appear (Villemagne et al. 2013; Jack et al. 2009; Braak et al. 2011; Gordon et al. 2018). AD is clinically distinguished by memory impairment and progressive decline in cognitive functions that can ultimately affect behaviour, speech, visuospatial orientation and the motor system (Schultz et al. 2004; DeTure et al. 2019; Nelson et al. 2009; Murray et al. 2011; Aisen et al. 2017; Masters et al. 2015). Clinical AD dementia cannot be definitively diagnosed until a post-mortem neuropathological examination is performed (Caselli et al. 2017). Currently, there are no effective therapies to intervene in the course of AD dementia. Several factors are thought to increase risk, so avoiding these is believed to reduce risk/age of onset (Lane et al. 2018; Cummings et al. 2018; Cummings et al. 2017; Edwards Iii et al. 2019; van der Flier et al. 2005; '2020 Alzheimer's disease facts and figures' 2020).

AD is characterized by widespread brain atrophy (Figure 1.1) (Braak and Del Tredici, 2011) and the combined presence of key histopathological hallmarks, extracellular amyloid-beta (Aβ) plaques and intracellular neurofibrillary tangles (NFTs) with abnormally phosphorylated tau (τ) protein in the brain (Thal et al. 2015; Hyman et al. 2012). The presence of these two features is required for the ultimate diagnosis. These changes are accompanied by the death of neurons and damage to brain tissue. In addition to this, extensive post-mortem immunohistochemical examinations often illustrate τ positive neuropil threads, dystrophic neurites and marked gliosis in AD patients which are associated with activation of microglia and astrocytes (Ransohoff 2016a; Itagaki et al. 1989). Additionally, the presence of eosinophilic Hirano bodies, granulovacuolar degeneration (GVD), cerebral amyloid angiopathy (CAA), inflammation and major synaptic changes are also common (Perl 2010; Dickson 1997; Katsumoto et al. 2018; Dansokho et al. 2018; Tonnies et al. 2017).

With the development in scientific techniques, research made a great lead in the understanding of the disease. Three well-established neuroimaging markers are now included in the revised criteria for amnestic forms of AD (Dubois et al. 2014): MRI, (to assess hippocampal atrophy), FDG-PET (to assess temporoparietal hypometabolism), and fibrillar amyloid PET (to check increased brain amyloid deposition). The availability of imaging biomarkers greatly increased the likelihood of diagnosing AD even in preclinical/predementia

stages (Dubois et al. 2014). Combining multiple imaging methods, such as τ and FDG-PET with fMRI (which can be done simultaneously using PET-MRI), would enable researchers to investigate the effects of pathological deposits on functional networks and gain a better understanding of the pathological course of AD over time. (Migliaccio et al. 2020).

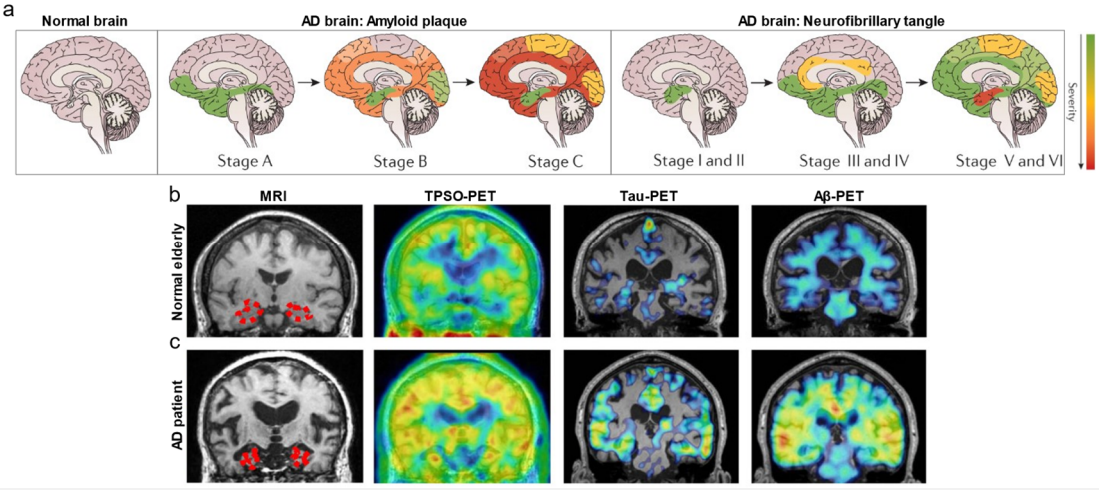

Figure 1.1 | Alzheimer's disease (AD) pathology in the human brain

(a) In AD, deposition of Aβ precedes neurofibrillary and neuritic changes with an apparent origin in the frontal and temporal lobes, hippocampus and limbic system. The NFTs and neuritic degeneration start in the medial temporal lobes and hippocampus and progressively spread to other areas of the neocortex. It is less common for AD to develop in other neocortical regions (frontal, parietal, and occipital lobes), showing relative sparing of the hippocampal structure. Comparison of **(b)** the normal elderly patient brain and **(c)** the AD patient brain by using molecular imaging techniques showing significant hippocampal atrophy in AD patient compared to control (red dotted area) in the magnetic resonance imaging (MRI) scanning. *In-vivo* positron emission tomography (PET) showed increased Aβ, τ signal and increased translocator protein (TSPO) signal marked by increased gliosis and inflammation in AD compared to healthy elderly cases. The PET imaging was done with [^{11}C]PiB (Aβ-PET), [^{11}C] PBB3 (τ-PET) and [^{11}C] DAA1106 (TSPO). *(Part (a) was adapted from (Masters et al. 2015), © 2015 Macmillan Publishers Limited, with permission from Springer Nature. (original source (Braak et al. 1997); part (b-c) was adapted from (Higuchi et al. 2016) © 2016 Japanese Society for Neuroimmunology, with permission from John Wiley and Sons)*

1.1.1 | Etiology of AD

To date, the cause of AD is not well understood. The greatest risk factor for sporadic AD is ageing (Guerreiro et al. 2015). Besides ageing, environmental (Dunn et al. 2019), epigenetic (Li et al. 2019; Coppieters et al. 2011), and genetic factors (Bellenguez et al. 2020) contribute to the risk of developing AD. Moreover, accumulating genetic and functional evidence strongly indicates an active role of the brain's innate immunity in AD pathogenesis and progression (Pimenova et al. 2018; Ennerfelt et al. 2020).

1.1.1.1 | Amyloid precursor protein (APP) processing

Amyloid precursor protein (APP) is crucial and central to understanding AD. APP is a type I transmembrane protein that mediates cell-to-cell adhesion to support synaptic connections as well as neuronal signals and neurotransmitter release by activating calcium channels. Alternate transcriptional splicing of the APP gene can generate isoforms, including the APP695 expressed predominantly in neurons, the APP751 and 770 expressed both in neurons, glial cells and many other cell types (Matsui et al. 2007; Nalivaeva et al. 2013; Cappai 2014; Zhang et al. 2011; Belyaev et al. 2010).

The major secretases of APP processing include α-secretase- mainly ADAM10 (A disintegrin and metalloproteinase domain-containing protein 10); β-secretase-BACE1 and 2; γ-secretase complex- PS1 and 2 (presenilin 1 &2), NCT (Nicastrin), PEN2 (presenilin enhancer 2), APH1 and 2 (anterior pharynx defective 1 & 2).

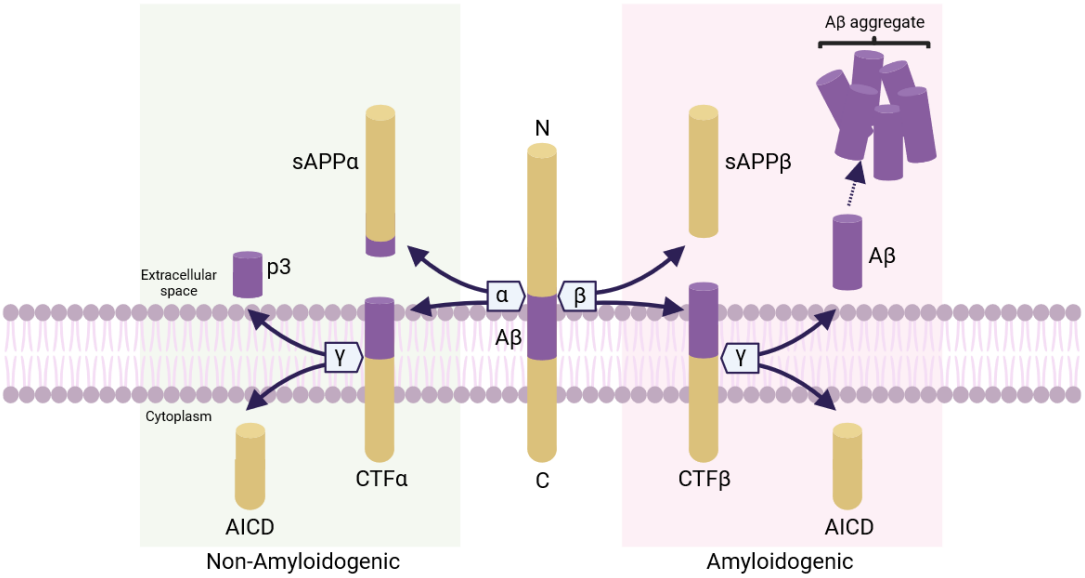

Figure 1.2 | Amyloid precursor protein (APP) processing pathway

In the canonical pathway, APP can be processed by either non-amyloidogenic α-secretase or amyloidogenic β-secretase pathway. In the non-amyloidogenic pathway, cleavage by α-secretase releases the soluble APP-fragment, sAPPα. The APP C-terminal fragment (CTFα) is then cleaved by γ-secretase to release the APP intracellular domain (AICD) and extracellular p3 fragment. In the amyloidogenic pathway, cleavage by β-secretase releases the soluble fragment, sAPPβ. The CTFβ is then cleaved by γ-secretase to produce Aβ40, Aβ42, and AICD. *(Figure was adopted from (Muller et al. 2017) and modified by Pranav Joshi using BioRender.com)*

The α-secretase cleavage initiates the so-called non-amyloidogenic pathway, which causes the formation of the APP-intracellular domain (AICD) and the soluble extracellularly secreted APPsα fragment. sAPPα has been well studied for its role in neuronal plasticity, synaptic transmission, cognition and neuroprotection during brain development as well as in the mature and ageing brain (O'Brien et al. 2011; Rice et al. 2019; Muller et al. 2017; Haass et al.

2019; Guo et al. 2020). In contrast, the abnormal proteolytic processing of APP via amyloidogenic pathways mediated by β- and γ-secretases produces a sAPPβ fragment, AICD and, importantly, amyloid peptides of varying lengths (Zhang et al. 2011; Bibl et al. 2006; Bibl et al. 2007) (Figure 1.2).

The γ-Secretase plays a central to intramembrane proteolysis by cleaving transmembrane APP domains, which, in turn, expose a C-terminal fragment (99 amino acids, C-99) to γ-secretase. This C-99 retains the transmembrane domain, in which γ-secretase first cuts between amino acids 48 and 49, or 49 and 50 (known as ε cleavage). This releases either of two APP intracellular domains, AICD49-99 or AICD50-99 into the cytosol. Following this, γ-secretase proceeds to chop off C-terminal amino acids from the remaining transmembrane domain, releasing the Aβ peptides into the lumen. Studies revealed that carboxypeptidase-like cleavage by γ-secretase occurs in increments: Epsilon cleavage at position 48 yields Aβ45, then Aβ42, while initial cleavage at amino acid 49 yields Aβ46, Aβ43, and finally Aβ40 (Takami et al. 2009; Bolduc et al. 2016; Olsson et al. 2014; Dimitrov et al. 2013; Lichtenthaler et al. 1999; Esler et al. 2004). Among these peptides, Aβ42 and Aβ40 are the predominant Aβ species in the brain (Bitan et al. 2003; Suzuki et al. 1994a; Iwatsubo et al. 1994; Waragai et al. 2012; Murray et al. 2012; Nutu et al. 2013). Although soluble Aβ40 is much more abundant than soluble Aβ42, Aβ42 exhibits a higher aggregation propensity, due to hydrophobicity within its two terminal residues. Indeed, Aβ42 is the main component of amyloid plaques depending on plaque size and stage and is also neurotoxic (Iwatsubo et al. 1994; Chen et al. 2017; Serrano-Pozo et al. 2012; Gu et al. 2013; Boon et al. 2020). Therefore, Aβ42 is thought to be a key player in initiating plaque formation and AD pathogenesis (Jan et al. 2008).

1.1.1.2 | Familial Alzheimer's Disease (fAD)

Dominantly inherited familial AD (fAD) can be caused by mutations in amyloid precursor protein (APP), and the two presenilin genes (PSEN1&2). These rare familial forms of AD account for less than 1% of all cases (Campion et al. 1999). Early-onset AD (EOAD) refers to cases diagnosed before age 65. Though slightly more common than fAD cases, EOAD cases account for less than 5% of pathologically diagnosed cases of AD (Ryman et al. 2014; Campion et al. 1999).

In addition to APP mutations, mutations in γ-secretase components PS1 or PS2 are also prevalent in fAD. Many of these mutations affect the γ-secretase cleavage of the APP which may alter Aβ40/42 ratios (Saito et al. 2011; Kretner et al. 2016; De Jonghe et al. 2001). One such example is the London APP mutation (V717I) which increases the Aβ40/42 ratio by modifying the γ-secretase cleavage (Goate et al. 1991). However, the well-known Swedish APP fAD mutation (APPswe, K595N/M596L) is located near the BACE1 cleavage site, enhancing BACE-mediated APP cleavage (Haass et al. 1995; Hardy et al. 2002). Not all APP mutations are

pathogenic. A recently identified rare Icelandic APP protective mutation, (A673T) based C-terminal to the β-secretase cleavage site reduces the AD risk onset through the attenuation of Aβ production and aggregation (Jonsson et al. 2012; Veugelen et al. 2016; Bergmans et al. 2010; De Strooper et al. 1999). These findings suggest that Aβ generation and accumulation play an important role in the initiation and development of AD.

1.1.1.3 | Sporadic Alzheimer's Disease (sAD)

Sporadic or late-onset AD (LOAD) is etiologically heterogeneous and results from a combination of many genetic and non-genetic (including lifestyle, injuries, and environmental) factors.

1.1.1.3.1 | Genetic risk factors

sAD is a complex genetic disorder, with an estimated heritability of 60-80% (Carmona et al. 2018). Despite uncertainty over environmental risk factors for sAD, one key genetic risk factor stands out in all studies: the polymorphism, ε4 associated with the gene encoding apolipoprotein E (ApoE) has a major effect in determining the risk/age/progression of AD (Masters et al. 2015) by modulating Aβ clearance and aggregation (Castellano et al. 2011; Holtzman et al. 2000). LOAD cases often display an increase in Aβ production resulting from an increase in β- or γ- secretase activity or deficits in Aβ clearance. (Mawuenyega et al. 2010; Selkoe 2001). Humans have three common alleles of ApoE, ε4 (Arginine 112, Arginine 158), ε3 (Cysteine 112, Arginine 158), and ε2 (Cysteine 112, Cysteine 158). Among these AD risk increases with an inheritance of the ε4 allele and there is a gene dosage effect wherein a single copy of ε4 increases AD risk by ~3-fold, while two copies increase the risk by ~12-fold, thereby affecting the age of onset and progression significantly (Corder et al. 1993; Saunders et al. 1993). Furthermore, the ε4 allele appears to confer risk for vascular dementia (VD), Lewy body dementia (LBD), Down's syndrome (DS) and traumatic brain injury (TBI) (Verghese et al. 2011). Genome-wide association studies (GWAS), a methodology that compares allele frequencies of polymorphisms between cases and controls revealed the genetic complexity of the disease in increasing susceptibility for LOAD. GWAS have identified polymorphisms in or near several genes that are associated with AD risk, including ABCA7, CLU, CR1, CD33, CD2AP, EPHA1, BIN1, PICALM, and MS4A (Karch et al. 2015; Kunkle et al. 2019). In contrast to the GWAS, whole genome or exome sequencing studies have identified rare coding variants that have moderate to large effects on LOAD risk such as the TREM2 (Figure 1.3).

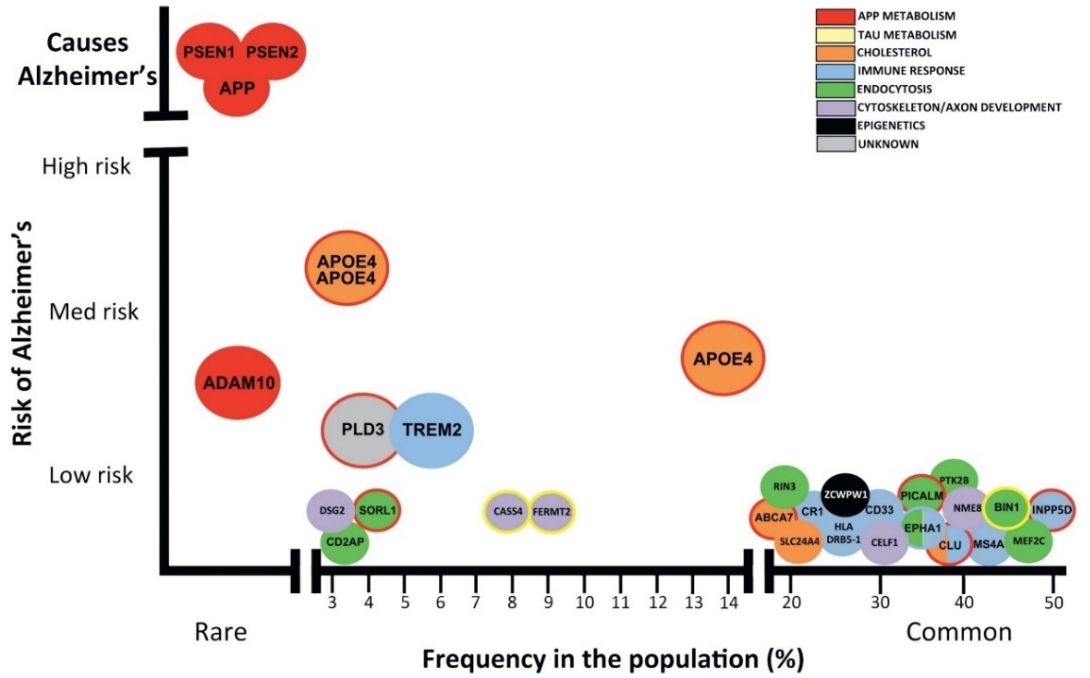

Figure 1.3 | Rare and common variants of AD genes and their risk

(Figure obtained from (Karch et al. 2015) Copyright @ 2015 Society of Biological Psychiatry, with permission from Elsevier. (original source (Guerreiro et al. 2013b))

1.1.1.3.2 | Non-genetic risk factors

Various environmental factors mediate the development and progression of LOAD at various levels (Wainaina et al. 2014). Such as at the systemic level, dysfunction of the hypothalamic-pituitary-adrenal (HPA) axis (Herman et al. 1995; Ostrander et al. 2006; Green et al. 2006) or at the intercellular level, cerebrovascular dysfunction, Aβ accumulation (De Felice et al. 2007; Shinkai et al. 1997), glial activation (Cornejo et al. 2013; Morales et al. 2013; Ogundele et al. 2014; Lee et al. 2013a), and metal toxicity (Moulton et al. 2012; Ayton et al. 2013; Bush 2013) creates abnormal milieu around neurons. In addition, at the intracellular level, the imbalance between the activities of enzymes such as τ-related kinases and phosphatases (Grundke-Iqbal et al. 1986; Alonso et al. 1994; Gendreau et al. 2013) and the abnormal epigenetic modification, especially DNA methylation and histone acetylation (Chouliaras et al. 2010; Kwok 2010; Babenko et al. 2012), are associated with neuronal dysfunction in LOAD (Wainaina et al. 2014).

1.1.2 | Amyloid cascade hypothesis

The amyloid cascade hypothesis states that excessive Aβ peptide accumulation, particularly of the longer, aggregation-prone Aβ species (Aβ42/43), is the causative agent in AD pathogenesis that sets a series of downstream events that ultimately leads to dementia and neurodegeneration (Selkoe et al. 2016; Hardy et al. 2002). Several pieces of evidence support the key role of Aβ dyshomeostasis in initiating AD (Selkoe et al. 2016). All AD patients have a

progressive accumulation of Aβ, which is followed by surrounding neuritic and glial cytopathology in brain regions responsible for memory and cognition (Selkoe et al. 2016; Haass et al. 2007). An extra copy of APP locus on chromosome 21 causes EOAD with CAA, strokes and intracerebral haemorrhage (ICH) of variable frequency (Rovelet-Lecrux et al. 2006; Cabrejo et al. 2006; Sleegers et al. 2006; Rovelet-Lecrux et al. 2007; Mann et al. 2018). While Down's syndrome patients (with trisomy 21) harbour 3 copies of APP and invariably develop neuropathologically typical AD (Delabar et al. 1987) showing progressive accumulation of abundant diffuse Aβ plaques with neuritic dystrophy, microgliosis, astrocytosis, and tangle formation (Selkoe et al. 2016). Patients with DS, have a high incidence of developing AD but also leukaemia, certain congenital heart defects, diverse autoimmune disorders, and autism but have a lower risk of developing many types of solid tumour cancers, some forms of adult cardiovascular diseases (such as hypertension and ischemic heart disease)(Snyder et al. 2020). As shown before, human Aβ42 oligomers form a penumbra around many neuritic plaques, causing τ hyperphosphorylation at AD-relevant epitopes and neuritic dystrophy (Selkoe et al. 2016; Jin et al. 2011). As a result, a decrease in synapse number occurs in a centrifugal gradient, with less abnormality at greater distances from the plaque edge (Selkoe et al. 2016; Yang et al. 2017b; Spires et al. 2005). According to many human biomarker studies, low CSF Aβ42 and positive amyloid-PET scans occur years before other AD-related changes (such as increased CSF τ, decreased cerebral glucose metabolism, brain atrophy, clinical dementia) (Selkoe et al. 2016).

The progressive accumulation of aggregation-prone Aβ species is thought to initiate the amyloid cascade in the AD brains (Selkoe et al. 2016; Haass et al. 2007; Selkoe 1991; Hardy et al. 1992; Hardy et al. 2002) (Figure 1.4). The fAD mutations cause a relative increase in Aβ42 species (Berezovska et al. 2005), which can cause severe and permanent changes in the synaptic function and also deposition as relatively visible benign diffuse (non-fibrillar) plaques in the brain parenchyma (Haass et al. 2007). Eventually, these diffuse plaques begin to accumulate Aβ fibrils which cause local inflammation, synaptic spine loss, and neuritic dystrophy. Over time, these events result in oxidative stress, endoplasmic reticulum (ER) stress, altered ion (e.g. calcium) homeostasis and a host of additional biochemical changes leading to an imbalance of phosphatases and kinases that could cause the τ hyperphosphorylation, enhance vascular and neuronal damage and induce widespread neuroinflammation observed as the disease progresses (Haass et al. 2007; Hardy et al. 1992; Selkoe et al. 2016). In addition to altered cellular dysfunction, Aβ has been shown to initiate τ phosphorylation both *in-vitro* and *in-vivo* (Jin et al. 2011; Zhang et al. 2014; Ma et al. 2009; Bloom 2014).

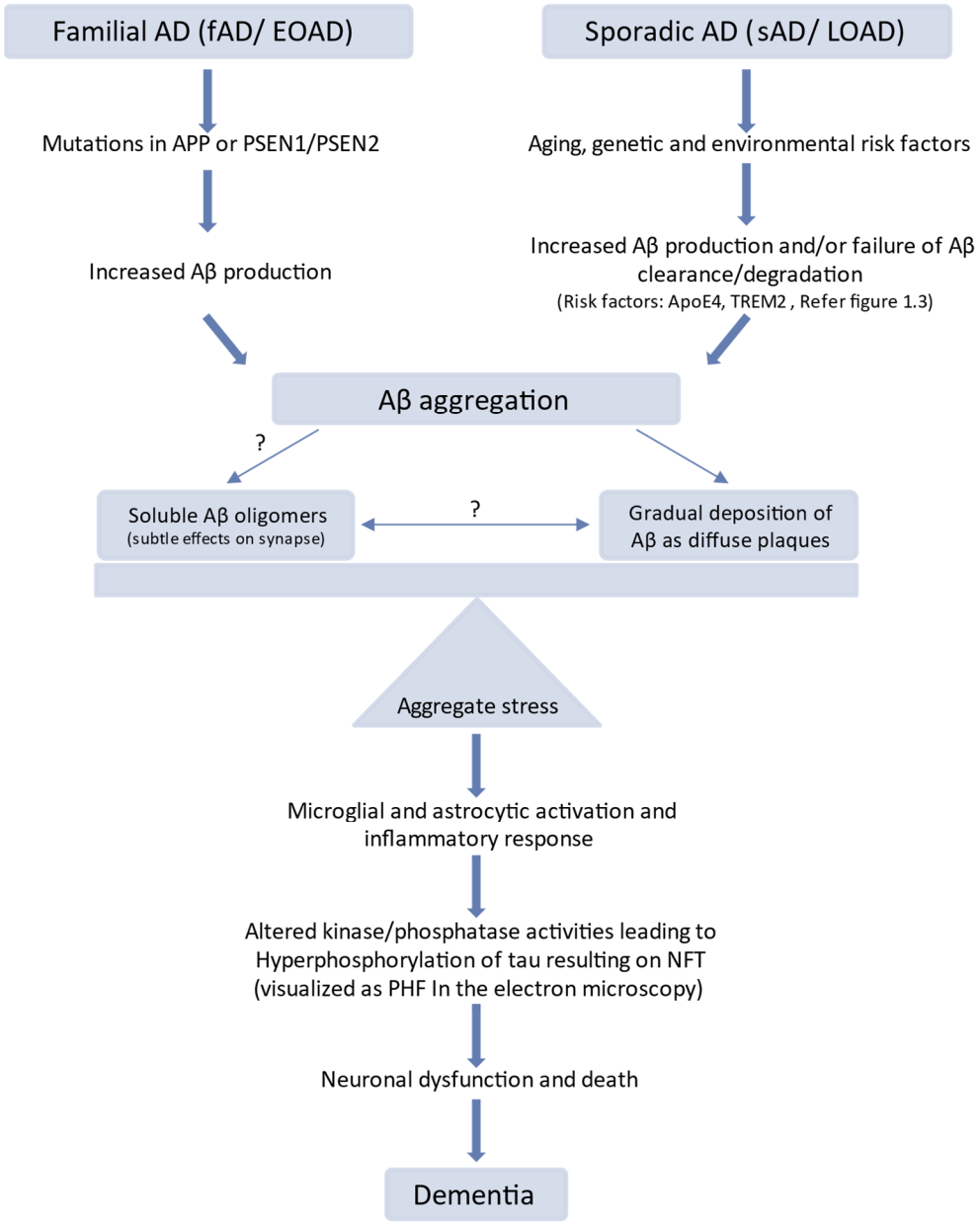

Figure 1.4 | The amyloid cascade hypothesis showing major pathogenic events leading to AD

This hypothesis represents the classic theory of the origins of both fAD caused by autosomal dominant mutations of three genes: PSEN1 and 2 and APP, while the sAD is caused by a combination of many genetic and environmental factors, ultimately leading to the altered production of Aβ. The classic theory has been modified over the years as it became clear that the correlation between dementia or other cognitive alterations and Aβ accumulation in the brain in the form of amyloid plaques is not linear. The theory now suggests that synaptotoxicity and neurotoxicity may be mediated by such soluble forms of multimeric Aβ peptide species which also deposit in the form of diffuse plaques. The dynamic nature of Aβ oligomers and the poorly defined mechanism/s of toxicity make this topic particularly controversial in the field. The term “aggregate stress” describes the potential mechanisms that may lead to Aβ aggregation (oligomers or the diffuse plaques). This leads to a chain of events such as microglial and astrocytic activation, inflammatory response, altered kinase/phosphatase activities leading to τ hyperphosphorylation resulting in NFT (visualized as PHFs in the electron microscopy) and,

ultimately, resulting in neuronal dysfunction/death. *(Figure is made by Pranav Joshi with the help of (Karran et al. 2011; Selkoe et al. 2016))*

The hyperphosphorylated τ leads to deposition as NFTs that contribute to additional defects, including some in axonal transport (Gendron et al. 2009; Mandelkow et al. 2012; Liu et al. 2020). The proposed cascade eventually leads to widespread synaptic/neuronal dysfunction and cell death, resulting in progressive dementia with extensive Aβ and τ pathology (Hardy et al. 2002; Rajmohan et al. 2017).

Contrary to the amyloid hypothesis, it is important to note that early symptoms of dementia and neuronal loss have been closely linked to NFTs deposits while Aβ plaques appear to be neurotoxic, particularly in the presence of NFTs (Rapoport et al. 2002). Here one could speculate the prerequisite of Aβ oligomers or deposits to be initially present to consequently trigger τ-mediated toxicity (Haass et al. 2007). The presence of senile Aβ plaques is not necessarily liked to cognitive abnormalities (Bennett et al. 2006; Morris et al. 2010) and this could suggest that Aβ may not necessarily initiate the downstream events but may instead be associated with ageing (Jack et al. 2008; Rodrigue et al. 2009).

Findings suggest that inflammatory pathways change during ageing and are specifically altered in AD (Cullen et al. 2021). It was suggested that the brain's innate immune system, and in particular the microglial response to plaque formation play a significant role in AD pathogenesis. Gene variants related to innate immunity and the complement cascade emerged as risk factors in AD (Jones et al. 2010; Torvell et al. 2021). The RNA-sequencing (RNA-seq) and single-cell RNA-sequencing (scRNA-seq) have revealed microglia-associated genes and provided insights into heterogeneous microglial activity changes in AD progression (Magusali et al. 2021; Tanzi 2012; Torvell et al. 2021). Indeed, blockade of complement receptor 1 (CR1) inhibits microglial activation and potentiates microglial phagocytosis (Lambert et al. 2009; Crehan et al. 2013), inactivation of sialoadhesin CD33 in primary microglia also potentiates microglial uptake of Aβ (Bertram et al. 2008; Griciuc et al. 2013) and TREM2, responsible for binding and sustaining microglial phagocytosis of Aβ (Wang et al. 2015; Zhao et al. 2018). All these studies suggest that it might be the failure of plaque clearance mechanisms one such mediated by microglia that could modulate the severity of plaque pathology and its clinical manifestations. In parallel, alterations in the cholesterol/sterol metabolism (Loera-Valencia et al. 2019; Varma et al. 2021) and increased inflammatory response promote neuroinflammation, synaptic degradation and neurodegeneration (Wyss-Coray et al. 2012; Petrov et al. 2016; Zhang et al. 2015; Kinney et al. 2018).

1.1.3 | Deposition and propagation of Aβ in the brain

The deposition of insoluble Aβ as an extracellular deposit with variable morphology has been documented in several studies. The human brains with different degrees of plaque accumulation show a spatiotemporal course of Aβ plaque formation (Thal et al. 2015; Thal et al. 2006; Thal et al. 2002; Walker 2020). In general, diffuse plaques emerge first, followed later by cored (amyloid) plaques (Braak et al. 2011). The neuropathological assessments followed by confirmation using cross-sectional Florbetapir-PET imaging have revealed a general pattern of Aβ-amyloid deposition (Serrano-Pozo et al. 2011; Grothe et al. 2017; Thal et al. 2006; Thal et al. 2002; Thal et al. 2000; Thal et al. 2015; Braak et al. 2011). Aβ plaques can be broadly categorized into amyloid plaques with varying sizes, shapes, densities and locations (Serrano-Pozo et al. 2011; Wisniewski et al. 1989; Ikeda et al. 1989; Armstrong 1998; Thal et al. 2000). Aβ-amyloid plaques are more or less spheroidal lesions that include 'classical' or 'mature' plaques and so-called compact/dense plaques (Walker 2020; Masters et al. 2001). Recently, another morphology called coarse-grain plaque has been described containing multiple small cores and a predominance of Aβ40 in advanced AD cases, often with CAA (Boon et al. 2020). Diffuse Aβ plaques comprise very small, and may or may not include amyloid fibrils (Davies et al. 1993; Yamaguchi et al. 1991; Yamaguchi et al. 1989).

Apart from extracellular deposition, Aβ accumulates in the vascular wall and perivascular zone in cases of primary Aβ-CAA involving APP mutations and to varying degrees in nearly all cases of AD (Walker 2020; Revesz et al. 2003; Greenberg et al. 2020; Biffi et al. 2011; Haan et al. 1990; Maat-Schieman et al. 1996). In the early stages of AD, Aβ42 is more commonly present than is Aβ40, but in later stages, Aβ40 predominates (Roher et al. 2000; Walker 2020). However, capillaries more often are positive for Aβ42 than for Aβ40 in CAA, presumably because of different mechanisms in the capillaries than that in large vessels and Aβ plaques (Richard et al. 2010; Attems et al. 2010; Walker 2020; Serrano-Pozo et al. 2011; Perl 2010).

As shown by many studies, Aβ can also accumulate intracellularly and is evident in many cellular models (Takeda et al. 2004; Ida et al. 1996; Knauer et al. 1992; Ard et al. 1996; Philipson et al. 2009; Takahashi et al. 2002; Takahashi et al. 2004; Gouras et al. 2010; Oddo et al. 2003; Aho et al. 2010; Wirths et al. 2004; Bayer et al. 2010; Wirths et al. 2010a; Jawhar et al. 2012; Wirths et al. 2009; Wirths et al. 2010c). Among these cell types, uptake by glial cells may reflect mainly clearance activity, whereas uptake by neurons may represent an alternative mechanism in the development of AD. The presence of intracellular Aβ has been shown in the postmortem human brain (Aho et al. 2010), AD transgenic mice (Philipson et al. 2009) and biochemically by micro dissecting human neurons (Hashimoto et al. 2010).

Aβ deposition follows distinct pathways spreading progressively rather than Aβ aggregation in different brain regions over time. This spread suggests self-propagating conformation upon misfolding and aggregation (Condello et al. 2018b). This was first demonstrated by *in-vivo*

experiments, wherein injecting Aβ aggregates from AD patients or aged transgenic mice into young mice expressing human Aβ-induced cerebral amyloidosis and recently it was found that microglia can propagate Aβ pathology in previously unaffected tissue (Meyer-Luehmann et al. 2006; d'Errico et al. 2022). It is also important to note that, APP overexpression is not a prerequisite for the prion-like induction of cerebral Aβ deposition (Ruiz-Riquelme et al. 2018). The inoculation of either purified Aβ aggregates derived from the brain or aggregates composed of synthetic Aβ demonstrates prion properties ultimately leading to widespread cerebral β-amyloidosis (Stohr et al. 2012; Jucker et al. 2018; Fritschi et al. 2014; Walker 2020; Condello et al. 2018b).

1.1.4 | Heterogeneity of Aβ in the AD brain

As explained in the preceding sections (1.1.1.2 and 1.1.1.3), the fAD is caused by the genetic abnormalities that result in accelerated Aβ accumulation in the brain causing early-onset dementia or CAA or both (Goate et al. 1991; Tsubuki et al. 2003; Tomiyama et al. 2008; Bettens et al. 2013; Levy et al. 1990) (Figure 1.5).

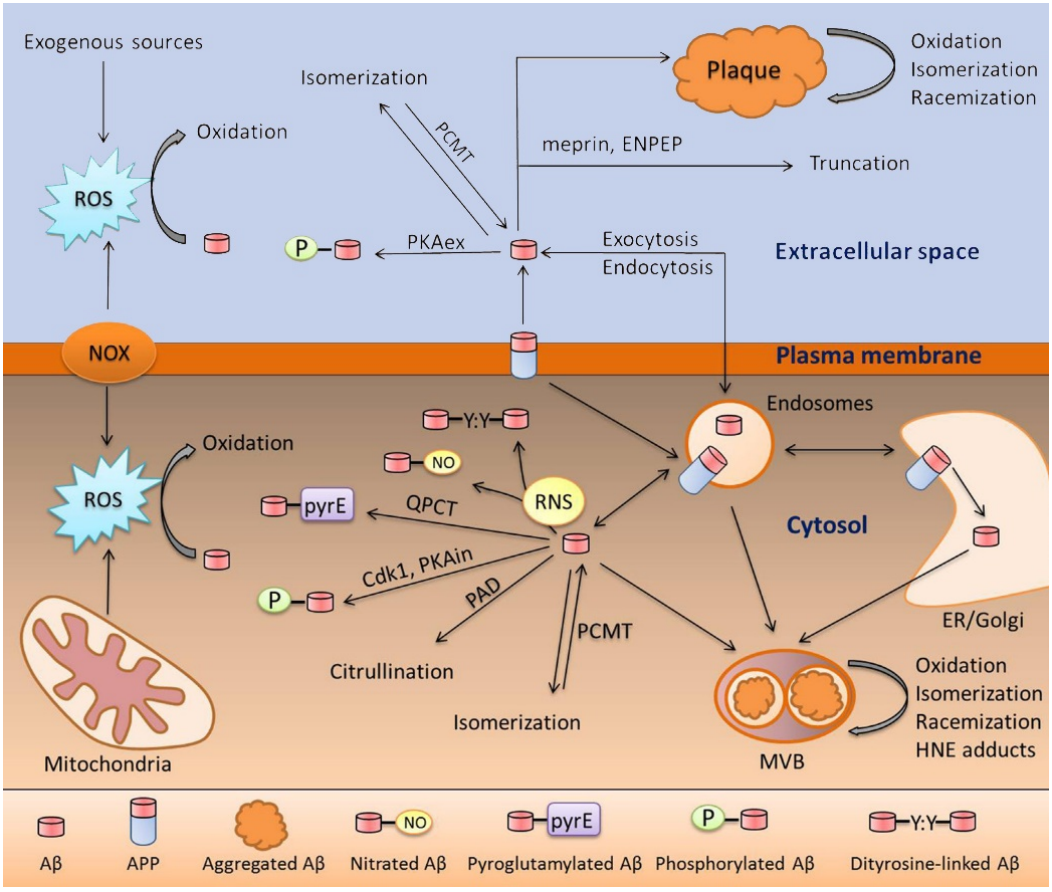

Figure 1.5 | Post-translational modifications (PTMs) of Aβ

APP is proteolytically processed to produce Aβ at the plasma membrane or inside the cell in the endosomal compartment or ER/Golgi or secretory compartment and the exchange of intra- and extracellular pools of Aβ can take place by endo- and exocytosis. Aβ in both of these pools can undergo modification by oxidation by enzymes due to interaction with reactive oxygen species (ROS), nitration

of Tyr10 residue by reactive nitrogen species (RNS), phosphorylation by protein kinase A (PKA) [extracellularly (ex) or intracellularly (in)] and cyclin-dependent kinase 1 kinase (Cdk1) (intracellularly), citrullination by peptidyl arginyl deiminase (PAD), isomerization or racemization of aspartic residues by protein carboxyl methyltransferase 1 (PCMT1), truncation by meprin and glutamyl aminopeptidase (ENPEP), pyroglutamylation by glutaminyl-peptide cyclotransferase (QPCT). Lastly, the oxidative stress due to Aβ in the amyloid deposits (plaques or multivesicular bodies (MVB)) form adducts with 4-hydroxynonenal (HNE); a product of lipid peroxidation. *(Figure adapted from (Barykin et al. 2017), CC BY © 2017 Barykin, Mitkevich, Kozin and Makarov)*

While the more common sAD is caused by failure of the Aβ clearance mechanism (Selkoe et al. 2016). While Aβ42 peptides appear to be the earliest form to accumulate in the brain, recent studies have revealed heterogeneity of both Aβ and other proteolytic products of APP processing (Selkoe et al. 2016). The analysis of Aβ plaque composition has shown that Aβ peptides are modified by different enzymes or are isomerized or racemized which leads to altered aggregation kinetics, neurotoxicity, and amyloidogenicity (Barykin et al. 2017; Welzel et al. 2014; Willem et al. 2015) (Figure 1.5).

The APP is processed by the α-, β-, and γ-secretases (Figure 1.2). β-secretase (such as BACE1) mediates the initial rate-limiting step leading to the production of Aβ peptides (Vassar et al. 1999). Cleavage by γ-secretase results in the production of a truncated Aβ peptide ranging from 37 to 43 amino acids in length; notably the 42 residue species are considered to be the most pathogenic (Haass et al. 2007). There are also minor cleavage sites at positions 34, 37, 39 and 43 (Takami et al. 2009) including the shorter forms (Aβ1-17, 18/19/20) with unknown mechanisms generated by γ-secretase cleavage (Beher et al. 2002; Portelius et al. 2011). Apart from Aβ generated during APP processing, many other modified Aβ species are produced by different enzymes and are reviewed previously (Barykin et al. 2017; Kummer et al. 2014) (refer to Figure 1.5). The following sections describe the modified Aβ species studied in this work.

1.1.4.1 | Pyroglutamation

The formation of N-terminally pyroglutamate-modified Aβ at position 3 (N3pE-Aβ) requires the removal of the first two amino acids from Aβ (Mori et al. 1992). For this modification, Aminopeptidase A (Sevalle et al. 2009) or spontaneous amide hydrolysis by Cu^{2+} have been reported (Drew et al. 2009). Another modification at glutamate 11 arising from the alternative BACE1 cleavage side in APP was discovered (N11pE-Aβ) (Liu et al. 2002; Naslund et al. 1994). In a subsequent step, the terminal glutamate is converted to pyroglutamate in a dehydration reaction (Schilling et al. 2004). This reaction can be catalyzed by the enzyme glutaminyl cyclase (Schilling et al. 2004), which is increased in AD (Schilling et al. 2008). *In-vitro*, NpEAβ(3-42) has similar toxicity compared to wild-type Aβ on neuronal cells (Tekirian

et al. 1999) and in mouse models that generate pyroglutamate-modified Aβ (Wirths et al. 2009; Alexandru et al. 2011).

This modification leads to altered biophysical and biochemical properties and tends to accumulate due to their limited degradation by enzymes (Saido et al. 1996; He et al. 1999). Also, this modification increases the aggregation propensity in aqueous and hydrophobic media compared to full-length Aβ (He et al. 1999). The N3pE-Aβ is proved to be more toxic for neurons and astrocytes compared to wild-type Aβ (Russo et al. 2002). However, some studies have demonstrated that the secondary structure and toxicity of the monomeric NpE(3-40/42) is similar to that of wild-type Aβ (1-40/42) peptides and exhibited similar effects on neuronal cytotoxicity in primary cortical neurons (Tekirian et al. 1999; Wirths et al. 2010b; Youssef et al. 2008).

1.1.4.2 | Nitration

The progression in accumulation of nitrated Aβ species has been observed in AD and is mediated by increased expression of nitric oxide synthase 2 (NOS2) leading to elevation in NO production (Heneka et al. 2001; Vodovotz et al. 1996; Butterfield et al. 2007; Castegna et al. 2003; Kummer et al. 2011; Luth et al. 2002). Considering the amino acid sequence of Aβ tyrosine 10 of Aβ is a potential target for protein nitration. This modification increases the propensity of Aβ to aggregate and also its deposition in the core of Aβ plaques (Kummer et al. 2011; Zhao et al. 2021). Nitrated Aβ was able to promote plaque formation in APP/PS1 mice, implying a key role in the early stages of AD (Kummer et al. 2011).

1.1.4.3 | Phosphorylation (pSer8, pSer26)

Phosphorylation of Aβ at serine residues 8 and 26 is widely studied. Phosphorylation of Aβ at serine 8 (pSer8-Aβ) increases the stability of its pathogenic aggregates against high-pressure and SDS-induced dissociation (Rezaei-Ghaleh et al. 2016). This pSer8 modification also inhibited the proteolytic degradation of Aβ monomers by the insulin-degrading enzyme and by the angiotensin-converting enzyme (Kumar et al. 2012; Kumar et al. 2011b). Using antibodies specifically recognizing Ser8 phosphorylated Aβ (described in Section 2.2), revealed the presence of phosphorylated Aβ in brains of human AD, DS cases as well as in different APP transgenic mouse models (Kumar et al. 2020a). In AD brains, pSer8-Aβ is localized to amyloid plaques (Kumar et al. 2011a; Joshi et al. 2021a), intracellularly (Kumar et al. 2013; Joshi et al. 2021a) and in CAA (Gerth et al. 2018; Joshi et al. 2021a).

Phosphorylation of β-amyloid at serine 26 by cyclin-dependent kinase 1 (cdk1) also known as cell division cycle protein 2 homolog (cdc2) (Milton 2001) leads to stable oligomeric assemblies and does not form larger fibrillar aggregates (Kumar et al. 2016). Using antibody detecting this modification, this species was detected in intracellular compartments of GVD,

but less frequently in extracellular plaques (Kumar et al. 2016). Furthermore, pSer26-Aβ species have been detected intracellularly, faintly in the plaques as well as CAA by using a novel monoclonal antibody described in Section 2.2(Kumar et al. 2020a).

The presence of phosphorylated Aβ species was verified by complementary biochemical methods using human brain samples (Kumar et al. 2011a; Rijal Upadhaya et al. 2014; Ashby et al. 2015; Kumar et al. 2016; Kumar et al. 2020a). In addition, recent studies demonstrated the existence of phosphorylated Aβ peptides by mass spectrometry (MS) in CAA patients and AD patients (Song et al. 2017a; Domingo et al. 2021), and by highly sensitive electrochemical impedance spectroscopy in human CSF (Yin et al. 2019), further demonstrating the existence of phosphorylated Aβ *in-vivo*.

1.2 | Mouse models of amyloid pathology

Transgenic mice were developed based on the amyloid hypothesis. In the first attempts to overexpress human APP in transgenic mice, none of these efforts resembled an amyloid plaque or any other recognizable AD-type pathology (Elder et al. 2010). After the discovery of fAD mutations in the APP and PS mutations, many groups started working with AD transgenic mouse models containing fAD mutations (Gotz et al. 2004; Reilly et al. 2003; Sasaguri et al. 2017; LaFerla et al. 2012). Importantly, sequence differences between mice and humans include 3 amino acids within the Aβ sequence (R5G, Y10F and H13R)(Tanzi et al. 1987; Xu et al. 2015). These prevent the formation of Aβ plaques in wild-type mice. Hence, the expression of human APP is necessary for the formation of Aβ plaques in mice. Various mouse models have been generated over years and the exact phenotype for each transgenic strain depends on the mutation, promoter, and mouse strain (Drummond et al. 2017; Boutajangout et al. 2014; Dujardin et al. 2015; Puzzo et al. 2015; Wisniewski et al. 2015; Wisniewski et al. 2010). Apart from Aβ plaque pathology, a limited number of studies have reported the animal models that display both plaques and tangles (Bolmont et al. 2007; Grueninger et al. 2010; Lewis et al. 2001; Oddo et al. 2003; Ribe et al. 2005).

Even though none of the existing transgenic models fully reproduce the full spectrum of AD pathology (plaques and tangles), critical aspects of AD pathology and disease processes can be experimentally recapitulated (LaFerla et al. 2012). These transgenic mouse models assisted in the understanding of disease mechanisms and have proven to be an important tool in the preclinical evaluation of potential therapeutic interventions (LaFerla et al. 2012; Sasaguri et al. 2017; Webster et al. 2014; Foley et al. 2015). Several efforts are being made by the researchers to recapitulate AD pathological stages in transgenic mouse models (Sasaguri et al. 2017). These studies demonstrated that Aβ accumulation as extracellular plaques and intracellular NFTs followed by chronic inflammation, neuronal loss, brain atrophy, along with decreased vascular, astroglial, and oligodendrocytic responses, leading to declining brain

homeostasis and resultant dementia (Sasaguri et al. 2017; Hyman et al. 2012; Braak et al. 1991) (Figure 1.6). Also, in most cases, animal models show behavioural abnormalities before Aβ pathology which arises much earlier than in humans. Several groups overexpressed APP with or without fAD mutations such as V717F (Indiana) in PDAPP mice (Games et al. 1995), KM670/671NL (Swedish) in APP23 that express APP751 isoform (Sturchler-Pierrat et al. 1997) and Tg2576 mice that express APP695 isoform (Hsiao et al. 1996; Sturchler-Pierrat et al. 1997; Hall et al. 2012), KM670/671NL+ V717F in J20 mice (Mucke et al. 2000), KM670/671NL+V717F in TgCRND8 mice (Chishti et al. 2001). It is obvious to notice mice carrying more than one mutation, with the most common mutation being the Swedish mutation (Citron et al. 1992). Several other combinations include Tg2576;PS1M146L (Holcomb et al. 1998), APPKM670/671NL;PS1A246E (Borchelt et al. 1996; Borchelt et al. 1997), APP751KM670/671NL-V717I; PS1M146L (Schmitz et al. 2004), APPKM670/671NL; PS1ΔE9/S290 (Jankowsky et al. 2004b), APPKM670/671NL and PS1L166P (Radde et al. 2006), and APPKM670/671NL-V717I; PSEN1M233T/L235P knock-in (Casas et al. 2004). PS1 mutations or PSEN1 knock-in alone did not induce Aβ pathology, presumably because the absolute amount of pathogenic longer Aβ (such as Aβ42 and Aβ43) generated from mouse APP was insufficient (De Strooper et al. 1995; Weggen et al. 2012; Xu et al. 2016). Notably, FAD mutations in APP are important to produce amyloidosis, and additional FAD PS1/2 expression increases amyloidosis.

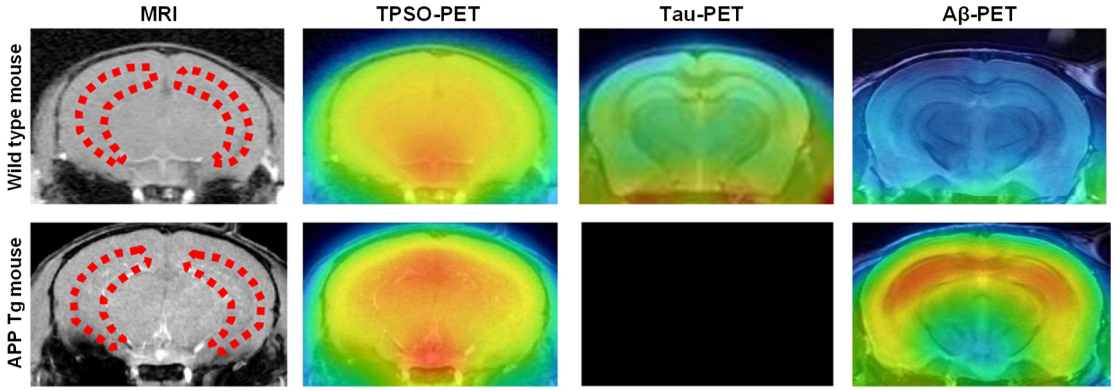

Figure 1.6 | Transgenic mouse brains with AD

Comparison of the wild-type mouse brain and the APP transgenic (Tg) mouse brain by using molecular imaging techniques showing significant hippocampal atrophy in APP-Tg mouse brain compared to wild-type mouse (red dotted area) in the magnetic resonance imaging (MRI) scanning. *In-vivo* positron emission tomography (PET) showed increased Aβ, τ signal and increased signal for 18kDa translocator protein (TSPO) marked by increased gliosis and inflammation in APP-Tg mouse brain compared to wild-type mouse. The PET imaging was done with [^{11}C] PiB (Aβ-PET), [^{11}C] PBB3 (τ-PET) and [18F] fluoroethoxy-DAA1106 (TSPO). *(Figure was adapted from (Higuchi et al. 2016) © 2016 Japanese Society for Neuroimmunology, with permission from John Wiley and Sons)*

In addition, 5XFAD mice carrying five FAD mutations in APP and PS1 transgenes (APPK670N/M671L/I716V/V717I; PS1M146L/L286V) was also generated that exhibited Aβ deposits and gliosis at 2 months of age, synaptic degeneration, neuronal loss and developed progressive cognitive deficits (Oakley et al. 2006). Since these mice models failed to develop NFTs, crossbreeding of mutant τ-Tg mice with APP-Tg mice enhanced τ pathology without affecting Aβ pathology (Lewis et al. 2001; Bolmont et al. 2007). Several other combinations of transgenic mouse models useful for specific applications were reviewed by (Sasaguri et al. 2017). The limitations in the APP and APP/PS overexpressing mouse models were several such as overproduction of APP full-length and fragments (Saito et al. 2014) that could also interact with cellular proteins (Chang et al. 2005; Mitani et al. 2012; Nicolas et al. 2014; Kerridge et al. 2015; Nhan et al. 2015; Willem et al. 2015), induce non-specific ER stress due to APP/PS overexpression (Barbero-Camps et al. 2018; Chaudhari et al. 2014; Reinhardt et al. 2014; Borkham-Kamphorst et al. 2016; Saito et al. 2016), production of different Aβ species other than those found in clinical AD brains (Saito et al. 2016; Saido et al. 1995), promoter driving of APP transgene may affect Aβ *in-vivo* propagation (Jucker et al. 2013) and so on (Sasaguri et al. 2017). To overcome the intrinsic drawbacks of the APP overexpression paradigm, APP knock-in mice were generated to overproduce pathogenic Aβ such as Aβ42 without overexpressing APP (Saito et al. 2016; Sasaguri et al. 2017). For this, the murine Aβ sequence was humanized by changing 3 amino acids that differ between mice and humans (G676R, F681Y, and H684R) and two additional fAD-associated mutations Swedish (KM670/671NL) and Beyreuther/Iberian (I716F) were introduced into the endogenous mouse APP gene (Saito et al. 2014). The Beyreuther/Iberian mutation caused an increase in the Aβ42/Aβ40 ratio and was identified to cause an aggressive form of fAD in Iberia (Guerreiro et al. 2010; Sasaguri et al. 2017).

Rodents and humans have different genetics, neuroanatomy, and behaviour (Emes et al. 2003; Molnar et al. 2012; Kaas 2013; Nithianantharajah et al. 2013; Sasaguri et al. 2017). Also, the sequence, pathogenicity, and a number of isoforms of Aβ, tau, and ApoE differ between mice and humans (Franco Bocanegra et al. 2018; Sasaguri et al. 2017). While the various mouse models were created using various strategies, they have limitations; however, they continue to be a tool for understanding the progression of AD.

1.2.1 | APPPS1 transgenic models

1.2.1.1 | APPKM670/671NL; PS1L166P

APPPS1 mice (line 21) contain human transgenes for both Swedish APP (K670N/M671L) and PS1 (L166P) mutation under the control of the Thymocyte differentiation antigen 1 (Thy1) promoter to ensure high levels of neuron-specific transgene expression in the postnatal brain (Radde et al. 2006). Human APP transgene expression is approximately three-fold higher in

these mice than endogenous murine APP. Human Aβ42 is preferentially generated over Aβ40, and levels of both peptides increase with age. Aβ levels were significantly higher at 8 months of age than at 1 month, with Aβ42 exceeding Aβ40 (Radde et al. 2006).

In human FAD, the L166P mutation in PS1 is associated with very early symptom onset as early as 24 years of age (Moehlmann et al. 2002; Wolfe et al. 1999; Steiner et al. 1999; Kimberly et al. 2000). When expressed in cultured cells, this mutation impaired carboxypeptidase-like γ-cleavage but spared APP endoproteolytic ε-cleavage. This resulted in lower intracellular and secreted levels of Aβ40 and an increased Aβ42/Aβ40 ratio (Bentahir et al. 2006; Koch et al. 2012; Li et al. 2016; Sannerud et al. 2016). L166P promotes the accumulation of APP β-CTFs, which appears to disrupt endosomes in addition to affecting Aβ peptide production (Kwart et al. 2019).

In the APP/PS1 model, cerebral amyloidosis begins at 6-8 weeks, and the ratio of human amyloid Aβ42 to Aβ40 observed was 1.5 and 5 respectively in pre-depositing and amyloid-depositing mice (Radde et al. 2006). At 2 months, deposits were mostly small and compact, whereas, at 8 months, amyloid deposits mostly consist of (i) dense core congophilic smaller plaques (ii) larger dense core plaques with a large halo of diffuse amyloid (iii) dense core plaques surrounded by a well-defined corona of diffuse amyloid, resembling the most abundant plaques in human AD (Radde et al. 2006). At 8 months, these plaques cover nearly the entire neocortex, are large-sized, and are surrounded by diffuse amyloid, and amyloid deposits develop later in the hippocampus (Radde et al. 2006). The presence of phosphorylated τ-positive neuritic processes was observed in the vicinity of all congophilic amyloid deposits, but there were no mature tangles found (Radde et al. 2006).

Amyloid-associated pathologies include dystrophic synaptic boutons, hyperphosphorylated τ positive neuritic structures, and increased gliosis, with the number of neocortical microglia increasing three-fold between 1 and 8 months of age (Radde et al. 2006). In this mouse model, modest neuron loss was observed in the granule cell layer (GCL) of the dentate gyrus (DG) and other high neuron density subregions at 17 months of age. The CSF levels of Aβ and τ in these mice have also been thoroughly investigated (Maia et al., 2013). Aβ42 concentrations in CSF of these mice decrease with age, with a 50% decrease by 6 months and an 80% decrease by 18 months of age. Aβ40 concentrations decrease as well, but less dramatically (45% by 18 months). This decrease in Aβ levels is strongly related to an increase in Aβ aggregates depositing in the brain. CSF concentrations of total τ rise in this mouse model, beginning at 6 months and reaching a 5-fold increase by 18 months (Radde et al. 2006; Maia et al. 2013; Bacioglu et al. 2016). These mice also show cognitive deficits in spatial learning and memory in the Morris water maze (MWM) test at 7 months (Serneels et al. 2009), as well as impaired reversal learning in a food-rewarded 4-arm spatial maze task at 8 months (Radde et al. 2006).

1.2.1.2 | APPKM670/671NL; PS1ΔE9

In addition to the Swedish APP (K670N/M671L) transgene, these mice a exclude exon 9 (ΔE9) human PS1 (Sato et al. 1998; Lee et al. 1997; Borchelt et al. 1996; Brooks et al. 2003). The expression of both genes was directed with murine prion protein promoter to the CNS (Jankowsky et al. 2004a; Garcia-Alloza et al. 2006). These mice begin to develop Aβ deposits by 6 months of age, with abundant plaques in the hippocampus and cortex by 9 months (Jankowsky et al. 2004a) which continue to increase up to around 12 months of age (Volianskis et al. 2010). Apart from the cerebral amyloid deposition, *in-vivo* multiphoton microscopy at weekly intervals and also immunohistochemistry showed Aβ deposition in the vessels as CAA (Garcia-Alloza et al. 2006; Shi et al. 2021; Duran-Aniotz et al. 2021). Astrocytosis develops alongside plaque deposition, with severe gliosis beginning around 6 months after plaque deposition, particularly in the vicinity of plaques (Kamphuis et al. 2014). A modest neuronal loss is observed adjacent to plaques within 8-10 months, while tangles are not observed in this model (Jackson et al. 2016).

The ΔE9 mutations can lead to deletion, insertion, or splice-site mutations within intron 8, resulting in the absence of exon 9 from transcripts and the production of presenilin protein lacking about 30 amino acids (Lanoiselee et al. 2017; Le Guennec et al. 2017; Hutton et al. 1996; Perez-Tur et al. 1995; Sato et al. 1998; Rovelet-Lecrux et al. 2015; Smith et al. 2001; Crook et al. 1998; Prihar et al. 1999). The ΔE9 mutations are also frequently associated with neuropathological features that are not typical of AD, most notably, "cotton-wool plaques" that lack an amyloid core. These plaques were first observed in the Finnish pedigree with exon 9 deletion and the brains of patients with ΔE9 mutations (Mann et al. 2001; Nelson et al. 2010; Hiltunen et al. 2000). In the mouse model with PS1ΔE9 generated by co-injection of K670M/N671L (Swedish) and PS1dE9 expression vectors, the cotton wool plaques have not been observed but instead have compact dense core deposits typical of AD (Jankowsky et al. 2004a).

A decline in CSF Aβ42 levels was observed between 6 and 9 months in APPswe/PS1ΔE9 mice with faster plaque pathology (Liu et al. 2004). These mice showed memory deficits across cognitive domains (Janus et al. 2015), with impaired contextual memory as early as 6 months of age, as shown by freezing behaviour in fear-conditioning tests (Kilgore et al. 2010), impaired spatial learning by 12 months as measured by performance in the MWM test but not at 7 months of age (Lalonde et al. 2005; Volianskis et al. 2010).

1.2.1.3 | 5xFAD

This model expresses human APP and PS1 transgenes with a total of five AD-linked mutations: the Swedish (K670N/M671L), Florida (I716V), and London (V717I) mutations in APP, and the M146L and L286V mutations in the PS1 gene each driven by the mouse Thy1 promoter. These

mice have a significant increase in Aβ42 compared to Aβ40, which is proportional to APP expression (Oakley et al. 2006) and an increased τ in CSF at 12 months of age (Mattsson-Carlgren et al. 2020).

At 2 months of age, these mice develop amyloid pathology in the subiculum, cortex, hippocampus, and thalamus, and is associated with dystrophic neurites, microgliosis, and astrogliosis (Richard et al. 2015; Jawhar et al. 2012; Giannoni et al. 2016). The composition of plaques has also been studied and found to contain N-terminally truncated Aβ in addition to Aβ42 (Wirths et al. 2017; Guzman et al. 2014; Savastano et al. 2016; Reinert et al. 2016; Forner et al. 2021). Mice exhibit extensive accumulation of intraneuronal Aβ42 within the neuronal soma and neurites at 1.5 months before plaque formation, indicating that intracellular Aβ deposits may be involved in plaque formation, neurodegeneration and neuronal loss (Braidy et al. 2012). Furthermore, progressive CAA in superficial, leptomeningeal vessels begins around 3 months of age (Giannoni et al. 2016) and lacks NFTs formation indicating a significant difference between the AD pathology of this model and human disease (Oblak et al. 2021; Forner et al. 2021; Oakley et al. 2006).

The mice exhibited normal locomotor activity in the open field for at least 12 months, with a progressive decrease in anxiety, as measured by the elevated plus-maze (EPM) and open field test (OFT), also appearing between 3 and 6 months (Jawhar et al. 2012). In addition, the impaired working memory in the Y-maze at an age of 4 to 5 months (Oakley et al. 2006), impaired contextual fear conditioning at 4 months age which correlated with the hippocampal synaptic dysfunction (Kimura et al. 2009), impaired spatial working memory, as measured by a cross-maze test, appears between 3 and 6 months of age and worsens with age (Jawhar et al. 2012). In the MWM test, two independent groups concluded conflicting findings attributed to how the memory impairment was defined. The first group concluded a normal memory function, since 5xFAD mice preferred the target quadrant in a probe test, the same as wild-type littermates (Richard et al. 2015), whereas two other studies compared target-quadrant occupancy between 5xFAD and wild-type (WT) mice and discovered that the 5xFAD mice spent slightly less time in the target quadrant, although both genotypes prefer this quadrant (Gu et al. 2018; Wu et al. 2018).

Altogether, these mouse models are in good agreement with amyloid pathology observed in AD patients, therefore serve as a suitable model for studying therapeutic strategies and pathways of amyloidosis.

1.3 | Neuroinflammation and microglia in AD

Neuroinflammation, an inflammatory response primarily protects the brain by removing or inhibiting diverse pathogens and cellular debris (Wyss-Coray et al. 2002) promotes CNS repair (Yong et al. 2019; Schwartz et al. 1999; Bollaerts et al. 2017). However, sustained

inflammatory responses are detrimental, and they inhibit regeneration (Kempuraj et al. 2016; Russo et al. 2016; Kwon et al. 2020). Neuroinflammation is associated with cognitive impairment and neurodegenerative diseases (Hemonnot et al. 2019; Gambino et al. 2019). In AD, misfolded and aggregated proteins bind pattern recognition receptors of the glial cells mainly, microglia and astrocytes, triggering an innate immune response characterized by the release of inflammatory mediators that promote disease progression and severity (Heneka et al. 2015; Guzman-Martinez et al. 2019; Lim et al. 2015; Garcia-Gonzalez et al. 2018; Venegas et al. 2017a).

Microglia are the resident macrophages in the brain (Lawson et al. 1992; Salter et al. 2017; Salter et al. 2014) and represent the first line of defence constantly scanning the microenvironment for signs of damage or debris, allowing them to respond quickly to focal injury or invading pathogens (Davalos et al. 2005; Bilbo et al. 2017; Wake et al. 2013; Nimmerjahn et al. 2005).

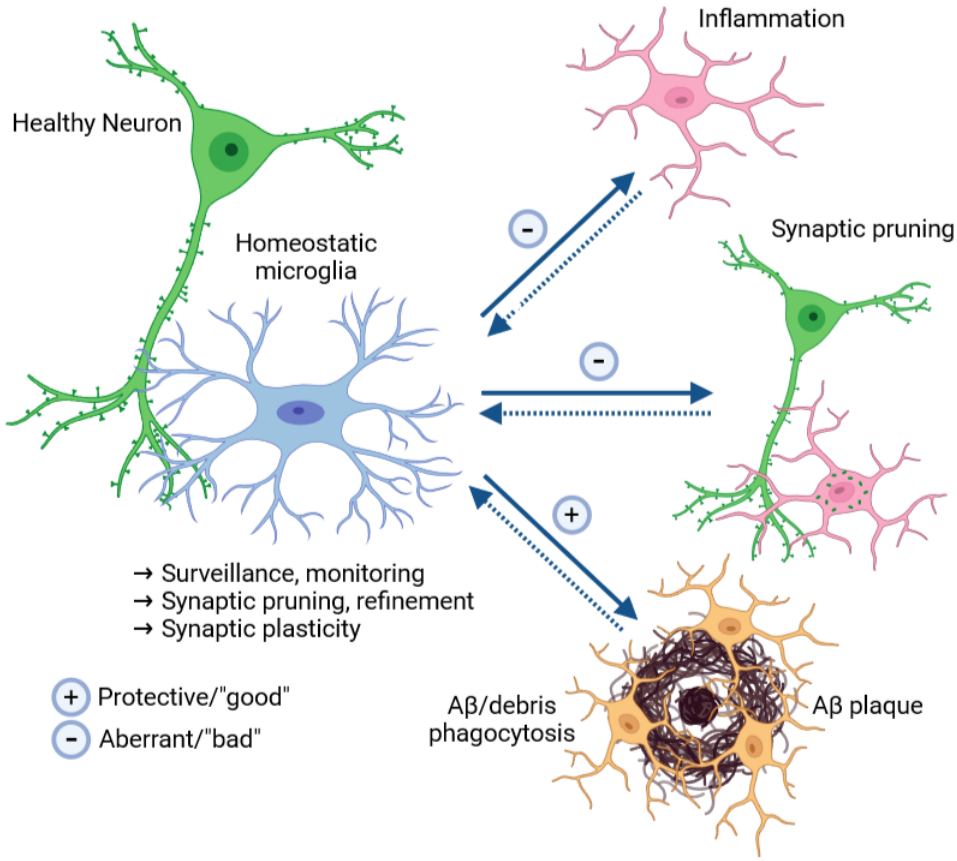

Figure 1.7 | Microglial functions in CNS

Microglial morphology and behaviour display variability across CNS regions and stages of the lifespan and brain lesions. Microglia play an important role in the brain by surveilling the local environment with their highly motile processes, structurally and functionally interact with neurons and the synaptic structures that include axonal terminals, dendritic spines (dark green), and are in direct contact with excitatory synaptic clefts for the exchanges of molecular signals. During disease progression, homeostatic microglia (blue colour) acquire a reactive phenotype of microglia (red colour) with

neuroinflammatory properties which secrete cytokines and upregulate particular cell surface molecules, which triggers oligodendrocyte damage, resulting in demyelination, axonal damage, neuronal loss, synaptic pruning and cognitive dysfunction in AD and other diseases (Geladaris et al. 2021). On the other side, activated microglia (orange colour) functions to maintain tissue homeostasis, restricts Aβ plaques, contribute to the restructuring of neuronal circuits by phagocytosing debris, synaptic elements as well as degrading toxic proteins (i.e., Aβ) resulting in neuroprotection. *(Figure was adopted from (Salter et al. 2017) and modified by Pranav Joshi using BioRender.com)*

Microglia represent the primary immune cells of the brain that plays a pivotal role in the CNS immune response and homeostasis (Bachiller et al. 2018) (Figure 1.7). Microglia play an important role in neuronal plasticity through their ability to prune synapses and axon terminals (Tremblay et al. 2011; Salter et al. 2014), shaping neuronal circuits, axon growth and synaptogenesis, modulation of adult neurogenesis, phagocytosis and elimination of microbes, dead cells, and protein aggregates (Ransohoff 2016b; Clayton et al. 2017; Bilbo et al. 2017; Parkhurst et al. 2013). Microglia change their morphology, number, and activity with pathological insults (Lourbopoulos et al. 2015; Norden et al. 2015; Bachiller et al. 2018) and during ageing (von Bernhardi et al. 2015). Microglia survey the brain milieu, sense pathogens and also express various cell surface receptors that affect the activation level, inflammatory status and phagocytic function (Nayak et al. 2014). Furthermore, microglia secrete a variety of soluble factors, including chemo-attractants, cytokines, and neurotrophic factors, which aid in various aspects of immune responses and tissue repair in the CNS (Colonna et al. 2017). However, whether microglia have beneficial or protective functions is debatable; their role may vary depending on the context such as it could be detrimental, especially in chronic inflammation (Colonna et al. 2017; Hickman et al. 2008; Lucin et al. 2009; Wake et al. 2013). Chronic microglial activation leads to the production of numerous cytokines and acute-phase reactants that damages the neurons (Bachiller et al. 2018; Akiyama et al. 2000).

In AD brains, resident microglia fail in their primary function as immune sentinels leading to the accumulation of Aβ peptides despite abundant microgliosis surrounding the amyloid plaques (Hansen et al. 2018; Casali et al. 2021; Arcuri et al. 2017; Galloway et al. 2019).

This suggests that there is a highly complex relationship between microglia and Aβ, which can be either beneficial or detrimental (Lee et al. 2010). If left unchecked, Aβ accumulation caused by impaired innate immune cell functions and the chronic neuroinflammatory process might cause neuronal injury; however, if controlled, reactive microgliosis can be used to clear the brain of harmful Aβ species (Guillot-Sestier et al. 2013; Heneka et al. 2015). Besides this, poor microglial Aβ phagocytosis or degradation could be at least partially due to ageing (Angelova et al. 2019; Candlish et al. 2021; Spittau 2017; Norden et al. 2013), the persistent release of pro-inflammatory molecules such as reactive oxygen species (ROS), cytokines and chemokines (Heiple et al. 1990), senescence/ dystrophic microglia (Flanary 2005; Greenwood et al. 2021;

Fossel 2000), or due to phenotype that the microglia adopt during disease (Guillot-Sestier et al. 2013). Recently, disease-associated microglia (DAM) were identified in the brain of AD patients and AD mouse models seem to have the potential to restrict neurodegeneration (Keren-Shaul et al. 2017) (Figure 1.8). Overall, the microglial response may be affected by the duration of activation, localization, involvement of other cells, ageing, genetic susceptibility, and disease progression (Sarlus et al. 2017).

Dynamic nature of microglia

Accumulating evidence suggests that inflammation plays a role in the pathogenesis and progression of AD, and new genetic and functional data support the role of innate immune components in the disease (Salani et al. 2019). The brain's innate immune cells, the microglia, act to protect against misfolded proteins by detecting and clearing them, but in AD they may acquire a dysfunctional phenotype, secreting neurotoxic cytokines, and instigating a persistent inflammatory state (Salani et al. 2019).

Two-photon imaging studies show microglia to be quite dynamic (Wake et al. 2009; Nimmerjahn et al. 2005; Davalos et al. 2005). The morphology of microglia reflects their interaction with their microenvironment. In homeostasis, microglia are considered ramified microglia (Brawek et al. 2017) with multiple branches and processes that extend from the somata and terminate with bulbous endings (Jurga et al. 2020; Bachiller et al. 2018; Brawek et al. 2021; Harry et al. 2008). In contrast, activated amoeboid microglia are associated with phagocytosis and proinflammatory function often characterized by the production of pro-inflammatory cytokines and nitric oxide (Wyss-Coray et al. 2012). In the brain, ramified (resting) microglia function as synaptic homeostasis, and surveillance, whereas amoeboid (phagocytic) microglia were typically associated with functions such as phagocytosis, motility to lesion site and mitotic proliferation, production of enzyme degrading proteins and increase secretion of inflammatory cytokines (Brawek et al. 2014; Edler et al. 2021; Clayton et al. 2017). Morphology is not a reliable indicator of function, dysfunction, or RNA expression profiles, but rather demonstrates that the cell is responding to altered homeostasis (Perry 2010).

Recent transcriptomics studies show that the activation of microglia is varied and context-dependent during disease progression/stages (Grubman et al. 2021; Grabert et al. 2016; Masuda et al. 2020). A comprehensive scRNA-seq analysis of AD, ALS, and ageing mouse models revealed a microglial heterogeneity with distinct spatiotemporal brain expression patterns (Kang et al. 2018; Keren-Shaul et al. 2017; Hammond et al. 2019; Masuda et al. 2020; Stratoulias et al. 2019). Among these subsets, microglia expressing disease-related genes and RNA signatures revealed a common disease-associated RNA signature known as disease-associated microglia (DAM) or amyloid-responsive microglia (ARM), conserved in mice and humans (Keren-Shaul et al. 2017; Holtman et al. 2015; Hickman et al. 2013; Orre et al. 2014;

Deczkowska et al. 2018; Krasemann et al. 2017; Chiu et al. 2013; Sala Frigerio et al. 2019) or microglia of neurodegenerative phenotype (Krasemann et al. 2017). DAM express typical markers for activated microglia, ionized calcium-binding adapter molecule 1 (Iba1), cystatin 3 (Cst3), and hexosaminidase subunit beta (Hexb), coincident with the downregulation of ‘‘homeostatic’’ microglial genes that include purinergic receptor P2Y, G-protein coupled, 12/13 (P2ry12 and 13), C-X3-C Motif Chemokine Receptor 1 (Cx3cr1), CD33, and Transmembrane Protein 119 (Tmem119) (Butovsky et al. 2014; Butovsky et al. 2015; Haynes et al. 2006; Hickman et al. 2013; Merino et al. 2016; Mildner et al. 2017), and upregulation of genes involved in phagocytic, lysosomal, and lipid metabolism pathways, including several known AD risk factors, such as ApoE (Corder et al. 1993), the gene encoding for cathepsin D (Ctsd) (Paz et al. 2016), Lipoprotein lipase (Lpl) (Scacchi et al. 2004), TYRO protein tyrosine kinase-binding protein (TYROBP)(Pottier et al. 2016b), and TREM2 (Lambert et al. 2013; Guerreiro et al. 2013d; Jonsson et al. 2013) (Figure 1.8).

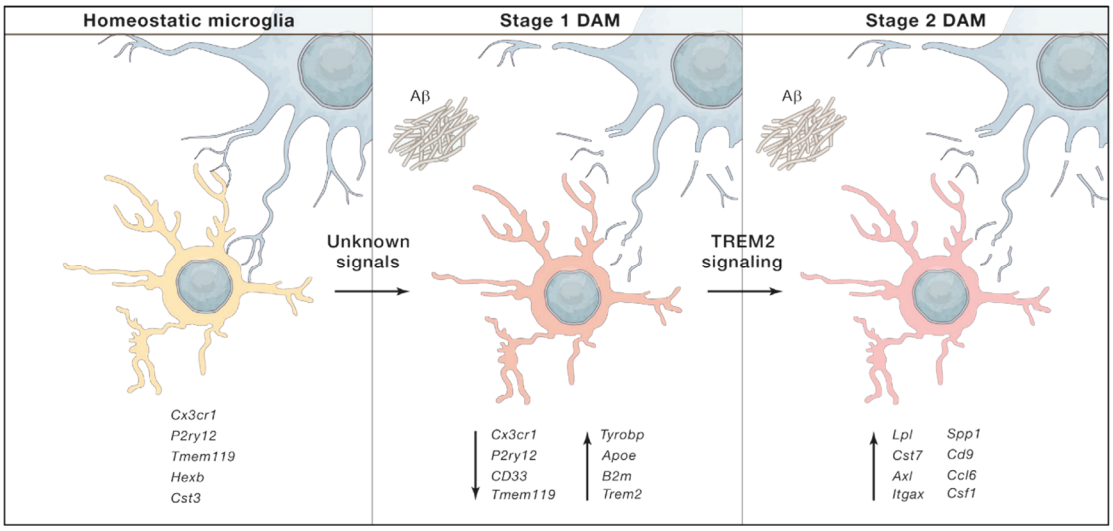

Figure 1.8 | Activation of disease-associated microglia (DAM) from homeostatic microglia

The single-cell RNA sequencing (scRNA-seq) analysis of AD, ALS, and ageing brains revealed a new and rare subset of microglia, conserved in mice and humans known as disease-associated microglia (DAM) (Keren-Shaul et al. 2017). These DAM are molecularly characterized as immune cells expressing typical microglial markers, Iba1, Cst3, and Hexb along with decreased expression of ‘‘homeostatic’’ microglial genes, including P2ry12 & 13, Cx3cr1, CD33, and Tmem119 (Butovsky et al. 2014). DAM further displays upregulation of genes involved in phagocytic, lysosomal and lipid metabolism pathways, including several known AD risk factors, such as ApoE, Ctsd, Lpl, TYROBP, and TREM2 (Lambert et al. 2013). DAM differentiation is a two-step process (Keren-Shaul et al. 2017; Friedman et al. 2018) and each stage is characterized by a unique transcriptional signature represented by the regulation of various genes mentioned in the figure above. *(Figure was adapted from (Deczkowska et al. 2018) © 2018 Elsevier Inc, with permission from Elsevier)*

Analysis of microglia from AD mouse models (5XFAD and APP/PS1) deficient in TREM2 revealed that differentiation to DAM is a sequential two-step process. The transition of stage

1 DAM is required for further activation of the stage 2 DAM (Friedman et al. 2018; Keren-Shaul et al. 2017). While the transition from stage 1 to stage 2 DAM requires TREM2, the transition from homeostatic microglia to stage 1 DAM is TREM2-independent, and the factors mediating this step are unknown at this time. TREM2-independent signalling causes a significant downregulation of homeostatic microglia genes (Cx3cr1, P2ry12), which are associated with an increase in the TREM2 adaptor TYROBP, upregulation of the phagocytic, lysosomal and lipid metabolism pathways (Deczkowska et al. 2018).

In AD brains, Aβ plaques are surrounded by DAM that expresses TREM2. This TREM2 has been shown to bind Aβ *in-vitro* (Zhao et al. 2018; Zhong et al. 2018; Lessard et al. 2018; Joshi et al. 2021b). Additionally, an array of negatively charged phospholipids, including phosphatidylinositol, phosphatidylcholine, and possibly others, that associate with Aβ and accumulate in the brain during Aβ deposition, also activate TREM2 signalling in TREM2-NFAT (Nuclear factor of activated T-cells) reporter cells (Ahyayauch et al. 2012; Nagarathinam et al. 2013; Wang et al. 2015). TREM2 was also found to bind lipoproteins (ApoE, LDL (low-density lipoproteins), CLU/Apoj (clusterin/ apolipoprotein J)), which form complexes with Aβ aggregates, facilitating microglial uptake (Song et al. 2017b; Yeh et al. 2016; Terwel et al. 2011). Thus, due to the diversity in ligands, TREM2 acts as a pattern recognition receptor (PRR) of CNS damage. Importantly, rare human TREM2 variants linked to an increased risk of neurodegenerative disease demonstrated impaired binding of many of these ligands *in-vitro* and *in-vivo* (Song et al. 2017b; Wang et al. 2015; Yeh et al. 2016; Zhao et al. 2018; Deczkowska et al. 2018). Among these, the rare variant (R47H) in TREM2 leads to a 3- to 4-fold increase in the risk of AD in humans (Guerreiro et al. 2013d; Jonsson et al. 2013). This was also supported by the findings observed in the 5xFAD mouse model (Song et al. 2018). Additionally, TYROBP, also known as DAP12 (DNAX-activating protein), which forms a receptor-signalling complex with TREM2, is upregulated in DAM and has been linked to pre-senile dementia (Paloneva et al. 2000). These findings suggest that TREM2 or its TREM2/DAP12 complex is required for full activation of the DAM cascade, which may protect from AD development.

1.4 | TREM2

The triggering receptor expressed on myeloid cells (TREM2) belongs to a family of innate immune receptors (Bouchon et al. 2000). Human TREM2 and murine TREM2 are highly homologous (77% protein homology) and 68% identical (Lee et al. 2018; Lessard et al. 2018). The human TREM2 gene is located on chromosome 6p21.1 and encodes 230 amino acid glycoprotein (Gratuze et al. 2018; Colonna et al. 2016; Allcock et al. 2003), and the murine TREM2 gene is located on chromosome 17 and encodes 227 amino acid glycoprotein (Ford et al. 2009; Klesney-Tait et al. 2006).

1.4.1 | TREM2 structure and expression

Human TREM2 is a polypeptide chain of 230 amino acids that consists of N -terminal mature extracellular domain (ECD) (aa19-174, with aa1-18 constituting signal peptide), a membrane-spanning region (aa175-195) and a C-terminal cytosolic tail (aa196-230). The TREM2 ectodomain contains a V-type Ig domain containing two disulfide bonds between residues C36 and C110 (bB–bF) and C51 and C60 (bC-bC')(Kober et al. 2016) (refer to Figure 1.9). Complete loss-of-function mutations of TREM2 are linked to Nasu-Hakola disease (NHD) and Frontotemporal dementia (FTD), which includes truncation (Q33X) or misfolding (Y38C) of the protein due to aberrant disulfide bond formation. However, the effects of mutations such as R47H, R62H, T66M and D87N on the structure and function of TREM2 are more subtle.

The crystal structure of TREM2 indicates that all amino acid residues responsible for AD (R47H, R62H, N68K, D87N and T96K) are surface exposed, but may instead impact ligand binding and the residues mutated in NHD (Y38C, T66M and V126G) were buried and could impact protein folding (Kober et al. 2016) (Figure 1.9).

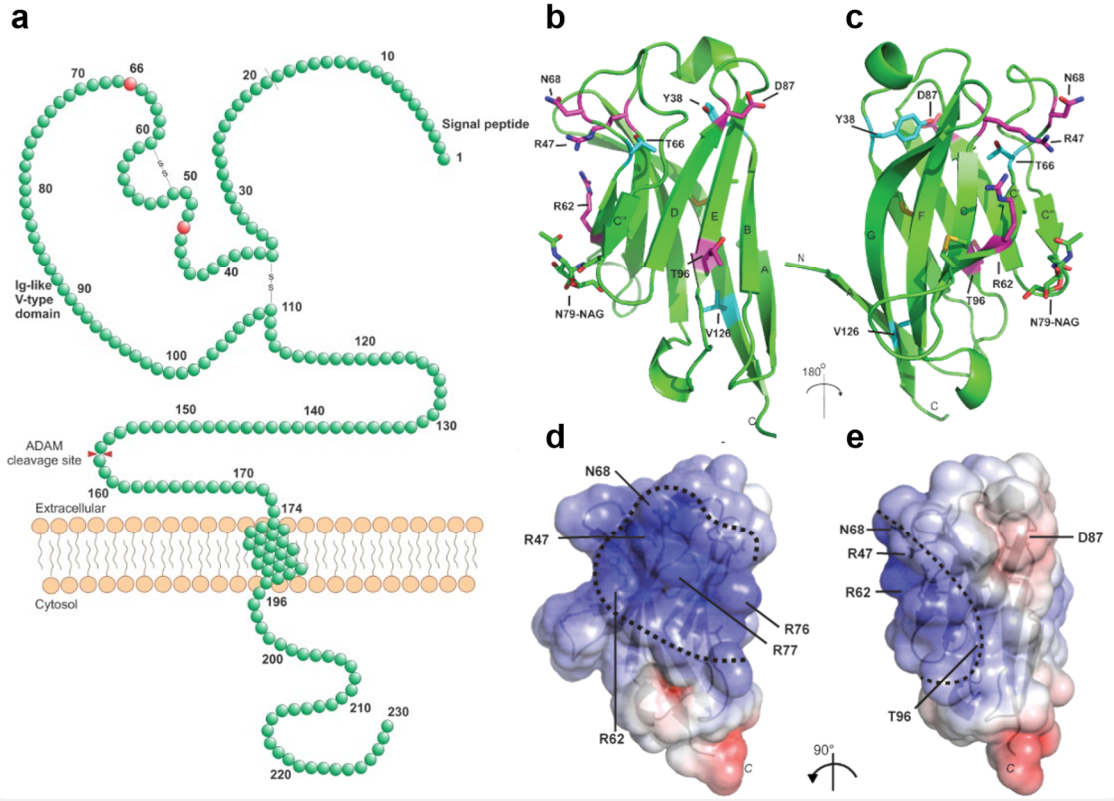

Figure 1.9 | Structural features of human TREM2

(a) Schematic illustration of TREM2 and with different mutations. Red colour circles indicate mutations of TREM2 in the ectodomain region, i.e., R47H and T66M are associated with AD and NHD respectively and are studied in this work. **(b-c)** The representations of TREM2 structures (in two orientations with disease-linked residues shown as sticks) is a V-type Ig domain containing two disulfide bonds, the canonical Ig disulfide between residues C36 and C110 (βB–βF) and an additional linkage between C51 and C60 (βC-βC'). The nine β-strands characteristics of proteins within this Ig domain class are present, and two short α-helix passages are observed spanning, β-sheets. The positions of AD risk variants are

shown in magenta, while the NHD mutations are shown in cyan. The side chains of verified AD risk variants (R47H and R62H) including possible AD risk variants (N68K, D87N and T96K) all lie on the protein surface whereas the side chains of NHD causing mutations (Y38, T66 and V126) are all buried within the core of the Ig fold. Analysis of the crystal structure showed the extended basic patch on hTREM2 (outlined with a dashed line) represented by **(d)** electrostatic surface of hTREM2 and **(e)** hTREM2 rotated 90°. Sequence analysis indicates that this basic patch is highly conserved within TREM2, but not within the rest of the TREM family, suggesting that it evolved for a specific function in TREM2. *(Part (a) was adapted and modified by Pranav Joshi after permission from ©Alzforum (Dr. Kathleen Zahs); part (b-e) was adapted from (Kober et al. 2016) CC BY © 2016 Kober et al.)*

The residue with the strongest link to AD is R47H, which is at the end of the loop that precedes β-sheet C (Guerreiro et al. 2013d; Kober et al. 2016). The side chains are parallel to the surface of the protein, and the side-chain amines interact with the carbonyl oxygen of T66 in an orderly manner (Kober et al. 2016). Another risk factor for AD is the R62H variant. R62H is located after the loop marked by the C51-C60 disulfide bond and with its outward side chain, makes no polar contacts (Song et al. 2017b; Jin et al. 2014; Kober et al. 2016) (Figure 1.9).

The detailed studies on the R47H variant revealed that Arg-47 (R-47) plays an important role in maintaining the structural characteristics of the complementarity-determining region 2 (CDR2) loop and the ligand-interacting surface, stabilizing conformations capable of interacting with ligands. The intracellular trafficking of WT and R47H variants, however, indicates both are predominantly localized in the Golgi compartment (pH 6.0-6.7) (Zhao et al. 2017) before moving to secretory granules (pH 5.5) and the cell surface (pH 7.4). While Arg47 would be protonated at different pH conditions existing in the Golgi compartment (pH 6-6.7), at the cell surface (pH 7.4), and in endocytic compartments to maintain the CDR2 loop conformation but the presence of histidine residue at this position would affect surface interactions significantly (Sudom et al. 2018).

In the brain, TREM2 is predominantly expressed by microglia (Garcia-Alloza et al. 2013; Kiialainen et al. 2005; Takahashi et al. 2005; Neumann et al. 2007; Sessa et al. 2004; Forabosco et al. 2013); however, there is some discordance regarding the level of its expression/translation (Jay et al. 2015; Satoh et al. 2011; Lue et al. 2015a) and whether or not TREM2 is present in all or only a subgroup of microglia (Schmid et al. 2002) in mice and humans. The TREM2 gene is also expressed in the periphery in a subgroup of myeloid cells including dendritic cells (Bouchon et al. 2001), bone osteoclasts (Cella et al. 2003; Humphrey et al. 2006; Paloneva et al. 2003), granulocytes, Kupfer cells (Goncalves et al. 2013), and alveolar macrophages (Koth et al. 2010).

TREM2 expression increases with ageing (Jay et al. 2015; Guerreiro et al. 2013b; Jiang et al. 2014; Brendel et al. 2017) and varies depending on the particular region of the CNS (Sessa et al. 2004; Chertoff et al. 2013), with a higher expression in the hippocampus, the white matter

and the spinal cord (Forabosco et al. 2013). TREM2 expression is up-regulated in pathological conditions such as AD (Lue et al. 2015a; Celarain et al. 2016; Ma et al. 2016; Perez et al. 2017), Parkinson's disease (PD) (Liu et al. 2016), Amyotrophic lateral sclerosis (ALS) (Cady et al. 2014), stroke (Kawabori et al. 2015) and traumatic brain injury (TBI) (Saber et al. 2017). In AD, increased TREM2 expression has been confirmed in patients (Lue et al. 2015a; Celarain et al. 2016; Ma et al. 2016; Perez et al. 2017; Gratuze et al. 2018) and in mouse models of amyloid and τ pathology, multiple sclerosis, ischemic stroke, and PD (Jay et al. 2015; Raha et al. 2017; Matarin et al. 2015; Savage et al. 2015; Jiang et al. 2014; Gratuze et al. 2018; Cignarella et al. 2020).

This increased expression is associated with DAM recruited to amyloid plaques (Perez et al. 2017; Yeh et al. 2017) and also DAM activation occurs in a TREM2-dependent manner during which microglia acquire a phagocytic phenotype (Keren-Shaul et al. 2017). Moreover, microglia appear to be locked in a homeostatic state with impaired chemotaxis and reduced responses to neuronal injury in TREM2-deficient mice (Mazaheri et al. 2017).

TREM2 modulates microglia-mediated inflammatory responses (Li et al. 2018a; Gratuze et al. 2018). Its expression is modulated by inflammation which appears to be the opposite *in-vitro*. While the expression of anti-inflammatory molecules enhances TREM2 expression (Turnbull et al. 2006), the expression of pro-inflammatory molecules, such as Tumor necrosis factor α (TNFα), Interleukin 1β (IL1β) or lipopolysaccharide (LPS) decreases TREM2 expression *in-vitro* (Bhattacharjee et al. 2016; Zheng et al. 2016; Bouchon et al. 2001). Thus, TREM2 can have both activating and inhibitory functions in the tissue macrophages.

TREM2 is transported in the secretory pathway and shuttles between the plasma membrane and cytoplasmic vesicles (Walter 2016; Prada et al. 2006). TREM2 also undergoes maturation by complex glycosylation during biosynthesis and secretory transport (Wunderlich et al. 2013; Park et al. 2015; Kleinberger et al. 2014), but the biological relevance of these modifications remains to be determined. TREM2 undergoes proteolytic processing by ADAM10 or ADAM17 resulting in the shedding between H157 and S158 residues generating a sTREM2 (Feuerbach et al. 2017; Schlepckow et al. 2017; Thornton et al. 2017).

1.4.2 | sTREM2

The sTREM2 is released into the extracellular space after proteolytic cleavage of the full-length protein, and it is detected in the plasma and CSF of healthy people and AD patients (Henjum et al. 2016), multiple sclerosis and other neurological inflammatory diseases (Piccio et al. 2008; Heslegrave et al. 2016). sTREM2 is abundantly detected in human CSF and its levels are elevated in the CSF of patients with sporadic AD, while the levels change dynamically during the progression of AD, with elevated levels at the early symptomatic stages of the AD (Piccio et al. 2016; Suarez-Calvet et al. 2016b; Heslegrave et al. 2016; Suarez-Calvet et al. 2016a).

More interestingly, the levels of sTREM2 have reduced in NHD cases but unchanged or elevated in human TREM2 variant AD cases suggesting a functional divergence in protein stability with the different variants (Piccio et al. 2016). There is a positive association between the amount of sTREM2 in the CSF and the amount of total and phosphorylated τ in the early symptomatic phase of AD (Heslegrave et al. 2016; Piccio et al. 2016). In multiple sclerosis patients, treatment with an immunomodulatory drug (natalizumab), reduced sTREM2 levels to normal levels, suggesting that sTREM2 may have a potential utility as a pharmacodynamic biomarker (Ohrfelt et al. 2016).

sTREM2 may be an effective biomarker of microglial activation in response to neurodegeneration and neuronal injury. Interestingly, sTREM2 functions independently of full-length TREM2 or its intracellular adaptor DAP12 to regulate interactions between neurons and the surrounding microenvironment (Zhong et al. 2017; Zhong et al. 2019; Sheng et al. 2021; Wunderlich et al. 2013). One study has shown that the sTREM2 may act as a decoy receptor to negatively modulate TREM2 signalling (Piccio et al. 2008). In support of this, *in-vitro*, a chimeric TREM2-Fc protein used to mimic sTREM2 inhibited osteoclastogenesis, a process that requires TREM2-DAP12 signalling (Kim et al. 2005). Recent data also demonstrate that sTREM2 treatment triggers microglial activation inducing inflammatory responses and promoting survival (Zhong et al. 2017). This study also found that sTREM2 strongly induced an inflammatory response in culture models of microglia (Zhong et al. 2017). sTREM2 also increased transcription of inflammatory cytokines in microglia through nuclear factor-kappa B (NF-κB) activation (Zhong et al. 2017), a pathway that was not activated by cellular TREM2 signalling (Bouchon et al. 2001). Furthermore, both studies have shown that sTREM2 acts independently of full-length TREM2. Recent studies showed that sTREM2 enhances microglial proliferation, migration, clustering in the vicinity of Aβ plaques, Aβ uptake and degradation (Zhong et al. 2019). The higher CSF levels of sTREM2 indicate the amount of signalling-competent TREM2 on the surface of microglia (Ewers et al. 2020; Kleinberger et al. 2014; Schlepckow et al. 2017). Interestingly, the H157Y mutant of TREM2 exhibited higher levels of sTREM2, reduced levels of TREM2 on the cell surface, as well as impaired phagocytosis *in-vitro* (Schlepckow et al. 2017) as well as being implicated as an AD risk variant depending on the cohort studied (Jiang et al. 2016b; Ghani et al. 2016; Miyashita et al. 2014; Jin et al. 2015; Jiang et al. 2016a). Further study will be necessary to gain insight into how these sTREM2 impact signalling both TREM2 and other pathways critical to innate immunity.

1.4.3 | TREM2 ligands and signalling

Early investigations found that the TREM2 extracellular domain can bind to polyanionic ligands, such as bacterial lipopolysaccharide (LPS) and phospholipids, lipoteichoic acids, peptidoglycans, and dextran sulfates (Daws et al. 2003; Poliani et al. 2015). Along with this,

many other TREM2 ligands have been reported while their physiological role and mechanism of signalling remain to be determined (Kober et al. 2017).

The fact that the majority of TREM2 disease-linked mutations are found in the extracellular Ig-like V-type domain of TREM2, including the two major AD-associated variants R47H and R62H, suggests that these mutations may affect the ability of TREM2 to interact with its ligands (Yeh et al. 2017), leading to an altered signalling pathway or activity, implying that the positively charged arginine residue may be critical for ligand binding. TREM2 also binds to nucleic acids, proteoglycans as well as heat shock protein 60 (Kober et al. 2016), high-density lipoproteins (HDL), low-density lipoproteins (LDL) as well as apolipoproteins (APO), such as APOA1 and APOA2, APOB (Atagi et al. 2015; Bailey et al. 2015; Yeh et al. 2016), CLU/APOJ (Yeh et al. 2016), and with APOE isoforms with similar affinities (Bailey et al. 2015; Atagi et al. 2015). Binding to APO was found to be dependent on lipidation, however, phosphocholine used for lipidation did not show significant binding to TREM2, suggesting that binding is enhanced through lipidation which reflects their natural state *in-vivo* (Yeh et al. 2016; Calero et al. 2000; DeMattos et al. 2001; Bailey et al. 2015; Calero et al. 1999). Recent studies also showed that Aβ binds in a conformation-specific way to TREM2 (Lessard et al. 2018; Zhao et al. 2018; Joshi et al. 2021b) and this binding leads to increased TREM2/DAP12 signalling (Zhao et al. 2018). It is important to note that DAP12 have a minimal extracellular region, and has no ligand-binding capacity (Lanier 2009).

TREM2 acts via intracellular adaptor DAP12 (DNAX-activation protein 12, also known as TYROBP). DAP12 is the transmembrane adapter protein and is abundantly expressed in immune cells such as natural killer cells, myeloid cells and neutrophils (Wilson et al., 2000(Lanier 2009)). TREM2 interacts with DAP12 within the transmembrane region through an electrostatic association (Bouchon et al., 2000), which is required for TREM2 signalling (Gratuze et al. 2018; Colonna et al. 2007).

DAP12 contains an immunoreceptor tyrosine-based activation motif (ITAM) with tyrosine residues that become phosphorylated when TREM2 binds a ligand. This then recruits the protein tyrosine kinase, Spleen tyrosine kinase (SYK) through its cytosolic ITAMs (Yeh et al. 2017; Colonna et al. 2016) which then activates signalling pathways involving phosphoinositide 3-kinase (PI3K), protein kinase C (PKC) activation, mitogen-activated protein kinase (MAPK), RAC serine/threonine-protein kinase (AKT), RAS/MEK/ERK activation, protein tyrosine phosphorylation leading to transcriptional regulation of pro-inflammatory molecules, and calcium (Ca^{2+}) modulation, leading to actin remodelling which controls adhesion and migration (Figure 1.10).

Together, these signals promote survival (Wang et al. 2015; Otero et al. 2012), proliferation (Otero et al. 2012), phagocytosis (Takahashi et al. 2005) and the secretion of chemokines and cytokines in myeloid cells (Bouchon et al. 2001). However, TREM2-induced signals attenuate

the production of proinflammatory cytokines in response to the activation of toll-like receptors (TLRs) (Yeh et al. 2017) and hence curtail macrophage inflammatory responses to various TLR ligands, such as lipopolysaccharide (LPS), lipoteichoic acid and unmethylated CpG oligodeoxyribonucleotides (Turnbull et al. 2006; Hamerman et al. 2006).

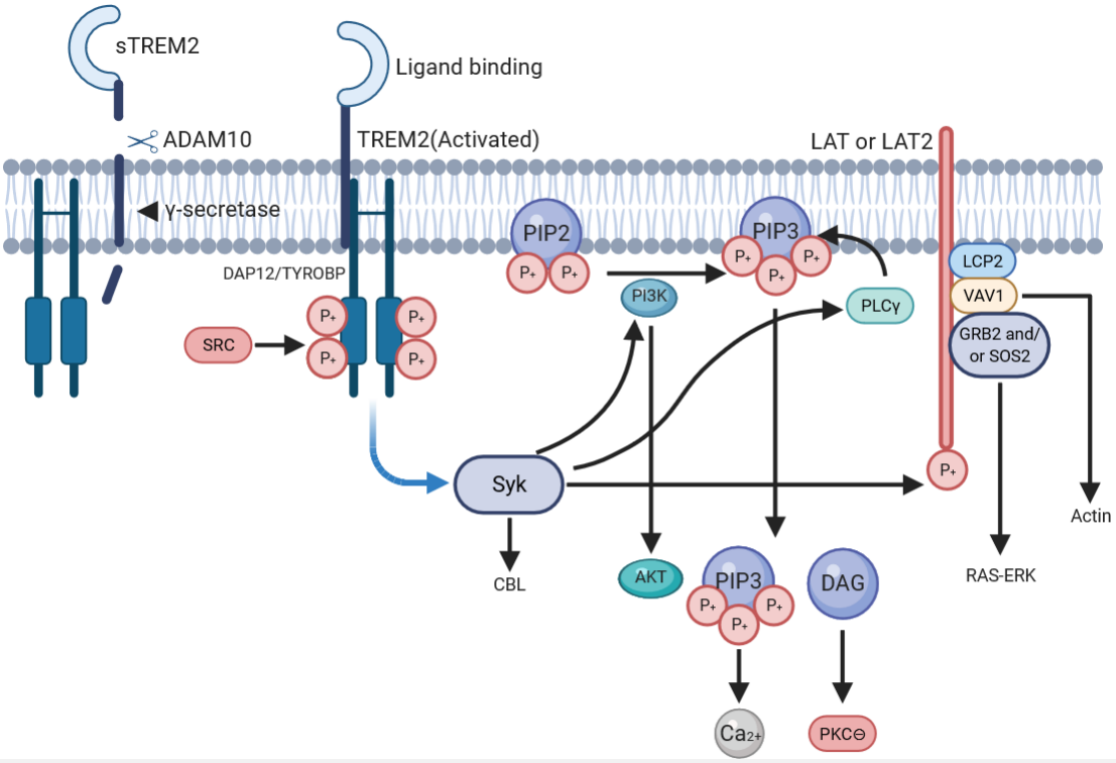

Figure 1.10 | TREM2 signalling

The extracellular domain of TREM2 can bind to negatively charged ligands. TREM2-associated adaptor DAP12 is tyrosine phosphorylated by the protein kinase SRC upon ligand binding and recruits the tyrosine-protein kinase SYK. SYK phosphorylates the adaptors LAT and/or LAT2 (linker for activation of T-cells family member), which in turn recruit phospholipase Cγ (PLCγ) (which degrades PIP3 (phosphatidylinositol-3,4,5-trisphosphate) into IP3 (inositol trisphosphate) and DAG (diacylglycerol)), LCP2 (lymphocyte cytosolic protein 2), VAV1 (proto-oncogene vav), GRB2 (growth factor receptor-bound protein 2) and members of the SOS (son of sevenless) homologue family. The downstream of the TREM2 signalling pathway leads to Ca^{2+} mobilization, activation of PKCθ (protein kinase Cθ), activation of the RAS–ERK pathway and actin remodelling. SYK also activates the PI3K (phosphoinositide 3-kinase)-AKT pathway as well as the E3 ubiquitin-protein ligase CBL (Casitas B-lineage Lymphoma), which negatively regulates the TREM2 signalling. TREM2 can be cleaved from the cell surface by ADAM10 and γ-secretase, thereby releasing sTREM2. *(Figure was adopted (Colonna et al. 2016), and modified by Pranav Joshi using BioRender.com)*

1.4.4 | TREM2 in AD

TREM2 is one of many immune receptors expressed in microglia, and researchers are looking into its role in the pathogenesis of AD because some TREM2 variants have been linked to an increased risk of AD. Recent genome-wide association studies (GWAS) and whole exome

sequencing (WES) have identified various genetic variants that increase the risk of developing LOAD. Several such heterozygous TREM2 variants are found to confer higher AD risk including R47H, R62H, D87N, H157Y, T96K, W191X, L211P and R136Q (Bonham et al. 2017; Guerreiro et al. 2013d; Jonsson et al. 2013; Jiang et al. 2016b; Jin et al. 2014; Jin et al. 2015) (Refer Table 1.1). These findings led scientists to investigate the role of TREM2 in AD, and studies have revealed that AD-associated TREM2 variants do not affect TREM2 folding, expression, stability, or structure (Ma et al. 2016; Song et al. 2017b; Kleinberger et al. 2014; Ibach et al. 2021).

Besides this, recent studies also focused to understand the relevance of TREM2 loss-of-function or mutation on amyloid pathology in mouse models of AD. Since TREM2 is implicated in phagocytosis, AD mice lacking TREM2 could display exacerbated amyloid plaque burden and inflammation (Condello et al. 2018c; Yeh et al. 2017). However, different groups have reported inconsistent findings regarding plaque pathology (Wang et al. 2015; Jay et al. 2015; Yuan et al. 2016; Wang et al. 2016). Human AD cases with the R47H variant show impaired microglial clustering around plaques (Yuan et al. 2016; Parhizkar et al. 2019), resulting in larger, more diffuse plaques (Yuan et al. 2016; Wang et al. 2016). Similarly, reduced plaque-surrounding microglia was also recently reported in 5xFAD mice overexpressing human $TREM2^{R47H}$ as compared to mice overexpressing human TREM2 WT/CV but lacking endogenous expression of murine TREM2 (Song et al. 2018). The microglial pathology of the R47H mice was comparable to TREM2 deficient 5xFAD mice, suggesting that the mutation causes a loss-of-function (Song et al. 2018). Murine R47H TREM2 knock-in also confirmed loss-of-function effects as a result of reduced TREM2 mRNA and protein production (Cheng-Hathaway et al. 2018). Among the observed findings, a consistent phenotype observed in the TREM2 knockout AD mice has been a lack of microglial barrier function and apparent microglial activation (Yeh et al. 2017) (Figure 1.11). Further, these deficits occurred in a gene dose-dependent manner (Ulrich et al. 2014). Microglia, via a TREM2-dependent mechanism, control the structure of amyloid plaques by forming a barrier around the plaques and this was further supported by the high-resolution microscopy and *in-vivo* imaging wherein the microglia processes appear to be stable surrounding the plaques (Condello et al. 2015). While smaller plaques were more efficiently enveloped by microglia, larger plaques presented more uncovered regions. Labelled Aβ42 peptides infused into the subarachnoid space accreted onto microregions of plaques, referred to as “hotspots”, and these corresponded to areas not covered by microglia (Condello et al. 2015). Because the hotspots were labelled with anti-Aβ antibodies but not with Thioflavin S (which labels densely packed fibrils), microglia may not only envelop but also locally compact or condense amyloid structures (Condello et al. 2015).

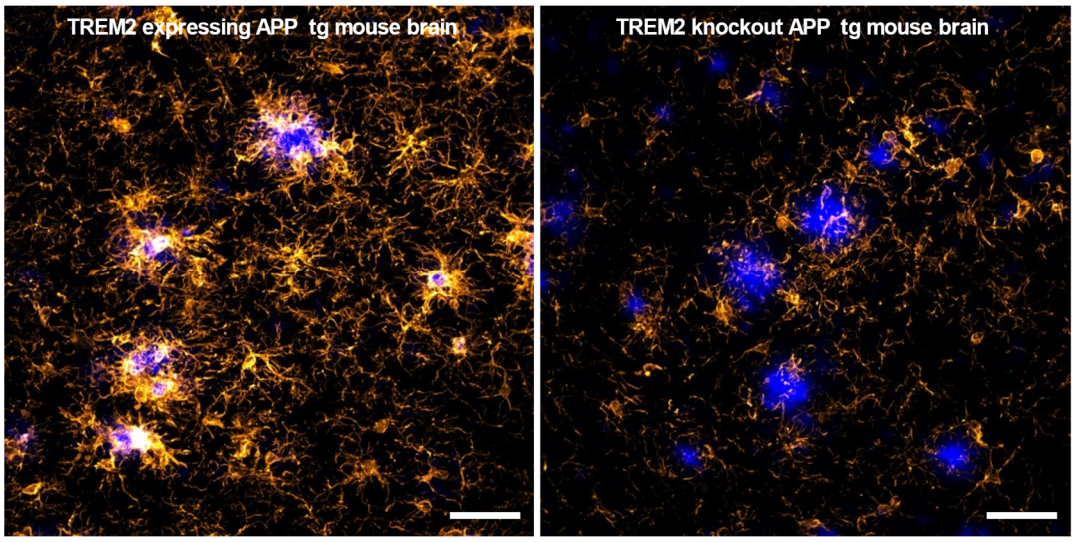

Figure 1.11 | Microglial dysfunction upon TREM2 loss in a mouse model of AD
Representative IF images of mouse brains stained with X-34 (for fibrillar Aβ) along with Iba1 (for microglia) revealed decreased plaque-associated microglia in 12-month-old APP/PS1L166P transgenic (tg) mice without TREM2 (right) compared to APP/PS1L166P mice expressing TREM2 (left) (Scale bar=50µm, 20x). *(Experiments performed and imaged by Pranav Joshi)*

It remains unclear whether the neurons in the vicinity of the plaques are protected by such barrier formed by the microglia or rather the compaction of plaques causes a decrease in the amounts of diffusible Aβ species. The barrier function of microglia decreases with ageing and even the small plaques showed less microglial coverage, enlarged protofibrillar Aβ hotspots and severe neuritic dystrophy (Condello et al. 2015; Yeh et al. 2017).

The failure of TREM2 deficient microglia to cluster and become activated around Aβ plaque would predict increased plaque load in these mice, given the widely believed function of microglia in the clearance of Aβ and/or plaques (McQuade et al. 2020; Yeh et al. 2017). Moreover, brains of AD cases with the R47H variant also displayed more phospho-τ-positive neurites around plaques than AD cases with the TREM2 common variant/WT, providing evidence that microglia can attenuate the neurotoxicity of the plaque environment via TREM2 (Yuan et al. 2016).

ApoE is the most abundant lipoprotein in the brain that is available for lipid transport and can aggregate with amyloid plaques (Wisniewski et al. 1992; Namba et al. 1991). Since it is known that the TREM2 acts as a lipid sensor and interacts with ApoE *in-vitro* (Atagi et al. 2015; Bailey et al. 2015), ApoE may be a ligand to stimulate microglial function through TREM2.

1.4.5 | TREM2 and FTD

Homozygous or compound heterozygosity in TREM2 such as Q33X, Y38C, T66M (Guerreiro et al. 2013c), D86V, W198X c.40 + 3delAGG (Chouery et al. 2008) has been documented in individuals that present with early-onset dementia akin to a behavioural variant form of FTD

(refer Table 1.1). In addition to typical FTD symptoms such as early-onset dementia and personality changes (euphoria, aggression, and impulsivity), these patients had atypical CNS features including seizures and corpus callosum atrophy (Guerreiro et al. 2013a; Guerreiro et al. 2013c; Yeh et al. 2017). Heterozygous expression of TREM2 variants has also been linked to cases of FTD, PD, and ALS (Cady et al. 2014; Borroni et al. 2014; Cuyvers et al. 2014; Rayaprolu et al. 2013). Although homozygous missense mutations of TREM2 such as Q33X, Y38C & T66M were also found in AD and NHD cases, they are more commonly associated with FTD (Guerreiro et al. 2013c; Jonsson et al. 2013). Others include T96K & L211P which increase the risk of developing FTD (Thelen et al. 2014; Rayaprolu et al. 2013). Since FTD mutations such as Q33X, Y38C, and T66M are mostly found in Ig-like domains, TREM2 misfolds in the ER (Kober et al. 2016; Park et al. 2015), and this affects cell surface trafficking and glycosylation (Kleinberger et al. 2014; Song et al. 2017b; Ibach et al. 2021), therefore could explain TREM2 loss-of-function causes FTD-like syndrome (Guerreiro et al. 2013c; Park et al. 2015).

A recent study using TREM2^{T66M} knock-In (KI) mice also supported previous *in-vitro* studies confirming a gene dose-dependent reduction in sTREM2 in the brain, serum, and CSF due to ER retention of mutant immature TREM2 (Kleinberger et al. 2014). A decrease in cell surface expression of the T66M likely underlies the observed decline in the phagocytic ability of bone marrow-derived macrophages (BMDMs) and *in-vivo* TSPO small animal fluorodeoxyglucose (FDG) PET (µPET) demonstrated an age-dependent reduction in microglial activity (Kleinberger et al. 2014). The perfusion MRI and FDG-µPET imaging revealed a significant reduction in cerebral blood flow (CBF) and brain glucose metabolism. This mouse model provided evidence of how T66M mutation causes dysfunction in microglia and macrophages which is associated with reduced CBF and brain energy metabolism (Kleinberger et al. 2014). Although no bone-related pathology was observed, this model can help to understand how CBF affects TREM2 maturation and whether brain-wide hypometabolic effects and neuronal activity are mediated by a cell-autonomous mechanism (microglia with TREM2) or a cell non-autonomous mechanism (microglia without TREM2) (via sTREM2).

1.4.6 | TREM2/DAP12 and Nasu Hakola disease (NHD)

Homozygous loss-of-function mutation in TREM2 or its signalling adapter TYROBP/DAP12 leads to a rare neurodegenerative disease associated with leukodystrophy, osteoporosis and a presenile form of frontal lobe dementia known as polycystic lipomembranous osteodysplasia with sclerosing leukoencephalopathy, PLOSL or also called as called Nasu Hakola disease (NHD) which is endemic to Finland, Japan and USA (Klunemann et al. 2005; Paloneva et al. 2001; Paloneva et al. 2002; Bird et al. 1983; Paloneva et al. 2000; Bianchin et al. 2004; Madry et al. 2007; Satoh et al. 2011). NHD patients develop bone cysts during the second decade of life, develop joint pain and fractures and also present a frontal lobe

syndrome (Paloneva et al. 2001) with cerebral white matter disease characterized by demyelination and the occurrence of axonal spheroids (Paloneva et al. 2001). These patients' functional imaging revealed hypoperfusion and changes in glucose metabolism in the thalamus and bilateral frontal lobes (Takeshita et al. 2005; Ueki et al. 2000; Klunemann et al. 2005). Other pathological changes include myelin loss, gliosis, and enlarged brain ventricles in the orbitofrontal and temporal cortex, which also affect motor functions resulting in the early death of NHD patients (Aoki et al. 2011; Paloneva et al. 2001). Furthermore, as the disease progresses, atrophy of the corpus callosum and frontal brain areas occurs, resulting in behavioural changes, progressive dementia, convulsions, and gait disturbances (Yeh et al. 2017). These patients usually perish in their 4th or 5th decades of life (Paloneva et al. 2001; Klunemann et al. 2005).

Given that TREM2 and its adaptor DAP12/TYROBP are specifically expressed in myeloid cells, NHD pathologies are likely due to microglial functional deficits in the brain and osteoclasts in the bones. Osteoclasts are giant, multinucleated syncytial cells involved in bone resorption that can be derived *in-vitro* when human blood monocytes are cultured with colony-stimulating factor 1 (CSF1) and receptor activator of nuclear factor kappa B ligand (RANKL) proteins, but this differentiation is impaired in cultures from TYROBP deficient or TREM2 deficient NHD patients (Pottier et al. 2016a). Recent studies have suggested that heterozygous TREM2 variants that cause NHD in homozygous carriers may confer an increased risk of AD (Guerreiro et al. 2013d; Jin et al. 2014; Song et al. 2017b), and also that rare coding variants of DAP12/TYROBP may give rise to autosomal dominant EOAD (Paloneva et al. 2002). Patients homozygous for the R47H mutation are extremely rare, and one such case exhibited amyloid and τ pathology, as well as marked frontal brain atrophy typical of NHD, albeit without the usual white matter lesions and bone fractures (Slattery et al. 2014). Additionally, extensive Aβ pathology was found by amyloid PET scanning in a patient carrying the Q33X variant (Ghezzi et al. 2017), which is more commonly found in FTD patients (Guerreiro et al. 2013c) Currently, there are no NHD mouse models available, however, TREM2- or DAP12-deficient mice display NHD related phenotypes including impaired remyelination (Cantoni et al. 2015; Piccio et al. 2007; Nataf et al. 2005), synaptic degeneration (Kaifu et al. 2003), reduced amyloid plaque-associated microglia and increased accumulation of diffuse Aβ plaques but no bone aberrations (Mazaheri et al. 2017; Parhizkar et al. 2019; Yuan et al. 2016; Wang et al. 2016; Keren-Shaul et al. 2017). The prevalence of AD-like neuropathology in NHD cases has yet to be determined. NHD is also linked to leukodystrophy (Oyanagi et al. 2017; Molina-Monasterios et al. 2003), which is not seen in AD or FTD (Walter 2016). Thus, it will be interesting to investigate the molecular mechanisms that contribute to the various pathologies associated with TREM2 mutations. Variants of TREM2 are summarized in Table 1.1 and on the Alzforum website: https://www.alzforum.org/mutations/trem2

Mutation/ polymorphism	Effect	Associated pathologies /Disease	References
40G→T	E14X, premature truncation	NHD	(Paloneva et al. 2002)
40 + 3delAGG	Altered splicing, decreased protein	FTD/FLTD	(Chouery et al. 2008)
97C→A	Q33X	AD; FTD/FTLD; NHD	(Guerreiro et al. 2013c; Klunemann et al. 2005; Lu et al. 2015; Bock et al. 2013; Soragna et al. 2003)
113A→G	Y38C	NHD, FTLD	(Guerreiro et al. 2013c; Klunemann et al. 2005; Guerreiro et al. 2013a)
132G→A	W44X, truncated, nonfunctional protein	NHD	(Paloneva et al. 2002)
c.140G→A	R47H	AD FTD/FLTD PD ALS	(Jonsson et al. 2013; Guerreiro et al. 2013d; Slattery et al. 2014; Lill et al. 2015; Hooli et al. 2014; Bertram et al. 2013; Mengel et al. 2016; Thelen et al. 2014; Rayaprolu et al. 2013; Huang et al. 2015; Kim et al. 2014; Cuyvers et al. 2014; Lu et al. 2015; Pottier et al. 2016a; Korvatska et al. 2015; Gonzalez Murcia et al. 2013; Benitez et al. 2013; Jin et al. 2014)
185G→A	R62H	AD	(Jin et al. 2014; Roussos et al. 2015)
197C→T	T66M	NHD, FTD/FTLD	(Klunemann et al. 2005; Guerreiro et al. 2013c)
233G→A	W78X	NHD	(Paloneva et al. 2002)
257A→T	D86V	FTD/FTLD	(Guerreiro et al. 2013a)
259C→T	D87N	AD	(Guerreiro et al. 2013d)
267delG	Frame-shift, nonfunctional protein	NHD	(Paloneva et al. 2002; Klunemann et al. 2005)
286C→A	T96K	FTD/FTLD	(Thelen et al. 2014)
313delG	Frame-shift, nonfunctional protein	NHD	(Paloneva et al. 2002; Klunemann et al. 2005)
377T→G	V126G	NHD	(Klunemann et al. 2005)
401A→G	D134G	NHD	(Klunemann et al. 2005; Paloneva et al. 2002)
469C→T	H157Y	AD	(Jiang et al. 2016b)
482 + 2T→C	Impaired splicing, decreased/nonfunctional protein	NHD	(Klunemann et al. 2005; Numasawa et al. 2011)
558G→A	K186N, no interaction with DAP12	NHD	(Paloneva et al. 2002)
598G→A	W198X	FTD/FLTD	(Giraldo et al. 2013)
632C→T	L211P	AD; FTD/FLTD	(Thelen et al. 2014; Jin et al. 2015)

Table 1.1 | Disease-associated mutations in TREM2

TREM2 mutations are found to be associated with many neurodegenerative disorders including Alzheimer's disease (AD), frontotemporal dementia (FTD) or frontotemporal lobar dementia (FTLD), Parkinson's Disease (PD), Amyotrophic lateral sclerosis (ALS), and Nasu-Hakola disease (NHD).

1.5 | Aim of the study

Recent GWAS have identified rare variants of TREM2 that increase the risk of developing AD. Such rare variants of TREM2 also increased the risk for FTD, PD, and ALS. Homozygous mutations or compound heterozygous mutations of TREM2 are known to cause NHD or early-onset FTD-like syndrome (Section 1.4.4 -1.4.6). TREM2 function is important for the proliferation and survival of macrophages such as microglia in the brain, however, it is still unclear whether the TREM2 function has a beneficial or detrimental effect. TREM2 binds to Aβ (Section 1.4.3) and with the progression of AD, this Aβ tends to aggregate and accumulate in the form of extracellular plaques. Also, several studies have shown that heterogeneity in proteolytic cleavages and additional post-translational modifications result in the production of several distinct Aβ variants, that could differ in their aggregation behaviour and toxic properties. Also, the deposition of non-modified (nm) Aβ peptides, pyroglutamate-modified Aβ (N3pE-Aβ) and phosphorylated Aβ (particularly, pSer8-Aβ) species in extracellular plaques follows a specific sequence during the progression from pre-clinical to clinical phases of AD (Section 1.1.4). So, the main objective of this work was to investigate the interaction of TREM2 with distinct Aβ species by biochemical as well as biophysical methods and to reveal the functional effects of TREM2 on the binding and uptake of various Aβ variants by microglia in cell culture models, and brains of transgenic mice and human AD cases. In addition, the specific deposition of a phosphorylated Aβ species in the brain and related functional implications should be analysed using a novel APP transgenic mouse model. It was also of interest to study the functional implications of TREM2 loss of function and disease-associated variants on the development and composition of different Aβ-associated lesions in the brain.

Chapter 2 | Materials and methods

2.1 | Chemicals and materials

2.1.1 | Chemicals

Chemicals were purchased from Sigma-Aldrich (St. Louis, USA), Roche (Basel, Switzerland), Merck KGaA (Darmstadt, Germany), MP Biomedicals (Santa Ana, USA), Invitrogen life technologies (Karlsruhe, Germany), Gibco (Karlsruhe, Germany), AppliChem (Darmstadt, Germany), Carl Roth (Karlsruhe, Germany), PSL (Heidelberg, Germany), New England Biolabs GmbH (Frankfurt am Main, Germany), CalBiochem (Darmstadt, Germany) or GE Healthcare (Solingen, Germany).

2.1.2 | Laboratory instruments and equipments

Device/Tools	Company
Aminopropylsilane (APS) sensors	ForteBio
Analytical balance (Labstyle 204)	Mettler Toledo
Autoclave	VARIOKLAV® HP Medizintechnik
Axio Scan.Z1	Carl Zeiss MicroImaging GmbH
AxioVert 200 fluorescence microscope	Zeiss
Beckman Ultracentrifuge Optima™ XPN-80	Beckman Coulter
Biophotometer	Eppendorf
CO_2 incubator 37°C	Binder
Cell culture-Laminar flow hood	Thermo Fisher Scientific/ Clean Air Products
Centrifuges (5415D, 5415R, 5804, 5804R)	Eppendorf
ChemiDoc™ XRS system with analysis	Bio-Rad Laboratories, Inc.
Column 10 kDA MWCO	Sartorius
Copper grid-400 mesh	Electron microscopy sciences
Ethovision XT version 13	Noldus information technology
Freezer -80°C	Thermo Fisher Scientific
Incubation hood TH 15	Edmund Bühler
InfiniteM200 PRO plate reader	Tecan
Leica TCS SP8 confocal microscope	Leica microsystems CMS GmbH
Magnetic stirrer	Velp Scientifica
Mice automatic monitoring system	TSE Systems
Nalgene® Mr Frosty freezing container	Thermo Fisher Scientific
NanoPhotometer® P-class P330	Implen P class
NuPAGE® 4-12% Bis-Tris protein gels	Thermo Fisher Scientific
Octet RED384	Forte Bio
Odyssey CLx Imager with analysis	LI-COR Biosciences
PCR cycler	Eppendorf
pH meter (MP225)	Mettler Toledo
Roto shake genie	Scientific Industries
Sonicator	Merck Eurolabs
Streptavidin (SA) biosensors	Forte Bio
Superose® 6 Increase 10/300 GL	GE Healthcare

Talos L120C	Thermo Fisher Scientific
Thermomixer R 5355	Eppendorf
VisiScope CSU-W1 spinning disk confocal microscope	Visitron Systems GmbH
Vortex (MS2 Minishaker)	IKA
Water bath	Labortechnik Medingen

Table 2.1 | Laboratory instruments and equipments

2.1.3 | Buffers and solutions

Name	Constituents with the final concentration
APS	10% Ammonium persulphate in water. Stored at 4 °C
BLI assay buffer	20mM HEPES, 500mM NaCl, 0.1%BSA, 0.02% Tween 20, prepared with dH_20 (pH 7.4)
Coomassie staining solution	0.4% Coomassie brilliant blue G-250, 5% Acetic Acid, 40% Methanol (Volume adjusted to 500 ml with dH_20, filtered through a Whatman filter paper and stored at RT)
Coomassie destaining solution	10% Acetic acid, 30% Methanol (Volume adjusted to 500 ml with dH_20)
Hypotone buffer	10 mM Tris-HCl (pH 7.5), 10mM NaCl, 0.1 mM EGTA, 25mM Glycerol phosphate, 1mM DTT, 1x protease inhibitor cocktail
Homogenisation buffer for mouse brains	1x PBS, 1 mM EDTA, 1 mM EGTA, 3 µl/ml protease inhibitor cocktail
Immunoblotting-antibody solution	Antibodies diluted in 1x TBS with 0.1% Tween 20 (prepared fresh)
Immunoblotting-washing buffer	100 ml 10x TBS, 0.1% Tween 20, volume adjusted to 1 L with dH_20
Immunoblotting-blocking solution-1	5% BSA, 1x TBS with 0.1% Tween 20 (prepared fresh)
Immunoblotting-blocking solution-2	5% Non-fat Skimmed milk powder, 1x TBS with 0.1% Tween 20 (prepared fresh)
Laemmli sample buffer (5x)	50 mM Sodium phosphate (pH 6.8), 5% SDS, 40 mM DTT, 5 mM EDTA, 5 mM EGTA, 20% Glycerol, 0.01% Bromophenol blue (Mixed thoroughly, aliquoted and stored at -20 °C)
Loading buffer (5X)	312.5 mM Tris-HCl (pH 6.8), Glycerol 50 % (V/V), 2-mercaptoethanol 7.5 % (V/V), SDS 10 % (m/V), Bromophenol blue 0.1 % (m/V)
NuPAGE Gel running buffer	50 ml 20x NuPAGE MES SDS running buffer, Volume adjusted to 1 L with dH_20
NuPAGE LDS sample buffer (1x)	2.5 µl of LDS (Lithium dodecyl sulfate) sample buffer (4x), 1 µl of NuPAGE reducing agent (10x), x µl of the sample. Volume adjusted to 10µl with dH_20
Phosphatase inhibitor	One tablet in 1 ml dH_20 (10x stock solution), aliquoted and stored up to 6 months at -20 °C
Phosphate Buffered Saline (PBS) (10x)	137 mM NaCl, 2.7 mM KCl, 10 mM $Na_2HPO_4\,2H_2O$, 2mM KH_2PO_4 (salts were dissolved in 4.5 L dH_20 (pH 7.4), volume adjusted to 5 L with dH_20, autoclaved and stored at RT)
Ponceau S staining solution	0.5% Ponceau S, 1% Acetic acid, prepared with dH_20 and filtered. Stored in dark at RT
Protease inhibitor	One tablet in 2 ml dH_20 (25x stock solution), aliquoted and stored up to 6 months at -20 °C
RIPA buffer	25 mM Tris-HCl (pH 7.5), 150 mM NaCl, 1% NP40, 0.5% NaDOC, 0.1% SDS
STEN-Buffer (1x)	50 mM Tris-HCl (pH 7.6), 150 mM NaCl, 2 mM EDTA, 0.2% NP-40 (Igepal CA-630). Stored at RT

STEN-Lysis Buffer with BSA (1x)	50 mM Tris-HCl (pH 7.4), 150 mM NaCl, 2 mM EDTA, 1% Triton X-100, 1% NP-40, 2% BSA, 1x complete protease inhibitor
STEN-NaCl Buffer (1x)	50 mM Tris-HCl (pH 7.6), 500 mM NaCl, 2 mM EDTA, 0.2% NP-40. Stored at RT
Thioflavin-T (ThT) solution	20µM stock prepared in Millipore H_20, sterilised by filtration
Transfer buffer (10x)	390 mM Tris, 480 mM Glycine dissolved in 1 L dH_20 (pH 8.0). Stored at 4 °C
Tris-buffered saline (10x)	0.1 M Tris, 1.5 M NaCl, dissolved in 750 ml dH_20 (pH 7.5), Volume adjusted to 1 L. Sterilized by autoclaving and stored at RT.

Table 2.2 | Buffers and solutions

2.1.4 | Solutions for Immunofluorescence/immunostainings

Name	Constituents with the final concentration
ICC- Blocking solution	2.5 % BSA, 0.125 % Trition X-100 in 1xPBS (prepared fresh)
ICC- Permeabilisation solution	0.25 % Triton X-100 solution in 1xPBS (prepared fresh) or 0.1 % Triton X-100 solution in 1xPBS (prepared fresh)
ICC- Antibody solution	0.125 % BSA, 0.1 % Tween-20 in 1xPBS (prepared fresh)
ICC- Washing solution	0.1 % Tween-20 in 1xPBS (prepared fresh)
IF (mouse brain sections)- Blocking solution	5% NHS, 2.5% BSA, 0.2% Triton X-100 prepared in 1xPBS (prepared fresh)
IF (mouse brain sections)- Washing solution	0.10% Triton X-100 in 1xPBS (prepared fresh)
IF/IHC (mouse brain/human sections)- Sodium citrate solution	10 mM sodium citrate, 0.05% Tween 20 in dH_2O (pH- 6.0)
IF (mouse brain sections)- Permeabilization solution	0.25% Triton X-100 in 1xPBS (prepared fresh)
IF (mouse brain sections)- Antibody solution	3% NHS, 1% BSA, 0.1% Tween 20, prepared in 1xPBS (prepared fresh)

Table 2.3 | Solutions for Immunofluorescence/immunostainings

2.1.5 | Assay kits

Kits/ ready to use reagents	Company
ABC-kit	Vector laboratories
Diaminobenzidine-HCl (DAB)	Vector laboratories
DPX Mountant for histology	Sigma
Immu-Mount	Thermo Fisher Scientific
Lipofectamin 2000	Thermo Fisher Scientific
Mouse on Mouse blocking reagent	Vector laboratories
NucleoSpin plasmid easy pure kit	Macherey and Nagel
Pierce™ BCA protein assay kit	Thermo Fisher Scientific
Protein G (SureBeads™) beads	Bio-Rad
SeeBlue™ Pre-stained protein standard	Thermo Fisher Scientific
QuikChange II site-directed mutagenesis kit	Agilent Technologies
Reveal decloaker	Biocare Medical
VECTASHIELD® antifade mounting medium	Vector laboratories

Table 2.4 | Assay kits

2.2 | Antibodies

Phosphorylation-state-specific antibodies were generated and validated as described in the previous papers (Milton 2001; Kumar et al. 2013; Kumar et al. 2020a). For specific detection of modified Aβ, particularly, the phosphorylated Aβ species was done using, the brain sections were stained with monoclonal antibodies, murine 1E4E11, specifically recognizing Aβ phosphorylated at Ser8 (pSer8Aβ) that did not cross-react with other post-translationally modified variants of Aβ, including N-terminally truncated (N3pE-Aβ42), nitrated (3NTyr10-Aβ), pyroglutamated (N3pE-Aβ), or Aβ phosphorylated at Ser 26 (Kumar et al. 2013). Rat 7H3D6 specifically detects Aβ species with a non-modified N-terminus (nmAβ) and does not recognize phosphorylated Ser8-Aβ but also does not recognize other Aβ variants with N-terminal modifications, including pyroglutamated, nitrated, and N-terminally truncated Aβ species (Ashby et al. 2015; Kumar et al. 2013; Kumar et al. 2018; Gerth et al. 2018). Rabbit polyclonal antibody 2964 was raised against aggregated Aβ (Wahle et al. 2006; Tamboli et al. 2010). TREM2 antibodies (AF1729, AF1828 and 4B2A3) were verified for immunostainings (Parhizkar et al. 2019; Jay et al. 2015). Recently reported mouse monoclonal antibody, clone 5H10C11, selectively detects Aβ phosphorylated at Ser26 which was characterized and validated by ELISA, western immunoblotting, and control staining's with non-transgenic mice, pre-absorption with pSer26-Aβ synthetic peptides and secondary antibody alone (Kumar et al. 2020a). Since phosphorylation at this site occurs after the generation of Aβ, the antibody does also not recognize full-length APP or APP CTFs (Kumar et al. 2020a; Joshi et al. 2021a; Joshi et al. 2021b). All the other antibodies used in the study were verified for immunostaining and immunoblotting in mouse and human samples according to the company websites (Table 2.5).

Antibody	Source/Catalog number	Species	Dilution
Primary antibodies			
Aβ- 4G8	Sigma-Aldrich Cat# A1349, RRID:AB_476683	Mouse monoclonal	IF-1:250; IHC-1:4000; ICC-250; WB-1:1000
Aβ- 82E1	Immuno-Biological Laboratories Cat# JP10323, RRID:AB_1630806	Mouse monoclonal	IF-1:250
Aβ- 2964	In-house made (Genscript)	Rabbit polyclonal	IF-1:250; WB-1:1000
Aβ- 6E10	BioLegend Cat# 803001, RRID:AB_2564653	Mouse monoclonal	IF-1:200
Aβ- MOAB2	Abcam Cat#Ab126649	Mouse monoclonal	IF-1:100
Aβ- 11A1	Immuno-Biological Laboratories Cat#10379	Mouse monoclonal	IF-1:100
Aβ- A11	Thermo Fisher Scientific Cat# AHB0052, RRID:AB_2536236	Rabbit polyclonal	IF-1:100; DB-1:1000
Non-modified Aβ (nmAβ)-7H3D6	In-house made (Genscript)	Rat monoclonal	IF-1:250; IHC-1:100; WB-1:250

pSer8-Aβ-1E4E11	In-house made (Genscript)	Mouse monoclonal	IF-1:250; IHC-1:50; WB-1:250
pSer26-Aβ-5H11C10	In-house made (Genscript)	Mouse monoclonal	IF-1:250
N3pE-Aβ	Immuno-Biological Laboratories Cat# JP18591, RRID:AB_1630801	Rabbit polyclonal	IF-1:100
Lamp1	Abcam Cat# ab25245, RRID:AB_449893	Rat monoclonal	IF-1:100; ICC-1:250
Laminin	Sigma-Aldrich Cat# L9393, RRID:AB_477163	Rabbit polyclonal	IF-1:25
Bip/GRP78	BD Biosciences Cat# 610978, RRID:AB_398291	Mouse monoclonal	1:100
CHOP	Cell Signaling Technology Cat# 2895, RRID:AB_2089254	Mouse monoclonal	1:100
Calnexin	Millipore Cat# AB2301, RRID:AB_10948000	Rabbit polyclonal	ICC-1:500; IF- 1:100
	Thermo Fisher Scientific Cat# MA3-027, RRID:AB_2069043	Mouse monoclonal	ICC-1:500; IF- 1:100
TGN46	Abcam Cat# ab16059, RRID:AB_443307	Rabbit polyclonal	ICC-1:500
	Sigma-Aldrich Cat# T7576, RRID:AB_1080261	Rabbit polyclonal	ICC-1:500
TREM2- AF1828	R and D Systems Cat# AF1828, RRID:AB_2208689	Goat polyclonal	ICC-1:100; WB-1:3000
TREM2- 4B2A3	In-house made (Genscript)	Mouse monoclonal	ICC-1:300; WB-1:3000; DB-1:3000
TREM2- AF1729	R and D Systems Cat# AF1729, RRID:AB_354956	Sheep polyclonal	IF-1:50
Iba1	Synaptic Systems Cat# 234 003, RRID:AB_10641962	Rabbit polyclonal	IF-1:1000; ICC-1:500
	Millipore Cat# MABN92, RRID:AB_10917271	Mouse monoclonal	IF-1:300
NeuN	Abcam Cat# ab104225, RRID:AB_10711153	Rabbit polyclonal	IF-1:500
β-actin	Sigma-Aldrich Cat# A1978, RRID:AB_476692	Mouse monoclonal	WB: 1:5000
Secondary antibodies			
Alexa Fluor 488	Thermo Fisher Scientific Cat# A-11055, RRID:AB_2534102	Donkey anti-goat	IF-1:500; ICC-1:1000
Alexa Fluor 488	Thermo Fisher Scientific Cat# A-21202, RRID:AB_141607	Donkey anti-mouse	IF-1:500
Alexa Fluor 488	Thermo Fisher Scientific Cat# A-11029, RRID:AB_2534088	Goat anti-mouse	IF-1:500; ICC-1:1000
Alexa Fluor 488	Thermo Fisher Scientific Cat# A-21208, RRID:AB_2535794	Donkey anti-rat	IF-1:500
Alexa Fluor 488	Thermo Fisher Scientific Cat# A-11034, RRID:AB_2576217	Goat anti-rabbit	IF-1:500; ICC-1:1000
Alexa Fluor 546	Thermo Fisher Scientific Cat# A-21098, RRID:AB_2535752	Donkey anti-sheep	IF-1:500
Alexa Fluor 546	Thermo Fisher Scientific Cat# A-10040, RRID:AB_2534016	Donkey anti-rabbit	IF-1:500; ICC-1:1000
Alexa Fluor 546	Thermo Fisher Scientific Cat# A-10036, RRID:AB_2534012	Donkey anti-mouse	IF-1:500; ICC-1:1000
Alexa Fluor 546	Thermo Fisher Scientific Cat# A-11035, RRID:AB_2534093	Goat anti-rabbit	IF-1:500; ICC-1:1000

Alexa Fluor 546	Thermo Fisher Scientific Cat# A10040, RRID:AB_2534016	Donkey anti-rabbit	IF-1:500; ICC-1:1000
Alexa Fluor 546	Thermo Fisher Scientific Cat# A-11081, RRID:AB_2534125	Goat anti-rat	IF-1:500
Alexa Fluor 647	Thermo Fisher Scientific Cat# A-21236, RRID:AB_2535805	Goat anti-mouse	IF-1:500; ICC-1:1000
Alexa Fluor 647	Thermo Fisher Scientific Cat# A-21245, RRID:AB_2535813	Goat anti-rabbit	IF-1:500; ICC-1:1000
Anti-Fc HRP	Thermo Fisher Scientific Cat# 62-8420, RRID:AB_2533962	Goat polyclonal	WB-1:500-1:2000
Mouse HRP	Sigma-Aldrich Cat# A9044, RRID:AB_258431	Mouse polyclonal	WB-1:15000
Rabbit HRP	Sigma-Aldrich Cat# A9169, RRID:AB_258434	Rabbit polyclonal	WB-1:15000
IRDye® 800CW	LI-COR Biosciences Cat# 926-32212, RRID:AB_621847	Donkey anti-mouse	WB-1:5000
	LI-COR Biosciences Cat# 926-32219, RRID:AB_1850025	Goat anti-rat	
	LI-COR Biosciences Cat# 926-32213, RRID:AB_621848	Donkey anti-rabbit	
	LI-COR Biosciences Cat# 926-32214, RRID:AB_621846	Donkey anti-goat	
	LI-COR Biosciences Cat# 926-32232, RRID:AB_10806644	Goat anti-human	
IRDye® 680CW	LI-COR Biosciences Cat# 926-68074, RRID:AB_10956736	Donkey anti-goat	WB-1:5000
	LI-COR Biosciences Cat# 926-68073, RRID:AB_10954442	Donkey anti-rabbit	
	LI-COR Biosciences Cat# 926-68076, RRID:AB_10956590	Goat anti-rat	
	LI-COR Biosciences Cat# 926-68072, RRID:AB_10953628	Donkey anti-mouse	

Table 2.5 | Primary and secondary antibodies

DB- Dot blot, IF-Immunofluorescence, ICC-Immunocytochemistry, WB-Western blotting, HRP-Horseradish peroxidase (Joshi et al. 2021a; Joshi et al. 2021b).

2.3 | Oligomerisation of Aβ peptides

The synthetic Aβ (1-42 and 1-40) and Aβ (3-42 and 3-40) peptide variants were obtained from PSL, GmBH. Synthetic Biotin-LC-Aβ (1-42) (LC: 6-carbon long-chain) was obtained from AnaSpec (Joshi et al. 2021b). The reconstitution of Aβ peptide variants was done by adding 10 mM NaOH directly to the vial containing the lyophilised peptides to make a stock solution of 230 µM followed by sonication for 5 min, aliquoted and snap-frozen. Biotin-LC-Aβ (1-42) was reconstituted with DMSO and biolayer interferometry (BLI) assay buffer (consisting of 20 mM HEPES and 1 M NaCl) thus giving a stock concentration of 100 µM, aliquoted and snap-frozen. For Aβ monomer-rich fractions, Aβ were prepared from freshly reconstituted Aβ stocks by dilution to 23 µM in ice-cold PBS and ultracentrifugation at 4°C at 100,000g for 1 h. Aβ in the[*]

[*] *Italicized text is taken from the manuscript published in GLIA by Joshi et al. 2021*

supernatant was considered as monomer rich preparation (Joshi et al. 2021b). For the preparation of Aβ oligomers two different methods were used:

Method 1- *For the dot blot, and BLI experiments, oAβ(1-42) preparation was used that was made by gently mixing freshly prepared Aβ(1-42) variants separately with a suitable concentration of Biotin-LC-Aβ(1-42) to make the final concentration of 23 µM in PBS (pH 7.4) followed by incubation at 37°C for 3 h[*] 0*

Method 2- *For the pulldown, cellular binding and phagocytosis experiments, we followed protocol to prepare oAβ as described previously (Kim et al. 2013). Briefly, monomeric Aβ stock was diluted to 100 µM in PBS and incubated at 23°C for 16 h followed by incubation at 4°C for 24 h. The preparation was further centrifuged at 16,000g and the supernatant was aliquoted, flash-frozen in liquid nitrogen and stored at -20°C[*] (Joshi et al. 2021b)[*].*

2.4 | Experimental animals

Wild-type (WT, Charles River Laboratories, USA) and homozygous TREM2^{T66M} (Taconic Biosciences GmbH, Germany), were of C57BL/6 genetic background. Mice were housed under standard conditions at 22°C and a 12 h light-dark cycle with free access to food and water. Animal care and handling of these mice were performed according to the Declaration of Helsinki and approved by the local ethical committees (LANUV NRW 84-02.04.2017.A226) (Joshi et al. 2021b)[*].

APP695KM670/671NL; PS1L166P TREM2$^{+/+}$ and APP695KM670/671NL; PS1L166P TREM2$^{-/-}$ transgenic mice, and 5xFAD TREM2$^{+/+}$ and 5xFAD TREM2$^{-/-}$ transgenic mice were described previously (Parhizkar et al. 2019; Turnbull et al. 2006; Wang et al. 2015). 12 M old female APPKM670/671NL; PS1ΔE9 transgenic mice endogenously expressing TREM2 WT or the homozygous TREM2T66M knock-in (KI) mutation were obtained from Taconic Biosciences GmbH, Germany (Joshi et al. 2021a; Joshi et al. 2021b; Kleinberger et al. 2017)[*]. The different AD mouse models are described in Table 6.1 and Table 2.6.

Genotype	Description
C57BL/6	Wild type mice with black colour for breeding and backcrossing
APP/PS1	APP695KM670/671NL; PS1L166P- Mice contain human APP transgenes for both containing Swedish mutation and PS1 containing an L166P mutation, both under the control of the Thy1 promoter.
	APPKM670/671NL; PS1ΔE9- Mice contain human APP transgene for both containing Swedish mutation and ΔE9 knock-out mutation in PS1, both under the control of mouse prion protein promoter.
	5xFAD- Mice express human APP and PSEN1 transgenes with a total of five AD-linked mutations: the Swedish (K670N/M671L), Florida (I716V), and London (V717I) mutations in APP, and the M146L and L286V mutations in PS1, each driven by the mouse Thy 1 promoter.

Table 2.6 | Experimental mouse models

[*] *Italicized text is taken from the manuscript published in GLIA by Joshi et al. 2021*

AβS26D-Tg mouse model

To understand the role of phosphorylation of Aβ at serine 26, we generated a novel transgenic AβS26D-Tg mouse model, which expresses the human APP751 variant carrying the Swedish (KM→NL) and phosphomimicking (S→D) mutations at Ser26 residue of Aβ, under the control of the neuron-specific Thy1 promoter. The AβS26D-Tg transgenic male and female mice produced in-house at different age groups were used in this study. Animals were maintained in a group of 3-5 at 25°C under a reversed light-dark cycle (lights on-19:00; lights off-9:00) and provided with food and water ad libitum. All animals were originally purchased from Charles River Laboratories and bred in the institutional animal house were used in this study. All animal procedures were carried out following the approved guidelines of the LANUV NRW (Approval Number: 81-02.04.2019.A047).

2.5 | Animal behaviour tests

2.5.1 | Open-Field Test (OFT)

It was performed as described previously (Bilkei-Gorzo et al. 2005). In brief, the mice were placed in the centre of a dimly lit (20-30 lux) chamber of the open-field apparatus (44 × 44 × 25 cm). At the end of each trial, the arena was thoroughly cleaned. Movements of the animals were tracked by an automatic monitoring system (TSE Systems, Germany) for 20 min. Horizontal motor activity was evaluated by calculating the distance that the animals travelled. The data were represented as the mean value and standard error.

2.5.2 | Partner Recognition Test (PRT)

It was performed to check the social recognition associated with long-term memory as described previously (Bilkei-Gorzo et al. 2017; Vorhees et al. 2006). The test was conducted in an open-field arena (44 × 44 cm × 25 cm) in a dimly lit, sound-isolated environment. The floor of the arena was covered with sawdust saturated with the odour of mice. Initially, the animals were habituated to the arena containing two small metal grid cages placed at two opposite corners 6-7 cm from the walls (Figure 5.5a) for 5 min daily for 3 days. The main tests started on the fourth day and consisted of two sessions. The first session of 6 min wherein the one mouse has kept in the metal grid cage whilst the other grid cage (same dimensions) was kept empty and then the second session of 3 min was carried out at different time intervals of (1h, 2h, 4h, 8h) on consecutive days. This session consists of introducing a new partner to the other metal grid cage in presence of the previous partner. The PRT was carried out by introducing the new mouse in each mouse enclosure during each new interval timepoint on consecutive days. In this test, recognition of the previously seen partner was defined by a novelty preference and was calculated by when the animal approached the vicinity (3 cm) of metal grid cage by using Ethovision XT version 13 (Noldus information technology, Netherlands). The

preference ratio was calculated by using the formula, preference = TA/(TA + TB) × 100; TA, the time social; TB, time at the objects that remained in their original positions. Novelty preference was calculated by the formula, %novelty= PA/(PA- PB)× 100; PA, time spent with the novel partner; PB is the time spent with the previous partner. Groups were compared using two-way ANOVA (Sidak multiple comparison tests). A significant reduction in the time the animals spent with social interactions in the second presentation (student's paired-t test) was considered as an indication that the animals recognized the partner. The test was repeated until the animals failed to recognize the partner in the second presentation.

2.5.3 | Morris water maze (MWM) test

It is well discerning behavioural test to explore spatial learning and memory in rodent models (Koistinaho et al. 2001; Wahul et al. 2018). Animals were subjected to training for 6 days in a circular tank (diameter of 120 cm) filled with opacified water (at 25-27°C) with visual clues and a hidden sub-merged platform usually below 1 cm of the water surface (1 cm) placed in Q3 (quadrant 3) during which their latency to find the hidden platform was measured up to a maximum of 60 s. During each day, the animal underwent three trials from different starting points marked as Q1 (quadrant 1), Q2 (quadrant 2) and Q4 (quadrant 4). If the mouse did not locate the platform within 60 s, the experimenter guided the mouse to the platform by hand and was allowed to remain on the platform for 10 s to allow the mouse to sufficiently assess distal cues. At the end of the trial, the mouse was returned to a holding cage, while the other mouse in the group were tested (<5-7 min inter-trial-interval). At the end of 3 trials, the mice were returned to their home cages in the colony room. Drop location varied between time-point/trials/days but was maintained between subjects. Time to reach the platform (i.e., escape latency), total distance, and velocity were calculated for each trial and averaged within a day. On the 7th day, the probe trial was carried out wherein the platform was removed and the search pattern was analyzed for 60 s with the help of video tracking software Ethovision XT version 13 (Noldus information technology, Netherlands). The cumulated duration the animal spends in each quadrant was calculated. Statistical analysis was carried out by using either student's t-test to check the variance within two groups or two-way ANOVA (sidak multiple comparison test) to check the variance within the genotype and quadrants.

2.6 | Human brain samples

Tissue samples of patient autopsy cases were provided by the Neurobiobank Munich, Ludwig-Maximilians-University (LMU) Munich. Detailed clinical characteristics were ascertained from an integrated autopsy database. Written informed consent for autopsy and analysis of tissue sample data was obtained for all patients, either from the patients themselves or their kin and the samples were collected according to the guidelines of the local ethics committee following

all ethical regulations. Information regarding cases, clinical diagnosis, age at death, post-mortem delay, fixation time, AD Braak & Braak stage, Thal phase, and TREM2 coding variant is given in Table 6.2. The genotyping and identification of TREM2 variant carriers were done as described before (Parhizkar et al. 2019). Sample sizes were based on the availability of patient material. For all analyses, the temporal neocortex was used which included the cortex of the medial temporal gyrus at the level of the anterior hippocampus[*]*.*

2.7 | Molecular biological methods

2.7.1 | Plasmids

The commercially available vector, pcDNA5^{TM}/FRT designed for use with the Flp-In System for the expression of proteins in mammalian cells was obtained from Thermo Fisher Scientific (Waltham, USA). The site-directed mutagenesis was performed using the full-length TREM2 construct made with pcDNA5^{TM}/FRT reported previously by (Ibach et al. 2021).

2.7.2 | Site-directed mutagenesis of plasmid DNA

Site-directed mutagenesis of plasmid DNA, mutant strand synthesis reaction, DpnI digestion of the amplification product, and transformation of XL 1-blue super-competent *E. coli* was accomplished using the QuikChange II Site-Directed Mutagenesis Kit from Agilent Technologies according to the manufacturer's instructions (Table 2.7).

No.	Name	Gene	Primers used for site directed mutagenesis	Resis-tance
488	sTREM2-WT	hTREM2-WT	**Fwd-**GAGGATGCCCATGTGGAGCACTGAATCTCCAGGAGCC **Rev-**GGCTCCTGGAGATTCAGTGCTCCACATGGGCATCCTCG	Amp/Hygr
489	sTREM2-R47H	hTREM2-R47H	**Fwd-**GAGGATGCCCATGTGGAGCACTGAATCTCCAGGAGCC **Rev-**GGCTCCTGGAGATTCAGTGCTCCACATGGGCATCCTCG	Amp/Hygr
506	sTREM2-T66M	hTREM2-T66M	**Fwd-**GAGGATGCCCATGTGGAGCACTGAATCTCCAGGAGCC **Rev-**GGCTCCTGGAGATTCAGTGCTCCACATGGGCATCCTCG	Amp/Hygr

Table 2.7 | Primers used for site-directed mutagenesis

2.8 | Bacterial culture and transformation

Media were prepared with dH_2O and autoclaved. To obtain a solid medium, 1.5% (w/v) agar was added (Table 2.8).

Name	Composition
Lysogeny broth (LB) medium	10 g tryptone,10 g NaCl, 5 g yeast extract, dH_2O; pH 7.5
Super Optimal Broth (SOC) medium	20 g tryptone, 0.59 g NaCl, 0.19 g KCl, 5 g yeast extract, 5 mM $MgCl_2$, 5 mM $MgSO_4$, 20 mM glucose, dH_2O; pH 7.0

Table 2.8 | Composition of culture media in bacterial cell culture

Masses refer to a volume of 1L.

[*] *Italicized text is taken from the manuscript published in Acta neuropathologica communications by Joshi et al. 2021*

2.8.1 | Bacterial strain for cloning

Following competent *E. coli* strain was used for maintenance and propagation of plasmid DNA. *XL1-blue, Agilent Technologies, Cat No: 200249, genotype: recA1 endA1 gyrA96 thi-1 hsdR17 supE44 relA1 lac [F´ proAB lacIq ZΔM15 Tn10 (Tetr)].*

2.8.2 | Transformation of competent *E. Coli*

The transformation was performed as per the standard protocol from Agilent technologies. For this, a total volume of 50 µl of competent *E. coli* bacterial cells was thawed 10 min on ice beforehand and gently mixed with 50 ng of the experimental DNA (or 2 µl of a ligation mixture). After a 30 min incubation on ice, the mixture was exposed to a heat shock for 30 s at 42°C (Eppendorf) and incubated for 2 min on ice. Then, 800 µl of SOC medium were added and bacterial cells were incubated for 1 h at 37°C under permanent shaking (750 rpm) in a thermomixer (Eppendorf). Plate ≤200 µl of the transformation mixture on LB agar plates containing the appropriate antibiotic. Agar plates were incubated at 37°C overnight and single colonies were tested for intake of the correct construct. For this purpose, 5 ml ampicillin-containing LB medium was inoculated with a single colony and incubated (Incubation hood TH 15) overnight at 37°C under permanent shaking (250 rpm).

2.8.3 | Small and large scale plasmid preparation

DNA mini preparations were performed on 5 ml of bacterial overnight cultures using NucleoSpin Plasmid EasyPure Kit (Macherey-Nagel, Germany) according to the manufacturer's instructions. DNA was eluted in an appropriate volume of either DNase/RNase-free H_2O or TE buffer. Similarly, DNA maxi preparations were performed on 200ml of bacterial overnight cultures using NucleoBond Xtra Maxi Kit (Macherey-Nagel, Germany) according to the manufacturer's protocol. The purity was measured spectrophotometrically using a NanoPhotometer (Implen P class, Germany). To control and verify DNA sequences, samples were sent for sequencing (GATC Biotech, Germany). Purified DNA was stored at -20°C.

Transformed bacteria were stored in glycerol 80% v/v of glycerol stocks at -80°C. To generate glycerol stocks, 800 µL of bacterial suspension were mixed with 200 µL of glycerol and stored at -80° C. Small amounts of this mixture were added to LB medium to enable reconstitution of the bacteria.

2.9 | Cell culture and transfection

2.9.1 | Culture of HEK293 Flp-In and stable cell lines

Handling of all the cells was performed inside a laminar flow hood (Clean Air Products, USA) using sterile equipment. The sTREM2-WT as well other mutants expressing HEK293 Flp-In cells were cultured in growth medium GlutaMAX™ (DMEM containing high glucose (4.5 g/l), 1 mM phenol red, sodium pyruvate additive, 10mM HEPES), supplemented with 10% heat-

inactivated FCS, 1% penicillin and streptomycin solution, and 100 µg/ml hygromycin in incubators maintained at 37°C and 5% CO_2 (Ibach et al. 2021; Joshi et al. 2021b). HEK293 Flp-In cells and HEK293 cells were cultured with and without antibiotics (Zeocin 100 µg/ml) in a growth medium respectively. The other culture medium conditions are described below in Table 2.9.

Name	Composition
DMEM$^{(+/+)}$ hygromycin B: culture and growth medium for TREM2 expressing HEK293 Flp-In cells	4.5 g/l D-glucose, 1 mM sodium pyruvate additive, 1% penicillin and streptomycin (100 U/ml penicillin, 100 µg/ml streptomycin), 10% heat-inactivated FCS, 10 mM HEPES, 100 µg/ml hygromycin B (while selecting single-cell clones, 200 µg/ml hygromycin B was used)
DMEM$^{(+/+)}$: culture and growth medium for HEK293 cells	4.5 g/l D-glucose, 1 mM sodium pyruvate additive, 1% penicillin and streptomycin (100 U/ml penicillin, 100 µg/ml streptomycin), 10% heat-inactivated FCS, 10 mM HEPES
DMEM$^{(+/+)}$ DMSO: cryopreservation medium	4.5 g/l D-glucose, 1 mM sodium pyruvate additive, 1% penicillin and streptomycin (100 U/ml penicillin, 100 µg/ml streptomycin), 10% heat-inactivated FCS, 10 mM HEPES, 10% DMSO
DMEM$^{(-/-)}$	4.5 g/l D-glucose, 1 mM sodium pyruvate additive, 10 mM HEPES

Table 2.9 | Composition of culture media in eukaryotic cell culture

+/+ = FCS/penicillin and streptomycin, -/- = without FCS/penicillin and streptomycin

2.9.2 | Transient transfection

Cells were cultured until 70-80% confluency and briefly washed with Dulbecco's Phosphate-Buffered Saline (DPBS). Transient transfections were performed using Lipofectamine 2000 (Thermo Fisher Scientific) using 8 µg of construct in reduced serum media, OptiMEM (Thermo Fisher Scientific) as a transfection medium according to the manufacturer's recommendations. Cells were maintained at 37°C and 5% CO_2. Subsequently, the transfection medium was collected after 24 h, all 6 cm dishes were collected for cell lysate (or membrane) preparation and also the medium was collected for further immunoblotting.

2.9.3 | Generation of stable cell clones

Culture dishes were pre-coated with poly-l-lysine for a minimum of 1-2 h. Further, the cells were cultured until 70-80% confluency and briefly washed with DPBS. Co-transfection was carried out using mammalian Flp-In™ host cells with pOG44:pcDNA5/FRT (9:1 ratio) plasmid DNA using Lipofectamine 2000 (Thermo Fisher Scientific) in OptiMEM. By co-transfecting pOG44 and pcDNA5/FRT, Flp recombinase is expressed and the pcDNA5/FRT plasmid is integrated into the genome via FRT sites. The pOG44 plasmid does not contain an antibiotic resistance marker for selection in mammalian cells. Consequently, the plasmid, and therefore, Flp recombinase expression, will gradually be lost from transfected cells as they are cultured and selected in hygromycin. 24 h after the transfections, fresh medium was exchanged with

fresh medium without antibiotics. The medium was replaced after 24 h with an antibiotic-containing medium for selection. The selection of the stable clones was done by the limiting-dilution method. For this, the cells were seeded into 96 well plate with a density of one cell per well. After this, the cells were allowed to grow for 1-2 weeks, expanded further in 24 well plates and the selection was done by checking the protein expression in the supernatant by acetone precipitation followed by immunoblotting (described in sections 2.13.1 and 2.15) or by performing immunocytochemistry (described in section 2.16.1)

2.9.4 | Passaging and cryopreservation of stable cell lines

Passaging of stable cell lines was performed when cells had reached at least 90% confluency. For this purpose, the cell culture medium was aspirated and cells were washed twice followed by the addition of trypsin solution. Cells were incubated with trypsin solution for 1-2 min in the incubator. Upon detachment of the cells, the trypsin reaction was terminated by the addition of a culture medium containing 10 % heat-inactivated FCS. The cell solution was then centrifuged for 1 min at RT 1000 rpm. The supernatant was aspirated and the cell pellet was resuspended in 1 ml. The cell number was determined using a Neubauer chamber. Passaging of the cells was completed by seeding the cells onto new culture dishes/flasks.

For cryopreservation, cells were detached and washed as described above. Upon cell counting, cells were transferred to cryogenic vials containing a cryopreservation medium (Table 2.9). The cryogenic vials were then stored for 48 h at -80°C in the Nalgene® Mr Frosty freezing container (Thermo Fisher Scientific) and then transferred to the liquid nitrogen tank for long-term storage. Revitalization of frozen cells was performed by transferring the vials to a 37°C water bath (< 1 min) by gently swirling the vial and rapid reconstitution in 10 ml of the pre-warmed medium. The cell suspension was centrifuged at 2000rpm for 1 min followed by discarding the supernatant and resuspending the cells in a fresh complete growth medium in an appropriate cell culture dish/flask.

2.9.5 | Culture of Expi293F™ cells

Expi293F™ cells were grown in suspension with serum-free FreeStyle™ expression medium (Thermo Fisher Scientific) and were kept at 37°C and 8% CO_2 (Joshi et al. 2021b)[*].

For thawing of cells, a vial of frozen cells was removed from liquid nitrogen and thawed in a water bath (Labortechnik, Germany). at 37°C (< 1 min) by gently swirling the vial. Cells were pipetted slowly in the pre-warmed culture medium, centrifuged at 2000rpm for 1 min followed by discarding the supernatant and resuspending the cells in a fresh complete growth medium in an appropriate cell culture dish/flask. Cells were routinely passaged for which the cells were trypsinized, resuspended in a culture medium, and gently pipetted up and down to

[*] *Italicized text is taken from the manuscript published in GLIA by Joshi et al. 2021*

disrupt cell clumps. Then, a fraction of cells with the adequate cell number was transferred to a new culture dish. Finally, the desired pre-warmed culture medium was added. For long-term storage, cells were resuspended in a cryopreservation medium (Table 2.9), transferred to a vial and placed in the Nalgene® Mr Frosty freezing container (Thermo Fisher Scientific), and kept for 48 h at -80°C. Subsequently, cells were stored in liquid nitrogen.

2.9.6 | Culture of WT and TREM2^{T66M} primary microglia cells

The cells were isolated by the previously described method (Giulian et al. 1986). Briefly, brains from neonatal mice were stripped of the meninges and dissociated using mechanical shearing and trypsin (Life Technologies, USA). Cells of two brains were plated on poly-L-lysine (PLL, Sigma-Aldrich, Germany) coated T75 culture flasks (Greiner bio-one, Kremsmünster, Austria) and cultivated in DMEM (Gibco by Thermo Fisher Scientific, Waltham, MA, USA) supplemented with 10% heat-inactivated fetal calf serum (FCS; Gibco) and 1% penicillin/streptomycin (P/S; Gibco). On the next day, cells were washed three times with DPBS (Gibco) to remove cellular debris and cultured with DMEM supplemented with 10% FCS, 1% P/S and 1% L929 conditioned medium as a source of growth factors. After 7-10 days loosely attached mature microglia were shaken off the astrocytic layer with a repetition of the harvesting procedure for two to three days up to three times. For experiments, primary microglia were seeded on poly-D-lysine (PDL, Sigma-Aldrich, Germany) coated glass coverslips at a density of 100,000/well into 24 well plates and allowed to adhere overnight in serum-free DMEM complemented with 1% N-2 supplement (Gibco) (Joshi et al. 2021b).*

2.10 | Binding and phagocytosis assays

oAβ variants prepared as described in method-2 (Section 2.3) were incubated with primary microglia from WT or TREM2^{T66M} transgenic mice. Cells were incubated with 1 µM of Aβ oligomers in DMEM GlutaMAX™ at 37°C and 5% CO_2 for 2 h before they were fixed, permeabilized and stained. Coverslips were mounted on glass slides and observed using a VisiScope CSU-W1 spinning disk confocal microscope. As a control, cells were also pretreated with DMSO at a final concentration of less than 0.01% and 10 µM Cytochalasin D (CytoD) dissolved in DMSO, keeping the final concentration of DMSO less than 0.01% for 30 min to block actin polymerization and thereby macropinocytosis before changing to the assay conditions described before (Kim et al., 2017; Xiang et al., 2016).*

To assess the binding of oAβ variants prepared as described in method-2 (Section 2.3, primary microglia from WT and TREM2^{T66M} transgenic mice seeded as described above were treated with 1 µM of oAβ in DMEM GlutaMAX™ and incubated on ice for 2 h followed by fixation and staining. To assess the uptake of bound Aβ, primary microglia were first incubated with 1 µM

*Italicized text is taken from the manuscript published in GLIA by Joshi et al. 2021

of oAβ in DMEM GlutaMAX™ on ice for 2 h. After this, the cells were washed and further incubated at 37°C and 5% CO_2 for 2 h. The cells were then fixed, permeabilized and stained[*]*(Joshi et al. 2021b).*

2.11 | TREM2 ectodomain purification

2.11.1 | sTREM2 for the dot blot experiments

The sTREM2 constructs were made as described above in section 2.7.2 (Ibach et al. 2021; Joshi et al. 2021b). The culture of cells for the transfection for the generation of a stable cell line was described previously in sections 2.9.3 and. *For the dot blot assay, cell supernatant from three 15 cm dishes of HEK293 Flp-In control or sTREM2-WT expressing HEK293 Flp-In cells was collected after 24 h of incubation. A saturated solution of ammonium sulphate (AS) was made (3.9 M at 0°C) and the total protein was precipitated with 40% AS solution. Because the addition of AS acidifies the solution, a 1 M Tris–HCl buffer (pH 8.0) was added to the supernatant so that the final concentration was 50 mM (Burgess 2009; Wingfield 2001). The mixture is gently mixed and incubated for 1 h on ice and then centrifuged for 30 min at 4°C at 16,000 rcf. The supernatant was discarded and the pellet was resuspended in 5 ml of 1X PBS and this solution was used for dot blot assay (Figure 2.1a)* [*] *(Joshi et al. 2021b).*

2.11.2 | sTREM2 ectodomain for BLI studies

The sTREM2 ectodomain (Figure 2.1b) was kindly provided by Prof. Dr Peter St George-Hyslop and is described in (Joshi et al. 2021b).

2.11.3 | sTREM2-Fc and Fc for Pulldown experiments

The sTREM2-Fc1 vector was generated by inserting the human sTREM2 (aa1-aa157) sequence into the pFUSE-hIgG1-Fc1 expression vector. Expression of the Fc-fusion proteins was done following the protocol described by (Fang et al. 2017)[*]*. Briefly one day before transfection, cells were seeded at 1.5 million viable cells per millilitre (mvc/ml) in a fresh medium. The next day, cells were transfected at 3 mvc/ml in half of the final volume with a 1 mg/ml linear 40kDa PEI Max solution (Polysciences, #24765-1) and the respective DNA (1µg/ml) in a 6:1 ratio. The efficiency of transfection was further increased by the addition of 0.1% Pluronic® F-68 (Thermo Fisher Scientific, #24040032). After 24h the transfection mix was diluted with fresh medium 1:1 and supplemented with 0.5 M valproic acid (Sigma Aldrich, #VPA P4543,) at a final concentration of 3.5 mM. The desired protein was collected after 4-5 days. Following centrifugation, filtration and pH adjustment the medium was loaded on a HiTrap™ Protein G HP 1 ml column and affinity-purified via FPLC. Eluted fractions were neutralized by the addition of 1 M Tris (pH 9.0). Concentration and buffer exchange against PBS was performed by*[*]

[*] *Italicized text is taken from the manuscript published in GLIA by Joshi et al. 2021*

ultrafiltration with a 10 kDa MWCO column (Sartorius, Germany). The concentration of the purified proteins was determined by a spectrophotometer measuring the absorbance at 280nm (Figure 2.1c)[*] (Joshi et al. 2021b).

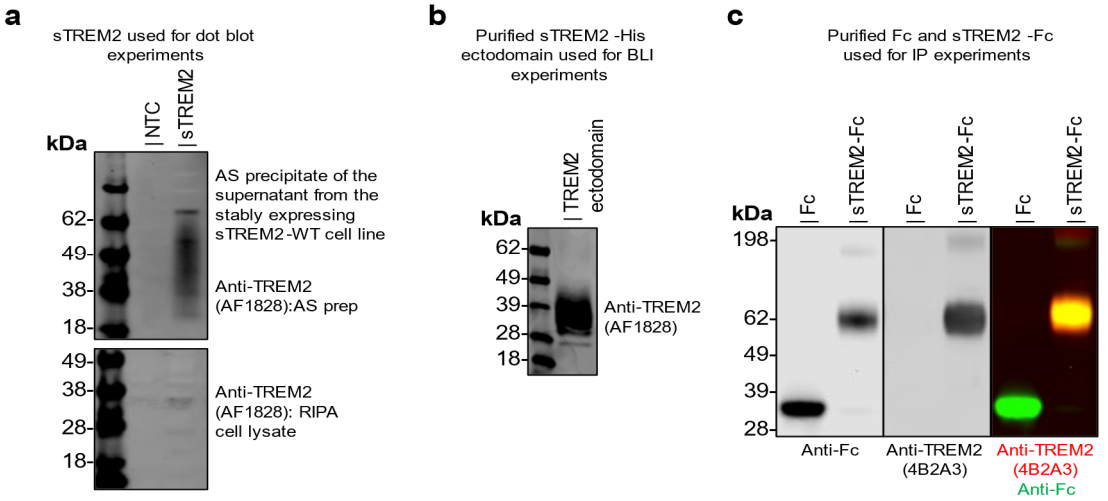

Figure 2.1 | Purified sTREM2 for various binding experiments

(a) Immunoblot of sTREM2 obtained from ammonium sulphate (AS) precipitated supernatant of single-cell clones of the sTREM2 Flp-In stable cell line detected with AF1828 antibody. **(b)** Immunoblot of TREM2 ectodomain detected with AF1828 antibody. **(c)** Immunoblot of purified Fc and sTREM2-Fc detected using anti-Fc and anti-TREM2 (in-house:4B2A3) antibody. *(Experiments were performed by Pranav Joshi and are now published as a part of (Joshi et al. 2021b), CC BY © 2021 Joshi et al.*

2.12 | Protein biochemical techniques

2.12.1 | Subcellular fractionation

For separation of cytosolic, membranous and nuclear fractions, transfected HEK293 cells (24h after post-transfection) were washed three times with ice-cold PBS, harvested in 300-500 µl hypotonic buffer D containing 1x protease inhibitor and 1 mM Dithiothreitol (DTT), and incubated for 15 min on ice (Ibach et al. 2021). Subsequently, cells were homogenized by passing the suspension through a cannula (0.6 mm) and a syringe (1 ml) 20 times. Cell homogenates were centrifuged for 10 min at 2000g at 4°C. Supernatants were transferred to new 1.5 ml reaction tubes, and pellets considered as nuclear fractions were stored at -20°C. Supernatants were centrifuged for 60 min at 4°C at 13,000 rpm (Eppendorf), and resulting supernatants (cytosolic fractions) were transferred to 1.5 ml reaction tubes, and likewise stored at -20°C. Further followed by resuspension of pellets (membrane fraction) in an appropriate volume of STEN lysis buffer; lysed for 10 min on ice, and centrifuged for 15 min at 4°C at 13,000 rpm (Eppendorf). The resulting supernatants (membrane fractions) were transferred to new 1.5 ml reaction tubes and the final protein concentration was determined using Pierce™ BCA Protein Assay kit (Thermo Fisher Scientific) according to the user's manual.

[*] *Italicized text is taken from the manuscript published in GLIA by Joshi et al. 2021*

2.12.2 | Extractions of proteins from mouse brains

Snap-frozen brain hemispheres were extracted as previously described (Heneka et al. 2013; Venegas et al. 2017b). *Briefly, hemispheres were homogenized and extracted in RIPA buffer (Section 2.1.3). Homogenates were centrifuged at 100,000g for 30 min and the pellet containing insoluble Aβ was solubilized in 2% SDS, 25 mM Tris-HCl, pH 7.5. The final protein concentration was determined using Pierce™ BCA protein assay kit (Thermo Fisher Scientific) according to the user's manual*[*]*(Joshi et al. 2021a).*

2.12.3 | Extractions of proteins from cultured cells

The cell lysates were prepared by using RIPA buffer for which the cells were grown on 60 mm or 100 mm dishes were washed three times with ice-cold PBS, centrifuged for 5 min at 4°C at 3,000 rpm and the resulting pellets were resuspended in an appropriate volume of RIPA buffer, and lysed for 20 min on ice. Subsequently, samples were transferred to new 1.5 ml reaction tubes and centrifuged for 10 min at 4°C at 13,000 rpm (Eppendorf). The resulting supernatants were transferred to new 1.5 ml reaction tubes, whereas pellets were discarded.

2.13 | Protein precipitation methods

2.13.1 | Acetone precipitation

For the selection of sTREM2 stable single-cell clones, the supernatant collected from each of the single-cell clones were precipitated using acetone. For this, the supernatant was collected in an acetone-compatible tube from each single cell clone followed by the addition of chilled acetone (-20°C) at a ratio of 1:4 (supernatant: acetone). The tubes containing the mixture were gently mixed and incubated for 60 min or overnight at -20°C. The samples were then centrifuged for 10 min at 4°C at 13,000 rpm. The supernatant was decanted without dislodging the protein pellet. The acetone was allowed to evaporate from the uncapped tube for 30 min at RT. An appropriate volume of STEN lysis buffer was added for the downstream process and vortexed thoroughly to dissolve the protein pellet.

2.13.2 | Ammonium sulphate (AS) precipitation

For interaction studies using the dot blot method, a saturated solution of ammonium sulphate (AS) was made (3.9 M at 0°C) and the total protein was precipitated with 40% AS solution. Because the addition of AS acidifies the solution, 1 M Tris-HCl buffer (pH 8.0) was added to the supernatant so that the final concentration was 50 mM (Wingfield 2001; Burgess 2009; Joshi et al. 2021b). The mixture is gently mixed and incubated for 1 h on ice and then centrifuged for 30 min at 4°C at 16,000 rcf. The supernatant was discarded and the pellet was resuspended in 5 ml of 1X PBS and this solution was used for dot blot assay[*] *(Joshi et al. 2021b).*

[*] *Italicized text is taken from the manuscript published in Acta neuropathologica communications by Joshi et al. 2021*
[*] *Italicized text is taken from the manuscript published in GLIA by Joshi et al. 2021*

2.13.3 | Trichloroacetic acid (TCA) precipitation

In addition to the acetone precipitation method, the TCA method was also followed to further assess the sTREM2 stable single-cell clones. For this up to 1 ml of supernatant were mixed with sodium deoxycholate to a final concentration of 0.02% and incubated for 15 min at RT. Samples were gently mixed following the addition of TCA (final concentration of 10%), then incubated for at least 60 min on ice, and precipitated proteins were collected by centrifugation for 10 min at 4°C at 13,200 rpm (Eppendorf). After aspiration of the supernatants, 700 µl of ice-cold acetone was added and samples were incubated for 15 min on ice. Subsequently, samples were centrifuged for 10 min at 4°C at 13,200 rpm (Eppendorf) and acetone was aspirated. Washing with acetone was repeated and pellets were dried for 1 h at 37°C in an incubator. Then, pellets were dissolved in of Tris-SDS buffer. NuPAGE LDS sample buffer with DTT was added to the samples and incubated for 10 min at 70°C in a block heater. Samples were analyzed by the SDS-PAGE system followed by immunoblotting and the remaining aliquot was stored at -20°C.

2.14 | Measurement of protein concentration

Bicinchoninic acid (BCA) Assay: Protein concentration was measured by using the Pierce™ BCA protein assay kit (Thermo Fisher Scientific) according to the user's manual. 10 µL of samples were pipetted in a 96-well plate and a 200 µL of working reagent mix from the kit was added. The 96-well plate was gently shaken for 30 s and incubated at 37°C for 30 min. The plate was cooled down to RT and absorbance was photometrically measured at 562 nm by the InfiniteM200 PRO plate reader (Tecan). A standard curve was generated by the measurement of different known BSA concentrations. Sample protein concentrations were calculated based on the standard curve. Samples were adjusted to similar protein concentrations and either used directly or stored at -80°C.

2.15 | Western blotting (WB)

2.15.1 | Sodium dodecyl sulfate-polyacrylamide gel electrophoresis (SDS-PAGE)

Separation of proteins according to their molecular weight was performed with the Novex Midi Gel SDS-PAGE system. NuPAGE Novex 4 to 12% Bis-Tris Mini/Midi protein gels allowing for separation of proteins with very different molecular weights were used with the XCell4 Sure-Lock Mini/Midi Cell for electrophoresis. SeeBlue™ prestained protein standard (Thermo Fisher Scientific, #LC5625) served as an estimate of protein sizes. A constant voltage of 150 V was applied for electrophoresis for 60 min in NuPAGE MES-SDS running buffer. Subsequently, proteins were electro-transferred to NC membranes by the wet transfer method. For this, 0.45 µm nitrocellulose (NC) membrane was arranged between soaked filter papers (GE Healthcare) in a blotting cassette. The blotting cassette was put into the blotting apparatus filled with

blotting buffer (30 mM Tris, 48 mM Glycine, 10% Methanol, pH 9.0) and transferred at 300 V and 400 mA for 2 h.

2.15.2 | Native-PAGE

The samples were prepared as described above in a Native Sample buffer and loaded on NativePAGE™ 4-16% Bis-Tris protein gels and separated using Novex ™ Tris-Glycine running anode and cathode buffers respectively, for 90 min at 150 V and 300 mA. The separated proteins were transferred onto a preactivated polyvinylidene difluoride (PVDF) membrane.

For immunodetection of proteins, membranes were blocked for 1 h in 5% nonfat dry milk in TBST (Tween 20-0.1%), then incubated with the primary antibodies in TBST overnight at 4 °C, followed by three washing steps for 10 min with TBST, and addition of appropriate secondary antibodies (conjugated to IRDyes or HRP) in TBST. After an incubation period of 60 min at RT, membranes were washed three times for 10 min with TBST, and once for 5 min with TBS. For signal detection, the enhanced chemiluminescence ECL imager (Bio-Rad laboratories) or Odyssey CLx™ (LI-COR, Biosciences) were used. The quantification was done by using Image Studio-Lite (Ver. 5.2)[*] (Joshi et al. 2021a; Joshi et al. 2021b). Primary and secondary antibodies are summarized in Table 2.5.

2.16 | Immunochemical staining techniques

2.16.1 | Immunocytochemistry (ICC)

For surface TREM2 staining- The cells were seeded at a density of $0.4x10^6$ cells on a poly-l-lysine coated coverslip in 6 well dish. The cells were then deprived of antibiotics for 24 h to remove the antibiotics from the medium. The cells were washed twice with warm with $DMEM^{-/-}$ media. The dishes were then kept on ice and the cells were incubated for 1 h with 4B2A3 antibody in $DMEM^{-/-}$ media. This was followed by washing three times and incubating with secondary antibody diluted in DPBS for 1 h on ice. Cells were washed three times with $DMEM^{-/-}$ media and twice with DPBS. Cells were fixed with 4 % PFA for 20 min and then washed three times with PBS before mounting on microscopic slides using Immu-Mount (Thermo Fisher Scientific).

For detection of intracellular proteins- The 4% PFA fixed cells were washed three times with PBS and incubated with 0.25 % Triton X-100 solution for 2 min at RT for permeabilization of the cellular membrane. The cells were incubated for 1 h with 2.5 % BSA in 0.125 % Triton X-100 followed by incubation for 1 h at RT with primary antibodies (Table 2.5) in 0.125 % BSA in 0.1 % Tween-20 in a humidified chamber. The cells were washed three times with 0.1 % Tween-20 solution followed by 1 h incubation at RT with DAPI and the appropriate secondary

[*] *Italicized text is taken from the manuscript published in Acta neuropathologica communications by Joshi et al. 2021*

antibody conjugated with fluorophores (Table 2.5). Cells were washed three times with 0.1 % Tween-20 solution, followed by two wash steps with PBS and shortly dipped in distilled water before mounting on microscopic slides using Immu-Mount.

2.16.2 | Immunocytochemistry (ICC) of primary microglia

For ICC of primary microglia- Cells were fixed for 15 min in 4% paraformaldehyde (PFA) before permeabilization with 0.1% Triton-X100 (PBS) for 5 min. After blocking with 3% BSA in PBS-T, 100 µl of primary antibody in 1% BSA was added to each coverslip and incubated at RT for 1 h. Coverslips were subsequently washed three times with 0.5% BSA in PBS-T. Afterwards, respective secondary antibodies in 1% BSA solution were added and coverslips were incubated for 1 h at RT in the dark, followed by another three washing steps. Finally, the coverslips were mounted on a microscopy slide using VECTASHIELD® antifade mounting medium with DAPI (Vector lab, #H-1200)[*] (Joshi et al. 2021b).

2.16.3 | Immunohistochemistry of mouse brains

Mouse brains were processed as described previously (Joshi et al. 2021b; Kumar et al. 2020a; Parhizkar et al. 2019). In brief, 20-25 µm sections were sequentially collected in Phosphate-buffered saline (PBS), placed on charged slides, and stained. For IF staining, Reveal Decloaker (Biocare Medical, #RV1000) was used for antigen retrieval at 95 °C for 30 min[*].

For X-34 staining (if required), just after the antigen retrieval step, sections were treated with 100µM of X-34 prepared in 60% PBS/40% EtOH mix; pH was adjusted with 1 N NaOH for 10 min at RT followed by washing steps with 60% PBS/40% EtOH. After this, the sections were washed with PBS and subjected to permeabilization with 0.25% Triton X-100 for 20 min before blocking for 2 h in 5% NHS and 3% BSA prepared in 1xPBST (Triton X100-0.2%). *Mouse on Mouse Blocking Reagent (Vector laboratories, #MKB-2213) was used for primary antibodies generated in mice or rats at a dilution of 1 drop/1000 µl. Primary antibodies were diluted in 3%NHS and 1.5% BSA prepared in 1xPBST (Tween 20-0.1%), added on sections and incubated at 4°C overnight. For TREM2 staining, sections were incubated in the primary antibody at 4 °C for 48 h. After washing steps, appropriate secondary antibodies diluted in 3% NHS and 1.5% BSA prepared in 1xPBST (Tween 20-0.1%) were added to the sections and incubated for 1 h at RT. The sections were then washed and mounted with VECTASHIELD® Hardset™ antifade mounting medium (Vector laboratories, #H-1400) or VECTASHIELD® antifade mounting medium with DAPI (Vector laboratories, #H-1200)[*](Joshi et al. 2021a).* Primary and secondary antibodies are summarized in Table 2.5.

[*] *Italicized text is taken from the manuscript published in GLIA by Joshi et al. 2021*

2.16.4 | Immunohistochemistry (IHC) on human post-mortem brain tissue

IHC on human post-mortem brain tissue was done as described in (Parhizkar et al. 2019). In brief, 5µm temporal neocortex sections were mounted on slides, deparaffinized and rehydrated in a series of xylene and graded ethanol. The sections were subjected to citric acid antigen retrieval (1M sodium citrate in PBS, pH 6.0) and boiled in a microwave for 20 min. After cooling, endogenous peroxidase activity was quenched using 30% hydrogen peroxide for 20 min. Sections were blocked and incubated with primary antibody (Table 2.5) overnight at 4°C. Primary antibodies were detected with biotinylated anti-mouse and anti-rabbit IgG secondary antibodies and visualized with avidin-biotin-complex (ABC-Kit, Vector laboratories) followed by development with diaminobenzidine-HCl (DAB, Vector laboratories) for 5 min. Lastly, sections were counterstained with haematoxylin. Stainings were performed in serially cut sections to compare the same region of interest through all immunostainings. Brightfield images were taken with Axio Scan.Z1 (Carl Zeiss MicroImaging GmbH, Germany)[*] (Joshi et al. 2021a).

2.16.5 | Data analysis of Aβ deposits in mouse and human brain

Initial optimization of antibodies was carried out for the detection of the different Aβ species as reported previously (Kumar et al. 2013; Kumar et al. 2016; Joshi et al. 2021b). Quantification for mouse tissue was excluded if tissue folds were present or the quality of the staining was poor. To represent and quantify plaque densities (number and size distribution) from three sections/mouse brains regions, the somatosensory cortex (SSC), the retrosplenial cortex (RSC), and the dentate gyrus (DG) (Figure 2.2a), acquired images were imported into Fiji software and data channels were separated (image/colour/split channels). All layers from a single image stack were projected on a single slice (stack/Z-projection) to test the feasibility of quantifying the area and number of plaques[*](Figure 2.2b).

[*] *Italicized text is taken from the manuscript published in Acta neuropathologica communications by Joshi et al. 2021*

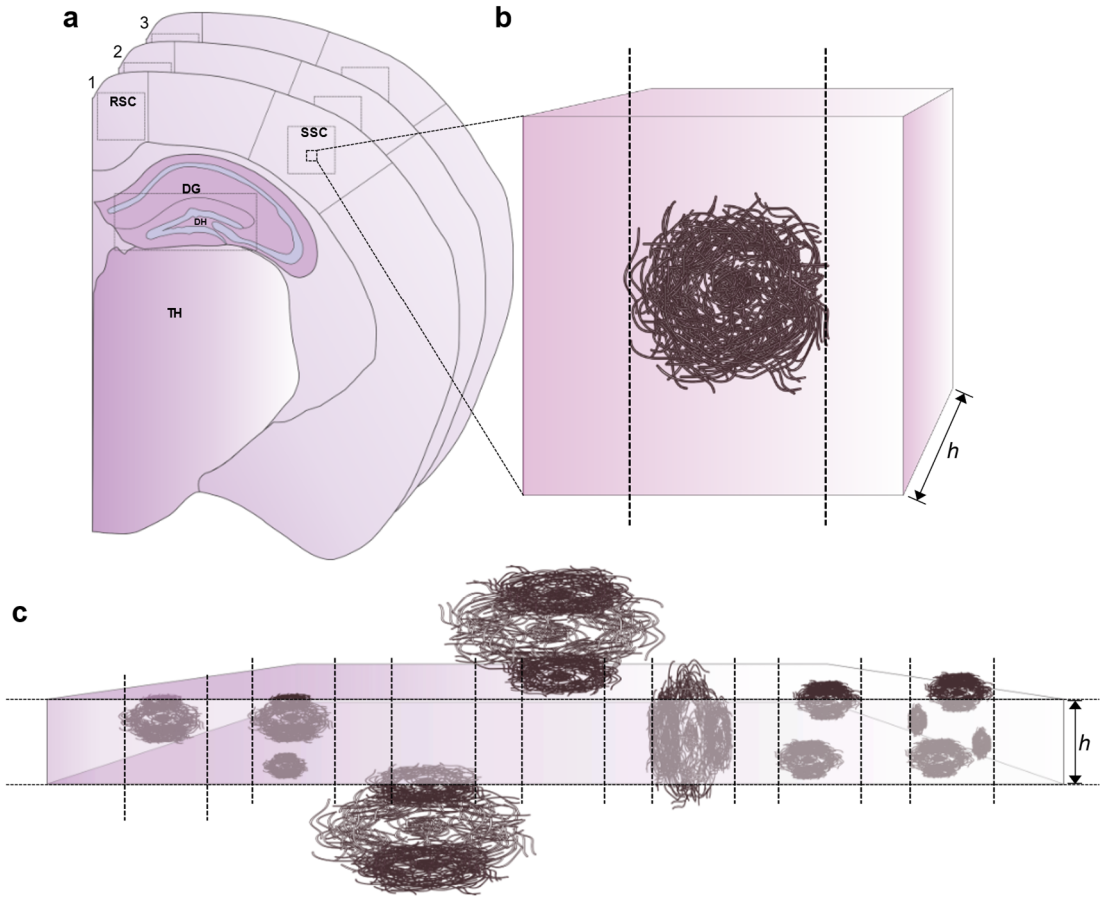

Figure 2.2 | Visualization and approach of analysis of area and number of Aβ plaques

(a) Showing different regions, RSC, SSC and DG regions in the coronal section of AD transgenic mouse brain analyzed in this study. For analysis of the area and number of Aβ plaques, three sections were used as depicted. **(b)** Showing the magnified region of interest (ROI) with Aβ plaque in a 3D view with a perspective. **(c)** Showing area and the number of hypothetical Aβ plaque from **"b"** embedded in the brain section of thickness "h" µm at a different visualizing plane. The Aβ plaque represented in **"b"** could be single, larger (outside the thickness), or multiple in the same region of interest hence the plaques and their quantified combined area in this study constitute the "lower boundary" of the plaque number volume density (Joshi et al. 2021a).

The plaques were then segmented and quantified in Fiji using automatic thresholding methods. Due to the thickness of brain sections and the limited penetration of antibodies to plaques through the mounted sections, lightly embedded stained plaques may or may not be detected depending on image adjustment values (Figure 2.2c). Therefore, the plaques and their quantified combined area in this study constitute the "lower boundary" of the plaque number volume density[*]*(Joshi et al. 2021a).*

[*] *Italicized text is taken from the manuscript published in Acta neuropathologica communications by Joshi et al. 2021*

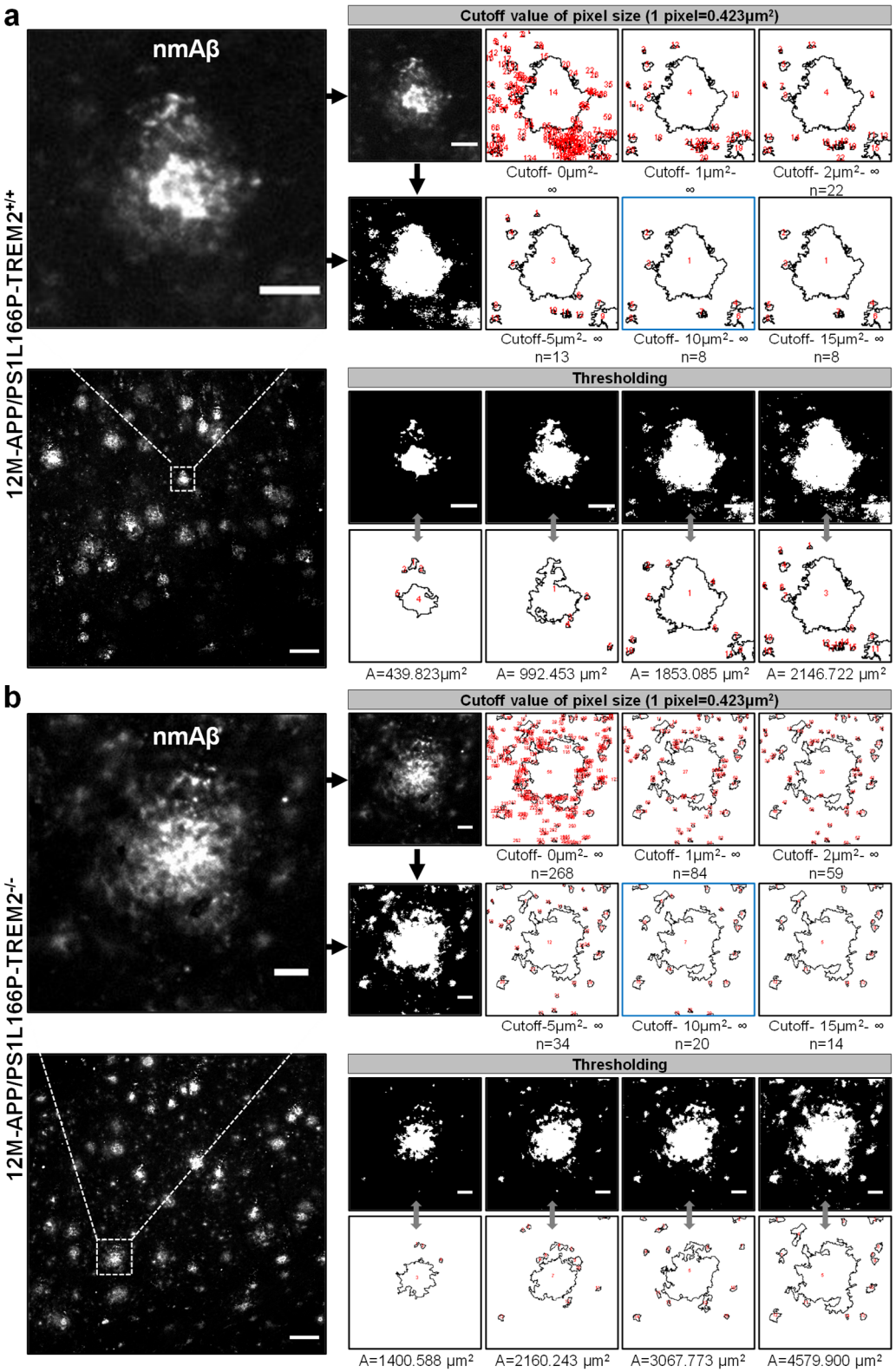

Figure 2.3 | Analysis of area and size of Aβ plaque in the transgenic mouse brains

(a-b) Representative images of SSC region of female 12M-APP/PS1L166P transgenic mouse brain with both TREM2 genotypes stained with 7H3D6 antibody. The cutoff value for the plaque size analysis determined the number of plaques hence default cutoff of 10μm^2 (blue box) was considered for the analysis. At this cutoff value, the number of plaques in TREM2$^{-/-}$ brains was significantly more as compared to TREM2$^{+/+}$ brains as shown in this study. Furthermore, the default thresholding also

determined the area of plaques. Hence, the same thresholding was set for both groups and analyses were carried out. It is also important to note that the area of plaque was significantly larger in TREM2 $^{-/-}$ mouse brains as compared to TREM2$^{+/+}$ mouse brains even at the lowest threshold (scale bar=200µm and 20µm for the magnified images) (Joshi et al. 2021a).

Furthermore, as demonstrated with digitalized plaques (SSC region stained with nmAβ as an example (Figure 2.3a-b), the number of plaques assessed using an image analysis method in a given brain region varied depending upon the cut-off value of pixel size and the thresholding of plaques. Initial analysis of optical images revealed that plaque-like images that were digitalized often displayed plaque-like artefacts. Therefore, plaques >10µm^2 were considered as the reliable "digital plaques". Adjustment of thresholding of certain digitalized plaques appeared to vary in the number of valuables due to irregularity in plaque shapes or depending upon the value of image distribution. It was found that the staining intensity cut-off had a significant impact on the number of plaques. Interestingly, TREM2 knockout mouse brain, showed large size plaques as well as an increased total number of plaques >10m^2 even at lower thresholding, confirming the validity of the analysis[*] (Joshi et al. 2021a).

For the quantification of plaque ratio of different Aβ species within plaques in the IF experiments, we considered 300 plaques/region/group (each for SSC and RSC) and 150 plaques/region/group (for DG) (so, SSC=60 plaques/mouse, RSC=60 plaques/mouse, DG=30 plaques/mouse) so making total of 750 plaques/group containing 5 animals or 450 plaques/group containing 3 animals (from at least 3 sections/animal). For this analysis, randomly selected plaques that were positive with all three antibodies detecting Aβ species/staining in 1000×1000µm ROI were analyzed by manually drawing a boundary around each plaque by using a freehand draw tool in Fiji and determining the IntDen (Condello et al. 2015) of total Aβ-immunoreactive area for each plaque stained with various antibodies specific to Aβ species within each section for all channels (Figure 2.4)[*](Joshi et al. 2021a).

The total number of neurons was manually counted in a 1000×1000µm area of SSC, in 2 independently stained sections and represented as a ratio of pSer8-Aβ positive neurons/total neurons[*] (Joshi et al. 2021a). For analysis of internalized pSer26-Aβ in the transgenic mouse brain, the number of plaque-associated microglia was manually counted in 500 × 500 µm areas of somatosensory cortex (SSC) on 1-2 independently stained sections and then represented as the ratio of pSer26-Aβ positive microglia/total Iba1 positive microglia (Joshi et al. 2021b). Similarly, the total number of neurons was manually counted in a 500 × 500 µm area of SSC, in 2 independently stained sections and represented as a ratio of pSer26-Aβ positive neurons/total neurons.

[*]*Italicized text is taken from the manuscript published in Acta neuropathologica communications by Joshi et al. 2021*

For quantification of microglial binding and uptake of Aβ, IntDen was calculated by manually drawing a border around randomly selected Aβ-positive microglia. Representation of ratio of Aβ positive microglia/total microglia was done by manually counting Aβ positive cells and automatically counting DAPI positive total cells for 10 images/experiment (5 images per coverslips and the experiments were in duplicates)[*] (Joshi et al. 2021b).

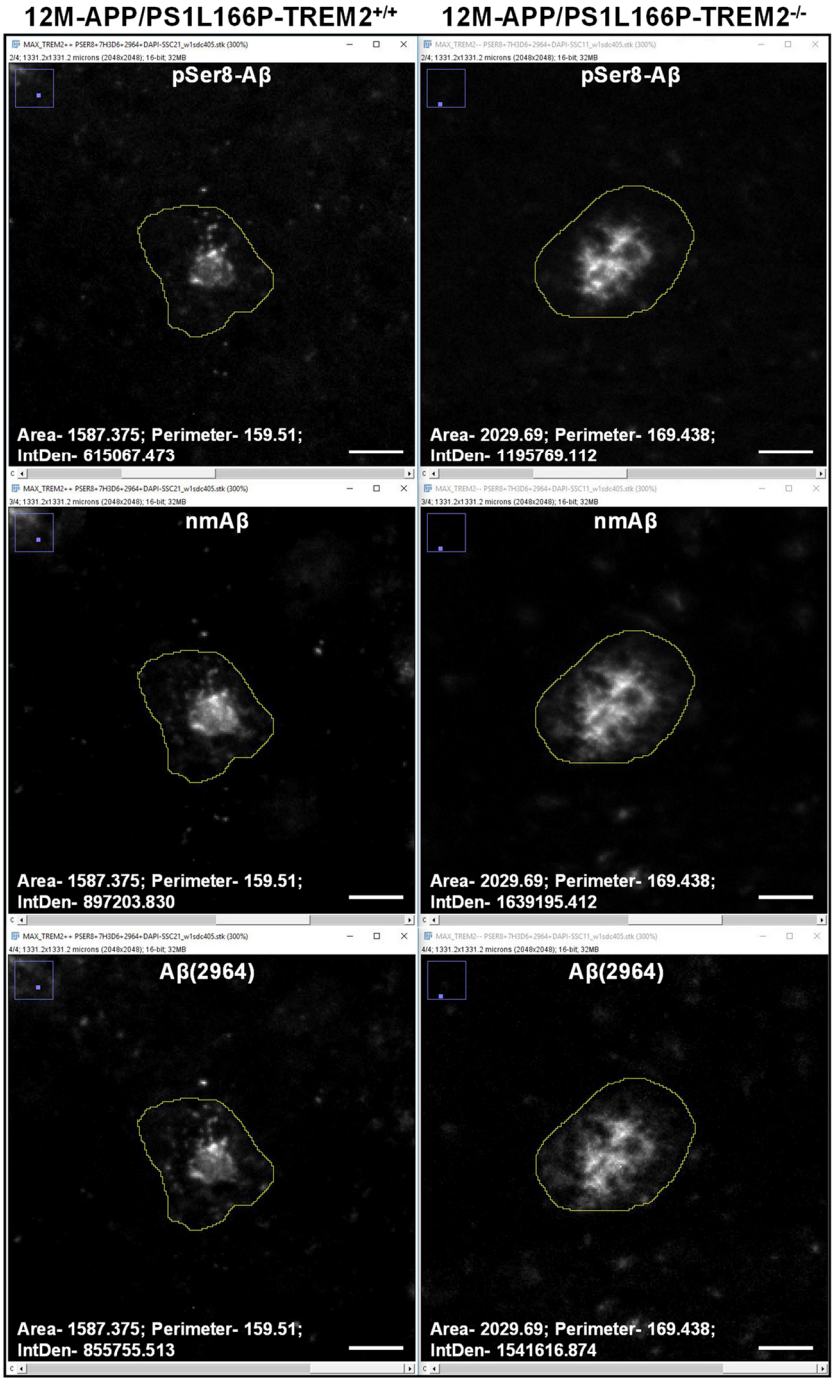

Figure 2.4 | Analysis of staining intensity of Aβ plaque stained with different antibodies
Representative three confocal channels of SSC region of female 12M-APP/PS1L166P transgenic mouse brain with both TREM2 genotypes stained with three different Aβ antibodies. For the analysis of the

[*] *Italicized text is taken from the manuscript published in Acta neuropathologica communications by Joshi et al. 2021*

staining intensity ratio for the two different antibody-stained plaques, a manual boundary surrounding the Aβ plaque (yellow colour shown above) was made with the "freehand selection" tool and the IntDen was measured keeping the same area for all three channels (scale bar=20µm) (Joshi et al. 2021a).

For the human brain data analysis, plaque densities of 4G8 and pSer8-Aβ stained plaques were manually quantified by randomly selecting, 10 cortical 2 × 2 mm regions of interest (ROIs) per case. ROIs were selected to allow the analysis of the same region for all four consecutive brain sections stained with different antibodies without interference by cuts, folds, or other irregularities. Also, the total number of plaques along with area measurements were considered for the analysis. The border around plaques was manually drawn by using the "spline contour" tool in the ZEN 3.2 software, for the area stained with different antibodies. With 4G8 antibody-stained sections, an area cut-off of 10 µm^2 was determined, while with pSer8-Aβ antibody-stained sections, an area cut-off of 30 µm^2 was determined, below which were considered as either artefacts or intracellular deposits (quantified separately). Case#3, with the highest fixation time, was omitted for the plaque count and size quantification as it was difficult to define boundaries of extracellular plaques stained with 1E4E11 (pSer8-Aβ) antibody. Aβ plaque load was calculated by summing the areas of all counted plaques divided by the total area of all ROIs. The intracellular deposits of nmAβ and phosphorylated Aβ were manually counted from 10 cortical consecutive 2 × 2 mm randomly selected ROIs per case[*] (Joshi et al. 2021a).*

2.17 | Microscopy

2.17.1 | Transmission Electron Microscopy

The characterization of Aβ preparations (monomers, section 2.3 and 2.17.1) and oligomers (prepared by method-1, section 2.3) by TEM was done as described by (Anderson et al. 2010). *Briefly, 5-10µL of Aβ (monomers and Oligomers) at a concentration of 1µM were placed onto a freshly glow-discharged (by Glow discharge cleaning system: PELCO easiGlow™ Glow Discharge System), carbon-coated formvar, copper grid-400 mesh (Electron microscopy sciences #CF400-CU). After 2 min, the sample solution was wicked off with filter paper, the grid rinsed with deionized water, and a 5µL of 2% (w/v) phosphotungstic acid stain (pH 7.0) was placed on the grid. After 1 min, the staining solution was wicked away and the grid air-dried. The negatively stained sample was then examined by using Talos L120C (Thermofischer scientific) at an acceleration voltage of 120 kV imaged with a 4k × 4K Ceta CMOS camera at 45,000x*[*] (Joshi et al. 2021b).* Representative images are shown in Figure 4.1a.

[*] *Italicized text is taken from the manuscript published in Acta neuropathologica communications by Joshi et al. 2021*
[*] *Italicized text is taken from the manuscript published in GLIA by Joshi et al. 2021*

2.17.2 | Confocal and bright field imaging

All ICC staining images for all cell culture experiments were acquired using the AxioVert microscope (Zeiss, Germany). ICC images for the cell culture experiments and all mouse brain *IF images were acquired using VisiScope CSU-W1 spinning disk confocal microscope and VisiView Software (Visitron Systems GmbH, Germany). Laser and detector settings were maintained constant for the acquisition of each immunostaining. All stainings were repeated at least three times to ensure reproducibility in the staining protocol. Images were acquired at 10×, 20×, 40×W or 63×W (W-water immersion) objective at 2048 × 2048 pixels, with a z-step size of 1 µm (for 10×, 20×, 40×W, 63×W images) or 4-5 µm (for 10× montage image). Human brain immunostaining data were acquired by Axio Scan.Z1 at Plan-Apochromat 20x/0.8M27 objective imaged by Hitachi HV-F202SCL with ZEN 3.2 software (Carl Zeiss MicroImaging GmbH, Germany)[*] (Joshi et al. 2021a; Joshi et al. 2021b).* High-resolution stacks imaged by confocal microscopy were 3D reconstructed using IMARIS 9.0.2 (Bitplane) software. FIJI (ImageJ) or ZEN 3.2 software was used for all immunohistochemical analyses.

2.18 | TREM2-Aβ Interaction studies

2.18.1 | Dot blot assay

Aβ binding assay: *Monomer- and oligomer-rich fractions of Aϐ (Section 2.3and Figure 4.1c) were spotted on nitrocellulose (NC) membranes, and the membranes were allowed to dry. The NC membranes were then incubated with AS precipitated cell supernatant overnight at 4°C. The membranes were washed with TBS-T (Tween 20-0.1%) (3 × 5 min) and then blocked with Odyssey blocking buffer (LI-COR Bioscience) for 1.5 h at RT. The membranes were then incubated overnight in primary antibody (monoclonal antibody 4B2A3 for detection of TREM2) at 4°C. The NC membranes were then washed with TBS-T (Tween 20-0.1%) (3 × 5 min) and incubated with LI-COR fluorescent secondary antibody for 1 h at RT, washed with TBS-T (3 × 5 min), then once with TBS (5 min) and imaged with Odyssey® CLx (LI-COR Biosciences). To detect Aϐ on the same membranes after detection of bound TREM2, the dot blots were washed with TBS-T (3 × 5 min) followed by incubation with 4G8 antibody overnight to detect Aϐ variants. The NC membranes were washed with TBS-T (3 × 5 min) and incubated with LI-COR fluorescent secondary antibody for 1 h at RT, washed with TBS-T (3 × 5 min), then once with TBS (5 min) and developed with LI-COR Odyssey® CLx (LI-COR Biosciences)[*](Joshi et al. 2021b).*

2.18.2 | Biolayer Interferometry (BLI) studies

Bio-layer Interferometry (BLI) is a label-free technology for measuring biomolecular interactions (Muller-Esparza et al. 2020). BLI measures the interference pattern of white light that is reflected from a layer of biomolecules immobilized on the surface of a sensor tip (bio-

[*] *Italicized text is taken from the manuscript published in GLIA by Joshi et al. 2021*

layers) in real-time and in solution (Muller-Esparza et al. 2020) (Figure 2.5). BLI experiments were carried out using Octet RED384 (Forte Bio) using either Streptavidin (SA)-coated biosensor and/or Aminopropylsilane (APS) biosensors. The interpretations of kinetic binding data are based on a mathematical model of the interaction, from which kinetic and equilibrium binding constants can be calculated based on rates of association and dissociation. Kinetic data were analysed using Octet data Analysis software and processed by Savitsky-Golay filtering specifying methods for reference subtraction, y-axis alignment, and inter-step correction. The data was then analyzed by specifying steps to analyze, selecting the curve fit model, fitting method (local or global) and window of interest (Tobias R et al. 2017).

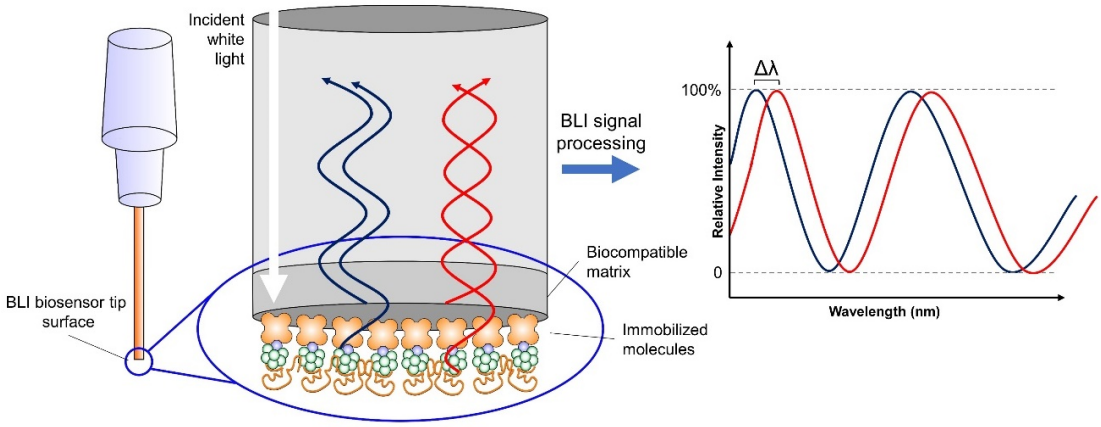

Figure 2.5 | Principle of Bio-layer interferometry

BLI is an analytical technique that analyzes the interference pattern of white light reflected from two surfaces. Changes in the number of molecules bound to the biosensor cause a shift in the interference pattern that is measured in real-time. *(Figure is created by Pranav Joshi by referring to the forte bio website as well as (Nirschl et al. 2011; Muller-Esparza et al. 2020; Tobias R et al. 2017))*

For BLI studies with TREM2 ectodomain by using Octet RED384 (Forte Bio), 5% of Biotin-LC-Aβ(1-42) was used for mixing with Aβ variants compared with only Biotin-LC-Aβ(1-42) (unpublished data). Further, we optimized the concentration of already mixed oAβ to immobilize onto the biosensors. Initial experiments revealed that 5% of 1 µM Biotin-LC-Aβ mixed with 1 µM of oAβ when immobilized onto the streptavidin (SA) biosensors (Forte Bio #18-0009) showed a similar loading and binding as compared with 100%, 5% Biotin-LC-Aβ[*] (Figure 2.6a-b) and hence the same concentration of mixed Aβ variants was used in this study. In addition to this, we also checked the differential loading of oAβ onto the SA biosensors in which oAβ(1-42)pSer26 showed higher loading as compared with other variants (Figure 2.6c)[*] (Joshi et al. 2021b).

[*] *Italicized text is taken from the manuscript published in GLIA by Joshi et al. 2021*

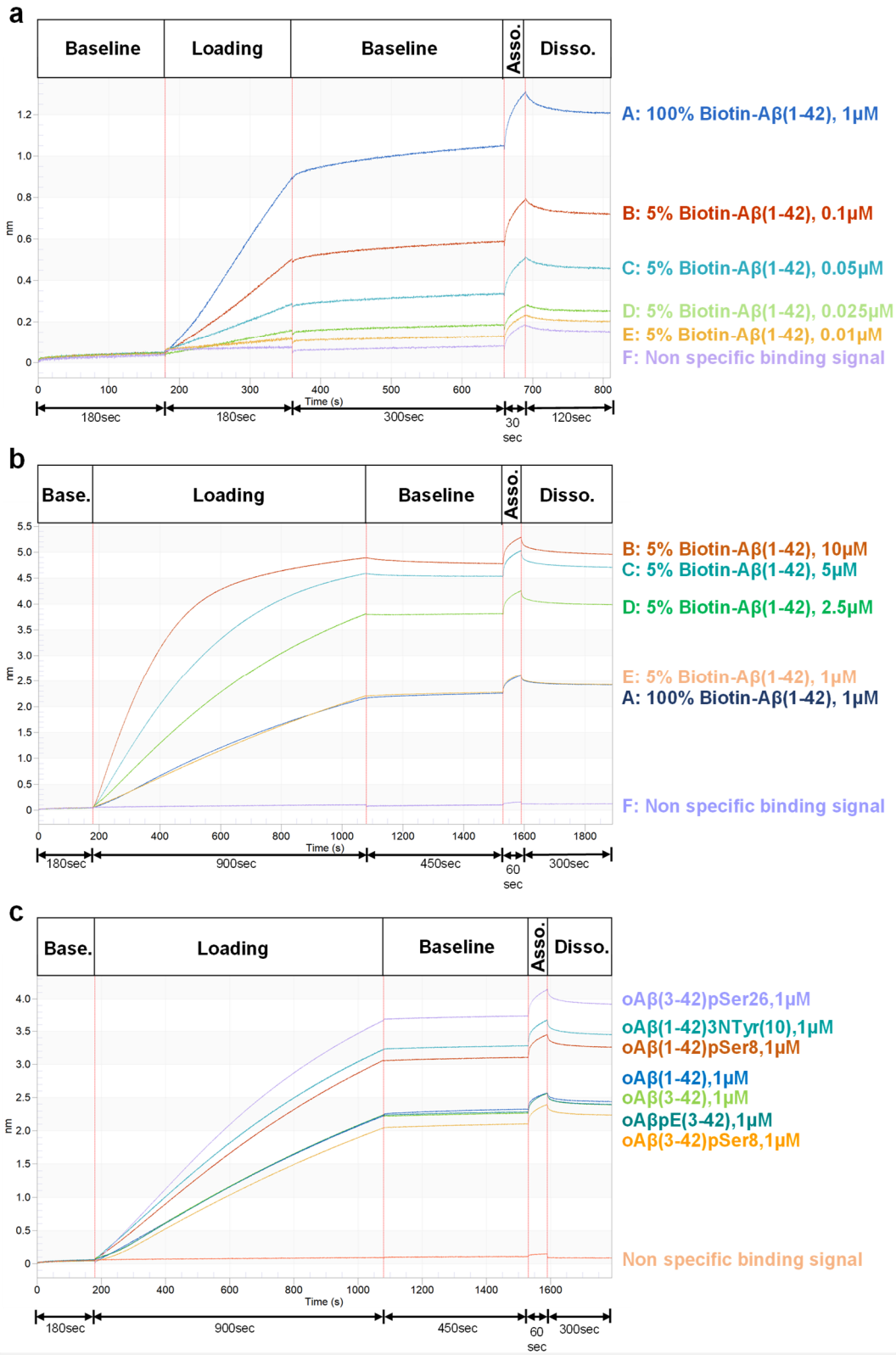

Figure 2.6 | Optimization of BLI experiments with varying concentrations of Aβ peptides

(a-b) Showing BLI association/dissociation of 2μM TREM2 ectodomain with different concentrations of 5% Biotin-Aβ mixed with Aβ (1-42) variants from 0.01μM to 10μM. We found that 1μM 5% Biotin-Aβ mixed with Aβ (1-42) showed a similar association/dissociation curve as compared to 1μM of 100% Biotin-Aβ. **(c)** Showing differential loading of 5% Biotin-Aβ mixed with modified Aβ variants followed by association/dissociation of 2μM TREM2 ectodomain (Joshi et al. 2021b).

Kinetic assay of TREM2 ectodomain binding with oAβ.

For BLI kinetic measurements, Streptavidin (SA) biosensors were hydrated with 220 µl assay buffer (20 mM HEPES, 500 mM NaCl, 0.1% BSA, 0.02% Tween 20 (pH 7.4) for 30 min (96 well plate). Further, biosensors were exposed to 220 µl buffer to determine the initial baseline. The biosensors were exposed to oligomer-rich preparations obtained from mixtures of the respective Aβ variants and Biotin-LC-Aβ in a 20:1 ratio. Biosensors were then exposed to 220 µl of assay buffer for 450 s for another baseline measurement. The biosensors were exposed to 220 µl assay buffer containing TREM2 ectodomain at different concentrations (1, 2, 5, and 10 µM) prepared in BLI assay buffer for 60 s to measure association. The biosensors were then exposed to 220 µl of assay buffer for 150 s to measure dissociation. The kinetic constants of BLI were obtained with four different concentrations of TREM2 ectodomain and data was aligned at the y-axis and smoothed by Savitzky–Golay filtering. Curves were processed by adjusting to the BLI control buffer, and curve fitting was performed using a 2:1 heterogenous ligand as a model due to the heterogenicity of Aβ. KD1 measures interaction that occupies the highest percentage of the binding surface area and KD2 characterizes the secondary interaction, determined mathematically by the Octet Data Analysis software[*] (Joshi et al. 2021b).

In another approach to carry out BLI studies with monomeric Aβ variants (1-40), monomeric Aβ was immobilised onto the biosensors by using Aminopropylsilane (APS) sensors (ForteBio, #18-0010). In this approach, the stock (230µM) Aβ (1-40) variants were centrifuged at 16,000g for 30 min at 4°C (Palhano et al. 2013; Li et al. 2018b) and then the supernatant was immediately collected on ice and then diluted with pre-cooled BLI assay buffer (20mM HEPES, 500mM NaCl, (pH 7.4)) to make the final concentration of 1µM for the BLI studies. For BLI measurements the APS sensors were hydrated with 220µL assay buffer (20mM HEPES, 500mM NaCl, (pH 7.4)) for 30 min (96 well plate). During this hydration period of the biosensors, the plate with Aβ (1-40) solution was prepared on ice for the BLI measurement to avoid any aggregation during this incubation time. The 96 well plate with Aβ (1-40) was placed inside the BLI machine to perform further steps wherein the biosensors were exposed to 220µl buffer containing 20mM HEPES, 500mM NaCl (pH 7.4) to get an initial baseline reading (60 s). The biosensors were exposed to mAβ (1-40) variants for 400 s, which the association curve of Aβ onto the biosensors. The biosensors are then exposed to 220 µl of assay buffer containing 20mM HEPES, 500mM NaCl, 0.1%BSA, 0.02% Tween 20 (pH 7.4) for 400 s for another baseline measurement. For binding/association curve, the biosensors were exposed to 220 µl assay buffer containing 2µM hTREM2 ectodomain prepared in BLI assay buffer for 300 s. The biosensors were then exposed to 220 µl of assay buffer for 150 s to obtain the dissociation

[*] *Italicized text is taken from the manuscript published in GLIA by Joshi et al. 2021*

curve/measurement. TREM2 binding response of 1 µM oAβ42 variants (without Biotin-LC-Aβ (1-42)) was also analysed with another approach by using APS biosensors. The experiment was carried out in triplicate and the average response value (in nm) was calculated to plot the graph.

2.18.3 | Immunoprecipitation (IP) of Aβ using sTREM2-Fc

For assessing differential binding of mAβ and oAβ variants to TREM2, 2 µg of sTREM2-Fc or hIgG1-Fc were pre-coupled to magnetic 50 µl of Protein G beads (SureBeads™, Bio-Rad) for 20 min at 23°C. The coupled beads were then further incubated with 2 µg of the oAβ preparation (prepared by Method-2) for 1 h at 23°C in PBS buffer containing 0.1% Tween-20 (PBS-T). After precipitation and subsequent thorough washing steps, the bound proteins were eluted from the beads by the addition of 20 mM glycine solution at pH 2.5. Finally, the eluate was neutralized with 1 M Tris-HCl pH 8 and boiled at 95°C in Laemmli buffer before being subjected to immunoblot analysis. For a quantitative assessment, this protocol was slightly altered by reducing beads (300 µg) and Aβ (1 µg) while increasing the amount of sTREM2-Fc and hIgG1-Fc to 10 µg to ensure complete saturation of the beads with recombinant protein[*] (Joshi et al. 2021b).

2.19 | Thioflavin T (ThT) aggregation assay

Aβ aggregation was monitored by fluorescence spectroscopy for which the concentration of 1 µM ThT and 5µM non-aggregated Aβ (Keskitalo et al. 2014) was used. To ensure a monomeric state of Aβ at the beginning of the aggregation assay, the freshly reconstituted Aβ solution was ultrasonicated for 5 min, centrifuged for 30 min at 16,000×g and added at the start of the measurement. Samples (100µL) were incubated at 37°C in 96-microwell plates that were sealed to prevent evaporation. ThT fluorescence intensity of each sample was recorded every 10 min using the InfiniteM200 PRO plate reader (Tecan, Switzerland) with 446/482nm excitation/emission filters respectively, with a slit width of 5 nm. After the ThT assay, select samples were separated by native PAGE followed by western immunodetection with A11 antibody or with 4G8 antibody (Figure 4.6).

2.20 | Statistics

Microsoft Excel was used to organize all data and calculate the averages of each repeated experiment. Graph Pad (Prism v8.0) was used to build graphs and perform statistical analyses. *Since the plaque area distribution showed a positively skewed distribution (Serrano-Pozo et al. 2012) and varied from the normal distribution confirmed by D'Agostino & Pearson and the Shapiro–Wilk normality test, we considered the non-parametric, Mann-Whitney test (which*

[*] *Italicized text is taken from the manuscript published in GLIA by Joshi et al. 2021*

*compares the distributions of ranks in two groups) and Kolmogorov–Smirnov test (which compares the cumulative distributions) for the frequency distribution of all values. Besides this, since the data were not formally tested, we assumed it followed Gaussian distribution and that the variance between groups was comparable (Parhizkar et al. 2019); thus, unless otherwise stated, a two-sided, unpaired t-test with Welch's correction was used to determine the statistical difference between groups in analyses requiring only single comparisons. The degree of significance between groups is represented as *p < 0.05, **p < 0.01, ***p < 0.001, ****p < 0.0001, and $^{ns}p > 0.05$[*](Joshi et al. 2021a).* In the statistical test requiring the comparison of two or more groups, two-way ANOVA (sidak multiple comparison test) was used.

[*] *Italicized text is taken from the manuscript published in Acta neuropathologica communications by Joshi et al. 2021*

Chapter 3 | Mutation specific effects of TREM2 variants on secretory transport and ER stress response

Brief introduction: TREM2 is proteolytically processed by ADAM proteases to generate a soluble ectodomain of TREM2 (sTREM2). This soluble form is found in both CSF as well as blood and has biological functions. Interestingly, studies on patients with early stages of AD onset showed a significantly increased level of sTREM2 in cerebrospinal fluid (CSF). Studies have also shown that sTREM2 can enhance microglial activation and survival associated with enhanced pro-inflammatory cytokine expression. TREM2 ectodomain FTD-associated mutations such as T66M result in altered processing and secretion of sTREM2 that can lead to an accumulation of immature TREM2 in the cytoplasm. The T66M mutation in TREM2 can impair trafficking of TREM2 from the ER to the Golgi and plasma membrane, resulting in accumulation in the ER. To investigate the potential role of sTREM2, compare sTREM2 with various mutations, and characterize ligand interactions, the Flp-In system was implemented to generate stable HEK 293 cell lines expressing sTREM2 as well as its disease-associated mutations (R47H and T66M). It is also demonstrated that accumulation of T66M mutant in the cells leads to increased levels of BiP/GRP78 and CHOP in response to the unfolded protein response (UPR) in the stable cells and plaque-associated microglia in transgenic mice brains.

3.1 | Generation of TREM2 expressing HEK293 Flp-In cell lines

The Flp-In system aims at the generation of constitutive mammalian expression cell lines by taking an advantage of an *S. Cerevisiae* derived DNA recombination system that uses recombinase (Flp) and site-specific recombination to integrate gene(s) of interest (GOI) into the genome of mammalian cells (Craig 1988; Sauer 1994; Buchholz et al. 1996).

The cDNA constructs encoding sTREM2 variants were generated by site-directed mutagenesis for inserting a stop codon at the amino acid 158 in place of serine (S-*) of the full-length TREM2 constructs (Figure 3.1). After confirmation by sequencing, these constructs were first transiently transfected in HEK293 cell lines to check the translation and overall subcellular localization as well as secretion of the respective sTREM2 variants.

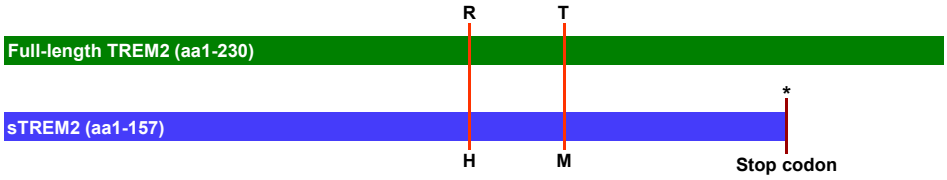

Figure 3.1 | Illustration of TREM2 and the cleaved sTREM2 fraction with different mutations

sTREM2 constructs were prepared by inserting a stop codon at 158 positions of full-length TREM2 in the pcDNA5^{TM}/FRT genomic integration vector. Similarly, a point mutation was inserted by using site-directed mutagenesis to produce the sTREM2-R47H and sTREM2-T66M mutants used in this study. *(The constructs were made by Pranav Joshi)*

An increase of sTREM2 was observed in the conditioned media collected from the cells transfected with the sTREM2 construct in comparison to the cells transfected with full-length TREM2, while sAPP secretion was unaltered (Figure 3.2a-e). Furthermore, decreased secretion and an increased accumulation in cellular membrane and vesicular fractions were observed in sTREM2-T66M mutants as compared to sTREM2-WT (Kleinberger et al. 2017; Ibach et al. 2021) (Figure 3.2b-f). The secreted sTREM2 in the culture medium was detected as a smear between 35-55kDa rather than as distinct bands due to the complex N-glycosylation within the TREM2 ectodomain (Ibach et al. 2021; Kleinberger et al. 2014; Park et al. 2015). It was reported that deglycosylation of the conditioned media collected from full-length TREM2 construct transfected cells resulted in the disappearance of the diffuse smear and formation of a distinct 17 kDa band, representing deglycosylated TREM2 (Ibach et al. 2021).

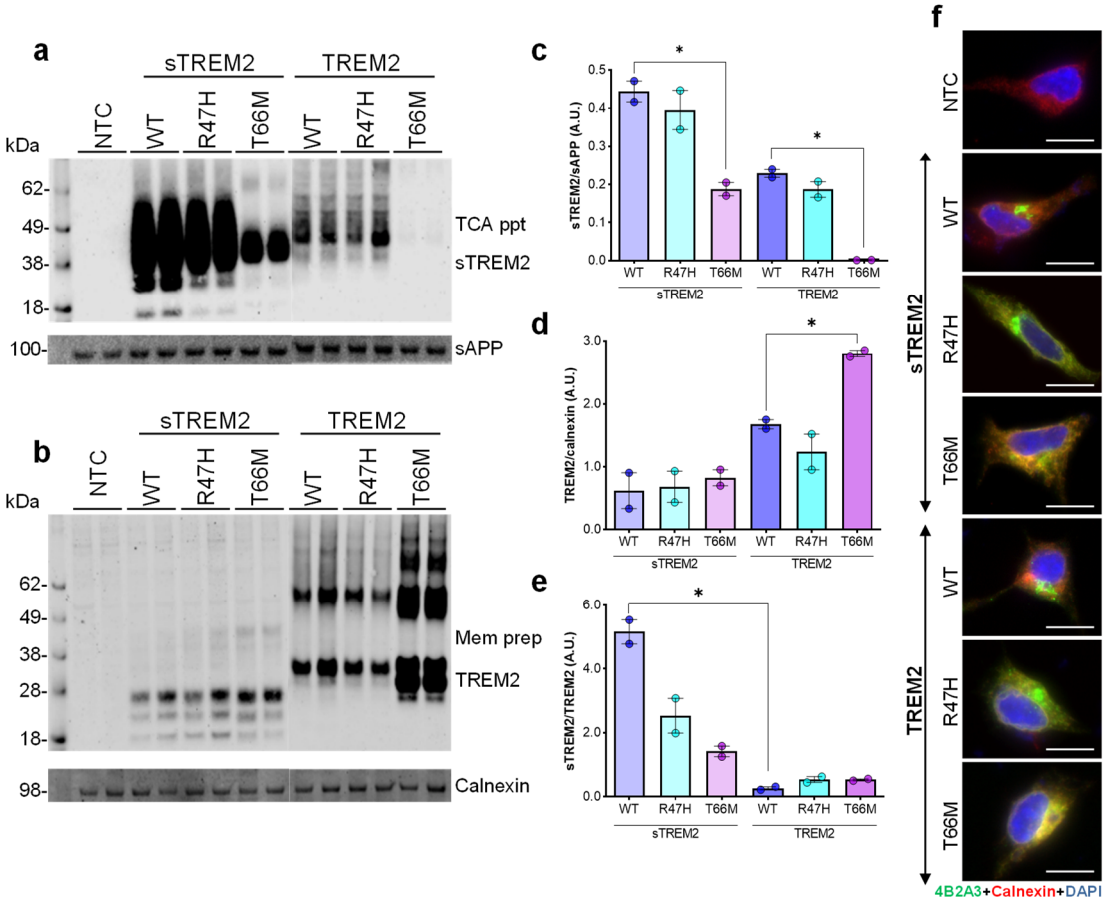

Figure 3.2 | Comparison of sTREM2 and full-length TREM2 after transient transfection

(a) Western immunoblots of the TCA precipitated supernatant collected after 24 h of transient transfection in the HEK293 cell line and **(b)** the purified cellular membrane fractions. **(c)** Box and whiskers plots represent decreased sTREM2-T66M mutant while no change in the sTREM2-R47H levels as compared to sTREM2-WT (normalized to sAPP) in the supernatant. **(d)** Box and whiskers plots represent no change in the sTREM2-R47H while a slight increase in sTREM2-T66M compared to sTREM2-WT and a significant increase in the sTREM2-T66M mutant accumulation as compared to full-

length TREM2-WT in the membrane fractions (normalized to calnexin) after 24 h of transient transfection. **(e)** Box and whiskers plots representing a significant increase in the ratio of secreted sTREM2 from the sTREM2 constructs as compared to full-length TREM2 constructs transiently transfected to HEK293 cell line **(f)** Representative ICC images of sTREM2 and TREM2 constructs transfected cells stained with anti-TREM2 (4B2A3) antibody (green), calnexin (red) and DAPI (blue) (scale bar=10µm, 20x). Each dot represents an average value per experiment and all data represent mean ± SEM (n= 2 experiments in duplicates), unpaired t-test with Welch's correction, *p< 0.05)

Also, it is interesting to note that the conditioned media collected from the cells transfected with the sTREM2 construct showed a distinct band at ~17kDa in addition to a smear between 35-55kDa. The conditioned media, therefore, contain both the complex glycosylated, deglycosylated or even degradation product of sTREM2. This might be due to the increased sTREM2 generated by transient transfection of sTREM2 constructs, as compared to full-length TREM2 constructs.

In the next step, stable cell lines were generated and for this, HEK293 Flp-In cells, having an endogenous Flp recombination target (FRT) site, were co-transfected with a plasmid encoding for the Flp recombinase (pOG44) and the other plasmid with the gene of interest (sTREM2-WT, R47H and T66M, respectively). Following transfection, single-cell clones were screened to identify cells expressing sTREM2 by ICC and western immunoblotting to examine protein expression in cells and supernatant, respectively. For the analysis of sTREM2 secretion, the supernatants from the selected single-cell clones were collected, followed by acetone precipitation and then detected with the TREM2 antibody. Consistently, the stable secretion of sTREM2 was observed including its mutants.

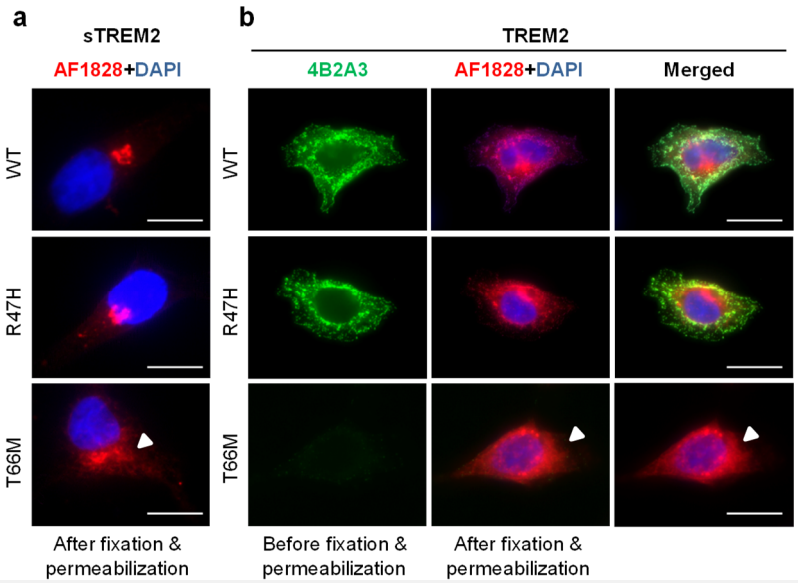

Figure 3.3 | sTREM2 and full-length TREM2 stable cell line with ectodomain mutations

Representative ICC images showing stably expressing **(a)** sTREM2 and **(b)** TREM2 stable cells stained with anti-TREM2 antibody, AF1828 for staining intracellular TREM2 and in-house 4B2A3 antibody for staining cell surface TREM2. In line with previous studies, we could see the accumulation of the T66M

mutant within the cell leading to decreased TREM2 cell surface expression (arrowheads) (scale bar=10µm, 40x).

After the generation of recombinant mammalian cell lines, a high degree of interclonal heterogeneity may remain (Grav et al. 2018; Giuliano et al. 2019). To test this possibility, we compared two independent single-cell clones for each sTREM2 mutant/variant. A similar expression level of sTREM2 was observed between two single-cell clones (data not shown). While the surface expression of wild-type full-length TREM2 was unchanged as compared to full-length TREM2 with R47H mutant, the T66M mutant was observed to be accumulated predominantly in the cellular membrane fraction of both sTREM2 and full-length TREM2 stable cell lines (Figure 3.3a-b).

Next, to check the retention of sTREM2 mutants in the ER, we treated the stable sTREM2 cell lines with Brefeldin A (BFA), an inhibitor of protein transport to the Golgi apparatus and performed ICC (Park et al. 2015) by staining the cells with TREM2 and Calnexin antibody to test the localisation of TREM2 upon treatment with BFA. After 4 h BFA treatment led to inhibition of sTREM2 transport from ER to Golgi in both WT and other mutants (Figure 3.4). This result suggests the transport differences between T66M and other variants. While sTREM2-T66M showed a reticular distribution, indicative for ER, the other variants were predominantly juxtanuclear indicative for Golgi apparatus.

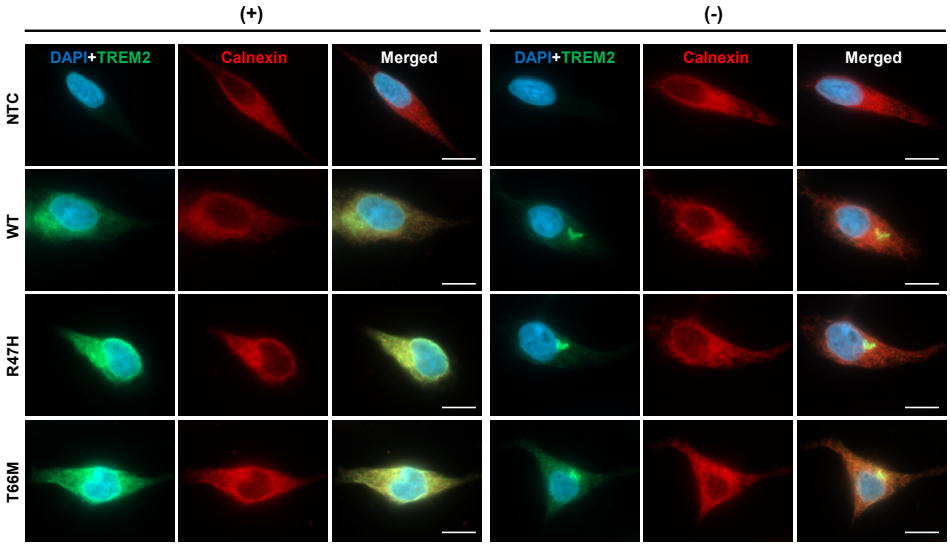

Figure 3.4 | Effect of protein transport inhibitor on sTREM2-WT and mutants

Representative ICC images of sTREM2 stable cell line and various mutants stained with anti-TREM2 (4B2A3) (green), calnexin (red) and DAPI (blue) upon treatment with (+) or without (-) Brefeldin A (BFA) at a concentration of 5µg/ml for 4 h at 37°C (scale bar=10µm, 40x).

3.2 | Ectodomain mutations alter the cellular localization of sTREM2 leading to ER stress

Disease-associated mutations of TREM2 such as T66M have previously been reported to alter intracellular trafficking and thus the localization of TREM2 (Park et al. 2015; Kleinberger et al. 2014; Kober et al. 2016). In ICC, sTREM2-T66M mutant was predominantly detected in the

endoplasmic reticulum (ER) while sTREM2-WT and sTREM2-R47H were predominantly localised to the Golgi apparatus (Figure 3.5a). The stable cell lines of sTREM2 showed similar characteristics of secretion of sTREM2 and accumulation of the mutant TREM2 in ER to those of full-length TREM2. These observations correlate with previous results (Kleinberger et al. 2014; Park et al. 2015).

The accumulation of T66M mutant upregulates ER chaperone proteins such as BiP/GRP78 in response to stress, which is supposed to be a sensor of unfolded protein in the ER that regulates the activation of ER stress transducers (Bertolotti et al. 2000; Sommer et al. 2002).

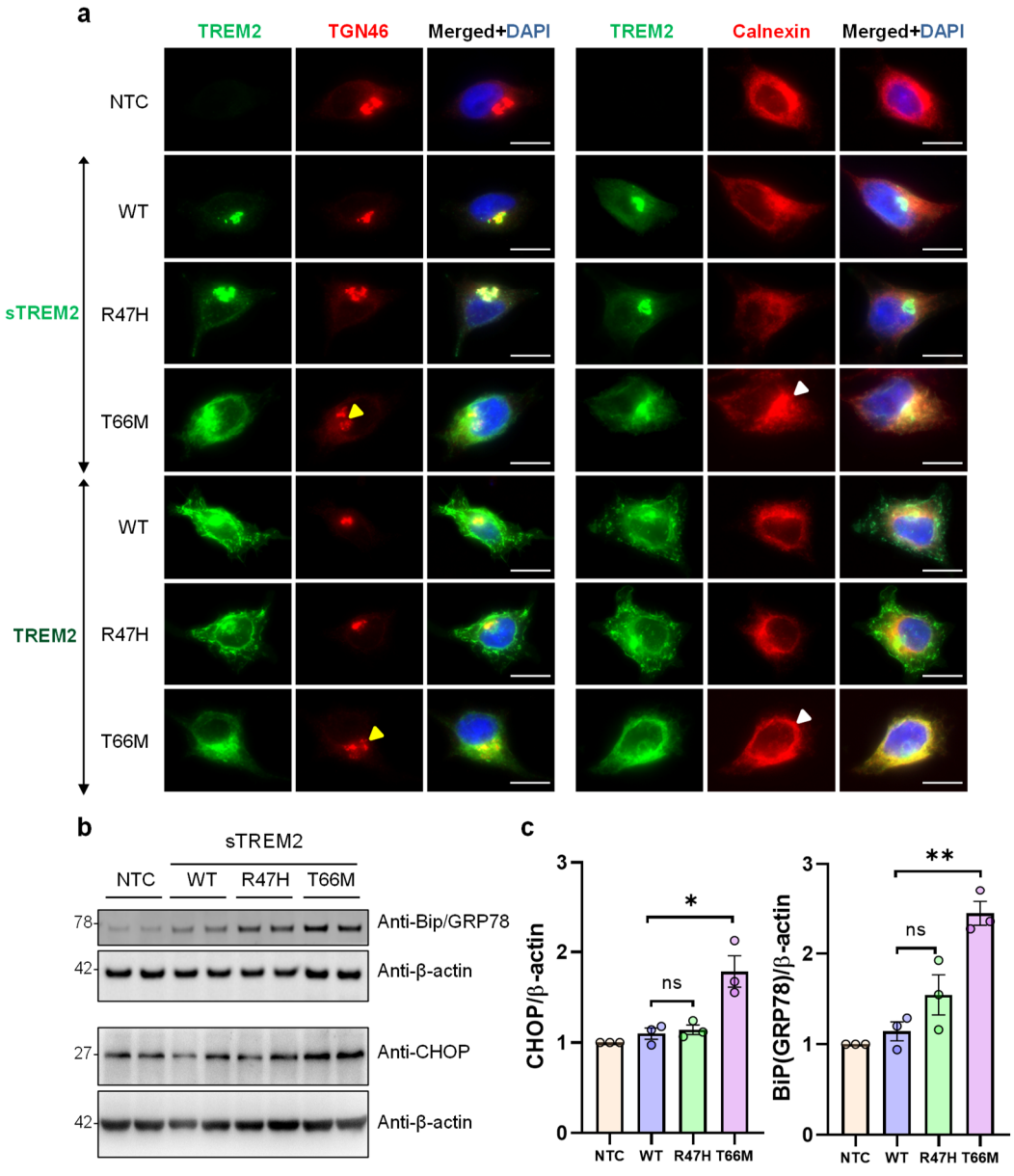

Figure 3.5 | T66M mutation alters the cellular accumulation of sTREM2 leading to ER stress

(a) Representative ICC images of sTREM2 and TREM2 stable cell line stained with an ER marker (Calnexin) and trans-Golgi network marker (TGN46). TREM2-WT and TREM2-R47H colocalize very well with TGN46. T66M mutant partially colocalizes with TGN46 (yellow arrowheads), but predominantly

colocalizes with calnexin (white arrowheads) in both sTREM2 and full-length TREM2 stable cells, indicating its ER accumulation (scale bar=10µm, 40x). **(b)** Immunoblots **(c)** and quantification show an increase in Bip/GRP78 and CHOP protein expression levels in the cell lysates in TREM2-T66M mutant as compared to TREM2-WT. Each dot represents a ratio per experiment normalized to non-transfected control (NTC, i.e., HEK293 Flp-In cells) and the dot plots represent mean ± SEM (n=3 experiments in duplicates, unpaired t-test with Welch's correction, $^{ns}p>0.05$, $*p< 0.05$, $**p<0.01$)

Besides, C/EBP homologous protein (CHOP) which is ubiquitously expressed at very low levels (Ron et al. 1992; Oyadomari et al. 2004), is robustly expressed by perturbations that induce stress and even serum deprivation increases the CHOP levels in a wide variety of cells (Bennett et al. 2010). Accumulation of misfolded sTREM2-T66M causes an increase in the expression of BiP/GRP78 and CHOP in sTREM2-T66M stable cell (Figure 3.5b-c).

3.3 | Increased expression of BiP/GRP78 in the plaque-associated microglia in transgenic mouse brains

In the IF studies using mouse brain sections, BiP/GRP78 was detected in the cytoplasm of neurons in the brains of wild-type and APP/PS1 transgenic mice but was not detected in microglia in wild-type mice. Also, BiP/GRP78 was hardly detectable in the resting microglia of both WT and T66M mice (hence not quantified). Interestingly, the plaque-associated microglia showed an increase in BiP/GRP78 in the cytoplasm indicating increased response to stress in APP/PS1 and APP/PS1-TREM2^{T66M} as compared to WT or TREM2^{T66M} (Figure 3.6a).

Quantification of the integrated density (Int/Den) of BiP/GRP78 and the size of the cell body of plaque-associated microglia (Figure 3.6b), revealed no difference in the Int/Den of BiP/GRP78 and size of the cell body of plaque-associated microglia in brains of APP/PS1 and APP/PS1-TREM2^{T66M} transgenic mice (Figure 3.6c-d).

3.4 | T66M mutation increases translocation of CHOP into the nucleus in plaque-associated microglia

Consistent with previous studies, CHOP expression was observed in the microglial cytosol of wild-type mice (Oyadomari et al. 2004; Ron et al. 1992) and its cytoplasmic expression increases within plaque-associated microglia of APP/PS1 transgenic mice brains. Notably, faint reactivity of antibody detecting CHOP was observed in the nuclei of the microglia in APP/PS1 mouse brains (Figure 3.7). Furthermore, the TREM2^{T66M} mouse microglia showed rather the nuclear localization of CHOP in addition to cytosolic expression. Also, the plaque-associated microglia in APP/PS1-TREM2^{T66M} mouse showed increased nuclear translocation. Additional quantification such as colocalization analysis and the integrated density (IntDen) measurement of both cytoplasmic and nuclear CHOP levels will be needed to conclude this data (Figure 3.7). Thus, FTD-associated TREM2 mutation resulted in UPR including

upregulation and nuclear translocation of CHOP in the APP transgenic mouse brains. In addition to the ER stress induced by Aβ plaque pathology in plaque-associated microglia, the TREM2^{T66M} mutation might exacerbate this stress condition in plaque-associated microglia in transgenic mice, resulting in nuclear translocation of CHOP.

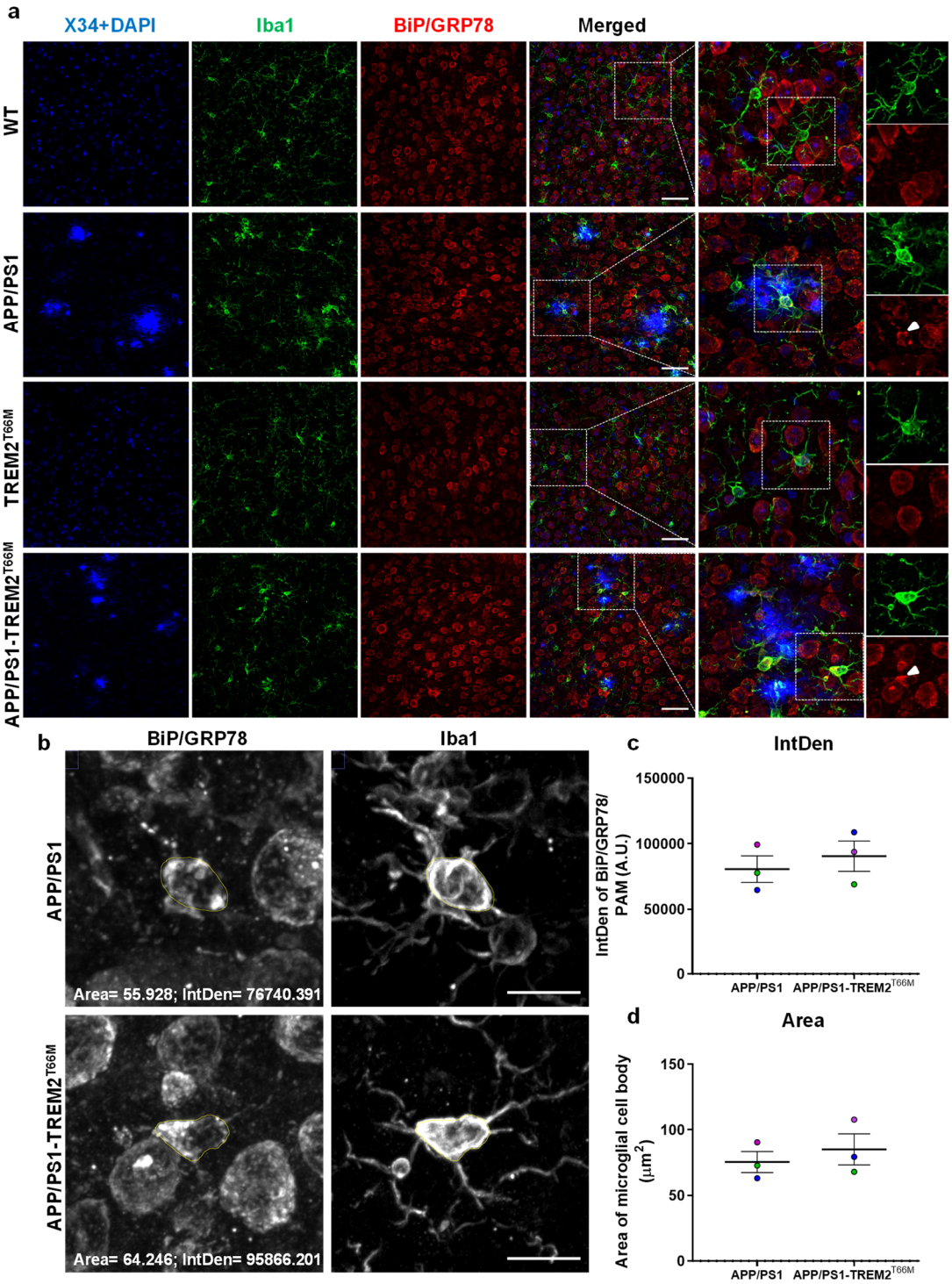

Figure 3.6 | Accumulation of T66M mutant led to an increased BiP/GRP78 expression in plaque-associated microglia

(a) Representative IF images of brain sections stained with BiP/GRP78, as well as markers for microglia (Iba1) and fibrilar Aβ (X34). The expression of BiP/GRP78 was observed in the plaque-associated

microglia in APP/PS1 and APP/PS1-TREM2^{T66M} microglia (arrowheads). Dotted white boxes indicate the area shown at higher magnification (Scale bar=50µm, 40xW). **(b)** Method of analysis for the quantification of IntDen and the area of the cell body of the plaque-associated microglia by using Fiji. A manual outline surrounding the microglial cell body was made by using the freehand selection tool (yellow line), (scale bar=20µm, 40xW). **(c-d)** Quantification of IntDen and area of the cell body of the plaque-associated microglia expressing BiP/GRP78. Each dot represents the average value of 100 plaque-associated microglia/animal. The dot plots represent mean ± SEM (n = 3 male mice, unpaired t-test with Welch's correction, $^{ns}p > 0.05$, $^{*}p < 0.05$).

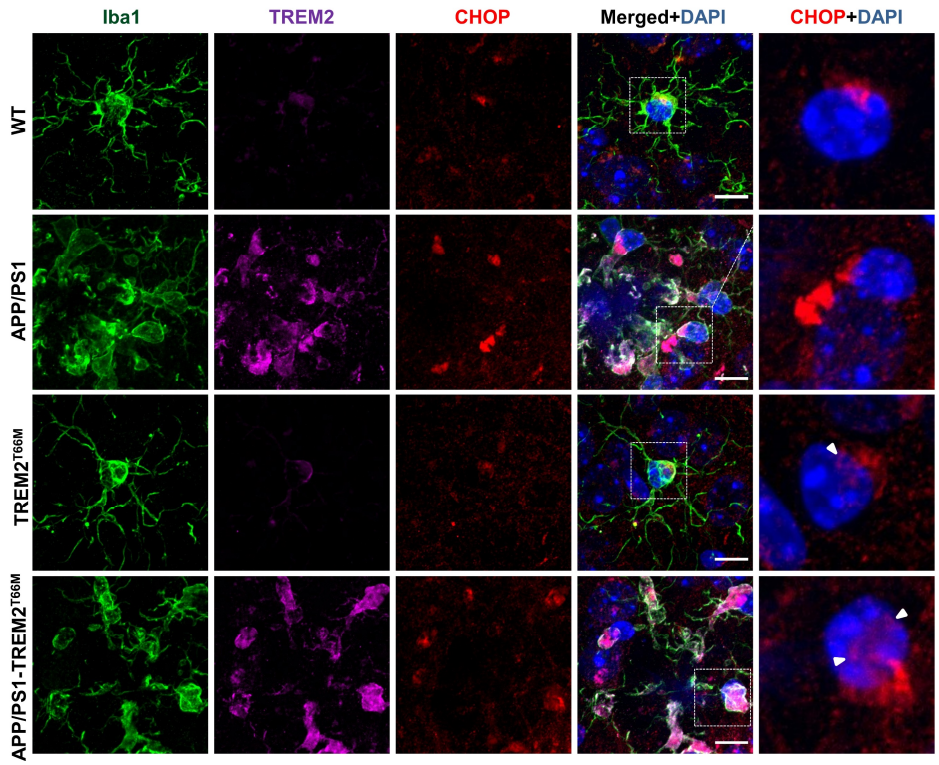

Figure 3.7 | Accumulation of T66M mutant led to nuclear translocation of CHOP in plaque-associated microglia

Representative IF images of brain sections stained with CHOP along with the microglial marker (Iba1) and TREM2. CHOP appears to be localized in the cytoplasm of the microglia in the wild-type mouse while it increases in the cytoplasm of plaque-associated microglia in APP/PS1 mice. Moreover, CHOP translocation into the nucleus was observed in TREM2^{T66M} mice microglia with an intense signal in APP/PS1-TREM2^{T66M} the plaque-associated microglia (arrowheads). Additional quantification such as colocalization analysis and the integrated density (IntDen) measurement of both cytoplasmic and nuclear CHOP levels will be needed to conclude this data. Dotted white boxes indicate the area shown at higher magnification (Scale bar=10µm, 40xW).

Chapter 4 | Differential interaction with TREM2 modulates microglial uptake of modified Aβ species

A significant portion of this chapter is published in Glia, 2021 (Appendix-1)

***Authors: Pranav Joshi**, Florian Riffel, Kanayo Satoh, Masahiro Enomoto, Seema Qamar, Hannah Scheiblich, Nàdia Villacampa, Sathish Kumar, Sandra Theil, Samira Parhizkar, Christian Haass, Michael T. Heneka, Paul E. Fraser, Peter St George-Hyslop, Jochen Walter.*[†]

Brief introduction: *Rare coding variants of the microglial triggering receptor expressed on myeloid cells 2 (TREM2) confer an increased risk for Alzheimer's disease (AD) characterized by the progressive accumulation of aggregated forms of amyloid ß peptides (Aß). Aß peptides are generated by proteolytic processing of the amyloid precursor protein (APP). Heterogeneity in proteolytic cleavages and additional post-translational modifications result in the production of several distinct Aß variants that could differ in their aggregation behaviour and toxic properties. Here, it was assessed whether post-translational modifications of Aß affect the interaction with TREM2. Biophysical and biochemical methods revealed that TREM2 preferentially interacts with oligomeric Aß and that phosphorylation of Aß increases this interaction. Phosphorylation of Aß also affected the TREM2-dependent interaction and phagocytosis by primary microglia and in APP transgenic mouse models. Thus, the TREM2 function is important for sensing phosphorylated Aß variants in distinct aggregation states and reduces the accumulation and deposition of these toxic Aß species in preclinical models of Alzheimer's disease*[*]*(Joshi et al. 2021b).*

4.1 | Characterisation of Aβ preparation for the BLI studies

The aggregation state of the different Aß variants (prepared by Method-1) was controlled by TEM; (Figure 4.1a). No significant change in the size distribution of oligomers formed by unlabeled Aß, Biotin-LC-Aß or by mixtures of unlabeled Aß and Biotin-LC-Aß (at a ratio of 20:1) was observed (Figure 4.1b) indicating that the conjugation of Aß with biotin does not affect the average size of oligomers. Mixtures of Biotin-LC-Aß with the different N-terminal truncated or post-translationally modified Aß variants (also at a 20:1 ratio) also yielded very similar size

[†] *Author contributions: Pranav Joshi, Paul E. Fraser, Peter St George-Hyslop, and Jochen Walter conceived the study. Pranav Joshi performed most of the experiments and analyzed data. Florian Riffel contributed to cell biological and biochemical interaction studies. Pranav Joshi, Kanayo Satoh, and Masahiro Enomoto performed and analyzed BLI experiments. Seema Qamar purified TREM2 ectodomain for the BLI experiments. Sandra Theil and Sathish Kumar purified modification-specific monoclonal antibodies. Hannah Scheiblich, Nàdia Villacampa, and Michael T. Heneka prepared primary mouse microglia and provided mouse brains. Pranav Joshi and Jochen Walter wrote the manuscript with help from Kanayo Satoh, Paul E. Fraser, and further input from all co-authors. All of the authors read, edited, and approved the final version of the manuscript.*

[*] *Italicized text is taken from the manuscript published in GLIA by Joshi et al. 2021*

distribution of oligomers between 8 and 55 nm. Only the oligomer preparation with pSer8-Aβ also contained larger oligomers with sizes between 55 and 90 nm. This was observed for both, Aβ(1-42) and Aβ(3-42) variants. However, also for pSer8-Aβ variants, >95% of the oligomers were in the size range of 8-55 nm. The monomer-rich fractions of Aβ were prepared from freshly reconstituted Aβ stocks by dilution to 23 µM in ice-cold PBS and ultracentrifugation at 4°C at 100,000g for 1 h. Aβ in the supernatant was considered as a monomer-rich preparation and characterized by western immunoblot(Joshi et al. 2021b) (Figure 4.1c).*

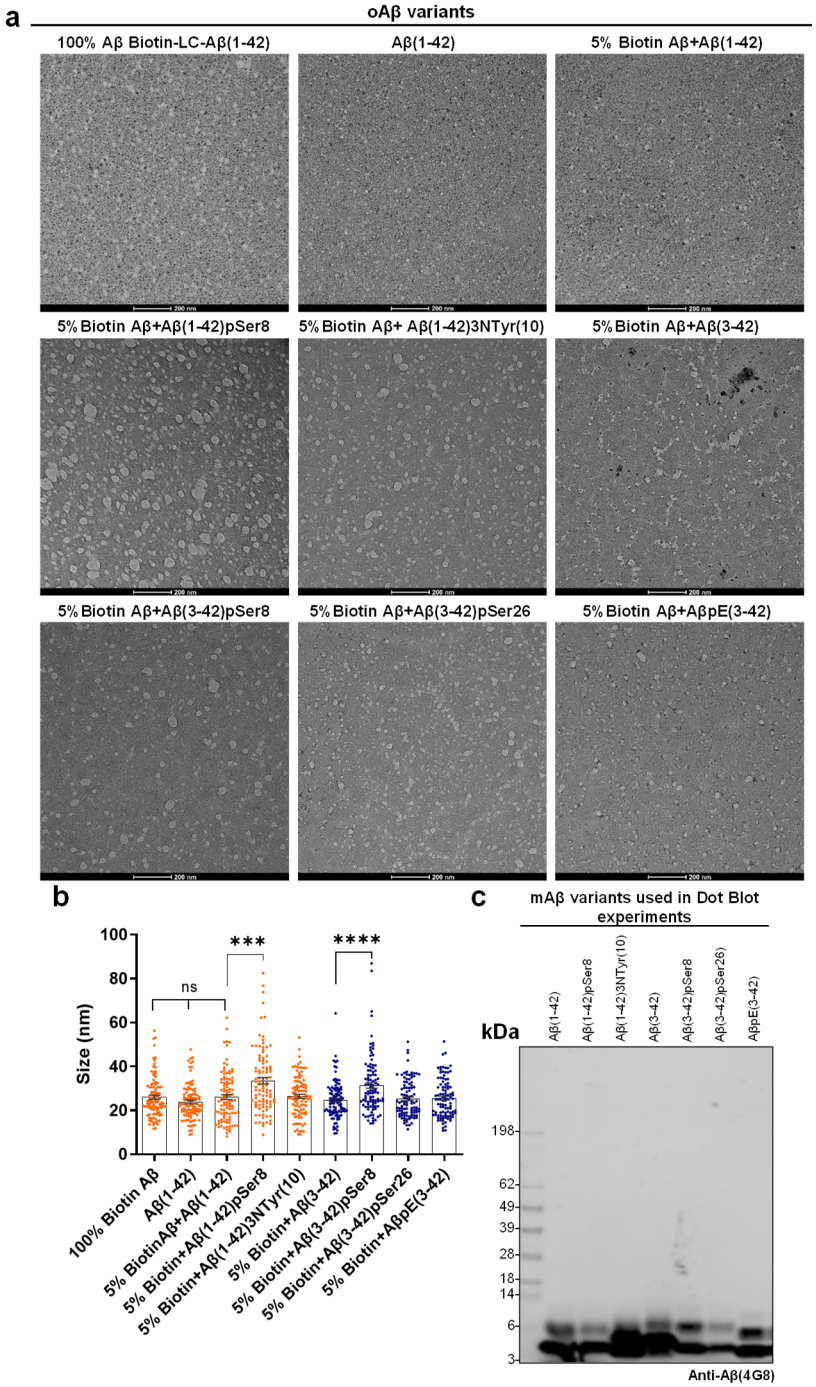

Figure 4.1 | Characterization of synthetic Aβ preparations used for the BLI and dot blot experiments

(a) Negative-stain TEM images of the oligomerized Aβ variants after mixing with 5% Biotin-LC-Aβ as described in the methods sections 2.3 and 2.17.1 (scale bar=200nm, 45,000x). **(b)** The scattered plot shows the diameter of randomly selected oAβ measured by manual marking using FIJI software. Dots represents individual oligomers and the the bars represents mean±SEM (n=100, Mann-Whitney test, ***p<0.001, ****p<0.0001, ^{ns}p>0.05). **(c)** Immunoblot representing mAβ variants detected with 4G8 antibody that was used for dot blot experiments prepared as described in the method section (Joshi et al. 2021b).

4.2 | Differential binding of TREM2 to post-translationally modified Aβ species

4.2.1 | Interaction of Aβ monomers with TREM2 measured by BLI

Interaction of the TREM2 ectodomain was tested with monomeric Aβ (mAβ) using Aβ40 variants that have a much lower propensity to aggregate (Figure 4.2 and section 2.18.2) since mixing of the different variants with biotin-labelled Aβ(1-42) as used for oligomer preparation was not applicable for experiments with mAβ, Aminopropylsilane (APS) sensors were used to immobilize mAβ and then performed the binding assay with purified TREM2 ectodomain. It is important to note that the binding curves for monomeric Aβ40 variants were biphasic, which may be due to the strong binding of Aβ with the sensor itself, making dissociation curves evaluation difficult. However, considering the binding response values at 300 s, the pSer8 and pSer26 phosphorylated monomeric Aβ showed increased binding to TREM2 as compared to unmodified, and pyro-glutamate modified Aβ variants.

The binding of soluble TREM2 (sTREM2) to monomeric (mAβ) and oligomeric (oAβ) forms of distinct post-translationally modified and non-modified Aβ variants (Figure 4.3a) was assessed in dot blot assays. For this, different Aβ variants in monomeric and oligomeric forms were spotted onto Nitrocellulose (NC) membranes and incubated with sTREM2 obtained from conditioned media of transgenic cells expressing a TREM2 variant with a stop codon at position 158 thereby representing the soluble TREM2 ectodomain that is physiologically generated by proteolytic processing of full-length TREM2 (Wunderlich et al. 2013; Schlepckow et al. 2020; Thornton et al. 2017; Feuerbach et al. 2017). sTREM2 bound to the different Aβ species was detected by an anti-TREM2 antibody (4B2A3). This antibody recognizes an epitope within the stalk region of TREM2 (aa 131-148) (Ibach et al. 2021), thereby avoiding possible competition with ligands bound to the ligand-binding domain of sTREM2. Consistent with previous reports, TREM2 showed strongly increased interaction with oligomeric as compared to monomeric Aβ variants (Figure 4.3b-c). Oligomers formed by Aβ variants phosphorylated at Ser8 (pSer8-Aβ) or Ser26 (pSer26-Aβ) showed significantly increased interaction with TREM2 as compared to non-modified, nitrated or pyroglutamate-modified variants. With monomeric forms, pSer26-Aβ also showed strongly increased binding to TREM2 as compared to non-modified Aβ or[*]

[*] *Italicized text is taken from the manuscript published in GLIA by Joshi et al. 2021*

otherwise modified Aß variants. However, it should be noted that pSer26-Aß has the highest tendency to form oligomeric assemblies (Kumar et al. 2016), and it cannot be excluded that pSer26-Aß formed some oligomeric assemblies during this assay (Joshi et al. 2021b)[*].*

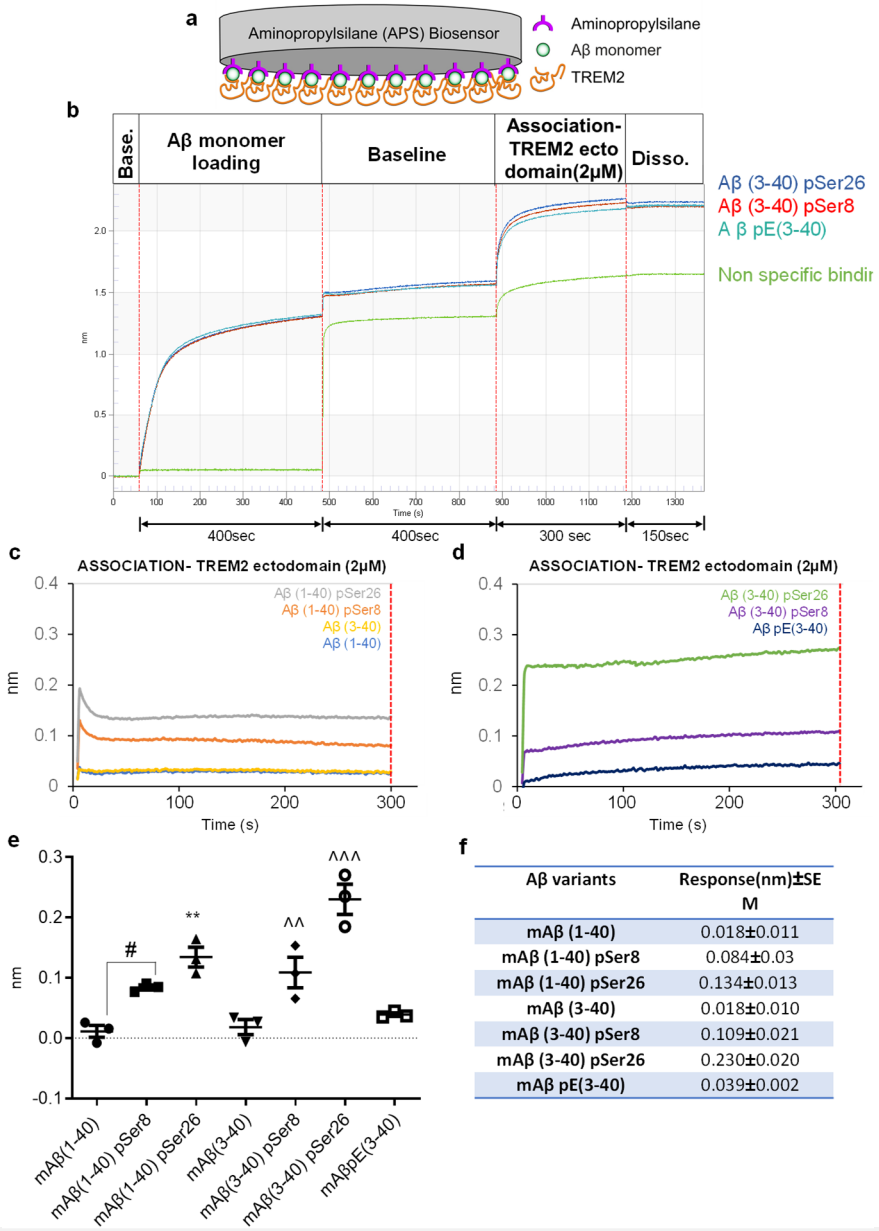

f

Aβ variants	Response(nm)±SEM
mAβ (1-40)	0.018±0.011
mAβ (1-40) pSer8	0.084±0.03
mAβ (1-40) pSer26	0.134±0.013
mAβ (3-40)	0.018±0.010
mAβ (3-40) pSer8	0.109±0.021
mAβ (3-40) pSer26	0.230±0.020
mAβ pE(3-40)	0.039±0.002

Figure 4.2 | BLI studies of mAβ with TREM2 ectodomain using Aminopropylsilane (APS) biosensors

(a) Schematics of BLI strategy using APS biosensors wherein mAβ were immobilized on the APS biosensors to check its interactions with 2μM of TREM2 ectodomain. **(b)** Raw image showing one trial loading of 1μM concentration of mAβ(3-40) variants followed by association of 2μM of TREM2 ectodomain. **(c-d)** Association of TREM2 ectodomain with mAβ(1-40) and mAβpE(3-40) variants. For plotting these graphs, the average response values calculation at 300 s by using octet software from three trials were used. **(e)** The scattered plot showing binding response values from the independent experiment (nm) measured at 300 s by octet software. The average values of ratio from experimental triplicate of Aβ(1-40) variants are represented as "●" while of Aβ(3-40) variants are represented as "▲".

[*]*Italicized text is taken from the manuscript published in GLIA by Joshi et al. 2021*

* or ^ represents a comparison of Aβ(1-40) or Aβ(3-40) variants respectively. Data represents mean±SEM (n=3, unpaired t-test with Welch correction, ** or^^p<0.01, $^{\#}p$=0.0517 and ^{ns}p>0.05) **(f)** Representing the absolute values mean±SEM response values from the BLI studies of mAβ(x-40) variants.

4.2.2 | Interaction of Aβ oligomers with TREM2 by using BLI studies

Next, to validate these findings with an independent method, Biolayer interferometry (BLI) was utilized (Figure 4.3d). The different Aβ variants were mixed with Biotin-labelled-Aβ at a ratio of 20:1 and oligomerized as described previously (Vilalta et al. 2021). Oligomer preparations were immobilized on streptavidin biosensors (Figure 4.3d) and kinetic binding assays were performed using purified TREM2 ectodomain at different concentrations (1, 2, 5 and 10μM).

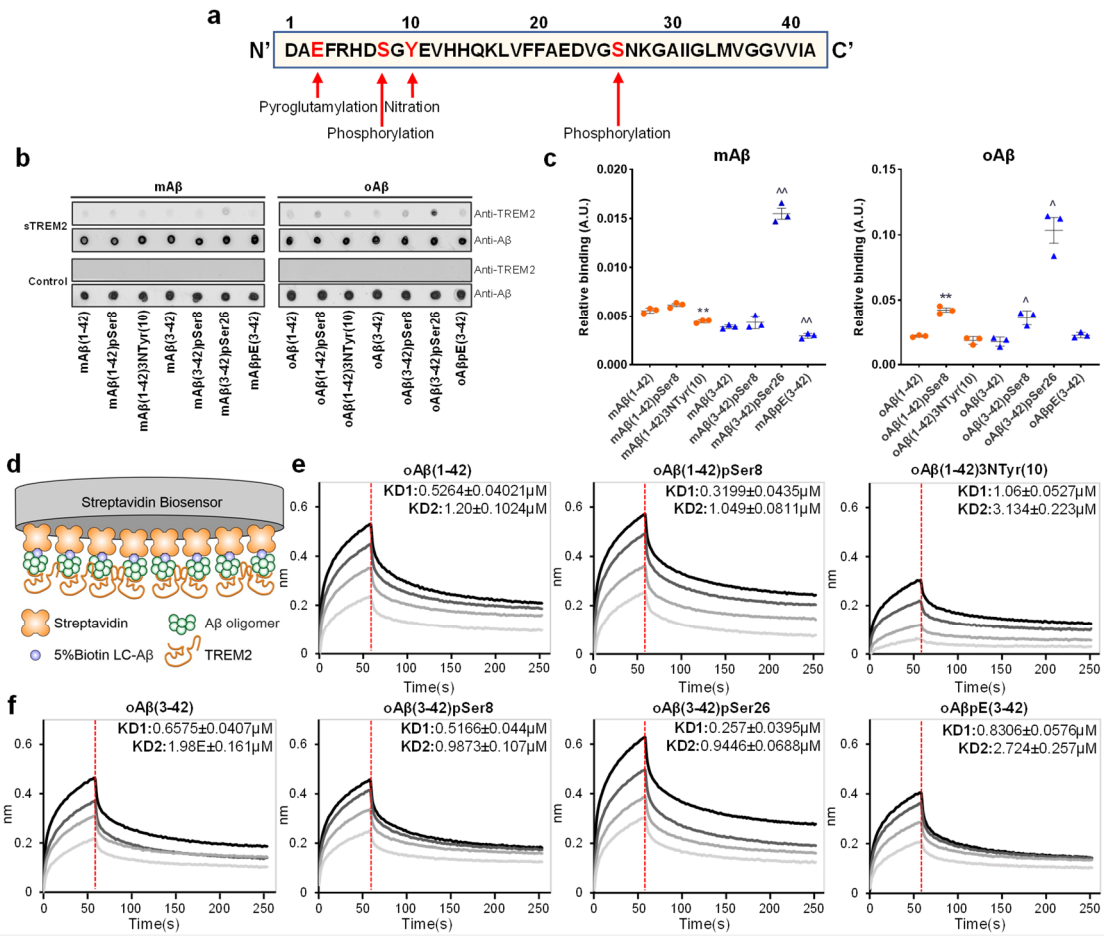

Figure 4.3 | Differential interaction of TREM2 with modified Aβ variants

(a) Pictorial illustration of various PTMs of Aβ peptides used for binding assessment in this study. **(b)** Representative dot blot of various mAβ and oAβ variants probed on the NC membrane followed by incubation with precipitated protein from the supernatant of HEK293 Flp-In or sTREM2 secreting stable HEK293 Flp-In cell line. **(c)** Quantification of the ratio of signal intensity of sTREM2 detected with Anti-TREM2 antibody and respective Aβ variants detected with 4G8 antibody. The average values of ratio from experimental triplicate of Aβ(1-42) variants are represented as "●" while that of Aβ(3-42) variants are represented as "▲". * or ^ represents a comparison of Aβ(1-42) or Aβ(3-42) variants respectively. (n=3, unpaired t-test with Welch correction, $*^{or}$^p<0.05, $**^{or}$^^p<0.01). **(d)** Schematics of BLI strategy

using streptavidin (SA) biosensors. Biotinylated oAβ variants were immobilized on the SA biosensor to assess its interaction with the TREM2 ectodomain at concentrations of 1, 2, 5, and 10µM. **(e-f)** Representative association/dissociation curves of varying TREM2 ectodomain concentrations and calculated KD1/KD2 values of TREM2 ectodomain binding with oAβ variants (Refer to Table 4.1 for another set of values). (n=2, which includes repetition of the entire experiment including preparation and dilution of oAβ oligomers, KD-equilibrium dissociation constant)(Joshi et al. 2021b)

BLI kinetic studies also revealed increased binding of the TREM2 ectodomain to oligomers that contained pSer8-Aβ or pSer26-Aβ (Figure 4.3e-f). The lowest binding was measured for nitrated Aβ3NTyr(10) as compared to non-modified Aβ (Figure 4.3e). Oligomeric pyroglutamate modified Aβ (pEAβ) also showed lower binding to the TREM2 ectodomain as compared to non-modified Aβ (Figure 4.3f) [*] *(Joshi et al. 2021b).*

5% Biotin-LC-Aβ +	Trial	KD1 (µM)	KD2 (µM)	kon1(1/Ms)	kon2(1/Ms)	kdis1(1/s)	kdis2(1/s)	KD1 (%)	KD1 (%)
oAβ (1-42)	1	0.5264 ±0.04021	1.20 ±0.1024	5.57E+03 ±1.68E+02	1.32E+05 ±1.02E+04	2.93E-03 ±2.06E-04	1.58E-01 ±5.69E-03	68	32
	2	0.643 ±0.0504	1.143 ±0.118	5.12E+03 ±1.86E+02	1.51E+05 ±1.43E+04	3.29E-03 ±2.28E-04	1.73E-01 ±7.30E-03	68	32
oAβ (1-42) pSer8	1	0.3199 ±0.0435	1.049 ±0.0811	5.81E+03 ±1.83E+02	1.14E+05 ±7.87E+03	1.86E-03 ±2.46E-04	1.19E-01 ±4.12E-03	64	36
	2	0.448 ±0.477	0.853 ±0.0712	5.55E+03 ±2.06E+02	1.38E+05 ±1.04E+04	2.49E-03 ±2.48E-04	1.18E-01 ±4.28E-03	62	38
oAβ (1-42) 3NTyr(10)	1	1.06 ±0.0527	3.134 ±0.223	3.42E+03 ±9.81E+01	6.01E+04 ±3.85E+03	3.63E-03 ±1.47E-04	1.88E-01 ±5.84E-03	66	34
	2	1.01 ±0.0808	2.776 ±0.330	3.69E+03 ±1.59E+02	6.32E+04 ±6.73E+03	3.73E-03 ±2.51E-04	1.75E-01 ±9.31E-03	67	37
oAβ (3-42)	1	0.6575 ±0.0407	1.98E ±0.161	5.53E+03 ±1.72E+02	9.28E+04 ±6.86E+03	3.63E-03 ±1.94E-04	1.84E-01 ±6.27E-03	61	39
	2	0.698 ±0.0411	1.969 ±0.182	5.25E+03 ±1.59E+02	1.05E+05 ±8.90E+03	3.67E-03 ±1.85E-04	2.07E-01 ±7.83E-03	66	34
oAβ (3-42) pSer8	1	0.5166 ±0.044	0.9873 ±0.107	5.75E+03 ±2.18E+02	1.89E+05 ±1.89E+04	2.97E-03 ±2.29E-04	1.87E-01 ±7.97E-03	64	36
	2	0.404 ±0.0404	0.987 ±0.0887	5.84E+03 ±1.90E+02	1.52E+05 ±1.24E+04	2.36E-03 ±2.23E-04	1.50E-01 ±5.60E-03	65	35
oAβ (3-42) pSer26	1	0.257 ±0.0395	0.9446 ±0.0688	6.01E+03 ±1.76E+02	1.23E+05 ±8.04E+03	1.55E-03 ±2.33E-04	1.16E-01 ±3.76E-03	64	36
	2	0.5297 ±0.0434	1.329 ±0.103	5.36E+03 ±1.64E+02	1.10E+05 ±7.62E+03	2.84E-03 ±2.16E-04	1.46E-01 ±4.87E-03	64	36
oAβ pE(3-42)	1	0.8306 ±0.0576	2.724 ±0.257	4.52E+03 ±1.86E+02	7.94E+04 ±6.86E+03	3.75E-03 ±2.10E-04	2.16E-01 ±8.29E-03	59	41
	2	0.77 ±0.0443	2.045 ±0.171	4.85E+03 ±1.39E+02	8.45E+04 ±6.37E+03	3.73E-03 ±1.86E-04	1.73E-01 ±6.16E-03	67	33

Table 4.1 | BLI kinetic assay representing values from two trials

(Kon-constant of association, Kdis-constant of dissociation, KD- equilibrium constant of dissociation). (Joshi et al. 2021b)

[*] *Italicized text is taken from the manuscript published in GLIA by Joshi et al. 2021*

Pull-down assays from mixtures containing monomeric and oligomeric forms of Aß using sTREM2-Fc fusion proteins further demonstrated that sTREM2 preferentially binds to oligomeric Aß assemblies. Again, the highest binding was detected for phosphorylated Aß oligomers as compared to non-modified Aß species (Figure 4.4a-b). The combined data from different biochemical and biophysical assays demonstrate that phosphorylation of Aß at Ser8 or Ser26 increased binding to TREM2 in particular for oligomeric Aß assemblies[*](Joshi et al. 2021b).*

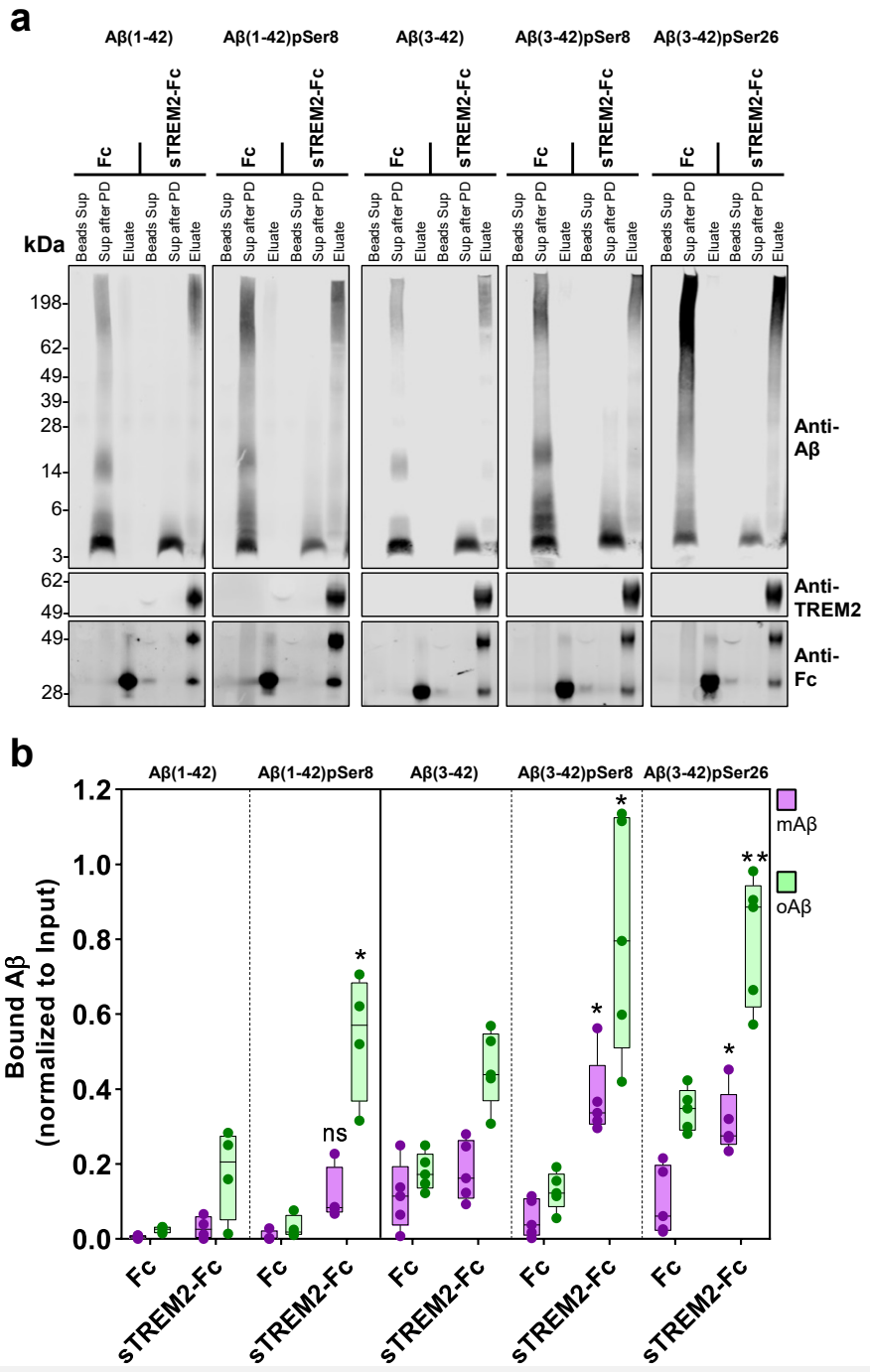

Figure 4.4 | Increased interaction of TREM2 with oligomeric phosphorylated Aβ variants

[*]*Italicized text is taken from the manuscript published in GLIA by Joshi et al. 2021*

(a) IP of oAβ fractions with Fc or sTREM2-Fc pre-coupled to protein-G magnetic beads confirmed by clear "beads sup" showed a preferential pull-down (PD) of oAβ while a large portion of mAβ remains in the supernatant **(b)** Box and whiskers plot of IntDen of either the monomer band or oligomeric fraction was determined and normalized to the respective input. Each dot represents an independent experiment. All data represent mean ± SEM. (n=4 for Aβ(1-42) or n=5 for Aβ(3-42) variants, unpaired t-test with Welch correction, *p<0.05, **p<0.01, ^{ns}p>0.05).

4.3 | TREM2 inhibits the aggregation of Aβ variants

A previous study reported that TREM2 could prevent the aggregation of Aβ (Kober et al. 2020; Vilalta et al. 2021) by inhibiting the fibrillization of Aβ40 and Aβ42 by targeting the secondary nucleation of fibril formation (Belsare et al. 2022). This suggests that TREM2 not only mediates uptake of Aβ by microglia but its soluble ectodomain also could modulate Aβ aggregation. Thus, the effect of sTREM2 on the aggregation of the different Aβ species was assessed by real-time fluorescence spectrometry. Interestingly, sTREM2 inhibited the aggregation of all Aβ variants in a concentration-dependent manner (Figure 4.5). Notably, the aggregation of pSer8-Aβ(1-42) was completely suppressed at 0.1 µM concentration of TREM2, while complete suppression of aggregation of non-modified Aβ(1-42), and 3NTyr10-Aβ(1-42) required higher concentrations of TREM2. This shows that sTREM2 can inhibit of aggregation of pSer8-Aβ modified species more efficiently as compared to that of non-phosphorylated Aβ or other Aβ variants, in line with a stronger binding of TREM2 to phosphorylated Aβ. Stronger suppression of aggregation of Ser8 phosphorylated Aβ was also observed for N-terminally truncated pSer8-Aβ(3-42) as compared to non-phosphorylated Aβ(3-42). The Aβ(3-42) species were included for better comparison with the N-terminally truncated pE-Aβ(3-42) variant. Notably, the inhibitory effect of sTREM2 on the aggregation of pyroglutamate-modified pE-Aβ(3-42) and pSer26-Aβ(3-42) was lower, likely due to the higher propensity of these variants to self-assemble (Figure 4.6a-c). Moreover, the aggregation of pSer26-Aβ differs from that of other variants as pSer26-Aβ does not form mature fibrils, but has a high propensity to rapidly form stable oligomers. When ThT assay endpoint samples were loaded on the Native-PAGE, the phosphorylated Aβ, particularly pSer26-Aβ showed the presence of stable oligomers after 15 h of aggregation as compared to other Aβ variants. Along with this, pSer8-Aβ also formed stable oligomers while fibrils were detected in the pockets of the gel. When ThT assay endpoint samples were used to perform the dot blot assay, only phosphorylated Aβ formed stable oligomers and in particular, pSer26-Aβ showed the presence of stable oligomers as compared to all other Aβ variants used in the study (Figure 4.6d-e). In the experiments, the oligomer-specific detection of Aβ species was achieved by using a previously reported A11 antibody (Ho et al. 2020; Yang et al. 2017a). Thus, the effect of TREM2 on the kinetics of aggregation of pSer26-Aβ and 3NTyr10-Aβ(1-42) cannot be directly compared to other fibrillization competent Aβ variants (Figure 4.6). However, sTREM2 also potently inhibited

oligomerization of both Aβ species. Among the tested Aβ variants, sTREM2 increases the lag phase and elongation phase in a concentration-dependent manner indicating inhibition of fibrillization. These new data provide an additional mechanism for how TREM2 could prevent the accumulation of different toxic Aβ species. These findings further support the differential binding of TREM2 to modified Aβ species, and additionally also indicate a protective function of TREM2 against the formation of Aβ aggregates.

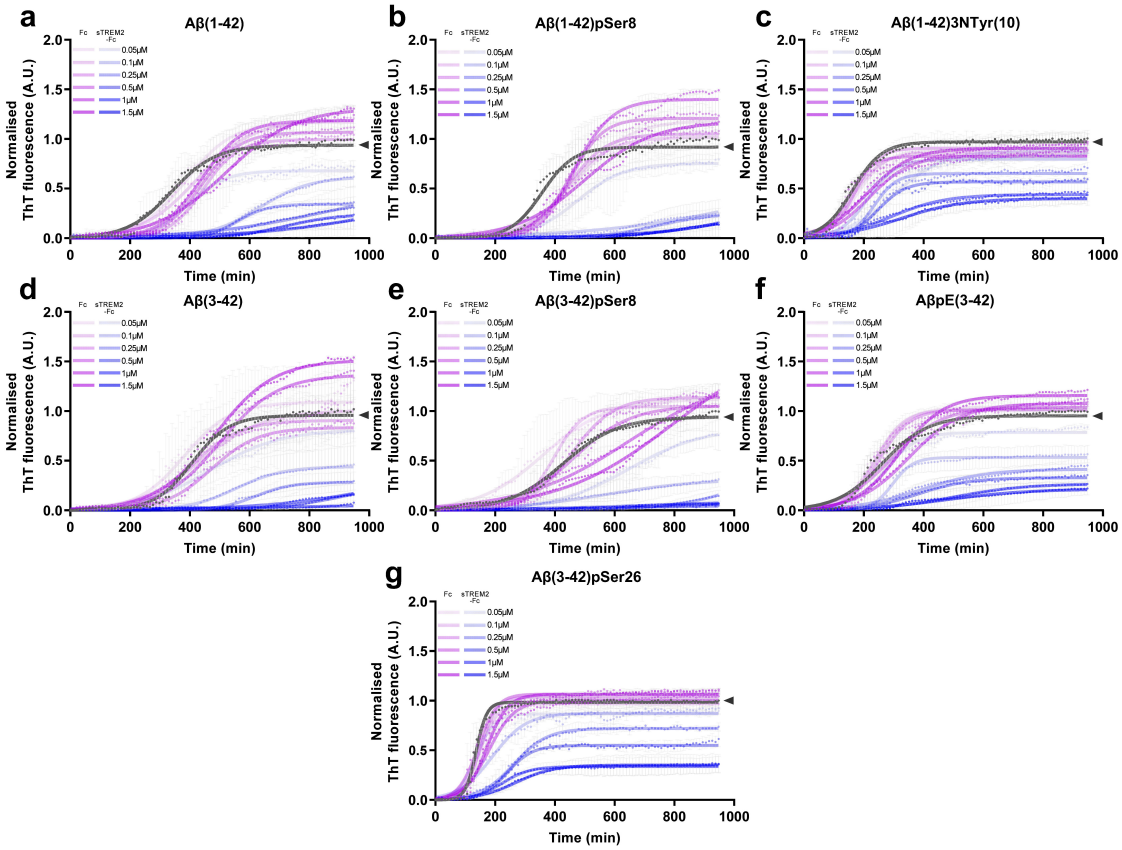

Figure 4.5 | TREM2 inhibits aggregation of modified Aβ(x-42) variants

Thioflavin-T (ThT) fluorescence assay of varying concentrations of sTREM2-Fc (blue colour gradient non-linear fit lines) co-incubated with **(a-c)** Aβ(1-42) variants or **(d-g)** Aβ(3-42) variants wherein Fc (pink colour gradient non-linear fit lines) was used as a control aggregated for 15 h. Values for each graph were normalized to the respective Aβ variant (marked with ◀). Data represent mean ± SEM (n=2, which includes repetition of the entire experiment including preparation and dilution of Aβ variants, A.U.-arbitrary units).

4.4 | TREM2 dependent binding and phagocytosis of modified Aβ species by primary microglia

Since microglia can phagocytose Aβ, the role of TREM2 in the uptake of different Aβ species was analyzed using primary microglia from wild-type (WT) mice expressing endogenous TREM2 and mice with the TREM2^{T66M} knock-in (KI) mutation. The TREM2^{T66M} mutation confers misfolding and a strong loss-of-function and is associated with NHD or frontal lobe dementia

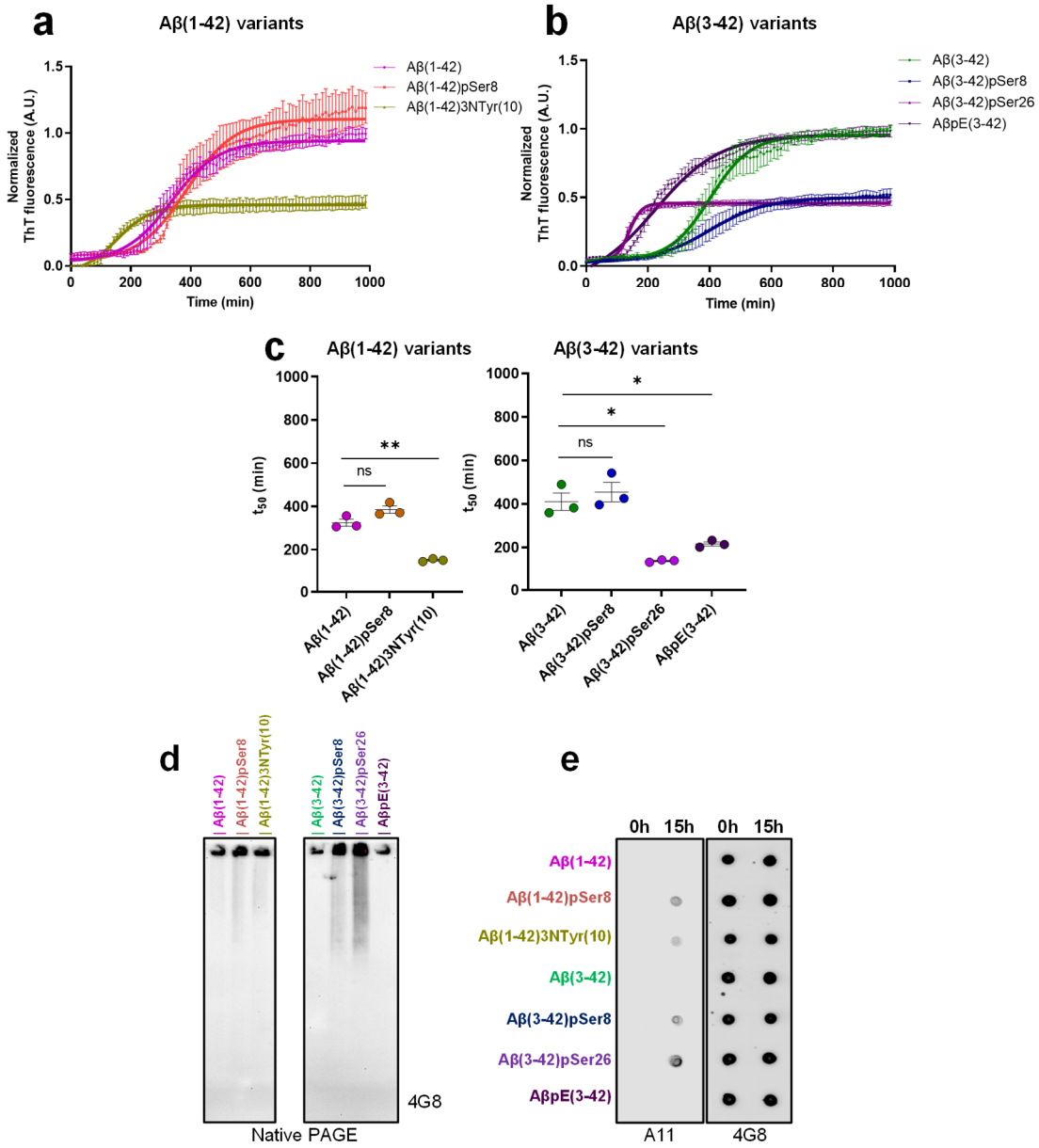

Figure 4.6 | Modified Aβ(x-42) variants showed differences in the aggregation kinetics

Thioflavin-T (ThT) fluorescence assay curve fit of 5µM non-aggregated **(a)** Aβ(1-42) variants and **(b)** Aβ(3-42) variants aggregated for 15 h and normalized to the respective wild-type Aβ variant (n=3). **(c)** Scattered plot of the t_{50} values showed a significant decrease in t_{50} or faster aggregation for Aβ(1-42)3NTyr(10) (t(2.23)=10.34,**p=0.0063), while no change in Aβ(1-42)pSer8 (t(3.997)=2.578,^{ns}p=0.0615) as compared to Aβ(1-42). Likewise, there was a decrease in t_{50} or faster aggregation of Aβ(3-42)pSer26 (t(2.026)=6.768,*p=0.0204) and AβpE(3-42) (t(2.216)=4.725,*p=0.0343), while no change in Aβ(3-42)pSer8 (t(3.956)=0.7345,^{ns}p=0.5038) as compared to Aβ(3-42). Each dot represents t_{50} of an independent experiment obtained by non-linear fitting to the Boltzmann function of each independent kinetics. Data represent mean ± SEM (n=3, unpaired t-test with Welch correction, A.U.- arbitrary units). **(d)** native-PAGE and **(e)** dot blot showed the presence of stable oligomers of phosphorylated Aβ(x-42) variants after 15h aggregation, detected by using A11 and 4G8 antibodies.

(Kleinberger et al. 2017; Le Ber et al. 2014). Consistent with previous findings (Kleinberger et al. 2014), TREM2^{T66M} primary microglia showed reduced phagocytosis of latex beads as compared to WT microglia (Figure 4.7a-c).

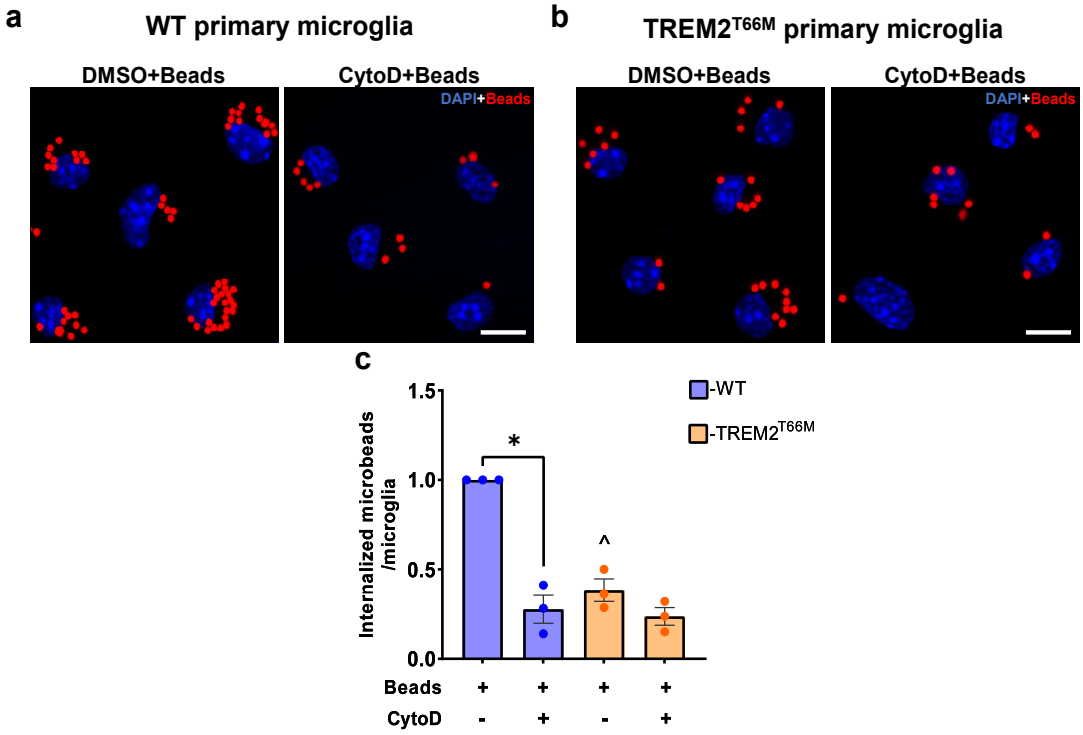

Figure 4.7 | Reduced uptake of latex beads by TREM2^{T66M} primary microglia

(a-b) Differences in the internalization of fluorescent latex beads (red) by primary microglia from wild-type (WT) and TREM2^{T66M} mice after 2h at 37°C were determined by ICC (Scale bar=10µm, 40xW). **(c)** Scattered dot plot representing internalized microbeads/microglia. Each dot represents the average ratio of beads per microglia normalized to WT microglia. Values were calculated by randomly selecting bead-positive microglia. Data represent mean ± SEM (n=300 cells/group, experimental n=3, unpaired t-test with Welch correction, (t(2.0)=9.213, *p=0.0116), (t(2.0)=9.851, ^p=0.0101) * for comparison CytoD treated to non-treated cells, ^ for comparison WT and TREM2^{T66M}).

*To further characterize the interaction of Aß species with TREM2 and its functional implications, primary microglia were used from wild-type (WT) mice expressing endogenous TREM2 and mice with the TREM2^{T66M} knock-in (KI) mutation. The TREM2^{T66M} mutation is associated with NHD or frontal lobe dementia (FTD) and strongly impairs ectodomain folding and cell surface transport of the receptor thereby causing a loss of function (Kleinberger et al. 2017; Le Ber et al. 2014). First, we assessed the binding of phosphorylated and non-modified Aß species to the plasma membrane of primary microglia from WT mice by incubation of cells on ice to halt endocytosis (Wesen et al. 2017; Tamboli et al. 2008). While the membrane-association of pSer8-Aß was lower, that of pSer26-Aß was increased as compared to binding**

[*] *Italicized text is taken from the manuscript published in GLIA by Joshi et al. 2021*

of non-modified Aß (Figure 4.8a-b), indicating phosphorylation-site and phosphorylation-state specific interaction of Aß with the microglial surface[*]*(Joshi et al. 2021b).*

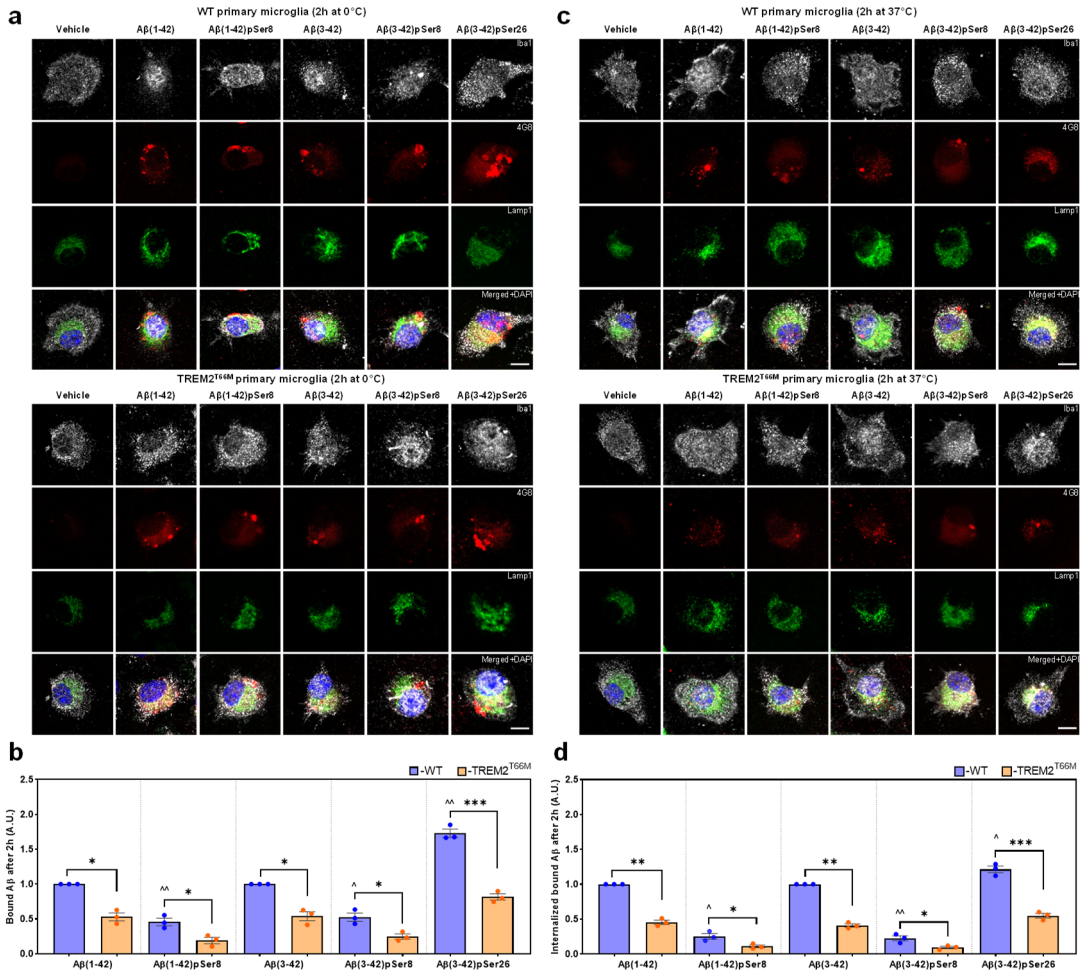

Figure 4.8 | Phosphorylated Aβ variants showed differential binding and uptake by the primary microglia with and without functional mutation of TREM2

(a) Representative immunocytochemical staining images of primary microglia from wild-type (WT) and TREM2^{T66M} mice, and **(b)** the scattered plot representing the normalized IntDen of oAβ positive cells after treatment with 1µM oAβ for 2h at 0°C followed by fixation and staining. **(c)** Representative immunocytochemical staining images of primary microglia from WT and TREM2^{T66M} mice, and **(d)** the scattered plot representing the uptake of bound oAβ levels calculated from IntDen of oAβ positive cells after treatment with 1µM oAβ variants for 2h at 0°C, followed by washing and incubating at 37°C for 2h followed by fixation and staining. Microglial cells were stained using the Iba1 antibody (white) while Aβ was stained via the generic antibody 4G8 (red). Lamp1 antibody was employed as a lysosomal marker (green) (Scale bar=10µm, 63xW). In the scattered plots, IntDen of oAβ (either 1-42 or 3-42) is considered as value one for the WT primary microglia and accordingly values for TREM2^{T66M} were calculated. Each dot represents the average value of normalized IntDen/experiment. Data represent mean ± SEM (n=300 cells/group, experimental n=3, unpaired t-test with Welch correction, *^{or}^p<0.05, **^{or}^^p<0.01***p<0.001 for comparison of WT and TREM2^{T66M}, A.U.-arbitrary units). ^represents

[*]*Italicized text is taken from the manuscript published in GLIA by Joshi et al. 2021*

comparison of phosphorylated Aβ variants with Aβ (1-42 or 3-42) treated to WT primary microglia (Joshi et al. 2021b).

Decreased binding of pSer8-Aβ was observed for the two length variants of Aβ, 1-42 and 3-42. Since Aβ(1-42)pSer26 could not be chemically synthesized, the analysis was restricted to Aβ(3-42)pSer26 and compared to non-modified Aβ(3-42) and Aβ(3-42)pSer8 species, respectively. Importantly, the binding of the different Aβ species was reduced by about 50% in TREM2^{T66M} expressing microglia as compared to TREM2 WT expressing microglia (Figure 4.8a-b). On one hand, these results demonstrate the involvement of functional TREM2 in the binding of the different Aβ species, and on the other hand, support previous reports showing that the association of Aβ to microglia could also involve additional proteins or lipids present in the cell surface (Yu et al. 2015; Verdier et al. 2004). When cells were further incubated at 37°C upon binding of Aβ to the surface, we observed differential uptake of bound Aβ depending on the phosphorylation state (Figure 4.8c-d). While the amount of internalized pSer8-Aβ was lower, the amount of internalized pSer26-Aβ was higher as compared to that of unphosphorylated Aβ. The phosphorylation-state dependent internalization of Aβ variants in TREM2 WT microglia might involve differences in the aggregation and/or conformation of pSer8-Aβ and pSer26-Aβ (Kumar et al. 2011a; Kumar et al. 2016; Kumar et al. 2012)[*].*

Phosphorylation-state dependent uptake of Aβ was also observed when cells were exposed to Aβ without a precedent binding period and was reduced by cytochalasin D (CytoD), indicating the involvement of phagocytosis (Figure 4.9a-c). In addition, the number of Aβ-positive microglia was lower for pSer8-Aβ exposed cells, but higher for pSer26-Aβ exposed cells as compared to the number of microglia that internalized unphosphorylated Aβ (Figure 4.9d). Again, the phagocytosis of the different Aβ species was strongly reduced in microglia from TREM2^{T66M} KI mice, demonstrating that the differential uptake of phosphorylation state variants of Aβ depends on functional TREM2 (Figure 4.9) (Joshi et al. 2021b). Co-staining with Lamp-1 revealed partial localization of internalized Aβ in lysosomal compartments (Figure 4.8 and Figure 4.9). Lysosomal localization was particularly pronounced for pSer26-Aβ, indicating lysosomal accumulation of this phosphorylated Aβ form. These results indicate that the phosphorylation state of Aβ affects its TREM2 dependent binding and phagocytosis by microglia. However, in addition to the differential interaction with TREM2, peculiar differences in the aggregation characteristics and conformation of the phosphorylation-state variants of Aβ could contribute to the differential interaction and uptake by microglia[*] *(Joshi et al. 2021b).*

[*] *Italicized text is taken from the manuscript published in GLIA by Joshi et al. 2021*

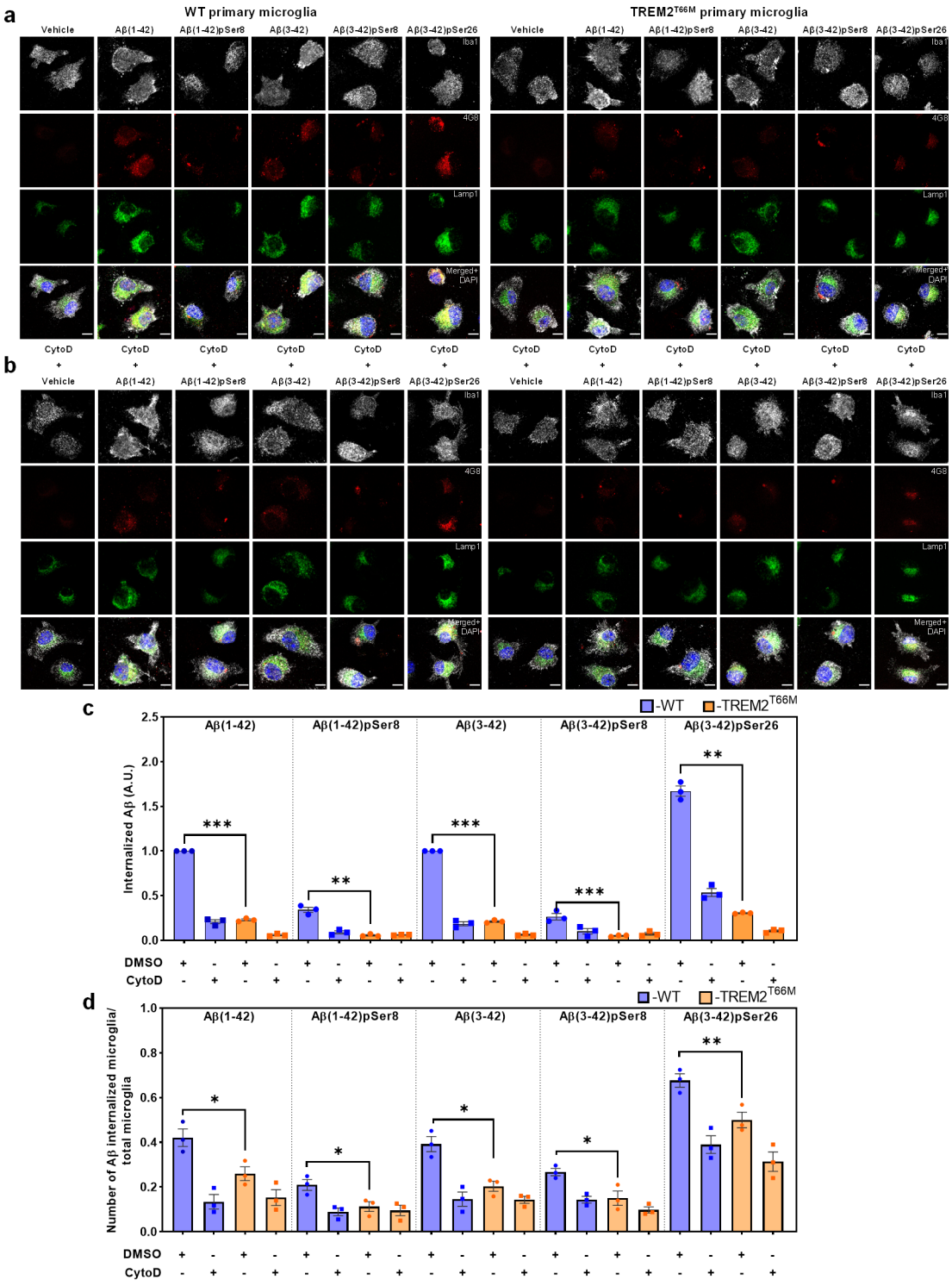

Figure 4.9 | Phosphorylated Aβ variants showed differential internalization by primary microglia

(a) Representative immunocytochemical staining images of primary microglia from wild-type (WT) and TREM2^{T66M} mice after pretreatment with vehicle (DMSO) or **(b)** CytoD treatment for 30 min followed by treatment with 1μM oAβ for 2h at 37°C (Scale bar=10μm, 63xW). **(c)** Scattered plot representing the differences in the internalization of different oAβ variants by primary microglia from WT and TREM2^{T66M} mice calculated by the IntDen of internalized Aβ. Each dot represents the average value of normalized IntDen of Aβ positive microglia/experiment. **(d)** Scattered dot plot representing the number of Aβ

positive microglia normalized to the total number of microglia. Each dot represents the average value of ratio/experiment; calculated by manually counting Aβ positive cells and automatically counting DAPI positive total cells for 10 images/experiment (5 images per coverslips and the experiments were in duplicates). Data represent mean ± SEM (experimental n=3, unpaired t-test with Welch correction, *p< 0.05, **p<0.01, ***p<0.001 for comparison of WT and TREM2^{T66M}) (Joshi et al. 2021b).

4.5 | TREM2 deletion leads to altered deposition of phosphorylated Aβ variants

To further investigate the role of TREM2 in the interaction of different phosphorylated Aβ species with microglia in-vivo, APP transgenic mice expressing endogenous TREM2 or mice with a TREM2 knock-out were used. Similar to previous studies (Yuan et al. 2016; Zhao et al. 2018; Wang et al. 2015), a decreased microglial clustering around X-34 positive plaques was observed in the brains of TREM2$^{-/-}$ mice as compared to TREM2$^{+/+}$ mice (Figure 4.10a-b) [*].*

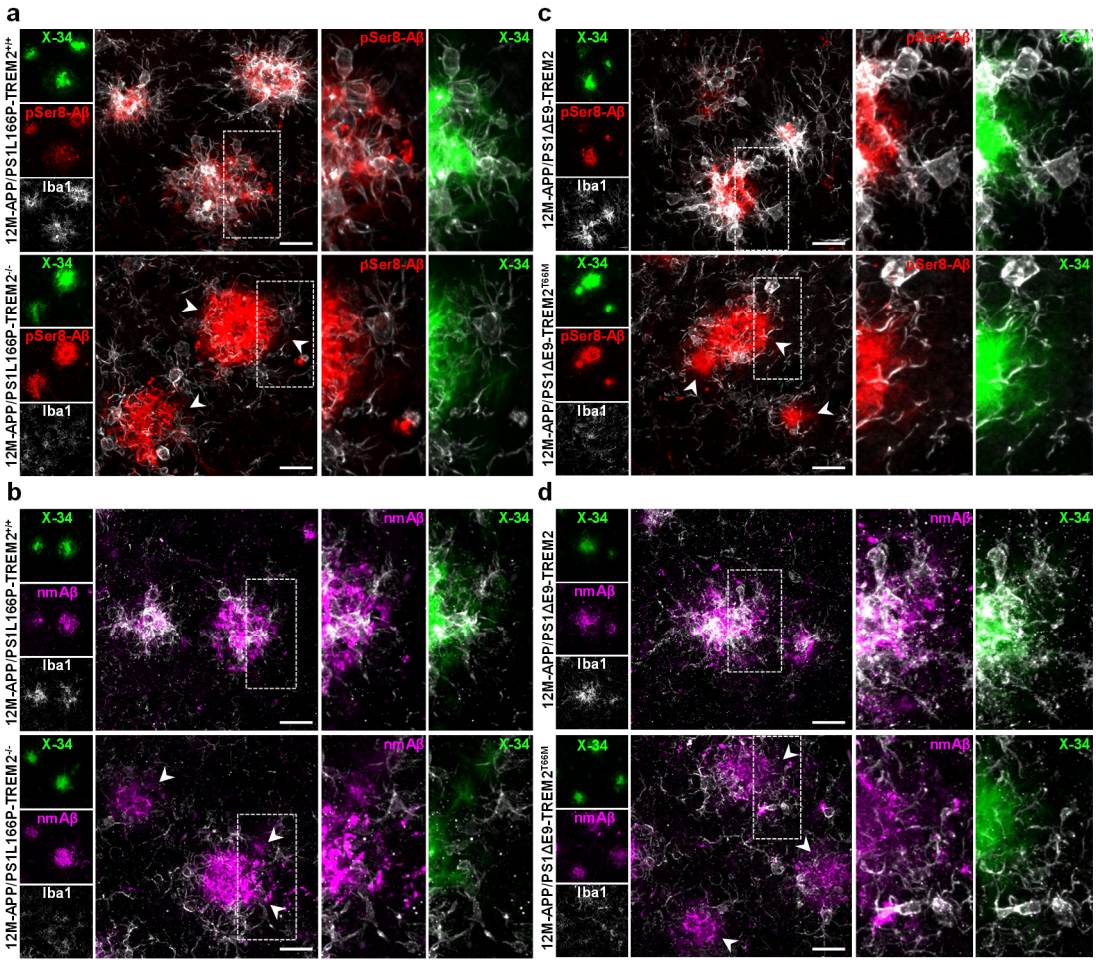

Figure 4.10 | Decreased microglial barrier function alters deposition of pSer8-Aβ and nmAβ in the transgenic mouse brain

(a-b) Representative IF images of extracellular plaques stained with pSer8-Aβ, nmAβ, and microglia stained with Iba1 in 12M-APP/PS1L166P-TREM2$^{+/+}$ and TREM2$^{-/-}$ mice. **(c-d)** Representative IF images of extracellular plaques stained with pSer8-Aβ, nmAβ, and microglia stained with Iba1 in 12M-

[*] *Italicized text is taken from the manuscript published in GLIA by Joshi et al. 2021*

APP/PS1ΔE9-TREM2 and APP/PS1ΔE9-TREM2^{T66M} mice. Dotted white boxes indicate the area shown at higher magnification while the arrow indicates the mesh-like structures that surround the plaques of various compaction in TREM2$^{-/-}$ or TREM2^{T66M} mice. (Scale bar=20µm, 40xW) (Joshi et al. 2021b).

Interestingly, mice homozygous for the TREM2^{T66M} mutation also showed reduced clustering around X-34 positive plaques that contain fibrillar Aβ (Figure 4.10c-d). Immunostaining of brain sections with antibodies against the microglial marker protein Iba1 together with phosphorylation-state specific antibodies for Aβ with Ser8 in the phosphorylated or non-modified state (nmAβ) revealed that X-34 positive plaques also contained pSer8-phosphorylated and unphosphorylated (nmAβ) species that are surrounded by microglia in TREM2 WT mice (Figure 4.10). In contrast, brains of TREM2$^{-/-}$ (Figure 4.10a-b) or TREM2^{T66M} expressing mice (Figure 4.10c-d) showed increased radial extensions of fibrillar Aβ that are intermingled with microglial processes thereby forming mesh-like structures with various degrees of compaction (indicated by arrowheads, Figure 4.10). Very similar observations on the morphology of Aβ deposits and interactions with microglia in brains of TREM2$^{+/+}$ and TREM2$^{-/-}$ mice were also made when Aβ was detected by a monoclonal antibody (82E1) that detects the N-terminus of Aβ independent of its phosphorylation state (Figure 4.11)[*]. These findings are consistent with the function of TREM2 to restrict plaque size or growth (Wang et al. 2015; Yuan et al. 2016). It is important to note that TREM2 positive plaque-associated microglia also restrict pSer8-Aβ deposits, which could be due to enhanced TREM2 binding. However, little if any pSer8-Aβ was detected within microglia (Figure 4.10 a and c)[*] (Joshi et al. 2021b).

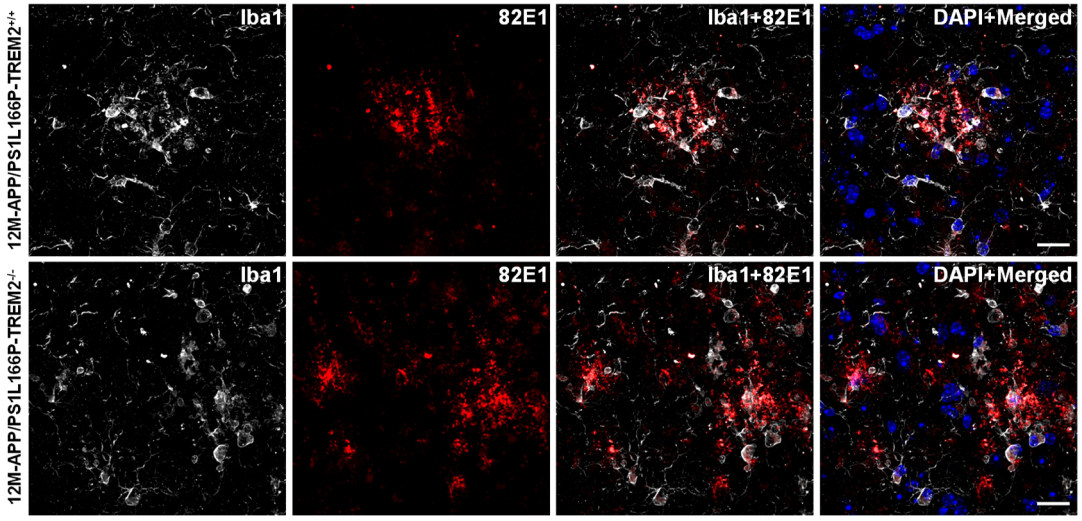

Figure 4.11 | Decreased microglial barrier function alters deposition of Aβ in the transgenic mouse brain

Representative IF images of extracellular plaques stained with 82E1 and microglia stained with Iba1 in 12M-APP/PS1L166P-TREM2$^{+/+}$ and TREM2$^{-/-}$ mice (Scale bar=20µm, 40xW) (Joshi et al. 2021b).

[*]*Italicized text is taken from the manuscript published in GLIA by Joshi et al. 2021*

In contrast to pSer8-Aβ, pSer26-Aβ was abundant within microglia (Figure 4.12), consistent with the observed increased binding and TREM2-dependent internalization by microglia (see Figure 4.8 and Figure 4.9).

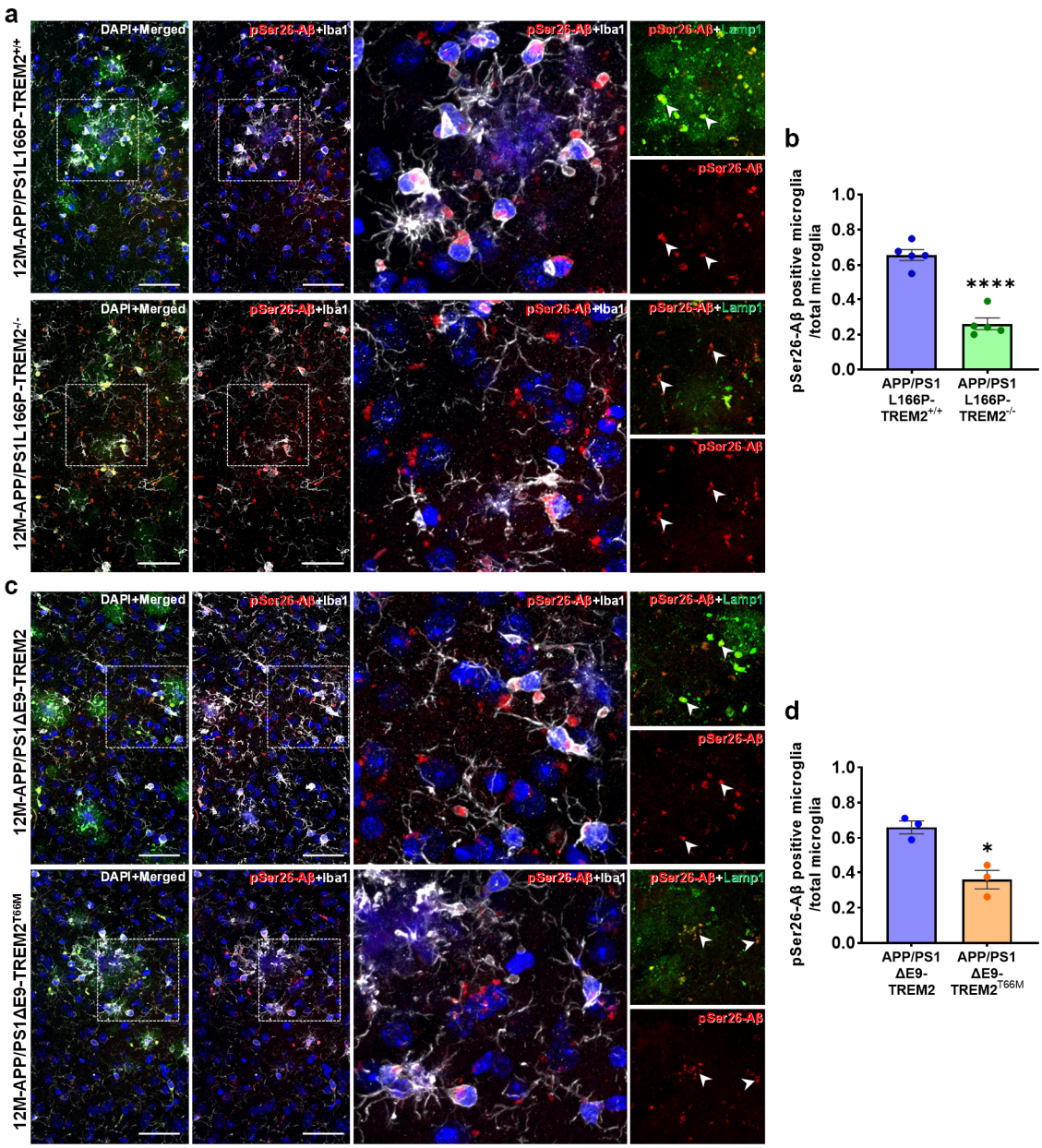

Figure 4.12 | TREM2 deletion or mutation leads to decreased microglial pSer26-Aβ deposits in TREM2 transgenic mouse brain

(a) Representative IF images of pSer26-Aβ stained SSC of 12M-APP/PS1L166P-TREM2$^{+/+}$ and TREM2$^{-/-}$ mice along with the lysosomal marker, Lamp1 and microglial marker, Iba1 (Scale bar=50µm, 40xW, dotted white boxes indicate the area shown at higher magnification). **(b)** Quantified number of microglia/cortical region of interest (ROI) showed a decreased number of pSer26-Aβ, Lamp1 positive microglia (indicated with an arrow) in the 12M-APP/PS1L166P-TREM2$^{-/-}$ compared to TREM2$^{+/+}$ mice (t(7.976)=8.615, ****p<0.0001). **(c)** Representative IF images of pSer26-Aβ stained SSC of 12M-APP/PS1ΔE9-TREM2 and TREM2^{T66M} mice along with the lysosomal marker, Lamp1 and microglial marker, Iba1 (Scale bar=50µm, 40xW, dotted white boxes indicate the area shown at higher

magnification). **(d)** Quantified number of microglia/cortical region of interest (ROI) showed a decreased number of pSer26-Aβ, Lamp1 positive microglia (indicated with an arrow) in the 12M-APP/PS1ΔE9-TREM2^{T66M} compared to APP/PS1ΔE9-TREM2 mice (t(3.577)=4.739,**p*=0.0118). All data represent mean ± SEM. (n=5(6b) or n=3(6d), unpaired t-test with Welch correction) (Joshi et al. 2021b).

Deposition of pSer26-Aβ was detected in the two independent APP transgenic mouse models used in this study (Figure 4.12). However, in contrast to fibrillar Aβ detected by X-34 or pSer8-Aβ, pSer26-Aβ species were only faintly detected in the core of dense Aβ plaques and rather appeared as small deposits in close proximity of extracellular plaques (Kumar et al. 2020b) (Figure 4.12a and c). Co-immunostaining of pSer26 with Iba1 and Lamp1 revealed lysosome-associated pSer26-Aβ within plaque-associated microglia in the different APP transgenic mouse models expressing TREM2$^{+/+}$, which was strongly reduced in APP transgenic mice deficient of TREM2 (Figure 4.12a-b) or expressing the TREM2^{T66M} KI mutation (Figure 4.12c-d) [*](Joshi et al. 2021b).

[*] *Italicized text is taken from the manuscript published in GLIA by Joshi et al. 2021*

Chapter 5 | Amyloid phosphorylation at Ser26 causes intraneuronal and vascular Aβ deposits leading to impaired memory in the S26D pseudophosphorylated transgenic mouse model

Brief introduction: Altered processing of APP results in the generation of Aβ peptides that coalesces to form insoluble, extracellular amyloid deposits. In addition, combinations of several enzymatic activities lead to multiple isoforms, including post-translationally modified Aβ variants, which might modulate disease progression. Previous studies showed that phosphorylation at Ser26 of Aβ increases the stability of oligomeric assembly and exists as abundant intraneuronal deposits at very early stages of AD, but much less in extracellular plaques, unlike other modified and unmodified Aβ variants. This work reports the generation and characterization of a novel transgenic AβS26D-Tg mouse model that expresses the human APP751 variant carrying the Swedish (KM→NL) and phosphomimicking (S→D) mutations at Ser26 residue of Aβ. Furthermore, this study demonstrates that the oligomers generated by phosphomimicking mutations at Ser26 residue of Aβ (AβS26D) do not form fibrillary assemblies in transgenic mice, presenting a new tool for understanding intracellular Aβ deposition and Aβ oligomer-induced disease in the absence of amyloid plaques.

5.1 | AβS26D-Tg mice showed intraneuronal accumulation of Aβ without extracellular deposits at 4,8 and 24 months of age

IF stainings were performed with brain coronal sections at different ages (4, 8 and 24 months) with Aβ-specific antibodies, 7H3D6 which detects N-terminally non-modified Aβ species and 6E10 detects Aβ along with APP and its CTFs (Section 2.2). Co-staining the sections with an antibody against the neuronal nuclear protein (NeuN) revealed intraneuronal immunoreactivity of Aβ in the brains of the AβS26D-Tg mice already at the age of 4 months (4M) in the cortex (Figure 5.1) and hippocampus (Figure 5.2), but not in non-Tg littermates (Figure 5.1 and Figure 5.2). It is important to note that, AβS26D-Tg mice exhibited no extracellular amyloid plaques in any regions that were examined at 4M, 8M and 24M of age. Instead, intraneuronal deposits were observed in the cortex (Figure 5.1), amygdala and hippocampal (CA1 and CA3) regions of 4M, 8M and 24M mice (Figure 5.1 and Figure 5.2). Also, vascular deposits of Aβ were observed in male and female mice (refer to Table 5.1).

It is important to note that the monoclonal 6E10 antibody is specific to the N-terminal region of human Aβ, showed reactivity that was apparent already at 4 months of age and accumulated in an age-dependent fashion in the cortex (layer V) (Figure 5.1), hippocampus (CA1 and CA3) (Figure 5.2) and amygdala.

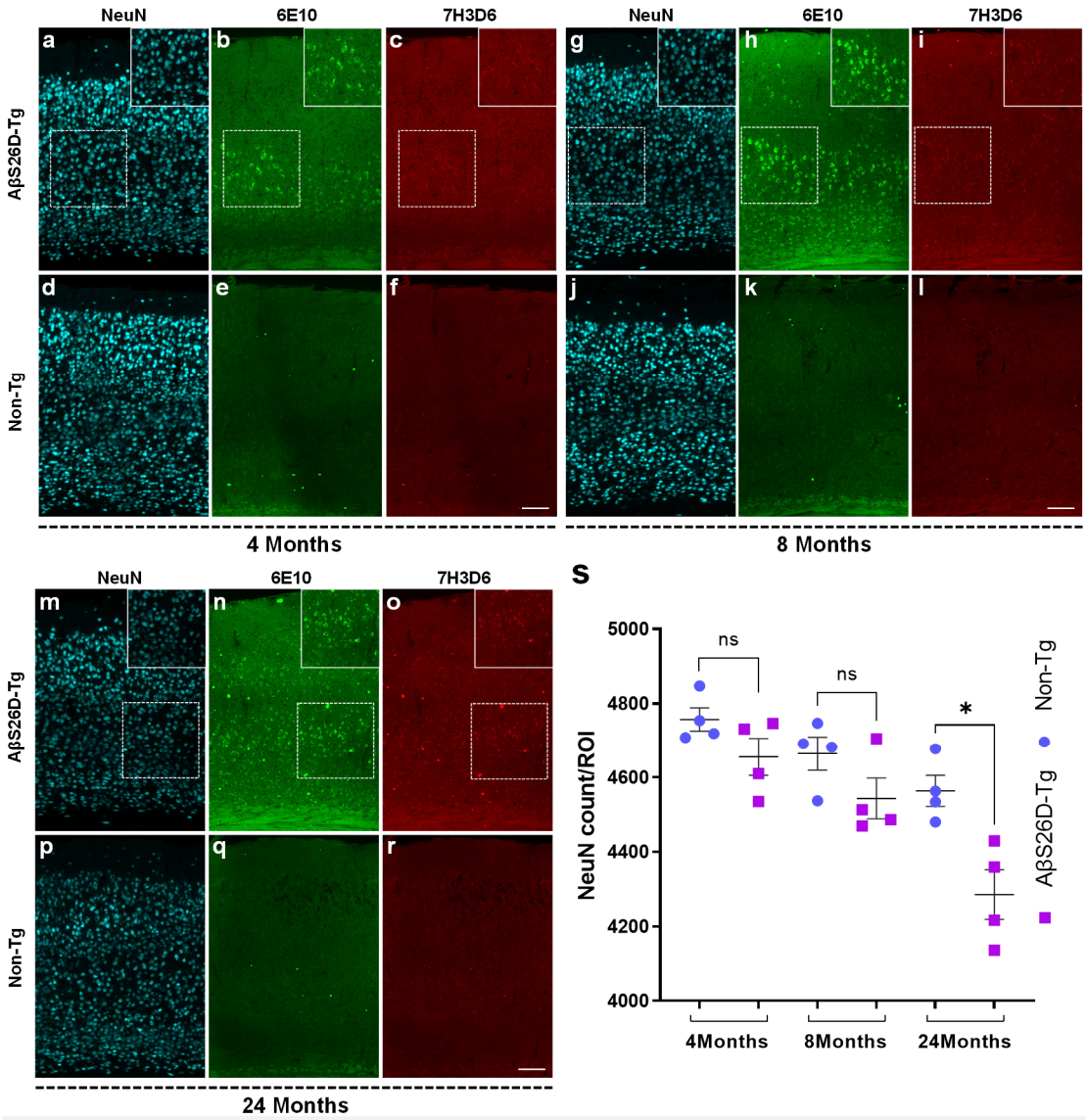

Figure 5.1 | Intraneuronal Aβ accumulation in the cortex of 4M, 8M, and 24M old AβS26D-Tg mice

IF staining of coronal brain sections of male 4M **(a-f)**, 8M **(g-l)**, and 24M **(m-r)** old AβS26D-Tg and non-Tg mice stained with 6E10 (green), 7H3D6 (red), NeuN (cyan) antibodies. Intracellular Aβ accumulation was evident already at 4M of age which is also observed predominantly at 8M of age with a slight decrease in the intraneuronal Aβ reactivity at 24M of age. Immunostaining with the 7H3D6 antibody that specifically recognizes the Aβ peptides confirms the intracellular Aβ deposition. Intracellular Aβ reactivity was observed uniformly distributed inside cells at 4M and 8M of age and many small dots throughout the cell bodies at 24M of age. Non-Tg littermates exhibited no 6E10 and 7H3D6 positive intracellular Aβ staining at 4M, 8M, and 24M of age. Dotted white boxes indicate the area shown at higher magnification (scale bars= 5mm, 10x). **(s)** Dot plots showing quantified cortical neuronal cell counts. For this quantification, the binarized images obtained after automatic thresholding are then processed by watershed segmentation, to separate touching cells, followed by manually checking/counting the cells that were not separated after segmentation. The counting was done automatically using Fiji software and the total number of NeuN positive cells was represented as the sum of all cells in the ROI (45.5x45.5mm) of the cortex counted over three consecutive coronal

sections/animal. Each dot represents the number of NeuN count/animal and dot plots represent mean ± SEM (n=4 animals, unpaired t-test with Welch's correction, $^{ns}p>0.05$, $^{*}p< 0.05$)

Furthermore, co-stainings of the sections with 7H3D6 antibody specifically recognizing the non-modified Aβ peptides also showed intraneuronal deposition of Aβ peptides in a different brain region in these AβS26D-Tg mice at 4M, 8M and 24M of age (Figure 5.1, Figure 5.2 and Table 5.1). The 7H3D6 antibody detects N-terminally unmodified Aβ without detection of APP or APP-CTFs and, confirms the intracellular accumulation of Aβ in the brains of AβS26D-Tg mice and no extracellular amyloid plaques deposition in the cortex (Figure 5.1) and hippocampus (Figure 5.2). Non-Tg littermates show no 6E10 or 7H3D6 positive immunostaining in any of the brain regions examined.

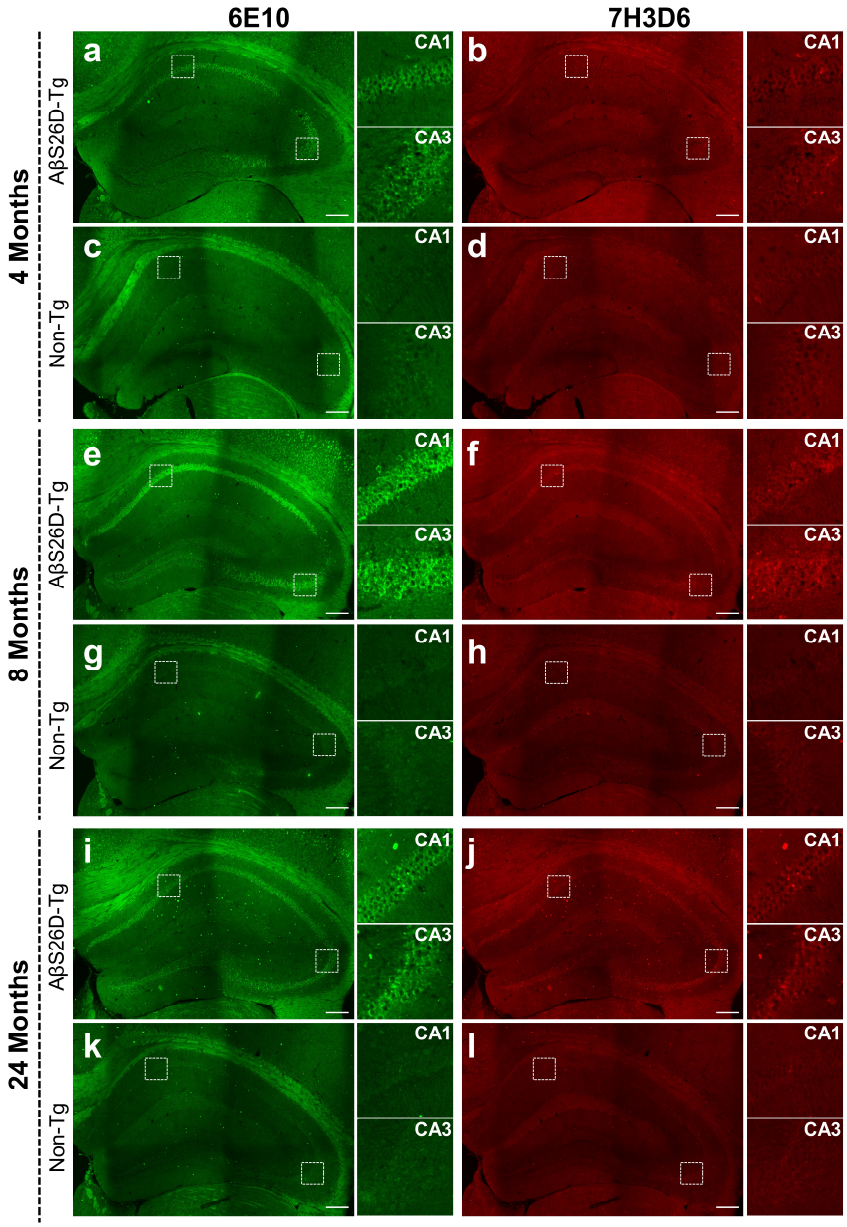

Figure 5.2 | Intraneuronal Aβ accumulation in the hippocampus of 4M, 8M, and 24M old AβS26D-Tg mice

Showing IF staining of coronal brain sections of male **(a-d)** 4M, **(e-h)** 8M, and **(i-l)** 24M month old AβS26D-Tg and non-Tg mice stained with 6E10 (green) and 7H3D6 (red) antibodies. Intracellular Aβ accumulation was evident already at 4M of age which is also observed predominantly at 8M of age with a slight decrease in the intraneuronal Aβ reactivity at 24M of age. Immunostaining with the 7H3D6 antibody that specifically recognizes the Aβ peptides confirm the intracellular Aβ deposition. Intraneuronal Aβ-reactivity was observed in the hippocampal CA1 and CA3 regions already at 4M of age **(a-d)**. At 8M age intraneuronal Aβ dramatically increases in the pyramidal cell layer hippocampal of CA1 and CA3 region **(e-h)**. In 24M old AβS26D-Tg mice, intraneuronal Aβ reactivity was reduced, but Aβ accumulation in and around blood vessels was found to be more abundant **(i-l)**. White boxes indicate the hippocampal CA1 and CA3 areas shown at higher magnification. Non-Tg littermates exhibited no 6E10 and 7H3D6 positive intracellular Aβ staining at 4M, 8M, and 24M of age (scale bars= 10mm, 10x).

At 24 months, AβS26D-Tg mice had a lesser amount of intraneuronal Aβ deposition in the cortex and hippocampus (Figure 5.1). Additionally, diffuse Aβ immunoreactivity was observed along with the molecular layer of the dentate gyrus (DG) together with abundant Aβ accumulation in and around blood vessels at 24 months of age (Figure 5.2). Also, the AβS26D-Tg mice displayed no extracellular amyloid plaque deposits in the cortex and hippocampus. Notably, the 6E10 and 7H3D6 antibodies showed no reactivity in Non-Tg mice (Figure 5.1, Figure 5.2). We noted, however, that the AβS26D-Tg mice exhibited abundant intraneuronal Aβ staining in the cortex and hippocampus (particularly the CA1 and CA3 region) and amygdala. Aβ deposition in vessels and intense intraneuronal accumulation of Aβ were observed in the cortex, hippocampus, striatum, and amygdala (Figure 5.1 and Table 5.1). Intraneuronal Aβ accumulation was strongest in the molecular layers 2 and 5 of the cortex, olfactory areas and hippocampal pyramidal cells in CA1 and CA3 regions (Figure 5.1, Figure 5.2 and Table 5.1). By comparison, deposition of Aβ was relatively weak in CA2 and dentate gyrus (DG) (Figure 5.2). In the cortex, intraneuronal Aβ expressing cells were scattered in all cell layers (Figure 5.1). While in the hippocampal pyramidal cells, Aβ accumulation was observed as many small dots throughout the cell bodies (Figure 5.2). These results suggest that AβS26D peptides are assembled as oligomers and accumulated intracellularly in cell bodies and vessels. Since the reactivity was mostly found in the SDS soluble fractions (immunoblotting data not shown) suggests that the AβS26D-Tg mice may not form amyloid fibrils and instead accumulate intracellularly and in vessels, as has been observed in other APP-Tg mouse models specifically generating oligomeric Aβ species (Tomiyama et al. 2008; Knobloch et al. 2007). The vascular deposition of Aβ was prominently detected with the 7H3D6 antibody in addition to the 6E10 antibody, and female transgenic mice showed a more intense vascular deposition than male transgenic mice. However, a thorough analysis of CAA staging and co-staining with a marker for blood vessels such as Laminin will be required to quantify the observed vascular Aβ deposits.

Next, to check the distribution of microglia in this model, the brain sections were stained with an Iba1 antibody (Schwabe et al. 2020; Keren-Shaul et al. 2017; Butovsky et al. 2018; Zhou et al. 2018) (Figure 5.3). The AβS26D-Tg and non-Tg mice exhibited age-dependent activation of microglia represented by increased Iba1 immunoreactivity. Interestingly, changes in the microglial phenotype were prominent at 24M of AβS26D-Tg as compared to WT mice. Also, no extracellular Aβ plaques in the whole brain but a prominent deposition of Aβ as an intraneuronal and a vascular deposit were observed. The summary of region-specific distribution at 4M, 8M and 24M old male and female AβS26D-Tg is given in Table 5.1.

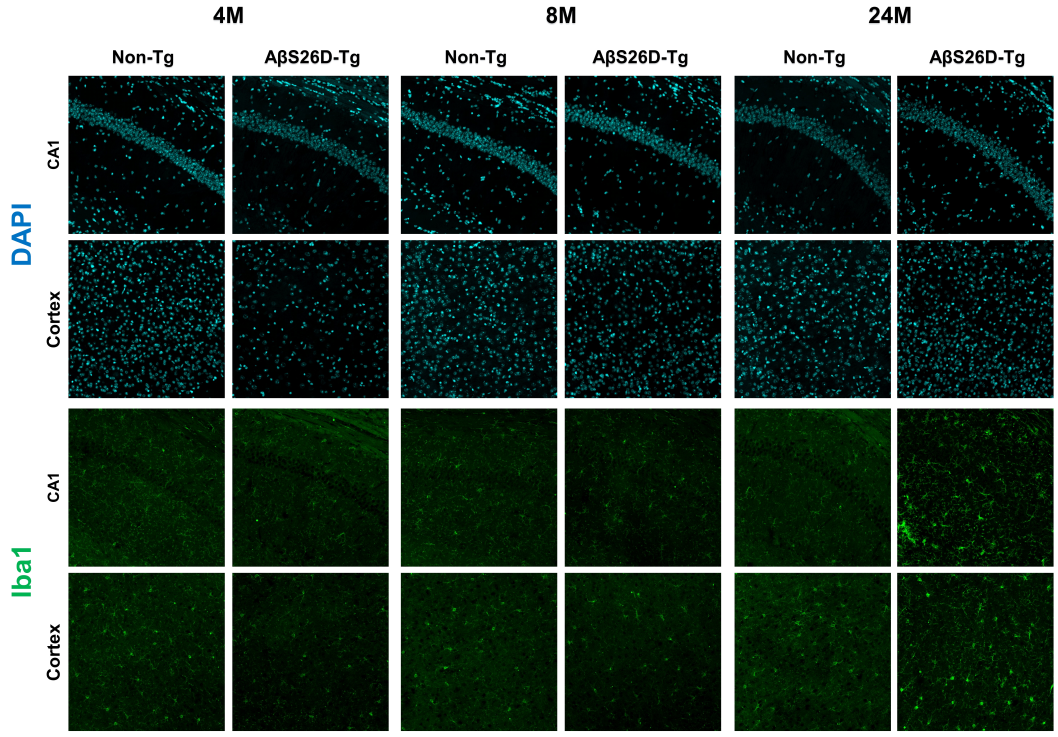

Figure 5.3 | AβS26D-Tg mice show changes in the microglial phenotype at 24M of age

Representative images showing the cortical region of 4M, 8M and 24M old male AβS26D-Tg and non-Tg mice stained with Iba1 (green) antibody counterstained with DAPI (cyan) (scale bar=100µm, 20x).

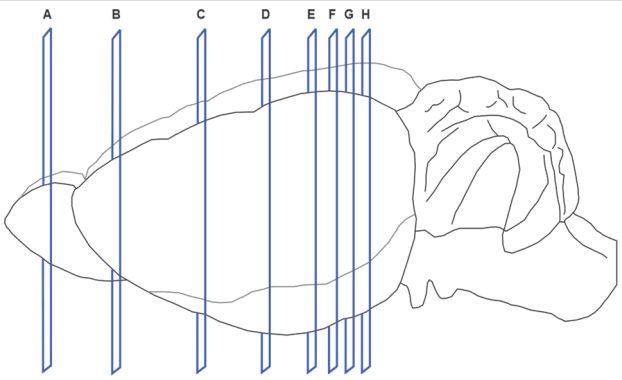

	Section	4M-Male		4M-Female	
		Characteristics	**Region**	**Characteristics**	**Region**
A	**Olfactory bulb**	Intraneuronal deposits of Aβ	Olfactory bulb	Intraneuronal and few	Olfactory bulb

				vascular deposits of Aβ	
B	**Prefrontal cortex (PFC)**	Intraneuronal deposits of Aβ	Prefrontal cortex	Intraneuronal and few vascular deposits of Aβ	Prefrontal cortex
C	**Striatum-Caudoputamen, Nucleus accumbens**	Intraneuronal deposits of Aβ	Cortex	Intraneuronal and few vascular deposits of Aβ	Cortex
D	**Striatum-Lateral ventricle**	Intraneuronal deposits of Aβ	Cortex, Piriform area-pyramidal layer, No Deposits at the SVZ	Intraneuronal and few vascular deposits of Aβ	Cortex, Piriform area-pyramidal layer, striatum (vascular deposits of Aβ), No Deposits at the SVZ
E	**Hippocampus-Start**	Intraneuronal deposits of Aβ	Cortex-Layer 5, Hippocampal CA1 and CA3 pyramidal layer, Piriform area-pyramidal layer, No CA2 pyramidal layer deposits	Intraneuronal and vascular deposits of Aβ	Cortex-Layer 5, Hippocampal CA1 and CA3 pyramidal layer, Piriform area-pyramidal layer, No CA2 pyramidal layer deposits
F	**Hippocampus- Early section**	Intraneuronal deposits of Aβ	Cortex-Layer 5, Hippocampal CA1 and CA3 pyramidal layer, Piriform area-pyramidal layer, Amygdala, No CA2 pyramidal layer deposits	Intraneuronal and vascular deposits of Aβ	Cortex-Layer 5, Hippocampal CA1 and CA3 pyramidal layer, Piriform area-pyramidal layer, Amygdala, No CA2 pyramidal layer deposits
G	**Hippocampus-Middle section**	Intraneuronal deposits of Aβ	Cortex-Layer 5, Hippocampal CA1 and CA3 pyramidal layer Piriform area-pyramidal layer, Amygdala, Subiculum, No CA2 pyramidal layer deposits	Intraneuronal and vascular deposits of Aβ	Cortex-Layer 5, Hippocampal CA1 and CA3 pyramidal layer, Piriform area-pyramidal layer, Amygdala (increased surface area), Subiculum, Retrosplenial cortex, No CA2 pyramidal layer deposits
H	**Hippocampus-Late section**	Intraneuronal deposits of Aβ	Cortex-Layer 5, Hippocampal CA1 and CA3 pyramidal layer- Piriform area, pyramidal & polymorph layer, Subiculum,	Intraneuronal and vascular deposits of Aβ	Cortex-Layer 5, Hippocampal CA1 and CA3 pyramidal layer, , Piriform area-pyramidal & polymorph layer, Subiculum, Retrosplenial cortex,

			No CA2 pyramidal layer deposits		No CA2 pyramidal layer deposits
	Section	**8M-Male**		**8M-Female**	
		Characteristics	**Region**	**Characteristics**	**Region**
A	**Olfactory bulb**	Intraneuronal deposits of Aβ	Olfactory bulb	Intraneuronal and few vascular deposits of Aβ	Olfactory bulb
B	**Prefrontal cortex (PFC)**	Intraneuronal deposits of Aβ	Prefrontal cortex	Intraneuronal and few vascular deposits of Aβ	Prefrontal cortex
C	**Striatum-Caudoputamen, Nucleus accumbens**	Intraneuronal deposits of Aβ	Cortex	Intraneuronal and few vascular deposits of Aβ	Cortex
D	**Striatum-Lateral ventricle**	Intraneuronal deposits of Aβ	Cortex, Piriform area-pyramidal layer, No Deposits at the SVZ	Intraneuronal and few vascular deposits of Aβ	Cortex, Piriform area-pyramidal layer, striatum (vascular deposits of Aβ), No Deposits at the SVZ
E	**Hippocampus-Start**	Intraneuronal deposits of Aβ	Cortex-Layer 5, Hippocampal CA1 and CA3 pyramidal layer, Piriform area-pyramidal layer, No CA2 pyramidal layer deposits	Intraneuronal deposits of Aβ, vascular deposits of Aβ	Cortex-Layer 5, Hippocampal CA1 and CA3 pyramidal layer, Piriform area-pyramidal layer, No CA2 pyramidal layer deposits
F	**Hippocampus- Early section**	Intraneuronal deposits with few vascular deposits (in the cortex) of Aβ	Cortex-Layer 5, Hippocampal CA1 and CA3 pyramidal layer, Piriform area-pyramidal layer, Amygdala, No CA2 pyramidal layer deposits	Intraneuronal and vascular deposits of Aβ	Cortex-Layer 5, Hippocampal CA1 and CA3 pyramidal layer, Piriform area-pyramidal layer, Amygdala, No CA2 pyramidal layer deposits
G	**Hippocampus-Middle section**	Intraneuronal deposits with few vascular deposits (in the cortex) of Aβ	Cortex-Layer 5, Hippocampal CA1 and CA3 pyramidal layer, Piriform area-pyramidal layer, Amygdala, Subiculum, No CA2 pyramidal layer deposits	Intraneuronal and vascular deposits of Aβ	Cortex-Layer 5, Hippocampal CA1 and CA3 pyramidal layer, Piriform area-pyramidal layer, Amygdala (increased surface area), Subiculum, Retrosplenial cortex, No CA2 pyramidal layer deposits

H	**Hippocampus-Late section**	Intraneuronal deposits with few vascular deposits (in the cortex) of Aβ	Cortex-Layer 5, Hippocampal CA1 and CA3 pyramidal layer, Piriform area-pyramidal & polymorph layer, Subiculum, Amygdala, No CA2 pyramidal layer deposits	Intraneuronal and vascular deposits of Aβ	Cortex, Hippocampal CA1 and CA3 pyramidal layer, , Piriform area-pyramidal & polymorph layer, Subiculum, Retrosplenial cortex, No CA2 pyramidal layer deposits
	Section	**24M-Male**		**24M-Female**	
		Characteristics	**Region**	**Characteristics**	**Region**
A	**Olfactory bulb**	Vascular deposits of Aβ	Olfactory bulb	Vascular deposits of Aβ	Olfactory bulb
B	**Prefrontal cortex (PFC)**	Intraneuronal deposits of Aβ	Prefrontal cortex	Intraneuronal and vascular deposits of Aβ	Prefrontal cortex
C	**Striatum-Caudoputamen, Nucleus accumbens**	Intraneuronal deposits of Aβ	Cortex	Intraneuronal and vascular deposits of Aβ	Cortex
D	**Striatum-Lateral ventricle**	Intraneuronal and vascular deposits of Aβ	Cortex, Piriform area-pyramidal layer, No Deposits at the SVZ	Intraneuronal and vascular deposits of Aβ	Cortex, Piriform area-pyramidal layer, No Deposits at the SVZ
E	**Hippocampus-Start**	Intraneuronal deposits of Aβ, Vascular deposits of Aβ	Cortex-Layer 5, Hippocampal CA1 and CA3 pyramidal layer, Piriform area-pyramidal layer, No CA2 pyramidal layer deposits	Intraneuronal deposits of Aβ, Vascular deposits of Aβ	Cortex-Layer 5, Hippocampal CA1 and CA3 pyramidal layer, Piriform area-pyramidal layer, No CA2 pyramidal layer deposits
F	**Hippocampus- Early section**	Intraneuronal and Vascular deposits of Aβ	Cortex-Layer 5 (few in layer 2/3), Hippocampal CA1 and CA3 pyramidal layer, Piriform area-pyramidal layer, No CA2 pyramidal layer deposits	Intraneuronal and Vascular deposits of Aβ	Cortex-Layer 5, Hippocampal CA1 and CA3 pyramidal layer, Piriform area-pyramidal layer, No CA2 pyramidal layer deposits
G	**Hippocampus-Middle section**	Intraneuronal deposits of Aβ, Vascular deposits of Aβ in the cortex	Cortex-Layer 5 (few in cortex layer 2/3), Hippocampal CA1	Intraneuronal and vascular deposits of Aβ in the cortex & hippocampus	Cortex-Layer 5, few in cortex layer 2/3 intraneuronal deposits, Hippocampal

			and CA3 pyramidal layer Piriform area-pyramidal layer, Amygdala, Subiculum, No CA2 pyramidal layer deposits		CA1 and CA3 pyramidal layer Piriform area-pyramidal layer, Amygdala, (increased surface area), Subiculum, Retrosplenial cortex, No CA2 pyramidal layer deposits
H	**Hippocampus-Late section**	Intraneuronal deposits of Aβ, Vascular deposits of Aβ in the cortex.	Cortex-Layer 5 & layer 2/3, Hippocampal CA1 and CA3 pyramidal layer, Piriform area-pyramidal & polymorph layer, Amygdala, Subiculum, Retrosplenial cortex, No CA2 pyramidal layer deposits	Intraneuronal and Vascular deposits of Aβ in the cortex, hippocampus.	Cortex-Layer 5, Layer 2/3, Hippocampal CA1 and CA3 pyramidal layer Piriform area-pyramidal & polymorph layer, Amygdala (increased surface area), Subiculum, Retrosplenial cortex, No CA2 pyramidal layer deposits

Table 5.1 | Region-specific distribution of Aβ at different ages of male and female AβS26D-Tg mice

5.2 | AβS26D-Tg mice did not show a change in the exploratory behaviour as compared to non-transgenic mice in the Open field test (OFT)

Aβ oligomers have been demonstrated to cause synaptic and cognitive dysfunction (Oddo et al. 2003; Shankar et al. 2008). To determine whether the AβS26D-Tg mice develop behavioural deficits in exploration, motor activity and working memory, cognitive function was examined at 24 months of age in a spontaneous motor activity task (open-field test) followed by a spatial learning test (Morris water maze) (Figure 5.4a).

The locomotor/exploratory activity was assessed in an open field for 20 min and it was found that there was no significant difference in total distance travelled in the arena, velocity in the arena and the time spent in the centre between non-Tg and AβS26D-Tg mice with both male and female mice (Figure 5.4b-c, male and female). This indicates that general locomotor activity and exploratory behaviour were intact in 24M old AβS26D-Tg mice.

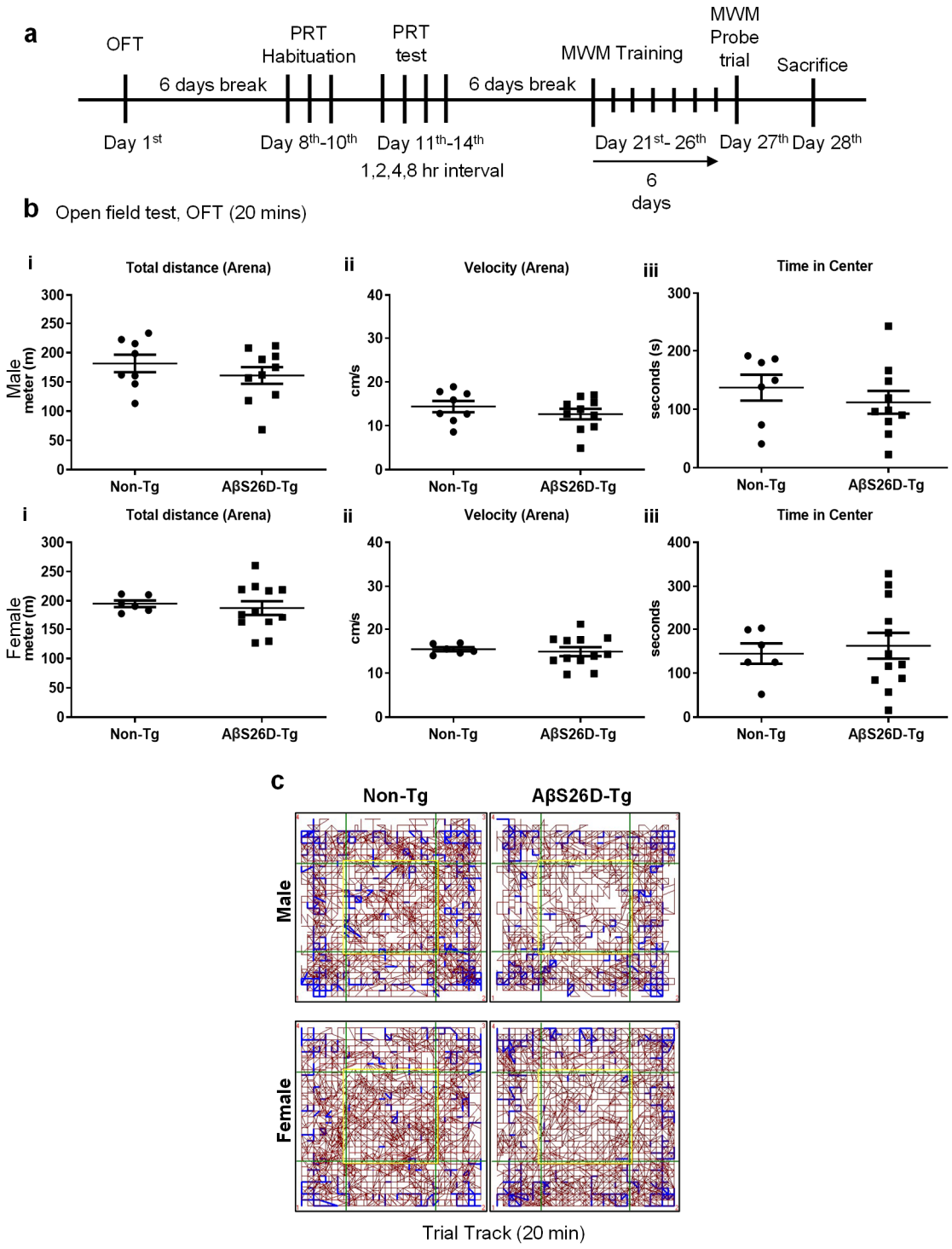

Figure 5.4 | No change in the locomotion as well as anxiety phenotype at 24M of male and female AβS26D-Tg mice in the OFT

(a) Schematic representation of the experimental design. **(b)** Upper panel: showing total distance (arena), velocity (arena), and time (centre) in male mice for 20 min of OFT. Lower panel: showing total distance (arena), velocity (arena), and time (centre) in female mice. The data is represented as mean±SEM (males (n=8-10) and females (n=6-12) per group, two-tailed unpaired student's t-test). **(c)** Representative track profile of mouse movement during 20 min of acquisition during OFT.

5.3 | Social recognition was not impaired in AβS26D-Tg mice as compared to non-Tg mice

The partner recognition test (PRT) was performed to check the impairment of social recognition associated with long-term memory.

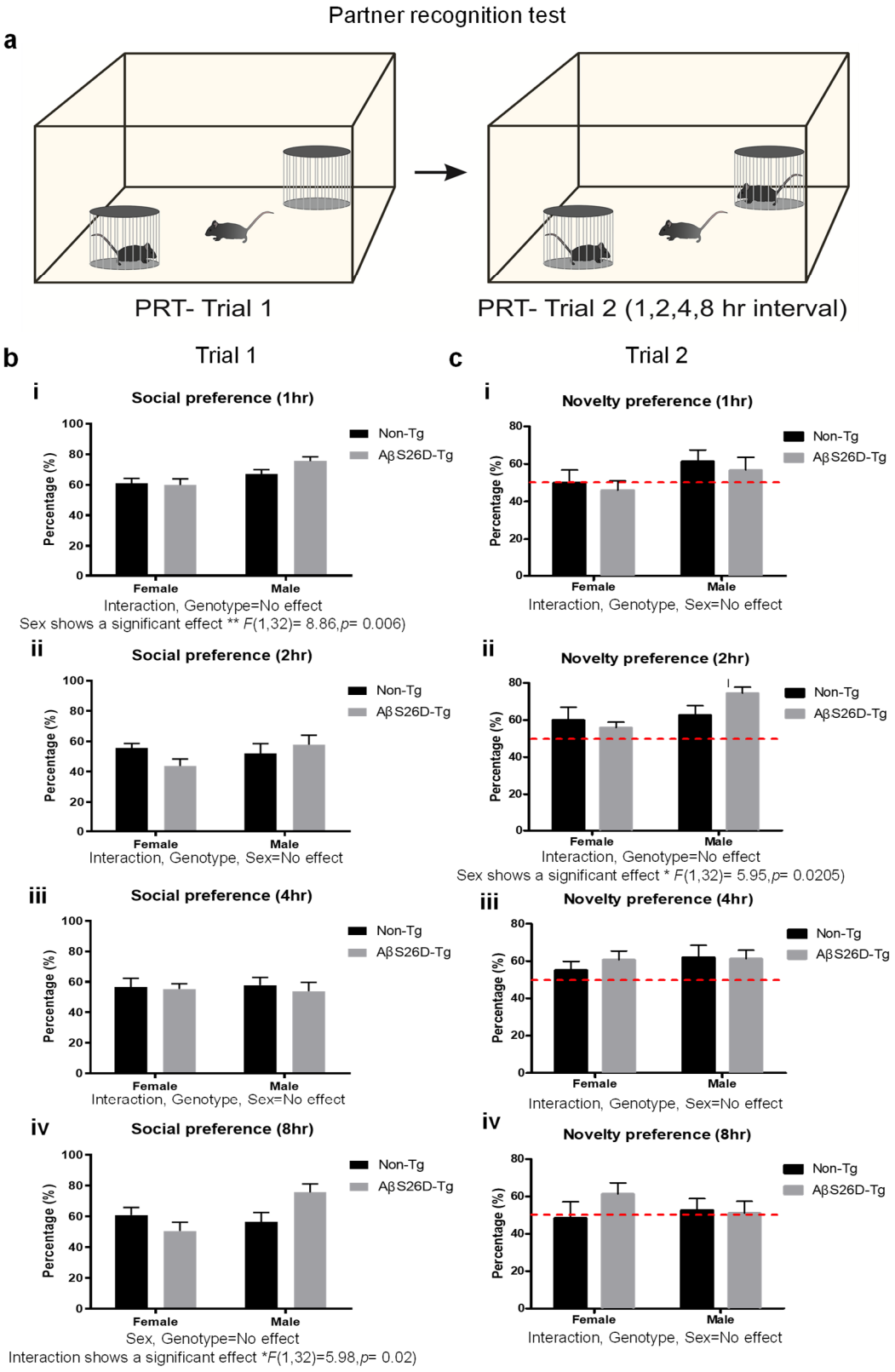

Figure 5.5 | Social recognition was not impaired at 24M of male and female AβS26D-Tg mice in partner recognition test (PRT)

No change in the percent social preference and novelty preference as well as impairment in the recognition memory after 4 h interval time in male and female AβS26D-Tg mice compared to non-Tg mice, while females showed poor performance in PRT irrespective of genotype. **(a)** Showing schematic representation of PRT test (trial 1 and trial 2 with 4 intervals). **(b)** Showing column graphs of percent social preference at **1 h** (i, Interaction- $F(1,32)=1.71$,$p=0.20$; genotype- $F(1,32)=1.0$,$p=0.32$; sex- $F(1,32)=8.86$,$p=0.005$) , **2 h** (ii, Interaction- $F(1,32) = 2.34$,$p=0.14$; genotype- $F(1, 32)=0.24$,$p=0.63$; sex- $F(1,32)=0.83$,$p=0.39$), **4 h** (iii, Interaction- $F(1,32)= 0.072$,$p=0.79$; genotype- $F(1,32)=0.26$,$p=0.614$; sex- $F(1,32)= 0.00028$,$p=0.987$) and **8 h** (iv, Interaction- $F(1,32)=5.984$, $p=0.020$; genotype- $F(1,32)=0.54$,$p=0.47$; sex- $F(1,32)=2.91$,$p=0.098$). In trial 1 we could see effect in sex only at 1 h and interaction only at 8 h while no change in genotype and at other time intervals. **(c)** Showing column graphs of percent novelty preference **1 h** (i, Interaction- $F(1,31)=0.003$,$p=0.9502$; genotype- $F(1,31)=0.44$,$p= 0.5141$;sex- $F(1,31)= 2.95$,$p= 0.0961$), **2 h** (ii, Interaction- $F(1,32)=3.32$,$p=0.0777$; genotype-$F(1,32)=0.80$,$p= 0.3767$;sex- $F(1,32)= 5.95$,$p= 0.0205$), **4 h** (iii, Interaction- $F(1,31)= 0.35$,$p= 0.5610$; genotype- $F(1,31)= 0.21$,$p= 0.6475$;sex- $F(1,31)= 0.49$,$p= 0.4872$) and **8 h** (iv, Interaction- $F(1,33)= 1.13$,$p= 0.2953$; genotype- $F(1,33)= 0.70$,$p= 0.4073$;sex- $F(1,33)= 0.21$,$p= 0.6530$). The data is represented as mean±SEM (males (n=8-10) and females (n=6-12) per group, two-way ANOVA (Sidak multiple comparison tests)). Here, a significant increase in the percent novelty preference was observed in males as compared to females at 2 h time interval and not at other time intervals.

PRT relies on the animal's innate tendency to explore a novel social partner and decreases the exploration of a known familiar social partner (Bilkei-Gorzo et al. 2005). In other words, if the mice remember the previous partner from the first session of the test then mice will show a high preference represented by time spent by the mice in the vicinity of a new partner. On the contrary, if there is an impairment in the recognition memory then mice will show no discrimination between previous and novel partners (refer to section 2.5.2 and Figure 5.5a). PRT was carried out at four different interval time points (1, 2, 4, 8h) it was found that no prominent differences between the genotypes in terms of percent social preference in trial 1 (Figure 5.5b) and percent novelty preference in trial 2 (Figure 5.5c) at all time intervals. In trial 1, it was observed a significant effect on sex only at 1 h but no genotype effect and the interaction between both the genotypes of male and female mice at 1h, 2h and 4 h time intervals. While at 8 h intervals a significant effect in the interaction was observed. Similarly, in trial 2, a significant effect was observed between sex only at 2 h time intervals but no change in interaction, sex, and genotype at all other time points. A general observation is that the females (both genotypes) showed poor performance in this test compared to males.

5.4 | AβS26D-Tg mice showed impairment in the spatial memory as compared to non-transgenic mice in the MWM test

Next, the cognitive function was examined by using the Morris water maze (MWM) test. MWM test is used for assessing spatial learning and reference memory (Wahul et al. 2018;

Vorhees et al. 2006). It is a spatial learning test for rodents that uses distal cues to navigate from start locations around the perimeter of an open swimming arena to a submerged escape platform (Vorhees et al. 2006). MWM test was performed that started with 6 days of training followed by a probe trial (Figure 5.4a). During the first 6 days of training, mice remembered the location of a hidden platform in the water maze, and the time required to reach the platform called an escape latency was measured in every trial. No significant change was observed in the total distance, velocity and escape latency (Figure 5.6 a-b, male and female) during the training period of MWM in both sex and genotypes.

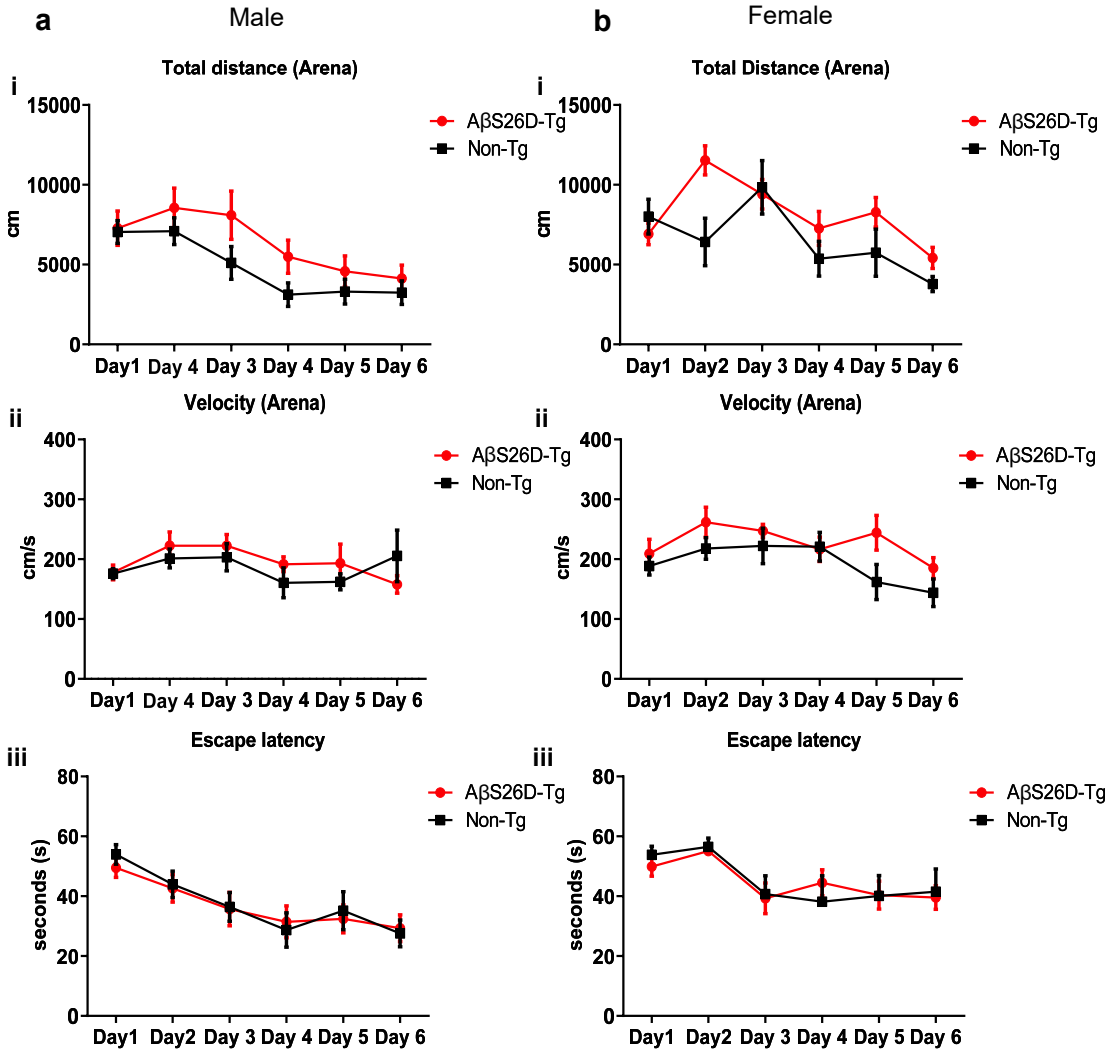

Figure 5.6 | No change in the spatial learning at 24M of male and female AβS26D-Tg mice in the MWM training

No significant difference in spatial learning was assessed by the escape latency between the sex and genotypes during MWM training. **(a)** Line graph showing total distance, velocity and escape latency plots during the 6 days of training in 24M old male AβS26D-Tg mice. **(b)** Line graph showing total distance, velocity and escape latency plots during the 6 days of training in 24M old female AβS26D-Tg mice. The data is represented as mean±SEM (males (n=8-10) and females (n=6-12) per group, two-tailed unpaired student's t-test).

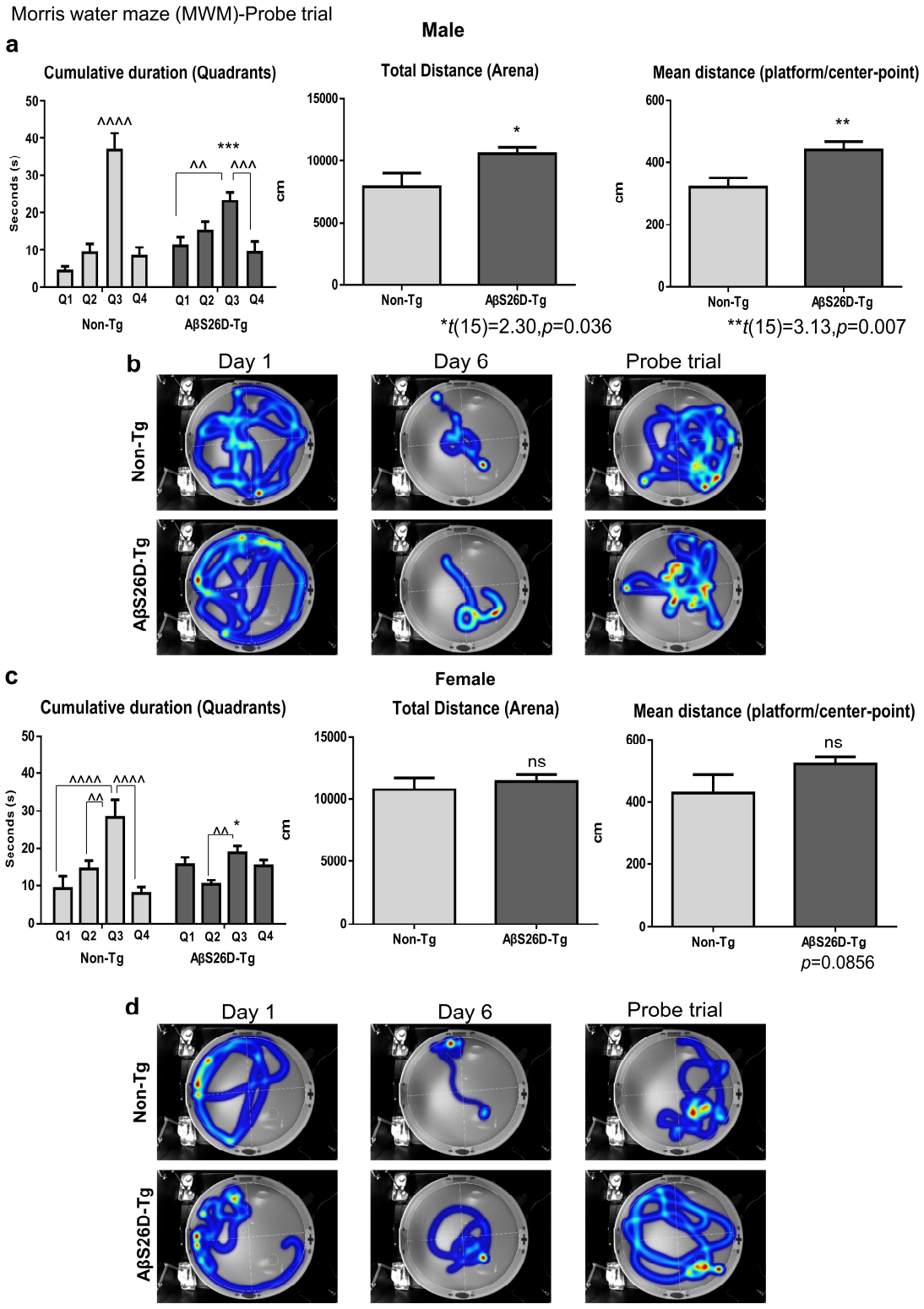

Figure 5.7 | Memory impairment in the male and female AβS26D-Tg mice in MWM probe trial.

(a) Showing cumulative duration (target quadrant of AβS26D-Tg compared with non-Tg), total distance- t(15)=2.30,p=0.036, and mean distance- t(15)=3.13,p=0.007 in MWM probe trial with male AβS26D-Tg and non-Tg mice. The data is represented as mean±SEM, (males (n=8-10) and females (n=6-12) per group, ***p=0.0005 ^^p=0.0020, ^^^p=0.0003, ^^^^p<0.0001) **(b)** Representative images of heatmaps (right panel) of mouse movement during the day 1st day, 6th day of acquisition, and probe trial of male

AβS26D-Tg and non-Tg mice. The heatmaps represent the cumulated merging in which the colour of the pixel represents the total time spent by the mice at that location. **(c)** Showing cumulative duration (target quadrant of AβS26D-Tg compared with non-Tg), total distance- t(16)=0.66,*p*=0.52, and mean distance- t(16)=1.832,*p*=0.086 in MWM probe trial test with female AβS26D-Tg and non-Tg mice. The data is represented as mean±SEM, (males (n=8-10) and females (n=6-12) per group, **p*=0.0194, ^*p*=0.0013 (Non-Tg), ^^*p*=0.0057 (AβS26D-Tg), ^^^^*p*<0.0001 and ns=non-significant). **(d)** Representative images of heatmaps (right panel) of mouse movement during the day 1st day, 6th day of acquisition, and probe trial of female AβS26D-Tg and non-Tg mice. The heatmaps represent the cumulated merging in which the colour of the pixel represents the total time spent by the mice at that location (*represents the comparison between genotypes carried out by two-way ANOVA, Sidak multiple comparison test and ^ represents the comparison within genotypes and analyzed by two-way ANOVA (Sidak multiple comparison test))

However, during the probe trial, there was a significant decrease in the total cumulative duration in the target quadrants by AβS26D-Tg mice as compared to non-Tg in males as well as females (Figure 5.7a&c). In addition to this, male AβS26D-Tg mice could still recall the target quadrant, shown by increased total cumulative duration in the target quadrants compared with other quadrants compared within the group while in females, failure to recall the target quadrant was observed compared to males. A significant increase in the total distance and the mean distance (platform/centre point) was observed in male AβS26D-Tg mice compared to non-Tg mice (Figure 5.7a-b). Moreover, female AβS26D-Tg mice showed no change in total distance and mean distance (platform/centre point) compared to non-Tg mice (Figure 5.7c-d). In summary, the AβS26D-Tg mice exhibited cognitive dysfunction in association with intraneuronal accumulation of Aβ oligomers and neuronal loss at 24M of age, but in the absence of extracellular plaques. These features indicate that the AβS26D-Tg mouse is a suitable model for the investigation of Aβ oligomer induced changes in the brain without the Aβ plaques even at old ages.

Chapter 6 | TREM2 modulates differential deposition of modified and non-modified Aβ species in extracellular plaques and intraneuronal deposits

A significant portion of this chapter is published in Acta Neuropathologica Communications, 2021 (Appendix-2)

***Authors: Pranav Joshi**, Florian Riffel, Sathish Kumar, Nàdia Villacampa, Sandra Theil, Samira Parhizkar, Christian Haass, Marco Colonna, Michael T. Heneka, Thomas Arzberger, Jochen Herms and Jochen Walter.*[‡]

Brief introduction: *Progressive accumulation of Amyloid-β (Aβ) deposits in the brain is a characteristic neuropathological hallmark of Alzheimer's disease (AD). During disease progression, extracellular Aβ plaques undergo specific changes in their composition by the sequential deposition of different modified Aβ species. Microglia are implicated in the restriction of amyloid deposits and play a major role in the internalization and degradation of Aβ. Recent studies showed that rare variants of the Triggering Receptor Expressed on Myeloid cells 2 (TREM2) are associated with an increased risk for AD. Post-translational modifications of Aβ could modulate the interaction with TREM2 and the uptake by microglia. Here, it is shown that genetic deletion of TREM2 or expression of a disease-associated TREM2 variant in mice leads to differential accumulation of modified and non-modified Aβ species in extracellular plaques and intraneuronal deposits. Human brains with rare TREM2 AD risk variants also showed altered deposition of modified Aβ species in the different brain lesions as compared to cases with the common variant of TREM2. These findings indicate that TREM2 plays a critical role in the development and the composition of Aβ deposits, not only in extracellular plaques but also intraneuronally, that both could contribute to the pathogenesis of AD*[*] *(Joshi et al. 2021a).*

6.1 | Selective accumulation of Ser8-phosphorylated Aβ species upon loss of TREM2 function in brains of transgenic mice

Phosphorylated Aβ variants were previously detected in brains of transgenic mouse models and human AD cases shown to exert increased toxicity in Drosophila models and human[*]

[‡] *Author contributions: Pranav Joshi and Jochen Walter conceived the study. Pranav Joshi performed most of the experiments and analyzed data. Sathish Kumar, Florian Riffel, and Sandra Theil contributed to biochemical and immunohistochemical experiments and interpretation. Samira Parhizkar, Christian Haass, Marco Colonna, Nàdia Villacampa, and Michael T. Heneka provided mouse brains. Pranav Joshi, Thomas Arzberger and Jochen Herms selected and analyzed human brains. Pranav Joshi and Jochen Walter wrote the manuscript with help all co-authors. All of the authors read, edited and approved the final version of the manuscript.*

[*] *Italicized text is taken from the manuscript published in Acta neuropathologica communications by Joshi et al. 2021*

neurons derived from the embryonic stem or induced pluripotent stem cells (Gerth et al. 2018; Gouras et al. 2005; Kumar et al. 2016; Kumar et al. 2013; Rijal Upadhaya et al. 2014). To assess the role of TREM2 in the deposition of modified Aβ species in-vivo, 5xFAD transgenic mice were crossed with TREM2$^{+/+}$ or TREM2$^{-/-}$ mice as described previously (Joshi et al. 2021b; Parhizkar et al. 2019) (Table 6.1), and the deposition of different Aβ species was analyzed using several antibodies selectively detecting modified and non-modified variants of Aβ. Monoclonal antibody 1E4E11 specifically detects pSer8-Aβ species, while monoclonal antibody 7H3D6 selectively recognizes Aβ with Ser8 in a non-phosphorylated state. Antibody 7H3D6 also does not recognize other Aβ variants with N-terminal modifications, including pyroglutaminated, nitrated, and N-terminally truncated Aβ species (Kumar et al. 2013)[*].

Sr. No.	Transgenic mouse models	Age (months)	Sex	Genotype	No. of animals (n)		Total number of Aβ plaques/ROI stained with various antibodies														
							Somatosensory cortex (SSC)					Retrosplenialcortex (RSC)					Dentate gyrus (DG)				
							pSer8-Aβ	N3p3-Aβ	nmAβ	Aβ (4G8)	Aβ (2964)	pSer8-Aβ	N3p3-Aβ	nmAβ	Aβ (4G8)	Aβ (2964)	pSer8-Aβ	N3p3-Aβ	nmAβ	Aβ (4G8)	Aβ (2964)
1	5xFAD	5 M	Male	TREM2$^{+/+}$	5	Total plaque count/group	1117	1664	1791	1847	1842	1353	1770	1724	1777	1815	933	1263	1932	1872	1857
						Plaque load (%)	2.89	8.11	10.91	11.42	11.46	4.35	7.49	7.70	9.27	8.52	2.89	5.12	8.76	8.98	8.93
				TREM2$^{-/-}$	5	Total plaque count/group	1631	1836	2247	2314	2305	1734	1899	2120	2169	2198	1257	1403	2258	2196	2183
						Plaque load (%)	9.53	10.80	17.90	19.08	17.49	7.66	9.29	13.82	14.41	14.45	5.27	6.94	13.56	14.29	14.22
		15 M	Male	TREM2$^{+/+}$	5	Total plaque count/group	1565	2322	3616	3725	3833	2057	2559	3641	3802	3778	1530	2535	3426	3537	3461
						Plaque load (%)	4.59	17.26	27.31	28.10	29.38	7.09	13.19	25.04	25.84	26.41	5.49	10.24	21.40	21.51	21.00
				TREM2$^{-/-}$	5	Total plaque count/group	2250	3013	4414	4417	4523	2846	3285	4398	4520	4488	2153	3139	4033	4144	4096
						Plaque load (%)	13.06	23.76	41.46	41.37	42.44	15.73	21.93	32.66	35.63	33.95	10.99	16.07	32.16	32.39	31.95
2	APP/PS1L166P	4 M	Male	TREM2$^{+/+}$	5	Total plaque count/group	422	n.d.	1027	967	982	420	n.d.	852	892	917	245	n.d.	626	760	776
						Plaque load (%)	1.93	n.d.	5.51	4.96	5.25	2.46	n.d.	5.59	6.52	6.62	1.35	n.d.	4.14	5.03	4.63
				TREM2$^{-/-}$	5	Total plaque count/group	607	n.d.	1215	1156	1193	631	n.d.	1062	1115	1132	446	n.d.	845	957	988
						Plaque load (%)	2.93	n.d.	8.19	9.03	9.88	4.09	n.d.	7.64	9.14	9.18	2.46	n.d.	6.57	7.01	7.63
		12 M	Female	TREM2$^{+/+}$	5	Total plaque count/group	804	1935	4003	4090	3959	942	2096	3776	4050	3943	649	1584	2437	2482	2485
						Plaque load (%)	4.81	14.99	28.03	27.91	26.88	6.57	15.42	30.03	32.66	32.23	3.83	9.56	17.92	17.82	15.41
				TREM2$^{-/-}$	5	Total plaque count/group	1424	2545	4655	4770	4571	1391	2562	4226	4518	4398	972	1951	2766	2835	2835
						Plaque load (%)	9.94	21.24	39.43	41.24	40.67	13.65	21.88	47.34	47.87	47.04	7.12	12.86	24.29	22.81	25.31
3	APP/PS1ΔE9	12 M	Female	TREM2	3	Total plaque count/group	491	1068	2044	2233	2331	414	889	1489	1785	1685	183	548	717	874	965
						Plaque load (%)	4.09	12.58	30.05	30.40	35.16	3.21	11.29	21.13	24.68	23.77	1.87	6.58	9.13	12.23	13.03
				TREM2^{T66M}	3	Total plaque count/group	757	1397	2570	2581	2605	735	1349	1975	2073	2060	255	770	1001	1119	1086
						Plaque load (%)	8.02	18.63	39.91	39.44	41.83	7.36	18.89	30.25	31.31	33.08	3.37	12.10	14.19	16.75	15.94

Table 6.1 | Details of transgenic mouse models and quantification of Aβ plaque pathology
n.d.-not detected, ROI-Region of Interest (Joshi et al. 2021a)

Triple staining with mouse monoclonal 1E4E11, rat monoclonal 7H3D6 and rabbit polyclonal 2964 antibodies revealed that TREM2$^{-/-}$ mice at 15 months (15 M) of age had significantly more plaques detected by all three antibodies. Elevated plaque deposition, as measured by[*] the plaque number (Figure 6.1a-b, Figure 6.2 and plaque load (Table 6.1), was detected in the

[*]*Italicized text is taken from the manuscript published in Acta neuropathologica communications by Joshi et al. 2021*

three different brain regions analyzed, the somatosensory cortex (SSC), the retrosplenial cortex (RSC), and the dentate gyrus (DG). Consistent with a preferential deposition in the core of plaques, pSer8-Aβ positive deposits are of smaller size than those containing nmAβ that is also deposited in the corona of plaques (Figure 6.1c, Figure 6.4)[*].*

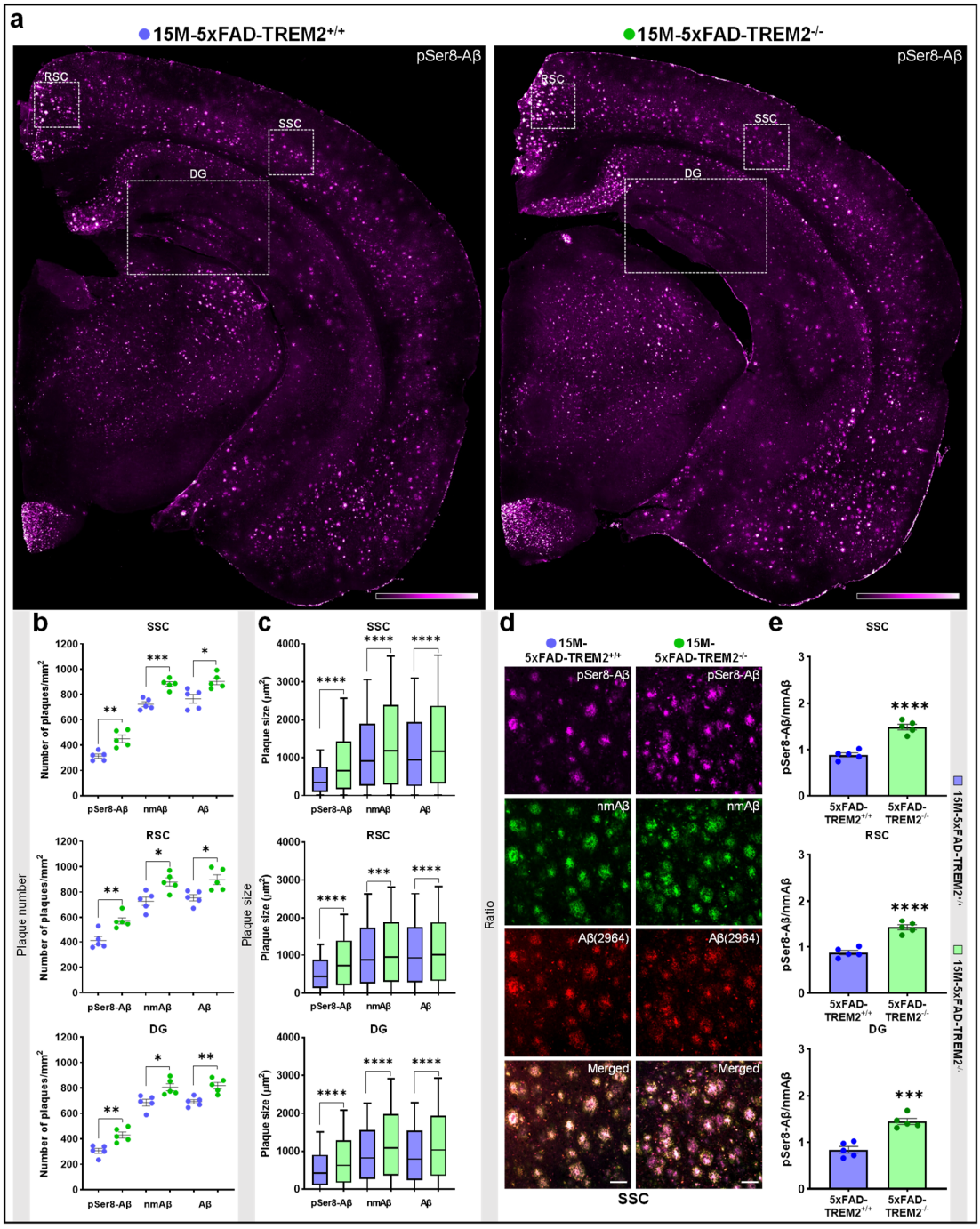

Figure 6.1 | TREM2 deletion leads to increased deposition of pSer8-Aβ in 15M old 5xFAD transgenic mouse brains

(a) Representative pSer8-Aβ stained male 15 M old-5xFAD-TREM2$^{+/+}$ and TREM2$^{-/-}$ mouse brain sections (color scale bar = 35 mm, represents min/max pixel intensities, 10x). **(b)** Dot plots representing

[*] *Italicized text is taken from the manuscript published in Acta neuropathologica communications by Joshi et al. 2021*

number of plaques/mm2, **(c)** Box and whiskers plots showing plaque size (µm^2) stained with pSer8-Aβ, nmAβ and Aβ (2964) antibodies in the SSC, RSC, and DG of male 15 M-5xFAD-TREM2$^{-/-}$ and TREM2$^{+/+}$ mice. **(d)** Representative images showing deposition of pSer8-Aβ, nmAβ, and Aβ (2964) in SSC of male 15 M-5xFAD-TREM2$^{-/-}$ and TREM2$^{+/+}$ mice (scale bar = 50 µm, 40xW). **(e)** Ratios of pSer8/nmAβ in SSC (t(7.41) = 7.856,****p < 0.0001), RSC (t(7.696) = 7.611,****p < 0.0001), and DG (t(7.945) = 6.345,***p = 0.0002) of male 15 M-5xFAD-TREM2$^{-/-}$ compared with TREM2$^{+/+}$ mice. Each dot represents an average value of the number of plaques or the ratio of pSer8-Aβ/nmAβ per animal. The box and whiskers plots represent min/max values of distribution of plaque size with the median (shown by the line dividing the box) and the dot plots represent mean ± SEM (n = 5 animals, color- blue (5xFAD-TREM2$^{+/+}$) and green (5xFAD-TREM2$^{-/-}$), unpaired t-test with Welch's correction for analysis of the number and ratio while Mann-Whitney test for plaque size, ^{ns}p > 0.05, *p < 0.05, **p < 0.01, ***p < 0.001 or ****p < 0.0001) (Joshi et al. 2021a).

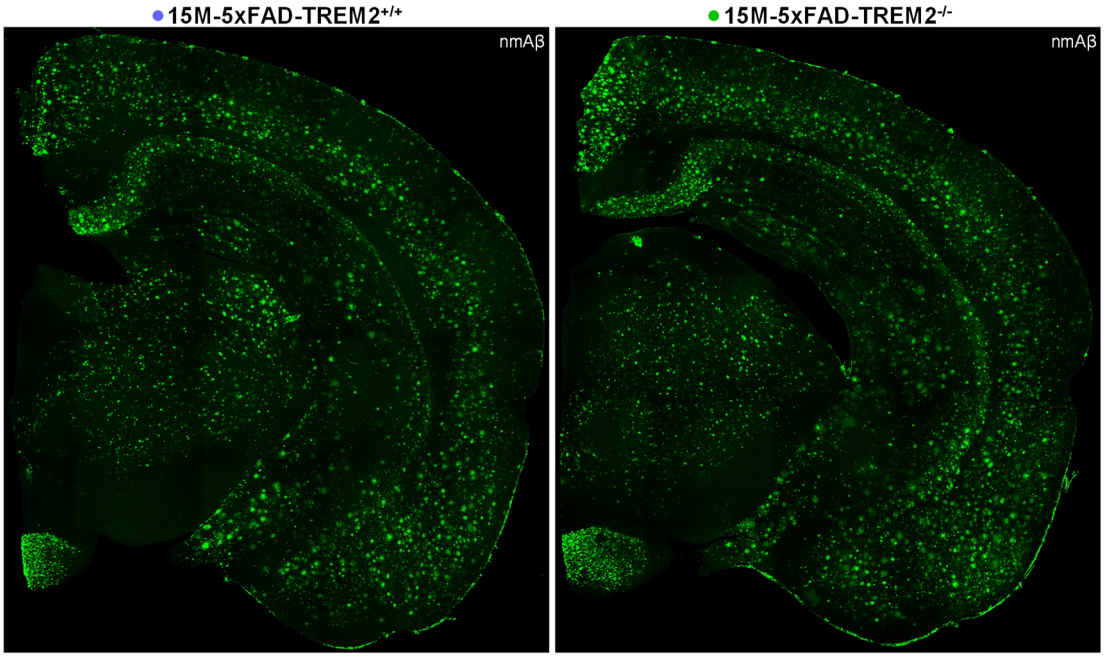

Figure 6.2 | TREM2 deletion leads to increased deposition of Aβ in 5xFAD transgenic mouse brains
Representative nmAβ stained male 15M-5xFAD-TREM2$^{+/+}$ and TREM2$^{-/-}$ mouse brain sections (color scale bar=35mm,10x) (Joshi et al. 2021a).

These findings are consistent with the function of TREM2 to restrict plaque size or growth (Wang et al. 2015; Yuan et al. 2016), and also demonstrate the importance of TREM2 to limit the accumulation of pSer8-Aβ in the core of plaques (Joshi et al. 2021a). A selective increase in pSer8-Aβ was detected by analyzing the mean fluorescence signal intensities within Aβ deposits (Figure 6.1d-e)[*] (Joshi et al. 2021a).

Furthermore, increased number and size of pSer8-Aβ and nmAβ positive plaques in 5xFAD TREM2$^{-/-}$ compared to TREM2$^{+/+}$ mouse brains were already observed in 5 M old mice (Figure

[*] *Italicized text is taken from the manuscript published in Acta neuropathologica communications by Joshi et al. 2021*

6.3a-b, Figure 6.4d-f). Analysis of plaque size distribution at both ages revealed overall[*] increased numbers of deposits of various sizes in all three analyzed brain regions of TREM2$^{-/-}$ mice (Figure 6.4). In particular, the number of deposits > 1200 µm^2 that are also positive for pSer8-Aß were strongly increased in TREM2$^{-/-}$ mice already at 5 M of age, suggesting that TREM2 decreases the formation and growth of plaques already at the early stages of deposition. However, the ratio of the mean fluorescence intensity for pSer8-Aß and nmAß was similar in TREM2$^{-/-}$ and TREM2$^{+/+}$ at this young age (Figure 6.3c-d), indicating that TREM2 deficiency promotes co-deposition of different Aß species[*](Joshi et al. 2021a).

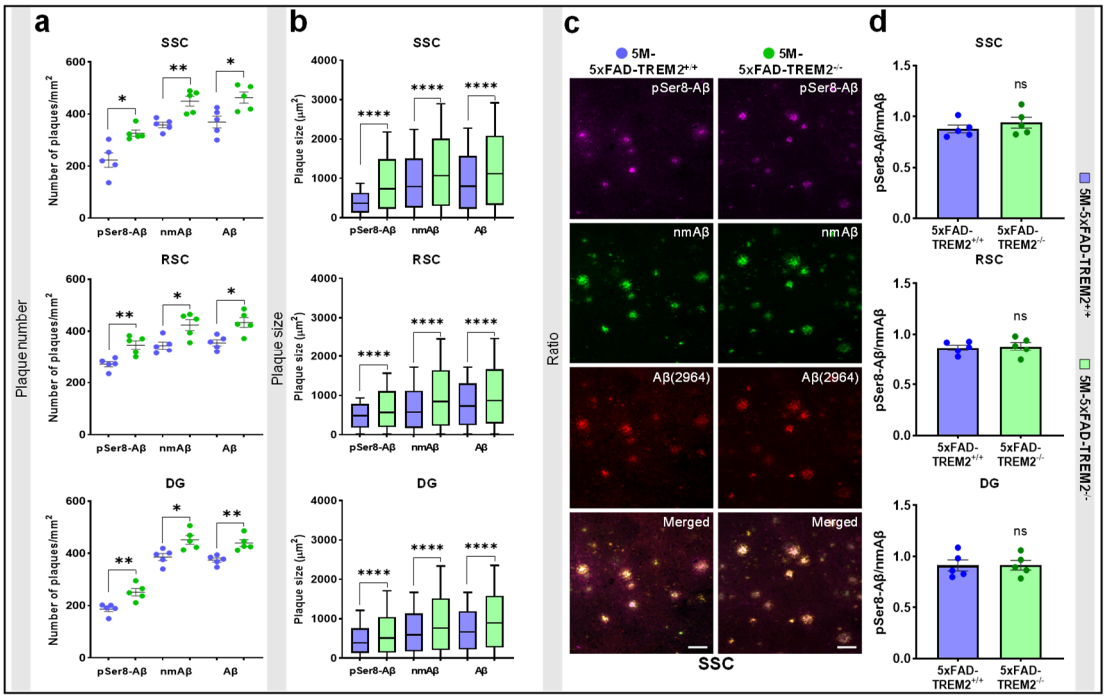

Figure 6.3 | TREM2 deletion leads to increased deposition of pSer8-Aβ in 5M old 5xFAD transgenic mouse brains

(a) Dot plots representing the increased number of plaques/mm^2, **(b)** Box and whiskers plots representing increased plaque size (µm^2) stained with pSer8-Aβ, nmAβ and Aβ (2964) antibodies in the SSC, RSC, and DG of male 5M-5xFAD-TREM2$^{-/-}$ compared to TREM2$^{+/+}$ mice. **(c)** Representative images showing increased accumulation of pSer8-Aβ, nmAβ, and Aβ (2964) in SSC of male 5M-5x-FAD-TREM2$^{-/-}$ compared to TREM2$^{+/+}$ mice (scale bar=50µm, 40xW). **(d)** Ratio of pSer8/nmAβ in SSC, RSC and DG in male 5M-5xFAD-TREM2$^{-/-}$ compared to TREM2$^{+/+}$ mice. Each dot represents an average value of the number of plaques or the ratio of pSer8-Aβ/nmAβ per animal. The box and whiskers plots represent min/max values of the distribution of plaque size with the median (shown by the line dividing the box) and the dot plots represent mean ± SEM (n = 5 animals, colour- blue (5xFAD-TREM2$^{+/+}$) and green (5xFAD-TREM2$^{-/-}$), unpaired t-test with Welch's correction for analysis of the number and ratio while Mann–Whitney test for plaque size, $^{ns}p > 0.05$, $*p < 0.05$, $**p < 0.01$ or $****p < 0.0001$) (Joshi et al. 2021a).

[*]*Italicized text is taken from the manuscript published in Acta neuropathologica communications by Joshi et al. 2021*

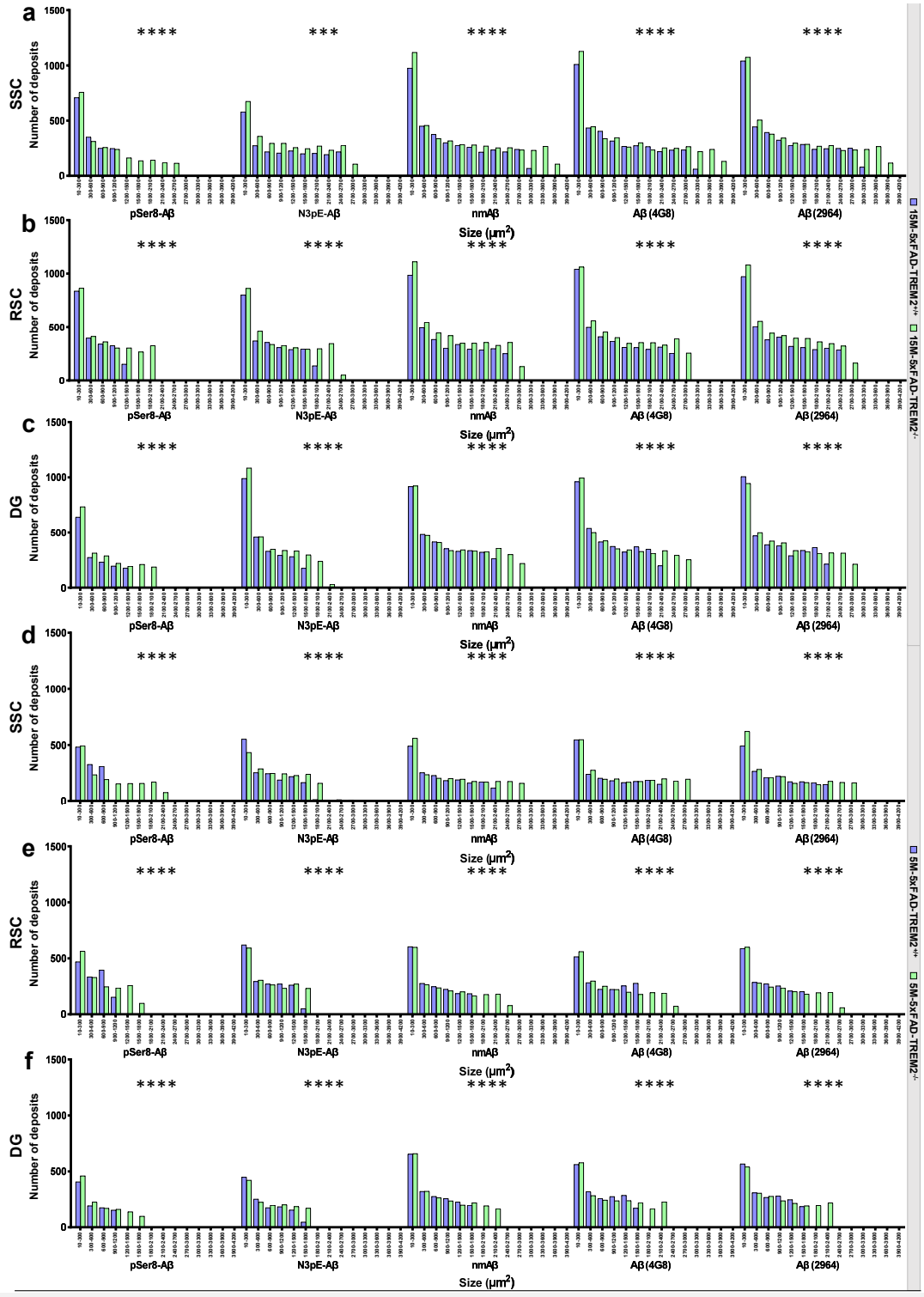

Figure 6.4 | Size distribution of Aβ plaques stained with different Aβ antibodies in 5xFAD-TREM2$^{+/+}$ and 5xFAD-TREM2$^{-/-}$ mice

Frequency distribution histogram representing plaque size (μm^2) distribution of total counted Aβ plaques stained with antibodies detecting modified and non-modified forms of Aβ in SSC, RSC and DG regions of **(a-c)** 15M old male and **(d-f)** 5M old male mice. A comparison of two frequency distributions with the total number of deposits was done by the Kolmogorov-Smirnov test. (n= 5 animals, size of all individual plaques counted/group (refer Table 6.1), colour-blue (5xFAD-TREM2$^{+/+}$) and green (5xFAD-TREM2$^{-/-}$), ***p<0.001 or ****p<0.0001) (Joshi et al. 2021a).

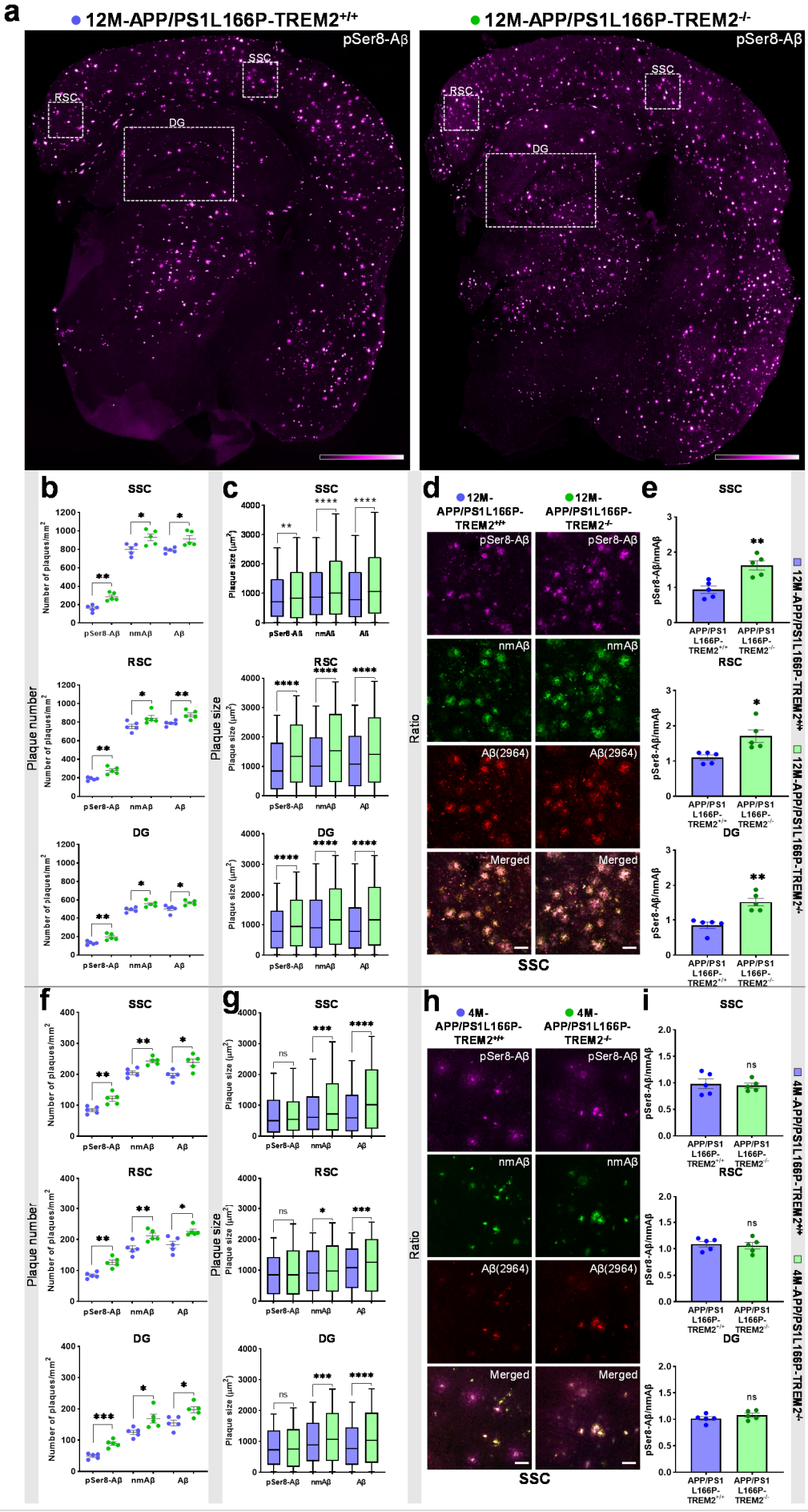
a
12M-APP/PS1L166P-TREM2+/+
12M-APP/PS1L166P-TREM2-/-
pSer8-Aβ
SSC
RSC
DG
b
c
d
e
f
g
h
i
Plaque number
Plaque size
Ratio
Number of plaques/mm2
Plaque size (µm2)
pSer8-Aβ/nmAβ
nmAβ
Aβ(2964)
Merged
APP/PS1 L166P-TREM2+/+
APP/PS1 L166P-TREM2-/-
12M-APP/PS1L166P-TREM2+/+
12M-APP/PS1L166P-TREM2-/-
4M-APP/PS1L166P-TREM2+/+
4M-APP/PS1L166P-TREM2-/-

Figure 6.5 | TREM2 deletion leads to increased deposition of pSer8-Aβ in APP/PS1L166P transgenic mouse brains

(a) Representative pSer8-Aβ stained female 12M-APP/PS1L166P-TREM2$^{+/+}$ and TREM2$^{-/-}$ mouse brain sections (color scale bar=35mm, represents min/max pixel intensities, 10x). **(b)** Dot plots representing the increased number of plaques/mm^2, **(c)** Box and whiskers plots representing increased plaque size (μm^2) stained with pSer8-Aβ, nmAβ, and Aβ (2964) antibodies in the SSC, RSC, and DG of female 12M-APP/PS1L166P-TREM2$^{-/-}$ compared to TREM2$^{+/+}$ mice. **(d)** Representative images showing increased accumulation of pSer8-Aβ, nmAβ, and Aβ (2964) in SSC of female 12M-APP/PS1L166P-TREM2$^{-/-}$ compared to TREM2$^{+/+}$ mice (scale bar=50μm, 40xW). **(e)** Ratio of pSer8/nmAβ in SSC (t(7.66)=4.053,**p=0.004), RSC (t(5.29)=3.19,*p=0.0241), and DG (t(7.48)=4.434,**p=0.0026) of 12M-APP/PS1L166P-TREM2$^{-/-}$ compared with TREM2$^{+/+}$ mice. **(f)** Dot plots representing the increased number of plaques/mm^2, **(g)** Box and whiskers plots representing increased plaque size (μm^2) stained with nmAβ and Aβ antibodies in the SSC, RSC, and DG of male 4M-APP/PS1L166P-TREM2$^{-/-}$ compared to TREM2$^{+/+}$ mice. **(h)** Representative images showing increased accumulation of pSer8-Aβ, nmAβ, and Aβ (2964) in SSC of male 4M-APP/PS1L166P-TREM2$^{-/-}$ compared to TREM2$^{+/+}$ mice (scale bar=50μm, 40xW). **(i)** Ratio of pSer8/nmAβ in SSC, RSC, and DG in male 4M-APP/PS1L166P-TREM2$^{-/-}$ compared with TREM2$^{+/+}$ mice. Each dot represents an average value of the number of plaques or ratio/animal. The box and whiskers plots represent min/max values of the distribution of plaque size with the median (shown by the line dividing the box) and the dot plots represent mean ± SEM (n=5 animals, colour- blue (APP/PS1L166P-TREM2$^{+/+}$) and green (APP/PS1L166P-TREM2$^{-/-}$), unpaired t-test with Welch's correction for analysis of the number and ratio while Mann-Whitney test for plaque size, ^{ns}p>0.05, *p< 0.05, **p<0.01, ***p<0.001 or ****p<0.0001) (Joshi et al. 2021a).

Very similar findings were obtained with an independent double-transgenic APP/PS1L166P mouse model (Table 6.1, Figure 6.5 and Figure 6.6)[*] (Joshi et al. 2021a).

[*] *Italicized text is taken from the manuscript published in Acta neuropathologica communications by Joshi et al. 2021*

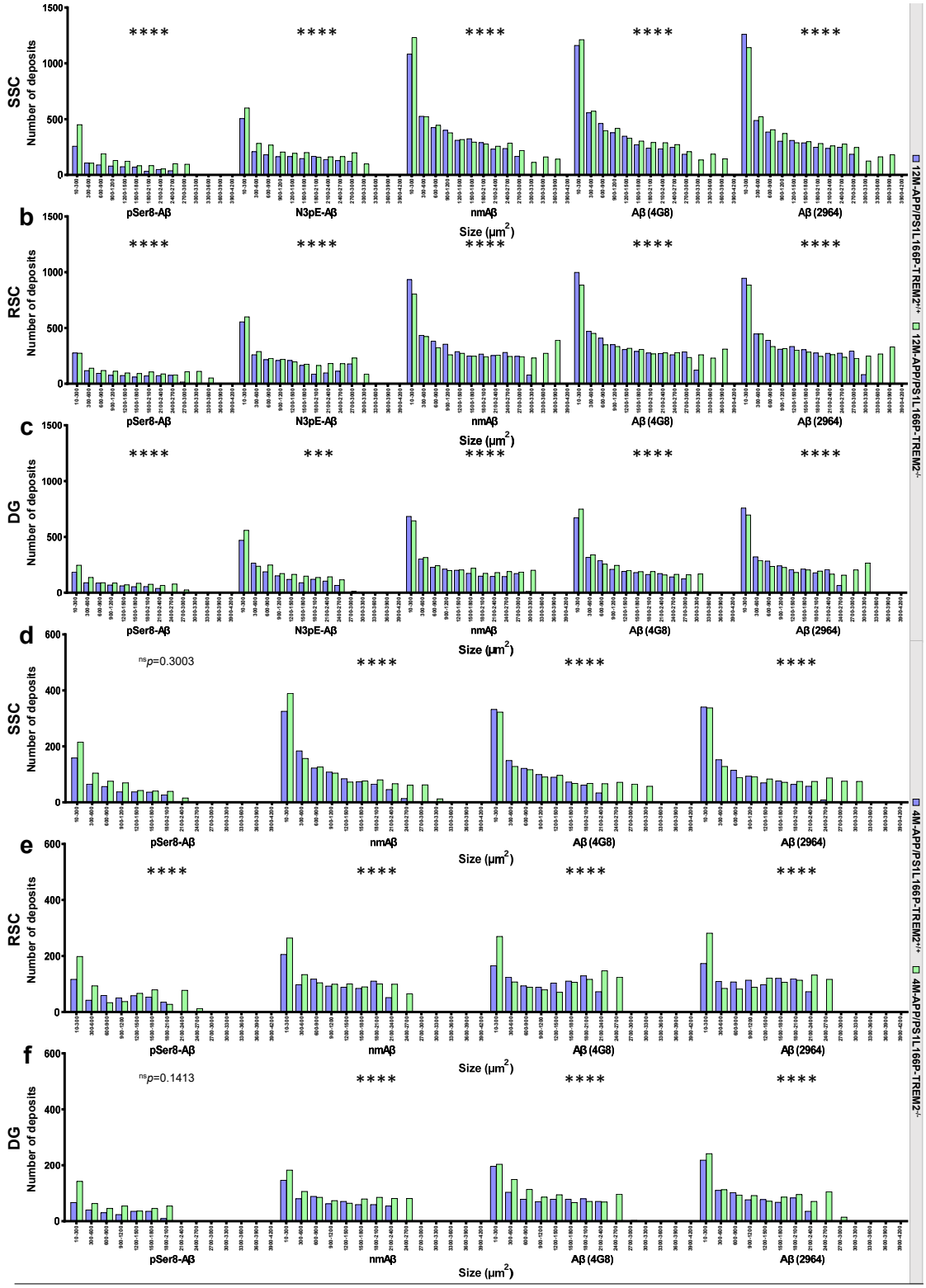

Figure 6.6 | Size distribution of Aβ plaques stained with different Aβ antibodies in APP/PS1L166P-TREM2$^{+/+}$ and TREM2$^{-/-}$ mice

Frequency distribution histogram representing plaque size (μm^2) distribution of total counted Aβ plaques stained with antibodies detecting modified and non-modified forms of Aβ in SSC, RSC and DG regions of **(a-c)** 12M old female and **(d-f)** 4M old male mice. A comparison of two frequency distributions with the total number of deposits was done by the Kolmogorov-Smirnov test. (n=5

animals, size of all individual plaques counted/group (refer Table 6.1), colour- blue (APP/PS1L166P-TREM2$^{+/+}$) and green (APP/PS1L166P-TREM2$^{-/-}$), $^{ns}p>0.05$, ***$p<0.001$ or ****$p<0.0001$) (Joshi et al. 2021a).

Pyroglutamate-modified Aβ (N3pE-Aβ) also accumulates during the pathogenesis of AD in the cortex and hippocampus (Portelius et al. 2010; Saido et al. 1995). Immunohistochemical analyses showed that TREM2$^{-/-}$ mice had significantly more N3pE-Aβ positive plaques at 15 M of age in the SSC, RSC, and the DG as compared to TREM2$^{+/+}$ mice. Consistent with data shown in Figure 6.1, TREM2$^{-/-}$ mice showed a higher number of plaques, (Figure 6.7a-b), increased size of plaques (Figure 6.7c, Figure 6.4a-c) and elevated plaque load (Table 6.1) in all three regions as revealed by co-staining with antibodies detecting N-terminally non-modified Aβ and total Aβ species at 15 M of age. In contrast to pSer8-Aβ, N3pE-Aβ was not selectively increased in plaques as compared to nmAβ at 15 M of age, as evidenced by similar ratios of N3pE-Aβ/nmAβ in all analyzed brain regions (Figure 6.7d)[*](Joshi et al. 2021a).

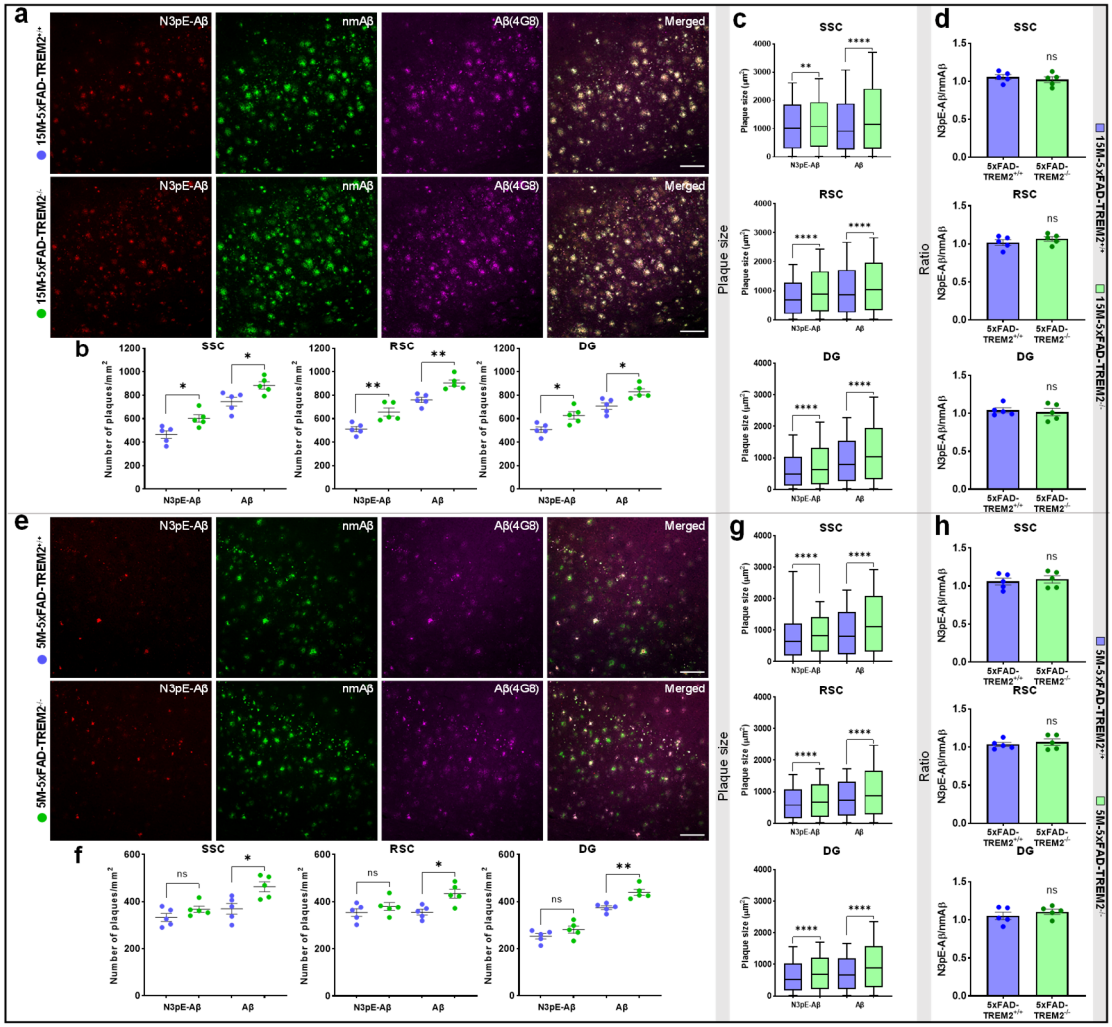

Figure 6.7 | TREM2 deletion leads to increased N3pE-Aβ deposits in 5xFAD transgenic mouse brains

[*]*Italicized text is taken from the manuscript published in Acta neuropathologica communications by Joshi et al. 2021*

(a) Representative images showing increased accumulation of N3pE-Aβ, nmAβ, and Aβ (4G8) in SSC of male 15M-5xFAD-TREM2$^{-/-}$ compared to TREM2$^{+/+}$ mice (scale bar=200µm,20x). **(b)** Dot plots representing the increased number of plaques/mm^2, **(c)** Box and whiskers plots representing increased plaque size (µm^2) stained with N3pE-Aβ and Aβ(4G8) antibodies in the SSC, RSC, and DG of the male 15M-5xFAD-TREM2$^{-/-}$ compared to TREM2$^{+/+}$ mice. **(d)** Ratio of N3pE-Aβ/nmAβ in the SSC, RSC, and DG of male 15M-5xFAD-TREM2$^{-/-}$ compared with TREM2$^{+/+}$ mice. **(e)** Representative images showing increased accumulation of N3pE-Aβ, nmAβ, and Aβ (4G8) in SSC of male 5M-5xFAD-TREM2$^{-/-}$ compared to TREM2$^{+/+}$ mice (scale bar=200µm,20x). **(f)** Dot plots representing the number of plaques/mm^2, **(g)** Box and whiskers plots representing increased plaque size (µm^2) stained with N3pE-Aβ and Aβ (4G8) antibodies in the SSC, RSC, and DG of male 5M-5xFAD-TREM2$^{-/-}$ compared to TREM2$^{+/+}$ mice. **(h)** Ratio of N3pE-Aβ/nmAβ in the SSC, RSC, and DG of male 5M-5xFAD-TREM2$^{-/-}$ compared with TREM2$^{+/+}$ mice. Each dot represents an average value of the number of plaques or ratio/animal. The box and whiskers plots represent min/max values of the distribution of plaque size with the median (shown by the line dividing the box) and the dot plots represent mean ± SEM (n=5 animals, colour- blue (5xFAD-TREM2$^{+/+}$) and green (5xFAD-TREM2$^{+/+}$), unpaired t-test with Welch's correction for analysis of the number and ratio while Mann-Whitney test for plaque size, ^{ns}p>0.05, *p< 0.05, **p<0.01 or ****p<0.0001) (Joshi et al. 2021a).

At 5 M of age, the total number of N3pE-Aβ deposits was only slightly, but not significantly increased in 5xFAD TREM2$^{-/-}$ mice as compared to TREM2$^{+/+}$ 5xFAD mice (Figure 6.7e-f). However, as observed with 15 M old mice, there was a significant increase in the size of N3pE-Aβ positive plaques, especially for larger deposits > 1500 µm^2 already at 5 M in 5xFAD TREM2$^{-/-}$ mice (Figure 6.7g, Figure 6.4d-f). Analysis of plaque size distribution revealed that there was an increase in the number of N3pE-Aβ deposits in both age groups, again particularly pronounced for deposits > 1500 µm^2. An increase of pSer8-Aβ and N3pE-Aβ deposits < 600 µm^2 in the three analyzed brain regions of TREM2$^{-/-}$ mice, as compared to TREM2+/+ mice, was only observed at 15 M of age (Figure 6.4). The N3pE-Aβ/nmAβ intensity ratio in the analyzed brain regions was not different between TREM2$^{-/-}$ and TREM2$^{+/+}$ mice at both ages (Figure 6.7d, h)[*]*(Joshi et al. 2021a).*

Very similar findings were obtained with the independent double-transgenic APP/PS1L166P mouse model (Figure 6.8 and Figure 6.6). These findings indicate that N3pE-Aβ species showed increased deposition upon deletion of TREM2. However, N3pE-Aβ, in contrast to pSer8-Aβ, did not selectively accumulate upon deletion of TREM2 in relation to nmAβ[*]*(Joshi et al. 2021a).*

[*] *Italicized text is taken from the manuscript published in Acta neuropathologica communications by Joshi et al. 2021*

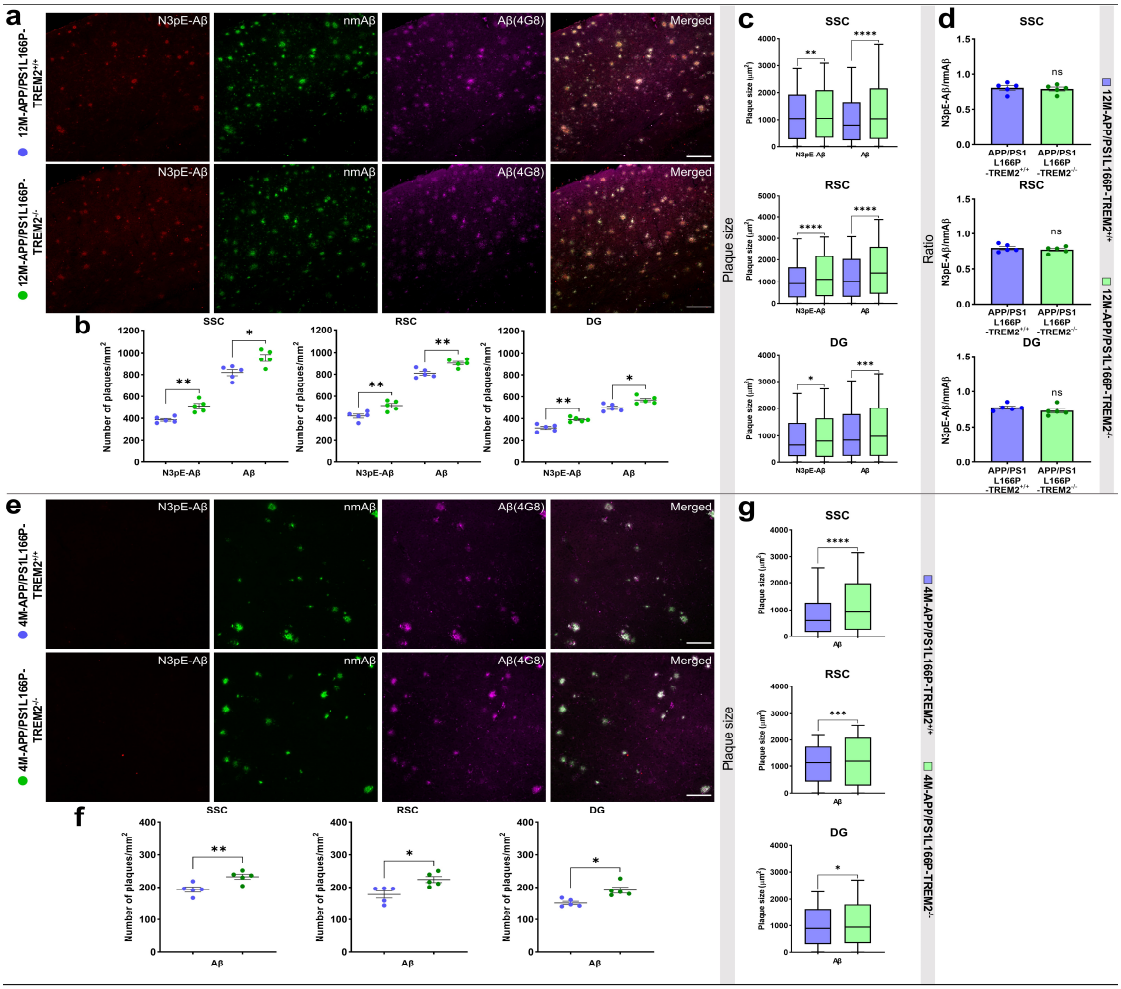

Figure 6.8 | TREM2 deletion leads to increased deposition of N3pE-Aβ in APP/PS1L166P transgenic mouse brains

(a) Representative images showing increased accumulation of N3pE-Aβ, and Aβ (4G8) in SSC of female 12M-APP/PS1L166P-TREM2$^{-/-}$ compared to TREM2$^{+/+}$ mice (scale bar=200µm,20x). **(b)** Dot plots representing the increased number of plaques/mm^2, **(c)** Box and whiskers plots representing increased plaque size (µm^2) stained with N3pE-Aβ, and Aβ (4G8) antibodies in the SSC, RSC, and DG of female 12M-APP/PS1L166P-TREM2$^{-/-}$ compared to TREM2$^{+/+}$ mice. **(d)** Ratio of N3pE-Aβ/nmAβ in the SSC, RSC, and DG of female 12M-APP/PS1L166P-TREM2$^{-/-}$ compared with TREM2$^{+/+}$ mice. **(e)** Representative images showing increased accumulation of Aβ (4G8) in SSC of male 4M-APP/PS1L166P-TREM2$^{-/-}$ compared to TREM2$^{+/+}$ mice (scale bar=200µm,20x). **(f)** Dot plots representing the increased number of plaques/mm^2, **(g)** Box and whiskers plots representing increased plaque size (µm^2) stained with Aβ(4G8) antibody in the SSC, RSC, and DG of male 4M-APP/PS1L166P-TREM2$^{-/-}$ compared to TREM2$^{+/+}$ mice. Each dot represents an average value of the number of plaques or ratio/animal. The box and whiskers plots represent min/max values of the distribution of plaque size with the median (shown by the line dividing the box) and the dot plots represent mean ± SEM (n=5 animals, colour- blue (APP/PS1L166P-TREM2$^{+/+}$) and green (APP/PS1L166P-TREM2$^{-/-}$), unpaired t-test with Welch's correction for analysis of the number and ratio while Mann-Whitney test for plaque size, ^{ns}p>0.05, *p< 0.05, **p<0.01, ***p<0.001 or ****p<0.0001) (Joshi et al. 2021a)

6.2 | TREM2^{T66M} mutation leads to increased deposition of pSer8-Aβ in transgenic mouse brain

To assess the potential effects of a disease-associated TREM2 mutant, knock-in (KI) mice were used that carry the TREM2^{T66M} variant (Table 6.1). The TREM2^{T66M} variant is associated with Nasu–Hakola disease (NHD) and frontal lobe degeneration (Guerreiro et al. 2013a; Guerreiro et al. 2013c; Paloneva et al. 2001). Importantly, the genetic modification at this site in the mouse genome does not result in aberrant splicing and lower mRNA levels as observed previously for knock-in mice expressing the Alzheimer-associated R47H variant[*] *(Xiang et al. 2018; Joshi et al. 2021a).*

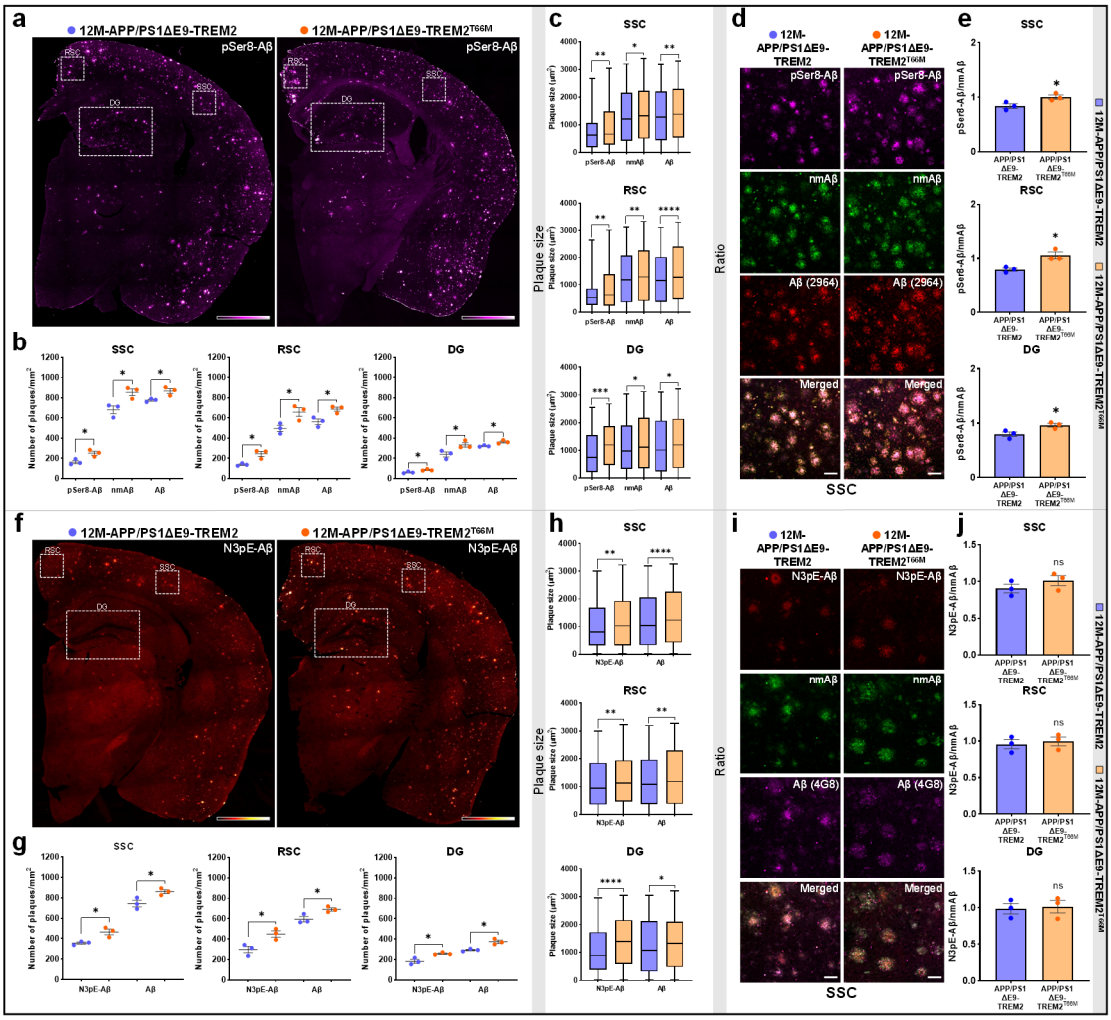

Figure 6.9 | TREM2^{T66M} causes increased deposition of pSer8-Aβ and N3pE-Aβ in APP/PS1 transgenic mouse brains

(a) Representative pSer8-Aβ stained female 12M-APP/PS1ΔE9-TREM2 and APP/PS1ΔE9-TREM2^{T66M} mouse brain sections (colour scale bar=35mm, represents min/max pixel intensities, 10x). **(b)** Dot plots represent increased the number of plaques/mm^2, **(c)** Box and whiskers plots represent an increase in plaque size (µm^2) stained with N3pE-Aβ, nmAβ, and Aβ (2964) antibodies in the SSC, RSC, and DG of female 12M-APP/PS1ΔE9-TREM2^{T66M} compared to APP/PS1ΔE9-TREM2 mice. **(d)** Representative

[*] *Italicized text is taken from the manuscript published in Acta neuropathologica communications by Joshi et al. 2021*

images showing increased accumulation of pSer8-Aβ, nmAβ, and Aβ (2964) in SSC of female 12M-APP/PS1ΔE9-TREM2^{T66M} compared to APP/PS1ΔE9-TREM2 mice (scale bar=50µm, 40xW). **(e)** Ratio of pSer8/nmAβ in SSC (t(3.953)=2.863, *p=0.0464), RSC (t(2.915)=3.94,*p=0.0307), and DG (t(3.743)=3.018,*p=0.0427) of female 12M-APP/PS1ΔE9-TREM2^{T66M} compared with APP/PS1ΔE9-TREM2 mice. **(f)** Representative N3pE-Aβ stained female 12M-APP/PS1ΔE9-TREM2 and APP/PS1ΔE9-TREM2^{T66M} mouse brain sections (colour scale bar=35mm, represents min/max pixel intensities, 10x). **(g)** Dot plots representing the increased number of plaques/mm^2, **(h)** Box and whiskers plots representing the increase in plaque size (µm^2) stained with N3pE-Aβ and Aβ (4G8) antibodies in the SSC, RSC, and DG of the female 12M-APP/PS1ΔE9-TREM2^{T66M} compared to APP/PS1ΔE9-TREM2 mice. **(i)** Representative images showing increased accumulation of N3pE-Aβ, nmAβ, and Aβ (4G8) in SSC of female 12M-APP/PS1ΔE9-TREM2^{T66M} compared to APP/PS1ΔE9-TREM2 mice (scale bar=50µm, 40xW). **(j)** Ratio of N3pE-Aβ/nmAβ in SSC, RSC, and DG of female 12M-APP/PS1ΔE9-TREM2^{T66M} compared with APP/PS1ΔE9-TREM2 mice. Each dot represents an average value of the number of plaques or ratio/animal. The box and whiskers plots represent min/max values of the distribution of plaque size with the median (shown by the line dividing the box) and the dot plots represent mean ± SEM (n=3 animals, colour- blue (APP/PS1ΔE9-TREM2) and orange (APP/PS1ΔE9-TREM2^{T66M}), unpaired t-test with Welch's correction for analysis of the number and ratio while Mann-Whitney test for plaque size, ^{ns}p>0.05, *p< 0.05, **p<0.01, ***p<0.001 or ****p<0.0001) (Joshi et al. 2021a).

TREM2^{T66M} KI mice were crossed with APP/PS1ΔE9 double transgenic mice. Mice homozygous for endogenous TREM2 or the TREM2^{T66M} KI mutation were analyzed at 12 M of age. Homozygous TREM2^{T66M} KI mice showed an increase in the number and size of plaques (Figure 6.9a-c and Figure 6.10) as well as increased plaque load (Table 6.1). TREM2^{T66M} KI mice also showed a selective accumulation of pSer8-Aβ in plaques as compared to nmAβ (Figure 6.9d-e). Moreover, there was an increase in the number of larger sized (> 1500 µm^2) as well as smaller sized (< 600 µm2) deposits of N3pE-Aβ along with pSer8-Aβ, nmAβ and total Aβ species in the analyzed brain regions of TREM2^{T66M} mice (Figure 6.9f-h and Figure 6.10). Again, no selective accumulation of N3pE-Aβ as compared to that of nmAβ was observed in the brains of TREM2^{T66M} expressing mice (Figure 6.9i-j)[*](Joshi et al. 2021a). These findings further support a selective increase of pSer8-Aβ in parenchymal plaques in mice with impaired TREM2 function[*](Joshi et al. 2021a).

6.3 | Loss of TREM2 function increases intraneuronal and vascular deposition of Aβ species

Clustering of Iba1 positive microglia around plaques was apparent in the different APP transgenic mouse models expressing endogenous TREM2 at advanced and earlier stages of Aβ deposition but was strongly reduced in brains of the respective TREM2$^{-/-}$ (Figure 6.11a-b) and TREM2^{T66M} KI mice (Figure 6.12a-b). Consistent with previous reports (Condello et al. 2015; Jay et al. 2015; Parhizkar et al. 2019), TREM2$^{-/-}$ mice showed much less compact Aβ deposits as[*]

[*]*Italicized text is taken from the manuscript published in Acta neuropathologica communications by Joshi et al. 2021*

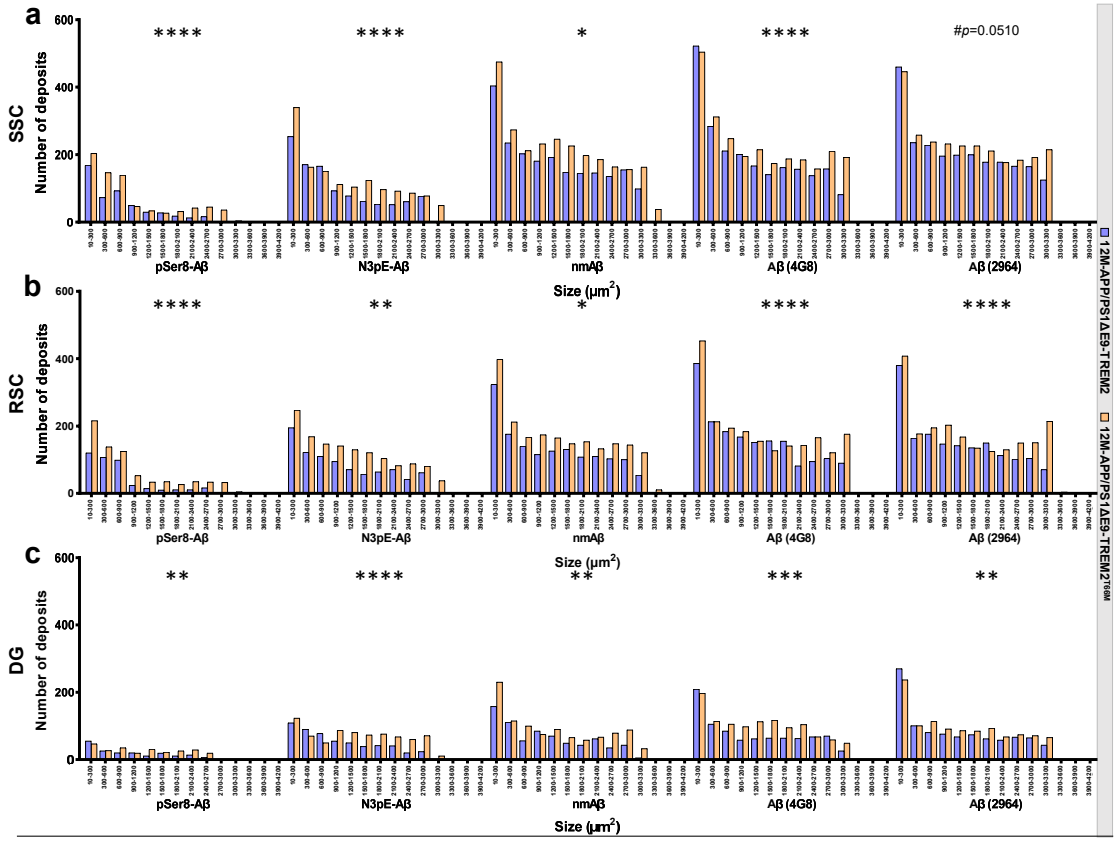

Figure 6.10 | Size distribution of Aβ plaques stained with different Aβ antibodies in APP/PS1ΔE9-TREM2 and APP/PS1ΔE9-TREM2^{T66M} mice

Frequency distribution histogram representing plaque size (μm^2) distribution of total counted Aβ plaques stained with antibodies detecting modified and non-modified forms of Aβ in SSC, RSC and DG regions of **(a-c)** 12M old female mice. A comparison of two frequency distributions with the total number of deposits was done by the Kolmogorov-Smirnov test. (n=3 animals, size of all individual plaques counted/group (refer Table 6.1), colour- blue (APP/PS1ΔE9-TREM2) and orange (APP/PS1ΔE9-TREM2^{T66M}), $^{\#}p>0.05$, $*p< 0.05$, $**p<0.01$, $***p<0.001$ or $****p<0.0001$) (Joshi et al. 2021a).

compared to TREM2$^{+/+}$ mice. Similar observations were made with the APP/PS1ΔE9-TREM2^{T66M} KI mice as compared to APP/PS1ΔE9-TREM2 mice indicating that impaired barrier function of TREM2 deficient microglia promotes the deposition of smaller plaques containing pSer8-Aβ. In addition, brains of the different APP transgenic TREM2$^{-/-}$ and TREM2^{T66M} KI mice showed strongly elevated deposition of pSer8-Aβ within neurons as compared to brains from APP transgenic mice expressing endogenous TREM2 (Figure 6.11c-d and Figure 6.12c-d)* (Joshi et al. 2021a).

**Italicized text is taken from the manuscript published in Acta neuropathologica communications by Joshi et al. 2021*

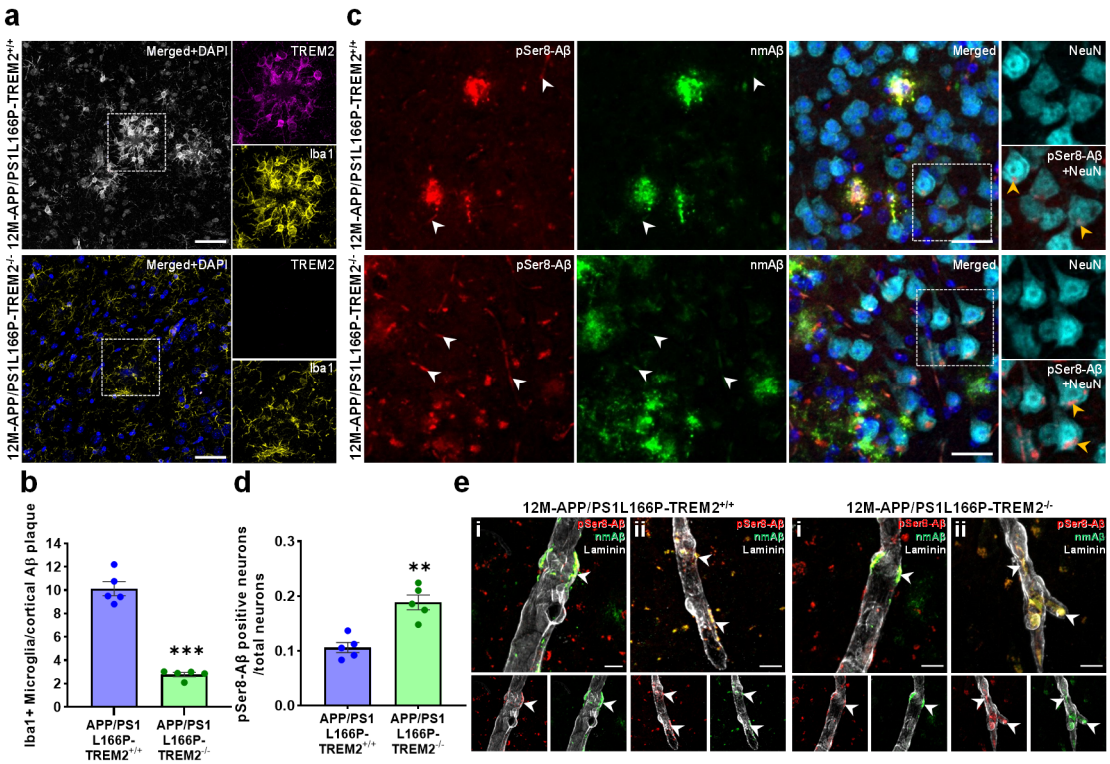

Figure 6.11 | Loss of microglial barrier functions upon TREM2 deletion leads to increased intraneuronal pSer8-Aβ deposits in the APP/PS1L166P transgenic mouse brains

(a) Representative IF images of TREM2 along with microglial marker, Iba1, in female 12M-APP/PS1L166P-TREM2$^{+/+}$ and TREM2$^{-/-}$ mice. Dotted white boxes indicate the area shown at higher magnification (scale bar=50µm, 20x). **(b)** Quantification showing decreased Iba1^{+ve} plaque-associated microglia surrounding cortical plaques in the female 12M-APP/PS1L166P-TREM2$^{-/-}$ compared with TREM2$^{+/+}$ mice (t(4.67)=11.68,***p=0.0001). Each dot represents the mean value of the microglia count surrounding 30 cortical plaques/animal. **(c)** Representative IF images of pSer8-Aβ and nmAβ localized in extracellular plaques, vessels (white arrowheads) and within NeuN positive neurons (yellow arrowheads) in SSC of female 12M-APP/PS1L166P-TREM2$^{+/+}$ and TREM2$^{-/-}$ mice. Dotted white boxes indicate the area shown at higher magnification (scale bar=50µm, 40xW). **(d)** Quantification of intraneuronal pSer8-Aβ normalized to the total number of neurons showed significantly increased neuronal pSer8-Aβ deposits in the SSC of female 12M-APP/PS1L166P-TREM2$^{-/-}$ as compared to TREM2$^{+/+}$ mice (t(7.078)=5.06, **p=0.0014). **(e)** Representative cortical artery (i) and capillary (ii) stained with Laminin showing pSer8-Aβ and nmAβ deposits in the SSC of female 12M-APP/PS1L166P-TREM2$^{+/+}$ and TREM2$^{-/-}$ mice (indicated with an arrow) (Scale bar=10µm, 63xW). All data represent mean ± SEM (n=5 animals, colour- blue (APP/PS1L166P-TREM2$^{+/+}$) and green (APP/PS1L166P-TREM2$^{-/-}$), unpaired t-test with Welch's correction) (Joshi et al. 2021a).

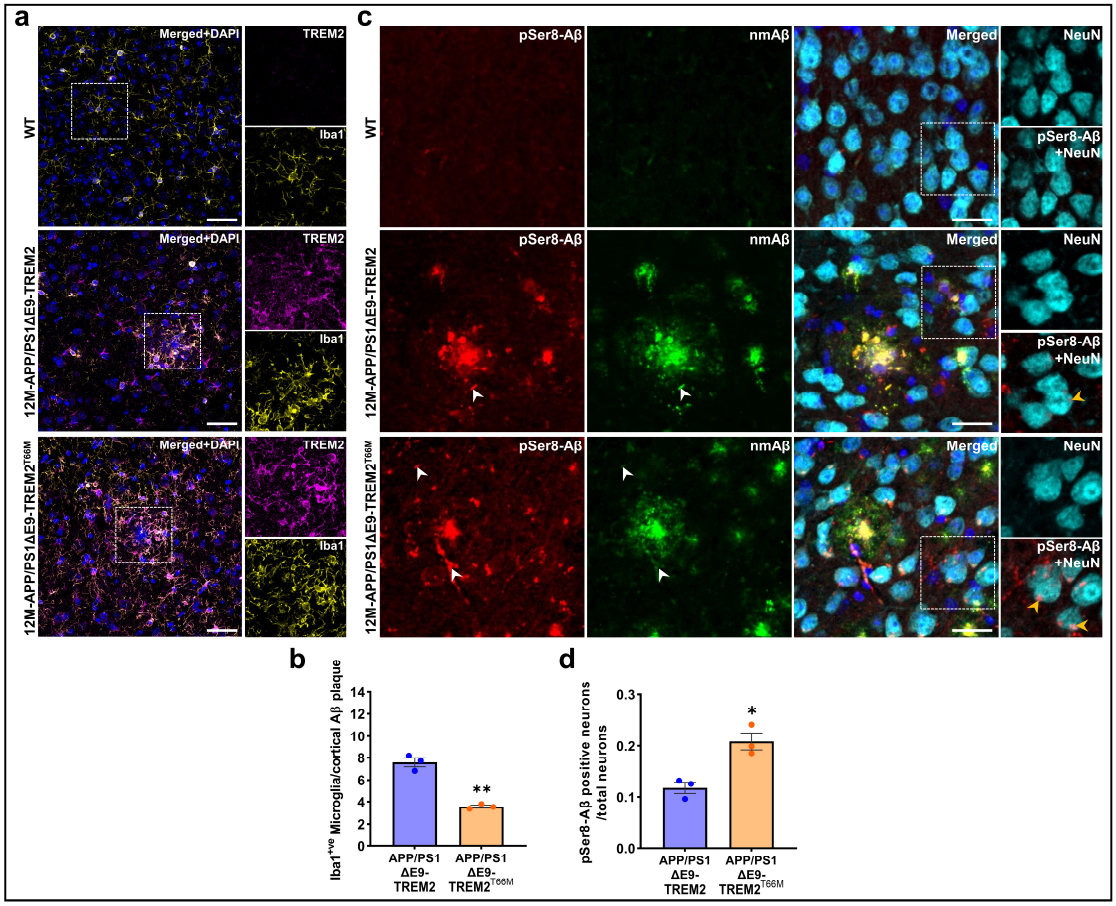

Figure 6.12 | TREM2^{T66M} causes increased Aβ in the APP/PS1 transgenic mouse brains

(a) Representative IF images of TREM2 along with microglial marker, Iba1 in female 12M- APP/PS1ΔE9 and APP/PS1ΔE9-TREM2^{T66M} mice. Dotted white boxes indicate the area shown at higher magnification (Scale bar=50µm, 20x). **(b)** Quantification showing decreased Iba1^{+ve} plaque-associated microglia surrounding cortical plaques in female 12M-APP/PS1ΔE9-TREM2^{T66M} as compared to APP/PS1ΔE9-TREM2 mice (t(2.392)=9.566,**p=0.0058). Each dot represents the mean value of the microglia count surrounding 30 cortical plaques/animal. **(c)** Representative IF images of pSer8-Aβ and nmAβ localized in extracellular plaques, vessels (white arrowheads) and within NeuN positive neurons (yellow arrowheads) in SSC of female APP/PS1ΔE9-TREM2 and APP/PS1ΔE9-TREM2^{T66M} mice. Dotted white boxes indicate the area shown at higher magnification (Scale bar=50µm, 40xW). **(d)** Quantification of intraneuronal pSer8-Aβ normalized to the total number of neurons/ROI showed significantly increased intraneuronal pSer8-Aβ deposits in the SSC of female 12M-APP/PS1ΔE9-TREM2^{T66M} as compared to APP/PS1ΔE9-TREM2 mice (t(3.466)=4.459, *p<0.0154). All data represent mean ± SEM (n=3 animals, colour-blue (APP/PS1ΔE9-TREM2) and orange (APP/PS1ΔE9-TREM2^{T66M}), unpaired t-test with Welch's correction).

*We also performed Western immunoblotting analyses with different fractions of brain extracts from APP/PS1L166P-TREM2$^{+/+}$ and APP/PS1ΔE9-TREM2^{T66M} KI mice. Levels of pSer8-Aβ, nmAβ, and total Aβ (immunostained with 4G8 or 2964 antibody) were significantly increased in the**

*Italicized text is taken from the manuscript published in Acta neuropathologica communications by Joshi et al. 2021

RIPA extracts with low detergent concentration that could contain extracellular and membrane-associated monomeric and oligomeric Aβ species (Figure 6.13a-h)(Joshi et al. 2021a).*

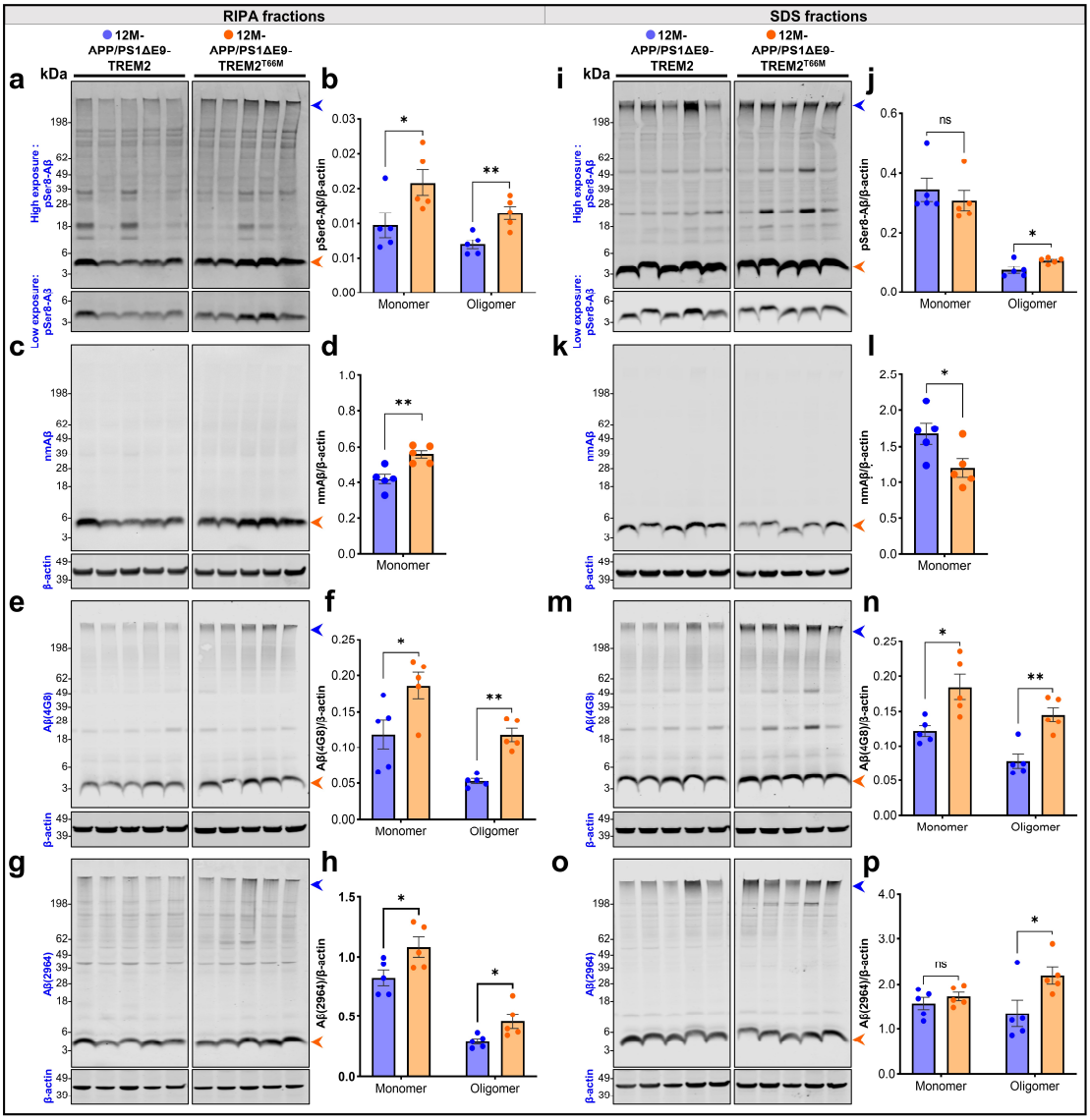

Figure 6.13 | Increased pSer8-Aβ in brain extracts of APP/PS1 ΔE9-TREM2^{T66M} transgenic mouse brains

(a-h) Immunoblots and quantification showing levels of monomeric and oligomeric Aβ variants in RIPA extracts of brains of female 12M-APP/PS1ΔE9-TREM2^{T66M} as compared to APP/PS1ΔE9-TREM2 mice; pSer8-Aβ immunostained with antibody 1E4E11, (monomer: t(7.993)=2.391, **p*=0.0438; oligomer: t(7.074)=3.925, ***p*=0.0056), nmAβ detected with antibody 7H3D6 (monomer: t(7.608)=3.849, ***p*=0.0054), Aβ immunostained with antibody 4G8 (monomer: t(7.847)=2.454, **p*=0.0402; oligomer: t(5.134)=6.604, ***p*=0.0011) or antibody 2964 (monomer: t(7.607)=2.46, **p*=0.0408; oligomer: t(5.181)=2.63, **p*=0.045) antibodies. **(i-p)** Immunoblots and quantification showing levels of monomeric and oligomeric Aβ variants in SDS extracts of brains of female 12M-APP/PS1ΔE9-TREM2^{T66M} as compared to APP/PS1ΔE9-TREM2 mice; pSer8-Aβ immunostained with antibody 1E4E11, (monomer:

*Italicized text is taken from the manuscript published in Acta neuropathologica communications by Joshi et al. 2021

t(7.81)=0.708, ^{ns}p=0.4995; oligomer: t(5.14)=2.62, *p=0.0458), nmAβ detected with antibody 7H3D6 (monomer: t(7.886)=2.449, *p=0.0404), Aβ immunostained with antibody 4G8 (monomer: t(5.396)=3.255, *p=0.0202; oligomer: t(7.999)=4.642, **p=0.0017) or antibody 2964 (monomer: t(7.153)=0.939, ^{ns}p=0.3784; oligomer: t(6.775)=2.434, *p=0.0463) antibodies. Each dot represents ratio of Aβ signal to β-actin per animal. All data represent mean ± SEM (n=5 animals, monomer: orange arrowheads and oligomer: blue arrowheads, color- blue (APP/PS1ΔE9-TREM2) and orange (APP/PS1ΔE9-TREM2^{T66M}), unpaired t-test with Welch's correction) (Joshi et al. 2021a).

Consistent with the higher aggregation propensity of pSer8-Aβ, pSer8-Aβ reactivity was also observed in the upper region of the blot that likely represents SDS-stable oligomers. These species were also detected by antibodies 4G8 or 2964 that detect Aβ independently of the modification state. In contrast, non-modified Aβ was almost exclusively detected as monomers. However, levels of monomeric non-modified Aβ were also increased in RIPA extracts of APP/PS1ΔE9-TREM2^{T66M} KI as compared to that of APP/PS1ΔE9-TREM2 WT mouse brains. In the SDS fractions that were obtained subsequently after extraction with RIPA buffer, and could also contain intracellular Aβ, levels of pSer8-Aβ migrating in the monomeric band were similar between TREM2 WT and TREM2^{T66M} brains. Notably, levels of oligomeric pSer8-Aβ were elevated in TREM2^{T66M} brains, indicating higher levels of pSer8-Aβ containing oligomers upon loss of TREM2 function. As observed for the RIPA extracts, nmAβ was also not detected as oligomers in the SDS fraction. Levels of monomeric nmAβ were decreased in the SDS fraction of TREM2^{T66M} mice as compared to that of TREM2 WT mice (Figure 6.13i-l). Increased levels of oligomeric Aβ in the brains of TREM2^{T66M} mice were confirmed with antibodies 4G8 and 2964 in both, RIPA and SDS extracts (Figure 6.13m-p). Together these data indicate that TREM2 could limit the accumulation of oligomeric Aβ assemblies which contain Ser8-Aβ. These oligomers might further aggregate to form Aβ deposits consistent with the increased plaque deposition observed in brains of mice with TREM2 deletion or expression dysfunctional TREM2^{T66M} variant. Notably, increased deposition of pSer8-Aβ and nmAβ was not only observed in form of extracellular plaques but also in brain vessels of APP/PS1L166P$^{-/-}$ mice as compared to APP/PS1L166P$^{+/+}$ mice (Figure 6.11e). This vascular deposition of Aβ resembles CAA pathology observed in different APP transgenic mouse models, and very commonly in human AD brains[*] (Thal et al. 2015; Kumar et al. 2020b; Gerth et al. 2018; Joshi et al. 2021a).

6.4 | TREM2 variants are associated with quantitative and qualitative differences in the deposition of distinct Aβ species in human brains

To assess the effect of rare disease-associated TREM2 variants in human brain tissue, AD cases with TREM2$^{R62H/R62C}$ variants and the clinical diagnosis for dementia were compared to[*] cases

[*] *Italicized text is taken from the manuscript published in Acta neuropathologica communications by Joshi et al. 2021*

with the TREM2 common variant (CV) also diagnosed with dementia. All cases fulfilled the criteria for neuropathological diagnosis of AD (Table 6.2). Sequential temporal neocortical sections were stained separately with the phosphorylation-state specific antibodies 7H3D6 (nmAβ), 1E4E11 (pSer8-Aβ), and 4G8 that detect Aβ independently of the phosphorylation state. In addition to extracellular plaques, all cases showed Aβ depositions in the wall of cerebral blood vessels, and inside of neurons (Figure 6.14a and Figure 6.15a)[*].

Case # number	Clinical diagnosis	Age at death (yr)	Sex	Post-mortem Delay (h)	Fixation time (days)	CERAD	Braak& BraakAD stage	Thal phase	ApoE status	TREM2 variant	Total number of Aβ plaques counted/ analyzed ROIs	Total number of pSer8-Aβ plaques counted/ analyzed ROIs	Total nmAβ intracellular deposits counted/ analyzed ROIs	Total pSer8-Aβ intracellular deposits counted/ analyzed ROIs
#1	Dementia (rapidly progressive without further specification)	75	M	24	n.i.	C	6	5	E3/E4	R62H (G>A)	13053	2286	2871	1663
#2	Dementia of the Alzheimer type	78	F	21	15	C	6	5	E3/E4	R62H (G>A)	14125	2270	2616	1496
#3	Dementia (without further specification)	81	F	11-35	613	C	5	5	E3/E4	R62H (G>A)	17147	-	2764	2740
#4	Frontotemporal dementia (FTD)	77	M	5	25	C	5	5	E3/E4	R62H (G>A)	15782	4894	4415	3825
#5	Dementia (without further specification)	86	M	16-40	156	C	5	4	E3/E4	R62H (G>A)	14296	1984	3731	3675
#6	Frontotemporal dementia (FTD)	77	M	26	297	C	5	4	E3/E4	R62C (C>T)	14432	1857	3832	2190
#7	Dementia of the Alzheimer type	81	F	60	39	C	6	n.i.	E3/E4	None	9384	2057	3304	1052
#13	Dementia, probably of the Alzheimer type	82	M	15	104	C	6	5	E3/E4	None	9816	2759	1850	1841
#14	Dementia (without further specification)	85	M	27	27	C	6	5	E3/E4	None	9892	2386	2157	1021
#15	Dementia (without further specification)	85	M	49	136	C	6	5	E3/E4	None	16160	4104	2404	2834
#16	Dementia (without further specification)	88	F	9	76	C	4	5	E3/E4	None	14698	3894	2891	1224
#17	Dementia of the Alzheimer type	75	M	3-13	141	C	5	5	E3/E4	None	8681	2256	2295	837

Table 6.2 | Demographic and clinical characteristics of the TREM2 coding variants and control (CV) groups

n.i.-no information, ROI-Region of Interest. Case#3, with the highest fixation time, was omitted for the plaque count and size quantification as it was difficult to draw boundaries surrounding the extracellular plaques stained with 1E4E11(pSer8-Aβ) antibody (Joshi et al. 2021a).

$TREM2^{R62H/R62C}$ variant cases had an increased number and size of 4G8 positive plaques resulting in a higher plaque load (% area) as compared to cases with the TREM2 common variant. Apart from this, we also observed a higher number of smaller extracellular deposits stained with 4G8 antibody in TREM2 CV cases (Figure 6.14a-d and Figure 6.15b-c). Interestingly, only two of the six $TREM2^{R62H/R67C}$ cases showed very few extracellular nmAβ positive deposits, while five out of six cases with the TREM2 CV showed abundant deposition of nmAβ (detected by antibody 7H3D6) in extracellular plaques, indicating that deposition of N-terminally non-modified Aβ species is reduced in cases with disease-associated TREM2 variants. In contrast, pSer8-Aβ was present in extracellular plaques in $TREM2^{R62H/R62C}$ and

[*] *Italicized text is taken from the manuscript published in Acta neuropathologica communications by Joshi et al. 2021*

TREM2 CV cases and prominently[*] detected in the core of plaques. The number of pSer8-Aβ positive extracellular plaques and plaque load (% area) was not significantly different between TREM2$^{R62H/R62C}$ and TREM2 CV cases (Figure 6.14e-f), pSer8-Aβ deposits stained with 1E4E11 were overall smaller as deposits stained with antibody 4G8 that detects total Aβ with positively skewed plaque size distribution with both antibodies and in all cases (Figure 6.14g and Figure 6.158d-e). However, analysis of plaque size distribution revealed that the number and size of pSer8-Aβ positive extracellular deposits were decreased in TREM2$^{R62H/R62C}$ cases as compared to TREM2 CV cases (Figure 6.15d-e)[*]. pSer8-Aβ and nmAβ were also detected in vessels in TREM2$^{R62H/R62C}$ and TREM2 CV cases. However, further analyses on the regional and quantitative deposition of phosphorylated Aβ species in different disease stages would be required to assess the potential effect of TREM2 genotypes on CAA in mouse and human brains (Figure 6.11e, Figure 6.14a and Figure 6.15a).

We also observed intraneuronal deposition of nmAβ and pSer8-Aβ species. Interestingly, the number of neurons with nmAβ and pSer8-Aβ positive intracellular deposits (Figure 6.14h-i) was significantly higher in TREM2$^{R62H/62C}$ carriers as compared to TREM2 CV cases[*] (Joshi et al. 2021a).

[*] *Italicized text is taken from the manuscript published in Acta neuropathologica communications by Joshi et al. 2021*

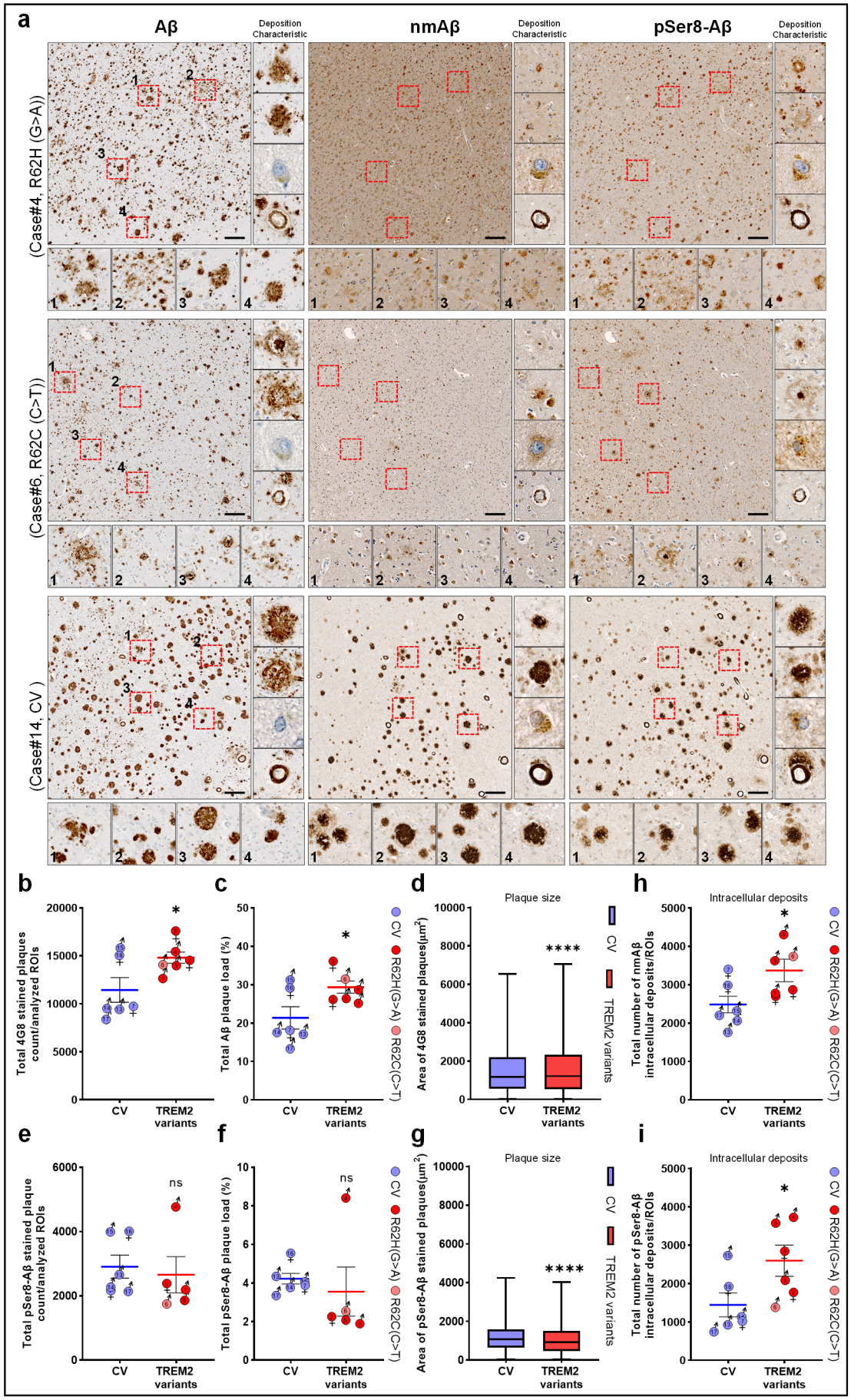
a
Aβ
Deposition Characteristic
nmAβ
Deposition Characteristic
pSer8-Aβ
Deposition Characteristic
(Case#4, R62H (G>A))
(Case#6, R62C (C>T))
(Case#14, CV)
b
Total 4G8 stained plaques count/analyzed ROIs
CV
TREM2 variants
c
Total Aβ plaque load (%)
CV
TREM2 variants
CV
R62H(G>A)
R62C(C>T)
d
Plaque size
Area of 4G8 stained plaques(μm²)
****
CV
TREM2 variants
h
Intracellular deposits
Total number of nmAβ intracellular deposits/ROIs
CV
TREM2 variants
e
Total pSer8-Aβ stained plaque count/analyzed ROIs
ns
CV
TREM2 variants
f
Total pSer8-Aβ plaque load (%)
ns
CV
TREM2 variants
g
Plaque size
Area of pSer8-Aβ stained plaques(μm²)
****
CV
TREM2 variants
i
Intracellular deposits
Total number of pSer8-Aβ intracellular deposits/ROIs
CV
TREM2 variants

Figure 6.14 | Differential deposition of phosphorylated Aβ species in human brains with the common and rare variants of TREM2

(a) Temporal neocortex of human AD patients with the indicated TREM2 variants (see **Table 6.2**) stained to detect total Aβ (with 4G8), nmAβ, and pSer8-Aβ on consecutive sections. Immunostaining indicated decreased deposition of N-terminally non-modified Aβ species in the TREM2 variants. pSer8-Aβ stained the plaques along with vascular as well as intracellular deposits. (Scale bar=200µm, 20x, the magnified dotted 4 red boxes within ROI and the small square boxes of 120×120µm on the right side (for plaques and vessels) represent deposition characteristics on consecutive sections except for the square box of 45×45µm for the neuronal deposits). **(b-c)** Quantification of the number of plaques (t(6.997)=2.378, **p*=0.0490) and percent plaque load (t(7.786)=2.412, **p*=0.0432) stained with 4G8 antibody in the analyzed ROIs of TREM2 risk allele carriers (Plaque area cutoff=10µm^2, n=6 cases each for TREM2 variants and CV, unpaired t-test with Welch's correction). **(d)** Box and whiskers plot showing a significant increase in the plaque size of TREM2 variants compared to CV cases (n= 68631 (CV) and n=88835 (TREM2 variants), *****p*<0.0001, Mann-Whitney test. Additional data are provided in Figure 6.15b-c. **(e-f)** Quantification of the numbers of plaques (t(6.96)=0.3754, ^{ns}p=0.7185) and the percent plaque load (t(4.366)=0.5145, ^{ns}p=0.6319) stained with pSer8-Aβ antibody in the analyzed ROIs of TREM2 risk allele carriers (Plaque area cutoff=30µm^2, n=5 cases for TREM2 variants and n=6 cases for CV, unpaired t-test with Welch's correction). Case#3, with the highest fixation time, was omitted for the plaque count and size quantification as it was difficult to identify extracellular plaques stained with 1E4E11 (pSer8-Aβ) antibody. **(g)** Box and whiskers plot showing a significant decrease in the plaque size of TREM2 variants compared to CV cases (n= 17456 (CV) and 13291 (TREM2 variants), ****p<0.0001, Mann-Whitney test. Additional data are provided in Figure 6.15d-e. There was a significant increase of intracellular deposits of **(h)** nmAβ (t(9.138)=2.429, **p*=0.0377) and **(i)** pSer8-Aβ (t(9.389)=2.251, **p*=0.0497) in the analyzed cortical ROIs of TREM2 variant as compared to CV cases (n=6 cases each for TREM2 variants and CV, unpaired t-test with Welch's correction). No data or the numerical value was excluded unless otherwise stated. Each coloured dot with the respective gender symbol represents a single case. Except for the box and whiskers plot, all data represent mean ± SEM (Joshi et al. 2021a).

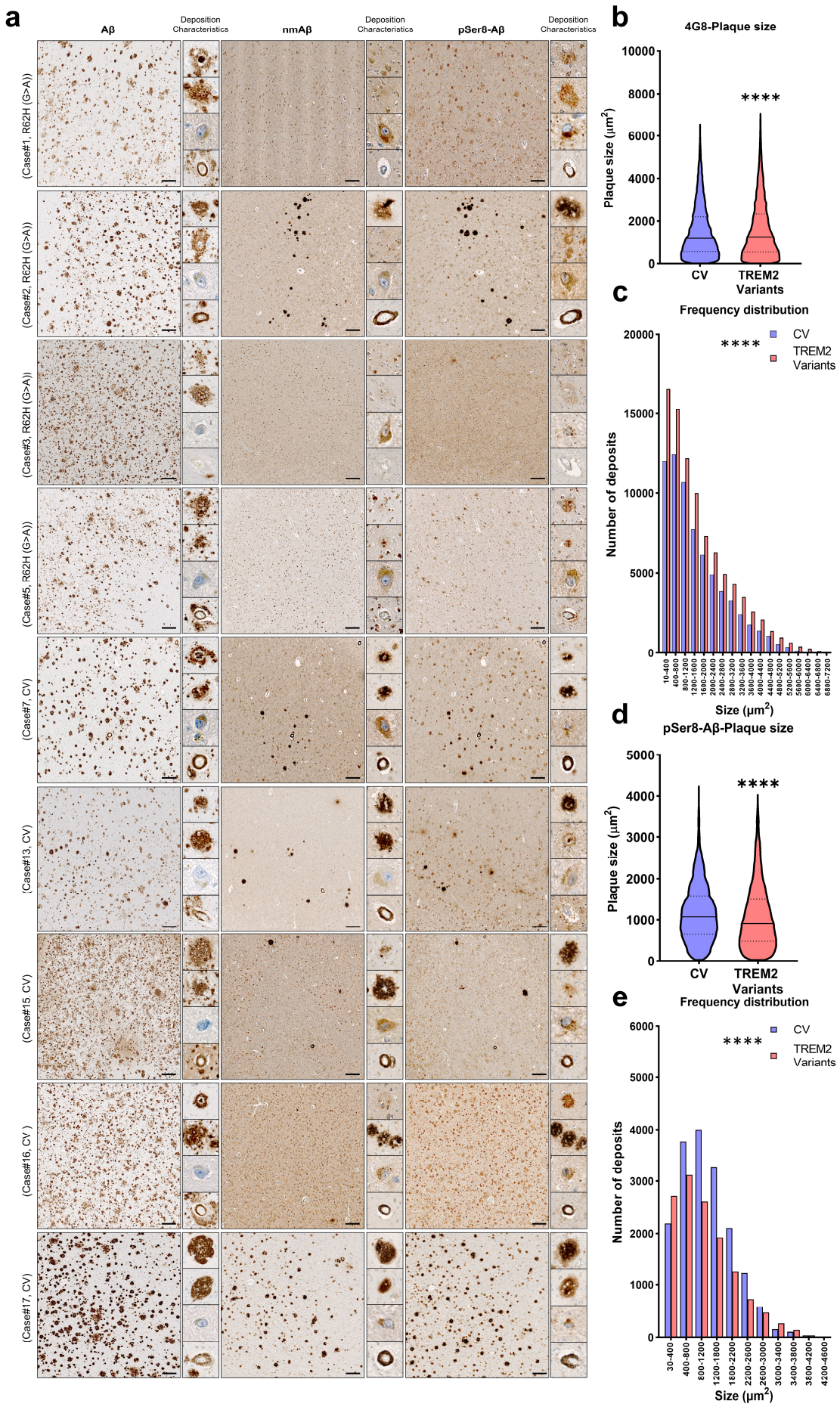
a
Aβ
Deposition Characteristics
nmAβ
Deposition Characteristics
pSer8-Aβ
Deposition Characteristics
(Case#1, R62H (G>A))
(Case#2, R62H (G>A))
(Case#3, R62H (G>A))
(Case#5, R62H (G>A))
(Case#7, CV)
(Case#13, CV)
(Case#15 CV)
(Case#16, CV)
(Case#17, CV)
b
4G8-Plaque size
Plaque size (μm²)
10000
8000
6000
4000
2000
0
****
CV
TREM2 Variants
c
Frequency distribution
****
CV
TREM2 Variants
Number of deposits
20000
15000
10000
5000
0
10-400
400-800
800-1200
1200-1600
1600-2000
2000-2400
2400-2800
2800-3200
3200-3600
3600-4000
4000-4400
4400-4800
4800-5200
5200-5600
5600-6000
6000-6400
6400-6800
6800-7200
Size (μm²)
d
pSer8-Aβ-Plaque size
Plaque size (μm²)
5000
4000
3000
2000
1000
0
****
CV
TREM2 Variants
e
Frequency distribution
****
CV
TREM2 Variants
Number of deposits
6000
5000
4000
3000
2000
1000
0
30-400
400-800
800-1200
1200-1800
1600-2200
2200-2600
2600-3000
3000-3400
3400-3800
3800-4200
4200-4600
Size (μm²)

Figure 6.15 | TREM2 ectodomain mutation leads to differential deposition of post-translationally modified Aβ species in the human brains

(a) Temporal neocortex of human AD patients with and without the indicated TREM2 variants stained for Aβ, nmAβ, and pSer8-Aβ by IHC (scale bar=200µm, 20x). Each small square box on the right side is either 120×120-140×140µm (for plaques/vessels) or 45×45µm for neurons **(b)** Violin plot represents 4G8 stained plaque size (in μm^2) distribution and **(c)** frequency distribution histogram with total counted 4G8 stained plaques in analyzed cortical ROIs/group. (Plaque area cutoff=10μm^2, n=68631 (CV) and n=88835 (TREM2 variants)).**(d)** Violin plot represents plaque size distribution (in μm^2) and **(e)** frequency distribution histogram with total counted pSer8-Aβ stained plaques in analyzed cortical ROIs/group. (Plaque area cutoff=30μm^2, n=17456 (CV) and 13291 (TREM2 variants)). Case#3, with the highest fixation time, was omitted for the plaque count and size quantification as it was difficult to identify extracellular plaques stained with 1E4E11 (pSer8-Aβ) antibody. A comparison of two groups of violin plots was done by the Mann-Whitney test and the frequency distribution of all values by the Kolmogorov-Smirnov test wherein ****p<0.0001 (Joshi et al. 2021a).

6.5 | TREM2 modulates intraneuronal deposition of pSer26-Aβ in mouse and human brains

Next, to analyze the deposition of pSer26-Aβ, since this species like pSer8-Aβ, showed increased binding to TREM2 and TREM2-dependent internalization by microglia (see Figure 4.8 and Figure 4.9), but has striking differences in its aggregation characteristics (see Figure 4.6 and (Kumar et al. 2016; Rezaei-Ghaleh et al. 2014)). A recently reported murine monoclonal antibody, 5H11C10 that selectively recognizes Aβ with Ser26 in a phosphorylated state was used (Kumar et al. 2020a). As described in Section 2.2, this antibody selectively detects Aβ species with Ser26 in a phosphorylated state, but not pSer8-Aβ or otherwise modified Aβ species. Since phosphorylation at this site occurs after the generation of Aβ, the antibody does also not recognize full-length APP or APP CTFs (Kumar et al. 2020a).

The immunostaining experiment using this antibody revealed deposition of pSer26-Aβ in all three APP transgenic mouse models used in this study (Figure 4.12 and Figure 6.16). However, as previously discussed in Section 4.5, pSer26-Aβ species were faintly detected in the core of dense Aβ plaques, and rather appeared as small deposits in close proximity to extracellular plaques (Joshi et al. 2021b). Co-immunostaining of pSer26-Aβ with Iba1 and Lamp1 revealed lysosome-associated pSer26-Aβ within plaque-associated microglia in the different APP transgenic mouse models expressing $TREM2^{+/+}$, which was strongly reduced in APP transgenic mice deficient of TREM2 or expressing the $TREM2^{T66M}$ KI (Joshi et al. 2021b).

Notably, pSer26-Aβ was also found to increase as intraneuronal deposits in the analysed somatosensory cortex (SSC) and the hippocampal dentate hilus (DH) regions of $TREM2^{-/-}$ or the $TREM2^{T66M}$ KI mice as compared to brains from the respective control mice expressing endogenous $TREM2^{+/+}$ at 12 or 15 months of age (Figure 6.16a-e). pSer26-Aβ was also found in deposits in the cerebral vasculature, and was more prominent in the brains of APP

transgenic TREM2$^{-/-}$ or the TREM2^{T66M} KI mice as compared to the respective APP transgenic mice expressing TREM2$^{+/+}$ (Figure 6.16f).

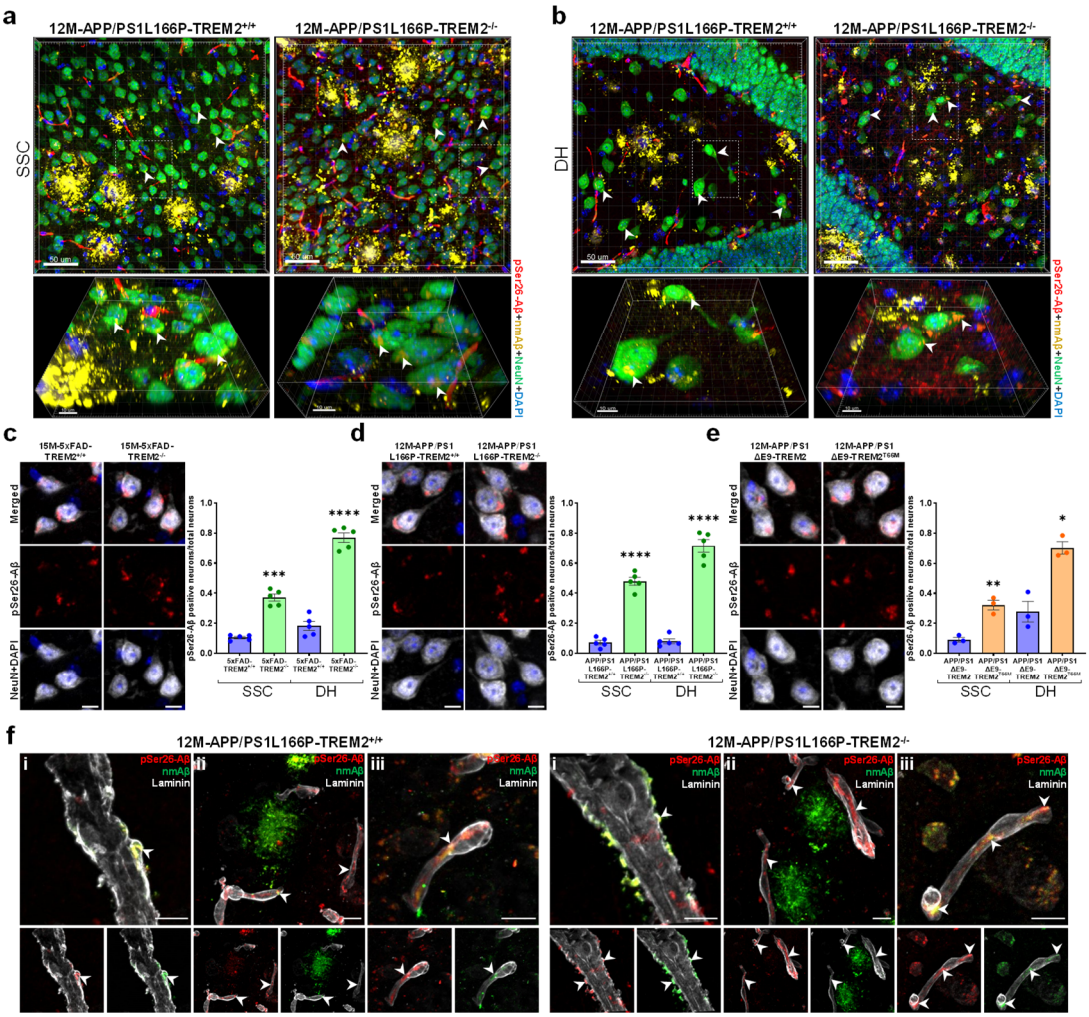

Figure 6.16 | TREM2 deletion or mutation leads to increased intraneuronal pSer26-Aβ deposits in TREM2 transgenic mouse brain

(a-b) Representative 3D reconstructed images showing increased pSer26-Aβ (red) accumulation in vessels and inside of neurons (indicated with arrow) in SSC and DG of 12M-APP/PS1L166P-TREM2$^{-/-}$ (scale bar =50µm, 40xW, dotted white boxes indicate 45° perspective area in each staining that is merged and shown at higher magnification. **(c-e)** Representative images and quantification of pSer26-Aβ neuronal deposits in the SSC and DH of male 15M-5xFAD-TREM2$^{-/-}$ (SSC- t(4.93)=10.89, ***p=0.0001, DH- t(7.963)=13.44, ****p<0.0001) (n=5), female 12M-APP/PS1L166P-TREM2$^{-/-}$ (SSC- t(6.21)=13.62, ****p<0.0001, DH- t(5.144)=14.05, ****p<0.0001) (n=5), and female 12M-APP/PS1ΔE9-TREM2^{T66M} (SSC- t(2.902)=6.56, **p=0.008, DH- t(3.284)=5.312, *p=0.0103) (n=3), in comparison to respective control mice (scale bar=10µm, 63xW). All data represent mean ± SEM. (unpaired t-test with Welch correction). **(f)** Representative images showing localization of pSer26-Aβ and nmAβ in the vessels stained with pSer26-Aβ in the SSC of 12M APP/PS1L166P-TREM2$^{-/-}$ compared to TREM2$^{+/+}$ mice. Representative cortical artery (i) and capillary (ii & iii) stained with Laminin showing increased pSer26-Aβ deposits (indicated with arrow) in the SSC of female 12M-APP/PS1L166P-TREM2$^{-/-}$ compared to TREM2$^{+/+}$ mice (Scale bar=10µm, 63xW).

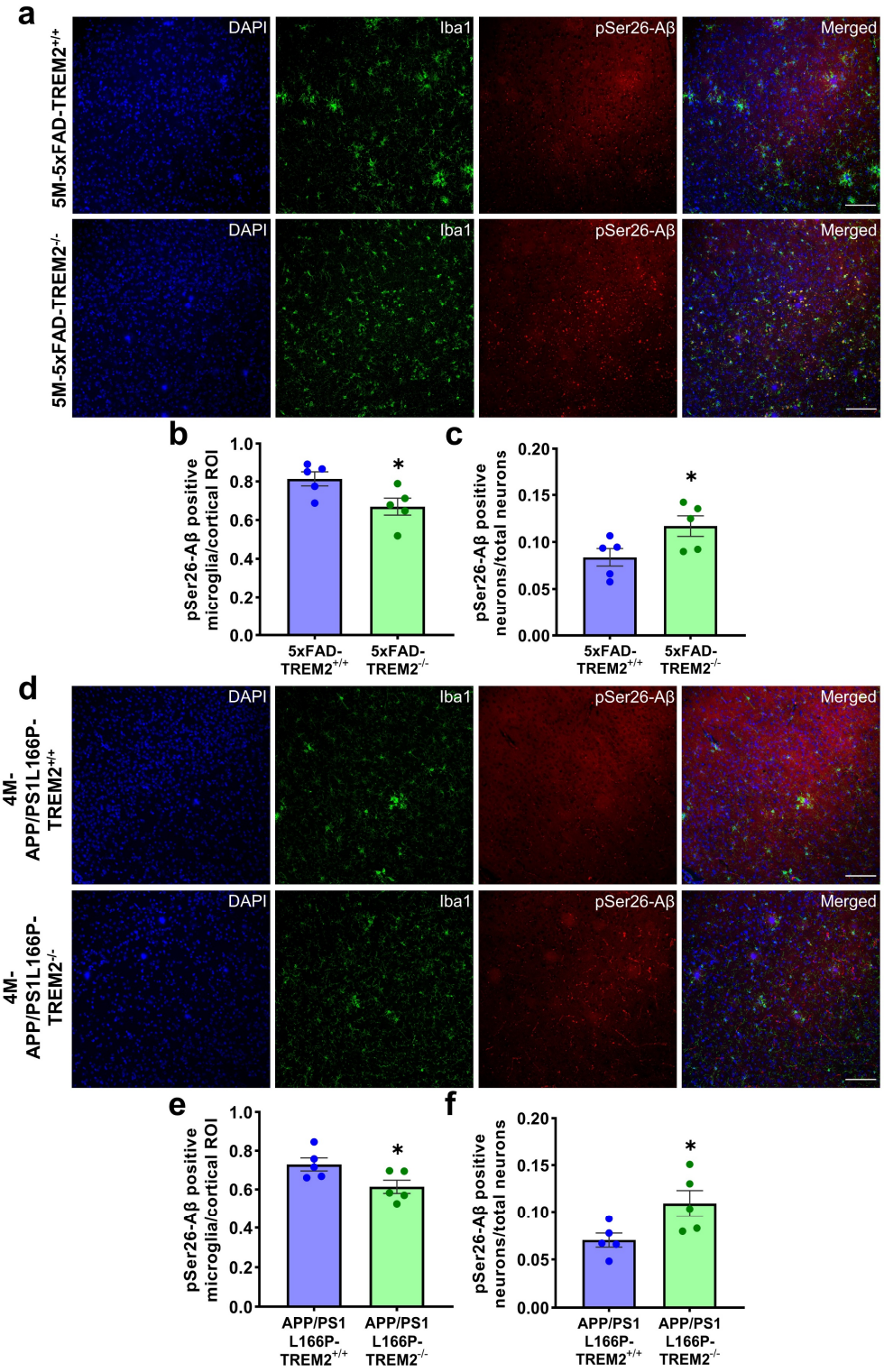

Figure 6.17 | TREM2 deletion leads to increased intracellular pSer26-Aβ deposits in young age transgenic mouse brains

(a) Representative SSC of male 5M-5xFAD-TREM2$^{+/+}$ and TREM2$^{-/-}$ mouse brain sections stained with pSer26-Aβ and Iba1 antibodies (scale bar=200µm, 20x). Scattered plot representing the **(b)** decreased microglial (t(7.734)=2.50,**p*=0.0379), and **(c)** increased pSer26-Aβ neuronal deposits (t(7.799)=2.321,**p*=0.0497) in male 5M-5xFAD-TREM2$^{-/-}$ compared to TREM2$^{+/+}$ mice. **(d)** Representative SSC of male 4M-APP/PS1L166P-TREM2$^{+/+}$ and TREM2$^{-/-}$ mouse brain sections stained

similarly (scale bar=200µm, 20x). Scattered plot representing the **(e)** decreased microglial (t(7.998)=2.384,*p=0.044), and **(f)** increased pSer26-Aβ neuronal deposits (t(6.065)=2.495,*p=0.046) in male 4M-APP/PS1L166P-TREM2$^{-/-}$ compared to TREM2$^{+/+}$ mice. All data represent mean ± SEM (n=5, unpaired t-test with Welch correction).

A lower association of pSer26-Aβ with TREM2 deficient microglia was also observed already at earlier stages of plaque deposition (4 or 5 months of age) (Figure 6.17).

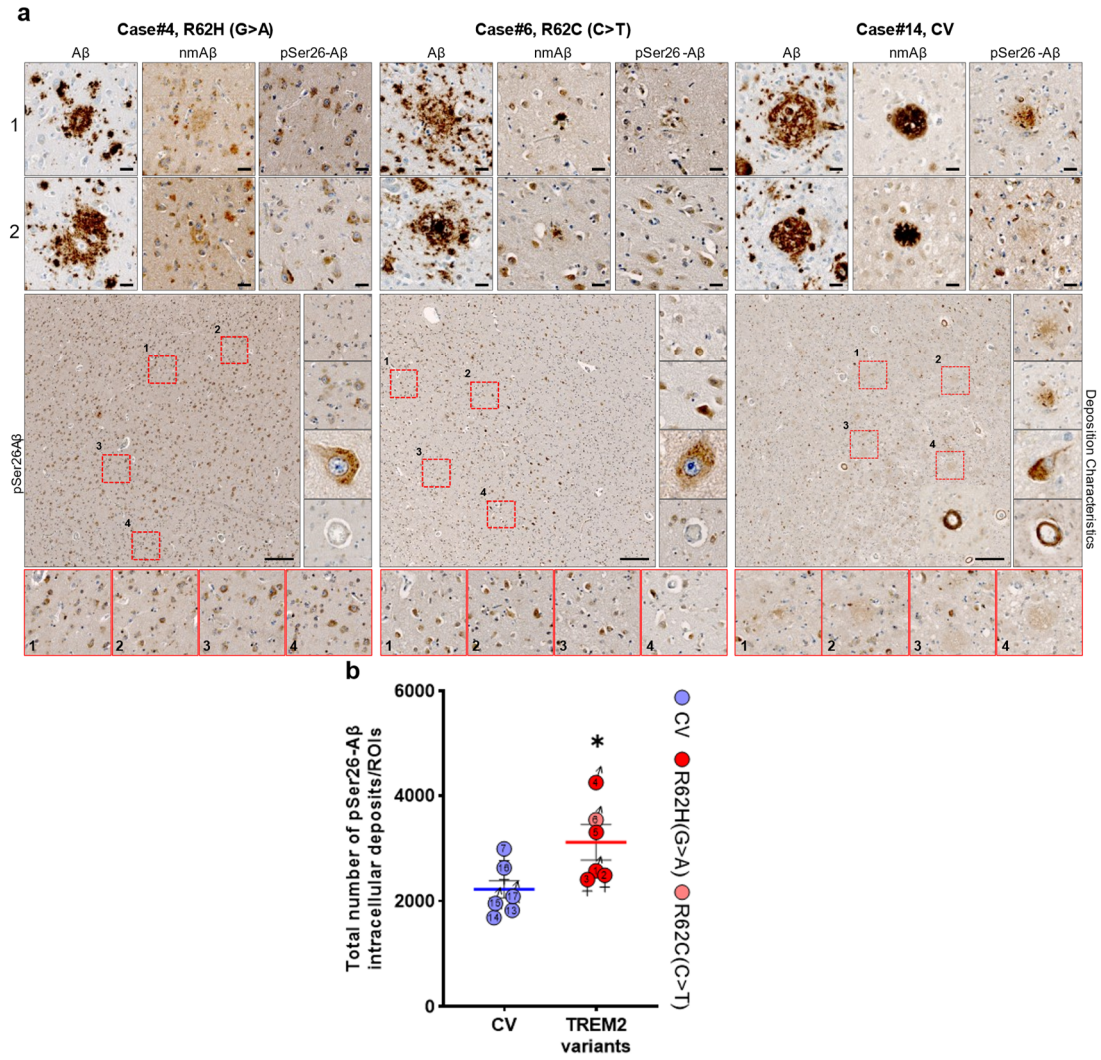

Figure 6.18 | TREM2 ectodomain mutation leads to increased intracellular pSer26-Aβ deposits in the human brain

(a-b) There was a significant increase in the intracellular deposits of pSer26-Aβ (t(7.203)=2.392, *p=0.0470) in the analyzed cortical ROIs of the TREM2 variant as compared to CV cases (n=6 cases each for TREM2 variants and CV, unpaired t-test with Welch correction). No data/numerical value was excluded unless otherwise stated. Each coloured dot with the respective gender symbol represents a single case. All data represent mean ± SEM.

In addition, it was observed a decreased microglial (Figure 6.17a-b, d-e) and increased neuronal pSer26-Aβ (Figure 6.17c, f) at this age in the analysed SSC region of $TREM2^{-/-}$ mice as compared to brains from the respective control mice expressing endogenous $TREM2^{+/+}$ mice.
The combined data with different transgenic mouse models indicate that a loss of TREM2 function not only leads to alterations in the Aβ composition and morphology of extracellular plaques but also promotes the formation of Aβ deposits in the cerebral vasculature and inside of neurons containing distinct phosphorylated Aβ.
Consistent with the data obtained from transgenic mice, pSer26-Aβ was only weakly detected in extracellular plaques, and rather appeared as plaque-associated smaller granules that were more abundant in brains of TREM2 CV cases than in $TREM2^{R62H/R62C}$ cases. Interestingly, a significant increase in the number of pSer26-Aβ positive neurons (Figure 6.18a-b) in $TREM2^{R62H/62C}$ carriers as compared to TREM2 CV cases was observed. pSer26-Aβ could only weakly be detected in brain vessels and was variable in both $TREM2^{R62H/R62C}$ and TREM2 CV cases. However, further analyses on the regional and quantitative deposition of phosphorylated Aβ species in different disease stages would be required to assess the potential effect of TREM2 genotypes on CAA in the human brain.
In conclusion, this data supports the hypothesis that TREM2 not only plays a critical role in the sensing of different Aβ species but also modulates the composition of these Aβ deposits in the brain. Furthermore, our data provide evidence for a critical role of TREM2 in the restriction of other characteristic AD-related lesions, including intraneuronal and vascular Aβ deposits that are highly correlated with clinical presentation and disease progression (Welikovitch et al. 2020; Condello et al. 2018a; Thal et al. 2008a). These findings are important since changes in the composition of extracellular plaques and CAA, in particular the occurrence of phosphorylated Aβ, are associated with clinical manifestation and progression of AD (Rijal Upadhaya et al. 2014; Gerth et al. 2018).

Chapter 7 | Discussion

To investigate the potential roles of sTREM2 and to characterize ligand interactions, cell lines stably expressing sTREM2 were generated by using the Flp-In system. Cell biological and biochemical studies revealed differential secretion of different sTREM2 variants very similar to the effects observed for full-length TREM2 variants. Variants of sTREM2 also affected the subcellular transport. Purified sTREM2 was then used for binding studies with Aβ. In particular, the post-translationally modified Aβ with distinct aggregation kinetics showed differences in the TREM2 mediated binding and uptake in the *in-vitro* experiments followed by a characteristic Spatio-temporal deposition of modified Aβ variants in extracellular plaques, vessels and intraneuronal deposits in brains of transgenic mice and human AD cases with rare TREM2 variants. These findings are discussed in detail in the following sections:

7.1 | Effects of disease-associated TREM2 mutations on secretory transport and cellular stress response

TREM2 disease-associated variants are rare (population frequency ~0.3%) and their effect size (odds ratio >3) is similar to that of ApoE-ε4 (Kleinberger et al. 2014). Among these mutations, R47H causes a threefold increase in the risk of developing AD (Guerreiro et al. 2013d; Jonsson et al. 2013), while a complete loss of TREM2 and/or DAP12 leads to early-onset dementia known as NHD (Klunemann et al. 2005). Moreover, patients with T66M mutation present clinically with FTD-like syndrome without bone involvement (Guerreiro et al. 2013c) most likely due to loss of TREM2 function caused by misfolding (Kober et al. 2016) and reduced expression of the mutant receptor at the cell surface (Kleinberger et al. 2014). Recently, in-silico studies indicate that the identified disease-associated variants could potentially hinder the function of TREM2 (Guerreiro et al. 2013d; Cuyvers et al. 2014; Kober et al. 2016). For example, R47H mutation does not severely impact the protein folding or stability of TREM2 but induces a subtle change in secondary structure detectable by circular dichroism (CD) and crystal structure leading to impaired ligand binding (Kober et al. 2016; Sudom et al. 2018) whereas, the T66M mutation which is buried within the core of Ig fold, causes protein misfolding or aggregation (Kober et al. 2016).

TREM2 is processed into a soluble form (sTREM2) by ADAM-mediated cleavage (Kleinberger et al. 2014; Wunderlich et al. 2013) of the full-length TREM2 (Thornton et al. 2017; Schlepckow et al. 2017), and this form may have biological functions (Ulrich et al. 2017; Zhong et al. 2019; Ewers et al. 2020). To investigate the potential roles of sTREM2 and to characterize ligand interactions, the cell lines stably expressing sTREM2 were generated by using the Flp-In system. In this study, it is shown that sTREM2 was effectively synthesized and released from the stable cells and that the differential secretion of different sTREM2 variants was similar to the effects observed for full-length TREM2 variants.

sTREM2^{T66M} showed an accumulation in the cells similar to this mutation in full-length TREM2 variants with no surface expression. The immunocytochemical analysis of the stable cell lines showed localization of full-length TREM2 in the plasma membrane and the vesicular structures in the cytoplasm; and these results are in line with previously published studies showing localization of TREM2 in various vesicular compartments, including endosomes, the Golgi complex, and the trans-Golgi network (Sessa et al. 2004; Prada et al. 2006; Wunderlich et al. 2013; Kleinberger et al. 2014; Ibach et al. 2021; Park et al. 2015). Consistent with other studies, T66M mutation in full-length TREM2 showed accumulation in the ER. Interestingly, the retention of the T66M mutant in the ER was also observed with the sTREM2 variant. Thus, membrane insertion of TREM2^{T66M} is not required for retention of the protein in ER (Park et al. 2015; Kleinberger et al. 2014). The accumulation of misfolded full-length TREM2^{T66M} in the ER has been shown to elicit the unfolded protein response (UPR) leading to ER stress which may have an impact on the function and survival of microglial cells as reported previously (Sprenkle et al. 2017; Wang et al. 2017; Yang et al. 2020b; Ulland et al. 2017; Sirkis et al. 2017). ER chaperone proteins such as BiP/GRP78, which is supposed to be a sensor of unfolded protein in the ER and regulate the activation of ER stress transducers (Bertolotti et al. 2000; Sommer et al. 2002). Besides this, C/EBP homologous protein (CHOP) is ubiquitously expressed at very low levels (Ron et al. 1992; Oyadomari et al. 2004), is robustly expressed by perturbations that induce stress in a wide variety of cells and even the serum deprivation increases the CHOP levels (Bennett et al. 2010). Both BiP/GRP78 and CHOP tend to increase in the sTREM2-T66M stable cell line but not in sTREM2-R47H and sTREM2-WT.

As described before, TREM2 is predominantly expressed in microglia (Colonna et al. 2016; Butovsky et al. 2014). Disease-associated TREM2 ectodomain sequence variants lead to a reduction of its microglial functions (Jendresen et al. 2017; Kleinberger et al. 2014; Yeh et al. 2017). Studies conducted using focal CNS damage in the somatosensory cortex (SSC) using a focused laser beam showed a decreased response of TREM2 knockout microglia in the vicinity of the injury and not the distant microglia. Besides, microglial activation was highly increased in APPPS1-Trem2$^{+/+}$ mice at 12 months compared with age-matched C57BL/6 mice (Mazaheri et al. 2017; Brendel et al. 2017; Parhizkar et al. 2019). APP/PS1 mice with TREM2 loss-of-function showed a significantly reduced longitudinal progression of microglial activity from 3 to 12 months and reduced ability of microglial activation at 12 months of age in APPPS1/TREM2$^{-/-}$ compared with APPPS1/TREM2$^{+/+}$ mice (Parhizkar et al. 2019).

Since microglia are activated with the pathological insults, the APP/PS1 mouse model was implemented to characterize microglia with different TREM2 genotypes. Consistent with other studies (Colonna et al. 2016), a significant reduction in the number of microglia surrounding plaques was observed in TREM2 knockout and FTD mutation mice. The plaque-associated microglia with T66M mutation showed increased TREM2 expression as compared

to TREM2-WT probably this could be due to its cellular accumulation due to the misfolding. Microglia tend to be locked in a homeostatic stage in the absence of TREM2 leading to impaired chemotaxis, reduced responses of microglia to neuronal injury, and loss of plaque barrier function of microglia causing decreased amyloid compaction and severe axonal dystrophy (Mazaheri et al. 2017; Yuan et al. 2016). While sTREM2-WT binds to neurons and this binding increases to apoptotic neurons, FTD mutations impair neuron function (Jadhav et al. 2020; Yang et al. 2020a; Song et al. 2018; Kober et al. 2017; Kawabori et al. 2015; Hsieh et al. 2009). This can be an important aspect of further examining the functional relevance of sTREM2 in the neuronal functions in normal and disease brains.

Analysis of post-mortem tissue from AD, PD, and multiple sclerosis patients showed increased levels of CHOP, BiP, pPERK (phosphorylated protein kinase R-like ER kinase), p-eIF2α (phosphorylated eukaryotic initiation factor-2α), pIRE1 (phosphorylated inositol-requiring kinase 1), and XBP1 (X-box binding protein 1) indicating increased activation of the UPR (Hoozemans et al. 2009; Mhaille et al. 2008; Wheeler et al. 2019; Yu et al. 2018). UPR in these pathologies is connected to immune cells. An increase in transcriptional signatures associated with protein folding and response to unfolded proteins was also observed in post-mortem microglia from patients with AD (Mathys et al. 2019). Also, microglia expression of BIP, CHOP, and p-eIF2α was shown to increase in multiple sclerosis patients (Mhaille et al. 2008; McMahon et al. 2012; Cunnea et al. 2011). Even so, it is still unclear whether microglial UPR relates to neurodegeneration. By IF studies, we found increased microglial expression of BiP/GRP78 in the plaque-associated microglia in both APP/PS1-TREM2 and APP/PS1-TREM2^{T66M} compared to non-transgenic wild-type mice. This effect thus shows that increased expression of BiP/GRP78 in the microglia is independent of the TREM2 genotype, but mainly caused by increased levels of Aβ. Nuclear translocation of CHOP in plaque-associated microglia of TREM2^{T66M} mice and a further increase in cytoplasmic as well as nuclear translocation of CHOP in the plaque-associated microglia in APP/PS1-TREM2^{T66M} mice were observed. Thus, these molecular chaperones could be triggered by the microglial response which might rescue the misfolding and restoration of microglial function in a disease state. This suggests the potential therapeutic importance of these chaperones that could be pursued for patient-specific FTD/NHD treatments.

7.2 | Increased interaction with TREM2 modulates microglial uptake of phosphorylated Aβ species

Previous studies have shown that TREM2 binds to Aβ oligomers and that the TREM2 contribute to the internalization of Aβ while Aβ oligomers induce NFAT signalling through TREM2 (Zhao et al. 2018; Lessard et al. 2018). As mentioned earlier that Aβ can exist in varying lengths and as modified variants as a result of proteolytic processing as well as variants from

post-translational modification by different enzymes. These post-translational modifications not only affect the structure of the Aβ but also alter its toxicity, stability and aggregation kinetics (Grochowska et al. 2017; Rezaei-Ghaleh et al. 2016; Vugmeyster et al. 2019; Kumar et al. 2011b; Barykin et al. 2017). In recent years, several monoclonal antibodies (mAbs) targeting Aβ have been or are in clinical trials. These antibodies recognize different epitopes in Aβ, and, even within a given epitope, bind the peptide in different conformations or display different selectivity for polymorphic variants (Arndt et al. 2018). Among these, antibodies mostly targeted the N terminus of the Aβ peptide. The precise molecular basis by which antibodies recognize Aβ may impact the outcome of their use in therapeutic regimes (Arndt et al. 2018). Also, post-translational modifications likely affect the binding affinities of the respective antibody. One such example is Aducanumab. Truncations at 3 or 4 (Aβ4-42 or Aβ5-42) substantially decreased the binding affinity of Aducanumab by more than 40-fold (Arndt et al. 2018). This suggests that understanding the post-translational modifications is important for the further development of therapeutic antibodies.

Alternative proteolytic processing of APP and post-translational modifications result in the formation and deposition of a variety of Aϐ peptides during the pathogenesis of AD (Barykin et al. 2017; Kummer et al. 2014). Among the different modifications, phosphorylation at Ser8 promotes the fibrillization of Aϐ, while phosphorylation at Ser26 stabilizes oligomeric assemblies, and rather decreased fibrillization (Kumar et al. 2011a; Rezaei-Ghaleh et al. 2016; Kumar et al. 2016). In addition, the phosphorylation at Ser8 increased the stability of Aϐ against degradation by microglial cells (Kumar et al. 2012) also pSer8-Aϐ could seed aggregation of unphosphorylated Aϐ (Kumar et al. 2011a; Hu et al. 2017)[*].

Many studies have shown that TREM2 binds to Aβ, so we wanted to determine if post-translationally modified Aβ variants interact with TREM2. So, this work demonstrates *the differential interaction of TREM2 with post-translationally modified Aϐ species with oligomers formed by phosphorylated Aϐ variants binding most avidly to TREM2*[*] *(Joshi et al. 2021b).*

Here the focus was on oligomer-rich fractions of Aβ in this study because of their toxicity, and functional effects on synapse (Wang et al. 2019; Benilova et al. 2012; Walsh et al. 2002; He et al. 2019; Kim et al. 2013; Ding et al. 2019), and ability to act as a seed to accelerate Aβ seeding (Katzmarski et al. 2020). Besides this, recent investigations also reported interactions of TREM2 with Aβ oligomers (Lessard et al. 2018; Zhao et al. 2018). The post-translational modifications of Aβ lead to alteration in the aggregation kinetics, such as pSer8 modification promotes aggregation into oligomeric and fibrillar assemblies (Kumar et al. 2011a) and pSer26 modification leads to the formation of stable oligomers as compared to non-modified Aβ (Kumar et al. 2016); thus, experiments on fibrils were not possible due to differences in the

[*] *Italicized text is taken from the manuscript published in GLIA by Joshi et al. 2021*

aggregation kinetics of all modified Aβ variants. Nevertheless, TREM2 binds to fibrillar Aβ in the pull-down assay in the absence of detergent, as shown previously (Lessard et al. 2018).

The three approaches for BLI studies were: (1) biotinylate all Aβ variants; (2) immobilize Aβ on Aminopropylsilane (APS) biosensors via hydrophobic or electrostatic immobilization; and (3) mix Aβ species with low amounts of biotinylated Aβ(1-42) so that the ratio of the two peptides does not affect the oligomeric conformation and the overall binding assessment. The first approach was not chosen because first due to the limitation of its synthesis of all Aβ variants and next is the possibility of forming higher aggregates during biotinylation. In the second approach, immobilisation of monomeric Aβ40 variants, which have a much lower propensity to aggregate as compared to Aβ42, onto APS sensors displayed biphasic curves with TREM2 due to the strong binding of Aβ with the sensor itself resulting in difficulties in the evaluation of dissociation curves. However, among the tested variants, considering the binding response values at 300 s, the pSer8 and pSer26 phosphorylated monomeric Aβ showed increased binding to TREM2 as compared to unmodified, and pyro-glutamate modified Aβ variants. The third approach was to implement the lowest concentration of biotinylated Aβ (5%) and mixed, oligomerized (method-1, mentioned in section 2.3) with modified Aβ variants and then used this mixture for kinetic BLI study using streptavidin (SA) biosensors. Since all modified Aβ42 couldn't be biotinylated, the kinetic BLI was not applied to monomeric Aβ42 variants.

Consistent with previous findings, we found that TREM2 binds much stronger to oligomeric Aβ assemblies than to monomeric Aβ (Zhao et al. 2018; Lessard et al. 2018). Furthermore, despite having distinct aggregation kinetics and stability, both phosphorylated Aβ species in oligomeric conformation showed the highest interaction with TREM2 (Joshi et al. 2021b)[*]. In previous studies, it was demonstrated that binding to monomeric Aβ is relatively weak whereas binding to oligomers is essentially irreversible and prior interaction of Aβ oligomers blocks the binding of a second ligand, lipidated ApoE (Lessard et al. 2018). Similarly, the binding of monomeric Aβ variants was assessed and weak binding was observed as compared to oligomeric Aβ. However, monomeric phosphorylated Aβ variants, pSer8-Aβ and pSer26-Aβ showed increased binding compared to other monomeric Aβ variants. Taken together this work along with previous studies support the notion that Aβ interacts with TREM2 with different affinity and that difference in affinity appears to be attributable to post-translational modifications and conformational differences of Aβ (Lessard et al. 2018; Joshi et al. 2021b). In line with the preferential interaction of TREM2 with anionic ligands (Sudom et al. 2018), the introduction of negatively charged phosphoryl groups at Ser8 or Ser26 of Aβ significantly increased the binding to TREM2 (Joshi et al. 2021b). Other post-translational modifications

[*] *Italicized text is taken from the manuscript published in GLIA by Joshi et al. 2021*

that do not increase the negative charge of Aβ, including nitration and pyroglutamination did not increase the interaction with TREM2 (Joshi et al. 2021b). Although oligomer assemblies formed by the different Aβ species might also have distinct ultrastructural characteristics that could also affect interaction with TREM2. However, since these potential differences would be a consequence of the modification, which would not change the conclusion that TREM2 binds phosphorylated Aβ species more avidly than non-modified Aβ.

A previous study reported that soluble ectodomain of TREM2 generated by proteolytic processing of the full-length receptor TREM2 (Kleinberger et al. 2014; Wunderlich et al. 2013), could prevent the aggregation of Aβ (Kober et al. 2020; Vilalta et al. 2021) suggesting that TREM2 not only mediates uptake of Aβ by microglia but its soluble ectodomain also could modulate Aβ aggregation. Thus, the effect of sTREM2 on the aggregation of the different Aβ species was assessed by real-time fluorescence spectrometry. Interestingly, sTREM2 inhibited the aggregation of all Aβ variants. In addition, titration with different concentrations of sTREM2 showed that the inhibition of aggregation is stronger for pSer8-Aβ modified species as compared to that of unphosphorylated Aβ or other Aβ variants, in line with a stronger binding of TREM2 to phosphorylated Aβ. The aggregation of pSer26-Aβ differs from that of other variants as pSer26-Aβ does not form mature fibrils, but has a high propensity to rapidly form stable oligomers. Thus, the effect of TREM2 on the kinetics of aggregation of pSer26-Aβ cannot be directly compared. However, sTREM2 also potently inhibited oligomerization of pSer26-Aβ. Thus, the deletion of TREM2 or mutations in the TREM2 ectodomain could not only impair microglial activation and Aβ clearance but also promote the deposition of different Aβ species by the impaired capacity to decrease Aβ aggregation (Vilalta et al. 2021).

Next, phosphorylation-state and phosphorylation-site specific uptake of Aβ by primary microglia is demonstrated (Joshi et al. 2021b). Notably, considerable differences in the uptake efficiency depending on the Aβ phosphorylation state were observed. *While the uptake of pSer8-Aβ was decreased, the internalization of pSer26-Aβ was increased as compared to that of unmodified Aβ (Joshi et al. 2021b)*[*]. These differences could be due to specific characteristics of the different Aβ species in the interaction with microglial surface molecules, including proteins and lipids, caused by phosphorylation-state specific differences in the aggregation behaviour. Here, it is important to note that pSer26-Aβ is not forming larger fibrils due to the formation of a salt bridge between the Asp23 and Lys28 that interferes with the formation of a fibril-specific β-turn conformation (Rezaei-Ghaleh et al. 2014). Thus, pSer26-Aβ in the soluble oligomeric state could be internalized by microglia more efficiently than pSer8-Aβ which forms larger fibrils (Kumar et al. 2013). Also, *the uptake of all Aβ species was significantly reduced in microglia expressing the TREM2^{T66M} loss-of-function mutation that is*

[*] *Italicized text is taken from the manuscript published in GLIA by Joshi et al. 2021*

associated with NHD and frontal lobe degeneration (Guerreiro et al. 2013a; Guerreiro et al. 2013c; Paloneva et al. 2001; Joshi et al. 2021b). This mutation causes misfolding and strongly decreases the expression of TREM2 at the cell surface (Kleinberger et al. 2017; Joshi et al. 2021b), reduced generation of soluble TREM2 similar to patients with the homozygous T66M mutation and significantly reduced phagocytic activity (Kleinberger et al. 2017; Joshi et al. 2021b). Thus, these data indicate that cell surface localized TREM2 is important for the regulation of Aβ phagocytosis. However, additional components of the microglial surface, including receptor proteins and membrane lipids could also be involved in the interaction and uptake of different Aβ variants (Yu et al. 2015; Verdier et al. 2004; Mandrekar et al. 2009; Joshi et al. 2021b)[*].*

In addition, peculiar effects of phosphorylation at Ser8 and Ser26 on the conformation and aggregation of Aβ could also contribute to the differential handling of the peptides by microglia (Kumar et al. 2012; Kumar et al. 2011a; Kumar et al. 2016; Joshi et al. 2021b)[*]. Thus, differential aggregation and metabolic stability of the phosphorylated Aβ species likely contribute to the specific accumulation and differential deposition in the brains of transgenic mice and humans.

TREM2 is associated with DAP12, and upon ligand binding, it activates Syk-PI3K/MAPK signalling and releases IP3/gated Ca^{2+} stores for phagocytosis (Glebov et al. 2016; Sasaki et al. 2015; Wunderlich et al. 2013; Bouchon et al. 2001; Daws et al. 2001; Takahashi et al. 2007; Parkhurst et al. 2013; Wang et al. 2015). Previously, the interaction between Aβ oligomers and TREM2 showed activation of NFAT signalling (Zhong et al. 2018; Lessard et al. 2018). Additional studies will be needed to investigate the functionality of interaction between Aβ oligomers and TREM2 signalling leading to SYK phosphorylation (Zhong et al. 2017; Zhao et al. 2018; Lessard et al. 2018). To do this, a reporter cell system expressing full-length TREM2/DAP12 complex (Ibach et al. 2021) reported previously could be of great importance. Further, it remains unclear whether Aβ could compete with other TREM2 ligands thereby interfering with activation. Also, it will be interesting to assess the effects of TREM2 ectodomain mutations in the binding to TREM2.

In light of the fact that TREM2 is expressed in the microglia that surround extracellular plaques, it would be interesting to study how TREM2 interacts with Aβ aggregates (Jiang et al. 2014; Yuan et al. 2016; Jay et al. 2017) and also decrease in the number of plaque-associated microglia have been observed in TREM2 knockout mouse models (Jay et al. 2017; Yuan et al. 2016; Ulrich et al. 2014; Jay et al. 2015; Wang et al. 2015; Wang et al. 2016).

With this approach in mind, *we demonstrate that the loss of TREM2 or TREM2 disease-associated variants leads to specific changes in the deposition and accumulation of*

[*] *Italicized text is taken from the manuscript published in GLIA by Joshi et al. 2021*

phosphorylated Aβ species in the brains of APP transgenic mice (Joshi et al. 2021b). To assess the role of TREM2 in the deposition of phosphorylated Aβ species in-vivo, two different APP/PS1 transgenic mouse models crossed to TREM2 WT, TREM2$^{-/-}$ mice or TREM2^{T66M} mice were used (Joshi et al. 2021b). Consistent with previous findings (Boon et al. 2020; Kumar et al. 2013; Kumar et al. 2016), pSer8-Aβ and pSer26-Aβ showed differential deposition (Prada et al. 2006). While pSer8-Aβ deposits primarily in the core of the plaques, pSer26-Aβ showed limited deposition in plaques (Kumar et al. 2020a; Boon et al. 2020). Importantly, pSer8-Aβ was hardly detected within microglia, but mainly as fibrillar Aβ in the plaque core which also contained N-terminally unmodified Aβ. These data are in line with the fibrillization-promoting effect of Ser8-phosphorylation (Kumar et al. 2011a; Yu et al. 2015). Thus, although microglia could bind to Ser8-Aβ containing aggregates, their internalization might be restricted by the high compaction of these peptides within the plaque core (Joshi et al. 2021b). In contrast, pSer26-Aβ was prominently detected within plaque-associated microglia. Since the phosphorylation at Ser26 prevents fibrillization but stabilizes oligomeric states of Aβ (Kumar et al. 2016; Rezaei-Ghaleh et al. 2014), soluble pSer26-Aβ assemblies might efficiently bind to TREM2 and be internalized (Joshi et al. 2021b)[*]*. Thus, phosphorylated Aβ species despite increased binding and pEAβ(3-42) with least binding to TREM2, differential aggregation and metabolic stability of Aβ species are likely to contribute to the specific accumulation and differential deposition in brains of transgenic mice in addition to the differential interaction with TREM2 (Joshi et al. 2021b). Further research is needed to determine whether TREM2 mediates the differential accumulation of various post-translationally modified Aβ variants in the brain.

Given the fact that Aβ oligomers are described as soluble, immunostainings with anti-oligomeric antibodies suggest that oligomeric Aβ is also present within the core of extracellular plaques (Koffie et al. 2009). This raises interesting speculation that TREM2 could interact with this plaque-associated oligomeric Aβ and one such modified Aβ we report is pSer26-Aβ which deposits in the extracellular plaques as well as is found in the plaque-associated microglia (Tanzi 2015; Yeh et al. 2017; Joshi et al. 2021b). Further research is needed with advanced imaging techniques such as 2-photon to investigate the biological effects of TREM2 engagement by the Aβ oligomers that are present in the extracellular plaques as well as also in the peri-plaque region.

Pyroglutamate-modified species, N3pE-Aβ, is known for its prion-like behaviour (Nussbaum et al. 2012), enhanced aggregation kinetics (Dammers et al. 2015), intraneuronal accumulation, and senile plaques (De Kimpe et al. 2013; Wirths et al. 2010b). Several studies have shown a sequential deposition starting with nmAβ peptides, followed by pEAβ (3-42) and pSer8-Aβ

[*] *Italicized text is taken from the manuscript published in GLIA by Joshi et al. 2021*

species in extracellular plaques during the progression from pre-clinical to clinical phases of AD (Thal et al. 2015; Yano et al. 2018; Rijal Upadhaya et al. 2014; Gerth et al. 2018). *In contrast to phosphorylation, pyro-glutamination and nitration do not change the overall charge of Aβ. Since TREM2 preferentially binds anionic ligands (Kober et al. 2017; Walter 2016; Ulrich et al. 2017), the additional negative charges introduced by phosphorylation, likely contribute to the increased association of phosphorylated Aβ with TREM2. However, additional effects of distinct post-translational modifications on the conformation and aggregation status of Aβ assemblies could also modulate binding to TREM2. Further, distinct post-translational modifications could affect phagocytosis and degradation pathways of these species as well as their deposition and neurotoxic properties independent of TREM2. Indeed, phosphorylation, nitration, and pyro-glutamination of Aβ differentially affect the aggregation and neurotoxicity of Aβ in-vitro systems without the involvement of TREM2 (Nussbaum et al. 2012; Dammers et al. 2015; Kummer et al. 2011; Kumar et al. 2016)*[*].*

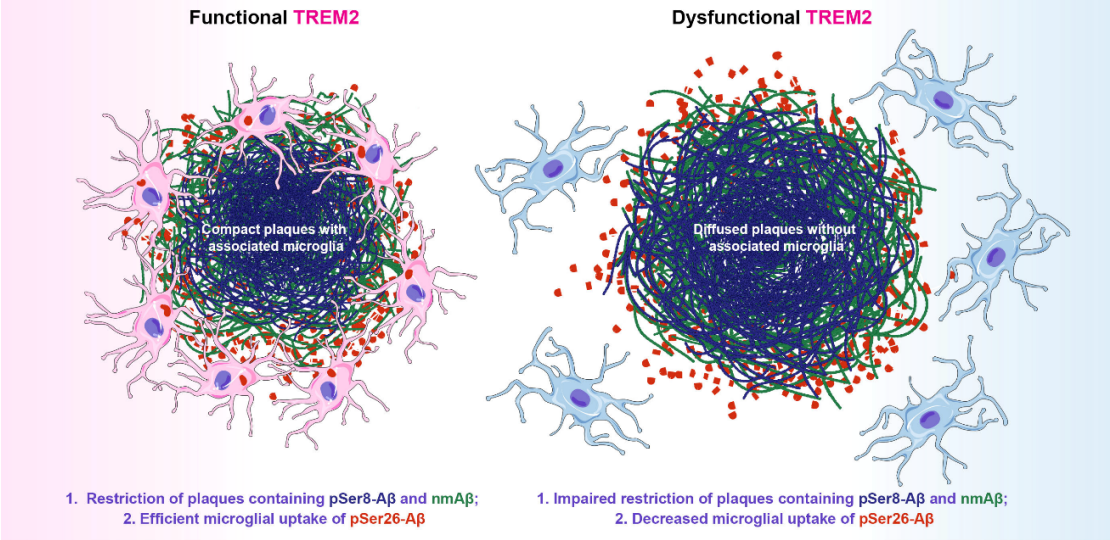

Figure 7.1 | Effect of dysfunctional TREM2 on the deposition of phosphorylated Aβ variants in transgenic mouse brains

TREM2 deletion or the disease-associated mutation in the microglia of APP/PS1 transgenic mice leads to diffuse plaques containing pSer8-Aβ and nmAβ due to impaired restriction and decreased plaque-associated microglia. Also, dysfunctional microglia lead to decreased uptake of pSer26-Aβ by the plaque-associated microglia in the APP/PS1 transgenic mice. *(Illustration was created by Pranav Joshi as now published as a part of (Joshi et al. 2021b), CC BY © 2021 Joshi et al.*

Thus, it will be interesting to further dissect the relative contribution of TREM2 and microglia in the deposition and neurotoxic properties of the different Aβ species in the brain during the pathogenesis of AD. It should be noted that the deposition of non-modified, pyroglutamate-[*] *modified and phosphorylated Aβ species follows a specific sequence in the brain with initial*

[*] *Italicized text is taken from the manuscript published in GLIA by Joshi et al. 2021*

deposits not containing detectable amounts of pyroglutaminated or phosphorylated Aϐ species (Thal et al. 2019; Rijal Upadhaya et al. 2014; Gerth et al. 2018)[*]. While pyroglutaminated Aϐ variants can also be detected in a subset of cases without clinical signs of dementia, detection of phosphorylated Ser8-Aϐ is mainly restricted to cases with clinical manifestation of AD (Rijal Upadhaya et al. 2014; Thal et al. 2019).

As mentioned above, pSer26-Aϐ species show limited deposition in extracellular plaques but are also found intra-neuronally and in vascular deposits (Kumar et al. 2016; Kumar et al. 2020a). Thus, post-translational modifications likely contribute to the specific accumulation and differential deposition in the brain and could represent interesting targets for AD therapy. Indeed, recent data from phase 2 clinical trials revealed positive effects of antibodies specifically recognizing pyroglutamate modified Aϐ (Donanemab) in early AD (Mintun et al. 2021). Thus, it will be important to further assess the potential of targeting phosphorylated Aϐ species in AD therapy and prevention[*].

In-vitro studies as well as studies reported before indicate that Aβ at varying aggregation states that include monomers, oligomers, and fibrils binds to sTREM2 (Lessard et al. 2018; Joshi et al. 2021b; Zhao et al. 2018). The binding of sTREM2 and Aβ oligomers is characterized by very slow dissociation, which can also block the binding with other ligands (Lessard et al. 2018). Upon assembly of the TREM2-Aβ complex, microglia are activated to initiate programmed cell phagocytosis to clear aggregated proteins (Wang et al. 2015). At the same time, one could speculate that TREM2, as well as sTREM2, settle around Aβ plaques, thereby preventing the plaques from spreading into the surrounding healthy tissues (Song et al. 2018; Yuan et al. 2016; Zhao et al. 2018; Condello et al. 2015) and the plaque-associated microglia release inflammation-related factors. In this regard, it is important to dissect the role of sTREM2 ectodomain in terms of the binding of sTREM2 to the Aβ plaques and its functional role in the microglial clearance of Aβ. To address this question a recent study showed that stereotaxic injection of recombinant sTREM2 protein could decrease Aβ deposition and rescue the behavioural deficits in 5XFAD mice which suggests that sTREM2 affects the Aβ-induced pathology directly exerting the neuroprotective effects (Zhong et al. 2019). This work revealed important aspects of TREM2 in the interaction and uptake of different modified Aβ variants by microglia that could contribute to the heterogeneity in Aβ-related pathology, and the changes in the composition of Aβ deposits during the progression of AD (Rijal Upadhaya et al. 2014; Thal et al. 2015; Gerth et al. 2018; Boon et al. 2020).

[*]*Italicized text is taken from the manuscript published in GLIA by Joshi et al. 2021*

7.3 | Intraneuronal and vascular deposition of Ser26 pseudophosphorylated Aβ is associated with impaired memory of transgenic mice

Extracellular deposits of Aβ consist of peptides of different lengths (Murphy et al. 2010; Kummer et al. 2014; Kumar et al. 2011b; Barykin et al. 2017) that make both diffuse pre-amyloid lesions and mature amyloid plaques (Serrano-Pozo et al. 2011). In addition, fibrillar Aβ deposition is also commonly observed in small and medium-sized cerebral vessels, known as CAA (Biffi et al. 2011; Weller et al. 2009). These Aβ peptides and the resulting deposits have cytotoxic properties and have a detrimental impact on neuronal signal transmission and thus have a central function in AD pathogenesis (Querfurth et al. 2010). *In-vivo* imaging using radioligands for Aβ deposits, strongly indicate that Aβ deposition in the brain occurs early in AD, perhaps even decades before overt symptoms (Scheltens et al. 2016; Villemagne et al. 2013). Aβ aggregation process leading to soluble oligomeric assemblies of amyloidogenic proteins are increasingly thought to initiate disease-specific cytopathology and subsequent symptoms (Haass et al. 2007; Benilova et al. 2012). Hence, the oligomeric species of Aβ could be the active targets for therapeutic intervention (Haass et al. 2007).

In the present study, a novel AβS26D-Tg mouse model expressing the phosphomimicking mutation (S→D) at Ser26 residue of Aβ peptide was generated to specifically analyze the neuropathological and cognitive effects of this particular Aβ peptide. The novel AβS26D-Tg mice with C57BL/6 background express the APP751 gene including the Swedish mutation driven by the neuron-specific Thy1 promoter. The well-characterized APP23-Tg mouse model expresses APP751 including the Swedish mutation driven by the neuron-specific Thy1 promoter (Sturchler-Pierrat et al. 1997), demonstrated classical AD-like neuropathology including extracellular Aβ plaque deposition at ~6 months of age and cognitive deficits that become more severe with age (Van Dam et al. 2003; Tomiyama et al. 2010). On immunostaining examination, AβS26D-Tg mice exhibited intracellular accumulation of Aβ within neurons in the brain regions such as the olfactory bulb, prefrontal cortex, striatum, hippocampus and amygdala from 4 months, but no amyloid plaques even at 24 months. Despite the similarities in the neuron-specific expression of human APP carrying the Swedish mutation, the phosphomimicking mutation introduced at Ser-26 residue stabilizes the Aβ oligomeric assembly and thus reduces the protofibril formation (Kumar et al. 2016; Kumar et al. 2020a). These peptides do not form amyloid fibrils *in-vitro* and are not deposited in amyloid plaques which are common to the APP23-Tg mouse model and AD patients' brains. Thus, enhanced formation of Aβ oligomers without amyloid plaques in this novel mouse model will help to understand the relative contribution of Aβ oligomers to the pathophysiological function in the progression of AD.

As previously stated, phosphorylation of the Aβ-peptide at Ser26 stabilizes oligomeric assembly (Kumar et al. 2016), preventing a distinct conformational rearrangement that is

required for the progression of Aβ aggregation toward fibrils (Rezaei-Ghaleh et al. 2014) and increases Aβ neurotoxicity (Kumar et al. 2016). The Ser26 is located at the centre of the turn motif, its phosphorylation interferes with the formation of a fibril-specific salt-bridge between amino acid residues Asp23 and Lys28 (Rezaei-Ghaleh et al. 2014), which plays a crucial role in Aβ monomer folding and oligomerization. Thus, rapid oligomerization of pSer26-Aβ and S26D-Aβ without proceeding to the protofibrils or fibrils was observed. Furthermore, in contrast to the wild-type Aβ peptide, pSer26Aβ and AβS26D are devoid of discernible secondary structure and exhibited little or no binding to thioflavin T dye (Kumar et al. 2016; Rezaei-Ghaleh et al. 2014).

In AD pathology, clustering of activated astrocytes and microglia around amyloid plaques is observed and is thought to be involved in neurodegeneration via cytokine and chemokine release from these cells. Activation of astrocytes and/or microglia has been observed in many APP-Tg mice, though again this was only after amyloid plaque formation and was in the vicinity of plaques (Duyckaerts et al. 2008). The immunohistochemical examination of WT and AβS26D-Tg mice exhibited age-dependent activation of microglia in both genotypes while the microglial activation was pronounced in AβS26D-Tg at 24 months of age as compared to sex and age-matched WT mice. Although we could not detect extracellular Aβ oligomers in the AβS26D-Tg mouse brain, the observed microglial activation may be caused by extracellular diffusible Aβ oligomers from neurons (Oddo et al. 2006). Alternatively, microglia might have been activated and recruited by cytokines or chemokines released from glial cells which neighboured and were in contact with aberrant neurons containing Aβ oligomers. In APP-Tg mice, the occurrence of neuronal loss has in several lines been reported only after the intense development of amyloid plaques (Duyckaerts et al. 2008). On immunohistochemical examination, AβS26DTg mice, despite their lack of amyloid plaques, exhibited a significant neuronal loss in the cortex region at 24 months. This supports that neuronal loss was induced by Aβ oligomers alone *in-vivo* in the absence of amyloid plaques. Consistent with other studies with oligomer mouse models, no neuronal loss was observed at younger ages, suggesting that Aβ oligomer-induced neuronal death requires long exposure of cells to Aβ oligomers *in-vivo* (Tomiyama et al. 2010). These findings suggest that neuroinflammation and extracellular amyloid plaques are likely to be triggered by insoluble higher-ordered Aβ assemblies.

It has been demonstrated that the accumulation of intraneuronal Aβ in the hippocampus (4 months) before amyloid plaque formation (12 months) is correlated with synaptic and cognitive dysfunction in the triple transgenic 3xTg-AD mice (Oddo et al. 2003; Billings et al. 2005). Also, in ArcAβ-Tg mice, cognitive dysfunction was observed at 6 months, after the intraneuronal accumulation of Aβ (3 months) but before amyloid plaque formation (7 months) (Knobloch et al. 2007), and in Tg2576 mouse brains, morphological alterations of synapses occurred in association with intraneuronal accumulation of Aβ (Takahashi et al. 2002), among

which some of the intraneuronal Aβ formed oligomers (Takahashi et al. 2004). Many other studies of cases with AD (Gouras et al. 2000; Fernandez-Vizarra et al. 2004) or Down syndrome (Mori et al. 2002), and with APP-Tg mice (Tomiyama et al. 2008; Billings et al. 2005; Oddo et al. 2003; Casas et al. 2004; Lord et al. 2006; Oakley et al. 2006) have demonstrated Aβ accumulation intraneuronally as an early pathological change observed before amyloid plaque formation. These findings imply that AβS26D stable oligomers can be found as intracellular, in particular, intraneuronal aggregates and are associated with cognitive abnormalities. A similar relationship between intracellular Aβ and cognitive abnormalities has been reported in various AD-Tg mice (Tomiyama et al. 2010; Ochiishi et al. 2019; Faucher et al. 2015).

According to previous studies, the incidence of CAA increases with age and 80-100% of the AD patients exhibits CAA (Vinters 1987; Attems 2005; Joachim et al. 1988; Thal et al. 2008b; Barker et al. 2002; Thal et al. 2008a). The majority of CAA patients also demonstrate parenchymal Aβ deposition, but there have been reports of CAA patients without parenchymal Aβ depositions, as well as AD patients without CAA (Kalaria 2016; Suzuki et al. 1994b; Vinters et al. 1983; Hamaguchi et al. 2021). In this study, the presence of vascular Aβ in AβS26D-Tg transgenic mice was detected prominently using 7H3D6 and 6E10 antibodies in both male and female mice. It is still necessary to further characterise these vascular deposits using C-terminal specific antibodies as well as Aβ40 and Aβ42 specific antibodies. Furthermore, CAA staging is required to quantify the severity of this vascular pathology.

In summary, these AβS26D-Tg mice demonstrate the accumulation of Aβ peptides inside of neurons and this resulted in neuronal loss and memory impairment, even though no AD typical pathology had appeared. These findings provide new insight into the pathogenesis of AD, that amyloid plaque formation is not an absolute requirement for the cognitive impairment in mice. Instead, Aβ oligomers play pivotal roles throughout the progression of AD. Indeed, the occurrence of NFTs has not been tested in these mice and thus needs further analysis of this model. Nevertheless, this novel Tg mice are represented as an animal model of Aβ oligomer-induced pathology avoiding the effects of extracellular Aβ plaques even at old ages, and are thus a valuable means of investigation of the pathological and physiological roles of Aβ oligomers and also shows the importance to further evaluate the potential of phosphorylated Aβ species in AD therapy and prevention.

7.4 | TREM2 modulates differential deposition of modified and non-modified Aβ species in extracellular plaques and intraneuronal deposits

One of the most well-documented molecular mechanisms by which fAD mutations underlie AD molecular pathogenesis is the alteration of cellular trafficking (Walter 2006; Yuksel et al. 2019) and/or proteolytic processing of the APP, leading to changes in the Aβ peptide at its N

or C terminus, which then alter aggregation (Barykin et al. 2017; Kummer et al. 2014). Considering the complexity of the Aβ species as a result of its modifications during and after APP processing by various enzymes, it will be a worthwhile endeavour to routinely assess modified Aβ species as they could serve as excellent diagnostic markers or therapeutic targets in the future. In this part of the work, the effects of TREM2 deficiency or disease-associated T66M mutation on the composition of amyloid plaques, with attention to phosphorylated Aβ species are demonstrated.

The effect of deletion of TREM2 on the deposition of Aβ in transgenic mice depends on models, age, and the region of the brain being analyzed (Jay et al. 2017; Parhizkar et al. 2019). Although a role for TREM2 in AD pathogenesis has been recently proposed, there exist conflicting data on the role of TREM2 in the deposition of Aβ plaque in transgenic AD mouse models (Jay et al. 2015; Wang et al. 2015). Deletion of TREM2 in APP/PS1 mouse model leads to reduction of Aβ plaque load at early stages of AD onset, yet exacerbates Aβ deposition at late stages of onset (Jay et al. 2017). In addition, NFTs may either increase or decrease while human τ protein studies in mice also show variable responses to deletion on TREM2 (Lee et al. 2021; Leyns et al. 2019; Bemiller et al. 2017; Gratuze et al. 2020). Moreover, TREM2 deletion is protective in the PS19 (P301S mutation of Microtubule Associated Protein τ) model of AD (Yoshiyama et al. 2007; Meilandt et al. 2020; Leyns et al. 2017). The conflicting results may be due to genetic differences and/or to additional effects of APP/PS1 overexpression (Cavanaugh et al. 2014; Lee et al. 2013b). It is important to note that several studies reported consistently that, TREM2 deficient or haplo-deficient APPPS1-21 and 5xFAD mice showed decreased microglial activation, leading to reduced plaque-associated microglia (Jay et al. 2015; Wang et al. 2015; Ulrich et al. 2014). Also, microglia failed to cluster around plaques in APPPS1-21 mice haplo-deficient or deficient for DAP12 (Yuan et al. 2016), suggesting that TREM2 is required for the recruitment of microglia to plaques. The inability of TREM2 deficient microglia to cluster around plaques was associated with defects in plaque compaction, microglia proliferation, and increased levels of dystrophic neurons (Wang et al. 2015; Wang et al. 2016; Yuan et al. 2016).

The role of TREM2 on Aβ deposition remains unclear, and a definitive model of how TREM2 contributes mechanistically to Aβ pathology and AD pathogenesis has yet to be established. TREM2 directly interacts with post-translationally modified Aβ, in particular, phosphorylated Aβ species and regulates Aβ aggregation, microglial binding and uptake, and demonstrates a novel role for TREM2 as a microglial receptor in phagocytosis of modified Aβ species in Aβ conformation and aggregation dependent manner (Joshi et al. 2021b).

To investigate the role of TREM2 in the deposition of Aβ in the brain validated antibodies detecting different modified Aβ species mentioned in Section-2.2 were used. This work demonstrates that the *deletion of TREM2 or TREM2 disease-associated variants leads to*

specific quantitative and qualitative changes of Aβ deposits in the brains of APP transgenic mice and human cases with the diagnosis of dementia and that TREM2 not only modulates the composition of extracellular plaques but also of intraneuronal deposits[*]*.*

TREM2 plays a fundamental role in the regulation of microglial activity and the deposition of Aβ in extracellular plaques (Jay et al. 2015; Jiang et al. 2014; Ulrich et al. 2014; Joshi et al. 2021b). However, Aβ exists in multiple variants with different lengths and post-translational modifications which differ in their aggregation behaviour, biostability, deposition and neurotoxic properties (Barykin et al. 2017; Kummer et al. 2014). It was shown recently that phosphorylation of Aβ modulates the direct interaction with TREM2 and the internalization by microglia (Joshi et al. 2021b). Phosphorylation at Ser8 also decreases the degradation of Aβ by the insulin-degrading enzyme that can be secreted by microglia (Kumar et al. 2012; Tamboli et al. 2010)[*]*.*

To assess the role of TREM2 in the deposition of modified Aβ species in-vivo, Aβ pathology was analyzed in three different mouse models of AD. Consistent with previous reports (Jay et al. 2015; Wang et al. 2016), TREM2 deletion was associated with increased Aβ deposition at younger (4-5 months) and older ages (12-15 months), and impaired microglial clustering around extracellular Aβ plaques (Joshi et al. 2021b). Importantly, the phosphorylated Aβ species, pSer8-Aβ, selectively increased as compared to other Aβ species in brains of 5xFAD and APP/PS1L166P transgenic mice upon deletion of TREM2. Increased accumulation of phosphorylated Aβ species was also observed in the brains of knock-in (KI) mice with the TREM2^{T66M} *mutation that causes FTD-like syndrome and NHD. In this regard, it is interesting to note that NHD cases could show AD characteristic neuropathological lesions, including senile plaques and neurofibrillary tangles (Bird et al. 1983). Consistent with previous findings (Kumar et al. 2016; Kumar et al. 2013; Kumar et al. 2020a; Joshi et al. 2021b), pSer8-Aβ is prominently detected in the core of extracellular plaques and also accumulated intraneuronally in the brains of 12M old TREM2*$^{-/-}$ *as compared with TREM2*$^{+/+}$ *in both 5xFAD and APP/PS1L166P mice. Very similar alterations in the deposition of the different Aβ species were also observed in TREM2*^{T66M} *KI mice as compared to mice expressing TREM2, indicating that disease-associated loss-of-function mutations also modulate the differential deposition of distinct Aβ variants*[*]*.*

In contrast, pSer26-Aβ was not enriched in the core of plaques but rather appeared as smaller deposits associated with plaques. Both phosphorylated species also accumulated in brain vessels and intraneuronally in brains of 12M old TREM2$^{-/-}$ as compared with TREM2$^{+/+}$ in both 5xFAD and APP/PS1L166P mice. Additionally, pSer26-Aβ was abundantly detected in TREM2 positive microglia surrounding the plaque core in TREM2$^{+/+}$ mice and less frequently in

[*] *Italicized text is taken from the manuscript published in Acta neuropathologica communications by Joshi et al. 2021*

microglia of TREM2$^{-/-}$ mice. Very similar alterations in the deposition of the different Aβ species were also observed in TREM2^{T66M} KI mice as compared to mice expressing TREM2$^{+/+}$ showing that disease-associated loss-of-function mutations also modulate the differential deposition of distinct Aβ variants. Altered plaque development and CAA related pathology has recently been observed upon depletion of microglia in the mouse brain (Spangenberg et al. 2019; Huang et al. 2021), showing that functional microglia are important to shape extracellular plaques and restrict the deposition of Aβ in the brain vasculature. The current study suggests that TREM2 deficiency could also result in increased deposition of phosphorylated Aβ in CAA.

Studies indicate that CAA preferentially contains Aβ40 species that are less prone to aggregate as compared to Aβ42 which has a much higher tendency to form fibrils and initially deposits in form of extracellular plaques (Kumar-Singh 2008; Miyakawa et al. 2000; Kakuda et al. 2017). Previously studies reported that pSer26-Aβ is much less prone to fibrilize and forms soluble oligomers. Thus, one could speculate that decreased clearance of these species by microglia with deleted or mutant TREM2 promotes deposition intraneuronally and in CAA. Indeed, binding and phagocytosis assays with primary microglia demonstrated increased phagocytosis of pSer26-Aβ as compared to other species, and strongly reduced uptake in TREM2^{T66M} mutant microglia.

Biochemical analysis of brain extracts revealed that TREM2 deficiency or the expression of the NHD associated T66M in APP transgenic mice increased the levels of pSer8-Aβ in form of oligomeric assemblies. Aβ oligomers exert neurotoxicity, and oligomer levels correlate with neuronal dysfunction in AD (Schutzmann et al. 2021; Sengupta et al. 2016; Tanokashira et al. 2017; Benilova et al. 2012; Yoo et al. 2020; He et al. 2019; Palop et al. 2010). Aβ oligomers also seed fibrillization and promote the deposition in form of extracellular plaques[*] (Katzmarski et al. 2020; Friesen et al. 2019; Hardy et al. 2002; Chen et al. 2017). In addition, oligomers can be internalized by neurons resulting in Aβ accumulation within neurons (Schutzmann et al. 2021; Bayer et al. 2010; Friedrich et al. 2010; Takahashi et al. 2004). Since TREM2 has been shown to selectively bind oligomeric assemblies of Aβ and promote microglial uptake (Zhao et al. 2018; Vilalta et al. 2021; Lessard et al. 2018; Joshi et al. 2021b), the loss of TREM2 function could result in decreased clearance of oligomers and thereby lead to increased uptake by neurons, and deposition in extracellular plaques and the vasculature. Indeed, altered plaque development and CAA related pathology has recently been observed in mouse brain upon depletion of microglia (Spangenberg et al. 2019; Huang et al. 2021), showing that functional microglia are important to shape extracellular plaques and restrict the deposition of Aβ in[*] the brain vasculature. pSer8-Aβ and nmAβ were also detected in vessels of transgenic mouse

[*] *Italicized text is taken from the manuscript published in Acta neuropathologica communications by Joshi et al. 2021*

brains, and it will be interesting the further investigate the role of TREM2 in the deposition and the potential pathophysiological implications of modified Aβ species in the vasculature[*].*

Human brain sections were analyzed with rare TREM2^{R62H} or TREM2^{R62C} mutation, another well-studied point mutation that increases the risk for late-onset AD (Parhizkar et al. 2019; Jin et al. 2014; Sims et al. 2017). *The analysis of human cases with rare TREM2^{R62H} or TREM2^{R62C} variants showed significantly increased accumulation of phosphorylated Aβ species inside neurons and alterations in plaque size, load and number, further indicating that impairment of TREM2 function mediates the formation and composition of AD characteristic lesions*[*]. Notably, pSer8-Aβ plaque size was not increased in the brains of carriers with rare TREM2 variants, suggesting a difference in the observations from transgenic mice and human brains. It should be noted that human cases all had advanced or end-stage AD pathology. Thus, potential differences during deposition and disease progression could not be assessed. Importantly, the intraneuronal deposition of pSer8-Aβ and pSer26-Aβ was significantly elevated in TREM2 rare variant carriers, confirming this aspect of pathological changes from transgenic mouse models. The present data are supporting the hypothesis that TREM2 plays a critical role in the sensing of different Aβ species, and that a loss of TREM2 function leads to altered deposition of these peptides.

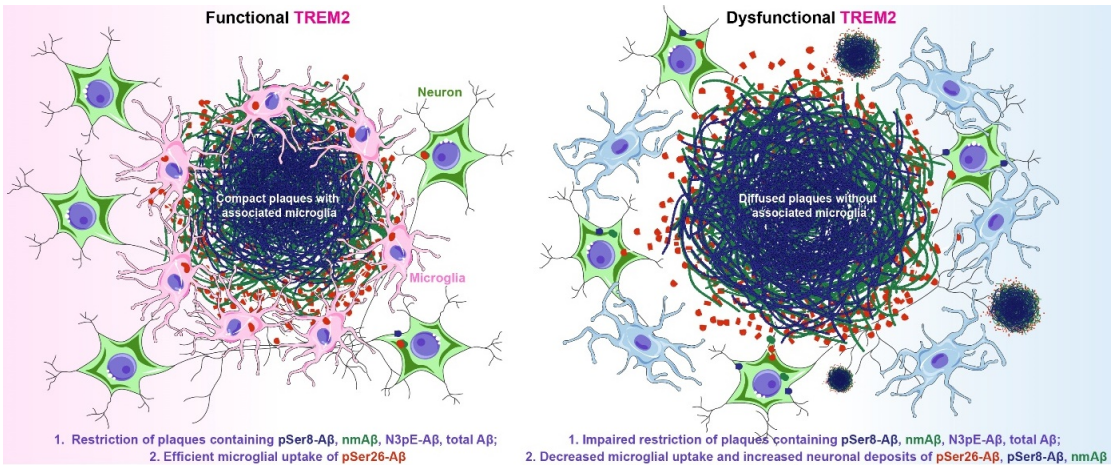

Figure 7.2| Effect of dysfunctional TREM2 on deposition of modified and non-modified Aβ species in extracellular plaques and intraneuronal deposits

TREM2 deletion or the disease-associated mutation in the microglia of APP/PS1 transgenic mice leads to an increase in the number and size of plaques containing pSer8-Aβ, nmAβ, and Aβ due to impaired restriction and decreased plaque-associated microglia. Also, dysfunctional microglia leads to decreased uptake of pSer26-Aβ by the plaque-associated microglia while increased neuronal deposits of pSer8-Aβ, pSer26-Aβ and nmAβ in the transgenic mice and human AD brains with rare TREM2 variants. *(Illustration was created by Pranav Joshi)*

[*] *Italicized text is taken from the manuscript published in Acta neuropathologica communications by Joshi et al. 2021*

It is important to mention that the abundance of intraneuronal Aβ in AD is still controversial (Gouras et al. 2010), and the cross-reactivity of several generic Aβ antibodies commonly used for immunohistochemical analyses and diagnosis (e.g. 4G8 and 6E10) with full-length APP or APP-CTFs complicates the interpretation of results. Additionally, the recognition of Aβ peptides by antibodies might be influenced by the conformation of intracellular Aβ assemblies, epitope masking and post-translational modifications. Previously it was demonstrated that the monoclonal antibody 6E10 that recognizes an N-terminal epitope does not detect Aβ when Ser8 is in a phosphorylated state (Kumar et al. 2011a). Also, see little reactivity was observed of the 4G8 with intracellular Aβ in the human brain, probably due to specific conformations of intracellular Aβ as compared to Aβ fibrils in extracellular plaques. By using several monoclonal and polyclonal antibodies that specifically detect Aβ in different phosphorylation states without cross-reacting with full-length APP or C-terminal fragments as demonstrated by western immunoblotting in previous studies and the present study, the occurrence of phosphorylated Aβ variants inside of neurons was demonstrated. Although the molecular mechanisms for neuronal Aβ internalization have remained unclear, the involvement of numerous receptors in the endocytosis of Aβ was described, as well as an accumulation of internalized Aβ in the endosomal/lysosomal system or late endosomes/multivesicular bodies (MVBs) (Mohamed et al. 2011b; Mohamed et al. 2011a; Gouras et al. 2010). The microglial Aβ uptake may reflect mainly clearance activity, whereas neuronal dysfunction mediated by neuronal Aβ deposition may represent an alternative mechanism in the progression of AD (LaFerla et al. 2007; Bayer et al. 2010; Lai et al. 2010; Christensen et al. 2014). Further studies will be required to reveal the mechanisms underlying the differential accumulation of phosphorylated Aβ peptides inside neurons. In addition, it will be also worth studying the potential role of TREM2 in regulating this deposition.

In addition to the previously described effects of TREM2 on plaque morphology, this study provides evidence for a critical role of TREM2 in the restriction of other characteristic AD-related lesions, including intraneuronal and vascular Aβ deposits that are highly correlated with clinical presentation and disease progression (Welikovitch et al. 2020; Condello et al. 2018a; Thal et al. 2008a). Further, it is demonstrated that TREM2 also modulates the composition of these lesions. This is interesting, because changes in the composition of extracellular plaques and CAA, in particular the occurrence of phosphorylated Aβ, are associated with clinical manifestation and progression of AD (Rijal Upadhaya et al. 2014; Gerth et al. 2018). Additional studies that analyze the temporal course of amyloid pathology in TREM2 deficient amyloidosis models will be necessary to clearly understand the role of TREM2 in plaque accumulation and clearance and for this, a less aggressive model of Aβ deposition will be useful to finely dissect the effect of TREM2 on Aβ accumulation.

Thus, in addition to the previously described effects of TREM2 on plaque morphology, this study provides evidence for a critical role of TREM2 in the restriction of intraneuronal Aβ deposits that are highly correlated with clinical presentation and disease progression (Welikovitch et al. 2020; Condello et al. 2018a; Thal et al. 2008a; Bayer et al. 2010; Gouras et al. 2000; Gouras et al. 2010; Jawhar et al. 2012). Further, it is shown that TREM2 also modulates the composition of these lesions. This is interesting, because changes in the composition of extracellular plaques and CAA, in particular the occurrence of phosphorylated Aβ, are associated with clinical manifestation and progression of AD (Rijal Upadhaya et al. 2014; Gerth et al. 2018; Libard et al. 2021; Thal et al. 2019)[*].*

Although TREM2 loss-of-function mutations could also contribute to neurodegeneration independently of Aβ by impairment of brain energy metabolism (Kleinberger et al. 2017), synapse dynamics (Mazaheri et al. 2017; Jadhav et al. 2020), and formation of neurofibrillary tangles (Leyns et al. 2017), a recent study suggests an important role of Aβ pathology in the TREM2 dependent formation of τ *pathology and brain atrophy (Lee et al. 2021). Thus, the differential interaction of TREM2 with modified Aβ species might not only be important for the deposition and composition of different Aβ lesions but also contribute to the development of* τ *pathology that together determines the onset and progression of AD*[*].

7.5 | Future Outlook

In recent years, TREM2 became the most important signalling molecule in the field of AD research. Researchers are trying to implement strategies to target TREM2 signalling in search of possible therapeutic intervention. One such approach was to activate the TREM2 to stimulate microglia to phagocytose and clear Aβ deposits. This was achieved by using an agonist monoclonal antibody against TREM2 (AL002) which is now in a phase I trial for AD patients (Wang et al. 2020). Another approach could be targeting condition- and/or tissue-specific TREM2 ligands, however in such cases, knowledge about such specific TREM2 ligands is limited. Moreover, TREM2 is constantly shed by the ADAMs to produce, sTREM2 which also exerts a neuroprotective effect by improving the Aβ clearance effect of microglia thus reducing the plaque load (Kim et al. 2017; Ewers et al. 2019), whereas sTREM2 can also trigger microglia to release pro-inflammatory cytokines, which may adversely affect neuronal function (Zheng et al. 2016). Although there are many pathophysiological effects, it is still unclear whether sTREM2 is formed in the early phase or as a response to changes in the microenvironment in the CNS (Finelli et al. 2015). It exerts a neuroprotective effect against AD by stimulating the innate immune system that drives microglial migration toward Aβ fibrils and abnormal neurons to facilitate phagocytosis (Yeh et al. 2017; Golde et al. 2013). In addition, sTREM2 plays a critical role in reducing the Aβ deposits (Zhong et al. 2019) and also

[*] *Italicized text is taken from the manuscript published in Acta neuropathologica communications by Joshi et al. 2021*

in τ phosphorylation. Inhibition or accelerating ADAMs is another potential point of intervention (Voytyuk et al. 2018). However, the limitation of this approach lies in the wide range of substrates of ADAM10/17 and inhibiting a specific protease activity is in most cases leads to unwanted side effects. So better understanding of the expression, localization and regulatory mechanisms of these ADAMs will help to uncover suitable targets for more specific blocking of TREM2 shedding. In a recent study, antibody 4D9 binds to the stalk region of TREM2 and reduces its proteolytic shedding. In addition, this antibody has also been shown to activate TREM2 signalling and promote microglia transitioning to the disease-associated state, microglial survival and Aβ uptake (Schlepckow et al. 2020). Inhibition or activation of specific intracellular signalling cascade downstream of TREM2 could be a different strategy, but because DAP10/12, Syk, and PI3K are involved in many other signal transduction pathways, they are unlikely to become effective therapeutic targets in the context of TREM2-specific therapy. The goal of these strategies is to stimulate macrophages and microglia by increasing TREM2 signalling.

Several studies have reported varying levels of sTREM2 in the CSF and blood at different stages of AD progression (Lue et al. 2015b) and also higher levels in the peripheral blood of AD patients compared to the healthy individuals (Hu et al. 2014; Casati et al. 2018), whereas other investigators reported no significant difference (Piccio et al. 2008; Liu et al. 2018) and the origins of serum sTREM2 are still under study (Fahrenhold et al. 2018). This discrepancy in the results might be attributed to the designation of groups and important patient characteristics (i.e., age, gender and disease stage). More research is needed to investigate the functions and metabolism of sTREM2 in the peripheral blood, as well as the pathology of AD.

TREM2 ectodomain interacts with Aβ (Lessard et al. 2018; Vilalta et al. 2021; Zhao et al. 2018; Joshi et al. 2021b) and this binding is stronger upon phosphorylation of Aβ in a conformation or aggregation state manner (Joshi et al. 2021b). Although there is experimental support for the hypothesis that reduced microglial interaction with Aβ plaques in TREM2 knockout mice leads to damage to nearby neuronal processes, microglial depletion by CSFR1 inhibitor in Aβ plaque-forming mice suggested that reduced microglial containment of plaques is not always harmful to neurons. In two independent mouse models, treatment with the CSFR1 inhibitor, eliminated microglia (Spangenberg et al. 2016) without affecting Aβ plaque levels. However, it did rescue dendritic spines, reduced neuronal loss in the subiculum and showed improvements in cognitive function without significant changes in Aβ plaque load (Spangenberg et al. 2016; Olmos-Alonso et al. 2016). This suggests a detrimental role of microglia on the neuronal function that is independent of effects on Aβ plaques and that a reduction in plaque- (and non-plaque)-associated microglia can be beneficial or that other pools of Aβ (not associated with plaques) are detrimental. Hence, identification/dissection of

TREM2 or Aβ dependent and independent pathways will help to understand the progression of AD.

It is shown that microglia are activated in two steps with an initial TREM2-independent process followed by a TREM2-dependent process (Keren-Shaul et al. 2017). The increase in CSF sTREM2 observed after the initial low levels may represent the second step of activation. Another possibility is that microglia initially form a barrier around plaques (Condello et al. 2015; Wang et al. 2016), and the sTREM2 released by microglia is retained within the plaque until the barrier fails and subsequent neural injury begins. Finally, it could be argued that subjects with low TREM2-function (and thus lower CSF sTREM2 levels) are more prone to early amyloidogenesis. This work reports that TREM2 regulate the deposition of post-translationally modified Aβ variants in three pathological lesions, extracellular plaques, intracellular deposits and also in vascular deposits in close resemblance to CAA. However, further studies are needed to dissect the relative contribution of sTREM2 ectodomain and its disease variants binding and deposition into distinct Aβ lesions. A study on AD-associated R62H/R62C and FTD/NHD associated T66M mutation or the TREM2 knockout compromise microglial functions leading to increased Aβ plaque load, provides a plausible mechanism for TREM2 and its disease-prone genetic variants in AD pathogenesis. This work is in line with recent structural analysis predicting that AD-associated TREM2 mutations might compromise a potential TREM2 ligand-binding interface (Kober et al. 2016) while misfolded T66M mutant is accumulated in the cells. So in such cases, the molecular chaperones might rescue the misfolding and restoration of microglial function in a disease state. This suggests the potential therapeutic importance of these chaperones that could be pursued for patient-specific FTD/NHD treatments. Since ApoE is the most potent genetic risk factor associated with late-onset AD (Kanekiyo et al. 2014) and has also been shown to be a TREM2 ligand along with other lipids (Atagi et al. 2015; Wang et al. 2015; Yeh et al. 2016), as well as evidence that dysfunctional lipid metabolism in AD (Di Paolo et al. 2011; Walter et al. 2013), it will be interesting to determine the interplay between these potential risk factors in TREM2 signalling in future studies.

References

'2020 Alzheimer's disease facts and figures'. 2020. Alzheimers Dement, 16: 391-460.

Aho, L., M. Pikkarainen, M. Hiltunen, V. Leinonen, and I. Alafuzoff. 2010. 'Immunohistochemical visualization of amyloid-beta protein precursor and amyloid-beta in extra- and intracellular compartments in the human brain', J Alzheimers Dis, 20: 1015-28.

Ahyayauch, H., M. Raab, J. V. Busto, N. Andraka, J. R. Arrondo, et al. 2012. 'Binding of beta-amyloid (1-42) peptide to negatively charged phospholipid membranes in the liquid-ordered state: modeling and experimental studies', Biophys J, 103: 453-63.

Aisen, P. S., J. Cummings, C. R. Jack, Jr., J. C. Morris, R. Sperling, et al. 2017. 'On the path to 2025: understanding the Alzheimer's disease continuum', Alzheimers Res Ther, 9: 60.

Akiyama, H., S. Barger, S. Barnum, B. Bradt, J. Bauer, et al. 2000. 'Inflammation and Alzheimer's disease', Neurobiol Aging, 21: 383-421.

Alexandru, A., W. Jagla, S. Graubner, A. Becker, C. Bauscher, et al. 2011. 'Selective hippocampal neurodegeneration in transgenic mice expressing small amounts of truncated Abeta is induced by pyroglutamate-Abeta formation', J Neurosci, 31: 12790-801.

Allcock, R. J., A. D. Barrow, S. Forbes, S. Beck, and J. Trowsdale. 2003. 'The human TREM gene cluster at 6p21.1 encodes both activating and inhibitory single IgV domain receptors and includes NKp44', Eur J Immunol, 33: 567-77.

Alonso, A. C., T. Zaidi, I. Grundke-Iqbal, and K. Iqbal. 1994. 'Role of abnormally phosphorylated tau in the breakdown of microtubules in Alzheimer disease', Proc Natl Acad Sci U S A, 91: 5562-6.

Alzheimer, A., R. A. Stelzmann, H. N. Schnitzlein, and F. R. Murtagh. 1995. 'An English translation of Alzheimer's 1907 paper, "Uber eine eigenartige Erkankung der Hirnrinde"', Clin Anat, 8: 429-31.

Alzheimers, Alois. 1911. 'On certain peculiar diseases of old age'.

Anderson, V. L., T. F. Ramlall, C. C. Rospigliosi, W. W. Webb, and D. Eliezer. 2010. 'Identification of a helical intermediate in trifluoroethanol-induced alpha-synuclein aggregation', Proc Natl Acad Sci U S A, 107: 18850-5.

Angelova, D. M., and D. R. Brown. 2019. 'Microglia and the aging brain: are senescent microglia the key to neurodegeneration?', J Neurochem, 151: 676-88.

Aoki, N., K. Tsuchiya, T. Togo, Z. Kobayashi, H. Uchikado, et al. 2011. 'Gray matter lesions in Nasu-Hakola disease: a report on three autopsy cases', Neuropathology, 31: 135-43.

Arcuri, C., C. Mecca, R. Bianchi, I. Giambanco, and R. Donato. 2017. 'The Pathophysiological Role of Microglia in Dynamic Surveillance, Phagocytosis and Structural Remodeling of the Developing CNS', Front Mol Neurosci, 10: 191.

Ard, M. D., G. M. Cole, J. Wei, A. P. Mehrle, and J. D. Fratkin. 1996. 'Scavenging of Alzheimer's amyloid beta-protein by microglia in culture', J Neurosci Res, 43: 190-202.

Armstrong, R. A. 1998. 'Beta-amyloid plaques: stages in life history or independent origin?', Dement Geriatr Cogn Disord, 9: 227-38.

Arndt, J. W., F. Qian, B. A. Smith, C. Quan, K. P. Kilambi, et al. 2018. 'Structural and kinetic basis for the selectivity of aducanumab for aggregated forms of amyloid-beta', Sci Rep, 8: 6412.

Ashby, E. L., J. S. Miners, S. Kumar, J. Walter, S. Love, and P. G. Kehoe. 2015. 'Investigation of Abeta phosphorylated at serine 8 (pAbeta) in Alzheimer's disease, dementia with Lewy bodies and vascular dementia', Neuropathol Appl Neurobiol, 41: 428-44.

Atagi, Y., C. C. Liu, M. M. Painter, X. F. Chen, C. Verbeeck, et al. 2015. 'Apolipoprotein E Is a Ligand for Triggering Receptor Expressed on Myeloid Cells 2 (TREM2)', J Biol Chem, 290: 26043-50.

Attems, J. 2005. 'Sporadic cerebral amyloid angiopathy: pathology, clinical implications, and possible pathomechanisms', Acta Neuropathol, 110: 345-59.

Attems, J., H. Yamaguchi, T. C. Saido, and D. R. Thal. 2010. 'Capillary CAA and perivascular Abeta-deposition: two distinct features of Alzheimer's disease pathology', J Neurol Sci, 299: 155-62.

Ayton, S., P. Lei, and A. I. Bush. 2013. 'Metallostasis in Alzheimer's disease', Free Radic Biol Med, 62: 76-89.

Babenko, O., I. Kovalchuk, and G. A. Metz. 2012. 'Epigenetic programming of neurodegenerative diseases by an adverse environment', Brain Res, 1444: 96-111.

Bachiller, S., I. Jimenez-Ferrer, A. Paulus, Y. Yang, M. Swanberg, T. Deierborg, and A. Boza-Serrano. 2018. 'Microglia in Neurological Diseases: A Road Map to Brain-Disease Dependent-Inflammatory Response', Front Cell Neurosci, 12: 1-17.

Bacioglu, M., L. F. Maia, O. Preische, J. Schelle, A. Apel, et al. 2016. 'Neurofilament Light Chain in Blood and CSF as Marker of Disease Progression in Mouse Models and in Neurodegenerative Diseases', Neuron, 91: 56-66.

Bailey, C. C., L. B. DeVaux, and M. Farzan. 2015. 'The Triggering Receptor Expressed on Myeloid Cells 2 Binds Apolipoprotein E', J Biol Chem, 290: 26033-42.

Barbero-Camps, E., V. Roca-Agujetas, I. Bartolessis, C. de Dios, J. C. Fernandez-Checa, et al. 2018. 'Cholesterol impairs autophagy-mediated clearance of amyloid beta while promoting its secretion', Autophagy, 14: 1129-54.

Barker, W. W., C. A. Luis, A. Kashuba, M. Luis, D. G. Harwood, et al. 2002. 'Relative frequencies of Alzheimer disease, Lewy body, vascular and frontotemporal dementia, and hippocampal sclerosis in the State of Florida Brain Bank', Alzheimer Dis Assoc Disord, 16: 203-12.

Barykin, E. P., V. A. Mitkevich, S. A. Kozin, and A. A. Makarov. 2017. 'Amyloid beta Modification: A Key to the Sporadic Alzheimer's Disease?', Front Genet, 8: 1-5.

Bayer, T. A., and O. Wirths. 2010. 'Intracellular accumulation of amyloid-Beta - a predictor for synaptic dysfunction and neuron loss in Alzheimer's disease', Front Aging Neurosci, 2: 1-10.

Beher, D., J. D. Wrigley, A. P. Owens, and M. S. Shearman. 2002. 'Generation of C-terminally truncated amyloid-beta peptides is dependent on gamma-secretase activity', J Neurochem, 82: 563-75.

Bellenguez, C., B. Grenier-Boley, and J. C. Lambert. 2020. 'Genetics of Alzheimer's disease: where we are, and where we are going', Curr Opin Neurobiol, 61: 40-48.

Belsare, K. D., H. Wu, D. Mondal, A. Bond, E. Castillo, et al. 2022. 'Soluble TREM2 inhibits secondary nucleation of Abeta fibrillization and enhances cellular uptake of fibrillar Abeta', Proc Natl Acad Sci U S A, 119.

Belyaev, N. D., K. A. Kellett, C. Beckett, N. Z. Makova, T. J. Revett, et al. 2010. 'The transcriptionally active amyloid precursor protein (APP) intracellular domain is preferentially produced from the 695 isoform of APP in a {beta}-secretase-dependent pathway', J Biol Chem, 285: 41443-54.

Bemiller, S. M., T. J. McCray, K. Allan, S. V. Formica, G. Xu, et al. 2017. 'TREM2 deficiency exacerbates tau pathology through dysregulated kinase signaling in a mouse model of tauopathy', Mol Neurodegener, 12: 74.

Benilova, I., E. Karran, and B. De Strooper. 2012. 'The toxic Abeta oligomer and Alzheimer's disease: an emperor in need of clothes', Nat Neurosci, 15: 349-57.

Benitez, B. A., B. Cooper, P. Pastor, S. C. Jin, E. Lorenzo, S. Cervantes, and C. Cruchaga. 2013. 'TREM2 is associated with the risk of Alzheimer's disease in Spanish population', Neurobiol Aging, 34: 1711 e15-7.

Bennett, D. A., J. A. Schneider, Z. Arvanitakis, J. F. Kelly, N. T. Aggarwal, R. C. Shah, and R. S. Wilson. 2006. 'Neuropathology of older persons without cognitive impairment from two community-based studies', Neurology, 66: 1837-44.

Bennett, H. L., J. T. Fleming, J. O'Prey, K. M. Ryan, and H. Y. Leung. 2010. 'Androgens modulate autophagy and cell death via regulation of the endoplasmic reticulum chaperone glucose-regulated protein 78/BiP in prostate cancer cells', Cell Death Dis, 1: e72.

Bentahir, M., O. Nyabi, J. Verhamme, A. Tolia, K. Horre, et al. 2006. 'Presenilin clinical mutations can affect gamma-secretase activity by different mechanisms', J Neurochem, 96: 732-42.

Berezovska, O., A. Lleo, L. D. Herl, M. P. Frosch, E. A. Stern, B. J. Bacskai, and B. T. Hyman. 2005. 'Familial Alzheimer's disease presenilin 1 mutations cause alterations in the conformation of presenilin and interactions with amyloid precursor protein', J Neurosci, 25: 3009-17.

Bergmans, B. A., and B. De Strooper. 2010. 'gamma-secretases: from cell biology to therapeutic strategies', Lancet Neurol, 9: 215-26.

Bertolotti, A., Y. Zhang, L. M. Hendershot, H. P. Harding, and D. Ron. 2000. 'Dynamic interaction of BiP and ER stress transducers in the unfolded-protein response', Nat Cell Biol, 2: 326-32.

Bertram, L., A. R. Parrado, and R. E. Tanzi. 2013. 'TREM2 and neurodegenerative disease', N Engl J Med, 369: 1565.

Bertram, L., and R. E. Tanzi. 2008. 'Thirty years of Alzheimer's disease genetics: the implications of systematic meta-analyses', Nat Rev Neurosci, 9: 768-78.

Bettens, K., K. Sleegers, and C. Van Broeckhoven. 2013. 'Genetic insights in Alzheimer's disease', Lancet Neurol, 12: 92-104.

Bhattacharjee, S., Y. Zhao, P. Dua, E. I. Rogaev, and W. J. Lukiw. 2016. 'microRNA-34a-Mediated Down-Regulation of the Microglial-Enriched Triggering Receptor and Phagocytosis-Sensor TREM2 in Age-Related Macular Degeneration', PLoS One, 11: e0150211.

Bianchin, M. M., H. M. Capella, D. L. Chaves, M. Steindel, E. C. Grisard, et al. 2004. 'Nasu-Hakola disease (polycystic lipomembranous osteodysplasia with sclerosing leukoencephalopathy--PLOSL): a dementia associated with bone cystic lesions. From clinical to genetic and molecular aspects', Cell Mol Neurobiol, 24: 1-24.

Bibl, M., B. Mollenhauer, H. Esselmann, P. Lewczuk, H. W. Klafki, et al. 2006. 'CSF amyloid-beta-peptides in Alzheimer's disease, dementia with Lewy bodies and Parkinson's disease dementia', Brain, 129: 1177-87.

Bibl, M., B. Mollenhauer, P. Lewczuk, H. Esselmann, S. Wolf, et al. 2007. 'Validation of amyloid-beta peptides in CSF diagnosis of neurodegenerative dementias', Mol Psychiatry, 12: 671-80.

Biffi, A., and S. M. Greenberg. 2011. 'Cerebral amyloid angiopathy: a systematic review', J Clin Neurol, 7: 1-9.

Bilbo, S., and B. Stevens. 2017. 'Microglia: The Brain's First Responders', Cerebrum, 2017: 1-14.

Bilkei-Gorzo, A., O. Albayram, A. Draffehn, K. Michel, A. Piyanova, et al. 2017. 'A chronic low dose of Delta(9)-tetrahydrocannabinol (THC) restores cognitive function in old mice', Nat Med, 23: 782-87.

Bilkei-Gorzo, A., I. Racz, O. Valverde, M. Otto, K. Michel, M. Sastre, and A. Zimmer. 2005. 'Early age-related cognitive impairment in mice lacking cannabinoid CB1 receptors', Proc Natl Acad Sci U S A, 102: 15670-5.

Billings, L. M., S. Oddo, K. N. Green, J. L. McGaugh, and F. M. LaFerla. 2005. 'Intraneuronal Abeta causes the onset of early Alzheimer's disease-related cognitive deficits in transgenic mice', Neuron, 45: 675-88.

Bird, T. D., R. M. Koerker, B. J. Leaird, B. W. Vlcek, and D. R. Thorning. 1983. 'Lipomembranous polycystic osteodysplasia (brain, bone, and fat disease): a genetic cause of presenile dementia', Neurology, 33: 81-6.

Bitan, G., M. D. Kirkitadze, A. Lomakin, S. S. Vollers, G. B. Benedek, and D. B. Teplow. 2003. 'Amyloid beta -protein (Abeta) assembly: Abeta 40 and Abeta 42 oligomerize through distinct pathways', Proc Natl Acad Sci U S A, 100: 330-5.

Bloom, G. S. 2014. 'Amyloid-beta and tau: the trigger and bullet in Alzheimer disease pathogenesis', JAMA Neurol, 71: 505-8.

Bock, V., A. Botturi, P. Gaviani, E. Lamperti, C. Maccagnano, et al. 2013. 'Polycystic Lipomembranous Osteodysplasia with Sclerosing Leukoencephalopathy (PLOSL): a new report of an Italian woman and review of the literature', J Neurol Sci, 326: 115-9.

Bolduc, D. M., D. R. Montagna, M. C. Seghers, M. S. Wolfe, and D. J. Selkoe. 2016. 'The amyloid-beta forming tripeptide cleavage mechanism of gamma-secretase', Elife, 5: 1-21.

Bollaerts, I., J. Van Houcke, L. Andries, L. De Groef, and L. Moons. 2017. 'Neuroinflammation as Fuel for Axonal Regeneration in the Injured Vertebrate Central Nervous System', Mediators Inflamm, 2017: 9478542.

Bolmont, T., F. Clavaguera, M. Meyer-Luehmann, M. C. Herzig, R. Radde, et al. 2007. 'Induction of tau pathology by intracerebral infusion of amyloid-beta -containing brain extract and by amyloid-beta deposition in APP x Tau transgenic mice', Am J Pathol, 171: 2012-20.

Bonham, L. W., D. W. Sirkis, J. Fan, R. E. Aparicio, M. Tse, et al. 2017. 'Identification of a rare coding variant in TREM2 in a Chinese individual with Alzheimer's disease', Neurocase, 23: 65-69.

Boon, B. D. C., M. Bulk, A. J. Jonker, T. H. J. Morrema, E. van den Berg, et al. 2020. 'The coarse-grained plaque: a divergent Abeta plaque-type in early-onset Alzheimer's disease', Acta Neuropathol, 140: 811-30.

Borchelt, D. R., T. Ratovitski, J. van Lare, M. K. Lee, V. Gonzales, et al. 1997. 'Accelerated amyloid deposition in the brains of transgenic mice coexpressing mutant presenilin 1 and amyloid precursor proteins', Neuron, 19: 939-45.

Borchelt, D. R., G. Thinakaran, C. B. Eckman, M. K. Lee, F. Davenport, et al. 1996. 'Familial Alzheimer's disease-linked presenilin 1 variants elevate Abeta1-42/1-40 ratio in vitro and in vivo', Neuron, 17: 1005-13.

Borkham-Kamphorst, E., B. T. Steffen, E. Van de Leur, U. Haas, L. Tihaa, S. L. Friedman, and R. Weiskirchen. 2016. 'CCN1/CYR61 overexpression in hepatic stellate cells induces ER stress-related apoptosis', Cell Signal, 28: 34-42.

Borroni, B., F. Ferrari, D. Galimberti, B. Nacmias, C. Barone, et al. 2014. 'Heterozygous TREM2 mutations in frontotemporal dementia', Neurobiol Aging, 35: 934 e7-10.

Bouchon, A., J. Dietrich, and M. Colonna. 2000. 'Cutting edge: inflammatory responses can be triggered by TREM-1, a novel receptor expressed on neutrophils and monocytes', J Immunol, 164: 4991-5.

Bouchon, A., C. Hernandez-Munain, M. Cella, and M. Colonna. 2001. 'A DAP12-mediated pathway regulates expression of CC chemokine receptor 7 and maturation of human dendritic cells', J Exp Med, 194: 1111-22.

Boutajangout, A., and T. Wisniewski. 2014. 'Tau-based therapeutic approaches for Alzheimer's disease - a mini-review', Gerontology, 60: 381-5.

Braak, H., and E. Braak. 1991. 'Demonstration of amyloid deposits and neurofibrillary changes in whole brain sections', Brain Pathol, 1: 213-6.

Braak, H., and E. Braak. 1997. 'Frequency of stages of Alzheimer-related lesions in different age categories', Neurobiol Aging, 18: 351-7.

Braak, H., D. R. Thal, E. Ghebremedhin, and K. Del Tredici. 2011. 'Stages of the pathologic process in Alzheimer disease: age categories from 1 to 100 years', J Neuropathol Exp Neurol, 70: 960-9.

Braidy, N., P. Munoz, A. G. Palacios, G. Castellano-Gonzalez, N. C. Inestrosa, et al. 2012. 'Recent rodent models for Alzheimer's disease: clinical implications and basic research', J Neural Transm (Vienna), 119: 173-95.

Brawek, B., Y. Liang, D. Savitska, K. Li, N. Fomin-Thunemann, et al. 2017. 'A new approach for ratiometric in vivo calcium imaging of microglia', Sci Rep, 7: 6030.

Brawek, B., B. Schwendele, K. Riester, S. Kohsaka, C. Lerdkrai, Y. Liang, and O. Garaschuk. 2014. 'Impairment of in vivo calcium signaling in amyloid plaque-associated microglia', Acta Neuropathol, 127: 495-505.

Brawek, B., M. Skok, and O. Garaschuk. 2021. 'Changing Functional Signatures of Microglia along the Axis of Brain Aging', Int J Mol Sci, 22: 1-21.

Brendel, M., G. Kleinberger, F. Probst, A. Jaworska, F. Overhoff, et al. 2017. 'Increase of TREM2 during Aging of an Alzheimer's Disease Mouse Model Is Paralleled by Microglial Activation and Amyloidosis', Front Aging Neurosci, 9: 8.

Brooks, W. S., J. B. Kwok, J. J. Kril, G. A. Broe, P. C. Blumbergs, et al. 2003. 'Alzheimer's disease with spastic paraparesis and 'cotton wool' plaques: two pedigrees with PS-1 exon 9 deletions', Brain, 126: 783-91.

Buchholz, F., L. Ringrose, P. O. Angrand, F. Rossi, and A. F. Stewart. 1996. 'Different thermostabilities of FLP and Cre recombinases: implications for applied site-specific recombination', Nucleic Acids Res, 24: 4256-62.

Burgess, Richard R. 2009. 'Chapter 20 Protein Precipitation Techniques.' in Richard R. Burgess and Murray P. Deutscher (eds.), Guide to Protein Purification, 2nd Edition (Academic Press) , Methods Enzymol, 463: 331-42.

Bush, A. I. 2013. 'The metal theory of Alzheimer's disease', J Alzheimers Dis, 33 Suppl 1: S277-81.

Butovsky, O., M. P. Jedrychowski, R. Cialic, S. Krasemann, G. Murugaiyan, et al. 2015. 'Targeting miR-155 restores abnormal microglia and attenuates disease in SOD1 mice', Ann Neurol, 77: 75-99.

Butovsky, O., M. P. Jedrychowski, C. S. Moore, R. Cialic, A. J. Lanser, et al. 2014. 'Identification of a unique TGF-beta-dependent molecular and functional signature in microglia', Nat Neurosci, 17: 131-43.

Butovsky, O., and H. L. Weiner. 2018. 'Microglial signatures and their role in health and disease', Nat Rev Neurosci, 19: 622-35.

Butterfield, D. A., T. T. Reed, M. Perluigi, C. De Marco, R. Coccia, et al. 2007. 'Elevated levels of 3-nitrotyrosine in brain from subjects with amnestic mild cognitive impairment: implications for the role of nitration in the progression of Alzheimer's disease', Brain Res, 1148: 243-8.

Cabrejo, L., L. Guyant-Marechal, A. Laquerriere, M. Vercelletto, F. De la Fourniere, et al. 2006. 'Phenotype associated with APP duplication in five families', Brain, 129: 2966-76.

Cady, J., E. D. Koval, B. A. Benitez, C. Zaidman, J. Jockel-Balsarotti, et al. 2014. 'TREM2 variant p.R47H as a risk factor for sporadic amyotrophic lateral sclerosis', JAMA Neurol, 71: 449-53.

Calero, M., A. Rostagno, E. Matsubara, B. Zlokovic, B. Frangione, and J. Ghiso. 2000. 'Apolipoprotein J (clusterin) and Alzheimer's disease', Microsc Res Tech, 50: 305-15.

Calero, M., T. Tokuda, A. Rostagno, A. Kumar, B. Zlokovic, B. Frangione, and J. Ghiso. 1999. 'Functional and structural properties of lipid-associated apolipoprotein J (clusterin)', Biochem J, 344 Pt 2: 375-83.

Campion, D., C. Dumanchin, D. Hannequin, B. Dubois, S. Belliard, et al. 1999. 'Early-onset autosomal dominant Alzheimer disease: prevalence, genetic heterogeneity, and mutation spectrum', Am J Hum Genet, 65: 664-70.

Candlish, M., and J. K. Hefendehl. 2021. 'Microglia Phenotypes Converge in Aging and Neurodegenerative Disease', Front Neurol, 12: 660720.

Cantoni, C., B. Bollman, D. Licastro, M. Xie, R. Mikesell, et al. 2015. 'TREM2 regulates microglial cell activation in response to demyelination in vivo', Acta Neuropathol, 129: 429-47.

Cappai, R. 2014. 'Making sense of the amyloid precursor protein: its tail tells an interesting tale', J Neurochem, 130: 325-7.

Carmona, S., J. Hardy, and R. Guerreiro. 2018. 'The genetic landscape of Alzheimer disease', Handb Clin Neurol, 148: 395-408.

Casali, B. T., and E. G. Reed-Geaghan. 2021. 'Microglial Function and Regulation during Development, Homeostasis and Alzheimer's Disease', Cells, 10: 1-28.

Casas, C., N. Sergeant, J. M. Itier, V. Blanchard, O. Wirths, et al. 2004. 'Massive CA1/2 neuronal loss with intraneuronal and N-terminal truncated Abeta42 accumulation in a novel Alzheimer transgenic model', Am J Pathol, 165: 1289-300.

Casati, M., E. Ferri, C. Gussago, P. Mazzola, C. Abbate, et al. 2018. 'Increased expression of TREM2 in peripheral cells from mild cognitive impairment patients who progress into Alzheimer's disease', Eur J Neurol, 25: 805-10.

Caselli, R. J., T. G. Beach, D. S. Knopman, and N. R. Graff-Radford. 2017. 'Alzheimer Disease: Scientific Breakthroughs and Translational Challenges', Mayo Clin Proc, 92: 978-94.

Castegna, A., V. Thongboonkerd, J. B. Klein, B. Lynn, W. R. Markesbery, and D. A. Butterfield. 2003. 'Proteomic identification of nitrated proteins in Alzheimer's disease brain', J Neurochem, 85: 1394-401.

Castellano, J. M., J. Kim, F. R. Stewart, H. Jiang, R. B. DeMattos, et al. 2011. 'Human apoE isoforms differentially regulate brain amyloid-beta peptide clearance', Sci Transl Med, 3: 89ra57.

Cavanaugh, S. E., J. J. Pippin, and N. D. Barnard. 2014. 'Animal models of Alzheimer disease: historical pitfalls and a path forward', ALTEX, 31: 279-302.

Celarain, N., J. Sanchez-Ruiz de Gordoa, M. V. Zelaya, M. Roldan, R. Larumbe, et al. 2016. 'TREM2 upregulation correlates with 5-hydroxymethycytosine enrichment in Alzheimer's disease hippocampus', Clin Epigenetics, 8: 37.

Cella, M., C. Buonsanti, C. Strader, T. Kondo, A. Salmaggi, and M. Colonna. 2003. 'Impaired differentiation of osteoclasts in TREM-2-deficient individuals', J Exp Med, 198: 645-51.

Chang, K. A., and Y. H. Suh. 2005. 'Pathophysiological roles of amyloidogenic carboxy-terminal fragments of the beta-amyloid precursor protein in Alzheimer's disease', J Pharmacol Sci, 97: 461-71.

Chaudhari, N., P. Talwar, A. Parimisetty, C. Lefebvre d'Hellencourt, and P. Ravanan. 2014. 'A molecular web: endoplasmic reticulum stress, inflammation, and oxidative stress', Front Cell Neurosci, 8: 213.

Chen, G. F., T. H. Xu, Y. Yan, Y. R. Zhou, Y. Jiang, K. Melcher, and H. E. Xu. 2017. 'Amyloid beta: structure, biology and structure-based therapeutic development', Acta Pharmacol Sin, 38: 1205-35.

Cheng-Hathaway, P. J., E. G. Reed-Geaghan, T. R. Jay, B. T. Casali, S. M. Bemiller, et al. 2018. 'The Trem2 R47H variant confers loss-of-function-like phenotypes in Alzheimer's disease', Mol Neurodegener, 13: 29.

Chertoff, M., K. Shrivastava, B. Gonzalez, L. Acarin, and L. Gimenez-Llort. 2013. 'Differential modulation of TREM2 protein during postnatal brain development in mice', PLoS One, 8: e72083.

Chishti, M. A., D. S. Yang, C. Janus, A. L. Phinney, P. Horne, et al. 2001. 'Early-onset amyloid deposition and cognitive deficits in transgenic mice expressing a double mutant form of amyloid precursor protein 695', J Biol Chem, 276: 21562-70.

Chiu, I. M., E. T. Morimoto, H. Goodarzi, J. T. Liao, S. O'Keeffe, et al. 2013. 'A neurodegeneration-specific gene-expression signature of acutely isolated microglia from an amyotrophic lateral sclerosis mouse model', Cell Rep, 4: 385-401.

Chouery, E., V. Delague, A. Bergougnoux, S. Koussa, J. L. Serre, and A. Megarbane. 2008. 'Mutations in TREM2 lead to pure early-onset dementia without bone cysts', Hum Mutat, 29: E194-204.

Chouliaras, L., B. P. Rutten, G. Kenis, O. Peerbooms, P. J. Visser, et al. 2010. 'Epigenetic regulation in the pathophysiology of Alzheimer's disease', Prog Neurobiol, 90: 498-510.

Christensen, D. Z., M. Huettenrauch, M. Mitkovski, L. Pradier, and O. Wirths. 2014. 'Axonal degeneration in an Alzheimer mouse model is PS1 gene dose dependent and linked to intraneuronal Abeta accumulation', Front Aging Neurosci, 6: 139.

Cignarella, F., F. Filipello, B. Bollman, C. Cantoni, A. Locca, et al. 2020. 'TREM2 activation on microglia promotes myelin debris clearance and remyelination in a model of multiple sclerosis', Acta Neuropathol, 140: 513-34.

Citron, M., T. Oltersdorf, C. Haass, L. McConlogue, A. Y. Hung, et al. 1992. 'Mutation of the beta-amyloid precursor protein in familial Alzheimer's disease increases beta-protein production', Nature, 360: 672-4.

Clayton, K. A., A. A. Van Enoo, and T. Ikezu. 2017. 'Alzheimer's Disease: The Role of Microglia in Brain Homeostasis and Proteopathy', Front Neurosci, 11: 680.

Colonna, M., and O. Butovsky. 2017. 'Microglia Function in the Central Nervous System During Health and Neurodegeneration', Annu Rev Immunol, 35: 441-68.

Colonna, M., I. Turnbull, and J. Klesney-Tait. 2007. 'The enigmatic function of TREM-2 in osteoclastogenesis', Adv Exp Med Biol, 602: 97-105.

Colonna, M., and Y. Wang. 2016. 'TREM2 variants: new keys to decipher Alzheimer disease pathogenesis', Nat Rev Neurosci, 17: 201-7.

Condello, C., T. Lemmin, J. Stohr, M. Nick, Y. Wu, et al. 2018a. 'Structural heterogeneity and intersubject variability of Abeta in familial and sporadic Alzheimer's disease', Proc Natl Acad Sci U S A, 115: E782-E91.

Condello, C., and J. Stoehr. 2018b. 'Abeta propagation and strains: Implications for the phenotypic diversity in Alzheimer's disease', Neurobiol Dis, 109: 191-200.

Condello, C., P. Yuan, and J. Grutzendler. 2018c. 'Microglia-Mediated Neuroprotection, TREM2, and Alzheimer's Disease: Evidence From Optical Imaging', Biol Psychiatry, 83: 377-87.

Condello, C., P. Yuan, A. Schain, and J. Grutzendler. 2015. 'Microglia constitute a barrier that prevents neurotoxic protofibrillar Abeta42 hotspots around plaques', Nat Commun, 6: 6176.

Coppieters, N., and M. Dragunow. 2011. 'Epigenetics in Alzheimer's disease: a focus on DNA modifications', Curr Pharm Des, 17: 3398-412.

Corder, E. H., A. M. Saunders, W. J. Strittmatter, D. E. Schmechel, P. C. Gaskell, et al. 1993. 'Gene dose of apolipoprotein E type 4 allele and the risk of Alzheimer's disease in late onset families', Science, 261: 921-3.

Cornejo, F., and R. von Bernhardi. 2013. 'Role of scavenger receptors in glia-mediated neuroinflammatory response associated with Alzheimer's disease', Mediators Inflamm, 2013: 895651.

Craig, N. L. 1988. 'The mechanism of conservative site-specific recombination', Annu Rev Genet, 22: 77-105.

Crehan, H., J. Hardy, and J. Pocock. 2013. 'Blockage of CR1 prevents activation of rodent microglia', Neurobiol Dis, 54: 139-49.

Crook, R., A. Verkkoniemi, J. Perez-Tur, N. Mehta, M. Baker, et al. 1998. 'A variant of Alzheimer's disease with spastic paraparesis and unusual plaques due to deletion of exon 9 of presenilin 1', Nat Med, 4: 452-5.

Cullen, N. C., A. N. Malarstig, E. Stomrud, O. Hansson, and N. Mattsson-Carlgren. 2021. 'Accelerated inflammatory aging in Alzheimer's disease and its relation to amyloid, tau, and cognition', Sci Rep, 11: 1965.

Cummings, J., and N. Fox. 2017. 'Defining Disease Modifying Therapy for Alzheimer's Disease', J Prev Alzheimers Dis, 4: 109-15.

Cummings, J., A. Ritter, and K. Zhong. 2018. 'Clinical Trials for Disease-Modifying Therapies in Alzheimer's Disease: A Primer, Lessons Learned, and a Blueprint for the Future', J Alzheimers Dis, 64: S3-S22.

Cunnea, P., A. N. Mhaille, S. McQuaid, M. Farrell, J. McMahon, and U. FitzGerald. 2011. 'Expression profiles of endoplasmic reticulum stress-related molecules in demyelinating lesions and multiple sclerosis', Mult Scler, 17: 808-18.

Cuyvers, E., K. Bettens, S. Philtjens, T. Van Langenhove, I. Gijselinck, et al. 2014. 'Investigating the role of rare heterozygous TREM2 variants in Alzheimer's disease and frontotemporal dementia', Neurobiol Aging, 35: 726 e11-9.

D'Errico, P., S. Ziegler-Waldkirch, V. Aires, P. Hoffmann, C. Mezo, et al. 2022. 'Microglia contribute to the propagation of Abeta into unaffected brain tissue', Nat Neurosci, 25: 20-25.

Dammers, C., L. Gremer, K. Reiss, A. N. Klein, P. Neudecker, et al. 2015. 'Structural Analysis and Aggregation Propensity of Pyroglutamate Abeta(3-40) in Aqueous Trifluoroethanol', PLoS One, 10: e0143647.

Dansokho, C., and M. T. Heneka. 2018. 'Neuroinflammatory responses in Alzheimer's disease', J Neural Transm (Vienna), 125: 771-79.

Davalos, D., J. Grutzendler, G. Yang, J. V. Kim, Y. Zuo, et al. 2005. 'ATP mediates rapid microglial response to local brain injury in vivo', Nat Neurosci, 8: 752-8.

Davies, C. A., and D. M. Mann. 1993. 'Is the "preamyloid" of diffuse plaques in Alzheimer's disease really nonfibrillar?', Am J Pathol, 143: 1594-605.

Daws, M. R., L. L. Lanier, W. E. Seaman, and J. C. Ryan. 2001. 'Cloning and characterization of a novel mouse myeloid DAP12-associated receptor family', Eur J Immunol, 31: 783-91.

Daws, M. R., P. M. Sullam, E. C. Niemi, T. T. Chen, N. K. Tchao, and W. E. Seaman. 2003. 'Pattern recognition by TREM-2: binding of anionic ligands', J Immunol, 171: 594-9.

De Felice, F. G., P. T. Velasco, M. P. Lambert, K. Viola, S. J. Fernandez, S. T. Ferreira, and W. L. Klein. 2007. 'Abeta oligomers induce neuronal oxidative stress through an N-methyl-D-aspartate receptor-dependent mechanism that is blocked by the Alzheimer drug memantine', J Biol Chem, 282: 11590-601.

De Jonghe, C., C. Esselens, S. Kumar-Singh, K. Craessaerts, S. Serneels, et al. 2001. 'Pathogenic APP mutations near the gamma-secretase cleavage site differentially affect Abeta secretion and APP C-terminal fragment stability', Hum Mol Genet, 10: 1665-71.

De Kimpe, L., E. S. van Haastert, A. Kaminari, R. Zwart, H. Rutjes, J. J. Hoozemans, and W. Scheper. 2013. 'Intracellular accumulation of aggregated pyroglutamate amyloid beta: convergence of aging and Abeta pathology at the lysosome', Age (Dordr), 35: 673-87.

De Strooper, B., W. Annaert, P. Cupers, P. Saftig, K. Craessaerts, et al. 1999. 'A presenilin-1-dependent gamma-secretase-like protease mediates release of Notch intracellular domain', Nature, 398: 518-22.

De Strooper, B., M. Simons, G. Multhaup, F. Van Leuven, K. Beyreuther, and C. G. Dotti. 1995. 'Production of intracellular amyloid-containing fragments in hippocampal neurons expressing human amyloid precursor protein and protection against amyloidogenesis by subtle amino acid substitutions in the rodent sequence', EMBO J, 14: 4932-8.

Deczkowska, A., H. Keren-Shaul, A. Weiner, M. Colonna, M. Schwartz, and I. Amit. 2018. 'Disease-Associated Microglia: A Universal Immune Sensor of Neurodegeneration', Cell, 173: 1073-81.

Delabar, J. M., D. Goldgaber, Y. Lamour, A. Nicole, J. L. Huret, et al. 1987. 'Beta amyloid gene duplication in Alzheimer's disease and karyotypically normal Down syndrome', Science, 235: 1390-2.

DeMattos, R. B., R. P. Brendza, J. E. Heuser, M. Kierson, J. R. Cirrito, et al. 2001. 'Purification and characterization of astrocyte-secreted apolipoprotein E and J-containing lipoproteins from wild-type and human apoE transgenic mice', Neurochem Int, 39: 415-25.

DeTure, M. A., and D. W. Dickson. 2019. 'The neuropathological diagnosis of Alzheimer's disease', Mol Neurodegener, 14: 32.

Di Paolo, G., and T. W. Kim. 2011. 'Linking lipids to Alzheimer's disease: cholesterol and beyond', Nat Rev Neurosci, 12: 284-96.

Dickson, D. W. 1997. 'The pathogenesis of senile plaques', J Neuropathol Exp Neurol, 56: 321-39.

Dimitrov, M., J. R. Alattia, T. Lemmin, R. Lehal, A. Fligier, et al. 2013. 'Alzheimer's disease mutations in APP but not gamma-secretase modulators affect epsilon-cleavage-dependent AICD production', Nat Commun, 4: 2246.

Ding, Y., J. Zhao, X. Zhang, S. Wang, K. L. Viola, et al. 2019. 'Amyloid Beta Oligomers Target to Extracellular and Intracellular Neuronal Synaptic Proteins in Alzheimer's Disease', Front Neurol, 10: 1140.

Domingo, G., L. Benussi, C. Saraceno, M. Bertuzzi, R. Nicsanu, et al. 2021. 'N-Terminally Truncated and Pyroglutamate-Modified Abeta Forms Are Measurable in Human Cerebrospinal Fluid and Are Potential Markers of Disease Progression in Alzheimer's Disease', Front Neurosci, 15: 708119.

Drew, S. C., C. L. Masters, and K. J. Barnham. 2009. 'Alanine-2 carbonyl is an oxygen ligand in Cu2+ coordination of Alzheimer's disease amyloid-beta peptide--relevance to N-terminally truncated forms', J Am Chem Soc, 131: 8760-1.

Drummond, E., and T. Wisniewski. 2017. 'Alzheimer's disease: experimental models and reality', Acta Neuropathol, 133: 155-75.

Dubois, B., H. H. Feldman, C. Jacova, H. Hampel, J. L. Molinuevo, et al. 2014. 'Advancing research diagnostic criteria for Alzheimer's disease: the IWG-2 criteria', Lancet Neurol, 13: 614-29.

Dujardin, S., M. Colin, and L. Buee. 2015. 'Invited review: Animal models of tauopathies and their implications for research/translation into the clinic', Neuropathol Appl Neurobiol, 41: 59-80.

Dunn, A. R., K. M. S. O'Connell, and C. C. Kaczorowski. 2019. 'Gene-by-environment interactions in Alzheimer's disease and Parkinson's disease', Neurosci Biobehav Rev, 103: 73-80.

Duran-Aniotz, C., I. Moreno-Gonzalez, N. Gamez, N. Perez-Urrutia, L. Vegas-Gomez, C. Soto, and R. Morales. 2021. 'Amyloid pathology arrangements in Alzheimer's disease brains modulate in vivo seeding capability', Acta Neuropathol Commun, 9: 56.

Duyckaerts, C., M. C. Potier, and B. Delatour. 2008. 'Alzheimer disease models and human neuropathology: similarities and differences', Acta Neuropathol, 115: 5-38.

Edler, M. K., I. Mhatre-Winters, and J. R. Richardson. 2021. 'Microglia in Aging and Alzheimer's Disease: A Comparative Species Review', Cells, 10: 1-30.

Edwards Iii, G. A., N. Gamez, G. Escobedo, Jr., O. Calderon, and I. Moreno-Gonzalez. 2019. 'Modifiable Risk Factors for Alzheimer's Disease', Front Aging Neurosci, 11: 146.

Elder, G. A., M. A. Gama Sosa, and R. De Gasperi. 2010. 'Transgenic mouse models of Alzheimer's disease', Mt Sinai J Med, 77: 69-81.

Emes, R. D., L. Goodstadt, E. E. Winter, and C. P. Ponting. 2003. 'Comparison of the genomes of human and mouse lays the foundation of genome zoology', Hum Mol Genet, 12: 701-9.

Ennerfelt, H. E., and J. R. Lukens. 2020. 'The role of innate immunity in Alzheimer's disease', Immunol Rev, 297: 225-46.

Esler, W. P., C. Das, and M. S. Wolfe. 2004. 'Probing pockets S2-S4' of the gamma-secretase active site with (hydroxyethyl)urea peptidomimetics', Bioorg Med Chem Lett, 14: 1935-8.

Ewers, M., G. Biechele, M. Suarez-Calvet, C. Sacher, T. Blume, et al. 2020. 'Higher CSF sTREM2 and microglia activation are associated with slower rates of beta-amyloid accumulation', EMBO Mol Med, 12: 1-18.

Ewers, M., N. Franzmeier, M. Suarez-Calvet, E. Morenas-Rodriguez, M. A. A. Caballero, et al. 2019. 'Increased soluble TREM2 in cerebrospinal fluid is associated with reduced cognitive and clinical decline in Alzheimer's disease', Sci Transl Med, 11: 1-28.

Fahrenhold, M., S. Rakic, J. Classey, C. Brayne, P. G. Ince, et al. 2018. 'TREM2 expression in the human brain: a marker of monocyte recruitment?', Brain Pathol, 28: 595-602.

Fang, X. T., D. Sehlin, L. Lannfelt, S. Syvanen, and G. Hultqvist. 2017. 'Efficient and inexpensive transient expression of multispecific multivalent antibodies in Expi293 cells', Biol Proced Online, 19: 11.

Faucher, P., N. Mons, J. Micheau, C. Louis, and D. J. Beracochea. 2015. 'Hippocampal Injections of Oligomeric Amyloid beta-peptide (1-42) Induce Selective Working Memory Deficits and Long-lasting Alterations of ERK Signaling Pathway', Front Aging Neurosci, 7: 245.

Fernandez-Vizarra, P., A. P. Fernandez, S. Castro-Blanco, J. Serrano, M. L. Bentura, et al. 2004. 'Intra- and extracellular Abeta and PHF in clinically evaluated cases of Alzheimer's disease', Histol Histopathol, 19: 823-44.

Feuerbach, D., P. Schindler, C. Barske, S. Joller, E. Beng-Louka, et al. 2017. 'ADAM17 is the main sheddase for the generation of human triggering receptor expressed in myeloid cells (hTREM2) ectodomain and cleaves TREM2 after Histidine 157', Neurosci Lett, 660: 109-14.

Finelli, D., S. Rollinson, J. Harris, M. Jones, A. Richardson, et al. 2015. 'TREM2 analysis and increased risk of Alzheimer's disease', Neurobiol Aging, 36: 546 e9-13.

Flanary, B. 2005. 'The role of microglial cellular senescence in the aging and Alzheimer diseased brain', Rejuvenation Res, 8: 82-5.

Foley, A. M., Z. M. Ammar, R. H. Lee, and C. S. Mitchell. 2015. 'Systematic review of the relationship between amyloid-beta levels and measures of transgenic mouse cognitive deficit in Alzheimer's disease', J Alzheimers Dis, 44: 787-95.

Forabosco, P., A. Ramasamy, D. Trabzuni, R. Walker, C. Smith, et al. 2013. 'Insights into TREM2 biology by network analysis of human brain gene expression data', Neurobiol Aging, 34: 2699-714.

Ford, J. W., and D. W. McVicar. 2009. 'TREM and TREM-like receptors in inflammation and disease', Curr Opin Immunol, 21: 38-46.

Forner, S., S. Kawauchi, G. Balderrama-Gutierrez, E. A. Kramar, D. P. Matheos, et al. 2021. 'Systematic phenotyping and characterization of the 5xFAD mouse model of Alzheimer's disease', Sci Data, 8: 270.

Fossel, M. 2000. 'Cell senescence in human aging: a review of the theory', In Vivo, 14: 29-34.

Franco Bocanegra, D. K., J. A. R. Nicoll, and D. Boche. 2018. 'Innate immunity in Alzheimer's disease: the relevance of animal models?', J Neural Transm (Vienna), 125: 827-46.

Friedman, B. A., K. Srinivasan, G. Ayalon, W. J. Meilandt, H. Lin, et al. 2018. 'Diverse Brain Myeloid Expression Profiles Reveal Distinct Microglial Activation States and Aspects of Alzheimer's Disease Not Evident in Mouse Models', Cell Rep, 22: 832-47.

Friedrich, R. P., K. Tepper, R. Ronicke, M. Soom, M. Westermann, et al. 2010. 'Mechanism of amyloid plaque formation suggests an intracellular basis of Abeta pathogenicity', Proc Natl Acad Sci U S A, 107: 1942-7.

Friesen, M., and M. Meyer-Luehmann. 2019. 'Abeta Seeding as a Tool to Study Cerebral Amyloidosis and Associated Pathology', Front Mol Neurosci, 12: 233.

Fritschi, S. K., F. Langer, S. A. Kaeser, L. F. Maia, E. Portelius, et al. 2014. 'Highly potent soluble amyloid-beta seeds in human Alzheimer brain but not cerebrospinal fluid', Brain, 137: 2909-15.

Galloway, D. A., A. E. M. Phillips, D. R. J. Owen, and C. S. Moore. 2019. 'Phagocytosis in the Brain: Homeostasis and Disease', Front Immunol, 10: 790.

Gambino, C. M., B. L. Sasso, G. Bivona, L. Agnello, and M. Ciaccio. 2019. 'Aging and Neuroinflammatory Disorders: New Biomarkers and Therapeutic Targets', Curr Pharm Des, 25: 4168-74.

Games, D., D. Adams, R. Alessandrini, R. Barbour, P. Berthelette, et al. 1995. 'Alzheimer-type neuropathology in transgenic mice overexpressing V717F beta-amyloid precursor protein', Nature, 373: 523-7.

Garcia-Alloza, M., L. A. Borrelli, D. H. Thyssen, S. E. Hickman, J. El Khoury, and B. J. Bacskai. 2013. 'Four-dimensional microglia response to anti-Abeta treatment in APP/PS1xCX3CR1/GFP mice', Intravital, 2: e25693-1-9.

Garcia-Alloza, M., E. M. Robbins, S. X. Zhang-Nunes, S. M. Purcell, R. A. Betensky, et al. 2006. 'Characterization of amyloid deposition in the APPswe/PS1dE9 mouse model of Alzheimer disease', Neurobiol Dis, 24: 516-24.

Garcia-Gonzalez, P., F. Cabral-Miranda, C. Hetz, and F. Osorio. 2018. 'Interplay Between the Unfolded Protein Response and Immune Function in the Development of Neurodegenerative Diseases', Front Immunol, 9: 2541.

Geladaris, A., D. Hausler, and M. S. Weber. 2021. 'Microglia: The Missing Link to Decipher and Therapeutically Control MS Progression?', Int J Mol Sci, 22: 1-19.

Gendreau, K. L., and G. F. Hall. 2013. 'Tangles, Toxicity, and Tau Secretion in AD - New Approaches to a Vexing Problem', Front Neurol, 4: 160.

Gendron, T. F., and L. Petrucelli. 2009. 'The role of tau in neurodegeneration', Mol Neurodegener, 4: 13.

Gerth, J., S. Kumar, A. Rijal Upadhaya, E. Ghebremedhin, C. A. F. von Arnim, D. R. Thal, and J. Walter. 2018. 'Modified amyloid variants in pathological subgroups of beta-amyloidosis', Ann Clin Transl Neurol, 5: 815-31.

Ghani, M., C. Sato, E. G. Kakhki, J. R. Gibbs, B. Traynor, P. St George-Hyslop, and E. Rogaeva. 2016. 'Mutation analysis of the MS4A and TREM gene clusters in a case-control Alzheimer's disease data set', Neurobiol Aging, 42: 217 e7-17 e13.

Ghezzi, L., T. Carandini, A. Arighi, C. Fenoglio, M. Arcaro, et al. 2017. 'Evidence of CNS beta-amyloid deposition in Nasu-Hakola disease due to the TREM2 Q33X mutation', Neurology, 89: 2503-05.

Giannoni, P., M. Arango-Lievano, I. D. Neves, M. C. Rousset, K. Baranger, et al. 2016. 'Cerebrovascular pathology during the progression of experimental Alzheimer's disease', Neurobiol Dis, 88: 107-17.

Giraldo, M., F. Lopera, A. L. Siniard, J. J. Corneveaux, I. Schrauwen, et al. 2013. 'Variants in triggering receptor expressed on myeloid cells 2 are associated with both behavioral variant frontotemporal lobar degeneration and Alzheimer's disease', Neurobiol Aging, 34: 2077 e11-8.

Giulian, D., and T. J. Baker. 1986. 'Characterization of ameboid microglia isolated from developing mammalian brain', J Neurosci, 6: 2163-78.

Giuliano, C. J., A. Lin, V. Girish, and J. M. Sheltzer. 2019. 'Generating Single Cell-Derived Knockout Clones in Mammalian Cells with CRISPR/Cas9', Curr Protoc Mol Biol, 128: e100.

Glebov, K., P. Wunderlich, I. Karaca, and J. Walter. 2016. 'Functional involvement of gamma-secretase in signaling of the triggering receptor expressed on myeloid cells-2 (TREM2)', J Neuroinflammation, 13: 17.

Goate, A., M. C. Chartier-Harlin, M. Mullan, J. Brown, F. Crawford, et al. 1991. 'Segregation of a missense mutation in the amyloid precursor protein gene with familial Alzheimer's disease', Nature, 349: 704-6.

Golde, T. E., W. J. Streit, and P. Chakrabarty. 2013. 'Alzheimer's disease risk alleles in TREM2 illuminate innate immunity in Alzheimer's disease', Alzheimers Res Ther, 5: 24.

Goncalves, L. A., L. Rodrigues-Duarte, J. Rodo, L. Vieira de Moraes, I. Marques, and C. Penha-Goncalves. 2013. 'TREM2 governs Kupffer cell activation and explains belr1 genetic resistance to malaria liver stage infection', Proc Natl Acad Sci U S A, 110: 19531-6.

Gonzalez Murcia, J. D., C. Schmutz, C. Munger, A. Perkes, A. Gustin, et al. 2013. 'Assessment of TREM2 rs75932628 association with Alzheimer's disease in a population-based sample: the Cache County Study', Neurobiol Aging, 34: 2889 e11-3.

Gordon, B. A., T. M. Blazey, Y. Su, A. Hari-Raj, A. Dincer, et al. 2018. 'Spatial patterns of neuroimaging biomarker change in individuals from families with autosomal dominant Alzheimer's disease: a longitudinal study', Lancet Neurol, 17: 241-50.

Gotz, J., J. R. Streffer, D. David, A. Schild, F. Hoerndli, et al. 2004. 'Transgenic animal models of Alzheimer's disease and related disorders: histopathology, behavior and therapy', Mol Psychiatry, 9: 664-83.

Gouras, G. K., C. G. Almeida, and R. H. Takahashi. 2005. 'Intraneuronal Abeta accumulation and origin of plaques in Alzheimer's disease', Neurobiol Aging, 26: 1235-44.

Gouras, G. K., D. Tampellini, R. H. Takahashi, and E. Capetillo-Zarate. 2010. 'Intraneuronal beta-amyloid accumulation and synapse pathology in Alzheimer's disease', Acta Neuropathol, 119: 523-41.

Gouras, G. K., J. Tsai, J. Naslund, B. Vincent, M. Edgar, et al. 2000. 'Intraneuronal Abeta42 accumulation in human brain', Am J Pathol, 156: 15-20.

Grabert, K., T. Michoel, M. H. Karavolos, S. Clohisey, J. K. Baillie, et al. 2016. 'Microglial brain region-dependent diversity and selective regional sensitivities to aging', Nat Neurosci, 19: 504-16.

Gratuze, M., C. E. G. Leyns, and D. M. Holtzman. 2018. 'New insights into the role of TREM2 in Alzheimer's disease', Mol Neurodegener, 13: 1-16.

Gratuze, M., C. E. Leyns, A. D. Sauerbeck, M. K. St-Pierre, M. Xiong, et al. 2020. 'Impact of TREM2R47H variant on tau pathology-induced gliosis and neurodegeneration', J Clin Invest, 130: 4954-68.

Grav, L. M., D. Sergeeva, J. S. Lee, I. Marin de Mas, N. E. Lewis, et al. 2018. 'Minimizing Clonal Variation during Mammalian Cell Line Engineering for Improved Systems Biology Data Generation', ACS Synth Biol, 7: 2148-59.

Green, K. N., L. M. Billings, B. Roozendaal, J. L. McGaugh, and F. M. LaFerla. 2006. 'Glucocorticoids increase amyloid-beta and tau pathology in a mouse model of Alzheimer's disease', J Neurosci, 26: 9047-56.

Greenberg, S. M., B. J. Bacskai, M. Hernandez-Guillamon, J. Pruzin, R. Sperling, and S. J. van Veluw. 2020. 'Cerebral amyloid angiopathy and Alzheimer disease - one peptide, two pathways', Nat Rev Neurol, 16: 30-42.

Greenwood, E. K., and D. R. Brown. 2021. 'Senescent Microglia: The Key to the Ageing Brain?', Int J Mol Sci, 22: 1-19.

Griciuc, A., A. Serrano-Pozo, A. R. Parrado, A. N. Lesinski, C. N. Asselin, et al. 2013. 'Alzheimer's disease risk gene CD33 inhibits microglial uptake of amyloid beta', Neuron, 78: 631-43.

Grochowska, K. M., P. Yuanxiang, J. Bar, R. Raman, G. Brugal, et al. 2017. 'Posttranslational modification impact on the mechanism by which amyloid-beta induces synaptic dysfunction', EMBO Rep, 18: 962-81.

Grothe, M. J., H. Barthel, J. Sepulcre, M. Dyrba, O. Sabri, S. J. Teipel, and Initiative Alzheimer's Disease Neuroimaging. 2017. 'In vivo staging of regional amyloid deposition', Neurology, 89: 2031-38.

Grubman, A., X. Y. Choo, G. Chew, J. F. Ouyang, G. Sun, et al. 2021. 'Transcriptional signature in microglia associated with Abeta plaque phagocytosis', Nat Commun, 12: 3015.

Grueninger, F., B. Bohrmann, C. Czech, T. M. Ballard, J. R. Frey, et al. 2010. 'Phosphorylation of Tau at S422 is enhanced by Abeta in TauPS2APP triple transgenic mice', Neurobiol Dis, 37: 294-306.

Grundke-Iqbal, I., K. Iqbal, Y. C. Tung, M. Quinlan, H. M. Wisniewski, and L. I. Binder. 1986. 'Abnormal phosphorylation of the microtubule-associated protein tau (tau) in Alzheimer cytoskeletal pathology', Proc Natl Acad Sci U S A, 83: 4913-7.

Gu, L., and Z. Guo. 2013. 'Alzheimer's Abeta42 and Abeta40 peptides form interlaced amyloid fibrils', J Neurochem, 126: 305-11.

Gu, L., D. Wu, X. Tang, X. Qi, X. Li, et al. 2018. 'Myelin changes at the early stage of 5XFAD mice', Brain Res Bull, 137: 285-93.

Guerreiro, R., B. Bilgic, G. Guven, J. Bras, J. Rohrer, et al. 2013a. 'Novel compound heterozygous mutation in TREM2 found in a Turkish frontotemporal dementia-like family', Neurobiol Aging, 34: 2890 e1-5.

Guerreiro, R., and J. Bras. 2015. 'The age factor in Alzheimer's disease', Genome Med, 7: 106.

Guerreiro, R., J. Bras, and J. Hardy. 2013b. 'SnapShot: genetics of Alzheimer's disease', Cell, 155: 968-68 e1.

Guerreiro, R. J., M. Baquero, R. Blesa, M. Boada, J. M. Bras, et al. 2010. 'Genetic screening of Alzheimer's disease genes in Iberian and African samples yields novel mutations in presenilins and APP', Neurobiol Aging, 31: 725-31.

Guerreiro, R. J., E. Lohmann, J. M. Bras, J. R. Gibbs, J. D. Rohrer, et al. 2013c. 'Using exome sequencing to reveal mutations in TREM2 presenting as a frontotemporal dementia-like syndrome without bone involvement', JAMA Neurol, 70: 78-84.

Guerreiro, R., A. Wojtas, J. Bras, M. Carrasquillo, E. Rogaeva, et al. 2013d. 'TREM2 variants in Alzheimer's disease', N Engl J Med, 368: 117-27.

Guillot-Sestier, M. V., and T. Town. 2013. 'Innate immunity in Alzheimer's disease: a complex affair', CNS Neurol Disord Drug Targets, 12: 593-607.

Guo, T., D. Zhang, Y. Zeng, T. Y. Huang, H. Xu, and Y. Zhao. 2020. 'Molecular and cellular mechanisms underlying the pathogenesis of Alzheimer's disease', Mol Neurodegener, 15: 40.

Guzman-Martinez, L., R. B. Maccioni, V. Andrade, L. P. Navarrete, M. G. Pastor, and N. Ramos-Escobar. 2019. 'Neuroinflammation as a Common Feature of Neurodegenerative Disorders', Front Pharmacol, 10: 1008.

Guzman, E. A., Y. Bouter, B. C. Richard, L. Lannfelt, M. Ingelsson, et al. 2014. 'Abundance of Abeta(5)-x like immunoreactivity in transgenic 5XFAD, APP/PS1KI and 3xTG mice, sporadic and familial Alzheimer's disease', Mol Neurodegener, 9: 13.

Haan, J., J. B. Lanser, I. Zijderveld, I. G. van der Does, and R. A. Roos. 1990. 'Dementia in hereditary cerebral hemorrhage with amyloidosis-Dutch type', Arch Neurol, 47: 965-7.

Haass, C., C. A. Lemere, A. Capell, M. Citron, P. Seubert, et al. 1995. 'The Swedish mutation causes early-onset Alzheimer's disease by beta-secretase cleavage within the secretory pathway', Nat Med, 1: 1291-6.

Haass, C., and D. J. Selkoe. 2007. 'Soluble protein oligomers in neurodegeneration: lessons from the Alzheimer's amyloid beta-peptide', Nat Rev Mol Cell Biol, 8: 101-12.

Haass, C., and M. Willem. 2019. 'Secreted APP Modulates Synaptic Activity: A Novel Target for Therapeutic Intervention?', Neuron, 101: 557-59.

Hall, A. M., and E. D. Roberson. 2012. 'Mouse models of Alzheimer's disease', Brain Res Bull, 88: 3-12.

Hamaguchi, T., J. H. Kim, A. Hasegawa, R. Goto, K. Sakai, et al. 2021. 'Exogenous Abeta seeds induce Abeta depositions in the blood vessels rather than the brain parenchyma, independently of Abeta strain-specific information', Acta Neuropathol Commun, 9: 151.

Hamerman, J. A., J. R. Jarjoura, M. B. Humphrey, M. C. Nakamura, W. E. Seaman, and L. L. Lanier. 2006. 'Cutting edge: inhibition of TLR and FcR responses in macrophages by triggering receptor expressed on myeloid cells (TREM)-2 and DAP12', J Immunol, 177: 2051-5.

Hammond, T. R., C. Dufort, L. Dissing-Olesen, S. Giera, A. Young, et al. 2019. 'Single-Cell RNA Sequencing of Microglia throughout the Mouse Lifespan and in the Injured Brain Reveals Complex Cell-State Changes', Immunity, 50: 253-71 e6.

Hansen, D. V., J. E. Hanson, and M. Sheng. 2018. 'Microglia in Alzheimer's disease', J Cell Biol, 217: 459-72.

Hardy, J. A., and G. A. Higgins. 1992. 'Alzheimer's disease: the amyloid cascade hypothesis', Science, 256: 184-5.

Hardy, J., and D. J. Selkoe. 2002. 'The amyloid hypothesis of Alzheimer's disease: progress and problems on the road to therapeutics', Science, 297: 353-6.

Harry, G. J., and A. D. Kraft. 2008. 'Neuroinflammation and microglia: considerations and approaches for neurotoxicity assessment', Expert Opin Drug Metab Toxicol, 4: 1265-77.

Hashimoto, M., N. Bogdanovic, I. Volkmann, M. Aoki, B. Winblad, and L. O. Tjernberg. 2010. 'Analysis of microdissected human neurons by a sensitive ELISA reveals a correlation between elevated intracellular concentrations of Abeta42 and Alzheimer's disease neuropathology', Acta Neuropathol, 119: 543-54.

Haynes, S. E., G. Hollopeter, G. Yang, D. Kurpius, M. E. Dailey, W. B. Gan, and D. Julius. 2006. 'The P2Y12 receptor regulates microglial activation by extracellular nucleotides', Nat Neurosci, 9: 1512-9.

He, W., and C. J. Barrow. 1999. 'The A beta 3-pyroglutamyl and 11-pyroglutamyl peptides found in senile plaque have greater beta-sheet forming and aggregation propensities in vitro than full-length A beta', Biochemistry, 38: 10871-7.

He, Y., M. Wei, Y. Wu, H. Qin, W. Li, et al. 2019. 'Amyloid beta oligomers suppress excitatory transmitter release via presynaptic depletion of phosphatidylinositol-4,5-bisphosphate', Nat Commun, 10: 1-18.

Heiple, J. M., S. D. Wright, N. S. Allen, and S. C. Silverstein. 1990. 'Macrophages form circular zones of very close apposition to IgG-coated surfaces', Cell Motil Cytoskeleton, 15: 260-70.

Hemonnot, A. L., J. Hua, L. Ulmann, and H. Hirbec. 2019. 'Microglia in Alzheimer Disease: Well-Known Targets and New Opportunities', Front Aging Neurosci, 11: 233.

Heneka, M. T., M. J. Carson, J. El Khoury, G. E. Landreth, F. Brosseron, et al. 2015. 'Neuroinflammation in Alzheimer's disease', Lancet Neurol, 14: 388-405.

Heneka, M. T., M. P. Kummer, A. Stutz, A. Delekate, S. Schwartz, et al. 2013. 'NLRP3 is activated in Alzheimer's disease and contributes to pathology in APP/PS1 mice', Nature, 493: 674-8.

Heneka, M. T., H. Wiesinger, L. Dumitrescu-Ozimek, P. Riederer, D. L. Feinstein, and T. Klockgether. 2001. 'Neuronal and glial coexpression of argininosuccinate synthetase and inducible nitric oxide synthase in Alzheimer disease', J Neuropathol Exp Neurol, 60: 906-16.

Henjum, K., I. S. Almdahl, V. Arskog, L. Minthon, O. Hansson, T. Fladby, and L. N. Nilsson. 2016. 'Cerebrospinal fluid soluble TREM2 in aging and Alzheimer's disease', Alzheimers Res Ther, 8: 17.

Herman, J. P., D. Adams, and C. Prewitt. 1995. 'Regulatory changes in neuroendocrine stress-integrative circuitry produced by a variable stress paradigm', Neuroendocrinology, 61: 180-90.

Heslegrave, A., W. Heywood, R. Paterson, N. Magdalinou, J. Svensson, et al. 2016. 'Increased cerebrospinal fluid soluble TREM2 concentration in Alzheimer's disease', Mol Neurodegener, 11: 3.

Hickman, S. E., E. K. Allison, and J. El Khoury. 2008. 'Microglial dysfunction and defective beta-amyloid clearance pathways in aging Alzheimer's disease mice', J Neurosci, 28: 8354-60.

Hickman, S. E., N. D. Kingery, T. K. Ohsumi, M. L. Borowsky, L. C. Wang, T. K. Means, and J. El Khoury. 2013. 'The microglial sensome revealed by direct RNA sequencing', Nat Neurosci, 16: 1896-905.

Higuchi, Makoto, Bin Ji, Jun Maeda, Naruhiko Sahara, and Tetsuya Suhara. 2016. 'In vivoimaging of neuroinflammation in Alzheimer's disease', Clinical and Experimental Neuroimmunology, 7: 139-44.

Hiltunen, M., S. Helisalmi, A. Mannermaa, I. Alafuzoff, A. M. Koivisto, et al. 2000. 'Identification of a novel 4.6-kb genomic deletion in presenilin-1 gene which results in exclusion of exon 9 in a Finnish early onset Alzheimer's disease family: an Alu core sequence-stimulated recombination?', Eur J Hum Genet, 8: 259-66.

Ho, P. W., C. T. Leung, H. Liu, S. Y. Pang, C. S. Lam, et al. 2020. 'Age-dependent accumulation of oligomeric SNCA/alpha-synuclein from impaired degradation in mutant LRRK2 knockin mouse model of Parkinson disease: role for therapeutic activation of chaperone-mediated autophagy (CMA)', Autophagy, 16: 347-70.

Holcomb, L., M. N. Gordon, E. McGowan, X. Yu, S. Benkovic, et al. 1998. 'Accelerated Alzheimer-type phenotype in transgenic mice carrying both mutant amyloid precursor protein and presenilin 1 transgenes', Nat Med, 4: 97-100.

Holtman, I. R., D. D. Raj, J. A. Miller, W. Schaafsma, Z. Yin, et al. 2015. 'Induction of a common microglia gene expression signature by aging and neurodegenerative conditions: a co-expression meta-analysis', Acta Neuropathol Commun, 3: 31.

Holtzman, D. M., K. R. Bales, T. Tenkova, A. M. Fagan, M. Parsadanian, et al. 2000. 'Apolipoprotein E isoform-dependent amyloid deposition and neuritic degeneration in a mouse model of Alzheimer's disease', Proc Natl Acad Sci U S A, 97: 2892-7.

Hooli, B. V., A. R. Parrado, K. Mullin, W. K. Yip, T. Liu, et al. 2014. 'The rare TREM2 R47H variant exerts only a modest effect on Alzheimer disease risk', Neurology, 83: 1353-8.

Hoozemans, J. J., E. S. van Haastert, D. A. Nijholt, A. J. Rozemuller, P. Eikelenboom, and W. Scheper. 2009. 'The unfolded protein response is activated in pretangle neurons in Alzheimer's disease hippocampus', Am J Pathol, 174: 1241-51.

Hsiao, K., P. Chapman, S. Nilsen, C. Eckman, Y. Harigaya, et al. 1996. 'Correlative memory deficits, Abeta elevation, and amyloid plaques in transgenic mice', Science, 274: 99-102.

Hsieh, C. L., M. Koike, S. C. Spusta, E. C. Niemi, M. Yenari, M. C. Nakamura, and W. E. Seaman. 2009. 'A role for TREM2 ligands in the phagocytosis of apoptotic neuronal cells by microglia', J Neurochem, 109: 1144-56.

Hu, N., M. S. Tan, J. T. Yu, L. Sun, L. Tan, et al. 2014. 'Increased expression of TREM2 in peripheral blood of Alzheimer's disease patients', J Alzheimers Dis, 38: 497-501.

Hu, Z. W., M. R. Ma, Y. X. Chen, Y. F. Zhao, W. Qiang, and Y. M. Li. 2017. 'Phosphorylation at Ser(8) as an Intrinsic Regulatory Switch to Regulate the Morphologies and Structures of Alzheimer's 40-residue beta-Amyloid (Abeta40) Fibrils', J Biol Chem, 292: 2611-23.

Huang, M., D. Wang, Z. Xu, Y. Xu, X. Xu, Y. Ma, and Z. Xia. 2015. 'Lack of genetic association between TREM2 and Alzheimer's disease in East Asian population: a systematic review and meta-analysis', Am J Alzheimers Dis Other Demen, 30: 541-6.

Huang, Y., K. E. Happonen, P. G. Burrola, C. O'Connor, N. Hah, et al. 2021. 'Microglia use TAM receptors to detect and engulf amyloid beta plaques', Nat Immunol, 22: 586-94.

Humphrey, M. B., M. R. Daws, S. C. Spusta, E. C. Niemi, J. A. Torchia, et al. 2006. 'TREM2, a DAP12-associated receptor, regulates osteoclast differentiation and function', J Bone Miner Res, 21: 237-45.

Hutton, M., F. Busfield, M. Wragg, R. Crook, J. Perez-Tur, et al. 1996. 'Complete analysis of the presenilin 1 gene in early onset Alzheimer's disease', Neuroreport, 7: 801-5.

Hyman, B. T., C. H. Phelps, T. G. Beach, E. H. Bigio, N. J. Cairns, et al. 2012. 'National Institute on Aging-Alzheimer's Association guidelines for the neuropathologic assessment of Alzheimer's disease', Alzheimers Dement, 8: 1-13.

Ibach, M., M. Mathews, B. Linnartz-Gerlach, S. Theil, S. Kumar, et al. 2021. 'A reporter cell system for the triggering receptor expressed on myeloid cells 2 reveals differential effects of disease-associated variants on receptor signaling and activation by antibodies against the stalk region', Glia, 69: 1126-39.

Ida, N., C. L. Masters, and K. Beyreuther. 1996. 'Rapid cellular uptake of Alzheimer amyloid betaA4 peptide by cultured human neuroblastoma cells', FEBS Lett, 394: 174-8.

Ikeda, S., D. Allsop, and G. G. Glenner. 1989. 'Morphology and distribution of plaque and related deposits in the brains of Alzheimer's disease and control cases. An immunohistochemical study using amyloid beta-protein antibody', Lab Invest, 60: 113-22.

Itagaki, S., P. L. McGeer, H. Akiyama, S. Zhu, and D. Selkoe. 1989. 'Relationship of microglia and astrocytes to amyloid deposits of Alzheimer disease', J Neuroimmunol, 24: 173-82.

Iwatsubo, T., A. Odaka, N. Suzuki, H. Mizusawa, N. Nukina, and Y. Ihara. 1994. 'Visualization of A beta 42(43) and A beta 40 in senile plaques with end-specific A beta monoclonals: evidence that an initially deposited species is A beta 42(43)', Neuron, 13: 45-53.

Jack, C. R., Jr., V. J. Lowe, M. L. Senjem, S. D. Weigand, B. J. Kemp, et al. 2008. '11C PiB and structural MRI provide complementary information in imaging of Alzheimer's disease and amnestic mild cognitive impairment', Brain, 131: 665-80.

Jack, C. R., Jr., V. J. Lowe, S. D. Weigand, H. J. Wiste, M. L. Senjem, et al. 2009. 'Serial PIB and MRI in normal, mild cognitive impairment and Alzheimer's disease: implications for sequence of pathological events in Alzheimer's disease', Brain, 132: 1355-65.

Jackson, R. J., N. Rudinskiy, A. G. Herrmann, S. Croft, J. M. Kim, et al. 2016. 'Human tau increases amyloid beta plaque size but not amyloid beta-mediated synapse loss in a novel mouse model of Alzheimer's disease', Eur J Neurosci, 44: 3056-66.

Jadhav, V. S., P. B. C. Lin, T. Pennington, G. V. Di Prisco, A. J. Jannu, et al. 2020. 'Trem2 Y38C mutation and loss of Trem2 impairs neuronal synapses in adult mice', Mol Neurodegener, 15: 62.

Jan, A., O. Gokce, R. Luthi-Carter, and H. A. Lashuel. 2008. 'The ratio of monomeric to aggregated forms of Abeta40 and Abeta42 is an important determinant of amyloid-beta aggregation, fibrillogenesis, and toxicity', J Biol Chem, 283: 28176-89.

Jankowsky, J. L., D. J. Fadale, J. Anderson, G. M. Xu, V. Gonzales, et al. 2004a. 'Mutant presenilins specifically elevate the levels of the 42 residue beta-amyloid peptide in vivo: evidence for augmentation of a 42-specific gamma secretase', Hum Mol Genet, 13: 159-70.

Jankowsky, J. L., H. H. Slunt, V. Gonzales, N. A. Jenkins, N. G. Copeland, and D. R. Borchelt. 2004b. 'APP processing and amyloid deposition in mice haplo-insufficient for presenilin 1', Neurobiol Aging, 25: 885-92.

Janus, C., A. Y. Flores, G. Xu, and D. R. Borchelt. 2015. 'Behavioral abnormalities in APPSwe/PS1dE9 mouse model of AD-like pathology: comparative analysis across multiple behavioral domains', Neurobiol Aging, 36: 2519-32.

Jawhar, S., A. Trawicka, C. Jenneckens, T. A. Bayer, and O. Wirths. 2012. 'Motor deficits, neuron loss, and reduced anxiety coinciding with axonal degeneration and intraneuronal Abeta aggregation in the 5XFAD mouse model of Alzheimer's disease', Neurobiol Aging, 33: 196 e29-40.

Jay, T. R., A. M. Hirsch, M. L. Broihier, C. M. Miller, L. E. Neilson, et al. 2017. 'Disease Progression-Dependent Effects of TREM2 Deficiency in a Mouse Model of Alzheimer's Disease', J Neurosci, 37: 637-47.

Jay, T. R., C. M. Miller, P. J. Cheng, L. C. Graham, S. Bemiller, et al. 2015. 'TREM2 deficiency eliminates TREM2+ inflammatory macrophages and ameliorates pathology in Alzheimer's disease mouse models', J Exp Med, 212: 287-95.

Jendresen, C., V. Arskog, M. R. Daws, and L. N. Nilsson. 2017. 'The Alzheimer's disease risk factors apolipoprotein E and TREM2 are linked in a receptor signaling pathway', J Neuroinflammation, 14: 59.

Jiang, T., J. K. Hou, Q. Gao, J. T. Yu, J. S. Zhou, H. D. Zhao, and Y. D. Zhang. 2016a. 'TREM2 p.H157Y Variant and the Risk of Alzheimer's Disease: A Meta-Analysis Involving 14,510 Subjects', Curr Neurovasc Res, 13: 318-20.

Jiang, T., L. Tan, Q. Chen, M. S. Tan, J. S. Zhou, et al. 2016b. 'A rare coding variant in TREM2 increases risk for Alzheimer's disease in Han Chinese', Neurobiol Aging, 42: 217 e1-3.

Jiang, T., L. Tan, X. C. Zhu, Q. Q. Zhang, L. Cao, et al. 2014. 'Upregulation of TREM2 ameliorates neuropathology and rescues spatial cognitive impairment in a transgenic mouse model of Alzheimer's disease', Neuropsychopharmacology, 39: 2949-62.

Jin, M., N. Shepardson, T. Yang, G. Chen, D. Walsh, and D. J. Selkoe. 2011. 'Soluble amyloid beta-protein dimers isolated from Alzheimer cortex directly induce Tau hyperphosphorylation and neuritic degeneration', Proc Natl Acad Sci U S A, 108: 5819-24.

Jin, S. C., B. A. Benitez, C. M. Karch, B. Cooper, T. Skorupa, et al. 2014. 'Coding variants in TREM2 increase risk for Alzheimer's disease', Hum Mol Genet, 23: 5838-46.

Jin, S. C., M. M. Carrasquillo, B. A. Benitez, T. Skorupa, D. Carrell, et al. 2015. 'TREM2 is associated with increased risk for Alzheimer's disease in African Americans', Mol Neurodegener, 10: 19.

Joachim, C. L., J. H. Morris, and D. J. Selkoe. 1988. 'Clinically diagnosed Alzheimer's disease: autopsy results in 150 cases', Ann Neurol, 24: 50-6.

Jones, L., P. A. Holmans, M. L. Hamshere, D. Harold, V. Moskvina, et al. 2010. 'Genetic evidence implicates the immune system and cholesterol metabolism in the aetiology of Alzheimer's disease', PLoS One, 5: e13950.

Jonsson, T., J. K. Atwal, S. Steinberg, J. Snaedal, P. V. Jonsson, et al. 2012. 'A mutation in APP protects against Alzheimer's disease and age-related cognitive decline', Nature, 488: 96-9.

Jonsson, T., H. Stefansson, S. Steinberg, I. Jonsdottir, P. V. Jonsson, et al. 2013. 'Variant of TREM2 associated with the risk of Alzheimer's disease', N Engl J Med, 368: 107-16.

Joshi, P., F. Riffel, S. Kumar, N. Villacampa, S. Theil, et al. 2021a. 'TREM2 modulates differential deposition of modified and non-modified Abeta species in extracellular plaques and intraneuronal deposits', Acta Neuropathol Commun, 9: 1-22.

Joshi, P., F. Riffel, K. Satoh, M. Enomoto, S. Qamar, et al. 2021b. 'Differential interaction with TREM2 modulates microglial uptake of modified Abeta species', Glia, 69: 2917-32.

Jucker, M., and L. C. Walker. 2013. 'Self-propagation of pathogenic protein aggregates in neurodegenerative diseases', Nature, 501: 45-51.

Jucker, M., and L. C. Walker. 2018. 'Propagation and spread of pathogenic protein assemblies in neurodegenerative diseases', Nat Neurosci, 21: 1341-49.

Jurga, A. M., M. Paleczna, and K. Z. Kuter. 2020. 'Overview of General and Discriminating Markers of Differential Microglia Phenotypes', Front Cell Neurosci, 14: 198.

Kaas, J. H. 2013. 'The evolution of brains from early mammals to humans', Wiley Interdiscip Rev Cogn Sci, 4: 33-45.

Kaifu, T., J. Nakahara, M. Inui, K. Mishima, T. Momiyama, et al. 2003. 'Osteopetrosis and thalamic hypomyelinosis with synaptic degeneration in DAP12-deficient mice', J Clin Invest, 111: 323-32.

Kakuda, N., T. Miyasaka, N. Iwasaki, T. Nirasawa, S. Wada-Kakuda, et al. 2017. 'Distinct deposition of amyloid-beta species in brains with Alzheimer's disease pathology visualized with MALDI imaging mass spectrometry', Acta Neuropathol Commun, 5: 73.

Kalaria, R. N. 2016. 'Neuropathological diagnosis of vascular cognitive impairment and vascular dementia with implications for Alzheimer's disease', Acta Neuropathol, 131: 659-85.

Kamphuis, W., J. Middeldorp, L. Kooijman, J. A. Sluijs, E. J. Kooi, et al. 2014. 'Glial fibrillary acidic protein isoform expression in plaque related astrogliosis in Alzheimer's disease', Neurobiol Aging, 35: 492-510.

Kanekiyo, T., H. Xu, and G. Bu. 2014. 'ApoE and Abeta in Alzheimer's disease: accidental encounters or partners?', Neuron, 81: 740-54.

Kang, S. S., M. T. W. Ebbert, K. E. Baker, C. Cook, X. Wang, et al. 2018. 'Microglial translational profiling reveals a convergent APOE pathway from aging, amyloid, and tau', J Exp Med, 215: 2235-45.

Karch, C. M., and A. M. Goate. 2015. 'Alzheimer's disease risk genes and mechanisms of disease pathogenesis', Biol Psychiatry, 77: 43-51.

Karran, E., M. Mercken, and B. De Strooper. 2011. 'The amyloid cascade hypothesis for Alzheimer's disease: an appraisal for the development of therapeutics', Nat Rev Drug Discov, 10: 698-712.

Katsumoto, A., H. Takeuchi, K. Takahashi, and F. Tanaka. 2018. 'Microglia in Alzheimer's Disease: Risk Factors and Inflammation', Front Neurol, 9: 978.

Katzmarski, N., S. Ziegler-Waldkirch, N. Scheffler, C. Witt, C. Abou-Ajram, et al. 2020. 'Abeta oligomers trigger and accelerate Abeta seeding', Brain Pathol, 30: 36-45.

Kawabori, M., R. Kacimi, T. Kauppinen, C. Calosing, J. Y. Kim, et al. 2015. 'Triggering receptor expressed on myeloid cells 2 (TREM2) deficiency attenuates phagocytic activities of microglia and exacerbates ischemic damage in experimental stroke', J Neurosci, 35: 3384-96.

Kempuraj, D., R. Thangavel, P. A. Natteru, G. P. Selvakumar, D. Saeed, et al. 2016. 'Neuroinflammation Induces Neurodegeneration', J Neurol Neurosurg Spine, 1: 1-15.

Keren-Shaul, H., A. Spinrad, A. Weiner, O. Matcovitch-Natan, R. Dvir-Szternfeld, et al. 2017. 'A Unique Microglia Type Associated with Restricting Development of Alzheimer's Disease', Cell, 169: 1276-90 e17.

Kerridge, C., D. I. Kozlova, N. N. Nalivaeva, and A. J. Turner. 2015. 'Hypoxia Affects Neprilysin Expression Through Caspase Activation and an APP Intracellular Domain-dependent Mechanism', Front Neurosci, 9: 426.

Keskitalo, S., M. Farkas, M. Hanenberg, A. Szodorai, L. Kulic, et al. 2014. 'Reciprocal modulation of Abeta42 aggregation by copper and homocysteine', Front Aging Neurosci, 6: 237.

Kiialainen, A., K. Hovanes, J. Paloneva, O. Kopra, and L. Peltonen. 2005. 'Dap12 and Trem2, molecules involved in innate immunity and neurodegeneration, are co-expressed in the CNS', Neurobiol Dis, 18: 314-22.

Kilgore, M., C. A. Miller, D. M. Fass, K. M. Hennig, S. J. Haggarty, J. D. Sweatt, and G. Rumbaugh. 2010. 'Inhibitors of class 1 histone deacetylases reverse contextual memory deficits in a mouse model of Alzheimer's disease', Neuropsychopharmacology, 35: 870-80.

Kim, J. H., P. Song, H. Lim, J. H. Lee, J. H. Lee, S. A. Park, and Initiative Alzheimer's Disease Neuroimaging. 2014. 'Gene-based rare allele analysis identified a risk gene of Alzheimer's disease', PLoS One, 9: e107983.

Kim, S. M., B. R. Mun, S. J. Lee, Y. Joh, H. Y. Lee, et al. 2017. 'TREM2 promotes Abeta phagocytosis by upregulating C/EBPalpha-dependent CD36 expression in microglia', Sci Rep, 7: 11118.

Kim, T., G. S. Vidal, M. Djurisic, C. M. William, M. E. Birnbaum, et al. 2013. 'Human LilrB2 is a beta-amyloid receptor and its murine homolog PirB regulates synaptic plasticity in an Alzheimer's model', Science, 341: 1399-404.

Kim, Y., K. Sato, M. Asagiri, I. Morita, K. Soma, and H. Takayanagi. 2005. 'Contribution of nuclear factor of activated T cells c1 to the transcriptional control of immunoreceptor osteoclast-associated receptor but not triggering receptor expressed by myeloid cells-2 during osteoclastogenesis', J Biol Chem, 280: 32905-13.

Kimberly, W. T., W. Xia, T. Rahmati, M. S. Wolfe, and D. J. Selkoe. 2000. 'The transmembrane aspartates in presenilin 1 and 2 are obligatory for gamma-secretase activity and amyloid beta-protein generation', J Biol Chem, 275: 3173-8.

Kimura, R., and M. Ohno. 2009. 'Impairments in remote memory stabilization precede hippocampal synaptic and cognitive failures in 5XFAD Alzheimer mouse model', Neurobiol Dis, 33: 229-35.

Kinney, J. W., S. M. Bemiller, A. S. Murtishaw, A. M. Leisgang, A. M. Salazar, and B. T. Lamb. 2018. 'Inflammation as a central mechanism in Alzheimer's disease', Alzheimers Dement (N Y), 4: 575-90.

Kleinberger, G., M. Brendel, E. Mracsko, B. Wefers, L. Groeneweg, et al. 2017. 'The FTD-like syndrome causing TREM2 T66M mutation impairs microglia function, brain perfusion, and glucose metabolism', EMBO J, 36: 1837-53.

Kleinberger, G., Y. Yamanishi, M. Suarez-Calvet, E. Czirr, E. Lohmann, et al. 2014. 'TREM2 mutations implicated in neurodegeneration impair cell surface transport and phagocytosis', Sci Transl Med, 6: 1-12.

Klesney-Tait, J., I. R. Turnbull, and M. Colonna. 2006. 'The TREM receptor family and signal integration', Nat Immunol, 7: 1266-73.

Klunemann, H. H., B. H. Ridha, L. Magy, J. R. Wherrett, D. M. Hemelsoet, et al. 2005. 'The genetic causes of basal ganglia calcification, dementia, and bone cysts: DAP12 and TREM2', Neurology, 64: 1502-7.

Knauer, M. F., B. Soreghan, D. Burdick, J. Kosmoski, and C. G. Glabe. 1992. 'Intracellular accumulation and resistance to degradation of the Alzheimer amyloid A4/beta protein', Proc Natl Acad Sci U S A, 89: 7437-41.

Knobloch, M., U. Konietzko, D. C. Krebs, and R. M. Nitsch. 2007. 'Intracellular Abeta and cognitive deficits precede beta-amyloid deposition in transgenic arcAbeta mice', Neurobiol Aging, 28: 1297-306.

Kober, D. L., J. M. Alexander-Brett, C. M. Karch, C. Cruchaga, M. Colonna, M. J. Holtzman, and T. J. Brett. 2016. 'Neurodegenerative disease mutations in TREM2 reveal a functional surface and distinct loss-of-function mechanisms', Elife, 5: 1-24.

Kober, D. L., and T. J. Brett. 2017. 'TREM2-Ligand Interactions in Health and Disease', J Mol Biol, 429: 1607-29.

Kober, D. L., M. D. Stuchell-Brereton, C. E. Kluender, H. B. Dean, M. R. Strickland, et al. 2020. 'Functional insights from biophysical study of TREM2 interactions with apoE and Abeta1-42', Alzheimers Dement: 1-10.

Koch, P., I. Y. Tamboli, J. Mertens, P. Wunderlich, J. Ladewig, et al. 2012. 'Presenilin-1 L166P mutant human pluripotent stem cell-derived neurons exhibit partial loss of gamma-secretase activity in endogenous amyloid-beta generation', Am J Pathol, 180: 2404-16.

Koffie, R. M., M. Meyer-Luehmann, T. Hashimoto, K. W. Adams, M. L. Mielke, et al. 2009. 'Oligomeric amyloid beta associates with postsynaptic densities and correlates with excitatory synapse loss near senile plaques', Proc Natl Acad Sci U S A, 106: 4012-7.

Koistinaho, M., M. Ort, J. M. Cimadevilla, R. Vondrous, B. Cordell, et al. 2001. 'Specific spatial learning deficits become severe with age in beta -amyloid precursor protein transgenic mice that harbor diffuse beta -amyloid deposits but do not form plaques', Proc Natl Acad Sci U S A, 98: 14675-80.

Korvatska, O., J. B. Leverenz, S. Jayadev, P. McMillan, I. Kurtz, et al. 2015. 'R47H Variant of TREM2 Associated With Alzheimer Disease in a Large Late-Onset Family: Clinical, Genetic, and Neuropathological Study', JAMA Neurol, 72: 920-7.

Koth, L. L., C. J. Cambier, A. Ellwanger, M. Solon, L. Hou, et al. 2010. 'DAP12 is required for macrophage recruitment to the lung in response to cigarette smoke and chemotaxis toward CCL2', J Immunol, 184: 6522-8.

Krasemann, S., C. Madore, R. Cialic, C. Baufeld, N. Calcagno, et al. 2017. 'The TREM2-APOE Pathway Drives the Transcriptional Phenotype of Dysfunctional Microglia in Neurodegenerative Diseases', Immunity, 47: 566-81 e9.

Kretner, B., J. Trambauer, A. Fukumori, J. Mielke, P. H. Kuhn, et al. 2016. 'Generation and deposition of Abeta43 by the virtually inactive presenilin-1 L435F mutant contradicts the presenilin loss-of-function hypothesis of Alzheimer's disease', EMBO Mol Med, 8: 458-65.

Kumar-Singh, S. 2008. 'Cerebral amyloid angiopathy: pathogenetic mechanisms and link to dense amyloid plaques', Genes Brain Behav, 7 Suppl 1: 67-82.

Kumar, S., J. L. Frost, C. W. Cotman, E. Head, R. Palmour, C. A. Lemere, and J. Walter. 2018. 'Deposition of phosphorylated amyloid-beta in brains of aged nonhuman primates and canines', Brain Pathol, 28: 427-30.

Kumar, S., A. Kapadia, S. Theil, P. Joshi, F. Riffel, M. T. Heneka, and J. Walter. 2020a. 'Novel Phosphorylation-State Specific Antibodies Reveal Differential Deposition of Ser26 Phosphorylated Abeta Species in a Mouse Model of Alzheimer's Disease', Front Mol Neurosci, 13: 1-12.

Kumar, S., C. A. Lemere, and J. Walter. 2020b. 'Phosphorylated Abeta peptides in human Down syndrome brain and different Alzheimer's-like mouse models', Acta Neuropathol Commun, 8: 1-14.

Kumar, S., N. Rezaei-Ghaleh, D. Terwel, D. R. Thal, M. Richard, et al. 2011a. 'Extracellular phosphorylation of the amyloid beta-peptide promotes formation of toxic aggregates during the pathogenesis of Alzheimer's disease', EMBO J, 30: 2255-65.

Kumar, S., S. Singh, D. Hinze, M. Josten, H. G. Sahl, M. Siepmann, and J. Walter. 2012. 'Phosphorylation of amyloid-beta peptide at serine 8 attenuates its clearance via insulin-degrading and angiotensin-converting enzymes', J Biol Chem, 287: 8641-51.

Kumar, S., and J. Walter. 2011b. 'Phosphorylation of amyloid beta (Abeta) peptides - a trigger for formation of toxic aggregates in Alzheimer's disease', Aging (Albany NY), 3: 803-12.

Kumar, S., O. Wirths, K. Stuber, P. Wunderlich, P. Koch, et al. 2016. 'Phosphorylation of the amyloid beta-peptide at Ser26 stabilizes oligomeric assembly and increases neurotoxicity', Acta Neuropathol, 131: 525-37.

Kumar, S., O. Wirths, S. Theil, J. Gerth, T. A. Bayer, and J. Walter. 2013. 'Early intraneuronal accumulation and increased aggregation of phosphorylated Abeta in a mouse model of Alzheimer's disease', Acta Neuropathol, 125: 699-709.

Kummer, M. P., and M. T. Heneka. 2014. 'Truncated and modified amyloid-beta species', Alzheimers Res Ther, 6: 1-9.

Kummer, M. P., M. Hermes, A. Delekarte, T. Hammerschmidt, S. Kumar, et al. 2011. 'Nitration of tyrosine 10 critically enhances amyloid beta aggregation and plaque formation', Neuron, 71: 833-44.

Kunkle, B. W., B. Grenier-Boley, R. Sims, J. C. Bis, V. Damotte, et al. 2019. 'Genetic meta-analysis of diagnosed Alzheimer's disease identifies new risk loci and implicates Abeta, tau, immunity and lipid processing', Nat Genet, 51: 414-30.

Kwart, D., A. Gregg, C. Scheckel, E. A. Murphy, D. Paquet, et al. 2019. 'A Large Panel of Isogenic APP and PSEN1 Mutant Human iPSC Neurons Reveals Shared Endosomal Abnormalities Mediated by APP beta-CTFs, Not Abeta', Neuron, 104: 256-70 e5.

Kwok, J. B. 2010. 'Role of epigenetics in Alzheimer's and Parkinson's disease', Epigenomics, 2: 671-82.

Kwon, H. S., and S. H. Koh. 2020. 'Neuroinflammation in neurodegenerative disorders: the roles of microglia and astrocytes', Transl Neurodegener, 9: 42.

LaFerla, F. M., and K. N. Green. 2012. 'Animal models of Alzheimer disease', Cold Spring Harb Perspect Med, 2: 1-13.

LaFerla, F. M., K. N. Green, and S. Oddo. 2007. 'Intracellular amyloid-beta in Alzheimer's disease', Nat Rev Neurosci, 8: 499-509.

Lai, A. Y., and J. McLaurin. 2010. 'Mechanisms of amyloid-Beta Peptide uptake by neurons: the role of lipid rafts and lipid raft-associated proteins', Int J Alzheimers Dis, 2011: 548380.

Lalonde, R., H. D. Kim, J. A. Maxwell, and K. Fukuchi. 2005. 'Exploratory activity and spatial learning in 12-month-old APP(695)SWE/co+PS1/DeltaE9 mice with amyloid plaques', Neurosci Lett, 390: 87-92.

Lambert, J. C., S. Heath, G. Even, D. Campion, K. Sleegers, et al. 2009. 'Genome-wide association study identifies variants at CLU and CR1 associated with Alzheimer's disease', Nat Genet, 41: 1094-9.

Lambert, J. C., C. A. Ibrahim-Verbaas, D. Harold, A. C. Naj, R. Sims, et al. 2013. 'Meta-analysis of 74,046 individuals identifies 11 new susceptibility loci for Alzheimer's disease', Nat Genet, 45: 1452-8.

Lane, C. A., J. Hardy, and J. M. Schott. 2018. 'Alzheimer's disease', Eur J Neurol, 25: 59-70.

Lanier, L. L. 2009. 'DAP10- and DAP12-associated receptors in innate immunity', Immunol Rev, 227: 150-60.

Lanoiselee, H. M., G. Nicolas, D. Wallon, A. Rovelet-Lecrux, M. Lacour, et al. 2017. 'APP, PSEN1, and PSEN2 mutations in early-onset Alzheimer disease: A genetic screening study of familial and sporadic cases', PLoS Med, 14: e1002270.

Lawson, L. J., V. H. Perry, and S. Gordon. 1992. 'Turnover of resident microglia in the normal adult mouse brain', Neuroscience, 48: 405-15.

Le Ber, I., A. De Septenville, R. Guerreiro, J. Bras, A. Camuzat, et al. 2014. 'Homozygous TREM2 mutation in a family with atypical frontotemporal dementia', Neurobiol Aging, 35: 2419 e23-19 e25.

Le Guennec, K., S. Veugelen, O. Quenez, M. Szaruga, S. Rousseau, et al. 2017. 'Deletion of exons 9 and 10 of the Presenilin 1 gene in a patient with Early-onset Alzheimer Disease generates longer amyloid seeds', Neurobiol Dis, 104: 97-103.

Lee, C. Y. D., A. Daggett, X. Gu, L. L. Jiang, P. Langfelder, et al. 2018. 'Elevated TREM2 Gene Dosage Reprograms Microglia Responsivity and Ameliorates Pathological Phenotypes in Alzheimer's Disease Models', Neuron, 97: 1032-48 e5.

Lee, C. Y., and G. E. Landreth. 2010. 'The role of microglia in amyloid clearance from the AD brain', J Neural Transm (Vienna), 117: 949-60.

Lee, D. C., J. Rizer, J. B. Hunt, M. L. Selenica, M. N. Gordon, and D. Morgan. 2013a. 'Review: experimental manipulations of microglia in mouse models of Alzheimer's pathology: activation reduces amyloid but hastens tau pathology', Neuropathol Appl Neurobiol, 39: 69-85.

Lee, J. E., and P. L. Han. 2013b. 'An update of animal models of Alzheimer disease with a reevaluation of plaque depositions', Exp Neurobiol, 22: 84-95.

Lee, M. K., D. R. Borchelt, G. Kim, G. Thinakaran, H. H. Slunt, et al. 1997. 'Hyperaccumulation of FAD-linked presenilin 1 variants in vivo', Nat Med, 3: 756-60.

Lee, S. H., W. J. Meilandt, L. Xie, V. D. Gandham, H. Ngu, et al. 2021. 'Trem2 restrains the enhancement of tau accumulation and neurodegeneration by beta-amyloid pathology', Neuron, 109: 1283-301 e6.

Lessard, C. B., S. L. Malnik, Y. Zhou, T. B. Ladd, P. E. Cruz, et al. 2018. 'High-affinity interactions and signal transduction between Abeta oligomers and TREM2', EMBO Mol Med, 10: 1-13.

Levy, E., M. D. Carman, I. J. Fernandez-Madrid, M. D. Power, I. Lieberburg, et al. 1990. 'Mutation of the Alzheimer's disease amyloid gene in hereditary cerebral hemorrhage, Dutch type', Science, 248: 1124-6.

Lewis, J., D. W. Dickson, W. L. Lin, L. Chisholm, A. Corral, et al. 2001. 'Enhanced neurofibrillary degeneration in transgenic mice expressing mutant tau and APP', Science, 293: 1487-91.

Leyns, C. E. G., M. Gratuze, S. Narasimhan, N. Jain, L. J. Koscal, et al. 2019. 'TREM2 function impedes tau seeding in neuritic plaques', Nat Neurosci, 22: 1217-22.

Leyns, C. E. G., J. D. Ulrich, M. B. Finn, F. R. Stewart, L. J. Koscal, et al. 2017. 'TREM2 deficiency attenuates neuroinflammation and protects against neurodegeneration in a mouse model of tauopathy', Proc Natl Acad Sci U S A, 114: 11524-29.

Li, J. T., and Y. Zhang. 2018a. 'TREM2 regulates innate immunity in Alzheimer's disease', J Neuroinflammation, 15: 107.

Li, N., K. Liu, Y. Qiu, Z. Ren, R. Dai, Y. Deng, and H. Qing. 2016. 'Effect of Presenilin Mutations on APP Cleavage; Insights into the Pathogenesis of FAD', Front Aging Neurosci, 8: 51.

Li, P., L. Marshall, G. Oh, J. L. Jakubowski, D. Groot, et al. 2019. 'Epigenetic dysregulation of enhancers in neurons is associated with Alzheimer's disease pathology and cognitive symptoms', Nat Commun, 10: 2246.

Li, S., M. Jin, L. Liu, Y. Dang, B. L. Ostaszewski, and D. J. Selkoe. 2018b. 'Decoding the synaptic dysfunction of bioactive human AD brain soluble Abeta to inspire novel therapeutic avenues for Alzheimer's disease', Acta Neuropathol Commun, 6: 121.

Libard, S., J. Walter, and I. Alafuzoff. 2021. 'In vivo Characterization of Biochemical Variants of Amyloid-beta in Subjects with Idiopathic Normal Pressure Hydrocephalus and Alzheimer's Disease Neuropathological Change', J Alzheimers Dis, 80: 1003-12.

Lichtenthaler, S. F., R. Wang, H. Grimm, S. N. Uljon, C. L. Masters, and K. Beyreuther. 1999. 'Mechanism of the cleavage specificity of Alzheimer's disease gamma-secretase identified by phenylalanine-scanning mutagenesis of the transmembrane domain of the amyloid precursor protein', Proc Natl Acad Sci U S A, 96: 3053-8.

Lill, C. M., A. Rengmark, L. Pihlstrom, I. Fogh, A. Shatunov, et al. 2015. 'The role of TREM2 R47H as a risk factor for Alzheimer's disease, frontotemporal lobar degeneration, amyotrophic lateral sclerosis, and Parkinson's disease', Alzheimers Dement, 11: 1407-16.

Lim, J., and Z. Yue. 2015. 'Neuronal aggregates: formation, clearance, and spreading', Dev Cell, 32: 491-501.

Liu, D., B. Cao, Y. Zhao, H. Huang, R. S. McIntyre, J. D. Rosenblat, and H. Zhou. 2018. 'Soluble TREM2 changes during the clinical course of Alzheimer's disease: A meta-analysis', Neurosci Lett, 686: 10-16.

Liu, G., Y. Liu, Q. Jiang, Y. Jiang, R. Feng, et al. 2016. 'Convergent Genetic and Expression Datasets Highlight TREM2 in Parkinson's Disease Susceptibility', Mol Neurobiol, 53: 4931-8.

Liu, K., R. W. Doms, and V. M. Lee. 2002. 'Glu11 site cleavage and N-terminally truncated A beta production upon BACE overexpression', Biochemistry, 41: 3128-36.

Liu, L., S. K. Herukka, R. Minkeviciene, T. van Groen, and H. Tanila. 2004. 'Longitudinal observation on CSF Abeta42 levels in young to middle-aged amyloid precursor protein/presenilin-1 doubly transgenic mice', Neurobiol Dis, 17: 516-23.

Liu, M., T. Dexheimer, D. Sui, S. Hovde, X. Deng, et al. 2020. 'Hyperphosphorylated tau aggregation and cytotoxicity modulators screen identified prescription drugs linked to Alzheimer's disease and cognitive functions', Sci Rep, 10: 16551.

Loera-Valencia, R., J. Goikolea, C. Parrado-Fernandez, P. Merino-Serrais, and S. Maioli. 2019. 'Alterations in cholesterol metabolism as a risk factor for developing Alzheimer's disease: Potential novel targets for treatment', J Steroid Biochem Mol Biol, 190: 104-14.

Lord, A., H. Kalimo, C. Eckman, X. Q. Zhang, L. Lannfelt, and L. N. Nilsson. 2006. 'The Arctic Alzheimer mutation facilitates early intraneuronal Abeta aggregation and senile plaque formation in transgenic mice', Neurobiol Aging, 27: 67-77.

Lourbopoulos, A., A. Erturk, and F. Hellal. 2015. 'Microglia in action: how aging and injury can change the brain's guardians', Front Cell Neurosci, 9: 54.

Lu, Y., W. Liu, and X. Wang. 2015. 'TREM2 variants and risk of Alzheimer's disease: a meta-analysis', Neurol Sci, 36: 1881-8.

Lucin, K. M., and T. Wyss-Coray. 2009. 'Immune activation in brain aging and neurodegeneration: too much or too little?', Neuron, 64: 110-22.

Lue, L. F., C. T. Schmitz, G. Serrano, L. I. Sue, T. G. Beach, and D. G. Walker. 2015a. 'TREM2 Protein Expression Changes Correlate with Alzheimer's Disease Neurodegenerative Pathologies in Post-Mortem Temporal Cortices', Brain Pathol, 25: 469-80.

Lue, L. F., C. Schmitz, and D. G. Walker. 2015b. 'What happens to microglial TREM2 in Alzheimer's disease: Immunoregulatory turned into immunopathogenic?', Neuroscience, 302: 138-50.

Luth, H. J., G. Munch, and T. Arendt. 2002. 'Aberrant expression of NOS isoforms in Alzheimer's disease is structurally related to nitrotyrosine formation', Brain Res, 953: 135-43.

Ma, L., M. Allen, N. Sakae, N. Ertekin-Taner, N. R. Graff-Radford, et al. 2016. 'Expression and processing analyses of wild type and p.R47H TREM2 variant in Alzheimer's disease brains', Mol Neurodegener, 11: 1-9.

Ma, Q. L., F. Yang, E. R. Rosario, O. J. Ubeda, W. Beech, et al. 2009. 'Beta-amyloid oligomers induce phosphorylation of tau and inactivation of insulin receptor substrate via c-Jun N-terminal kinase signaling: suppression by omega-3 fatty acids and curcumin', J Neurosci, 29: 9078-89.

Maat-Schieman, M. L., S. G. van Duinen, M. Bornebroek, J. Haan, and R. A. Roos. 1996. 'Hereditary cerebral hemorrhage with amyloidosis-Dutch type (HCHWA-D): II--A review of histopathological aspects', Brain Pathol, 6: 115-20.

Madry, H., J. Prudlo, A. Grgic, and J. Freyschmidt. 2007. 'Nasu-Hakola disease (PLOSL): report of five cases and review of the literature', Clin Orthop Relat Res, 454: 262-9.

Magusali, N., A. C. Graham, T. M. Piers, P. Panichnantakul, U. Yaman, et al. 2021. 'A genetic link between risk for Alzheimer's disease and severe COVID-19 outcomes via the OAS1 gene', Brain, 144: 3727-41.

Maia, L. F., S. A. Kaeser, J. Reichwald, M. Hruscha, P. Martus, M. Staufenbiel, and M. Jucker. 2013. 'Changes in amyloid-beta and Tau in the cerebrospinal fluid of transgenic mice overexpressing amyloid precursor protein', Sci Transl Med, 5: 194re2.

Mandelkow, E. M., and E. Mandelkow. 2012. 'Biochemistry and cell biology of tau protein in neurofibrillary degeneration', Cold Spring Harb Perspect Med, 2: a006247.

Mandrekar, S., Q. Jiang, C. Y. Lee, J. Koenigsknecht-Talboo, D. M. Holtzman, and G. E. Landreth. 2009. 'Microglia mediate the clearance of soluble Abeta through fluid phase macropinocytosis', J Neurosci, 29: 4252-62.

Mann, D. M. A., Y. S. Davidson, A. C. Robinson, N. Allen, T. Hashimoto, et al. 2018. 'Patterns and severity of vascular amyloid in Alzheimer's disease associated with duplications and missense mutations in APP gene, Down syndrome and sporadic Alzheimer's disease', Acta Neuropathol, 136: 569-87.

Mann, D. M., A. Takeuchi, S. Sato, N. J. Cairns, P. L. Lantos, et al. 2001. 'Cases of Alzheimer's disease due to deletion of exon 9 of the presenilin-1 gene show an unusual but characteristic beta-amyloid pathology known as 'cotton wool' plaques', Neuropathol Appl Neurobiol, 27: 189-96.

Masters, C. L., R. Bateman, K. Blennow, C. C. Rowe, R. A. Sperling, and J. L. Cummings. 2015. 'Alzheimer's disease', Nat Rev Dis Primers, 1: 15056.

Masters, C. L., and K. Beyreuther. 2001. 'Henryk M. Wisniewski and the amyloid theory of Alzheimer's disease', J Alzheimers Dis, 3: 83-86.

Masuda, T., R. Sankowski, O. Staszewski, and M. Prinz. 2020. 'Microglia Heterogeneity in the Single-Cell Era', Cell Rep, 30: 1271-81.

Matarin, M., D. A. Salih, M. Yasvoina, D. M. Cummings, S. Guelfi, et al. 2015. 'A genome-wide gene-expression analysis and database in transgenic mice during development of amyloid or tau pathology', Cell Rep, 10: 633-44.

Mathys, H., J. Davila-Velderrain, Z. Peng, F. Gao, S. Mohammadi, et al. 2019. 'Single-cell transcriptomic analysis of Alzheimer's disease', Nature, 570: 332-37.

Matsui, T., M. Ingelsson, H. Fukumoto, K. Ramasamy, H. Kowa, et al. 2007. 'Expression of APP pathway mRNAs and proteins in Alzheimer's disease', Brain Res, 1161: 116-23.

Mattsson-Carlgren, N., E. Andersson, S. Janelidze, R. Ossenkoppele, P. Insel, et al. 2020. 'Abeta deposition is associated with increases in soluble and phosphorylated tau that precede a positive Tau PET in Alzheimer's disease', Sci Adv, 6: eaaz2387.

Mawuenyega, K. G., W. Sigurdson, V. Ovod, L. Munsell, T. Kasten, et al. 2010. 'Decreased clearance of CNS beta-amyloid in Alzheimer's disease', Science, 330: 1774.

Mazaheri, F., N. Snaidero, G. Kleinberger, C. Madore, A. Daria, et al. 2017. 'TREM2 deficiency impairs chemotaxis and microglial responses to neuronal injury', EMBO Rep, 18: 1186-98.

McMahon, J. M., S. McQuaid, R. Reynolds, and U. F. FitzGerald. 2012. 'Increased expression of ER stress- and hypoxia-associated molecules in grey matter lesions in multiple sclerosis', Mult Scler, 18: 1437-47.

McQuade, A., Y. J. Kang, J. Hasselmann, A. Jairaman, A. Sotelo, et al. 2020. 'Gene expression and functional deficits underlie TREM2-knockout microglia responses in human models of Alzheimer's disease', Nat Commun, 11: 5370.

Meilandt, W. J., H. Ngu, A. Gogineni, G. Lalehzadeh, S. H. Lee, et al. 2020. 'Trem2 Deletion Reduces Late-Stage Amyloid Plaque Accumulation, Elevates the Abeta42:Abeta40 Ratio, and Exacerbates Axonal Dystrophy and Dendritic Spine Loss in the PS2APP Alzheimer's Mouse Model', J Neurosci, 40: 1956-74.

Mengel, D., M. Thelen, M. Balzer-Geldsetzer, C. Soling, J. P. Bach, et al. 2016. 'TREM2 rare variant p.R47H is not associated with Parkinson's disease', Parkinsonism Relat Disord, 23: 109-11.

Merino, M. M., R. Levayer, and E. Moreno. 2016. 'Survival of the Fittest: Essential Roles of Cell Competition in Development, Aging, and Cancer', Trends Cell Biol, 26: 776-88.

Meyer-Luehmann, M., J. Coomaraswamy, T. Bolmont, S. Kaeser, C. Schaefer, et al. 2006. 'Exogenous induction of cerebral beta-amyloidogenesis is governed by agent and host', Science, 313: 1781-4.

Mhaille, A. N., S. McQuaid, A. Windebank, P. Cunnea, J. McMahon, A. Samali, and U. FitzGerald. 2008. 'Increased expression of endoplasmic reticulum stress-related signaling pathway molecules in multiple sclerosis lesions', J Neuropathol Exp Neurol, 67: 200-11.

Migliaccio, R., F. Agosta, S. Basaia, C. Cividini, M. O. Habert, et al. 2020. 'Functional brain connectome in posterior cortical atrophy', Neuroimage Clin, 25: 102100.

Mildner, A., H. Huang, J. Radke, W. Stenzel, and J. Priller. 2017. 'P2Y12 receptor is expressed on human microglia under physiological conditions throughout development and is sensitive to neuroinflammatory diseases', Glia, 65: 375-87.

Milton, N. G. 2001. 'Phosphorylation of amyloid-beta at the serine 26 residue by human cdc2 kinase', Neuroreport, 12: 3839-44.

Mintun, M. A., A. C. Lo, C. Duggan Evans, A. M. Wessels, P. A. Ardayfio, et al. 2021. 'Donanemab in Early Alzheimer's Disease', N Engl J Med, 384: 1691-704.

Mitani, Y., J. Yarimizu, K. Saita, H. Uchino, H. Akashiba, et al. 2012. 'Differential effects between gamma-secretase inhibitors and modulators on cognitive function in amyloid precursor protein-transgenic and nontransgenic mice', J Neurosci, 32: 2037-50.

Miyakawa, T., T. Kimura, S. Hirata, N. Fujise, T. Ono, K. Ishizuka, and J. Nakabayashi. 2000. 'Role of blood vessels in producing pathological changes in the brain with Alzheimer's disease', Ann N Y Acad Sci, 903: 46-54.

Miyashita, A., Y. Wen, N. Kitamura, E. Matsubara, T. Kawarabayashi, et al. 2014. 'Lack of genetic association between TREM2 and late-onset Alzheimer's disease in a Japanese population', J Alzheimers Dis, 41: 1031-8.

Moehlmann, T., E. Winkler, X. Xia, D. Edbauer, J. Murrell, et al. 2002. 'Presenilin-1 mutations of leucine 166 equally affect the generation of the Notch and APP intracellular domains independent of their effect on Abeta 42 production', Proc Natl Acad Sci U S A, 99: 8025-30.

Mohamed, A., L. Cortez, and E. P. de Chaves. 2011a. 'Aggregation state and neurotoxic properties of alzheimer beta-amyloid peptide', Curr Protein Pept Sci, 12: 235-57.

Mohamed, A., and E. Posse de Chaves. 2011b. 'Abeta internalization by neurons and glia', Int J Alzheimers Dis, 2011: 127984.

Molina-Monasterios, M. C., and H. Molina-Abecia. 2003. '[Nasu Hakola disease: a report of the first two cases in Bolivia]', Rev Neurol, 36: 837-40.

Molnar, Z., and G. Clowry. 2012. 'Cerebral cortical development in rodents and primates', Prog Brain Res, 195: 45-70.

Morales, I., J. M. Jimenez, M. Mancilla, and R. B. Maccioni. 2013. 'Tau oligomers and fibrils induce activation of microglial cells', J Alzheimers Dis, 37: 849-56.

Mori, C., E. T. Spooner, K. E. Wisniewsk, T. M. Wisniewski, H. Yamaguch, et al. 2002. 'Intraneuronal Abeta42 accumulation in Down syndrome brain', Amyloid, 9: 88-102.

Mori, H., K. Takio, M. Ogawara, and D. J. Selkoe. 1992. 'Mass spectrometry of purified amyloid beta protein in Alzheimer's disease', J Biol Chem, 267: 17082-6.

Morris, J. C., C. M. Roe, C. Xiong, A. M. Fagan, A. M. Goate, D. M. Holtzman, and M. A. Mintun. 2010. 'APOE predicts amyloid-beta but not tau Alzheimer pathology in cognitively normal aging', Ann Neurol, 67: 122-31.

Moulton, P. V., and W. Yang. 2012. 'Air pollution, oxidative stress, and Alzheimer's disease', J Environ Public Health, 2012: 472751.

Mucke, L., E. Masliah, G. Q. Yu, M. Mallory, E. M. Rockenstein, et al. 2000. 'High-level neuronal expression of abeta 1-42 in wild-type human amyloid protein precursor transgenic mice: synaptotoxicity without plaque formation', J Neurosci, 20: 4050-8.

Muller-Esparza, H., M. Osorio-Valeriano, N. Steube, M. Thanbichler, and L. Randau. 2020. 'Bio-Layer Interferometry Analysis of the Target Binding Activity of CRISPR-Cas Effector Complexes', Front Mol Biosci, 7: 1-10.

Muller, U. C., T. Deller, and M. Korte. 2017. 'Not just amyloid: physiological functions of the amyloid precursor protein family', Nat Rev Neurosci, 18: 281-98.

Murphy, M. P., and H. LeVine, 3rd. 2010. 'Alzheimer's disease and the amyloid-beta peptide', J Alzheimers Dis, 19: 311-23.

Murray, M. E., N. R. Graff-Radford, O. A. Ross, R. C. Petersen, R. Duara, and D. W. Dickson. 2011. 'Neuropathologically defined subtypes of Alzheimer's disease with distinct clinical characteristics: a retrospective study', Lancet Neurol, 10: 785-96.

Murray, P. S., C. M. Kirkwood, M. C. Gray, M. D. Ikonomovic, W. R. Paljug, et al. 2012. 'Beta-Amyloid 42/40 ratio and kalirin expression in Alzheimer disease with psychosis', Neurobiol Aging, 33: 2807-16.

Nagarathinam, A., P. Hoflinger, A. Buhler, C. Schafer, G. McGovern, et al. 2013. 'Membrane-anchored Abeta accelerates amyloid formation and exacerbates amyloid-associated toxicity in mice', J Neurosci, 33: 19284-94.

Nalivaeva, N. N., and A. J. Turner. 2013. 'The amyloid precursor protein: a biochemical enigma in brain development, function and disease', FEBS Lett, 587: 2046-54.

Namba, Y., M. Tomonaga, H. Kawasaki, E. Otomo, and K. Ikeda. 1991. 'Apolipoprotein E immunoreactivity in cerebral amyloid deposits and neurofibrillary tangles in Alzheimer's disease and kuru plaque amyloid in Creutzfeldt-Jakob disease', Brain Res, 541: 163-6.

Naslund, J., A. Schierhorn, U. Hellman, L. Lannfelt, A. D. Roses, et al. 1994. 'Relative abundance of Alzheimer A beta amyloid peptide variants in Alzheimer disease and normal aging', Proc Natl Acad Sci U S A, 91: 8378-82.

Nataf, S., A. Anginot, C. Vuaillat, L. Malaval, N. Fodil, et al. 2005. 'Brain and bone damage in KARAP/DAP12 loss-of-function mice correlate with alterations in microglia and osteoclast lineages', Am J Pathol, 166: 275-86.

Nayak, D., T. L. Roth, and D. B. McGavern. 2014. 'Microglia development and function', Annu Rev Immunol, 32: 367-402.

Nelson, O., C. Supnet, H. Liu, and I. Bezprozvanny. 2010. 'Familial Alzheimer's disease mutations in presenilins: effects on endoplasmic reticulum calcium homeostasis and correlation with clinical phenotypes', J Alzheimers Dis, 21: 781-93.

Nelson, P. T., H. Braak, and W. R. Markesbery. 2009. 'Neuropathology and cognitive impairment in Alzheimer disease: a complex but coherent relationship', J Neuropathol Exp Neurol, 68: 1-14.

Neumann, H., and K. Takahashi. 2007. 'Essential role of the microglial triggering receptor expressed on myeloid cells-2 (TREM2) for central nervous tissue immune homeostasis', J Neuroimmunol, 184: 92-9.

Nhan, H. S., K. Chiang, and E. H. Koo. 2015. 'The multifaceted nature of amyloid precursor protein and its proteolytic fragments: friends and foes', Acta Neuropathol, 129: 1-19.

Nicolas, M., and B. A. Hassan. 2014. 'Amyloid precursor protein and neural development', Development, 141: 2543-8.

Nimmerjahn, A., F. Kirchhoff, and F. Helmchen. 2005. 'Resting microglial cells are highly dynamic surveillants of brain parenchyma in vivo', Science, 308: 1314-8.

Nirschl, M., F. Reuter, and J. Voros. 2011. 'Review of transducer principles for label-free biomolecular interaction analysis', Biosensors (Basel), 1: 70-92.

Nithianantharajah, J., and S. G. Grant. 2013. 'Cognitive components in mice and humans: combining genetics and touchscreens for medical translation', Neurobiol Learn Mem, 105: 13-9.

Norden, D. M., and J. P. Godbout. 2013. 'Review: microglia of the aged brain: primed to be activated and resistant to regulation', Neuropathol Appl Neurobiol, 39: 19-34.

Norden, D. M., M. M. Muccigrosso, and J. P. Godbout. 2015. 'Microglial priming and enhanced reactivity to secondary insult in aging, and traumatic CNS injury, and neurodegenerative disease', Neuropharmacology, 96: 29-41.

Numasawa, Y., C. Yamaura, S. Ishihara, S. Shintani, M. Yamazaki, H. Tabunoki, and J. I. Satoh. 2011. 'Nasu-Hakola disease with a splicing mutation of TREM2 in a Japanese family', Eur J Neurol, 18: 1179-83.

Nussbaum, J. M., S. Schilling, H. Cynis, A. Silva, E. Swanson, et al. 2012. 'Prion-like behaviour and tau-dependent cytotoxicity of pyroglutamylated amyloid-beta', Nature, 485: 651-5.

Nutu, M., H. Zetterberg, E. Londos, L. Minthon, K. Nagga, et al. 2013. 'Evaluation of the cerebrospinal fluid amyloid-beta1-42/amyloid-beta1-40 ratio measured by alpha-LISA to distinguish Alzheimer's disease from other dementia disorders', Dement Geriatr Cogn Disord, 36: 99-110.

O'Brien, R. J., and P. C. Wong. 2011. 'Amyloid precursor protein processing and Alzheimer's disease', Annu Rev Neurosci, 34: 185-204.

Oakley, H., S. L. Cole, S. Logan, E. Maus, P. Shao, et al. 2006. 'Intraneuronal beta-amyloid aggregates, neurodegeneration, and neuron loss in transgenic mice with five familial Alzheimer's disease mutations: potential factors in amyloid plaque formation', J Neurosci, 26: 10129-40.

Oblak, A. L., P. B. Lin, K. P. Kotredes, R. S. Pandey, D. Garceau, et al. 2021. 'Comprehensive Evaluation of the 5XFAD Mouse Model for Preclinical Testing Applications: A MODEL-AD Study', Front Aging Neurosci, 13: 713726.

Ochiishi, T., M. Kaku, K. Kiyosue, M. Doi, T. Urabe, et al. 2019. 'New Alzheimer's disease model mouse specialized for analyzing the function and toxicity of intraneuronal Amyloid beta oligomers', Sci Rep, 9: 17368.

Oddo, S., A. Caccamo, J. D. Shepherd, M. P. Murphy, T. E. Golde, et al. 2003. 'Triple-transgenic model of Alzheimer's disease with plaques and tangles: intracellular Abeta and synaptic dysfunction', Neuron, 39: 409-21.

Oddo, S., A. Caccamo, L. Tran, M. P. Lambert, C. G. Glabe, W. L. Klein, and F. M. LaFerla. 2006. 'Temporal profile of amyloid-beta (Abeta) oligomerization in an in vivo model of Alzheimer disease. A link between Abeta and tau pathology', J Biol Chem, 281: 1599-604.

Ogundele, O. M., A. O. Omoaghe, D. C. Ajonijebu, A. A. Ojo, T. D. Fabiyi, et al. 2014. 'Glia activation and its role in oxidative stress', Metab Brain Dis, 29: 483-93.

Ohrfelt, A., M. Axelsson, C. Malmestrom, L. Novakova, A. Heslegrave, et al. 2016. 'Soluble TREM-2 in cerebrospinal fluid from patients with multiple sclerosis treated with natalizumab or mitoxantrone', Mult Scler, 22: 1587-95.

Olmos-Alonso, A., S. T. Schetters, S. Sri, K. Askew, R. Mancuso, et al. 2016. 'Pharmacological targeting of CSF1R inhibits microglial proliferation and prevents the progression of Alzheimer's-like pathology', Brain, 139: 891-907.

Olsson, F., S. Schmidt, V. Althoff, L. M. Munter, S. Jin, et al. 2014. 'Characterization of intermediate steps in amyloid beta (Abeta) production under near-native conditions', J Biol Chem, 289: 1540-50.

Orre, M., W. Kamphuis, L. M. Osborn, A. H. P. Jansen, L. Kooijman, K. Bossers, and E. M. Hol. 2014. 'Isolation of glia from Alzheimer's mice reveals inflammation and dysfunction', Neurobiol Aging, 35: 2746-60.

Ostrander, M. M., Y. M. Ulrich-Lai, D. C. Choi, N. M. Richtand, and J. P. Herman. 2006. 'Hypoactivity of the hypothalamo-pituitary-adrenocortical axis during recovery from chronic variable stress', Endocrinology, 147: 2008-17.

Otero, K., M. Shinohara, H. Zhao, M. Cella, S. Gilfillan, et al. 2012. 'TREM2 and beta-catenin regulate bone homeostasis by controlling the rate of osteoclastogenesis', J Immunol, 188: 2612-21.

Oyadomari, S., and M. Mori. 2004. 'Roles of CHOP/GADD153 in endoplasmic reticulum stress', Cell Death Differ, 11: 381-9.

Oyanagi, K., M. Kinoshita, E. Suzuki-Kouyama, T. Inoue, A. Nakahara, et al. 2017. 'Adult onset leukoencephalopathy with axonal spheroids and pigmented glia (ALSP) and Nasu-Hakola disease: lesion staging and dynamic changes of axons and microglial subsets', Brain Pathol, 27: 748-69.

Palhano, F. L., J. Lee, N. P. Grimster, and J. W. Kelly. 2013. 'Toward the molecular mechanism(s) by which EGCG treatment remodels mature amyloid fibrils', J Am Chem Soc, 135: 7503-10.

Paloneva, J., T. Autti, R. Raininko, J. Partanen, O. Salonen, et al. 2001. 'CNS manifestations of Nasu-Hakola disease: a frontal dementia with bone cysts', Neurology, 56: 1552-8.

Paloneva, J., M. Kestila, J. Wu, A. Salminen, T. Bohling, et al. 2000. 'Loss-of-function mutations in TYROBP (DAP12) result in a presenile dementia with bone cysts', Nat Genet, 25: 357-61.

Paloneva, J., J. Mandelin, A. Kiialainen, T. Bohling, J. Prudlo, et al. 2003. 'DAP12/TREM2 deficiency results in impaired osteoclast differentiation and osteoporotic features', J Exp Med, 198: 669-75.

Paloneva, J., T. Manninen, G. Christman, K. Hovanes, J. Mandelin, et al. 2002. 'Mutations in two genes encoding different subunits of a receptor signaling complex result in an identical disease phenotype', Am J Hum Genet, 71: 656-62.

Palop, J. J., and L. Mucke. 2010. 'Amyloid-beta-induced neuronal dysfunction in Alzheimer's disease: from synapses toward neural networks', Nat Neurosci, 13: 812-8.

Parhizkar, S., T. Arzberger, M. Brendel, G. Kleinberger, M. Deussing, et al. 2019. 'Loss of TREM2 function increases amyloid seeding but reduces plaque-associated ApoE', Nat Neurosci, 22: 191-204.

Park, J. S., I. J. Ji, H. J. An, M. J. Kang, S. W. Kang, D. H. Kim, and S. Y. Yoon. 2015. 'Disease-Associated Mutations of TREM2 Alter the Processing of N-Linked Oligosaccharides in the Golgi Apparatus', Traffic, 16: 510-8.

Parkhurst, C. N., G. Yang, I. Ninan, J. N. Savas, J. R. Yates, 3rd, et al. 2013. 'Microglia promote learning-dependent synapse formation through brain-derived neurotrophic factor', Cell, 155: 1596-609.

Paz, Y. Mino C., M. J. Guillen Sacoto, and P. E. Leone. 2016. 'Genetics and genomic medicine in Ecuador', Mol Genet Genomic Med, 4: 9-17.

Perez-Tur, J., S. Froelich, G. Prihar, R. Crook, M. Baker, et al. 1995. 'A mutation in Alzheimer's disease destroying a splice acceptor site in the presenilin-1 gene', Neuroreport, 7: 297-301.

Perez, S. E., M. Nadeem, B. He, J. C. Miguel, M. H. Malek-Ahmadi, K. Chen, and E. J. Mufson. 2017. 'Neocortical and hippocampal TREM2 protein levels during the progression of Alzheimer's disease', Neurobiol Aging, 54: 133-43.

Perl, D. P. 2010. 'Neuropathology of Alzheimer's disease', Mt Sinai J Med, 77: 32-42.

Perry, V. H. 2010. 'Contribution of systemic inflammation to chronic neurodegeneration', Acta Neuropathol, 120: 277-86.

Petrov, A. M., M. R. Kasimov, and A. L. Zefirov. 2016. 'Brain Cholesterol Metabolism and Its Defects: Linkage to Neurodegenerative Diseases and Synaptic Dysfunction', Acta Naturae, 8: 58-73.

Philipson, O., L. Lannfelt, and L. N. Nilsson. 2009. 'Genetic and pharmacological evidence of intraneuronal Abeta accumulation in APP transgenic mice', FEBS Lett, 583: 3021-6.

Piccio, L., C. Buonsanti, M. Cella, I. Tassi, R. E. Schmidt, et al. 2008. 'Identification of soluble TREM-2 in the cerebrospinal fluid and its association with multiple sclerosis and CNS inflammation', Brain, 131: 3081-91.

Piccio, L., C. Buonsanti, M. Mariani, M. Cella, S. Gilfillan, et al. 2007. 'Blockade of TREM-2 exacerbates experimental autoimmune encephalomyelitis', Eur J Immunol, 37: 1290-301.

Piccio, L., Y. Deming, J. L. Del-Aguila, L. Ghezzi, D. M. Holtzman, et al. 2016. 'Cerebrospinal fluid soluble TREM2 is higher in Alzheimer disease and associated with mutation status', Acta Neuropathol, 131: 925-33.

Pimenova, A. A., T. Raj, and A. M. Goate. 2018. 'Untangling Genetic Risk for Alzheimer's Disease', Biol Psychiatry, 83: 300-10.

Poliani, P. L., Y. Wang, E. Fontana, M. L. Robinette, Y. Yamanishi, S. Gilfillan, and M. Colonna. 2015. 'TREM2 sustains microglial expansion during aging and response to demyelination', J Clin Invest, 125: 2161-70.

Portelius, E., N. Bogdanovic, M. K. Gustavsson, I. Volkmann, G. Brinkmalm, et al. 2010. 'Mass spectrometric characterization of brain amyloid beta isoform signatures in familial and sporadic Alzheimer's disease', Acta Neuropathol, 120: 185-93.

Portelius, E., E. Price, G. Brinkmalm, M. Stiteler, M. Olsson, et al. 2011. 'A novel pathway for amyloid precursor protein processing', Neurobiol Aging, 32: 1090-8.

Pottier, C., T. A. Ravenscroft, P. H. Brown, N. A. Finch, M. Baker, et al. 2016a. 'TYROBP genetic variants in early-onset Alzheimer's disease', Neurobiol Aging, 48: 222 e9-22 e15.

Pottier, C., T. A. Ravenscroft, M. Sanchez-Contreras, and R. Rademakers. 2016b. 'Genetics of FTLD: overview and what else we can expect from genetic studies', J Neurochem, 138 Suppl 1: 32-53.

Prada, I., G. N. Ongania, C. Buonsanti, P. Panina-Bordignon, and J. Meldolesi. 2006. 'Triggering receptor expressed in myeloid cells 2 (TREM2) trafficking in microglial cells: continuous shuttling to and from the plasma membrane regulated by cell stimulation', Neuroscience, 140: 1139-48.

Prihar, G., A. Verkkoniem, J. Perez-Tur, R. Crook, S. Lincoln, et al. 1999. 'Alzheimer disease PS-1 exon 9 deletion defined', Nat Med, 5: 1090.

Puzzo, D., W. Gulisano, A. Palmeri, and O. Arancio. 2015. 'Rodent models for Alzheimer's disease drug discovery', Expert Opin Drug Discov, 10: 703-11.

Querfurth, H. W., and F. M. LaFerla. 2010. 'Alzheimer's disease', N Engl J Med, 362: 329-44.

Radde, R., T. Bolmont, S. A. Kaeser, J. Coomaraswamy, D. Lindau, et al. 2006. 'Abeta42-driven cerebral amyloidosis in transgenic mice reveals early and robust pathology', EMBO Rep, 7: 940-6.

Raha, A. A., J. W. Henderson, S. R. Stott, R. Vuono, S. Foscarin, et al. 2017. 'Neuroprotective Effect of TREM-2 in Aging and Alzheimer's Disease Model', J Alzheimers Dis, 55: 199-217.

Rajmohan, R., and P. H. Reddy. 2017. 'Amyloid-Beta and Phosphorylated Tau Accumulations Cause Abnormalities at Synapses of Alzheimer's disease Neurons', J Alzheimers Dis, 57: 975-99.

Ransohoff, R. M. 2016a. 'How neuroinflammation contributes to neurodegeneration', Science, 353: 777-83.

Ransohoff, R. M. 2016b. 'A polarizing question: do M1 and M2 microglia exist?', Nat Neurosci, 19: 987-91.

Rapoport, M., H. N. Dawson, L. I. Binder, M. P. Vitek, and A. Ferreira. 2002. 'Tau is essential to beta -amyloid-induced neurotoxicity', Proc Natl Acad Sci U S A, 99: 6364-9.

Rayaprolu, S., B. Mullen, M. Baker, T. Lynch, E. Finger, et al. 2013. 'TREM2 in neurodegeneration: evidence for association of the p.R47H variant with frontotemporal dementia and Parkinson's disease', Mol Neurodegener, 8: 1-5.

Reilly, J. F., D. Games, R. E. Rydel, S. Freedman, D. Schenk, et al. 2003. 'Amyloid deposition in the hippocampus and entorhinal cortex: quantitative analysis of a transgenic mouse model', Proc Natl Acad Sci U S A, 100: 4837-42.

Reinert, J., B. C. Richard, H. W. Klafki, B. Friedrich, T. A. Bayer, et al. 2016. 'Deposition of C-terminally truncated Abeta species Abeta37 and Abeta39 in Alzheimer's disease and transgenic mouse models', Acta Neuropathol Commun, 4: 24.

Reinhardt, S., F. Schuck, S. Grosgen, M. Riemenschneider, T. Hartmann, et al. 2014. 'Unfolded protein response signaling by transcription factor XBP-1 regulates ADAM10 and is affected in Alzheimer's disease', FASEB J, 28: 978-97.

Revesz, T., J. Ghiso, T. Lashley, G. Plant, A. Rostagno, B. Frangione, and J. L. Holton. 2003. 'Cerebral amyloid angiopathies: a pathologic, biochemical, and genetic view', J Neuropathol Exp Neurol, 62: 885-98.

Rezaei-Ghaleh, N., M. Amininasab, K. Giller, S. Kumar, A. Stundl, et al. 2014. 'Turn plasticity distinguishes different modes of amyloid-beta aggregation', J Am Chem Soc, 136: 4913-9.

Rezaei-Ghaleh, N., M. Amininasab, S. Kumar, J. Walter, and M. Zweckstetter. 2016. 'Phosphorylation modifies the molecular stability of beta-amyloid deposits', Nat Commun, 7: 1-9.

Ribe, E. M., M. Perez, B. Puig, I. Gich, F. Lim, et al. 2005. 'Accelerated amyloid deposition, neurofibrillary degeneration and neuronal loss in double mutant APP/tau transgenic mice', Neurobiol Dis, 20: 814-22.

Rice, H. C., D. de Malmazet, A. Schreurs, S. Frere, I. Van Molle, et al. 2019. 'Secreted amyloid-beta precursor protein functions as a GABABR1a ligand to modulate synaptic transmission', Science, 363: 1-19.

Richard, B. C., A. Kurdakova, S. Baches, T. A. Bayer, S. Weggen, and O. Wirths. 2015. 'Gene Dosage Dependent Aggravation of the Neurological Phenotype in the 5XFAD Mouse Model of Alzheimer's Disease', J Alzheimers Dis, 45: 1223-36.

Richard, E., A. Carrano, J. J. Hoozemans, J. van Horssen, E. S. van Haastert, et al. 2010. 'Characteristics of dyshoric capillary cerebral amyloid angiopathy', J Neuropathol Exp Neurol, 69: 1158-67.

Rijal Upadhaya, A., I. Kosterin, S. Kumar, C. A. von Arnim, H. Yamaguchi, et al. 2014. 'Biochemical stages of amyloid-beta peptide aggregation and accumulation in the human brain and their association with symptomatic and pathologically preclinical Alzheimer's disease', Brain, 137: 887-903.

Rodrigue, K. M., K. M. Kennedy, and D. C. Park. 2009. 'Beta-amyloid deposition and the aging brain', Neuropsychol Rev, 19: 436-50.

Roher, A. E., Kuo Y.M., A.A. Roher, M. R. Emmerling, and Goux W.J. 2000. 'Chemical analysis of Amyloid beta protein in CAA.' in de Waal RMW Verbeek MM, and Vinters HV, (ed.), Cerebral Amyloid Angiopathy in Alzheimer's Disease and Related Disorders (Kluwer Academic Publishers: Dordrecht).

Ron, D., and J. F. Habener. 1992. 'CHOP, a novel developmentally regulated nuclear protein that dimerizes with transcription factors C/EBP and LAP and functions as a dominant-negative inhibitor of gene transcription', Genes Dev, 6: 439-53.

Roussos, P., P. Katsel, P. Fam, W. Tan, D. P. Purohit, and V. Haroutunian. 2015. 'The triggering receptor expressed on myeloid cells 2 (TREM2) is associated with enhanced inflammation, neuropathological lesions and increased risk for Alzheimer's dementia', Alzheimers Dement, 11: 1163-70.

Rovelet-Lecrux, A., C. Charbonnier, D. Wallon, G. Nicolas, M. N. Seaman, et al. 2015. 'De novo deleterious genetic variations target a biological network centered on Abeta peptide in early-onset Alzheimer disease', Mol Psychiatry, 20: 1046-56.

Rovelet-Lecrux, A., T. Frebourg, H. Tuominen, K. Majamaa, D. Campion, and A. M. Remes. 2007. 'APP locus duplication in a Finnish family with dementia and intracerebral haemorrhage', J Neurol Neurosurg Psychiatry, 78: 1158-9.

Rovelet-Lecrux, A., D. Hannequin, G. Raux, N. Le Meur, A. Laquerriere, et al. 2006. 'APP locus duplication causes autosomal dominant early-onset Alzheimer disease with cerebral amyloid angiopathy', Nat Genet, 38: 24-6.

Ruiz-Riquelme, A., H. H. C. Lau, E. Stuart, A. N. Goczi, Z. Wang, G. Schmitt-Ulms, and J. C. Watts. 2018. 'Prion-like propagation of beta-amyloid aggregates in the absence of APP overexpression', Acta Neuropathol Commun, 6: 26.

Russo, C., E. Violani, S. Salis, V. Venezia, V. Dolcini, et al. 2002. 'Pyroglutamate-modified amyloid beta-peptides--AbetaN3(pE)--strongly affect cultured neuron and astrocyte survival', J Neurochem, 82: 1480-9.

Russo, M. V., and D. B. McGavern. 2016. 'Inflammatory neuroprotection following traumatic brain injury', Science, 353: 783-5.

Ryman, D. C., N. Acosta-Baena, P. S. Aisen, T. Bird, A. Danek, et al. 2014. 'Symptom onset in autosomal dominant Alzheimer disease: a systematic review and meta-analysis', Neurology, 83: 253-60.

Saber, M., O. Kokiko-Cochran, S. S. Puntambekar, J. D. Lathia, and B. T. Lamb. 2017. 'Triggering Receptor Expressed on Myeloid Cells 2 Deficiency Alters Acute Macrophage Distribution and Improves Recovery after Traumatic Brain Injury', J Neurotrauma, 34: 423-35.

Saido, T. C., T. Iwatsubo, D. M. Mann, H. Shimada, Y. Ihara, and S. Kawashima. 1995. 'Dominant and differential deposition of distinct beta-amyloid peptide species, A beta N3(pE), in senile plaques', Neuron, 14: 457-66.

Saido, T. C., W. Yamao-Harigaya, T. Iwatsubo, and S. Kawashima. 1996. 'Amino- and carboxyl-terminal heterogeneity of beta-amyloid peptides deposited in human brain', Neurosci Lett, 215: 173-6.

Saito, T., Y. Matsuba, N. Mihira, J. Takano, P. Nilsson, et al. 2014. 'Single App knock-in mouse models of Alzheimer's disease', Nat Neurosci, 17: 661-3.

Saito, T., Y. Matsuba, N. Yamazaki, S. Hashimoto, and T. C. Saido. 2016. 'Calpain Activation in Alzheimer's Model Mice Is an Artifact of APP and Presenilin Overexpression', J Neurosci, 36: 9933-6.

Saito, T., T. Suemoto, N. Brouwers, K. Sleegers, S. Funamoto, et al. 2011. 'Potent amyloidogenicity and pathogenicity of Abeta43', Nat Neurosci, 14: 1023-32.

Sala Frigerio, C., L. Wolfs, N. Fattorelli, N. Thrupp, I. Voytyuk, et al. 2019. 'The Major Risk Factors for Alzheimer's Disease: Age, Sex, and Genes Modulate the Microglia Response to Abeta Plaques', Cell Rep, 27: 1293-306 e6.

Salani, F., V. Sterbini, E. Sacchinelli, M. Garramone, and P. Bossu. 2019. 'Is Innate Memory a Double-Edge Sword in Alzheimer's Disease? A Reappraisal of New Concepts and Old Data', Front Immunol, 10: 1768.

Salter, M. W., and S. Beggs. 2014. 'Sublime microglia: expanding roles for the guardians of the CNS', Cell, 158: 15-24.

Salter, M. W., and B. Stevens. 2017. 'Microglia emerge as central players in brain disease', Nat Med, 23: 1018-27.

Sannerud, R., C. Esselens, P. Ejsmont, R. Mattera, L. Rochin, et al. 2016. 'Restricted Location of PSEN2/gamma-Secretase Determines Substrate Specificity and Generates an Intracellular Abeta Pool', Cell, 166: 193-208.

Sarlus, H., and M. T. Heneka. 2017. 'Microglia in Alzheimer's disease', J Clin Invest, 127: 3240-49.

Sasaguri, H., P. Nilsson, S. Hashimoto, K. Nagata, T. Saito, et al. 2017. 'APP mouse models for Alzheimer's disease preclinical studies', EMBO J, 36: 2473-87.

Sasaki, A., A. Kakita, K. Yoshida, T. Konno, T. Ikeuchi, et al. 2015. 'Variable expression of microglial DAP12 and TREM2 genes in Nasu-Hakola disease', Neurogenetics, 16: 265-76.

Sato, S., K. Kamino, T. Miki, A. Doi, K. Ii, et al. 1998. 'Splicing mutation of presenilin-1 gene for early-onset familial Alzheimer's disease', Hum Mutat, Suppl 1: S91-4.

Satoh, J., H. Tabunoki, T. Ishida, S. Yagishita, K. Jinnai, et al. 2011. 'Immunohistochemical characterization of microglia in Nasu-Hakola disease brains', Neuropathology, 31: 363-75.

Sauer, B. 1994. 'Site-specific recombination: developments and applications', Curr Opin Biotechnol, 5: 521-7.

Saunders, A. M., W. J. Strittmatter, D. Schmechel, P. H. George-Hyslop, M. A. Pericak-Vance, et al. 1993. 'Association of apolipoprotein E allele epsilon 4 with late-onset familial and sporadic Alzheimer's disease', Neurology, 43: 1467-72.

Savage, J. C., T. Jay, E. Goduni, C. Quigley, M. M. Mariani, et al. 2015. 'Nuclear receptors license phagocytosis by trem2+ myeloid cells in mouse models of Alzheimer's disease', J Neurosci, 35: 6532-43.

Savastano, A., H. Klafki, U. Haussmann, T. J. Oberstein, P. Muller, et al. 2016. 'N-truncated Abeta2-X starting with position two in sporadic Alzheimer's disease cases and two Alzheimer mouse models', J Alzheimers Dis, 49: 101-10.

Scacchi, R., G. Gambina, E. Broggio, G. Moretto, M. Ruggeri, and R. M. Corbo. 2004. 'The H+ allele of the lipoprotein lipase (LPL) HindIII intronic polymorphism and the risk for sporadic late-onset Alzheimer's disease', Neurosci Lett, 367: 177-80.

Scheltens, P., K. Blennow, M. M. Breteler, B. de Strooper, G. B. Frisoni, S. Salloway, and W. M. Van der Flier. 2016. 'Alzheimer's disease', Lancet, 388: 505-17.

Schilling, S., T. Hoffmann, S. Manhart, M. Hoffmann, and H. U. Demuth. 2004. 'Glutaminyl cyclases unfold glutamyl cyclase activity under mild acid conditions', FEBS Lett, 563: 191-6.

Schilling, S., U. Zeitschel, T. Hoffmann, U. Heiser, M. Francke, et al. 2008. 'Glutaminyl cyclase inhibition attenuates pyroglutamate Abeta and Alzheimer's disease-like pathology', Nat Med, 14: 1106-11.

Schlepckow, K., G. Kleinberger, A. Fukumori, R. Feederle, S. F. Lichtenthaler, H. Steiner, and C. Haass. 2017. 'An Alzheimer-associated TREM2 variant occurs at the ADAM cleavage site and affects shedding and phagocytic function', EMBO Mol Med, 9: 1356-65.

Schlepckow, K., K. M. Monroe, G. Kleinberger, L. Cantuti-Castelvetri, S. Parhizkar, et al. 2020. 'Enhancing protective microglial activities with a dual function TREM2 antibody to the stalk region', EMBO Mol Med, 12: e11227.

Schmid, C. D., L. N. Sautkulis, P. E. Danielson, J. Cooper, K. W. Hasel, et al. 2002. 'Heterogeneous expression of the triggering receptor expressed on myeloid cells-2 on adult murine microglia', J Neurochem, 83: 1309-20.

Schmitz, C., B. P. Rutten, A. Pielen, S. Schafer, O. Wirths, et al. 2004. 'Hippocampal neuron loss exceeds amyloid plaque load in a transgenic mouse model of Alzheimer's disease', Am J Pathol, 164: 1495-502.

Schultz, Christian, Kelly Del Tredici, and Heiko Braak. 2004. 'Neuropathology of Alzheimer’s disease.' in Ralph W. Richter and Brigitte Zoeller Richter (eds.), Alzheimer’s disease: A physician’s guide to practical management (Humana Press: Totowa, NJ).

Schutzmann, M. P., F. Hasecke, S. Bachmann, M. Zielinski, S. Hansch, et al. 2021. 'Endo-lysosomal Abeta concentration and pH trigger formation of Abeta oligomers that potently induce Tau missorting', Nat Commun, 12: 4634.

Schwabe, T., K. Srinivasan, and H. Rhinn. 2020. 'Shifting paradigms: The central role of microglia in Alzheimer's disease', Neurobiol Dis, 143: 104962.

Schwartz, M., G. Moalem, R. Leibowitz-Amit, and I. R. Cohen. 1999. 'Innate and adaptive immune responses can be beneficial for CNS repair', Trends Neurosci, 22: 295-9.

Selkoe, D. J. 1991. 'The molecular pathology of Alzheimer's disease', Neuron, 6: 487-98.

Selkoe, D. J. 2001. 'Alzheimer's disease: genes, proteins, and therapy', Physiol Rev, 81: 741-66.

Selkoe, D. J., and J. Hardy. 2016. 'The amyloid hypothesis of Alzheimer's disease at 25 years', EMBO Mol Med, 8: 595-608.

Sengupta, U., A. N. Nilson, and R. Kayed. 2016. 'The Role of Amyloid-beta Oligomers in Toxicity, Propagation, and Immunotherapy', EBioMedicine, 6: 42-49.

Serneels, L., J. Van Biervliet, K. Craessaerts, T. Dejaegere, K. Horre, et al. 2009. 'gamma-Secretase heterogeneity in the Aph1 subunit: relevance for Alzheimer's disease', Science, 324: 639-42.

Serrano-Pozo, A., M. P. Frosch, E. Masliah, and B. T. Hyman. 2011. 'Neuropathological alterations in Alzheimer disease', Cold Spring Harb Perspect Med, 1: a006189.

Serrano-Pozo, A., M. L. Mielke, A. Muzitansky, T. Gomez-Isla, J. H. Growdon, et al. 2012. 'Stable size distribution of amyloid plaques over the course of Alzheimer disease', J Neuropathol Exp Neurol, 71: 694-701.

Sessa, G., P. Podini, M. Mariani, A. Meroni, R. Spreafico, et al. 2004. 'Distribution and signaling of TREM2/DAP12, the receptor system mutated in human polycystic lipomembraneous osteodysplasia with sclerosing leukoencephalopathy dementia', Eur J Neurosci, 20: 2617-28.

Sevalle, J., A. Amoyel, P. Robert, M. C. Fournie-Zaluski, B. Roques, and F. Checler. 2009. 'Aminopeptidase A contributes to the N-terminal truncation of amyloid beta-peptide', J Neurochem, 109: 248-56.

Shankar, G. M., S. Li, T. H. Mehta, A. Garcia-Munoz, N. E. Shepardson, et al. 2008. 'Amyloid-beta protein dimers isolated directly from Alzheimer's brains impair synaptic plasticity and memory', Nat Med, 14: 837-42.

Sheng, X., Y. Yao, R. Huang, Y. Xu, Y. Zhu, et al. 2021. 'Identification of the minimal active soluble TREM2 sequence for modulating microglial phenotypes and amyloid pathology', J Neuroinflammation, 18: 286.

Shi, H., Y. Koronyo, A. Rentsendorj, D. T. Fuchs, J. Sheyn, et al. 2021. 'Retinal Vasculopathy in Alzheimer's Disease', Front Neurosci, 15: 731614.

Shinkai, Y., M. Yoshimura, M. Morishima-Kawashima, Y. Ito, H. Shimada, K. Yanagisawa, and Y. Ihara. 1997. 'Amyloid beta-protein deposition in the leptomeninges and cerebral cortex', Ann Neurol, 42: 899-908.

Sims, R., S. J. van der Lee, A. C. Naj, C. Bellenguez, N. Badarinarayan, et al. 2017. 'Rare coding variants in PLCG2, ABI3, and TREM2 implicate microglial-mediated innate immunity in Alzheimer's disease', Nat Genet, 49: 1373-84.

Sirkis, D. W., R. E. Aparicio, and R. Schekman. 2017. 'Neurodegeneration-associated mutant TREM2 proteins abortively cycle between the ER and ER-Golgi intermediate compartment', Mol Biol Cell, 28: 2723-33.

Slattery, C. F., J. A. Beck, L. Harper, G. Adamson, Z. Abdi, et al. 2014. 'R47H TREM2 variant increases risk of typical early-onset Alzheimer's disease but not of prion or frontotemporal dementia', Alzheimers Dement, 10: 602-08 e4.

Sleegers, K., N. Brouwers, I. Gijselinck, J. Theuns, D. Goossens, et al. 2006. 'APP duplication is sufficient to cause early onset Alzheimer's dementia with cerebral amyloid angiopathy', Brain, 129: 2977-83.

Smith, M. J., J. B. Kwok, C. A. McLean, J. J. Kril, G. A. Broe, et al. 2001. 'Variable phenotype of Alzheimer's disease with spastic paraparesis', Ann Neurol, 49: 125-9.

Snyder, H. M., L. J. Bain, A. M. Brickman, M. C. Carrillo, A. J. Esbensen, et al. 2020. 'Further understanding the connection between Alzheimer's disease and Down syndrome', Alzheimers Dement, 16: 1065-77.

Sommer, T., and E. Jarosch. 2002. 'BiP binding keeps ATF6 at bay', Dev Cell, 3: 1-2.

Song, L., R. Xue, P. Ge, M. Li, L. Wang, et al. 2017a. 'Identification of post-translational modifications of Abeta peptide in platelet membranes from patients with cerebral amyloid angiopathy', J Neurol Sci, 383: 11-17.

Song, W., B. Hooli, K. Mullin, S. C. Jin, M. Cella, et al. 2017b. 'Alzheimer's disease-associated TREM2 variants exhibit either decreased or increased ligand-dependent activation', Alzheimers Dement, 13: 381-87.

Song, W. M., S. Joshita, Y. Zhou, T. K. Ulland, S. Gilfillan, and M. Colonna. 2018. 'Humanized TREM2 mice reveal microglia-intrinsic and -extrinsic effects of R47H polymorphism', J Exp Med, 215: 745-60.

Soragna, D., L. Papi, M. T. Ratti, R. Sestini, R. Tupler, and L. Montalbetti. 2003. 'An Italian family affected by Nasu-Hakola disease with a novel genetic mutation in the TREM2 gene', J Neurol Neurosurg Psychiatry, 74: 825-6.

Spangenberg, E. E., R. J. Lee, A. R. Najafi, R. A. Rice, M. R. Elmore, et al. 2016. 'Eliminating microglia in Alzheimer's mice prevents neuronal loss without modulating amyloid-beta pathology', Brain, 139: 1265-81.

Spangenberg, E., P. L. Severson, L. A. Hohsfield, J. Crapser, J. Zhang, et al. 2019. 'Sustained microglial depletion with CSF1R inhibitor impairs parenchymal plaque development in an Alzheimer's disease model', Nat Commun, 10: 3758.

Spires, T. L., M. Meyer-Luehmann, E. A. Stern, P. J. McLean, J. Skoch, et al. 2005. 'Dendritic spine abnormalities in amyloid precursor protein transgenic mice demonstrated by gene transfer and intravital multiphoton microscopy', J Neurosci, 25: 7278-87.

Spittau, B. 2017. 'Aging Microglia-Phenotypes, Functions and Implications for Age-Related Neurodegenerative Diseases', Front Aging Neurosci, 9: 194.

Sprenkle, N. T., S. G. Sims, C. L. Sanchez, and G. P. Meares. 2017. 'Endoplasmic reticulum stress and inflammation in the central nervous system', Mol Neurodegener, 12: 42.

Steiner, H., K. Duff, A. Capell, H. Romig, M. G. Grim, et al. 1999. 'A loss of function mutation of presenilin-2 interferes with amyloid beta-peptide production and notch signaling', J Biol Chem, 274: 28669-73.

Stohr, J., J. C. Watts, Z. L. Mensinger, A. Oehler, S. K. Grillo, et al. 2012. 'Purified and synthetic Alzheimer's amyloid beta (Abeta) prions', Proc Natl Acad Sci U S A, 109: 11025-30.

Stratoulias, V., J. L. Venero, M. E. Tremblay, and B. Joseph. 2019. 'Microglial subtypes: diversity within the microglial community', EMBO J, 38: e101997.

Sturchler-Pierrat, C., D. Abramowski, M. Duke, K. H. Wiederhold, C. Mistl, et al. 1997. 'Two amyloid precursor protein transgenic mouse models with Alzheimer disease-like pathology', Proc Natl Acad Sci U S A, 94: 13287-92.

Suarez-Calvet, M., M. A. Araque Caballero, G. Kleinberger, R. J. Bateman, A. M. Fagan, et al. 2016a. 'Early changes in CSF sTREM2 in dominantly inherited Alzheimer's disease occur after amyloid deposition and neuronal injury', Sci Transl Med, 8: 369ra178.

Suarez-Calvet, M., G. Kleinberger, M. A. Araque Caballero, M. Brendel, A. Rominger, et al. 2016b. 'sTREM2 cerebrospinal fluid levels are a potential biomarker for microglia activity in early-stage Alzheimer's disease and associate with neuronal injury markers', EMBO Mol Med, 8: 466-76.

Sudom, A., S. Talreja, J. Danao, E. Bragg, R. Kegel, et al. 2018. 'Molecular basis for the loss-of-function effects of the Alzheimer's disease-associated R47H variant of the immune receptor TREM2', J Biol Chem, 293: 12634-46.

Suzuki, N., T. T. Cheung, X. D. Cai, A. Odaka, L. Otvos, Jr., et al. 1994a. 'An increased percentage of long amyloid beta protein secreted by familial amyloid beta protein precursor (beta APP717) mutants', Science, 264: 1336-40.

Suzuki, N., T. Iwatsubo, A. Odaka, Y. Ishibashi, C. Kitada, and Y. Ihara. 1994b. 'High tissue content of soluble beta 1-40 is linked to cerebral amyloid angiopathy', Am J Pathol, 145: 452-60.

Takahashi, K., M. Prinz, M. Stagi, O. Chechneva, and H. Neumann. 2007. 'TREM2-transduced myeloid precursors mediate nervous tissue debris clearance and facilitate recovery in an animal model of multiple sclerosis', PLoS Med, 4: e124.

Takahashi, K., C. D. Rochford, and H. Neumann. 2005. 'Clearance of apoptotic neurons without inflammation by microglial triggering receptor expressed on myeloid cells-2', J Exp Med, 201: 647-57.

Takahashi, R. H., C. G. Almeida, P. F. Kearney, F. Yu, M. T. Lin, T. A. Milner, and G. K. Gouras. 2004. 'Oligomerization of Alzheimer's beta-amyloid within processes and synapses of cultured neurons and brain', J Neurosci, 24: 3592-9.

Takahashi, R. H., T. A. Milner, F. Li, E. E. Nam, M. A. Edgar, et al. 2002. 'Intraneuronal Alzheimer abeta42 accumulates in multivesicular bodies and is associated with synaptic pathology', Am J Pathol, 161: 1869-79.

Takami, M., Y. Nagashima, Y. Sano, S. Ishihara, M. Morishima-Kawashima, S. Funamoto, and Y. Ihara. 2009. 'gamma-Secretase: successive tripeptide and tetrapeptide release from the transmembrane domain of beta-carboxyl terminal fragment', J Neurosci, 29: 13042-52.

Takeda, K., W. Araki, and T. Tabira. 2004. 'Enhanced generation of intracellular Abeta42 amyloid peptide by mutation of presenilins PS1 and PS2', Eur J Neurosci, 19: 258-64.

Takeshita, T., T. Kaminaga, T. Tatsumi, Y. Hatanaka, and S. Furui. 2005. 'Regional cerebral blood flow in a patient with Nasu-Hakola disease', Ann Nucl Med, 19: 309-12.

Tamboli, I. Y., E. Barth, L. Christian, M. Siepmann, S. Kumar, et al. 2010. 'Statins promote the degradation of extracellular amyloid {beta}-peptide by microglia via stimulation of exosome-associated insulin-degrading enzyme (IDE) secretion', J Biol Chem, 285: 37405-14.

Tamboli, I. Y., K. Prager, D. R. Thal, K. M. Thelen, I. Dewachter, et al. 2008. 'Loss of gamma-secretase function impairs endocytosis of lipoprotein particles and membrane cholesterol homeostasis', J Neurosci, 28: 12097-106.

Tanokashira, D., N. Mamada, F. Yamamoto, K. Taniguchi, A. Tamaoka, M. K. Lakshmana, and W. Araki. 2017. 'The neurotoxicity of amyloid beta-protein oligomers is reversible in a primary neuron model', Mol Brain, 10: 4.

Tanzi, R. E. 2012. 'The genetics of Alzheimer disease', Cold Spring Harb Perspect Med, 2: 1-10.

Tanzi, R. E. 2015. 'TREM2 and Risk of Alzheimer's Disease--Friend or Foe?', N Engl J Med, 372: 2564-5.

Tanzi, R. E., J. F. Gusella, P. C. Watkins, G. A. Bruns, P. St George-Hyslop, et al. 1987. 'Amyloid beta protein gene: cDNA, mRNA distribution, and genetic linkage near the Alzheimer locus', Science, 235: 880-4.

Tekirian, T. L., A. Y. Yang, C. Glabe, and J. W. Geddes. 1999. 'Toxicity of pyroglutaminated amyloid beta-peptides 3(pE)-40 and -42 is similar to that of A beta1-40 and -42', J Neurochem, 73: 1584-9.

Terwel, D., K. R. Steffensen, P. B. Verghese, M. P. Kummer, J. A. Gustafsson, D. M. Holtzman, and M. T. Heneka. 2011. 'Critical role of astroglial apolipoprotein E and liver X receptor-alpha expression for microglial Abeta phagocytosis', J Neurosci, 31: 7049-59.

Thal, D. R., E. Capetillo-Zarate, K. Del Tredici, and H. Braak. 2006. 'The development of amyloid beta protein deposits in the aged brain', Sci Aging Knowledge Environ, 2006: re1.

Thal, D. R., W. S. Griffin, and H. Braak. 2008a. 'Parenchymal and vascular Abeta-deposition and its effects on the degeneration of neurons and cognition in Alzheimer's disease', J Cell Mol Med, 12: 1848-62.

Thal, D. R., W. S. Griffin, R. A. de Vos, and E. Ghebremedhin. 2008b. 'Cerebral amyloid angiopathy and its relationship to Alzheimer's disease', Acta Neuropathol, 115: 599-609.

Thal, D. R., A. Ronisz, T. Tousseyn, A. Rijal Upadhaya, K. Balakrishnan, et al. 2019. 'Different aspects of Alzheimer's disease-related amyloid beta-peptide pathology and their relationship to amyloid positron emission tomography imaging and dementia', Acta Neuropathol Commun, 7: 1-16.

Thal, D. R., U. Rub, M. Orantes, and H. Braak. 2002. 'Phases of A beta-deposition in the human brain and its relevance for the development of AD', Neurology, 58: 1791-800.

Thal, D. R., U. Rub, C. Schultz, I. Sassin, E. Ghebremedhin, et al. 2000. 'Sequence of Abeta-protein deposition in the human medial temporal lobe', J Neuropathol Exp Neurol, 59: 733-48.

Thal, D. R., J. Walter, T. C. Saido, and M. Fandrich. 2015. 'Neuropathology and biochemistry of Abeta and its aggregates in Alzheimer's disease', Acta Neuropathol, 129: 167-82.

Thelen, M., C. Razquin, I. Hernandez, A. Gorostidi, R. Sanchez-Valle, et al. 2014. 'Investigation of the role of rare TREM2 variants in frontotemporal dementia subtypes', Neurobiol Aging, 35: 2657 e13-57 e19.

Thornton, P., J. Sevalle, M. J. Deery, G. Fraser, Y. Zhou, et al. 2017. 'TREM2 shedding by cleavage at the H157-S158 bond is accelerated for the Alzheimer's disease-associated H157Y variant', EMBO Mol Med, 9: 1366-78.

Tobias R, and Kumaraswam S. 2017. "Biomolecular binding kinetics assays on the octet platform." In Pall Life Sciences, edited by ForteBio, 1-22. Pall Life Sciences.

Tomiyama, T., S. Matsuyama, H. Iso, T. Umeda, H. Takuma, et al. 2010. 'A mouse model of amyloid beta oligomers: their contribution to synaptic alteration, abnormal tau phosphorylation, glial activation, and neuronal loss in vivo', J Neurosci, 30: 4845-56.

Tomiyama, T., T. Nagata, H. Shimada, R. Teraoka, A. Fukushima, et al. 2008. 'A new amyloid beta variant favoring oligomerization in Alzheimer's-type dementia', Ann Neurol, 63: 377-87.

Tonnies, E., and E. Trushina. 2017. 'Oxidative Stress, Synaptic Dysfunction, and Alzheimer's Disease', J Alzheimers Dis, 57: 1105-21.

Torvell, M., S. M. Carpanini, N. Daskoulidou, R. A. J. Byrne, R. Sims, and B. P. Morgan. 2021. 'Genetic Insights into the Impact of Complement in Alzheimer's Disease', Genes (Basel), 12: 1-15.

Tremblay, M. E., and A. K. Majewska. 2011. 'A role for microglia in synaptic plasticity?', Commun Integr Biol, 4: 220-2.

Tsubuki, S., Y. Takaki, and T. C. Saido. 2003. 'Dutch, Flemish, Italian, and Arctic mutations of APP and resistance of Abeta to physiologically relevant proteolytic degradation', Lancet, 361: 1957-8.

Turnbull, I. R., S. Gilfillan, M. Cella, T. Aoshi, M. Miller, et al. 2006. 'Cutting edge: TREM-2 attenuates macrophage activation', J Immunol, 177: 3520-4.

Ueki, Y., N. Kohara, T. Oga, H. Fukuyama, I. Akiguchi, J. Kimura, and H. Shibasaki. 2000. 'Membranous lipodystrophy presenting with palilalia: a PET study of cerebral glucose metabolism', Acta Neurol Scand, 102: 60-4.

Ulland, T. K., W. M. Song, S. C. Huang, J. D. Ulrich, A. Sergushichev, et al. 2017. 'TREM2 Maintains Microglial Metabolic Fitness in Alzheimer's Disease', Cell, 170: 649-63 e13.

Ulrich, J. D., M. B. Finn, Y. Wang, A. Shen, T. E. Mahan, et al. 2014. 'Altered microglial response to Abeta plaques in APPPS1-21 mice heterozygous for TREM2', Mol Neurodegener, 9: 20.

Ulrich, J. D., T. K. Ulland, M. Colonna, and D. M. Holtzman. 2017. 'Elucidating the Role of TREM2 in Alzheimer's Disease', Neuron, 94: 237-48.

Van Dam, D., R. D'Hooge, M. Staufenbiel, C. Van Ginneken, F. Van Meir, and P. P. De Deyn. 2003. 'Age-dependent cognitive decline in the APP23 model precedes amyloid deposition', Eur J Neurosci, 17: 388-96.

Van der Flier, W. M., and P. Scheltens. 2005. 'Epidemiology and risk factors of dementia', J Neurol Neurosurg Psychiatry, 76 Suppl 5: v2-7.

Varma, V. R., H. Busra Luleci, A. M. Oommen, S. Varma, C. T. Blackshear, et al. 2021. 'Abnormal brain cholesterol homeostasis in Alzheimer's disease-a targeted metabolomic and transcriptomic study', NPJ Aging Mech Dis, 7: 11.

Vassar, R., B. D. Bennett, S. Babu-Khan, S. Kahn, E. A. Mendiaz, et al. 1999. 'Beta-secretase cleavage of Alzheimer's amyloid precursor protein by the transmembrane aspartic protease BACE', Science, 286: 735-41.

Venegas, C., and M. T. Heneka. 2017a. 'Danger-associated molecular patterns in Alzheimer's disease', J Leukoc Biol, 101: 87-98.

Venegas, C., S. Kumar, B. S. Franklin, T. Dierkes, R. Brinkschulte, et al. 2017b. 'Microglia-derived ASC specks cross-seed amyloid-beta in Alzheimer's disease', Nature, 552: 355-61.

Verdier, Y., M. Zarandi, and B. Penke. 2004. 'Amyloid beta-peptide interactions with neuronal and glial cell plasma membrane: binding sites and implications for Alzheimer's disease', J Pept Sci, 10: 229-48.

Verghese, P. B., J. M. Castellano, and D. M. Holtzman. 2011. 'Apolipoprotein E in Alzheimer's disease and other neurological disorders', Lancet Neurol, 10: 241-52.

Veugelen, S., T. Saito, T. C. Saido, L. Chavez-Gutierrez, and B. De Strooper. 2016. 'Familial Alzheimer's Disease Mutations in Presenilin Generate Amyloidogenic Abeta Peptide Seeds', Neuron, 90: 410-6.

Vilalta, A., Y. Zhou, J. Sevalle, J. K. Griffin, K. Satoh, et al. 2021. 'Wild-type sTREM2 blocks Abeta aggregation and neurotoxicity, but the Alzheimer's R47H mutant increases Abeta aggregation', J Biol Chem, 296: 100631.

Villemagne, V. L., S. Burnham, P. Bourgeat, B. Brown, K. A. Ellis, et al. 2013. 'Amyloid beta deposition, neurodegeneration, and cognitive decline in sporadic Alzheimer's disease: a prospective cohort study', Lancet Neurol, 12: 357-67.

Vinters, H. V. 1987. 'Cerebral amyloid angiopathy. A critical review', Stroke, 18: 311-24.

Vinters, H. V., and J. J. Gilbert. 1983. 'Cerebral amyloid angiopathy: incidence and complications in the aging brain. II. The distribution of amyloid vascular changes', Stroke, 14: 924-8.

Vodovotz, Y., M. S. Lucia, K. C. Flanders, L. Chesler, Q. W. Xie, et al. 1996. 'Inducible nitric oxide synthase in tangle-bearing neurons of patients with Alzheimer's disease', J Exp Med, 184: 1425-33.

Volianskis, A., R. Kostner, M. Molgaard, S. Hass, and M. S. Jensen. 2010. 'Episodic memory deficits are not related to altered glutamatergic synaptic transmission and plasticity in the CA1 hippocampus of the APPswe/PS1deltaE9-deleted transgenic mice model of ss-amyloidosis', Neurobiol Aging, 31: 1173-87.

Von Bernhardi, R., L. Eugenin-von Bernhardi, and J. Eugenin. 2015. 'Microglial cell dysregulation in brain aging and neurodegeneration', Front Aging Neurosci, 7: 124.

Vorhees, C. V., and M. T. Williams. 2006. 'Morris water maze: procedures for assessing spatial and related forms of learning and memory', Nat Protoc, 1: 848-58.

Voytyuk, I., B. De Strooper, and L. Chavez-Gutierrez. 2018. 'Modulation of gamma- and beta-Secretases as Early Prevention Against Alzheimer's Disease', Biol Psychiatry, 83: 320-27.

Vugmeyster, L., D. F. Au, D. Ostrovsky, B. Kierl, R. Fu, Z. W. Hu, and W. Qiang. 2019. 'Effect of Post-Translational Modifications and Mutations on Amyloid-beta Fibrils Dynamics at N Terminus', Biophys J, 117: 1524-35.

Wahle, T., D. R. Thal, M. Sastre, A. Rentmeister, N. Bogdanovic, et al. 2006. 'GGA1 is expressed in the human brain and affects the generation of amyloid beta-peptide', J Neurosci, 26: 12838-46.

Wahul, A. B., P. C. Joshi, A. Kumar, and S. Chakravarty. 2018. 'Transient global cerebral ischemia differentially affects cortex, striatum and hippocampus in Bilateral Common Carotid Arterial occlusion (BCCAo) mouse model', J Chem Neuroanat, 92: 1-15.

Wainaina, M. N., Z. Chen, and C. Zhong. 2014. 'Environmental factors in the development and progression of late-onset Alzheimer's disease', Neurosci Bull, 30: 253-70.

Wake, H., A. J. Moorhouse, S. Jinno, S. Kohsaka, and J. Nabekura. 2009. 'Resting microglia directly monitor the functional state of synapses in vivo and determine the fate of ischemic terminals', J Neurosci, 29: 3974-80.

Wake, H., A. J. Moorhouse, A. Miyamoto, and J. Nabekura. 2013. 'Microglia: actively surveying and shaping neuronal circuit structure and function', Trends Neurosci, 36: 209-17.

Walker, L. C. 2020. 'Abeta Plaques', Free Neuropathol, 1: 1-42.

Walsh, D. M., I. Klyubin, J. V. Fadeeva, W. K. Cullen, R. Anwyl, et al. 2002. 'Naturally secreted oligomers of amyloid beta protein potently inhibit hippocampal long-term potentiation in vivo', Nature, 416: 535-9.

Walter, J. 2006. 'Control of amyloid-beta-peptide generation by subcellular trafficking of the beta-amyloid precursor protein and beta-secretase', Neurodegener Dis, 3: 247-54.

Walter, J. 2016. 'The Triggering Receptor Expressed on Myeloid Cells 2: A Molecular Link of Neuroinflammation and Neurodegenerative Diseases', J Biol Chem, 291: 4334-41.

Walter, J., and G. van Echten-Deckert. 2013. 'Cross-talk of membrane lipids and Alzheimer-related proteins', Mol Neurodegener, 8: 34.

Wang, S., M. Mustafa, C. M. Yuede, S. V. Salazar, P. Kong, et al. 2020. 'Anti-human TREM2 induces microglia proliferation and reduces pathology in an Alzheimer's disease model', J Exp Med, 217: 1-19.

Wang, W., T. T. Hou, L. F. Jia, Q. Q. Wu, M. N. Quan, and J. P. Jia. 2019. 'Toxic amyloid-beta oligomers induced self-replication in astrocytes triggering neuronal injury', EBioMedicine, 42: 174-87.

Wang, Y., M. Cella, K. Mallinson, J. D. Ulrich, K. L. Young, et al. 2015. 'TREM2 lipid sensing sustains the microglial response in an Alzheimer's disease model', Cell, 160: 1061-71.

Wang, Y., T. K. Ulland, J. D. Ulrich, W. Song, J. A. Tzaferis, et al. 2016. 'TREM2-mediated early microglial response limits diffusion and toxicity of amyloid plaques', J Exp Med, 213: 667-75.

Wang, Y. W., Q. Zhou, X. Zhang, Q. Q. Qian, J. W. Xu, P. F. Ni, and Y. N. Qian. 2017. 'Mild endoplasmic reticulum stress ameliorates lipopolysaccharide-induced neuroinflammation and cognitive impairment via regulation of microglial polarization', J Neuroinflammation, 14: 233.

Waragai, M., M. Yoshida, M. Mizoi, R. Saiki, K. Kashiwagi, et al. 2012. 'Increased protein-conjugated acrolein and amyloid-beta40/42 ratio in plasma of patients with mild cognitive impairment and Alzheimer's disease', J Alzheimers Dis, 32: 33-41.

Webster, S. J., A. D. Bachstetter, P. T. Nelson, F. A. Schmitt, and L. J. Van Eldik. 2014. 'Using mice to model Alzheimer's dementia: an overview of the clinical disease and the preclinical behavioral changes in 10 mouse models', Front Genet, 5: 88.

Weggen, S., and D. Beher. 2012. 'Molecular consequences of amyloid precursor protein and presenilin mutations causing autosomal-dominant Alzheimer's disease', Alzheimers Res Ther, 4: 9.

Welikovitch, L. A., S. Do Carmo, Z. Magloczky, J. C. Malcolm, J. Loke, et al. 2020. 'Early intraneuronal amyloid triggers neuron-derived inflammatory signaling in APP transgenic rats and human brain', Proc Natl Acad Sci U S A, 117: 6844-54.

Weller, R. O., S. D. Preston, M. Subash, and R. O. Carare. 2009. 'Cerebral amyloid angiopathy in the aetiology and immunotherapy of Alzheimer disease', Alzheimers Res Ther, 1: 6.

Welzel, A. T., J. E. Maggio, G. M. Shankar, D. E. Walker, B. L. Ostaszewski, et al. 2014. 'Secreted amyloid beta-proteins in a cell culture model include N-terminally extended peptides that impair synaptic plasticity', Biochemistry, 53: 3908-21.

Wesen, E., G. D. M. Jeffries, M. Matson Dzebo, and E. K. Esbjorner. 2017. 'Endocytic uptake of monomeric amyloid-beta peptides is clathrin- and dynamin-independent and results in selective accumulation of Abeta(1-42) compared to Abeta(1-40)', Sci Rep, 7: 2021.

Wheeler, M. A., M. Jaronen, R. Covacu, S. E. J. Zandee, G. Scalisi, et al. 2019. 'Environmental Control of Astrocyte Pathogenic Activities in CNS Inflammation', Cell, 176: 581-96 e18.

Willem, M., S. Tahirovic, M. A. Busche, S. V. Ovsepian, M. Chafai, et al. 2015. 'eta-Secretase processing of APP inhibits neuronal activity in the hippocampus', Nature, 526: 443-7.

Wingfield, P. 2001. 'Protein precipitation using ammonium sulfate', Curr Protoc Protein Sci, Appendix 3: Appendix 3F.

Wirths, O., and T. A. Bayer. 2010a. 'Neuron loss in transgenic mouse models of Alzheimer's disease', Int J Alzheimers Dis, 2010: 1-19.

Wirths, O., T. Bethge, A. Marcello, A. Harmeier, S. Jawhar, et al. 2010b. 'Pyroglutamate Abeta pathology in APP/PS1KI mice, sporadic and familial Alzheimer's disease cases', J Neural Transm (Vienna), 117: 85-96.

Wirths, O., H. Breyhan, H. Cynis, S. Schilling, H. U. Demuth, and T. A. Bayer. 2009. 'Intraneuronal pyroglutamate-Abeta 3-42 triggers neurodegeneration and lethal neurological deficits in a transgenic mouse model', Acta Neuropathol, 118: 487-96.

Wirths, O., C. Erck, H. Martens, A. Harmeier, C. Geumann, et al. 2010c. 'Identification of low molecular weight pyroglutamate A{beta} oligomers in Alzheimer disease: a novel tool for therapy and diagnosis', J Biol Chem, 285: 41517-24.

Wirths, O., G. Multhaup, and T. A. Bayer. 2004. 'A modified beta-amyloid hypothesis: intraneuronal accumulation of the beta-amyloid peptide--the first step of a fatal cascade', J Neurochem, 91: 513-20.

Wirths, O., S. Walter, I. Kraus, H. W. Klafki, M. Stazi, et al. 2017. 'N-truncated Abeta4-x peptides in sporadic Alzheimer's disease cases and transgenic Alzheimer mouse models', Alzheimers Res Ther, 9: 80.

Wisniewski, H. M., C. Bancher, M. Barcikowska, G. Y. Wen, and J. Currie. 1989. 'Spectrum of morphological appearance of amyloid deposits in Alzheimer's disease', Acta Neuropathol, 78: 337-47.

Wisniewski, T., and B. Frangione. 1992. 'Apolipoprotein E: a pathological chaperone protein in patients with cerebral and systemic amyloid', Neurosci Lett, 135: 235-8.

Wisniewski, T., and F. Goni. 2015. 'Immunotherapeutic approaches for Alzheimer's disease', Neuron, 85: 1162-76.

Wisniewski, T., and E. M. Sigurdsson. 2010. 'Murine models of Alzheimer's disease and their use in developing immunotherapies', Biochim Biophys Acta, 1802: 847-59.

Wolfe, M. S., W. Xia, B. L. Ostaszewski, T. S. Diehl, W. T. Kimberly, and D. J. Selkoe. 1999. 'Two transmembrane aspartates in presenilin-1 required for presenilin endoproteolysis and gamma-secretase activity', Nature, 398: 513-7.

Wu, D., X. Tang, L. H. Gu, X. L. Li, X. Y. Qi, et al. 2018. 'LINGO-1 antibody ameliorates myelin impairment and spatial memory deficits in the early stage of 5XFAD mice', CNS Neurosci Ther, 24: 381-93.

Wunderlich, P., K. Glebov, N. Kemmerling, N. T. Tien, H. Neumann, and J. Walter. 2013. 'Sequential proteolytic processing of the triggering receptor expressed on myeloid cells-2 (TREM2) protein by ectodomain shedding and gamma-secretase-dependent intramembranous cleavage', J Biol Chem, 288: 33027-36.

Wyss-Coray, T., and L. Mucke. 2002. 'Inflammation in neurodegenerative disease--a double-edged sword', Neuron, 35: 419-32.

Wyss-Coray, T., and J. Rogers. 2012. 'Inflammation in Alzheimer disease-a brief review of the basic science and clinical literature', Cold Spring Harb Perspect Med, 2: a006346.

Xiang, X., T. M. Piers, B. Wefers, K. Zhu, A. Mallach, et al. 2018. 'The Trem2 R47H Alzheimer's risk variant impairs splicing and reduces Trem2 mRNA and protein in mice but not in humans', Mol Neurodegener, 13: 49.

Xu, G., Y. Ran, S. E. Fromholt, C. Fu, A. T. Yachnis, T. E. Golde, and D. R. Borchelt. 2015. 'Murine Abeta over-production produces diffuse and compact Alzheimer-type amyloid deposits', Acta Neuropathol Commun, 3: 72.

Xu, T. H., Y. Yan, Y. Kang, Y. Jiang, K. Melcher, and H. E. Xu. 2016. 'Alzheimer's disease-associated mutations increase amyloid precursor protein resistance to gamma-secretase cleavage and the Abeta42/Abeta40 ratio', Cell Discov, 2: 16026.

Yamaguchi, H., Y. Nakazato, S. Hirai, M. Shoji, and Y. Harigaya. 1989. 'Electron micrograph of diffuse plaques. Initial stage of senile plaque formation in the Alzheimer brain', Am J Pathol, 135: 593-7.

Yamaguchi, H., Y. Nakazato, M. Shoji, M. Takatama, and S. Hirai. 1991. 'Ultrastructure of diffuse plaques in senile dementia of the Alzheimer type: comparison with primitive plaques', Acta Neuropathol, 82: 13-20.

Yang, J., Z. Fu, X. Zhang, M. Xiong, L. Meng, and Z. Zhang. 2020a. 'TREM2 ectodomain and its soluble form in Alzheimer's disease', J Neuroinflammation, 17: 204.

Yang, S. H., D. K. Lee, J. Shin, S. Lee, S. Baek, et al. 2017a. 'Nec-1 alleviates cognitive impairment with reduction of Abeta and tau abnormalities in APP/PS1 mice', EMBO Mol Med, 9: 61-77.

Yang, T., S. Li, H. Xu, D. M. Walsh, and D. J. Selkoe. 2017b. 'Large Soluble Oligomers of Amyloid beta-Protein from Alzheimer Brain Are Far Less Neuroactive Than the Smaller Oligomers to Which They Dissociate', J Neurosci, 37: 152-63.

Yang, Z., Y. Shao, Y. Zhao, Q. Li, R. Li, et al. 2020b. 'Endoplasmic reticulum stress-related neuroinflammation and neural stem cells decrease in mice exposure to paraquat', Sci Rep, 10: 17757.

Yano, Y., A. Takeno, and K. Matsuzaki. 2018. 'Trace amounts of pyroglutaminated Abeta-(3-42) enhance aggregation of Abeta-(1-42) on neuronal membranes at physiological concentrations: FCS analysis of cell surface', Biochim Biophys Acta Biomembr, 1860: 1603-08.

Yeh, F. L., D. V. Hansen, and M. Sheng. 2017. 'TREM2, Microglia, and Neurodegenerative Diseases', Trends Mol Med, 23: 512-33.

Yeh, F. L., Y. Wang, I. Tom, L. C. Gonzalez, and M. Sheng. 2016. 'TREM2 Binds to Apolipoproteins, Including APOE and CLU/APOJ, and Thereby Facilitates Uptake of Amyloid-Beta by Microglia', Neuron, 91: 328-40.

Yin, Z., S. Wang, B. Shen, C. Deng, Q. Tu, et al. 2019. 'Coimmunocapture and Electrochemical Quantitation of Total and Phosphorylated Amyloid-beta40 Monomers', Anal Chem, 91: 3539-45.

Yong, H. Y. F., K. S. Rawji, S. Ghorbani, M. Xue, and V. W. Yong. 2019. 'The benefits of neuroinflammation for the repair of the injured central nervous system', Cell Mol Immunol, 16: 540-46.

Yoo, S. J., G. Son, J. Bae, S. Y. Kim, Y. K. Yoo, et al. 2020. 'Longitudinal profiling of oligomeric Abeta in human nasal discharge reflecting cognitive decline in probable Alzheimer's disease', Sci Rep, 10: 11234.

Yoshiyama, Y., M. Higuchi, B. Zhang, S. M. Huang, N. Iwata, et al. 2007. 'Synapse loss and microglial activation precede tangles in a P301S tauopathy mouse model', Neuron, 53: 337-51.

Youssef, I., S. Florent-Bechard, C. Malaplate-Armand, V. Koziel, B. Bihain, et al. 2008. 'N-truncated amyloid-beta oligomers induce learning impairment and neuronal apoptosis', Neurobiol Aging, 29: 1319-33.

Yu, Y., and R. D. Ye. 2015. 'Microglial Abeta receptors in Alzheimer's disease', Cell Mol Neurobiol, 35: 71-83.

Yu, Z., F. Dou, Y. Wang, L. Hou, and H. Chen. 2018. 'Ca(2+)-dependent endoplasmic reticulum stress correlation with astrogliosis involves upregulation of KCa3.1 and inhibition of AKT/mTOR signaling', J Neuroinflammation, 15: 316.

Yuan, P., C. Condello, C. D. Keene, Y. Wang, T. D. Bird, et al. 2016. 'TREM2 Haplodeficiency in Mice and Humans Impairs the Microglia Barrier Function Leading to Decreased Amyloid Compaction and Severe Axonal Dystrophy', Neuron, 90: 724-39.

Yuksel, M., and O. Tacal. 2019. 'Trafficking and proteolytic processing of amyloid precursor protein and secretases in Alzheimer's disease development: An up-to-date review', Eur J Pharmacol, 856: 172415.

Zhang, J., and Q. Liu. 2015. 'Cholesterol metabolism and homeostasis in the brain', Protein Cell, 6: 254-64.

Zhang, Y., L. Lu, J. Jia, L. Jia, C. Geula, et al. 2014. 'A lifespan observation of a novel mouse model: in vivo evidence supports abeta oligomer hypothesis', PLoS One, 9: e85885.

Zhang, Y. W., R. Thompson, H. Zhang, and H. Xu. 2011. 'APP processing in Alzheimer's disease', Mol Brain, 4: 3.

Zhao, J., Q. Shi, Y. Zheng, Q. Liu, Z. He, Z. Gao, and Q. Liu. 2021. 'Insights Into the Mechanism of Tyrosine Nitration in Preventing beta-Amyloid Aggregation in Alzheimer's Disease', Front Mol Neurosci, 14: 619836.

Zhao, Y., X. Li, T. Huang, L. L. Jiang, Z. Tan, et al. 2017. 'Intracellular trafficking of TREM2 is regulated by presenilin 1', Exp Mol Med, 49: e405.

Zhao, Y., X. Wu, X. Li, L. L. Jiang, X. Gui, et al. 2018. 'TREM2 Is a Receptor for beta-Amyloid that Mediates Microglial Function', Neuron, 97: 1023-31 e7.

Zheng, H., C. C. Liu, Y. Atagi, X. F. Chen, L. Jia, et al. 2016. 'Opposing roles of the triggering receptor expressed on myeloid cells 2 and triggering receptor expressed on myeloid cells-like transcript 2 in microglia activation', Neurobiol Aging, 42: 132-41.

Zhong, L., X. F. Chen, T. Wang, Z. Wang, C. Liao, et al. 2017. 'Soluble TREM2 induces inflammatory responses and enhances microglial survival', J Exp Med, 214: 597-607.

Zhong, L., Z. Wang, D. Wang, Z. Wang, Y. A. Martens, et al. 2018. 'Amyloid-beta modulates microglial responses by binding to the triggering receptor expressed on myeloid cells 2 (TREM2)', Mol Neurodegener, 13: 1-12.

Zhong, L., Y. Xu, R. Zhuo, T. Wang, K. Wang, et al. 2019. 'Soluble TREM2 ameliorates pathological phenotypes by modulating microglial functions in an Alzheimer's disease model', Nat Commun, 10: 1365.

Zhou, Y., T. K. Ulland, and M. Colonna. 2018. 'TREM2-Dependent Effects on Microglia in Alzheimer's Disease', Front Aging Neurosci, 10: 202.

List of publications

Manuscripts from the thesis (published):

1. **Joshi P**, Riffel F, Satoh K, Enomoto M, Qamar S, Scheiblich H, Villacampa N, Kumar S, Theil S, Parhizkar S, Haass C, Heneka MT, Fraser PE, Hyslop P.St George, Walter J. Differential interaction with TREM2 modulates microglial uptake and brain deposition of modified Aβ species. Glia 69:12, 2917-32 **(2021)**; PMID: 34427354 (https://doi.org/10.1002/glia.24077).
2. **Joshi P**, Riffel F, Kumar S, Villacampa N, Theil S, Parhizkar S, Haass C, Colonna M, Heneka MT, Arzberger T, Herms J, Walter J. TREM2 modulates differential deposition of modified and non-modified Aβ species in extracellular plaques and intraneuronal deposits. acta neuropathol commun 9:168; 1-22 **(2021)**; PMID: 34663480 (https://doi.org/10.1186/s40478-021-01263-x).

Poster presentations:

1. **Joshi P**, Satoh K, Enomoto M, Qamar S, Kumar S, Haass C, Fraser P, Hyslop PStG, Walter J. Effect of TREM2 deletion in deposition of pyroglutamate-3 Amyloid-β in transgenic mouse brain, at AD/PD™ **(2021)**.
2. **Joshi P**, Satoh K, Enomoto M, Qamar S, Parhizkar S, Riffel F, Kumar S, Haass C, Colonna M, Fraser P, Hyslop PStG, Walter J. Differential interaction of post-translationally modified Aβ variants with TREM2", at FENS 2020 virtual forum **(2020)**.
3. **Joshi P**, Riffel R, Ibach M, Kumar S, Walter J. Generation and characterization of isogenic cell lines expressing soluble TREM2 for ligand binding studies, at Düsseldorf-Jülich Symposium on Neurodegenerative Diseases: Aggregates, Autophagy, Prions and Biomarkers, Düsseldorf-Germany **(2019)**.
4. **Joshi P**, Ibach M, Kumar S, Walter J. Generation and characterization of isogenic cell line for the stable expression of sTREM2, at 4th BIGS Neuroscience Student Symposium, Kamen-Germany **(2018)**.

Conference talks:

1. **Title:** Interaction of TREM2 with Aβ variants, at 6th PHAGO general assembly virtual meeting **(2021)**.
2. **Title:** Phosphorylated Amyloid-β showed increased interaction with the TREM2 resulting in altered deposition in transgenic mouse brain, at 38th Annual Conference of Indian Academy of Neuroscience (IAN) virtual forum **(2020)**.
3. **Title:** Differential Interaction of TREM2 with modified Aβ variants phosphorylated Aβ as a TREM2 ligand, at 5th PHAGO general assembly virtual meeting **(2020)**.

Acknowledgement

First and foremost, I would like to thank Almighty Sri Ram and my guru, Gondawalekar Maharaj, who has given me this wonderful life and opportunity.

It is a great pleasure and honour for me to owe gratitude to my guide Prof. Dr Jochen Walter for his remarkable guidance, constant encouragement, and patience and also for his scientific and personal concern throughout the investigation and successful completion of this work. Professor, this journey was impossible without you!

With humble gratitude, I thank Prof. Dr Thorsten Lang, Prof. Dr Sven Burgdorf and Prof. Dr Michael Gütschow for their support, keen interest, cooperation, valuable time and willingness to review my thesis.

With pride and pleasure, I want to thank the University of Bonn, Department of Neurology, University Clinic Bonn, Microscopy Core Facility of the Medical Faculty at the University of Bonn, Bonn International Graduate School (BIGS) of Neuroscience for providing the suitable infrastructure and opportunities, and as well as PHAGO project, Deutscher Akademischer Austauschdienst (DAAD), Bonner Forum Biomedizin (BFB), Alzheimer Forschung Initiative (AFI) for providing grant/support that helped me to carry out experiments and for my career growth.

To Prof. Dr Peter St. George Hyslop, Prof. Dr Paul Fraser, Dr Masahiro Enomoto, and Dr Kanayo Satoh for hosting me in their laboratory in Toronto, Canada for performing biophysics experiments. Masa, I will always admire your scientific skills. Kanayo, I will never forget your help during the experiments and support throughout these years.

I would like to thank Prof. Christian Haass, Prof. Marco Colonna, Prof. Dr Michael Heneka and their lab members who contributed directly or indirectly to my research findings.

To Prof. Dr Jochen Hermes and Dr Thomas Arzberger, thank you for providing the human brain samples and helping with analysing the data.

To my dear current and former colleagues and the members of the neurobiology group, especially, Dr Naoto Oikawa, and Mr Florian Riffle for the discussions, advice, critical comments, and time, as well as for providing a very conducive environment in the lab. Dr Sathish Kumar and his wife Mrs Jayashree, especially, for guiding me all along by providing all necessary information needed for personal and professional development.

I am thankful and fortunate enough to get constant encouragement, support and guidance from my previous guides, Dr Sugato Banerjee, Dr Ashok Pattnaik, Dr Sumana Chakravarty, Dr Arvind Kumar and to my all dear friends in all institutions, organisations, and universities that I worked or studied before.

I am grateful to Mrs Petra and Mr Hansjörg Schneider, Mrs Vidya and Mr Revan Banakar, Mrs Shefali and Mr Harish Patel, for their moral support, love, concern and constant encouragement in making my stay in Bonn unforgettable.

I cannot forget to thank many people who contributed to my personal and professional growth over the years. To all my teachers from the school and the university who encouraged and kept faith in my capabilities. To all the fellow scientific community for their tremendous and intriguing research work/papers/books which helped me to gain insights into the subjects as well as helped me to direct my research work.

I also take this opportunity to express a deep sense of gratitude to my dear friends, Dr Abhipradnya Wahul, Dr Vandana and Dr Dnyaneshwar Kapote, Mr Anand Kumar, Mr Lorenz Haase, Dr Michael Klug, Dr Remi Avohou, Dr Dilek Mercan, Dr Nàdia Villacampa, for their cordial support, valuable information and suggestions necessary for successful completion of my project.

I cherish the affectionate encouragement, trust, faith, care and love of my mother, Mrs Sushama Joshi, my brother, Mr Amey Joshi and my father, Late Chintamani Joshi. To all who are responsible to make me who I am today, Late Vasant Joshi, Late Jayavant Misal, Late Narayan Hawaldar, Late Gajanan Vaze, Mrs Revati Vaze, Mrs Leena and Adv. Abhishek Sathe, Mrs Anagha and Mr Arun Sathe, Mr Nagesh Vaze, Mrs Jyostna and Mr Sudesh Vaze and all my well-wishers and all the people who kept their faith and cared for me beyond my imagination. And to my wife, Dr Gargi. I simply could not have done this without you. Thank you for your patience, support, love and most importantly believing in me during this stressful time. And not the least, Mrs Kirti and Prof. Dr Milind Ray for the constant support encouragement and faith in me and finally my Champ, Mast. Parth Ray for encouraging me.

Finally, I take this opportunity to express my gratitude to all the people involved directly or indirectly in the successful completion of this journey. No words can express how grateful I am for your love and support.

We all did it! Thank you for everything.... always.

Check for updates

Received: 17 June 2021 | Revised: 2 August 2021 | Accepted: 6 August 2021

DOI: 10.1002/glia.24077

GLIA

WILEY

RESEARCH ARTICLE

Differential interaction with TREM2 modulates microglial uptake of modified Aβ species

Pranav Joshi[1] | Florian Riffel[1] | Kanayo Satoh[2] | Masahiro Enomoto[3] | Seema Qamar[4] | Hannah Scheiblich[5,6] | Nàdia Villacampa[5,6] | Sathish Kumar[1] | Sandra Theil[1] | Samira Parhizkar[7] | Christian Haass[7,8,9] | Michael T. Heneka[5,6] | Paul E. Fraser[2] | Peter St George-Hyslop[2,4] | Jochen Walter[1]

[1]Department of Neurology, University of Bonn, Bonn, Germany

[2]Departments of Medical Biophysics and Medicine (Neurology), Tanz Centre for Research in Neurodegenerative Diseases and, Toronto, Ontario, Canada

[3]Princess Margaret Cancer Centre Research Institute, University Health Network, Toronto, Ontario, Canada

[4]Cambridge Institute for Medical Research, Department of Clinical Neurosciences, School of Clinical Medicine, University of Cambridge, Cambridge, UK

[5]Department of Neurodegenerative Diseases and Gerontopsychiatry, University Hospital Bonn, Bonn, Germany

[6]Neuroinflammation Unit, German Center for Neurodegenerative Diseases e. V. (DZNE), Bonn, Germany

[7]Chair of Metabolic Biochemistry, Biomedical Center (BMC), Faculty of Medicine, Ludwig-Maximilians-Universität München, Munich, Germany

[8]Munich Cluster for Systems Neurology (SyNergy), Munich, Germany

[9]Molecular Neurodegeneration Unit, German Center for Neurodegenerative Diseases e.V. (DZNE) Munich, Munich, Germany

Correspondence
Jochen Walter, Department of Neurology, University of Bonn, Venusberg-Campus 1, (Formerly Sigmund-Freud-Str. 25), 53127 Bonn, Germany.
Email: jochen.walter@ukbonn.de

Funding information
Canadian Institutes of Health Research; Deutsche Forschungsgemeinschaft, Grant/Award Number: WA1477/6-6; EU Innovative Medicines Initiative 2 Joint Undertaking, Grant/Award Number: 115976 (PHAGO); Alzheimer's Association (Zenith Award); Canadian Institutes of Health Research (CIHR) operating grant, Grant/Award Number: PJT17349; UK Alzheimer Society and ARUK; Wellcome Trust Collaborative Award in Science

Abstract

Rare coding variants of the microglial triggering receptor expressed on myeloid cells 2 (TREM2) confer an increased risk for Alzheimer's disease (AD) characterized by the progressive accumulation of aggregated forms of amyloid β peptides (Aβ). Aβ peptides are generated by proteolytic processing of the amyloid precursor protein (APP). Heterogeneity in proteolytic cleavages and additional post-translational modifications result in the production of several distinct Aβ variants that could differ in their aggregation behavior and toxic properties. Here, we sought to assess whether post-translational modifications of Aβ affect the interaction with TREM2. Biophysical and biochemical methods revealed that TREM2 preferentially interacts with oligomeric Aβ, and that phosphorylation of Aβ increases this interaction. Phosphorylation of Aβ also affected the TREM2 dependent interaction and phagocytosis by primary microglia and in APP transgenic mouse models. Thus, TREM2 function is important for sensing phosphorylated Aβ variants in distinct aggregation states and reduces the accumulation and deposition of these toxic Aβ species in preclinical models of Alzheimer's disease.

KEYWORDS
Alzheimer's disease, amyloid β, FTD mutation, phosphorylation, post-translational modification, TREM2

This is an open access article under the terms of the Creative Commons Attribution-NonCommercial License, which permits use, distribution and reproduction in any medium, provided the original work is properly cited and is not used for commercial purposes.
© 2021 The Authors. *GLIA* published by Wiley Periodicals LLC.

1 | INTRODUCTION

Progressive accumulation of amyloid-β (Aβ) in form of extracellular plaques along with intracellular deposition of hyperphosphorylated tau protein in neurofibrillary tangles (NFT) are classical pathological hallmarks of Alzheimer's disease (AD) (d'Errico & Meyer-Luehmann, 2020; Haass & Selkoe, 2007; Hyman et al., 2012; Selkoe & Hardy, 2016). Aβ deposits can also be detected intracellularly, particularly inside of neurons (Gouras et al., 2010; Gouras et al., 2012; Kumar et al., 2013; Wirths et al., 2009) and within the vasculature of the brain (Huang et al., 2021; Spangenberg et al., 2019; Thal et al., 2008; Thal et al., 2009). Aβ peptides can undergo post-translational modifications that alter aggregation and neurotoxic characteristics and might thereby modulate the pathogenesis of AD (Barykin et al., 2017; Kummer & Heneka, 2014). For example, N-terminal truncation and formation of pyroglutamate at position 3 of the Aβ peptide strongly promotes aggregation, and pyroglutamate modified Aβ species are abundant in AD brain (Saido et al., 1995; Schilling et al., 2008). Phosphorylation of Aβ at serine 8 also promotes aggregation into oligomeric and fibrillar assemblies (Kumar et al., 2011), while phosphorylation at serine 26 leads to formation of stable neurotoxic oligomers (Kumar et al., 2016).

During disease progression, brain-resident microglia cluster around extracellular Aβ plaques to prevent further growth or deposition thereby limiting neuritic dystrophy (Condello et al., 2015). Microglia depletion also altered parenchymal plaque development and promoted Aβ deposition in cortical blood vessels (Spangenberg et al., 2019).

Recent studies identified sequence variants in the triggering receptor expressed on myeloid cells 2 (TREM2) that are associated with an increased risk for several neurodegenerative disorders such as AD (Guerreiro, A. Wojtas, et al., 2013; Jonsson et al., 2013). TREM2 binds anionic ligands, including certain phospholipids and apolipoproteins (Bailey et al., 2015; Kober & Brett, 2017; Yeh et al., 2016). In addition, TREM2 has also been shown to bind Aβ, and affect its clearance and aggregation (Kober et al., 2020; Lessard et al., 2018; Vilalta et al., 2021; Zhao et al., 2018; Zhong et al., 2018). However, little is known about how post-translationally modified Aβ variants in various aggregation states are handled by microglia and whether this is TREM2 dependent.

In this study, we demonstrate that posttranslational modifications of Aβ differentially affect the binding to TREM2. Furthermore, we report that TREM2 is involved in the differential internalization of modified Aβ variants by microglia, and the characteristic deposition in brains of transgenic mouse models of AD.

2 | METHODS

2.1 | Processing of Aβ peptides

The synthetic Aβ(1–42) and Aβ(3–42) peptide variants were obtained from PSL, GmbH. Synthetic Biotin-LC-Aβ(1–42) (LC: 6-carbon long chain) was obtained from AnaSpec. The synthetic Aβ peptides used in this study showed greater than 95% purity by HPLC (data available on request). The reconstitution of Aβ peptide variants was done by adding 10 mM NaOH directly to the vial to make a stock solution of 230 μM followed by sonication for 5 min, aliquoted and snap-frozen. Biotin-LC-Aβ(1–42) was reconstituted with DMSO and biolayer interferometry (BLI) assay buffer (consisting of 20 mM HEPES and 1 M NaCl) thus giving a stock concentration of 100 μM, aliquoted and snap-frozen.

For the preparation of Aβ oligomers we used two different methods:

2.1.1 | Method 1

For the dot blot, and BLI experiments, we used oAβ(1–42) preparation made by gently mixing freshly prepared Aβ(1–42) variants separately with a suitable concentration of Biotin-LC-Aβ(1–42) to make the final concentration of 23 μM in PBS (pH 7.4) followed by incubation at 37°C for 3 h (Vilalta et al., 2021).

2.1.2 | Method 2

For the pulldown, and cellular binding and phagocytosis experiments, we followed protocol to prepare oAβ as described previously (T. Kim et al., 2013). Briefly, monomeric Aβ stock was diluted to 100 μM in PBS and incubated at 23°C for 16 h followed by an incubation at 4°C for 24 h. The preparation was further centrifuged at 16,000*g* and the supernatant aliquoted, flash frozen in liquid nitrogen and stored at −20°C.

2.2 | Transmission electron microscopy

oAβ prepared using method 1 were characterized by negative stain-transmission electron microscopy (TEM) as described by Anderson et al. (2010). Briefly, 5–10 μl of oAβ at a concentration of 1 μM were placed onto a freshly glow-discharged (by Glow discharge cleaning system: PELCO easiGlow™ Glow Discharge System), carbon-coated formvar, copper grid-400mesh (Electron microscopy sciences, #CF400-CU). After 2 min, the sample solution was wicked off with filter paper, the grid rinsed with deionized water, and 5 μl of 2% (wt/vol) phosphotungstic acid stain (pH 7.0) was placed on the grid. After 1 min, the staining solution was wicked away and the grid air-dried. The negatively stained sample was then examined by using Talos L120C (Thermo Fischer Scientific) at an acceleration voltage of 120 kV imaged with 4 k × 4 K Ceta CMOS camera at x45,000. Representative images are shown in Figure S1 a and b.

2.3 | Cell culture

2.3.1 | Culture of HEK293 Flp-In cells

HEK293 Flp-In and the sTREM2-WT expressing HEK293 Flp-In cells were cultured in growth medium GlutaMAX™ (DMEM containing

high glucose [4.5 g/L], phenol red, sodium pyruvate additive, 10 mM HEPES), supplemented with 10% heat-inactivated fetal calf serum (FCS), 1% penicillin and streptomycin (P/S) solution, and 100 μg/ml hygromycin in incubators maintained at 37°C and 5% CO_2 (Ibach et al., 2021). Using the QuikChange-II kit (Agilent Technologies), site directed mutagenesis was carried out according to the manufacturer's instructions in order to introduce the stop codon at aa158 of full length TREM2 construct. The generation of stable cell line was described previously (Ibach et al., 2021). Briefly, the cells were cultured until 70%–80% confluency and washed with DPBS. Co-transfection was carried our using mammalian Flp-In™ host cells with a 9:1 ratio of pOG44 coding for Flp recombinase and pcDNA5/FRT plasmid DNA containing sTREM2 (aa1–aa157) sequence using Lipofectamine 2000 (Thermo Fisher Scientific) in a transfection medium (OptiMEM, Thermo Fisher Scientific). After 24 h, the medium was replaced by medium containing 100 μg/ml Hygromycin B for selection of single cell clones by limiting dilution. Clones were screened by detection of secreted Trem2 in the supernatant.

2.3.2 | Culture of Expi293F™ cells

Expi293F™ cells were grown in suspension with serum free FreeStyle™ expression medium (Thermo Fisher Scientific) and were kept at 37°C and 8% CO_2.

2.3.3 | Culture of WT and TREM2^{T66M} primary microglia cells

The cells were isolated by the previously described method (Giulian & Baker, 1986). Briefly, brains from neonatal mice were stripped of the meninges and dissociated using mechanical shearing and trypsin (Life Technologies). Cells of two brains were plated on poly-L-lysine (PLL, Sigma-Aldrich) coated T75 culture flasks (Greiner bio-one) and cultivated in DMEM (Gibco by Thermo Fisher Scientific) supplemented with 10% FCS and 1% P/S (Gibco). On the next day cells were washed three times with DPBS (Gibco) to remove cellular debris and cultured with DMEM supplemented with 10% FCS, 1% P/S and 1% L929 conditioned medium as a source of growth factors. After 7–10 days loosely attached mature microglia were shaken off the astrocytic layer with a repetition of the harvesting procedure all 2–3 days for up to three times. For experiments, primary microglia were seeded on poly-D-lysine (PDL, Sigma-Aldrich) coated glass cover slips at a density of 100,000/well into 24 well plates and allowed to adhere overnight in serum-free DMEM complemented with 1% N-2 supplement (Gibco).

2.4 | TREM2 ectodomain purification

2.4.1 | sTREM2 for the dot blot experiments

For the dot blot assay, cell supernatant from three 15 cm dishes of HEK293 Flp-In controlk or sTREM2-WT expressing HEK293 Flp-In cells was collected after 24 h of incubation. Saturated solution of ammonium sulphate (AS) was made (3.9 M at 0°C) and the total protein was precipitated with 40% AS solution. Because the addition of AS acidifies the solution, a 1 M Tris–HCl buffer (pH 8.0) was added to the supernatant so that the final concentration was 50 mM (Burgess, 2009; Wingfield, 2001). The mixture is gently mixed and incubated for 1 h on ice and then centrifuged for 30 min at 4°C at 16,000 rcf. The supernatant was discarded and the pellet was resuspended in 5 ml of 1X PBS and this solution was used for dot blot assay (Data S1a for the immunoblot).

2.4.2 | TREM2 ectodomain for BLI studies

A cDNA construct encoding residues aa19–aa143 of TREM2 with a C-terminal His-tag was subcloned into a mammalian expression vector, pHLSec (Aricescu et al., 2006) and transfected into Expi293 cell line using polyethylenimine (PEI) (Backliwal et al., 2008) as the transfection reagent. Endotoxin-free chemicals and plastic ware were used. Recombinant protein was purified from the culture medium using Ni-Excel and size exclusion chromatography followed by Endo H_f (NEB, # P0703L) treatment and the buffer exchange to BLI assay buffer by using Superose® 6 Increase 10/300 GL (GE Healthcare, #29-0915-96) and the final concentration of the protein was determined by using Biophotometer (Eppendorf) (Vilalta et al., 2021). The obtained TREM2 was detected with Anti-TREM2 antibody (Data S1b for the immunoblot).

2.4.3 | sTREM2-Fc and Fc for pull down experiments

sTREM2-Fc1 vector was generated by inserting human sTREM2 (aa1–aa157) sequence into the pFUSE-hIgG1-Fc1 expression vector. Expression of the Fc-fusion proteins was done following the protocol described by Fang et al. (2017). Briefly, one day before transfection, cells were seeded at 1.5 million viable cells per milliliter (mvc/ml) in fresh medium. The next day, cells were transfected at 3 mvc/ml in half of the final volume with a 1 mg/ml linear 40 kDa PEI Max solution (Polysciences, #24765-1) and the respective DNA (1 μg/ml) in a 6:1 ratio. Efficiency of transfection was further increased by addition of 0.1% Pluronic® F-68 (Thermo Fisher Scientific, #24040032). After 24 h the transfection mix was diluted with fresh medium 1:1 and supplemented with 0.5 M valproic acid (Sigma Aldrich, #VPA P4543) to a final concentration of 3.5 mM. The conditioned media were collected after 4–5 days. Following centrifugation, filtration and pH adjustment the media were loaded on a HiTrap™ Protein G HP 1 ml column and affinity purified via FPLC. Eluted fractions were neutralized by addition of 1 M Tris (pH 9.0). Concentration and buffer exchange against PBS was performed by ultrafiltration with a 10 kDA MWCO column (Sartorius, Göttingen). The concentration of the purified proteins was determined by a spectrophotometer measuring the absorbance at 280 nm (Data S1c for the immunoblot).

2.5 | Dot blot assay

Monomer rich fractions of Aβ were prepared from freshly reconstituted Aβ stocks by dilution to 23 μM in ice cold PBS and ultracentrifugation at 4°C at 100,000*g* for 1 h. Aβ in the supernatant was considered as monomer rich preparation, and characterized by western immunoblot (please refer Figure S1c). Oligomer rich Aβ (oAβ) preparations were obtained as described in Method-1. Then, 2 μl from each of above equimolar preparations from the stock solution (23 μM) were spotted on nitrocellulose (NC) membranes, and the membranes were allowed to dry. The NC membranes were then incubated with concentrated cell supernatant overnight at 4°C. The membranes were washed with TBS-T (3 × 5 min) and then blocked with Odyssey Blocking Buffer (LI-COR Bioscience) for 1.5 h at RT. The membranes were then incubated overnight in primary antibody (monoclonal antibody 4B2A3 for detection of TREM2) at 4°C. The NC membranes were then washed with TBS-T (3 × 5 min) and incubated with LI-COR fluorescent secondary antibody for 1 h at RT, washed with TBS-T (3 × 5 min), then once with TBS (5 min) and imaged with Odyssey® CLx (LI-COR Biosciences). To detect Aβ on the same membranes after detection of bound TREM2, the dot blots were washed with TBS-T (3 × 5 min) followed by incubation with 4G8 antibody overnight to detect Aβ variants. The NC membranes were washed with TBS-T (3 × 5 min) and incubated with LI-COR fluorescent secondary antibody for 1 h at RT, washed with TBS-T (3 × 5 min), then once with TBS (5 min) and developed with LI-COR Odyssey® CLx (LI-COR Biosciences). (please refer Data S1d for the original dot blots cropped for Figure 1b).

2.6 | Bio-layer interferometry (BLI) studies

The aggregation state of the different Aβ variants (prepared by Method-1) was controlled by TEM; (Figure S1a). No significant changes in the size distribution of oligomers formed by unlabeled Aβ, Biotin-LC-Aβ or by mixtures of unlabeled Aβ and Biotin-LC-Aβ (at a ratio of 20:1) was observed (Figure S1b) indicating that the conjugation of Aβ with biotin does not affect the average size of oligomers. Mixtures of Biotin-LC-Aβ with the different N-terminal truncated or post-translationally modified Aβ variants (also at 20:1 ratio) also yielded very similar size distribution of oligomers between 8 and 55 nm. Only the oligomer preparation with pSer8-Aβ also contained larger oligomers with sizes between 55 and 90 nm. This was observed for both, Aβ(1–42) and Aβ(3–42) variants. However, also for pSer8-Aβ variants, >95% of the oligomers were in the size range of 8–55 nm. For BLI studies with TREM2 ectodomain by using Octet RED384 (Forte Bio), we used 5% of Biotin-LC-Aβ(1–42) for mixing with Aβ variants compared with only Biotin-LC-Aβ(1–42) (unpublished data). Further, we optimized the concentration of already mixed oAβ to immobilize onto the biosensors. Initial experiments revealed that 5% of 1 μM Biotin-LC-Aβ mixed with 1 μM of oAβ when immobilized onto the streptavidin (SA) biosensors (Forte Bio #18-0009) showed a similar loading and binding as compared with 100%, 5% Biotin-LC-Aβ (Data S2a,b) and hence the same concentration of mixed Aβ variants was used in this study. In addition to this, we also checked the differential loading of oAβ onto the SA biosensors in which oAβ(1–42) pSer26 showed higher loading as compared with other variants (Data S2c).

For BLI kinetic measurements, Streptavidin (SA) biosensors were hydrated with 220 μl assay buffer (20 mM HEPES, 500 mM NaCl, 0.1% BSA, 0.02% Tween 20 (pH 7.4) for 30 min (96 well plate). Further, biosensors were exposed to 220 μl buffer in order to determine the initial baseline. The Biosensors were exposed to oligomer rich preparations obtained from mixtures of the respective Aβ variants and Biotin-LC-Aβ in 20:1 ratios. Biosensors were then exposed to 220 μl of assay buffer for 450 s for another baseline measurement. The biosensors were exposed to 220 μl assay buffer containing TREM2 ectodomain at different concentrations (1, 2, 5, and 10 μM) prepared in BLI assay buffer for 60 s to measure association. The biosensors were then exposed to 220 μl of assay buffer for 150 s to measure dissociation. The kinetic constants of BLI were obtained with four different concentrations of TREM2 ectodomain and data was aligned at the y-axis and smoothed by Savitzky–Golay filtering. Curves were processed by adjusting to BLI control buffer, and curve fitting was performed using 2:1 heterogenous ligand as a model due to the heterogenicity of Aβ. KD1 and KD2 values provide the measure of the relative coefficients for dissociation and binding, wherein KD1 measures interaction that occupies the highest percentage of the binding surface area and KD2 characterizes the secondary interaction, determined mathematically by the Octet Data Analysis software.

2.7 | Immunoprecipitation of Aβ using sTREM2-Fc

For assessing differential binding of mAβ and oAβ variants to TREM2, 2 μg of sTREM2-Fc or hIgG1-Fc were pre-coupled to magnetic Protein G beads (SureBeads™, Bio-Rad) for 20 min at 23°C. The coupled beads were then further incubated with 2 μg of the oAβ preparation (prepared by Method-2) for 1 h at 23°C in PBS buffer containing 0.1% Tween-20 (PBS-T). After precipitation and subsequent thorough washing steps, the bound proteins were eluted from the beads by addition of 20 mM glycine solution at pH 2.5. Finally, the eluate was neutralized with 1 M Tris–HCl pH 8 and boiled at 95°C in Laemmli buffer before being subjected to immunoblot analysis. For a quantitative assessment, this protocol was slightly altered by reducing the amount of beads (300 μg) and Aβ (1 μg) while increasing the amount of sTREM2-Fc and hIgG1-Fc to 10 μg to ensure complete saturation of the beads with recombinant protein.

2.8 | SDS-page

Protein separation was performed using the XCell SureLock®Mini-Cell or XCell4 SureLock® Midi-Cell SDS-PAGE system (Invitrogen™, #V601020). Samples prepared in 5x SDS sample buffer and boiled at

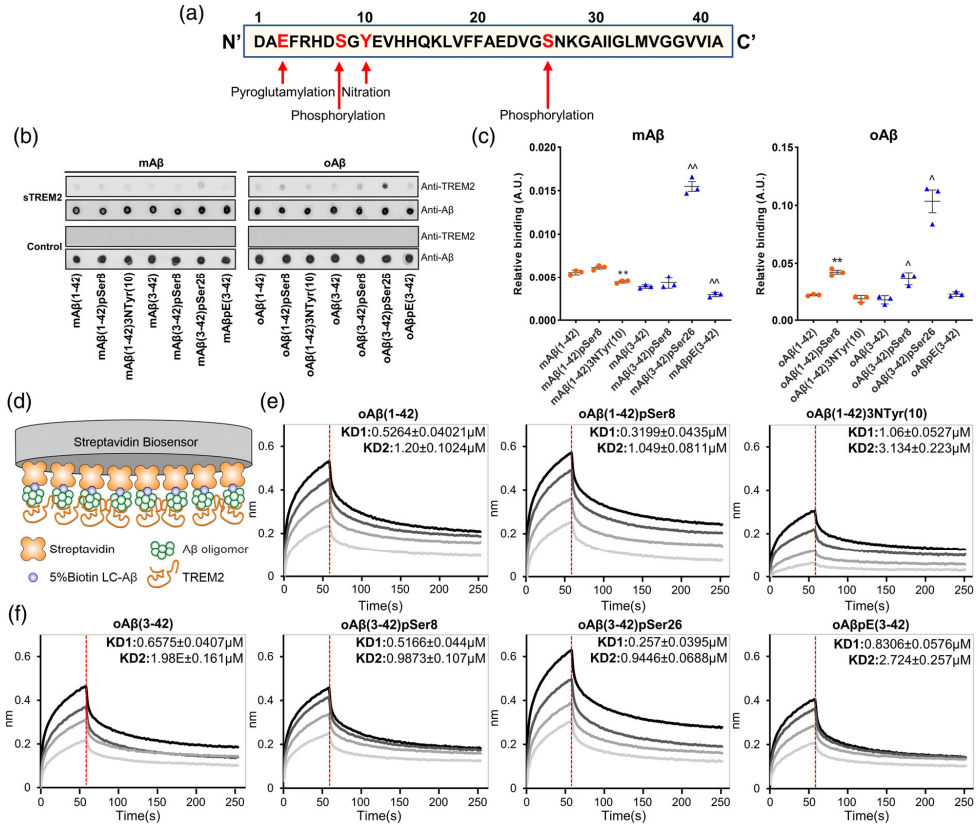

FIGURE 1 Differential interaction of TREM2 with modified Aβ variants. (a) Pictorial illustration of various PTMs of Aβ peptides used for binding assessment in this study. (b) Representative dot blot of various mAβ and oAβ variants spotted on the NC membrane followed by incubation with concentrated supernatant of control HEK293 Flp-In cells or transgenic sTREM2 expressing stable HEK293 Flp-In cells. (c) Quantification of ratio of signal intensity of sTREM2 detected with anti-TREM2 antibody and respective Aβ variants detected with 4G8 antibody. The average values of ratio from experimental triplicate of Aβ(1–42) variants are represented as "●" while of Aβ(3–42) variants are represented as "▲." * or ^represents a comparison of Aβ(1–42) or Aβ(3–42) variants respectively. (n = 3, unpaired *t* test with Welch correction, $^{*or\hat{}}p < .05$, $^{**or\hat{}\hat{}}p < .01$). (d) Schematics of BLI strategy using streptavidin (SA) biosensors. Biotinylated oAβ variants immobilized on SA biosensor to assess the interaction with TREM2 ectodomain at concentrations of 1, 2, 5, 10 μM. (e, f) Representative association/dissociation curves of varying TREM2 ectodomain concentrations and calculated KD1/KD2 values of TREM2 ectodomain binding with oAβ variants (see Table S1 for other set of values). *n* = 2, which includes repetition of the entire experiment including preparation and dilution of oAβ oligomers, KD-equilibrium dissociation constant

95°C for 5 min were separated according to their molecular weight on a precasted discontinuous Bis-Tris NuPAGE Novex 4%–12% gel (Invitrogen™, #V601020). Separation was achieved by using 1x NuPAGE™ MES SDS Running Buffer and a constant voltage of 120 V for 1 h. Gels were subsequently analyzed by western immunoblot analysis (Ibach et al., 2021; Kumar et al., 2021).

2.9 | Western immunoblotting

Proteins separated by SDS-PAGE were transferred to NC membranes as described previously (Ibach et al., 2021), at constant current of 400 mA and for 2 h. The membranes were then blocked for 1 h at constant agitation with a 5% milk solution, followed by incubation of the membrane over night at 4°C and constant agitation (orbital shaker) with a solution of the primary antibody in 1x TBS-T. The next day, the membranes were washed (3 × 5 min) followed by incubation with respective secondary antibody conjugated either to horseradish peroxidase or a fluorophore for 1 h at RT. The membranes were washed again (3 × 5 min) followed by detection of the protein with the Chemidoc XRS Imager (BioRad) or Odyssey® CLx (LI-COR Biosciences).

2.10 | Binding and phagocytosis assays

oAβ variants prepared as described in Method 2 were incubated with primary microglia from WT or TREM2^{T66M} transgenic mice. Cells were incubated with 1 μM of Aβ oligomers in DMEM GlutaMAX™ at 37°C

and 5% CO_2 for 2 h before they were fixed, permeabilized and stained. Coverslips were mounted on glass slides and observed using a VisiScope CSU-W1 spinning disk confocal microscope. As a control, cells were also pretreated with DMSO at a final concentration less than 0.01% and 10 μM Cytochalasin D (CytoD) dissolved in DMSO, keeping the final concentration of DMSO less than 0.01% for 30 min to block actin polymerization and thereby macropinoctytosis before changing to the assay conditions described before (Kim et al., 2017; Xiang et al., 2016).

In order to assess the binding of oAβ variants prepared as described in Method-2, primary microglia from WT and $TREM2^{T66M}$ transgenic mice seeded as described above were treated with 1 μM of oAβ in DMEM GlutaMAX™ and incubated on ice for 2 h followed by fixation and staining. In order to assess the uptake of bound Aβ, primary microglia were first incubated with 1 μM of oAβ in DMEM GlutaMAX™ on ice for 2 h. After this, the cells were washed and further incubated at 37°C and 5% CO_2 for 2 h. The cells were then fixed, permeabilized and stained.

2.11 | Immunocytochemistry of primary microglia

Cells were fixed for 15 min in 4% paraformaldehyde (PFA) before permeabilization with 0.1% Triton-X100 (PBS) for 5 min. After blocking with 3% BSA in PBS-T, 100 μl of primary antibody in 1% BSA was added to each coverslip and incubated at RT for 1 h. Coverslips were subsequently washed three times with 0.5% BSA in PBS-T. Afterwards, respective secondary antibodies in 1% BSA solution were added and coverslips were incubated for 1 h at RT in the dark, followed by another three washing steps. Finally, the coverslips were mounted on a microscopy slide using VECTASHIELD® antifade mounting medium with DAPI (Vector lab, #H-1200).

2.12 | Transgenic mice

Wild-type and homozygous $TREM2^{T66M}$ crossed to APPKM670/671NL; PS1ΔE9 transgenic mice were obtained from Taconic Biosciences GmbH, and were all of the C57BL/6 genetic background. Mice were housed under standard conditions at 22°C and a 12 h light–dark cycle with free access to food and water. Animal care and handling of these mice was performed according to the Declaration of Helsinki and approved by the local ethical committees (LANUV NRW 84–02.04.2017.A226).

APP695KM670/671NL; PS1L166P transgenic mice with endogenous TREM2 or the TREM2 deletion ($TREM2^{-/-}$) mice were described previously (Parhizkar et al., 2019; Turnbull et al., 2006).

2.13 | Immunofluorescence analysis of mouse brains

Mouse brain samples were processed as described previously (Kumar et al., 2021; Parhizkar et al., 2019), and 20–25 μm sections collected in PBS for staining. For immunofluorescence (IF) staining, heat-induced sodium citrate antigen retrieval (pH 6.0) using 10 mM sodium citrate with 0.05% Tween-20 at 95°C for 30 min or 80% formic acid treatment for 8 min (Gerth et al., 2018) was employed depending on various Aβ species. Sections were then washed once with PBS. For X-34 staining, sections were treated with 100 μM of X-34 prepared in 60% PBS/40% EtOH mix (pH was adjusted with 1 M NaOH) for 10 min at RT (Parhizkar et al., 2019; Styren et al., 2000). The sections were washed briefly with 60% PBS/40% EtOH and subjected to permeabilization with 0.3% Triton X-100 for 30 min before blocking for 2 h in 5% NHS and 2.5% BSA prepared in 1xPBS. Mouse on Mouse Blocking Reagent (Vector laboratories, #MKB-2213) was used for primary antibodies generated in mouse or rat at a dilution of 1 drop/1000 μl. Primary antibodies (Table S2) were added and the sections kept at 4°C overnight. After adding the appropriate secondary antibodies (Table S2), tissue sections were mounted onto slides by using VECTASHIELD® Hardset™ antifade mounting medium (Vector lab, #H-1400) or VECTASHIELD® antifade mounting medium with DAPI (Vector laboratories, #H-1200).

2.14 | Confocal imaging and data analysis

Images were acquired using VisiScope CSU-W1 spinning disk confocal microscope and VisiView Software (Visitron Systems GmbH). Laser and detector settings were maintained constant for the acquisition of each immunostaining. For all analyses, at least two images were acquired using x20, x40W or x63W (W: water immersion) objective at 2048 × 2048 pixels, with z-step size of 1 μm.

For quantification of microglial binding and uptake of Aβ, IntDen was calculated by manually drawing border around randomly selected Aβ positive microglia. Representation of ratio of Aβ positive microglia/total microglia was done by manually counting Aβ positive cells and automatically counting DAPI positive total cells for 10 images/experiment (5 images per coverslips and the experiments were in duplicates).

For analysis of internalized pSer26-Aβ in transgenic mouse brain, number of plaque associated microglia were manually counted in 500 × 500 μm areas of somatosensory cortex (SSC) on 1–2 independently stained sections and then represented as the ratio of pSer26-Aβ positive microglia/total Iba1 positive microglia.

2.15 | Statistical analysis

Statistical analyses were performed using Prism (GraphPad Software). Unless otherwise stated, two-sided, unpaired student's *t* tests with Welch's correction was used to determine the statistical difference between groups in analyses that only required single comparisons. The degree of significance between groups is represented as $^{*}p < .05$, $^{**}p < .01$, $^{***}p < .001$, $^{****}p < .0001$, and $^{ns}p > .05$.

2.16 | Randomization and blinding

The primary microglia experiments and the immunofluorescence analysis of mouse brains were initially performed blinded with coded slides. However, complete randomization was not possible with the stainings of mouse brain sections with a microglial marker depicting microglial clustering. Following the completion of the analysis, the groups were unblinded to perform statistics.

2.17 | Data collection

The BLI data were acquired and analyzed by using Octet RED384 and data analysis 9.0 (Forte Bio). The TEM images were acquired by using Talos L120C (Thermofischer Scientific). Confocal images were acquired by using VisiScope CSU-W1 spinning disk confocal microscope and VisiView Software (Visitron Systems). The western immunoblotting data were acquired by using by enhanced chemiluminescence using Chemidoc XRS Imager (BioRad) or Odyssey® CLx (LI-COR Biosciences). Microsoft Excel was used to organize and to calculate the averages of each repeated experiment. Graph Pad (Prism v7.0) was used to build graphs and perform statistical analyses presented throughout the manuscript.

3 | RESULTS

3.1 | Differential binding of TREM2 to post-translationally modified Aβ species

In order to investigate the interaction of TREM2 with different Aβ species (Figure 1a), we first assessed the binding of soluble TREM2 (sTREM2) to monomeric (mAβ) and oligomeric (oAβ) forms of distinct post-translationally modified and non-modified Aβ variants in dot blot assays. For this, different Aβ variants in monomeric and oligomeric form were spotted onto Nitrocellulose (NC) membranes and incubated with sTREM2 obtained from conditioned media of transgenic cells expressing a TREM2 variant with a stop codon at position 158 thereby representing the soluble TREM2 ectodomain that is physiologically generated by proteolytic processing of full-length TREM2 (Feuerbach et al., 2017; Schlepckow et al., 2017; Thornton et al., 2017; Wunderlich et al., 2013). sTREM2 bound to the different Aβ species was detected by an anti-TREM2 antibody (4B2A3). This antibody recognizes an epitope within the stalk region of TREM2 (aa 131–148) (Ibach et al., 2021), thereby avoiding possible competition with ligands bound to the ligand binding domain of sTREM2. Consistent with previous reports, TREM2 showed strongly increased interaction with oligomeric as compared with monomeric Aβ variants (Figures 1b,c and S1). Oligomers formed by Aβ variants phosphorylated at Ser8 (pSer8-Aβ) or Ser26 (pSer26-Aβ) showed significantly increased interaction with TREM2 as compared with non-modified, nitrated or pyroglutamate-modified variants. With monomeric forms, pSer26-Aβ also showed strongly increased binding to TREM2 as compared to non-modified Aβ or otherwise modified Aβ variants. However, it should be noted that pSer26-Aβ has the highest tendency to form oligomeric assemblies (Kumar et al., 2016), and it cannot be excluded that pSer26-Aβ formed some oligomeric assemblies during this assay.

To validate these findings with an independent method, we utilized BLI (Figure 1d). The different Aβ variants were mixed with Biotin-labeled-Aβ at a ratio of 20:1 and oligomerized as described previously (Vilalta et al., 2021). Oligomer preparations were immobilized on streptavidin biosensors (Figure 1d) and kinetic binding assays performed using purified TREM2 ectodomain at different concentrations (1, 2, 5, and 10 μM). BLI kinetic studies also revealed increased binding of the TREM2 ectodomain to oligomers that contained pSer8-Aβ or pSer26-Aβ (Figure 1e,f). The lowest binding was measured for nitrated Aβ3NTyr(10) as compared with non-modified Aβ (Figure 1e). Oligomeric pyroglutamate modified Aβ (pEAβ) also showed lower binding to the TREM2 ectodomain as compared with non-modified Aβ. (Figure 1f, Table S1).

Pull-down assays from mixtures containing monomeric and oligomeric forms of Aβ using sTREM2-Fc fusion proteins further demonstrated that sTREM2 preferentially binds to oligomeric Aβ assemblies. Again, highest binding was detected for phosphorylated Aβ oligomers as compared with non-modified Aβ species (Figure 2a,b). The combined data from different biochemical and biophysical assays demonstrate that phosphorylation of Aβ at Ser8 or Ser26 increased binding to TREM2 in particular for oligomeric Aβ assemblies.

3.2 | TREM2 dependent binding and phagocytosis of modified Aβ species by primary microglia

To further characterize the interaction of Aβ species with TREM2 and its functional implications, we used primary microglia from wild-type (WT) mice expressing endogenous TREM2 and mice with the $TREM2^{T66M}$ knock-in (KI) mutation. The $TREM2^{T66M}$ mutation is associated with Nasu Hakola disease (NHD) or frontal lobe dementia (FTD) and strongly impairs ectodomain folding and cell surface transport of the receptor thereby causing a loss of function (Kleinberger et al., 2014; Le Ber et al., 2014). First, we assessed the binding of phosphorylated and non-modified Aβ species to the plasma membrane of primary microglia from WT mice by incubation of cells on ice to halt endocytosis (Tamboli et al., 2008; Wesen et al., 2017). While the membrane-association of pSer8-Aβ was lower, that of pSer26-Aβ was increased as compared with binding of non-modified Aβ (Figure 3a,b), indicating phosphorylation-site and phosphorylation-state specific interaction of Aβ with the microglial surface. Decreased binding of pSer8-Aβ was observed for the two length variants of Aβ, 1–42 and 3–42. Since Aβ(1–42)pSer26 could not be chemically synthesized, the analysis was restricted to Aβ(3-42)pSer26 and compared with non-modified Aβ(3–42) and Aβ(3-42)pSer8 species, respectively. Importantly, binding of the different Aβ species was reduced by about 50% in $TREM2^{T66M}$ expressing microglia as compared with TREM2 WT expressing microglia (Figure 3a,b). On one hand, these results

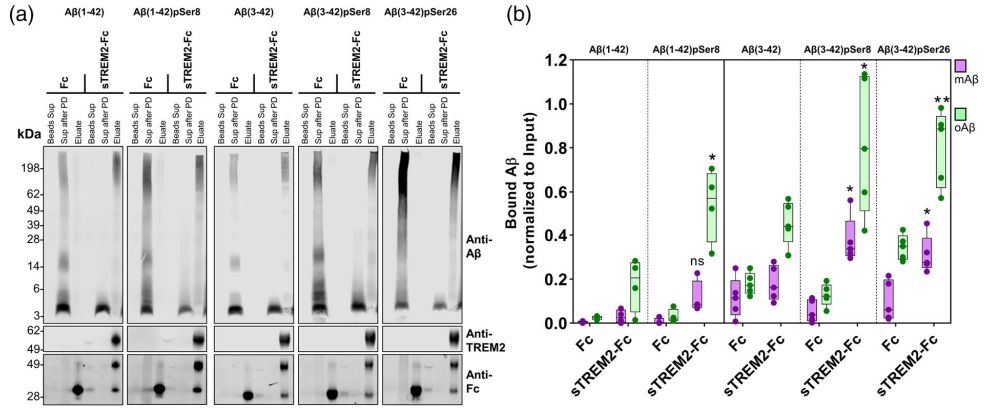

FIGURE 2 Increased interaction of TREM2 with oligomeric phosphorylated Aβ variants. (a) Representative western immunoblot of samples from pull-down (PD) experiments for oAβ with sTREM2-Fc or with Fc alone as a control. Efficient pre-coupling of sTREM2-Fc or Fc alone to protein-G magnetic beads is confirmed by the depletion of these proteins from the buffer solution in the supernatant after pre-incubation of beads ("Beads sup" lanes). A preferential pull-down of oAβ by sTREM2 is indicated by robust signals for aggregated forms of Aβ in the "Eluate" fractions detected in the upper regions of the gels, while large portions of mAβ remains in the supernatant after the pull-down ("Sup after PD"). (b) Box and whiskers plot of IntDen of signals for the monomer band or oligomeric forms. Values were normalized to the respective input. Each dot represents an independent experiment. All data represent mean ± *SEM* ($n = 4$ for Aβ(1–42) or $n = 5$ for Aβ(3–42) variants, unpaired *t* test with Welch correction, $^{*}p < .05$, $^{**}p < .01$, $^{ns}p > .05$)

demonstrate the involvement of functional TREM2 in the binding of the different Aβ species, and on the other hand, support previous reports showing that the association of Aβ to microglia could also involve additional proteins or lipids present at the cell surface (Verdier et al., 2004; Yu & Ye, 2015). When cells were further incubated at 37°C upon binding of Aβ to the surface, we observed differential uptake of bound Aβ depending on the phosphorylation state (Figure 3c,d). While the amount of internalized pSer8-Aβ was lower, the amount of internalized pSer26-Aβ was higher as compared with that of unphosphorylated Aβ. In addition, the number of Aβ positive microglia was lower for pSer8-Aβ exposed cells, but higher for pSer26-Aβ exposed cells as compared with the number of microglia that internalized unphosphorylated Aβ (Figure S2a,b). The phosphorylation-state dependent internalization of Aβ variants in TREM2 WT microglia might involve differences in the aggregation and/or conformation of pSer8-Aβ and pSer26-Aβ (Kumar et al., 2011; Kumar et al., 2012; Kumar et al., 2016). Phosphorylation-state dependent uptake of Aβ was also observed when cells were exposed to Aβ without a precedent binding period, and was reduced by cytochalasin D, indicating the involvement of phagocytosis (Figures 4a,b and S2). Again, the phagocytosis of the different Aβ species was strongly reduced in microglia from TREM2^{T66M} KI mice, demonstrating that the differential uptake of phosphorylation-state variants of Aβ depends on functional TREM2 (Figure 4). Co-staining with Lamp-1 revealed partial localization of internalized Aβ in lysosomal compartments (Figures 3 and 4). Lysosomal localization was particularly pronounced for pSer26-Aβ, indicating lysosomal accumulation of this phosphorylated Aβ form. These results indicate that the phosphorylation state of Aβ affects its TREM2 dependent binding and phagocytosis by microglia. However, in addition to the differential interaction with TREM2, peculiar differences in the aggregation characteristics and conformation of the phosphorylation-state variants of Aβ could contribute to the differential interaction and uptake by microglia.

3.3 | TREM2 deletion leads to altered deposition of phosphorylated Aβ variants

To further investigate the role of TREM2 in the interaction of different phosphorylated Aβ species with microglia in vivo, we used APP transgenic mice that express endogenous TREM2 or mice with a TREM2 knockout mutation. Similar to previous studies (Wang et al., 2015; Yuan et al., 2016; Zhao et al., 2018), we also observed decreased microglial clustering around X-34 positive plaques in brains of TREM2$^{-/-}$ mice as compared with TREM2$^{+/+}$ mice (Figure 5a,b). Interestingly, mice homozygous for the TREM2^{T66M} mutation also showed reduced clustering around X-34 positive plaques that contain fibrillar Aβ (Figure 5c,d). Immunostaining of brain sections with antibodies against the microglial marker protein Iba1 together with phosphorylation-state specific antibodies for Aβ with Ser8 in phosphorylated or non-modified state (nmAβ) revealed that X-34 positive plaques also contained Ser8-phosphorylated and unphosphorylated (nmAβ) species that are surrounded by microglia in TREM2 WT mice (Figure 5). In contrast, brains of TREM2$^{-/-}$ (Figure 5a,b) or TREM2^{T66M} expressing mice (Figure 5c,d) showed increased radial extensions of fibrillar Aβ that are intermingled with microglial processes thereby forming

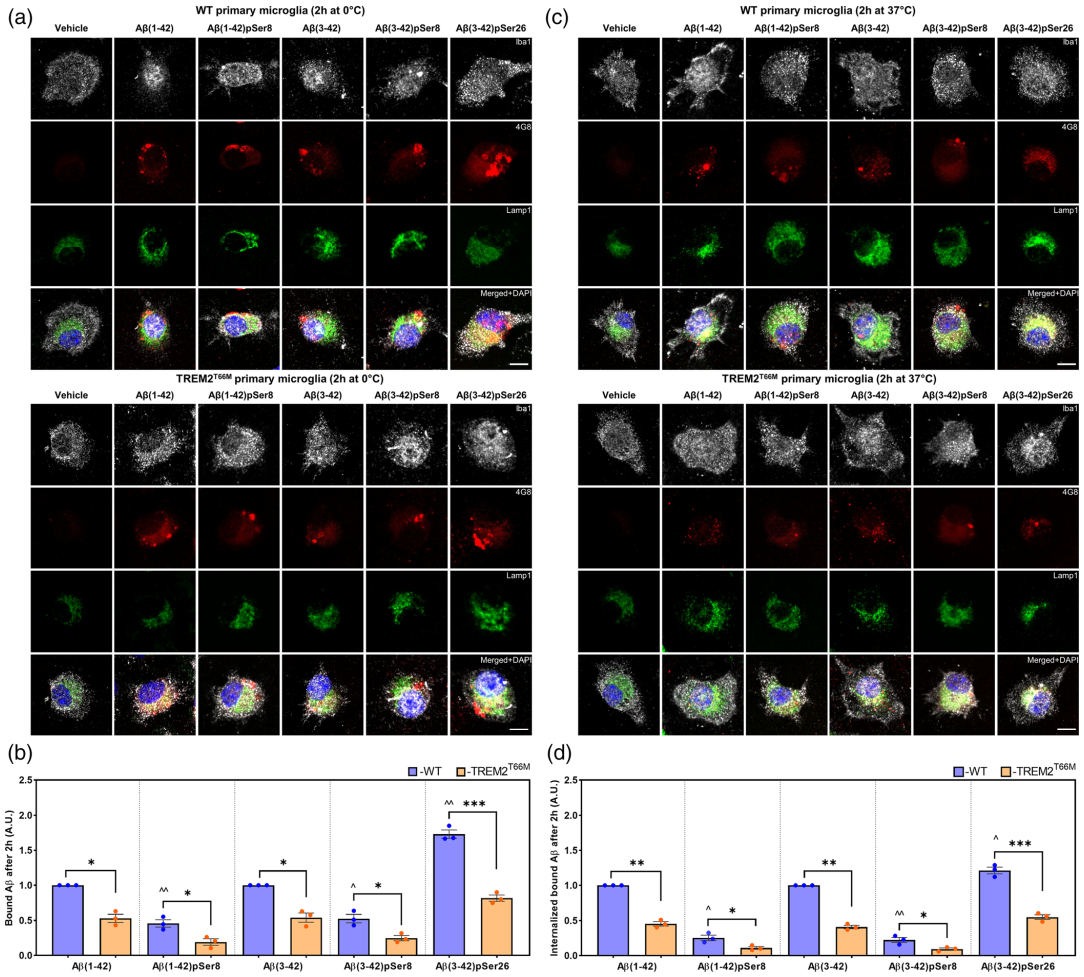

FIGURE 3 Involvement of functional TREM2 in surface binding and subsequent uptake of phosphorylated Aβ variants by primary microglia. (a) Representative immunocytochemical staining images of primary microglia from wild-type (WT) and TREM2^{T66M} mice, and (b) plot showing the normalized IntDen of oAβ positive cells after treatment with 1 μM oAβ for 2 h at 0°C followed by fixation and staining. (c) Representative immunocytochemical staining images of primary microglia from WT and TREM2^{T66M} mice, and (d) plot representing the uptake of bound oAβ levels calculated from IntDen of oAβ positive cells after treatment with 1 μM oAβ variants for 2 h at 0°C, followed by washing and incubating at 37°C for 2 h followed by fixation and staining. Microglial cells were stained using Iba1 antibody (white) while Aβ was stained via the generic antibody 4G8 (red). Lamp1 antibody was employed as a lysosomal marker (green) (Scale bar = 10 μm, 63xW). IntDen of oAβ (either 1–42 or 3–42) for WT primary microglia was set as 1 for normalization of values for pSer8 and pSer26-phosphorylated oAβ species and accordingly values for TREM2^{T66M} were calculated. Each dot represents the average value of normalized IntDen/experiment. Data represent mean ± *SEM* ($n = 300$ cells/group, experimental $n = 3$, unpaired *t* test with Welch correction, $^{*or\ \hat{}}p < .05$, $^{**or\ \hat{}\hat{}}p < .01$ $^{***}p < .001$ for comparison of WT and TREM2^{T66M}, A.U.-arbitrary units). $\hat{}$represents comparison of phosphorylated Aβ variants with Aβ (1–42 or 3–42) treated to WT primary microglia

mesh-like structures with various degrees of compaction (indicated by arrow heads, Figure 5). Very similar observations on the morphology of Aβ deposits and interactions with microglia in brains of TREM2$^{+/+}$ and TREM2$^{-/-}$ mice were also made when Aβ was detected by a monoclonal antibody (82E1) that detects the N-terminus of Aβ independent on its phosphorylation state (Figure S3). These findings are consistent with the function of TREM2 to restrict plaque size or growth (Wang et al., 2015; Yuan et al., 2016). It is important to note that TREM2 positive plaque associated microglia also restrict pSer8-Aβ deposits, which could

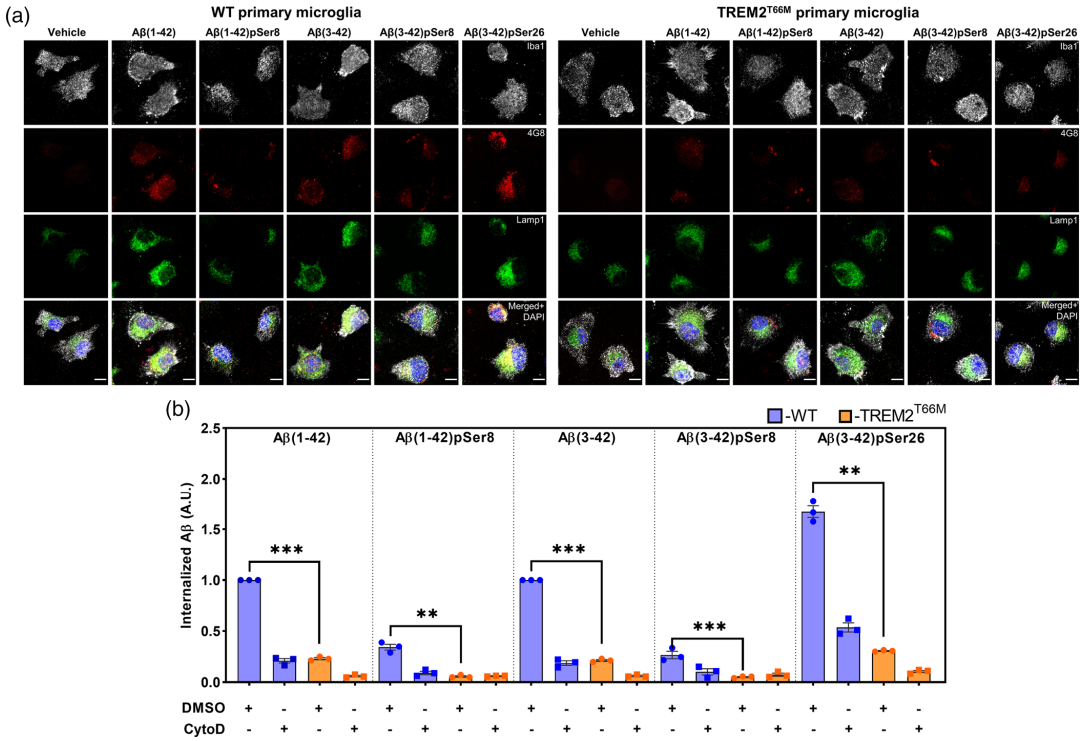

FIGURE 4 Differential phagocytosis of phosphorylated Aβ variants by primary microglia. (a) Representative immunocytochemical staining images of primary microglia from wild-type (WT) and TREM2^{T66M} mice after pretreatment with vehicle (DMSO) or CytoD (Figure S2a) treatment for 30 min followed by treatment with 1 μM oAβ for 2 h at 37°C. Microglial cells were stained using Iba1 antibody (white), and Aβ by antibody 4G8 (red). Lamp1 antibody was employed as a lysosomal marker (green) (Scale bar = 10 μm, 63xW). (Scale bar = 10 μm, 63xW). (b) Plot representing the internalization of different oAβ variants by primary microglia from WT and TREM2^{T66M} mice calculated by the IntDen of internalized Aβ. Each dot represents the average value of normalized IntDen of Aβ positive microglia/experiment. Data represent mean ± *SEM* ($n = 300$ cells/group, experimental $n = 3$, unpaired *t* test with Welch correction, $^{**}p < .01$, $^{***}p < .001$ for comparison of WT and TREM2^{T66M}, A.U.-arbitrary units)

be due to enhanced TREM2 binding. However, little if any pSer8-Aβ was detected within microglia (Figure 5a,c).

In contrast to pSer8-Aβ, pSer26-Aβ was abundant within microglia (Figure 6), consistent with the observed increased binding and TREM2-dependent internalization by microglia (see Figures 1–4). Deposition of pSer26-Aβ was detected in the two independent APP transgenic mouse models used in this study (Figure 6). However, in contrast to fibrillar Aβ detected by X-34 or pSer8-Aβ, pSer26-Aβ species were only faintly detected in the core of dense Aβ plaques and rather appeared as small deposits in close proximity of extracellular plaques (Figure 6a,c). Co-immunostaining of pSer26 with Iba1 and Lamp1 revealed lysosome associated pSer26-Aβ within plaque associated microglia in the different APP transgenic mouse models expressing TREM2$^{+/+}$, that was strongly reduced in APP transgenic mice deficient of TREM2 (Figure 6a,b) or expressing the TREM2^{T66M} KI mutation (Figure 6c,d).

4 | DISCUSSION

Here, we show the differential interaction of TREM2 and post-translationally modified Aβ species with oligomers formed by phosphorylated Aβ variants binding most avidly to TREM2. In addition, our data demonstrate the involvement of TREM2 in the binding and uptake of distinct phosphorylation-state variants of Aβ by microglia in vitro and in vivo.

Alternative proteolytic processing of APP and post-translational modifications results in the formation and deposition of a variety of Aβ peptides during the pathogenesis of AD (Barykin et al., 2017; Kummer & Heneka, 2014). Among the different modifications, phosphorylation at Ser8 promotes the fibrillization of Aβ, while phosphorylation at Ser26 rather decreases fibrillization, but stabilizes oligomeric assembly (Kumar et al., 2011; Kumar et al., 2016; Rezaei-Ghaleh et al., 2016). In addition, the phosphorylation at Ser8 increased the stability of Aβ against degradation by microglial cells (Kumar

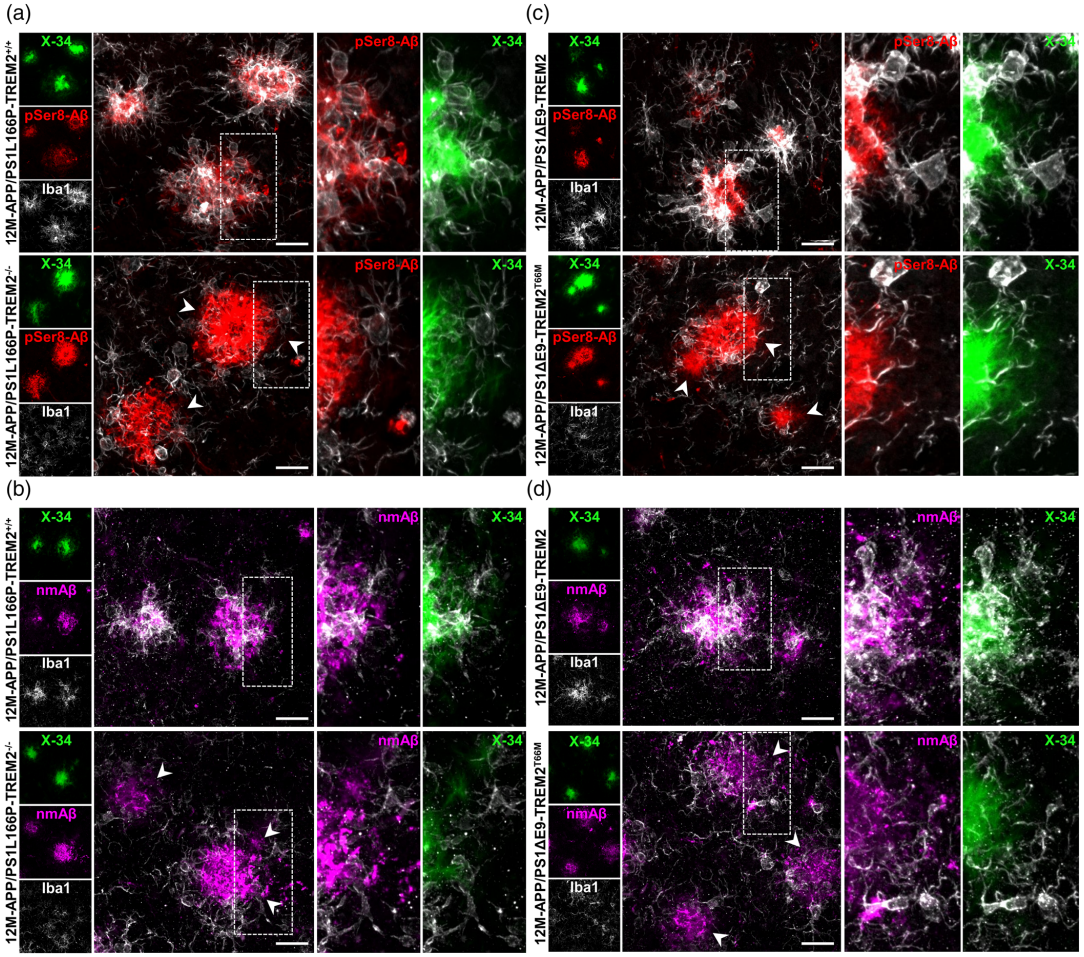

FIGURE 5 Decreased microglial barrier function alters deposition of pSer8-Aβ and nmAβ in brains of TREM2 deficient mice (a, b) Representative IF images of extracellular plaques stained for pSer8-Aβ (a) and nmAβ (b) in 12 M-APP/PS1L166P-TREM2$^{+/+}$ and TREM2$^{-/-}$ mice. Fibrillar Aβ was detected by X-34 and microglia were stained with Iba1. (c, d) Representative IF images of extracellular plaques stained for pSer8-Aβ (c) and nmAβ (d) in 12 M-APP/PS1ΔE9-TREM2 and APP/PS1ΔE9-TREM2^{T66M} mice. Fibrillar Aβ was detected by X-34 and microglia were stained with Iba1. Dotted white boxes indicate the area shown at higher magnification while the arrowheads indicate the mesh-like structures that surround the plaques of varying compaction in TREM2$^{-/-}$ or TREM2^{T66M} mice. (Scale bar = 20 μm, 40xW)

et al., 2012). pSer8-Aβ could also seed aggregation of unphosphorylated Aβ (Hu et al., 2017; Kumar et al., 2011). Consistent with previous findings, we found that TREM2 binds much stronger to oligomeric Aβ assemblies than to monomeric Aβ (Lessard et al., 2018; Zhao et al., 2018). Furthermore, despite having distinct aggregation kinetics and stability, both phosphorylated Aβ species in oligomeric form showed the strongest interaction with TREM2.

We also show phosphorylation-state and phosphorylation-site specific uptake of Aβ by primary microglia. Notably, while the uptake of pSer8-Aβ was decreased, the internalization of pSer26-Aβ was increased as compared with that of non-modified Aβ. The uptake of all Aβ species was significantly reduced in microglia expressing the TREM2^{T66M} loss of function mutation that is associated with NHD and frontal lobe degeneration (Guerreiro, Bilgic, et al., 2013; Guerreiro, Lohmann, et al., 2013; Paloneva BM et al., 2001). This mutation causes misfolding and strongly decreases the expression of TREM2 at the cell surface (Kleinberger et al., 2014). Thus, these data indicate that cell surface localized TREM2 is important for the regulation of Aβ phagocytosis. However, additional components of the microglial surface,

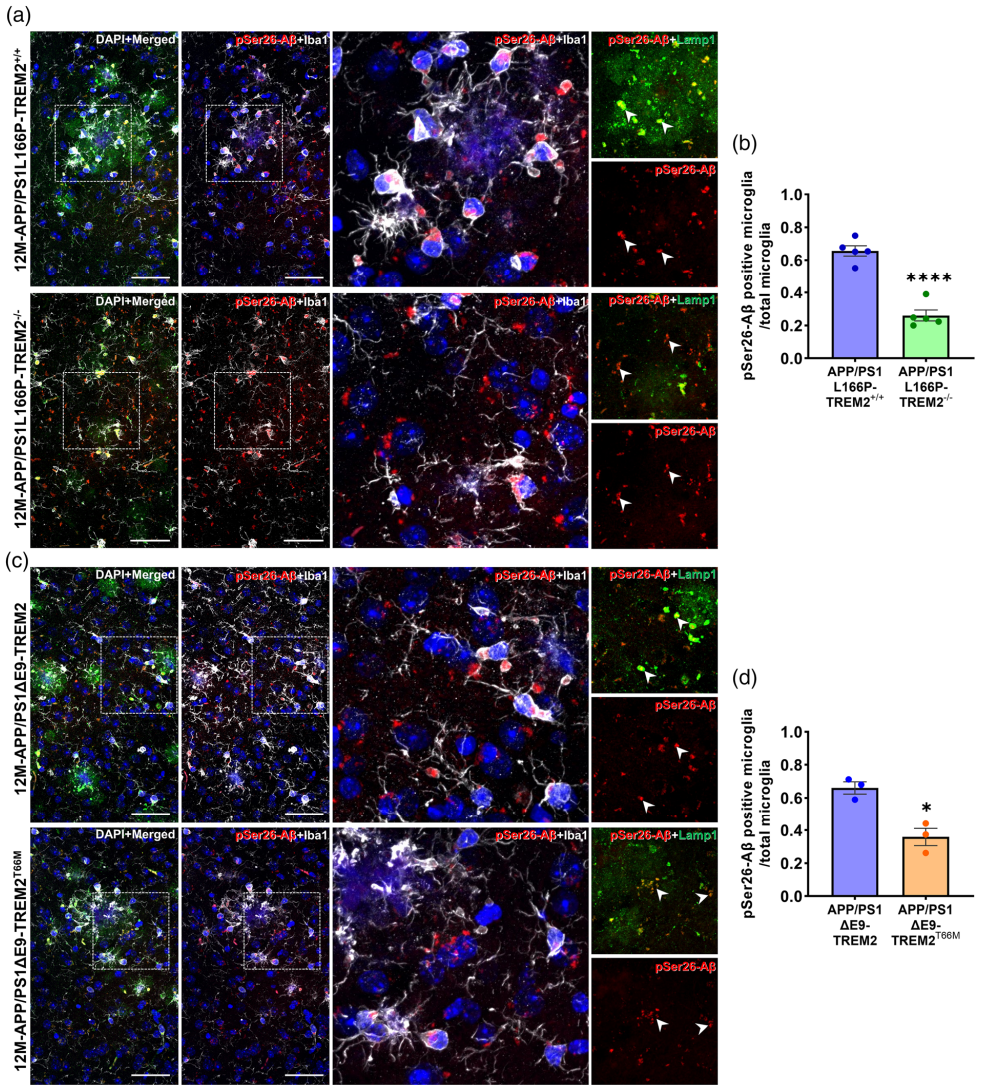

FIGURE 6 Loss of TREM2 function leads to decreased microglial pSer26-Aβ deposits in brains of TREM2 transgenic mice. (a) Representative IF images of SSC regions of 12 M-APP/PS1L166P-TREM2$^{+/+}$ and TREM2$^{-/-}$ mice co-stained for pSer26-Aβ along with the lysosomal marker Lamp1, and the microglial marker Iba1 (Scale bar = 50 μm, 40xW, dotted white boxes indicate the area shown at higher magnification). (b) Quantification of microglia per cortical region of interest (ROI) showed a decreased number of pSer26-Aβ positive microglia (indicated with arrowheads) in the 12 M-APP/PS1L166P-TREM2$^{-/-}$ compared with TREM2$^{+/+}$ mice (t[7.976] = 8.615, ****p < .0001). (c) Representative IF images of pSer26-Aβ stained SSC of 12 M-APP/PS1ΔE9-TREM2 and TREM2^{T66M} mice along with the lysosomal marker, Lamp1 and microglial marker, Iba1 (Scale bar = 50 μm, 40xW, dotted white boxes indicate the area shown at higher magnification). (d) Quantification of microglia per cortical region of interest (ROI) showed a decreased number of pSer26-Aβ positive microglia (indicated with arrowheads) in the 12 M-APP/PS1ΔE9-TREM2^{T66M} compared with APP/PS1ΔE9-TREM2 mice (t [3.577] = 4.739,*p = .0118). All data represent mean ± *SEM*. (n = 5 animals (6b) or n = 3 animals (6d), unpaired t test with Welch correction)

including receptor proteins and membrane lipids could also be involved in the interaction and uptake of different Aβ variants (Mandrekar et al., 2009; Verdier et al., 2004; Yu & Ye, 2015). In addition, peculiar effects of phosphorylation at Ser8 and Ser26 on the conformation and aggregation of Aβ could also contribute to the differential interaction with TREM2 and handling of the peptides by microglia (Kumar et al., 2011; Kumar et al., 2012; Kumar et al., 2016).

Appendix-1

To assess the role of TREM2 in the deposition of phosphorylated Aβ species in vivo, we used two different APP/PS1 transgenic mouse models crossed to TREM2 WT, TREM2$^{-/-}$ mice or TREM2^{T66M} mice. Consistent with previous findings (Boon et al., 2020; Kumar et al., 2013; Kumar et al., 2016), pSer8-Aβ and pSer26-Aβ showed differential deposition. While pSer8-Aβ deposits primarily in the core of extracellular plaques, pSer26-Aβ showed limited deposition in these lesions (Boon et al., 2020; Kumar et al., 2021). Importantly, pSer8-Aβ was hardly detected within microglia, but mainly deposited as fibrillar Aβ in the plaque core which also contained N-terminally non-modified Aβ. These data are in line with the fibrillization-promoting effect of Aβ phosphorylation at Ser8 (Kumar et al., 2011). Thus, although microglia could bind Ser8-Aβ containing aggregates, their internalization might be restricted by the high compaction of these peptides within the plaque core. In contrast, pSer26-Aβ was prominently detected within plaque-associated microglia. Since the phosphorylation at Ser26 prevents fibrillization but stabilizes oligomeric states of Aβ (Kumar et al., 2016; Rezaei-Ghaleh et al., 2014), soluble pSer26-Aβ assemblies might efficiently bind to TREM2 and be internalized.

Pyroglutamate modified and nitrated Aβ did not show increased binding to TREM2. In contrast to phosphorylation, pyro-glutamination and nitration do not change the overall charge of Aβ. Since TREM2 preferentially binds anionic ligands (Kober & Brett, 2017; Ulrich et al., 2017; Walter, 2016), the additional negative charges introduced by phosphorylation, likely contribute to the increased association of phosphorylated Aβ with TREM2. However, additional effects of distinct post-translational modifications on the conformation and aggregation status of Aβ assemblies could also modulate binding to TREM2. Further, distinct post-translational modifications could affect phagocytosis and degradation pathways of these species as well as their deposition and neurotoxic properties independent on TREM2. Indeed, phosphorylation, nitration, and pyro-glutamination of Aβ differentially affect the aggregation and neurotoxicity of Aβ in in vitro systems without the involvement of TREM2 (Dammers et al., 2015; Kumar et al., 2016; Kummer et al., 2011; Nussbaum et al., 2012). Thus, it will be interesting to further dissect the relative contribution of TREM2 and microglia in the deposition and neurotoxic properties of the different Aβ species in the brain during the pathogenesis of AD.

It should be noted that the deposition of non-modified, pyroglutamate-modified, and phosphorylated Aβ species follows a specific sequence in the brain with initial deposits not containing detectable amounts of pyro-glutaminated or phosphorylated Aβ species (Gerth et al., 2018; Rijal Upadhaya et al., 2014; Thal et al., 2019). While pyro-glutaminated Aβ variants can also be detected in a subset of cases without clinical signs of dementia, detection of phosphorylated Ser8-Aβ is mainly restricted to cases with clinical manifestation of AD (Rijal Upadhaya et al., 2014; Thal et al., 2019). As mentioned above, pSer26-Aβ species show limited deposition in extracellular plaques, but are also found intraneuronally and in vascular deposits (Kumar et al., 2016; Kumar et al., 2021). Thus, post-translational modifications likely contribute to the specific accumulation and differential deposition in the brain and could represent interesting targets for AD therapy. Indeed, recent data from phase 2 clinical trials revealed positive effects of antibodies specifically recognizing pyroglutamate modified Aβ (Donanemab) in early AD (Mintun et al., 2021). Thus, it will be important to further assess the potential of targeting phosphorylated Aβ species in AD therapy and prevention.

ACKNOWLEDGMENT

This work was supported by the Deutsche Forschungsgemeinschaft, Grant WA1477/6-6 (to Jochen Walter), the EU Innovative Medicines Initiative 2 Joint Undertaking (IMI2 JU), Grant/Award Number: No 115976 (PHAGO), the Canadian Institutes of Health Research (CIHR) operating grant PJT17349 (to Paul E. Fraser) and the Canadian Institutes of Health Research (Foundation Award to Peter St George-Hyslop), US Alzheimer Association (Zenith Award- to Peter St George-Hyslop); UK Alzheimer Society and ARUK (to Peter St George-Hyslop), Wellcome Trust Collaborative Award in Science (to Peter St George-Hyslop). Pranav Joshi thanks the BIGS neuroscience and the University of Bonn for IPID4all-DAAD travel grant. Authors thank the Microscopy Core Facility of the Medical Faculty at the University of Bonn for providing support and instrumentation funded by the Deutsche Forschungsgemeinschaft, Project number: 388169927. Open Access funding enabled and organized by Projekt DEAL.

CONFLICT OF INTEREST

The authors declare no competing financial interests.

AUTHOR CONTRIBUTIONS

Pranav Joshi, Paul E. Fraser, Peter St George-Hyslop, and Jochen Walter conceived the study. Pranav Joshi performed most of the experiments and analyzed data. Florian Riffel contributed to cell biological and biochemical interaction studies. Pranav Joshi, Kanayo Satoh, and Masahiro Enomoto performed and analyzed BLI experiments. Seema Qamar purified TREM2 ectodomain for the BLI experiments. Sandra Theil and Sathish Kumar purified modification-specific monoclonal antibodies. Hannah Scheiblich, Nàdia Villacampa, and Michael T. Heneka prepared primary mouse microglia and provided mouse brains. Pranav Joshi and Jochen Walter wrote the manuscript with help from Kanayo Satoh, Paul E. Fraser, and further input from all co-authors. All of the authors read, edited, and approved the final version of the manuscript.

DATA AVAILABILITY STATEMENT

The data of this study is available from the corresponding author upon reasonable request.

ORCID

Pranav Joshi https://orcid.org/0000-0002-1153-0440
Florian Riffel https://orcid.org/0000-0001-8594-100X
Nàdia Villacampa https://orcid.org/0000-0001-6513-0250
Sathish Kumar https://orcid.org/0000-0002-2792-7047
Samira Parhizkar https://orcid.org/0000-0001-5807-190X
Jochen Walter https://orcid.org/0000-0002-4678-2912

Appendix-1

REFERENCES

Anderson, V. L., Ramlall, T. F., Rospigliosi, C. C., Webb, W. W., & Eliezer, D. (2010). Identification of a helical intermediate in trifluoroethanol-induced alpha-synuclein aggregation. *Proceedings of the National Academy of Sciences of the United States of America*, *107*(44), 18850–18855. https://doi.org/10.1073/pnas.1012336107

Aricescu, A. R., Lu, W., & Jones, E. Y. (2006). A time- and cost-efficient system for high-level protein production in mammalian cells. *Acta Crystallographica. Section D, Biological Crystallography*, *62*(Pt 10), 1243–1250. https://doi.org/10.1107/S0907444906029799

Backliwal, G., Hildinger, M., Hasija, V., & Wurm, F. M. (2008). High-density transfection with HEK-293 cells allows doubling of transient titers and removes need for a priori DNA complex formation with PEI. *Biotechnology and Bioengineering*, *99*(3), 721–727. https://doi.org/10.1002/bit.21596

Bailey, C. C., DeVaux, L. B., & Farzan, M. (2015). The triggering receptor expressed on myeloid cells 2 binds Apolipoprotein E. *The Journal of Biological Chemistry*, *290*(43), 26033–26042. https://doi.org/10.1074/jbc.M115.677286

Barykin, E. P., Mitkevich, V. A., Kozin, S. A., & Makarov, A. A. (2017). Amyloid beta modification: A key to the sporadic Alzheimer's disease? *Frontiers in Genetics*, *8*, 58. https://doi.org/10.3389/fgene.2017.00058

Boon, B. D. C., Bulk, M., Jonker, A. J., Morrema, T. H. J., van den Berg, E., Popovic, M., Walter, J., Kumar, S., van der Lee, S. J., Holstege, H., Zhu, X., van Nostrand, W. E., Natté, R., van der Weerd, L., Bouwman, F. H., van de Berg, W. D. J., Rozemuller, A. J. M., & Hoozemans, J. J. M. (2020). The coarse-grained plaque: A divergent Abeta plaque-type in early-onset Alzheimer's disease. *Acta Neuropathologica*, *140*(6), 811–830. https://doi.org/10.1007/s00401-020-02198-8

Burgess, R. R. (2009). Protein precipitation techniques. *Methods in Enzymology*, *463*, 331–342. https://doi.org/10.1016/s0076-6879(09)63020-2

Condello, C., Yuan, P., Schain, A., & Grutzendler, J. (2015). Microglia constitute a barrier that prevents neurotoxic protofibrillar Abeta42 hotspots around plaques. *Nature Communications*, *6*, 6176. https://doi.org/10.1038/ncomms7176

Dammers, C., Gremer, L., Reiß, K., Klein, A. N., Neudecker, P., Hartmann, R., Sun, N., Demuth, H. U., Schwarten, M., & Willbold, D. (2015). Structural analysis and aggregation propensity of Pyroglutamate Abeta(3-40) in aqueous Trifluoroethanol. *PLoS One*, *10*(11), e0143647. https://doi.org/10.1371/journal.pone.0143647

d'Errico, P., & Meyer-Luehmann, M. (2020). Mechanisms of pathogenic tau and Abeta protein spreading in Alzheimer's disease. *Frontiers in Aging Neuroscience*, *12*, 265. https://doi.org/10.3389/fnagi.2020.00265

Fang, X. T., Sehlin, D., Lannfelt, L., Syvanen, S., & Hultqvist, G. (2017). Efficient and inexpensive transient expression of multispecific multivalent antibodies in Expi293 cells. *Biological Procedures Online*, *19*, 11. https://doi.org/10.1186/s12575-017-0060-7

Feuerbach, D., Schindler, P., Barske, C., Joller, S., Beng-Louka, E., Worringer, K. A., Kommineni, S., Kaykas, A., Ho, D. J., Ye, C., Welzenbach, K., Elain, G., Klein, L., Brzak, I., Mir, A. K., Farady, C. J., Aichholz, R., Popp, S., George, N., & Neumann, U. (2017). ADAM17 is the main sheddase for the generation of human triggering receptor expressed in myeloid cells (hTREM2) ectodomain and cleaves TREM2 after Histidine 157. *Neuroscience Letters*, *660*, 109–114. https://doi.org/10.1016/j.neulet.2017.09.034

Gerth, J., Kumar, S., Rijal Upadhaya, A., Ghebremedhin, E., von Arnim, C. A. F., Thal, D. R., & Walter, J. (2018). Modified amyloid variants in pathological subgroups of beta-amyloidosis. *Annals of Clinical Translational Neurology*, *5*(7), 815–831. https://doi.org/10.1002/acn3.577

Giulian, D., & Baker, T. J. (1986). Characterization of ameboid microglia isolated from developing mammalian brain. *The Journal of Neuroscience*, *6*(8), 2163–2178. https://doi.org/10.1523/JNEUROSCI.06-08-02163.1986

Gouras, G. K., Tampellini, D., Takahashi, R. H., & Capetillo-Zarate, E. (2010). Intraneuronal beta-amyloid accumulation and synapse pathology in Alzheimer's disease. *Acta Neuropathologica*, *119*(5), 523–541. https://doi.org/10.1007/s00401-010-0679-9

Gouras, G. K., Willen, K., & Tampellini, D. (2012). Critical role of intraneuronal Abeta in Alzheimer's disease: Technical challenges in studying intracellular Abeta. *Life Sciences*, *91*(23–24), 1153–1158. https://doi.org/10.1016/j.lfs.2012.06.004

Guerreiro, R., Bilgic, B., Guven, G., Brás, J., Rohrer, J., Lohmann, E., Hanagasi, H., Gurvit, H., & Emre, M. (2013). Novel compound heterozygous mutation in TREM2 found in a Turkish frontotemporal dementia-like family. *Neurobiology of Aging*, *34*(12), 2890.e1–2890.e5. https://doi.org/10.1016/j.neurobiolaging.2013.06.005

Guerreiro, R., Wojtas, A., Bras, J., Carrasquillo, M., Rogaeva, E., Majounie, E., Cruchaga, C., Sassi, C., Kauwe, J. S., Younkin, S., Hazrati, L., Collinge, J., Pocock, J., Lashley, T., Williams, J., Lambert, J. C., Amouyel, P., Goate, A., Rademakers, R., … Alzheimer Genetic Analysis Group. (2013). TREM2 variants in Alzheimer's disease. *The New England Journal of Medicine*, *368*(2), 117–127. https://doi.org/10.1056/NEJMoa1211851

Guerreiro, R. J., Lohmann, E., Brás, J. M., Gibbs, J. R., Rohrer, J. D., Gurunlian, N., Dursun, B., Bilgic, B., Hanagasi, H., Gurvit, H., Emre, M., Singleton, A., & Hardy, J. (2013). Using exome sequencing to reveal mutations in TREM2 presenting as a frontotemporal dementia-like syndrome without bone involvement. *JAMA Neurology*, *70*(1), 78–84. https://doi.org/10.1001/jamaneurol.2013.579

Haass, C., & Selkoe, D. J. (2007). Soluble protein oligomers in neurodegeneration: Lessons from the Alzheimer's amyloid beta-peptide. *Nature Reviews. Molecular Cell Biology*, *8*(2), 101–112. https://doi.org/10.1038/nrm2101

Hu, Z. W., Ma, M. R., Chen, Y. X., Zhao, Y. F., Qiang, W., & Li, Y. M. (2017). Phosphorylation at Ser(8) as an intrinsic regulatory switch to regulate the morphologies and structures of Alzheimer's 40-residue beta-amyloid (Abeta40) fibrils. *The Journal of Biological Chemistry*, *292*(7), 2611–2623. https://doi.org/10.1074/jbc.M116.757179

Huang, Y., Happonen, K. E., Burrola, P. G., O'Connor, C., Hah, N., Huang, L., et al. (2021). Microglia use TAM receptors to detect and engulf amyloid beta plaques. *Nature Immunology*, *22*(5), 586–594. https://doi.org/10.1038/s41590-021-00913-5

Hyman, B. T., Phelps, C. H., Beach, T. G., Bigio, E. H., Cairns, N. J., Carrillo, M. C., Dickson, D. W., Duyckaerts, C., Frosch, M. P., Masliah, E., Mirra, S. S., Nelson, P. T., Schneider, J. A., Thal, D. R., Thies, B., Trojanowski, J. Q., Vinters, H. V., & Montine, T. J. (2012). National Institute on Aging-Alzheimer's Association guidelines for the neuropathologic assessment of Alzheimer's disease. *Alzheimers Dement*, *8*(1), 1–13. https://doi.org/10.1016/j.jalz.2011.10.007

Ibach, M., Mathews, M., Linnartz-Gerlach, B., Theil, S., Kumar, S., Feederle, R., Brüstle, O., Neumann, H., & Walter, J. (2021). A reporter cell system for the triggering receptor expressed on myeloid cells 2 reveals differential effects of disease-associated variants on receptor signaling and activation by antibodies against the stalk region. *Glia*, *69*(5), 1126–1139. https://doi.org/10.1002/glia.23953

Jonsson, T., Stefansson, H., Steinberg, S., Jonsdottir, I., Jonsson, P. V., Snaedal, J., Bjornsson, S., Huttenlocher, J., Levey, A. I., Lah, J. J., Rujescu, D., Hampel, H., Giegling, I., Andreassen, O. A., Engedal, K., Ulstein, I., Djurovic, S., Ibrahim-Verbaas, C., Hofman, A., … Stefansson, K. (2013). Variant of TREM2 associated with the risk of Alzheimer's disease. *The New England Journal of Medicine*, *368*(2), 107–116. https://doi.org/10.1056/NEJMoa1211103

Kim, S. M., Mun, B. R., Lee, S. J., Joh, Y., Lee, H. Y., Ji, K. Y., Choi, H. R., Lee, E. H., Kim, E. M., Jang, J. H., Song, H. W., Mook-Jung, I., Choi, W. S., & Kang, H. S. (2017). TREM2 promotes Abeta phagocytosis by upregulating C/EBPalpha-dependent CD36 expression in microglia. *Scientific Reports*, *7*(1), 11118. https://doi.org/10.1038/s41598-017-11634-x

Kim, T., Vidal, G. S., Djurisic, M., William, C. M., Birnbaum, M. E., Garcia, K. C., Hyman, B. T., & Shatz, C. J. (2013). Human LilrB2 is a beta-amyloid receptor and its murine homolog PirB regulates synaptic plasticity in an Alzheimer's model. *Science*, *341*(6152), 1399–1404. https://doi.org/10.1126/science.1242077

Kleinberger, G., Yamanishi, Y., Suarez-Calvet, M., Czirr, E., Lohmann, E., Cuyvers, E., Struyfs, H., Pettkus, N., Wenninger-Weinzierl, A.,

Appendix-1

Mazaheri, F., Tahirovic, S., Lleo, A., Alcolea, D., Fortea, J., Willem, M., Lammich, S., Molinuevo, J. L., Sanchez-Valle, R., Antonell, A., … Haass, C. (2014). TREM2 mutations implicated in neurodegeneration impair cell surface transport and phagocytosis. *Science Translational Medicine*, *6*(243), 243ra86. https://doi.org/10.1126/scitranslmed.3009093

Kober, D. L., & Brett, T. J. (2017). TREM2-ligand interactions in health and disease. *Journal of Molecular Biology*, *429*(11), 1607–1629. https://doi.org/10.1016/j.jmb.2017.04.004

Kober, D. L., Stuchell-Brereton, M. D., Kluender, C. E., Dean, H. B., Strickland, M. R., Steinberg, D. F., Nelson, S. S., Baban, B., Holtzman, D. M., Frieden, C., Alexander-Brett, J., Roberson, E. D., Song, Y., & Brett, T. J. (2020). Functional insights from biophysical study of TREM2 interactions with apoE and Abeta1-42. *Alzheimer's & Dementia*, *17*, 475–488. https://doi.org/10.1002/alz.12194

Kumar, S., Kapadia, A., Theil, S., Joshi, P., Riffel, F., Heneka, M. T., & Walter, J. (2021). Novel phosphorylation-state specific antibodies reveal differential deposition of ser26 phosphorylated Aβ species in a mouse model of Alzheimer's disease. *Frontiers in Molecular Neuroscience*, *13*, 257. https://doi.org/10.3389/fnmol.2020.619639

Kumar, S., Rezaei-Ghaleh, N., Terwel, D., Thal, D. R., Richard, M., Hoch, M., Mc Donald, J. M., Wüllner, U., Glebov, K., Heneka, M. T., Walsh, D. M., Zweckstetter, M., & Walter, J. (2011). Extracellular phosphorylation of the amyloid beta-peptide promotes formation of toxic aggregates during the pathogenesis of Alzheimer's disease. *The EMBO Journal*, *30*(11), 2255–2265. https://doi.org/10.1038/emboj.2011.138

Kumar, S., Singh, S., Hinze, D., Josten, M., Sahl, H. G., Siepmann, M., & Walter, J. (2012). Phosphorylation of amyloid-beta peptide at serine 8 attenuates its clearance via insulin-degrading and angiotensin-converting enzymes. *The Journal of Biological Chemistry*, *287*(11), 8641–8651. https://doi.org/10.1074/jbc.M111.279133

Kumar, S., Wirths, O., Stüber, K., Wunderlich, P., Koch, P., Theil, S., Rezaei-Ghaleh, N., Zweckstetter, M., Bayer, T. A., Brüstle, O., Thal, D. R., & Walter, J. (2016). Phosphorylation of the amyloid beta-peptide at Ser26 stabilizes oligomeric assembly and increases neurotoxicity. *Acta Neuropathologica*, *131*(4), 525–537. https://doi.org/10.1007/s00401-016-1546-0

Kumar, S., Wirths, O., Theil, S., Gerth, J., Bayer, T. A., & Walter, J. (2013). Early intraneuronal accumulation and increased aggregation of phosphorylated Abeta in a mouse model of Alzheimer's disease. *Acta Neuropathologica*, *125*(5), 699–709. https://doi.org/10.1007/s00401-013-1107-8

Kummer, M. P., & Heneka, M. T. (2014). Truncated and modified amyloid-beta species. *Alzheimer's Research & Therapy*, *6*(3), 28. https://doi.org/10.1186/alzrt258

Kummer, M. P., Hermes, M., Delekarte, A., Hammerschmidt, T., Kumar, S., Terwel, D., Walter, J., Pape, H. C., König, S., Roeber, S., Jessen, F., Klockgether, T., Korte, M., & Heneka, M. T. (2011). Nitration of tyrosine 10 critically enhances amyloid beta aggregation and plaque formation. *Neuron*, *71*(5), 833–844. https://doi.org/10.1016/j.neuron.2011.07.001

le Ber, I., de Septenville, A., Guerreiro, R., Bras, J., Camuzat, A., Caroppo, P., Lattante, S., Couarch, P., Kabashi, E., Bouya-Ahmed, K., Dubois, B., & Brice, A. (2014). Homozygous TREM2 mutation in a family with atypical frontotemporal dementia. *Neurobiology of Aging*, *35*(10), 2419.e23–2419.e25. https://doi.org/10.1016/j.neurobiolaging.2014.04.010

Lessard, C. B., Malnik, S. L., Zhou, Y., Ladd, T. B., Cruz, P. E., Ran, Y., Mahan, T. E., Chakrabaty, P., Holtzman, D. M., Ulrich, J. D., Colonna, M., & Golde, T. E. (2018). High-affinity interactions and signal transduction between Abeta oligomers and TREM2. *EMBO Molecular Medicine*, *10*(11), e9027. https://doi.org/10.15252/emmm.201809027

Mandrekar, S., Jiang, Q., Lee, C. Y., Koenigsknecht-Talboo, J., Holtzman, D. M., & Landreth, G. E. (2009). Microglia mediate the clearance of soluble Abeta through fluid phase macropinocytosis. *The Journal of Neuroscience*, *29*(13), 4252–4262. https://doi.org/10.1523/JNEUROSCI.5572-08.2009

Mintun, M. A., Lo, A. C., Duggan Evans, C., Wessels, A. M., Ardayfio, P. A., Andersen, S. W., Shcherbinin, S., Sparks, J. D., Sims, J. R., Brys, M., Apostolova, L. G., Salloway, S. P., & Skovronsky, D. M. (2021). Donanemab in early Alzheimer's disease. *The New England Journal of Medicine*, *384*(18), 1691–1704. https://doi.org/10.1056/NEJMoa2100708

Nussbaum, J. M., Schilling, S., Cynis, H., Silva, A., Swanson, E., Wangsanut, T., Tayler, K., Wiltgen, B., Hatami, A., Rönicke, R., Reymann, K., Hutter-Paier, B., Alexandru, A., Jagla, W., Graubner, S., Glabe, C. G., Demuth, H. U., & Bloom, G. S. (2012). Prion-like behaviour and tau-dependent cytotoxicity of pyroglutamylated amyloid-beta. *Nature*, *485*(7400), 651–655. https://doi.org/10.1038/nature11060

Paloneva BM, J., Autti, T., Raininko, R., Partanen, J., Salonen, O., Puranen, M., Hakola, P., & Haltia, M. (2001). CNS manifestations of Nasu-Hakola disease: A frontal dementia with bone cysts. *Neurology*, *56*(11), 1552–1558. https://doi.org/10.1212/wnl.56.11.1552

Parhizkar, S., Arzberger, T., Brendel, M., Kleinberger, G., Deussing, M., Focke, C., Nuscher, B., Xiong, M., Ghasemigharagoz, A., Katzmarski, N., Krasemann, S., Lichtenthaler, S. F., Müller, S. A., Colombo, A., Monasor, L. S., Tahirovic, S., Herms, J., Willem, M., Pettkus, N., … Haass, C. (2019). Loss of TREM2 function increases amyloid seeding but reduces plaque-associated ApoE. *Nature Neuroscience*, *22*(2), 191–204. https://doi.org/10.1038/s41593-018-0296-9

Rezaei-Ghaleh, N., Amininasab, M., Giller, K., Kumar, S., Stündl, A., Schneider, A., Becker, S., Walter, J., & Zweckstetter, M. (2014). Turn plasticity distinguishes different modes of amyloid-beta aggregation. *Journal of the American Chemical Society*, *136*(13), 4913–4919. https://doi.org/10.1021/ja411707y

Rezaei-Ghaleh, N., Amininasab, M., Kumar, S., Walter, J., & Zweckstetter, M. (2016). Phosphorylation modifies the molecular stability of beta-amyloid deposits. *Nature Communications*, *7*, 11359. https://doi.org/10.1038/ncomms11359

Rijal Upadhaya, A., Kosterin, I., Kumar, S., von Arnim, C. A., Yamaguchi, H., Fändrich, M., Walter, J., & Thal, D. R. (2014). Biochemical stages of amyloid-beta peptide aggregation and accumulation in the human brain and their association with symptomatic and pathologically preclinical Alzheimer's disease. *Brain*, *137*(Pt 3), 887–903. https://doi.org/10.1093/brain/awt362

Saido, T. C., Iwatsubo, T., Mann, D. M., Shimada, H., Ihara, Y., & Kawashima, S. (1995). Dominant and differential deposition of distinct beta-amyloid peptide species, a beta N3(pE), in senile plaques. *Neuron*, *14*(2), 457–466. https://doi.org/10.1016/0896-6273(95)90301-1

Schilling, S., Zeitschel, U., Hoffmann, T., Heiser, U., Francke, M., Kehlen, A., Holzer, M., Hutter-Paier, B., Prokesch, M., Windisch, M., Jagla, W., Schlenzig, D., Lindner, C., Rudolph, T., Reuter, G., Cynis, H., Montag, D., Demuth, H. U., & Rossner, S. (2008). Glutaminyl cyclase inhibition attenuates pyroglutamate Abeta and Alzheimer's disease-like pathology. *Nature Medicine*, *14*(10), 1106–1111. https://doi.org/10.1038/nm.1872

Schlepckow, K., Kleinberger, G., Fukumori, A., Feederle, R., Lichtenthaler, S. F., Steiner, H., & Haass, C. (2017). An Alzheimer-associated TREM2 variant occurs at the ADAM cleavage site and affects shedding and phagocytic function. *EMBO Molecular Medicine*, *9*(10), 1356–1365. https://doi.org/10.15252/emmm.201707672

Selkoe, D. J., & Hardy, J. (2016). The amyloid hypothesis of Alzheimer's disease at 25 years. *EMBO Molecular Medicine*, *8*(6), 595–608. https://doi.org/10.15252/emmm.201606210

Spangenberg, E., Severson, P. L., Hohsfield, L. A., Crapser, J., Zhang, J., Burton, E. A., Zhang, Y., Spevak, W., Lin, J., Phan, N. Y., Habets, G., Rymar, A., Tsang, G., Walters, J., Nespi, M., Singh, P., Broome, S., Ibrahim, P., Zhang, C., … Green, K. N. (2019). Sustained microglial depletion with CSF1R inhibitor impairs parenchymal plaque development in an Alzheimer's disease model. *Nature Communications*, *10*(1), 3758. https://doi.org/10.1038/s41467-019-11674-z

Styren, S. D., Hamilton, R. L., Styren, G. C., & Klunk, W. E. (2000). X-34, a fluorescent derivative of Congo red: A novel histochemical stain for Alzheimer's disease pathology. *The Journal of Histochemistry and Cytochemistry*, *48*(9), 1223–1232. https://doi.org/10.1177/002215540004800906

Appendix-1

Tamboli, I. Y., Prager, K., Thal, D. R., Thelen, K. M., Dewachter, I., Pietrzik, C. U., St. George-Hyslop, P., Sisodia, S. S., de Strooper, B., Heneka, M. T., Filippov, M. A., Muller, U., van Leuven, F., Lutjohann, D., & Walter, J. (2008). Loss of gamma-secretase function impairs endocytosis of lipoprotein particles and membrane cholesterol homeostasis. *The Journal of Neuroscience*, *28*(46), 12097–12106. https://doi.org/10.1523/JNEUROSCI.2635-08.2008

Thal, D. R., Capetillo-Zarate, E., Larionov, S., Staufenbiel, M., Zurbruegg, S., & Beckmann, N. (2009). Capillary cerebral amyloid angiopathy is associated with vessel occlusion and cerebral blood flow disturbances. *Neurobiology of Aging*, *30*(12), 1936–1948. https://doi.org/10.1016/j.neurobiolaging.2008.01.017

Thal, D. R., Griffin, W. S., & Braak, H. (2008). Parenchymal and vascular Abeta-deposition and its effects on the degeneration of neurons and cognition in Alzheimer's disease. *Journal of Cellular and Molecular Medicine*, *12*(5B), 1848–1862. https://doi.org/10.1111/j.1582-4934.2008.00411.x

Thal, D. R., Ronisz, A., Tousseyn, T., Rijal Upadhaya, A., Balakrishnan, K., Vandenberghe, R., Vandenbulcke, M., von Arnim, C. A. F., Otto, M., Beach, T. G., Lilja, J., Heurling, K., Chakrabarty, A., Ismail, A., Buckley, C., Smith, A. P. L., Kumar, S., Farrar, G., & Walter, J. (2019). Different aspects of Alzheimer's disease-related amyloid beta-peptide pathology and their relationship to amyloid positron emission tomography imaging and dementia. *Acta Neuropathologica Communications*, *7*(1), 178. https://doi.org/10.1186/s40478-019-0837-9

Thornton, P., Sevalle, J., Deery, M. J., Fraser, G., Zhou, Y., Ståhl, S., Franssen, E. H., Dodd, R. B., Qamar, S., Gomez Perez-Nievas, B., Nicol, L. S. C., Eketjäll, S., Revell, J., Jones, C., Billinton, A., St George-Hyslop, P. H., Chessell, I., & Crowther, D. C. (2017). TREM2 shedding by cleavage at the H157-S158 bond is accelerated for the Alzheimer's disease-associated H157Y variant. *EMBO Molecular Medicine*, *9*(10), 1366–1378. https://doi.org/10.15252/emmm.201707673

Turnbull, I. R., Gilfillan, S., Cella, M., Aoshi, T., Miller, M., Piccio, L., Hernandez, M., & Colonna, M. (2006). Cutting edge: TREM-2 attenuates macrophage activation. *Journal of Immunology*, *177*(6), 3520–3524. https://doi.org/10.4049/jimmunol.177.6.3520

Ulrich, J. D., Ulland, T. K., Colonna, M., & Holtzman, D. M. (2017). Elucidating the role of TREM2 in Alzheimer's disease. *Neuron*, *94*(2), 237–248. https://doi.org/10.1016/j.neuron.2017.02.042

Verdier, Y., Zarandi, M., & Penke, B. (2004). Amyloid beta-peptide interactions with neuronal and glial cell plasma membrane: Binding sites and implications for Alzheimer's disease. *Journal of Peptide Science*, *10*(5), 229–248. https://doi.org/10.1002/psc.573

Vilalta, A., Zhou, Y., Sevalle, J., Griffin, J. K., Satoh, K., Allendorf, D. H., De, S., Puigdellívol, M., Bruzas, A., Burguillos, M. A., Dodd, R. B., Chen, F., Zhang, Y., Flagmeier, P., Needham, L.-M., Enomoto, M., Qamar, S., Henderson, J., Walter, J., … Brown, G. C. (2021). Wild-type sTREM2 blocks Aβ aggregation and neurotoxicity, but the Alzheimer's R47H mutant increases Aβ aggregation. *Journal of Biological Chemistry*, *296*, 100631. https://doi.org/10.1016/j.jbc.2021.100631

Walter, J. (2016). The triggering receptor expressed on myeloid cells 2: A molecular link of Neuroinflammation and neurodegenerative diseases. *The Journal of Biological Chemistry*, *291*(9), 4334–4341. https://doi.org/10.1074/jbc.R115.704981

Wang, Y., Cella, M., Mallinson, K., Ulrich, J. D., Young, K. L., Robinette, M. L., Gilfillan, S., Krishnan, G. M., Sudhakar, S., Zinselmeyer, B. H., Holtzman, D. M., Cirrito, J. R., & Colonna, M. (2015). TREM2 lipid sensing sustains the microglial response in an Alzheimer's disease model. *Cell*, *160*(6), 1061–1071. https://doi.org/10.1016/j.cell.2015.01.049

Wesen, E., Jeffries, G. D. M., Matson Dzebo, M., & Esbjorner, E. K. (2017). Endocytic uptake of monomeric amyloid-beta peptides is clathrin- and dynamin-independent and results in selective accumulation of Abeta (1-42) compared to Abeta(1-40). *Scientific Reports*, *7*(1), 2021. https://doi.org/10.1038/s41598-017-02227-9

Wingfield, P. (2001). Protein precipitation using ammonium sulfate. *Current Protocols in Protein Science*, *Appendix 3*, Appendix 3F. https://doi.org/10.1002/0471140864.psa03fs13

Wirths, O., Breyhan, H., Cynis, H., Schilling, S., Demuth, H. U., & Bayer, T. A. (2009). Intraneuronal pyroglutamate-Abeta 3-42 triggers neurodegeneration and lethal neurological deficits in a transgenic mouse model. *Acta Neuropathologica*, *118*(4), 487–496. https://doi.org/10.1007/s00401-009-0557-5

Wunderlich, P., Glebov, K., Kemmerling, N., Tien, N. T., Neumann, H., & Walter, J. (2013). Sequential proteolytic processing of the triggering receptor expressed on myeloid cells-2 (TREM2) protein by ectodomain shedding and gamma-secretase-dependent intramembranous cleavage. *The Journal of Biological Chemistry*, *288*(46), 33027–33036. https://doi.org/10.1074/jbc.M113.517540

Xiang, X., Werner, G., Bohrmann, B., Liesz, A., Mazaheri, F., Capell, A., Feederle, R., Knuesel, I., Kleinberger, G., & Haass, C. (2016). TREM2 deficiency reduces the efficacy of immunotherapeutic amyloid clearance. *EMBO Molecular Medicine*, *8*(9), 992–1004. https://doi.org/10.15252/emmm.201606370

Yeh, F. L., Wang, Y., Tom, I., Gonzalez, L. C., & Sheng, M. (2016). TREM2 binds to Apolipoproteins, including APOE and CLU/APOJ, and thereby facilitates uptake of amyloid-Beta by microglia. *Neuron*, *91*(2), 328–340. https://doi.org/10.1016/j.neuron.2016.06.015

Yu, Y., & Ye, R. D. (2015). Microglial Abeta receptors in Alzheimer's disease. *Cellular and Molecular Neurobiology*, *35*(1), 71–83. https://doi.org/10.1007/s10571-014-0101-6

Yuan, P., Condello, C., Keene, C. D., Wang, Y., Bird, T. D., Paul, S. M., Luo, W., Colonna, M., Baddeley, D., & Grutzendler, J. (2016). TREM2 Haplodeficiency in mice and humans impairs the microglia barrier function leading to decreased amyloid compaction and severe axonal dystrophy. *Neuron*, *90*(4), 724–739. https://doi.org/10.1016/j.neuron.2016.05.003

Zhao, Y., Wu, X., Li, X., Jiang, L.-L., Gui, X., Liu, Y., Sun, Y., Zhu, B., Piña-Crespo, J. C., Zhang, M., Zhang, N., Chen, X., Bu, G., An, Z., Huang, T. Y., & Xu, H. (2018). TREM2 is a receptor for β-amyloid that mediates microglial function. *Neuron*, *97*(5), 1023–1031.e7. https://doi.org/10.1016/j.neuron.2018.01.031

Zhong, L., Wang, Z., Wang, D., Wang, Z., Martens, Y. A., Wu, L., Xu, Y., Wang, K., Li, J., Huang, R., Can, D., Xu, H., Bu, G., & Chen, X. F. (2018). Amyloid-beta modulates microglial responses by binding to the triggering receptor expressed on myeloid cells 2 (TREM2). *Molecular Neurodegeneration*, *13*(1), 15. https://doi.org/10.1186/s13024-018-0247-7

SUPPORTING INFORMATION

Additional supporting information may be found in the online version of the article at the publisher's website.

How to cite this article: Joshi, P., Riffel, F., Satoh, K., Enomoto, M., Qamar, S., Scheiblich, H., Villacampa, N., Kumar, S., Theil, S., Parhizkar, S., Haass, C., Heneka, M. T., Fraser, P. E., St George-Hyslop, P., & Walter, J. (2021). Differential interaction with TREM2 modulates microglial uptake of modified Aβ species. *Glia*, 1–16. https://doi.org/10.1002/glia.24077

Joshi *et al. acta neuropathol commun (2021) 9:168*
https://doi.org/10.1186/s40478-021-01263-x

Acta Neuropathologica Communications

RESEARCH Open Access

TREM2 modulates differential deposition of modified and non-modified Aβ species in extracellular plaques and intraneuronal deposits

Pranav Joshi[1], Florian Riffel[1], Sathish Kumar[1], Nàdia Villacampa[2,3], Sandra Theil[1], Samira Parhizkar[4], Christian Haass[4,5,6], Marco Colonna[7], Michael T. Heneka[2,3], Thomas Arzberger[6,8,9], Jochen Herms[5,6,8] and Jochen Walter[1*]

Abstract

Progressive accumulation of Amyloid-β (Aβ) deposits in the brain is a characteristic neuropathological hallmark of Alzheimer's disease (AD). During disease progression, extracellular Aβ plaques undergo specific changes in their composition by the sequential deposition of different modified Aβ species. Microglia are implicated in the restriction of amyloid deposits and play a major role in internalization and degradation of Aβ. Recent studies showed that rare variants of the Triggering Receptor Expressed on Myeloid cells 2 (TREM2) are associated with an increased risk for AD. Post-translational modifications of Aβ could modulate the interaction with TREM2, and the uptake by microglia. Here, we demonstrate that genetic deletion of TREM2 or expression of a disease associated TREM2 variant in mice lead to differential accumulation of modified and non-modified Aβ species in extracellular plaques and intraneuronal deposits. Human brains with rare TREM2 AD risk variants also showed altered deposition of modified Aβ species in the different brain lesions as compared to cases with the common variant of TREM2. These findings indicate that TREM2 plays a critical role in the development and the composition of Aβ deposits, not only in extracellular plaques, but also intraneuronally, that both could contribute to the pathogenesis of AD.

Keywords: TREM2, Microglia, Post-translational modification, Aβ, Intraneuronal, Vascular deposits

Background

Alzheimer's disease (AD) is characterized neuropathologically by the combined occurrence of extracellular amyloid-beta (Aβ) plaques and intracellular neurofibrillary tangles (NFTs) with abnormally phosphorylated tau (τ) protein in the brain [24, 65]. Aβ deposits in the human brain contain different Aβ species, including N-terminal truncated, pyroglutamated, phosphorylated and nitrated variants that show significant differences in aggregation, stability, and toxicity [1, 42]. In particular, Aβ peptides with pyroglutamate-modification at glutamate residue 3 (N3pE-Aβ) or phosphorylated serine residue 8 (pSer8-Aβ) have increased propensity to form aggregates with increased neurotoxicity [38, 40–42, 53]. Previous investigations revealed a specific sequential deposition starting with non-modified Aβ (nmAβ) peptides, followed by N3pE-Aβ and pSer8-Aβ species in extracellular plaques during the progression from pre-clinical to clinical phases of AD [1, 54]. A similar sequence for the deposition of these Aβ species was also found in cerebral amyloid angiopathy (CAA) [11].

*Correspondence: jochen.walter@ukbonn.de
[1] Department of Neurology, University of Bonn, Venusberg-Campus 1, (Formerly Sigmund-Freud-Str. 25), 53127 Bonn, Germany
Full list of author information is available at the end of the article

© The Author(s) 2021. **Open Access** This article is licensed under a Creative Commons Attribution 4.0 International License, which permits use, sharing, adaptation, distribution and reproduction in any medium or format, as long as you give appropriate credit to the original author(s) and the source, provide a link to the Creative Commons licence, and indicate if changes were made. The images or other third party material in this article are included in the article's Creative Commons licence, unless indicated otherwise in a credit line to the material. If material is not included in the article's Creative Commons licence and your intended use is not permitted by statutory regulation or exceeds the permitted use, you will need to obtain permission directly from the copyright holder. To view a copy of this licence, visit http://creativecommons.org/licenses/by/4.0/. The Creative Commons Public Domain Dedication waiver (http://creativecommons.org/publicdomain/zero/1.0/) applies to the data made available in this article, unless otherwise stated in a credit line to the data.

Genome-wide association studies (GWAS) and exome sequencing have revealed genetic loci related to inflammatory pathways to be associated with an increased risk for AD [5, 18, 71]. Among these subsets of genes, rare variants of the microglial transmembrane receptor, Triggering Receptor Expressed on Myeloid cells (TREM2), confer a high risk for the development of AD, comparable to the risk exerted by the Apolipoprotein E4 allele (ApoE4) [18, 30]. TREM2 is preferentially expressed in microglia and functions as a receptor for different ligands, including anionic lipids, ApoE, and Aβ [12, 47, 74, 82]. Activation of TREM2 regulates microglial functions, including phagocytosis, cytokine production, proliferation and migration [16, 69, 75]. TREM2 is proteolytically processed by ADAM proteases to generate soluble variants of TREM2 (sTREM2) [25, 34, 78], that can be detected in extracellular fluids. sTREM2 could act as a decoy receptor to negatively modulate TREM2 signaling and inflammatory responses of microglia, and also shows trophic activity to promote microglial survival [35, 83].

TREM2 positive microglia cluster around extracellular plaques in brains of human AD cases and amyloid precursor protein (APP) transgenic mice, and the deletion of TREM2 in APP mouse models results in altered morphology and seeding of plaques, as well as decrease in number of plaque associated microglia [28, 51, 67], indicating an involvement of TREM2 in the restriction of Aβ deposits [11, 75]. Here, we sought to characterize the role of TREM2 in accumulation and distribution of modified and non-modified Aβ species in the brain. Deletion of TREM2 or the expression of the disease associated TREM2^{T66M} variant in different APP transgenic mouse models led to altered composition not only of extracellular plaques, but also of intraneuronal deposits containing modified and non-modified Aβ variants. Human cases with rare AD associated TREM2 variants also showed altered composition and morphology of the different Aβ pathological lesions as compared to AD cases with the common TREM2 variant. Together, the data indicate an important role of TREM2 in altering the composition of Aβ related brain lesions during the pathogenesis of AD.

Methods

Transgenic mice

APP695KM670/671NL; PS1L166P TREM2$^{+/+}$ and APP695KM670/671NL; PS1L166P TREM2$^{-/-}$ transgenic mice, and 5xFAD TREM2$^{+/+}$ and 5xFAD TREM2$^{-/-}$ transgenic mice were described previously [31, 51, 66, 75].

12 M old female APPKM670/671NL; PS1ΔE9 transgenic mice endogenously expressing TREM2 WT or the homozygous TREM2^{T66M} knock-in (KI) mutation were obtained from Taconic Biosciences GmbH, Cologne, Germany [31]. The different mouse models are described in Table 1.

Immunofluorescence (IF) analysis of mouse brains

Mouse brains were processed as described previously [31, 36, 51]. In brief, 20–25 µm sections were sequentially collected in Phosphate-buffered saline (PBS), placed on charged slides, and stained. For IF staining, Reveal Decloaker (Biocare Medical, #RV1000) was used for antigen retrieval [31] at 95 °C for 30 min. After this, the sections were washed with PBS and subjected to permeabilization with 0.25% Triton X-100 for 20 min before blocking for 2 h in 5% NHS and 3% BSA prepared in 1xPBST (Triton X100-0.2%). Mouse on Mouse Blocking Reagent (Vector laboratories, #MKB-2213) was used for primary antibodies generated in mouse or rat at a dilution of 1 drop/1000 µl. Primary antibodies were diluted in 3%NHS and 1.5% BSA prepared in 1xPBST (Tween 20-0.1%), added on sections and incubated at 4 °C overnight. For TREM2 staining, sections were incubated in the primary antibody at 4 °C for 48 h [31, 51]. After washing steps, appropriate secondary antibodies diluted in 3% NHS and 1.5% BSA prepared in 1xPBST (Tween 20–0.1%) were added on the sections and incubated for 1 h at RT. The sections were then washed and mounted with VECTASHIELD® Hardset™ antifade mounting medium (Vector laboratories, #H-1400) or VECTASHIELD® antifade mounting medium with DAPI (Vector laboratories, #H-1200). Primary and secondary antibodies are summarized in Additional file 1: Table S1.

Brain protein extraction

Snap-frozen brain hemispheres were extracted as previously described [22, 70]. Briefly, hemispheres were homogenized in PBS, 1 mM EDTA, 1 mM EGTA, 3 µl/ml protease inhibitor mix (Sigma). Homogenates were extracted in RIPA buffer (25 mM Tris–HCl, pH 7.5, 150 mM NaCl, 1% NP40, 0.5% NaDOC, 0.1% SDS), centrifuged at 100,000 g for 30 min and the pellet containing insoluble Aβ was solubilized in 2% SDS, 25 mM Tris–HCl, pH 7.5. The final protein concentration was determined using PierceTM BCA Protein Assay kit (Thermo Fisher) according to the user's manual.

Immunoblotting

The brain extracts were separated on 4–12% NuPAGE gels and transferred to 0.45 µm nitrocellulose (NC) membranes as described previously [36]. For immunodetection of proteins, membranes were blocked for 1 h in 5% nonfat dry milk in TBST (Tween 20–0.1%), then incubated with the primary antibodies in TBST (Tween 20–0.1%) overnight at 4 °C, followed by three washing steps for 10 min with TBST (Tween 20–0.1%), and

Table 1 Details of transgenic mouse models and quantification of Aβ plaque pathology. n.d.-not detected, ROI-Region of interest

Sr. No.	Transgenic mouse models	Age (months)	Sex	Genotype	No. of animals (n)		Total number of Aβ plaques/ROI stained with various antibodies													
							Somatosensory cortex (SSC)					Retrosplenial cortex (RSC)					Dentate gyrus (DG)				
							pSer8-Aβ	N3p3-Aβ	nmAβ	Aβ (4G8)	Aβ (2964)	pSer8-Aβ	N3p3-Aβ	nmAβ	Aβ (4G8)	Aβ (2964)	pSer8-Aβ	N3p3-Aβ	nmAβ	Aβ (4G8)	Aβ (2964)
1	5xFAD	5 M	Male	TREM2$^{+/+}$	5	Total plaque count/ group	1117	1664	1791	1847	1842	1353	1770	1724	1777	1815	933	1263	1932	1872	1857
						Plaque load (%)	2.89	8.11	10.91	11.42	11.46	4.35	7.49	7.71	9.27	8.52	2.89	5.12	8.76	8.98	8.93
				TREM2$^{-/-}$	5	Total plaque count/ group	1631	1836	2247	2314	2305	1734	1899	2120	2169	2198	1257	1403	2258	2196	2183
						Plaque load (%)	9.53	10.80	17.90	19.08	17.49	7.66	9.29	13.82	14.41	14.45	5.27	6.94	13.55	14.29	14.22
		15 M	Male	TREM2$^{+/+}$	5	Total plaque count/ group	1565	2322	3616	3725	3833	2057	2559	3641	3802	3778	1530	2535	3426	3537	3461
						Plaque load (%)	4.59	17.26	27.31	28.10	29.38	7.09	13.19	25.04	25.84	26.41	5.49	10.24	21.40	21.51	21.00
				TREM2$^{-/-}$	5	Total plaque count/ group	2250	3013	4414	4417	4523	2846	3285	4398	4520	4488	2153	3139	4033	4144	4096
						Plaque load (%)	13.06	23.76	41.46	41.37	42.44	15.73	21.93	32.66	35.63	33.95	10.99	16.07	32.16	32.39	31.95
2	APP/ PS1L166P	4 M	Male	TREM2$^{+/+}$	5	Total plaque count/ group	422	n.d.	1027	967	982	420	n.d.	852	892	917	245	n.d.	626	760	776
						Plaque load (%)	1.93	n.d.	5.51	4.96	5.25	2.46	n.d.	5.59	6.52	6.62	1.35	n.d.	4.14	5.03	4.63
				TREM2$^{-/-}$	5	Total plaque count/ group	607	n.d.	1215	1156	1193	631	n.d.	1062	1115	1132	446	n.d.	845	957	988
						Plaque load (%)	2.93	n.d.	8.19	9.03	9.88	4.09	n.d.	7.64	9.14	9.18	2.46	n.d.	6.57	7.01	7.63

Appendix-2

Appendix-2

Table 1 (continued)

Sr. No.	Transgenic mouse models	Age (months)	Sex	Genotype	No. of animals (n)		Total number of Aβ plaques/ROI stained with various antibodies													
							Somatosensory cortex (SSC)					Retrosplenial cortex (RSC)					Dentate gyrus (DG)				
							pSer8-Aβ	N3p3-Aβ	nmAβ	Aβ (4G8)	Aβ (2964)	pSer8-Aβ	N3p3-Aβ	nmAβ	Aβ (4G8)	Aβ (2964)	pSer8-Aβ	N3p3-Aβ	nmAβ	Aβ (4G8)	Aβ (2964)
		12 M	Female	TREM2$^{+/+}$	5	Total plaque count/ group	804	1935	4003	4090	3959	942	2096	3776	4050	3943	649	1584	2437	2482	2485
						Plaque load (%)	4.81	14.99	28.03	27.91	26.88	6.57	15.42	30.03	32.66	32.23	3.83	9.56	17.92	17.82	15.41
				TREM2$^{-/-}$	5	Total plaque count/ group	1424	2545	4655	4770	4571	1391	2562	4226	4518	4398	972	1951	2766	2835	2835
						Plaque load (%)	9.94	21.24	39.43	41.24	40.67	13.65	21.88	47.34	47.87	47.04	7.12	12.86	24.29	22.81	25.31
3	APP/PS1ΔE9	12 M	Female	TREM2	3	Total plaque count/ group	491	1068	2044	2233	2331	414	889	1489	1785	1685	183	548	717	874	965
						Plaque load (%)	4.09	12.58	30.05	30.40	35.16	3.21	11.29	21.13	24.68	23.77	1.87	6.58	9.13	12.23	13.03
				TREM2^{T66M}	3	Total plaque count/ group	757	1397	2570	2581	2605	735	1349	1975	2073	2060	255	770	1001	1119	1086
						Plaque load (%)	8.02	18.63	39.91	39.44	41.83	7.36	18.89	30.25	31.31	33.08	3.37	12.10	14.19	16.75	15.94

addition of appropriate secondary antibodies in TBST (Tween 20–0.1%). After an incubation period of 60 min at RT, membranes were washed three times for 10 min with TBST (Tween 20–0.1%), and once for 5 min with TBS. For signal detection, the enhanced chemiluminescence ECL imager (Bio-Rad laboratories, Inc.) or Odyssey CLx™ (LI-COR, Biosciences) were used. The quantification was done by using Image Studio-Lite (Ver. 5.2). Primary and secondary antibodies are summarized in Additional file 1: Table S1.

Patient material

Tissue samples of patient autopsy cases were provided by the Neurobiobank Munich, Ludwig-Maximilians-University (LMU) Munich. Detailed clinical characteristics were ascertained from an integrated autopsy database. Written informed consent for autopsy and analysis of tissue sample data was obtained for all patients, either from the patients themselves or their kin and the samples were collected according to the guidelines of the local ethics committee following all ethical regulations. Information regarding cases, clinical diagnosis, age at death, post-mortem delay, fixation time, AD Braak & Braak stage, Thal phase, TREM2 coding variant is given in Table 2. The genotyping and identification of TREM2 variant carriers were done as described before [51]. Sample sizes were based on availability of patient material. For all analyses, temporal neocortex was used which included cortex of medial temporal gyrus at the level of anterior hippocampus.

Immunohistochemistry (IHC) on human post-mortem brain tissue

IHC was done as described before [51]. In brief, 5 µm temporal neocortex sections were mounted on slides, deparaffinized and rehydrated in a series of xylene and graded ethanol. The sections were subjected to citric acid antigen retrieval (1 M sodium citrate in PBS, pH 6.0) and boiled in a microwave for 20 min. After cooling, endogenous peroxidase activity was quenched using 30% hydrogen peroxide for 20 min. Sections were blocked and incubated with primary antibodies (Additional file 1: Table S1) overnight at 4 °C. Primary antibodies were detected with biotinylated anti-mouse and anti-rat IgG secondary antibodies and visualized with avidin–biotin-complex (ABC-Kit, Vector laboratories) followed by development with diaminobenzidine-HCl (DAB, Vector laboratories) for 5 min. Lastly, sections were counterstained with haematoxylin. Stainings were performed in serially cut sections to compare the same region of interest through all immunostainings. Brightfield images were taken with Axio Scan.Z1 (Carl Zeiss MicroImaging GmbH, Germany).

Confocal imaging

All IF images were acquired using VisiScope CSU-W1 spinning disk confocal microscope and VisiView Software (Visitron Systems GmbH, Germany). Laser and detector settings were maintained constant for the acquisition of each immunostaining. All stainings were repeated at least three times to ensure reproducibility in the staining protocol. Images were acquired at 10×, 20×, 40×W or 63×W (W-water immersion) objective at 2048 × 2048 pixels, with z-step size of 1 µm (for 10×, 20×, 40×W, 63×W images) or 4-5 µm (for 10× montage image).

Data analysis of Aβ deposits in mouse and human brain

Initial optimization of dilutions and incubation times for the different antibodies was carried out for detection of the different Aβ species as reported previously [31, 40, 41]. Sections or areas with folds or poor staining quality were excluded from quantifications. To represent and quantify plaque densities (number and size distribution) from three sections/mouse brains regions, the somatosensory cortex (SSC), the retrosplenial cortex (RSC), and the dentate gyrus (DG) (Additional file 1: Figure S1a), acquired images were imported into Fiji software and data channels were separated (image/color/split channels). All layers from a single image stack were projected on a single slice (stack/Z-projection) to test the feasibility of quantifying the area and number of plaques (Additional file 1: Figure S1b). The plaques were then segmented and quantified in Fiji using automatic thresholding methods. Due to the thickness of brain sections and the limited penetration of antibody to plaques underneath the sectioned face, lightly embedded stained plaques may or may not be detected depending on image adjustment values (Additional file 1: Figure S1c). Therefore, the plaques and their quantified combined area in this study constitute the "lower boundary" of the plaque number volume density. Furthermore, as demonstrated with digitalized plaques (SSC region stained with nmAβ as an example (Additional file 1: Figure S2a-b), the number of plaques assessed using an image analysis method in a given brain region varied depending upon the cut-off value of pixel size and the thresholding of plaques. Initial analysis of optical images revealed that plaque-like images that were digitalized often displayed plaque-like artifacts. Therefore, plaques > $10\mu m^2$ were considered as reliable "digital plaques". Adjustment of thresholding of certain digitalized plaques appeared to vary in number valuables due to irregularity in plaque shapes or depending upon value of image distribution. It was found that the staining intensity cut-off had a significant impact on the number of plaques. Interestingly, TREM2 knockout

Table 2 Demographic and clinical characteristics of the TREM2 coding variants and control (CV) groups. n.i.- no information, ROI- Region of interest. Case#3, with highest fixation time, was omitted for the plaque count and size quantification as it was difficult to define boundaries of extracellular plaques stained with 1E4E11 (pSer8-Aβ) antibody

Case # number	Clinical diagnosis	Age at death (yr)	Sex	Post-mortem Delay (h)	Fixation time (days)	CERAD	Braak & Braak AD stage	Thal phase	ApoE status	TREM2 variant	Total number of Aβ plaques counted/ analyzed ROIs	Total number of pSer8-Aβ plaques counted/ analyzed ROIs	Total nmAβ intracellular deposits counted/ analyzed ROIs	Total pSer8-Aβ intracellular deposits counted/ analyzed ROIs
#1	Dementia (rapidly progressive; without further specification)	75	M	24	n.i	C	6	5	E3/E4	R62H (G > A)	13,053	2286	2871	1663
#2	Dementia of the Alzheimer type	78	F	21	15	C	6	5	E3/E4	R62H (G > A)	14,125	2270	2616	1496
#3	Dementia (without further specification)	81	F	11–35	613	C	5	5	E3/E4	R62H (G > A)	17,147	-	2764	2740
#4	Fronto-temporal dementia (FTD)	77	M	5	25	C	5	5	E3/E4	R62H (G > A)	15,782	4894	4415	3825
#5	Dementia (without further specification)	86	M	16–40	156	C	5	4	E3/E4	R62H (G > A)	14,296	1984	3731	3675
#6	Fronto-temporal dementia (FTD)	77	M	26	297	C	5	4	E3/E4	R62C (C > T)	14,432	1857	3832	2190
#7	Dementia of the Alzheimer type	81	F	60	39	C	6	n.i	E3/E4	None	9384	2057	3304	1052
#13	Dementia, probably of the Alzheimer type	82	M	15	104	C	6	5	E3/E4	None	9816	2759	1850	1841

Appendix-2

Table 2 (continued)

Case # number	Clinical diagnosis	Age at death (yr)	Sex	Post-mortem Delay (h)	Fixation time (days)	CERAD	Braak & Braak AD stage	Thal phase	ApoE status	TREM2 variant	Total number of Aβ plaques counted/ analyzed ROIs	Total number of pSer8-Aβ plaques counted/ analyzed ROIs	Total nmAβ intracellular deposits counted/ analyzed ROIs	Total pSer8-Aβ intracellular deposits counted/ analyzed ROIs
#14	Dementia (without further specification)	85	M	27	27	C	6	5	E3/E4	None	9892	2386	2157	1021
#15	Dementia (without further specification)	85	M	49	136	C	6	5	E3/E4	None	16,160	4104	2404	2834
#16	Dementia (without further specification)	88	F	9	76	C	4	5	E3/E4	None	14,698	3894	2891	1224
#17	Dementia of the Alzheimer type	75	M	3–13	141	C	5	5	E3/E4	None	8681	2256	2295	837

mouse brain, showed large size plaques as well as an increased total number of plaques > 10 μm^2 even at lower thresholding, confirming the validity of the analysis.

For the quantification of plaque ratio in the IF experiments, we considered 300 plaques/region/group (each for SSC and RSC) and 150 plaques/region/group (for DG) (so, SSC = 60 plaques/mouse, RSC = 60 plaques/mouse, DG = 30 plaques/mouse) so making total of 750 plaques/group containing 5 animals or 450 plaques/group containing 3 animals (from at least 3 sections/animal). For this analysis, randomly selected plaques that were positive with all three antibodies detecting Aβ species/staining in 1000 × 1000 µm ROI were analyzed by manually drawing boundary around each plaque by using freehand draw tool in Fiji and determining the IntDen [8] of total Aβ-immunoreactive area for each plaque stained with various antibodies specific to Aβ species within each section for all channels (Additional file 1: Figure S3).

For quantification of microglia surrounding plaques, microglia surrounding 30 cortical plaques of similar plaque area were manually counted and represented as a mean of 30 plaque associated microglia/animal. The total number of neurons was manually counted in a 1000 × 1000 µm area of SSC, in 2 independently stained sections and represented as a ratio of pSer8-Aβ positive neurons/total neurons.

For representation and quantification of plaque densities of 4G8 and pSer8-Aβ stained plaques in the human brain's sections, 10 cortical 2 × 2 mm regions of interest (ROIs) were randomly selected per case and manually quantified. ROIs were selected to allow analysis of the same region for all four consecutive brain sections stained with different antibodies without interference by cuts, folds, or other irregularities (Additional file 2: Source data 1). The total number of plaques along with area measurements were considered for the analysis. The border around plaques was manually drawn by using "spline contour" tool in the ZEN 3.2 software, for the area stained with different antibodies. With 4G8 antibody-stained sections, an area cutoff of 10 μm^2 was determined, while with pSer8-Aβ antibody-stained sections, an area cutoff of 30 μm^2 was determined, below which were considered as either artifacts or intracellular deposits (quantified separately). Case#3, with highest fixation time, was omitted for the plaque count and size quantification as it was difficult to define boundaries of extracellular plaques stained with 1E4E11 (pSer8-Aβ) antibody. Aβ plaque load was calculated by summing the areas of all counted plaques divided by the total area of all ROIs. The intracellular deposits of nmAβ and phosphorylated Aβ were manually counted from 10 cortical consecutive 2 × 2 mm randomly selected ROIs per case.

Statistical analysis

Statistical analyses were performed using GraphPad prism software. The plaque area distribution showed positively skewed distribution [58] and varied from the normal distribution confirmed by D'Agostino & Pearson and the Shapiro–Wilk normality test. Hence, for this analysis, we considered non-parametric, Mann Whitney test (compares the distributions of ranks in two groups) and Kolmogorov–Smirnov test (compares the cumulative distributions) for the frequency distribution of all values. Besides this, since the data were not formally tested, we assumed it followed Gaussian distribution and that the variance between groups was comparable [51]; thus, unless otherwise stated, two-sided, unpaired t-test with Welch's correction was used to determine the statistical difference between groups in analyses requiring only single comparisons. The degree of significance between groups is represented as $^{*}p < 0.05$, $^{**}p < 0.01$, $^{***}p < 0.001$, $^{****}p < 0.0001$, and $^{ns}p > 0.05$.

Randomization and blinding

The immunohistochemical analysis of mouse and human brains was initially performed blinded with coded slides. However, complete randomization was not possible in the staining with a microglial marker or when stained with anti-TREM2 antibody [31, 51], depicting microglial clustering. No randomization procedure was performed for selecting patient material as case inclusion was largely based on availability. Following the completion of the analysis, the groups were unblinded to perform statistics.

Data collection

Confocal images were acquired by using VisiScope CSU-W1 spinning disk confocal microscope and VisiView Software (Visitron Systems GmbH, Germany). Human brain immunostaining data were acquired by Axio Scan. Z1 at Plan-Apochromat 20x/0.8M27 objective imaged by Hitachi HV-F202SCL with ZEN 3.2 software (Carl Zeiss MicroImaging GmbH, Germany). FIJI (ImageJ) or ZEN 3.2 software was used for all immunohistochemical analyses. Microsoft Excel was used to organize and to calculate the averages of each repeated experiment. GraphPad (Prism v7.0) software was used to build graphs and perform statistical analyses presented throughout the manuscript.

Validation

Phosphorylation-state specific antibodies were generated and validated as described previously [38, 41]. Antibody 1E4E11 is specific for pSer8-Aβ and does not cross-react with other post-translationally modified variants of Aβ, including N-terminally truncated (Aβ 3–42), nitrated (3NTyr10-Aβ), pyroglutamated (N3pE-Aβ), or Aβ

phosphorylated at Ser 26 [41]. Rabbit polyclonal antibody 2964 was raised against aggregated Aβ [73]. TREM2 antibody was verified for immunostainings [28, 51]. 7H3D6 antibody specifically detects Aβ species with a non-modified N-terminus and does not recognize phosphorylated Ser8-Aβ, but also does not recognize other Aβ variants with N-terminal modifications, including pyroglutamated, nitrated, and N-terminally truncated Aβ species [41]. It is important to note that both antibodies 1E4E11, detecting pSer8-Aβ and 7H3D6 used for detection of N-terminally non-modified Aβ, do not cross-react with full-length APP or APP C-terminal fragments [40, 41]. All the other antibodies used in the study were verified for immunostaining and immunoblotting in mouse and human samples according to the company websites (Additional file 1: Table S1).

Results

Selective accumulation of Ser8-phosphorylated Aβ species upon loss of TREM2 function in brains of transgenic mice

Phosphorylated Aβ variants were previously detected in brains of transgenic mouse models and human AD cases, and shown to exert increased toxicity in Drosophila models and human neurons derived from embryonic stem or induced pluripotent stem cells [11, 13, 38, 40, 41, 54]. To assess the role of TREM2 in the deposition of modified Aβ species in-vivo, 5xFAD transgenic mice were crossed with $TREM2^{+/+}$ or $TREM2^{-/-}$ mice as described previously [31, 51] (Table 1), and the deposition of different Aβ species was analyzed using several antibodies selectively detecting modified and non-modified variants of Aβ. Monoclonal antibody 1E4E11 specifically detects pSer8-Aβ species, while monoclonal antibody 7H3D6 selectively recognizes Aβ with Ser8 in non-phosphorylated state. Antibody 7H3D6 also does not recognize other Aβ variants with N-terminal modifications, including pyroglutaminated, nitrated, and N-terminally truncated Aβ species [41].

Triple staining with mouse monoclonal 1E4E11, rat monoclonal 7H3D6, and rabbit polyclonal 2964 antibodies revealed that $TREM2^{-/-}$ mice at 15 months (15 M) of age had significantly more plaques detected by all three antibodies. Elevated plaque deposition, as measured by the plaque number (Fig. 1a–b, Additional file 1: Figure S4) and plaque load (Table 1), was detected in the three different brain regions analyzed, the somatosensory cortex (SSC), the retrosplenial cortex (RSC), and the dentate gyrus (DG). Consistent with a preferential deposition in the core of plaques, pSer8-Aβ positive deposits are of smaller size than those containing nmAβ that is also deposited in the corona of plaques (Fig. 1c, Additional file 2: Source data 2a-c). These findings are consistent with the function of TREM2 to restrict plaque size or growth [75, 81], and also demonstrate the importance of TREM2 to limit accumulation of pSer8-Aβ in the core of plaques. A selective increase in pSer8-Aβ was detected by analyzing the mean fluorescence signal intensities within Aβ deposits (Fig. 1d–e). Furthermore, increased number and size of pSer8-Aβ and nmAβ positive plaques in 5xFAD $TREM2^{-/-}$ compared to $TREM2^{+/+}$ mouse brains was already observed in 5 M old mice (Fig. 2a–b, Additional file 2: Source data 2d-f). Analysis of plaque size distribution at both ages revealed overall increased numbers of deposits of various sizes in all three analyzed brain regions of $TREM2^{-/-}$ mice (Additional file 2: Source data 2). In particular, the number of deposits > 1200 μm^2 that are also positive for pSer8-Aβ were strongly increased in $TREM2^{-/-}$ mice already at 5 M of age, suggesting that TREM2 decreases the formation and growth of plaques already at early stages of deposition. However, the ratio of the mean fluorescence intensity for pSer8-Aβ and nmAβ was similar in $TREM2^{-/-}$ and $TREM2^{+/+}$ at this young age (Fig. 2c–d), indicating that TREM2 deficiency promotes co-deposition of different Aβ species. Very similar findings were obtained with an independent double-transgenic APP/PS1L166P mouse model (Table 1, Additional file 1: Figure S5, Additional file 2: Source data 3).

Pyroglutamate-modified Aβ (N3pE-Aβ) also accumulates during the pathogenesis of AD in the cortex and hippocampus [52, 55]. Immunohistochemical analyses showed that $TREM2^{-/-}$ mice had significantly more

(See figure on next page.)

Fig. 1 TREM2 deletion leads to increased deposition of pSer8-Aβ in 15 M old 5xFAD transgenic mouse brains. **a** Representative pSer8-Aβ stained male 15 M old-5xFAD-$TREM2^{+/+}$ and $TREM2^{-/-}$ mouse brain sections (color scale bar = 35 mm, represents min/max pixel intensities, 10x). **b** Dot plots representing number of plaques/mm^2, **c** Box and whiskers plots showing plaque size (μm^2) stained with pSer8-Aβ, nmAβ and Aβ (2964) antibodies in the SSC, RSC, and DG of male 15 M-5xFAD-$TREM2^{-/-}$ and $TREM2^{+/+}$ mice. **d** Representative images showing deposition of pSer8-Aβ, nmAβ, and Aβ (2964) in SSC of male 15 M-5xFAD-$TREM2^{-/-}$ and $TREM2^{+/+}$ mice (scale bar = 50 μm, 40xW). **e** Ratios of pSer8/nmAβ in SSC ($t(7.41) = 7.856$,$^{****}p < 0.0001$), RSC ($t(7.696) = 7.611$,$^{****}p < 0.0001$), and DG ($t(7.945) = 6.345$,$^{***}p = 0.0002$) of male 15 M-5xFAD-$TREM2^{-/-}$ compared with $TREM2^{+/+}$ mice. Each dot represents average value of the number of plaques or the ratio of pSer8-Aβ/nmAβ per animal. The box and whiskers plots represent min/max values of distribution of plaque size with the median (shown by the line dividing the box) and the dot plots represent mean ± SEM (n = 5 animals, color- blue (5xFAD-$TREM2^{+/+}$) and green (5xFAD-$TREM2^{-/-}$), unpaired t-test with Welch's correction for analysis of the number and ratio while Mann–Whitney test for plaque size, $^{ns}p > 0.05$, $^{*}p < 0.05$, $^{**}p < 0.01$, $^{***}p < 0.001$ or $^{****}p < 0.0001$)

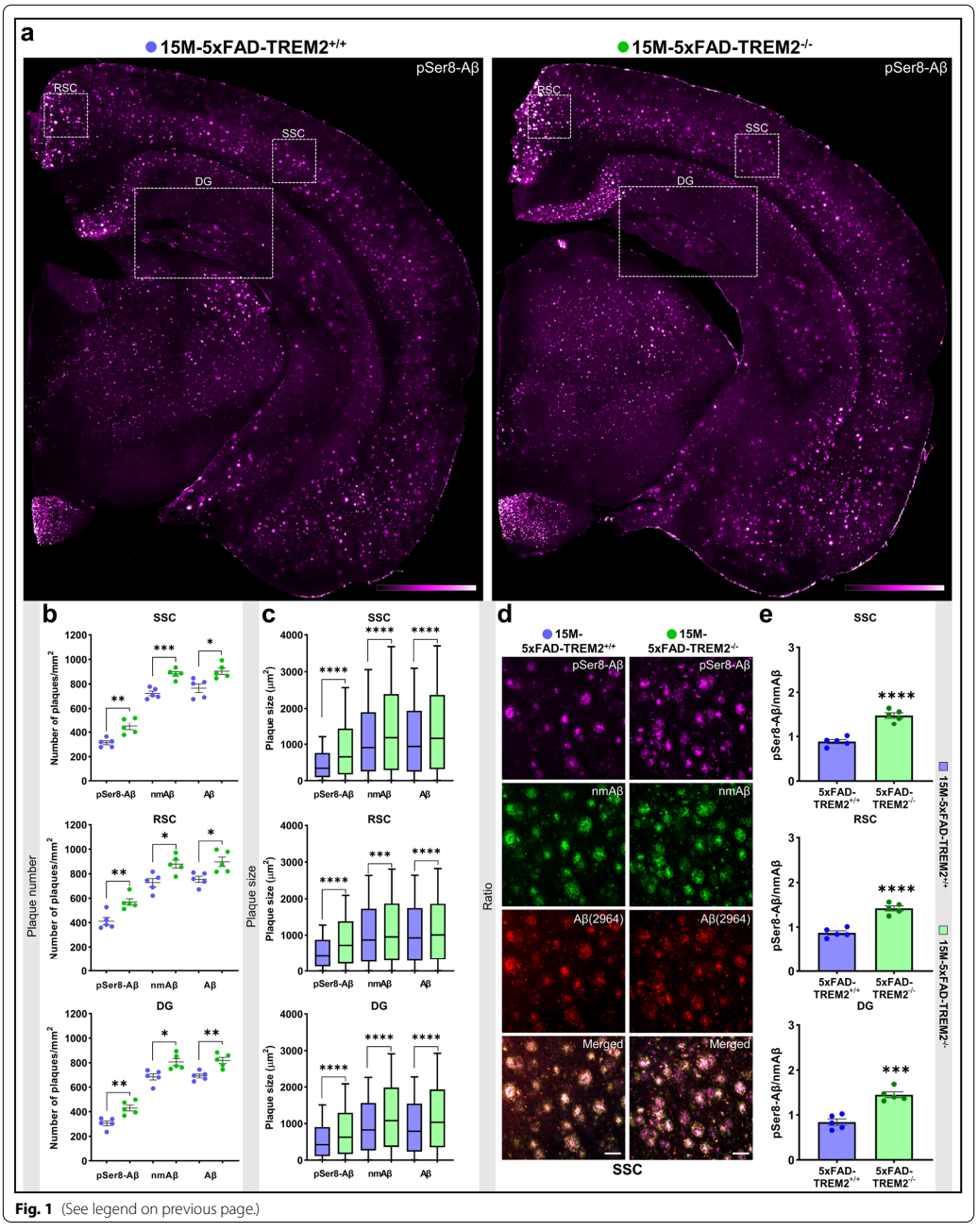

Fig. 1 (See legend on previous page.)

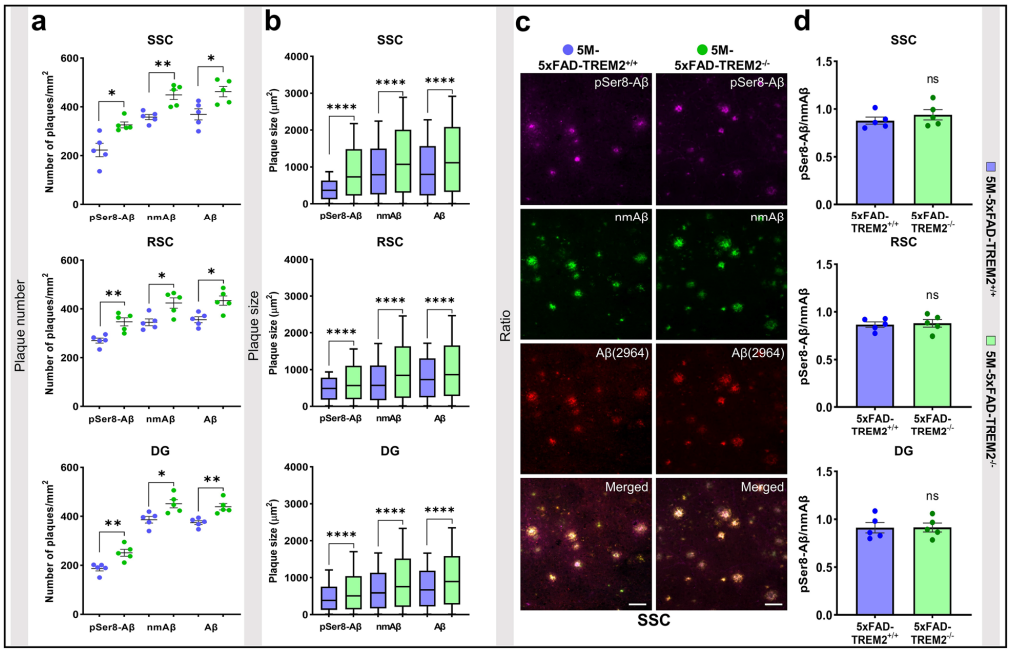

Fig. 2 TREM2 deletion leads to increased deposition of pSer8-Aβ in 5 M old 5xFAD transgenic mouse brains. **a** Dot plots representing number of plaques/mm^2, **b** Box and whiskers plots showing plaque size (µm^2) stained with pSer8-Aβ, nmAβ and Aβ (2964) antibodies in the SSC, RSC, and DG of male 5 M old-5xFAD-TREM2$^{-/-}$ and TREM2$^{+/+}$ mice. **c** Representative images showing deposition of pSer8-Aβ, nmAβ, and Aβ (2964) in SSC of male 5 M-5x-FAD-TREM2$^{-/-}$ and TREM2$^{+/+}$ mice (scale bar = 50 µm, 40xW). **d** Ratio of pSer8/nmAβ in SSC, RSC and DG in male 5 M-5xFAD-TREM2$^{-/-}$ compared to TREM2$^{+/+}$ mice. Each dot represents average value of the number of plaques or the ratio of pSer8-Aβ/nmAβ per animal. The box and whiskers plots represent min/max values of distribution of plaque size with the median (shown by the line dividing the box) and the dot plots represent mean ± SEM (n = 5 animals, color- blue (5xFAD-TREM2$^{+/+}$) and green (5xFAD-TREM2$^{-/-}$), unpaired t-test with Welch's correction for analysis of the number and ratio while Mann–Whitney test for plaque size, $^{ns}p > 0.05$, $^{*}p < 0.05$, $^{**}p < 0.01$ or $^{****}p < 0.0001$)

N3pE-Aβ positive plaques at 15 M of age in the SSC, RSC, and the DG as compared to TREM2$^{+/+}$ mice. Consistent with data shown in Fig. 1, TREM2$^{-/-}$ mice showed higher number of plaques, (Fig. 3a-b), increased size of plaques (Fig. 3c, Additional file 2: Source data 2a-c) and elevated plaque load (Table 1) in all three regions as revealed by co-staining with antibodies detecting N-terminally non-modified Aβ and total Aβ species at 15 M of age. In contrast to pSer8-Aβ, N3pE-Aβ was not selectively increased in plaques as compared to nmAβ at 15 M of age, as evidenced by similar ratios of N3pE-Aβ/nmAβ in all analyzed brain regions (Fig. 3d). At 5 M of age, the total number of N3pE-Aβ deposits were only slightly, but not significantly increased in 5xFAD TREM2$^{-/-}$ mice as compared to TREM2$^{+/+}$ 5xFAD mice (Fig. 3e–f). However, as observed with 15 M old mice, there was a significant increase in the size of N3pE-Aβ positive plaques especially for larger deposits > 1500 µm^2 already at 5 M in 5xFAD TREM2$^{-/-}$ mice (Fig. 3g, Additional file 2: Source data 2d–f). Analysis of plaque size distribution revealed that there was an increase in the number of N3pE-Aβ deposits at both age groups, again particularly pronounced for deposits > 1500 µm^2. An increase of pSer8-Aβ and N3pE-Aβ deposits < 600 µm^2 in the three analyzed brain regions of TREM2$^{-/-}$ mice as compared to TREM2$^{+/+}$ mice was only observed at 15 M of age (Additional file 2: Source data 2). The N3pE-Aβ/nmAβ intensity ratio in the analyzed brain regions was not different between TREM2$^{-/-}$ and TREM2$^{+/+}$ mice at both ages (Fig. 3d, h). Very similar findings were obtained with the independent double-transgenic APP/PS1L166P mouse model (Additional file 1: Figure S6, Additional file 2: Source data 3). These findings indicate that N3pE-Aβ species showed increased deposition upon deletion of TREM2. However, N3pE-Aβ, in contrast to pSer8-Aβ, did not selectively accumulate upon deletion of TREM2 in relation to nmAβ.

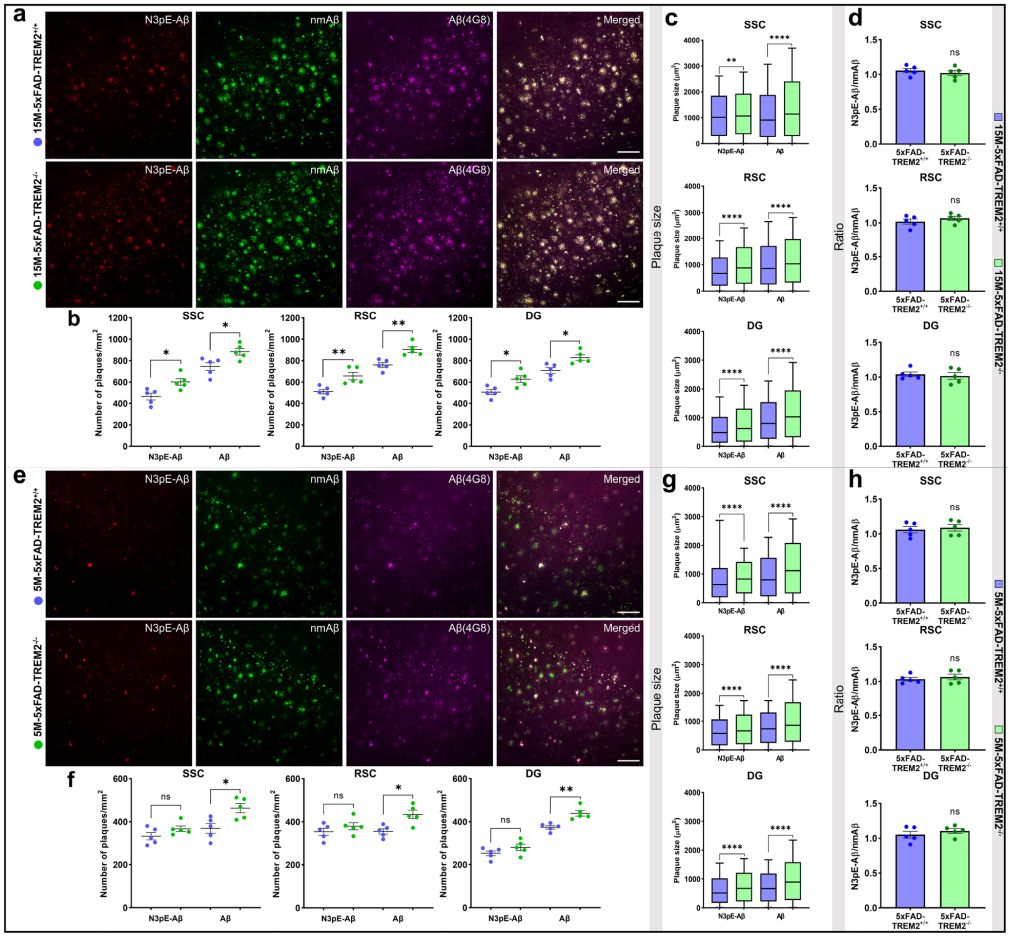

Fig. 3 TREM2 deletion leads to increased N3pE-Aβ deposits in 5xFAD transgenic mouse brains. **a** Representative images showing deposition of N3pE-Aβ, nmAβ, and Aβ (4G8) in SSC of male 15 M old-5xFAD-TREM2$^{-/-}$ and TREM2$^{+/+}$ mice (scale bar = 200 μm, 20x). **b** Dot plots representing number of plaques/mm^2, **c** Box and whiskers plots showing plaque size (μm^2) stained with N3pE-Aβ and Aβ(4G8) antibodies in the SSC, RSC, and DG of the male 15 M-5xFAD-TREM2$^{-/-}$ and TREM2$^{+/+}$ mice. **d** Ratio of N3pE-Aβ/nmAβ in the SSC, RSC, and DG of male 15 M-5xFAD-TREM2$^{-/-}$ compared with TREM2$^{+/+}$ mice. **e** Representative images showing deposition of N3pE-Aβ, nmAβ, and Aβ (4G8) in SSC of male 5 M-5xFAD-TREM2$^{-/-}$ and TREM2$^{+/+}$ mice (scale bar = 200 μm, 20x). **f** Dot plots representing number of plaques/mm^2, **g** Box and whiskers plots showing plaque size (μm^2) stained with N3pE-Aβ and Aβ (4G8) antibodies in the SSC, RSC, and DG of male 5 M-5xFAD-TREM2$^{-/-}$ and TREM2$^{+/+}$ mice. **h** Ratio of N3pE-Aβ/nmAβ in the SSC, RSC, and DG of male 5 M-5xFAD-TREM2$^{-/-}$ compared with TREM2$^{+/+}$ mice. Each dot represents average value of the number of plaques or the ratio of N3pE-Aβ/nmAβ per animal. The box and whiskers plots represent min/max values of distribution of plaque size with the median (shown by the line dividing the box) and the dot plots represent mean ± SEM (n = 5 animals, color- blue (5xFAD-TREM2$^{+/+}$) and green (5xFAD-TREM2$^{+/+}$), unpaired t-test with Welch's correction for analysis of the number and ratio while Mann–Whitney test for plaque size, $^{ns}p > 0.05$, $^{*}p < 0.05$, $^{**}p < 0.01$ or $^{****}p < 0.0001$)

TREM2^{T66M} mutation leads to increased deposition of pSer8-Aβ in transgenic mouse brain

To assess potential effects of a disease associated TREM2 mutant, we used knock-in (KI) mice that carry the TREM2^{T66M} variant (Table 1). The TREM2^{T66M} variant is associated with Nasu–Hakola disease (NHD) and frontal lobe degeneration [17, 19, 49]. Importantly, the genetic modification at this site in the mouse genome does not result in aberrant splicing and lower mRNA levels as observed previously for knock-in mice expressing the Alzheimer-associated R47H variant [79]. TREM2^{T66M} KI mice were crossed with APP/PS1ΔE9 double transgenic mice. Mice homozygous for endogenous TREM2 or the TREM2^{T66M} KI mutation were analyzed at 12 M of age. Homozygous TREM2^{T66M} KI mice showed an increase in the number and size of plaques (Fig. 4a–c, Additional file 2: Source data 4) as well as increased plaque load (Table 1). TREM2^{T66M} KI mice also showed a selective accumulation of pSer8-Aβ in plaques as compared to nmAβ (Fig. 4d–e). Moreover, there was an increase in the number of larger sized (> 1500 μm^2) as well as smaller sized (< 600 μm^2) deposits of N3pE-Aβ along with pSer8-Aβ, nmAβ and total Aβ species in the analyzed-brain regions of TREM2^{T66M} mice (Fig. 4f–h, Additional file 2: Source data 4). Again, no selective accumulation of N3pE-Aβ as compared to that of nmAβ was observed in brains of TREM2^{T66M} expressing mice (Fig. 4i–j). These findings further support a selective increase of pSer8-Aβ in parenchymal plaques in mice with impaired TREM2 function.

Loss of TREM2 function increases intraneuronal and vascular deposition of Aβ species

Clustering of Iba1 positive microglia around plaques was apparent in the different APP transgenic mouse models expressing endogenous TREM2 at advanced and earlier stages of Aβ deposition, but was strongly reduced in brains of the respective TREM2$^{-/-}$ (Additional file 1: Figure S7a-b) and TREM2^{T66M} KI mice (Fig. 5a-b). Consistent with previous reports [8, 28, 51], TREM2$^{-/-}$ mice showed much less compact Aβ deposits as compared to TREM2$^{+/+}$ mice. Similar observations were made with the APP/PS1ΔE9-TREM2^{T66M} KI mice as compared to APP/PS1ΔE9-TREM2 mice, indicating that impaired barrier function of microglia caused by dysfunctional TREM2 promotes the deposition of smaller plaques containing pSer8-Aβ. In addition, brains of APP transgenic TREM2$^{-/-}$ and TREM2^{T66M} KI mice showed strongly elevated deposition of pSer8-Aβ within neurons as compared to brains from APP transgenic mice expressing endogenous functional TREM2 (Fig. 5c–d, Additional file 1: Figure S7c-d).

We also performed western immunoblotting analyses with different fractions of brain extracts from APP/PS1ΔE9-TREM2 and APP/PS1ΔE9-TREM2^{T66M} KI mice. Levels of pSer8-Aβ, nmAβ, and total Aβ (immunostained with 4G8 or 2964 antibody) were significantly increased in the RIPA extracts with low detergent concentration that could contain extracellular and membrane-associated monomeric and oligomeric Aβ species (Fig. 6a–h). Consistent with the higher aggregation propensity of pSer8-Aβ, pSer8-Aβ reactivity was also observed in the upper region of the blot that likely represent SDS-stable oligomers. These species were also detected by antibodies 4G8 or 2964 that detect Aβ independently of the modification state. In contrast, non-modified Aβ was almost exclusively detected as monomers. However, levels of monomeric non-modified Aβ were also increased in RIPA extracts of APP/PS1ΔE9-TREM2^{T66M} KI as compared to that of APP/PS1ΔE9-TREM2 WT mouse brains. In the SDS fractions that were obtained subsequently after extraction with RIPA buffer, and could also contain intracellular Aβ, levels of pSer8-Aβ migrating in the monomeric band were similar between TREM2 WT and TREM2^{T66M} brains. Notably, levels of oligomeric pSer8-Aβ were elevated in TREM2^{T66M} brains, indicating higher levels of pSer8-Aβ containing oligomers upon loss of TREM2 function. As observed for the RIPA extracts, nmAβ was also not detected as oligomers in the SDS fraction. Levels of monomeric nmAβ were decreased in the SDS fraction of TREM2^{T66M} mice as compared to that of TREM2 WT mice (Fig. 6i–l). Increased levels of oligomeric Aβ in brains of TREM2^{T66M} mice were confirmed with antibodies 4G8 and 2964 in both, RIPA and SDS extracts (Fig. 6m–p). Together these data indicate that TREM2 could limit the accumulation of oligomeric Aβ assemblies which contain Ser8-Aβ. These oligomers might further aggregate to form Aβ deposits consistent with the increased plaque deposition observed in brains of mice with TREM2 deletion or expression of the dysfunctional TREM2^{T66M} variant. Notably, increased deposition of pSer8-Aβ and nmAβ was not only observed in form of extracellular plaques, but also in brain vessels of APP/PS1L166P-TREM2$^{-/-}$ mice as compared to APP/PS1L166P-TREM2$^{+/+}$ mice (Additional file 1: Figure S7e). This vascular deposition of Aβ resembles cerebral amyloid angiopathy (CAA) observed in different APP transgenic mouse models, and very commonly in human AD brains [11, 37, 65].

TREM2 variants are associated with quantitative and qualitative differences in the deposition of distinct Aβ species in human brains

To assess the effect of rare disease associated TREM2 variants in human brain tissue, AD cases with

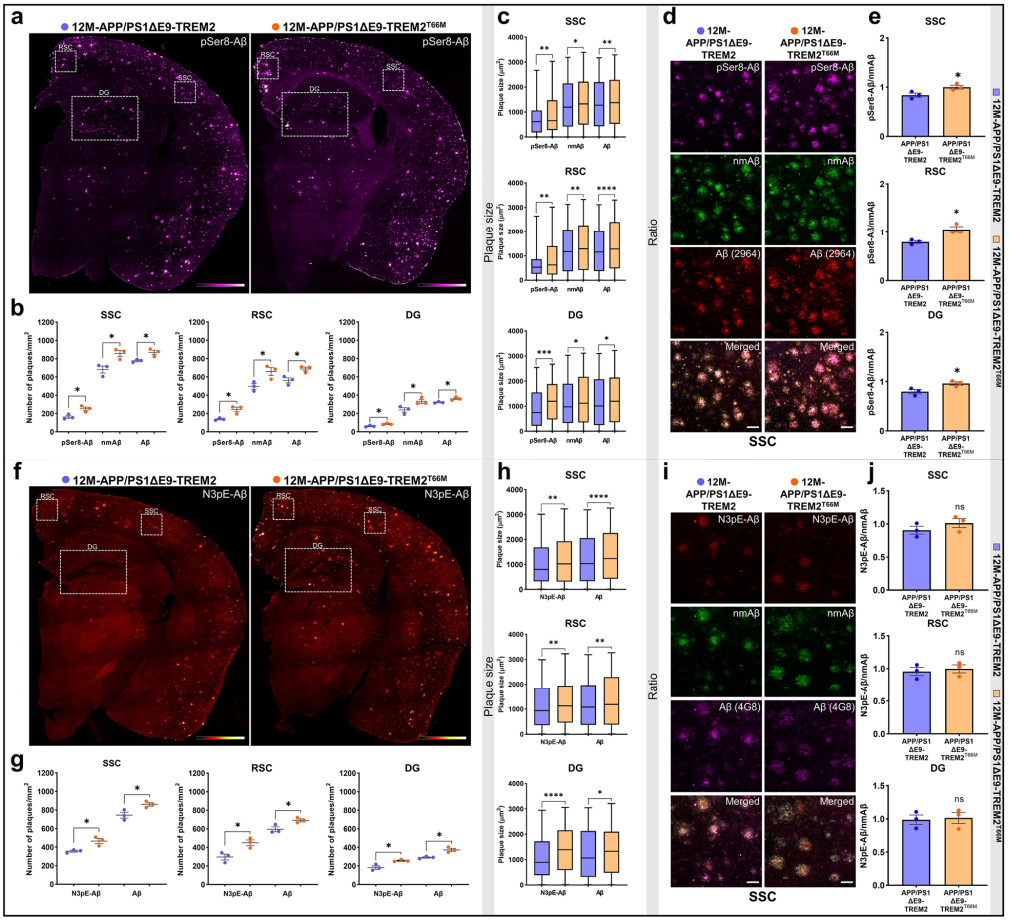

Fig. 4 TREM2^{T66M} causes increased deposition of pSer8-Aβ and N3pE-Aβ in APP/PS1 transgenic mouse brains. **a** Representative pSer8-Aβ stained female 12 M old-APP/PS1ΔE9-TREM2 and APP/PS1ΔE9-TREM2^{T66M} mouse brain sections (color scale bar = 35 mm, represents min/max pixel intensities, 10x). **b** Dot plots representing number of plaques/mm^2, **c** Box and whiskers plots showing sizes of plaques (μm^2) stained with N3pE-Aβ, nmAβ, and Aβ (2964) antibodies in the SSC, RSC, and DG of female 12 M APP/PS1ΔE9-TREM2^{T66M} and APP/PS1ΔE9-TREM2 mice. **d** Representative images showing deposition of pSer8-Aβ, nmAβ, and Aβ (2964) in SSC of female 12 M-APP/PS1ΔE9-TREM2^{T66M} and APP/PS1ΔE9-TREM2 mice (scale bar = 50 μm, 40xW). **e** Ratio of pSer8/nmAβ in SSC ($t(3.953) = 2.863$, $^*p = 0.0464$), RSC ($t(2.915) = 3.94$,$^*p = 0.0307$), and DG ($t(3.743) = 3.018$,$^*p = 0.0427$) of female 12 M-APP/PS1ΔE9-TREM2^{T66M} compared with APP/PS1ΔE9-TREM2 mice. **f** Representative N3pE-Aβ stained female 12 M-APP/PS1ΔE9-TREM2 and APP/PS1ΔE9-TREM2^{T66M} mouse brain sections (color scale bar = 35 mm, represents min/max pixel intensities, 10x). **g** Dot plots representing number of plaques/mm^2, **h** Box and whiskers plots representing size of plaques (μm^2) stained with N3pE-Aβ and Aβ (4G8) antibodies in the SSC, RSC, and DG of the female 12 M-APP/PS1ΔE9-TREM2^{T66M} and APP/PS1ΔE9-TREM2 mice. **i** Representative images showing deposition of N3pE-Aβ, nmAβ, and Aβ (4G8) in SSC of female 12 M-APP/PS1ΔE9-TREM2^{T66M} and APP/PS1ΔE9-TREM2 mice (scale bar = 50 μm, 40xW). **j** Ratio of N3pE-Aβ/nmAβ in SSC, RSC, and DG of female 12 M-APP/PS1ΔE9-TREM2^{T66M} compared with APP/PS1ΔE9-TREM2 mice. Each dot represents average value of number of plaques or ratio/animal. The box and whiskers plots represent min/max values of distribution of plaque size with the median (shown by the line dividing the box) and the dot plots represent mean ± SEM (n = 3 animals, color- blue (APP/PS1ΔE9-TREM2) and orange (APP/PS1ΔE9-TREM2^{T66M}), unpaired t-test with Welch's correction for analysis of the number and ratio while Mann–Whitney test for plaque size, $^{ns}p > 0.05$, $^*p < 0.05$, $^{**}p < 0.01$, $^{***}p < 0.001$ or $^{****}p < 0.0001$)

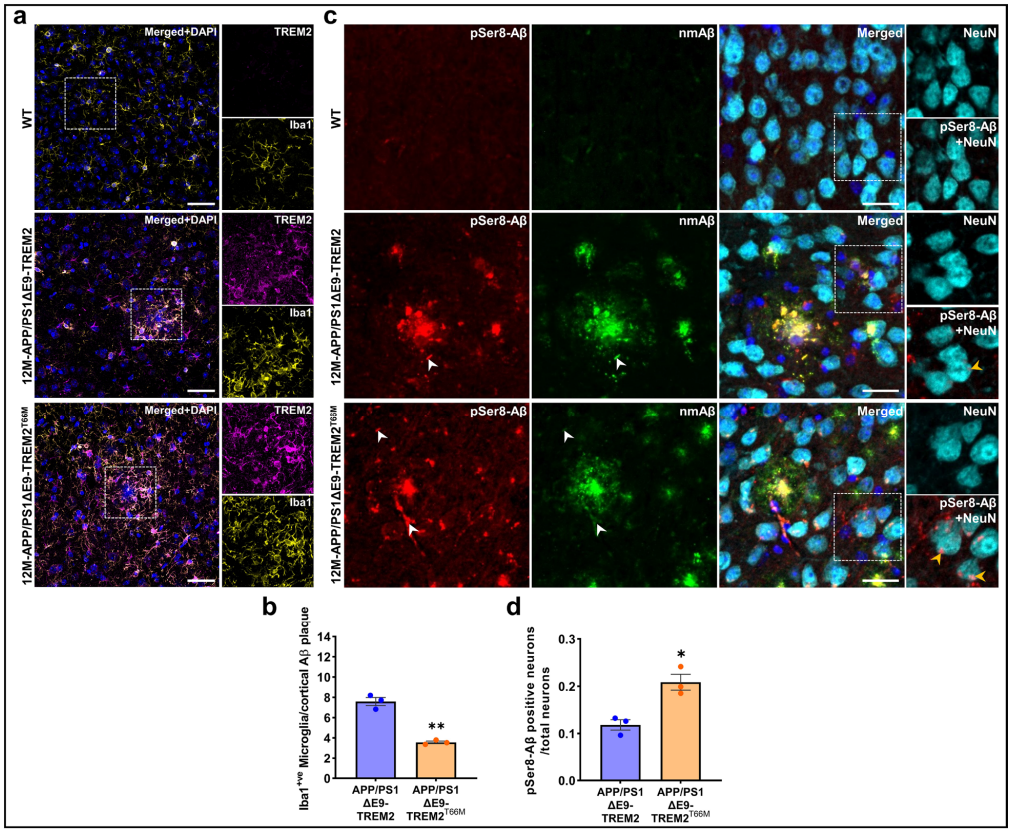

Fig. 5 TREM2^{T66M} causes increased Aβ in the APP/PS1 transgenic mouse brains. **a** Representative IF images of TREM2 along with microglial marker, Iba1 in female 12 M old- APP/PS1ΔE9 and APP/PS1ΔE9-TREM2^{T66M} mice. Dotted white boxes indicate the area shown at higher magnification (Scale bar = 50 µm, 20x). **b** Quantification showing decreased plaque associated Iba1^{+ve} microglia surrounding cortical plaques in female 12 M-APP/PS1ΔE9-TREM2^{T66M} as compared to APP/PS1ΔE9-TREM2 mice ($t(2.392) = 9.566$,$^{**}p = 0.0058$). Each dot represents the mean value of microglia count surrounding 30 cortical plaques/animal. **c** Representative IF images of pSer8-Aβ and nmAβ localized in extracellular plaques, vessels (white arrowheads) and within NeuN positive neurons (yellow arrowheads) in SSC of female APP/PS1ΔE9-TREM2 and APP/PS1ΔE9-TREM2^{T66M} mice. Dotted white boxes indicate the area shown at higher magnification (Scale bar = 50 µm, 40xW). **d** Quantification of intraneuronal pSer8-Aβ normalized to total number of neurons/ROI showed significantly increased intraneuronal pSer8-Aβ deposits in the SSC of female 12 M-APP/PS1ΔE9-TREM2^{T66M} as compared to APP/PS1ΔE9-TREM2 mice ($t(3.466) = 4.459$, $^{*}p < 0.0154$). All data represent mean ± SEM (n = 3 animals, color- blue (APP/PS1ΔE9-TREM2) and orange (APP/PS1ΔE9-TREM2^{T66M}), unpaired t-test with Welch's correction)

TREM2$^{R62H/R62C}$ variants and the clinical diagnosis for dementia were compared to cases with the TREM2 common variant (CV) also diagnosed with dementia. All cases fulfilled the criteria for neuropathological diagnosis of AD (Table 2). Sequential temporal neocortical sections were stained separately with the phosphorylation-state specific antibodies 7H3D6 (nmAβ), 1E4E11 (pSer8-Aβ), and with 4G8 that detects Aβ independently of the phosphorylation state. In addition to extracellular plaques, all cases showed Aβ depositions in the wall of cerebral blood vessels, and inside of neurons (Fig. 7a, Additional file 1: Figure S8a).

TREM2$^{R62H/R62C}$ variant cases had increased number and size of 4G8 positive plaques resulting in a higher plaque load (% area) as compared to cases with the TREM2 common variant. Further, we also observed a higher number of smaller extracellular deposits stained with 4G8 antibody in TREM2 CV cases (Fig. 7a–d,

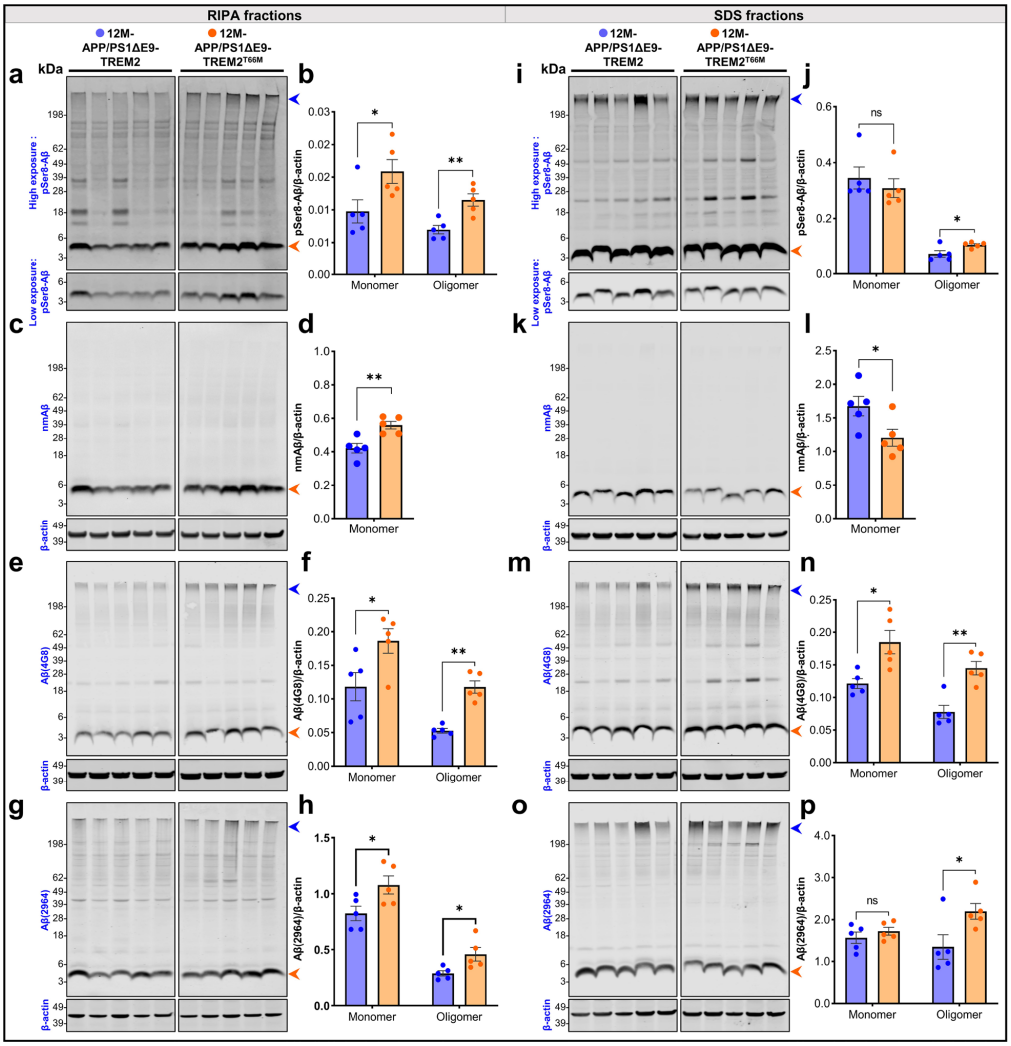

Fig. 6 Increased pSer8-Aβ in brain extracts of APP/PS1 ΔE9-TREM2^{T66M} transgenic mouse brains. **a–h** Immunoblots and quantification showing levels of monomeric and oligomeric Aβ variants in RIPA extracts of brains of female 12 M old-APP/PS1ΔE9-TREM2^{T66M} as compared to APP/PS1ΔE9-TREM2 mice; pSer8-Aβ immunostained with antibody 1E4E11, (*monomer:* $t(7.993) = 2.391$, $^{*}p = 0.0438$; *oligomer:* $t(7.074) = 3.925$, $^{**}p = 0.0056$), nmAβ detected with antibody 7H3D6 (*monomer:* $t(7.608) = 3.849$, $^{**}p = 0.0054$), Aβ immunostained with antibody 4G8 (*monomer:* $t(7.847) = 2.454$, $^{*}p = 0.0402$; *oligomer:* $t(5.134) = 6.604$, $^{**}p = 0.0011$) or antibody 2964 (*monomer:* $t(7.607) = 2.46$, $^{*}p = 0.0408$; *oligomer:* $t(5.181) = 2.63$, $^{*}p = 0.045$) antibodies. **i–p** Immunoblots and quantification showing levels of monomeric and oligomeric Aβ variants in SDS extracts of brains of female 12 M-APP/PS1ΔE9-TREM2^{T66M} as compared to APP/PS1ΔE9-TREM2 mice; pSer8-Aβ immunostained with antibody 1E4E11, (*monomer:* $t(7.81) = 0.708$, $^{ns}p = 0.4995$; *oligomer:* $t(5.14) = 2.62$, $^{*}p = 0.0458$), nmAβ detected with antibody 7H3D6 (*monomer:* $t(7.886) = 2.449$, $^{*}p = 0.0404$), Aβ immunostained with antibody 4G8 (*monomer:* $t(5.396) = 3.255$, $^{*}p = 0.0202$; *oligomer:* $t(7.999) = 4.642$, $^{**}p = 0.0017$) or antibody 2964 (*monomer:* $t(7.153) = 0.939$, $^{ns}p = 0.3784$; *oligomer:* $t(6.775) = 2.434$, $^{*}p = 0.0463$) antibodies. Each dot represents ratio of Aβ signal to β-actin per animal. All data represent mean ± SEM (n = 5 animals, *monomer: orange arrowheads and oligomer: blue arrowheads*, color- blue (APP/PS1ΔE9-TREM2) and orange (APP/PS1ΔE9-TREM2^{T66M}), unpaired t-test with Welch's correction). Original uncropped immunoblots are provided in the Additional file 2: Source data 5

Additional file 1: Figure S8b-c). Interestingly, only two of the six TREM2$^{R62H/R67C}$ cases showed very few extracellular nmAβ positive deposits, while five out of six cases with the TREM2 CV showed abundant deposition of nmAβ (detected by antibody 7H3D6) in extracellular plaques, indicating that deposition of N-terminally non-modified Aβ species is reduced in cases with disease associated TREM2 variants. In contrast, pSer8-Aβ was present in extracellular plaques in TREM2$^{R62H/R62C}$ and TREM2 CV cases, and prominently detected in the core of plaques. The number of pSer8-Aβ positive extracellular plaques and plaque load (% area) was not significantly different between TREM2$^{R62H/R62C}$ and TREM2 CV cases (Fig. 7e-f). pSer8-Aβ deposits stained with 1E4E11 were overall smaller as deposits stained with antibody 4G8 that detects total Aβ with positively skewed plaque size distribution with both antibodies and in all cases (Fig. 7g, Additional file 1: Figure S8d-e). However, analysis of plaque size distribution revealed that the number and size of pSer8-Aβ positive extracellular deposits were decreased in TREM2$^{R62H/R62C}$ cases as compared to TREM2 CV cases (Additional file 1: Figure S8d-e).

pSer8-Aβ and nmAβ was also detected in vessels in TREM2$^{R62H/R62C}$ and TREM2 CV cases. However, further analyses on the regional and quantitative deposition of phosphorylated Aβ species in different disease stages would be required to assess a potential effect of TREM2 genotypes on CAA in mouse and human brains (Additional file 1: Figures S7e, S8a; Fig. 7a).

We also observed intraneuronal deposition of nmAβ and pSer8-Aβ species. Interestingly, the number of neurons with nmAβ and pSer8-Aβ positive intracellular deposits was significantly higher in TREM2$^{R62H/62C}$ carriers as compared to TREM2 CV cases (Fig. 7h–i).

Discussion

Here, we show that deletion of TREM2 or TREM2 disease associated variants lead to specific quantitative and qualitative changes of Aβ deposits in brains of APP transgenic mice and human cases with the diagnosis of dementia, and that TREM2 not only modulates the composition of extracellular plaques, but also of intraneuronal deposits.

TREM2 plays a fundamental role in the regulation of microglial activity and the deposition of Aβ in extracellular plaques [28, 29, 31, 68]. Aβ exists in multiple variants with different lengths and post-translational modifications which differ in their aggregation behavior, biostability, deposition and neurotoxic properties [1, 42]. It was shown recently that phosphorylation of Aβ modulates the direct interaction with TREM2 and the internalization by microglia [31]. Phosphorylation at Ser8 also decreases the degradation of Aβ by the insulin degrading enzyme that can be secreted by microglia [39, 61].

To assess the role of TREM2 in the deposition of modified Aβ species in-vivo, we analyzed Aβ pathology in three different mouse models of AD. Consistent with previous reports [28, 76], TREM2 deletion was associated with increased Aβ deposition at younger (4–5 month) and older ages (12–15 month), and impaired microglial clustering around extracellular Aβ plaques [31]. Importantly, the phosphorylated Aβ species, pSer8-Aβ, selectively increased as compared to other Aβ species in brains of 5xFAD and APP/PS1L166P transgenic mice upon deletion of TREM2. Increased accumulation of phosphorylated Aβ species was also observed in brains of knock-in (KI) mice with the TREM2^{T66M} mutation that causes FTD-like syndrome and NHD in humans. In this regard,

(See figure on next page.)

Fig. 7 Differential deposition of phosphorylated Aβ species in human brains with the common and rare variants of TREM2. **a** Temporal neocortex of human AD patients with the indicated TREM2 variants (see Table 2) stained to detect total Aβ (with 4G8), nmAβ, and pSer8-Aβ on consecutive sections. Immunostaining clearly indicated decreased deposition of N-terminally non-modified Aβ species in the TREM2 variants. pSer8-Aβ stained the plaques along with vascular as well as intracellular deposits. (Scale bar = 200 µm, 20×, the magnified dotted 4 red boxes within ROI and the small square boxes of 120 × 120 µm on the right-side (for plaques and vessels) represents deposition characteristics on consecutive sections except the square box of 45 × 45 µm for the neuronal deposits). **b–c** Quantification of the number of plaques ($t(6.997) = 2.378$, $^{*}p = 0.0490$) and percent plaque load ($t(7.786) = 2.412$, $^{*}p = 0.0432$) stained with 4G8 antibody in the analyzed ROIs of TREM2 risk allele carriers (Plaque area cutoff = 10 µm^2, n = 6 cases each for TREM2 variants and CV, unpaired t-test with Welch's correction). **d** Box and whiskers plot showing a significant increase in the plaque size of TREM2 variants compared to CV cases (n = 68,631 (CV) and n = 88,835 (TREM2 variants), $^{****}p < 0.0001$, Mann–Whitney test. Additional data are provided in Additional file 1: Figure S8b-c. **e**, **f** Quantification of the numbers of plaques ($t(6.96) = 0.3754$, $^{ns}p = 0.7185$) and the percent plaque load ($t(4.366) = 0.5145$, $^{ns}p = 0.6319$) stained with pSer8-Aβ antibody in the analyzed ROIs of TREM2 risk allele carriers (Plaque area cutoff = 30 µm^2, n = 5 cases for TREM2 variants and n = 6 cases for CV, unpaired t-test with Welch's correction). Case#3, with highest fixation time, was omitted for the plaque count and size quantification as it was difficult to identify extracellular plaques stained with 1E4E11 (pSer8-Aβ) antibody. **g** Box and whiskers plot showing a significant decrease in the plaque size of TREM2 variants compared to CV cases (n = 17,456 (CV) and 13,291 (TREM2 variants), $^{****}p < 0.0001$, Mann–Whitney test. Additional data are provided in Additional file 1: Figure S8d-e. There was a significant increase of intracellular deposits of **h** nmAβ ($t(9.138) = 2.429$, $^{*}p = 0.0377$) and **i** pSer8-Aβ ($t(9.389) = 2.251$, $^{*}p = 0.0497$) in the analyzed cortical ROIs of TREM2 variant as compared to CV cases (n = 6 cases each for TREM2 variants and CV, unpaired t-test with Welch's correction). No data or numerical value was excluded unless otherwise stated. Each colored dot with respective gender symbol represents single case. Except for bot and whiskers plot, all data represent mean ± SEM

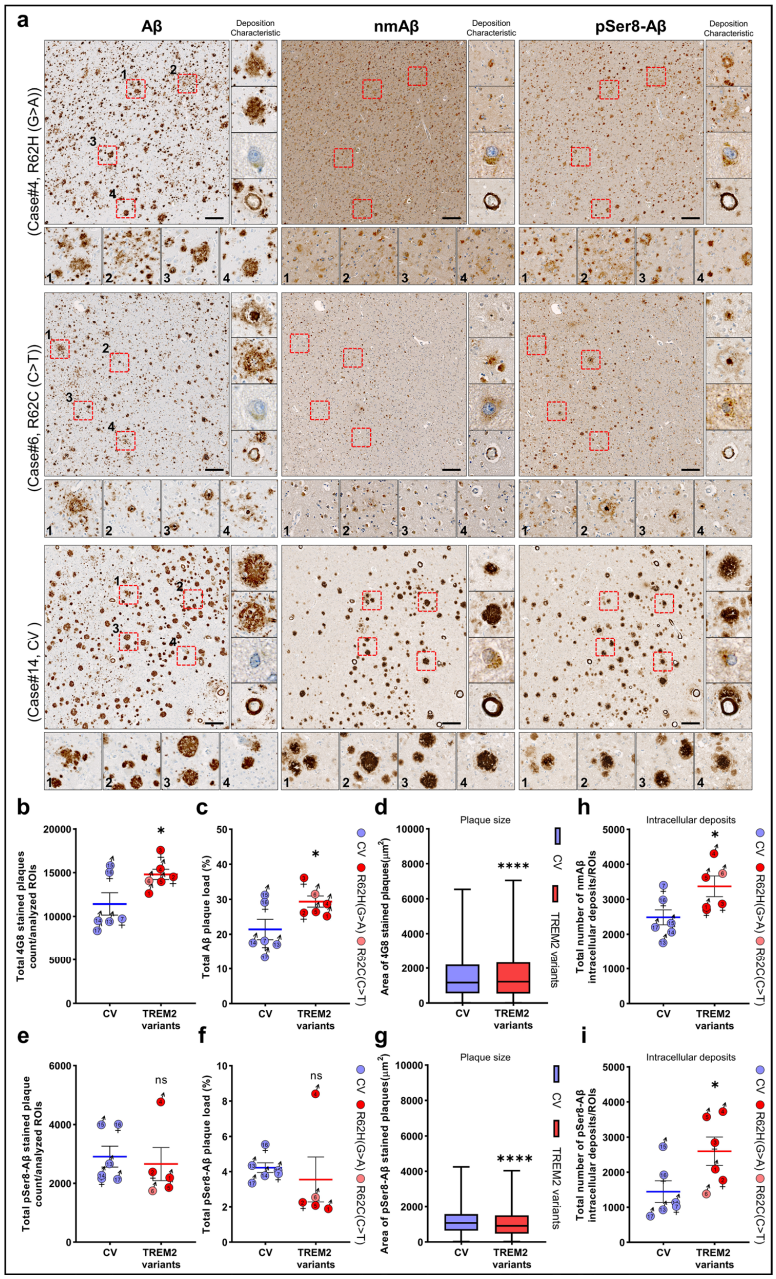

Fig. 7 (See legend on previous page.)

it is interesting to note that NHD cases could show AD characteristic neuropathological lesions, including senile plaques and neurofibrillary tangles [4]. Consistent with previous findings [31, 36, 40, 41], pSer8-Aβ is prominently detected in the core of extracellular plaques and intraneuronally. The deposition of pSer8-Aβ in both lesions was increased in brains of 12 M old TREM2$^{-/-}$ as compared with TREM2$^{+/+}$ in 5xFAD as well as APP/PS1L166P transgenic mice. Very similar alterations in the deposition of the different Aβ species were also observed in TREM2^{T66M} KI mice as compared to mice expressing functional TREM2, indicating that disease associated loss of function mutations also modulate the differential deposition of distinct Aβ variants.

Biochemical analysis of brain extracts revealed that TREM2 deficiency or the expression of the NHD associated T66M in APP transgenic mice increased the levels of pSer8-Aβ in form of oligomeric assemblies. Aβ oligomers exert neurotoxicity, and oligomer levels correlate with neuronal dysfunction in AD [3, 21, 50, 56, 57, 62, 80]. Aβ oligomers also seed fibrillization and promote the deposition in form of extracellular plaques [6, 10, 20, 32]. In addition, oligomers can be internalized by neurons resulting in Aβ accumulation within neurons [2, 9, 13, 56, 60]. Since TREM2 has been shown to selectively bind oligomeric assemblies of Aβ and promote microglial uptake [31, 44, 72, 82], the loss of TREM2 function could result in decreased clearance of oligomers and thereby lead to increased uptake by neurons, and deposition in extracellular plaques and the vasculature. Indeed, altered plaque development and CAA related pathology has recently been observed in mouse brain upon depletion of microglia [23, 59], showing that functional microglia are important to shape extracellular plaques and to restrict the deposition of Aβ in the brain vasculature. We also detected pSer8-Aβ and nmAβ in vessels of transgenic mouse brains, and it will be interesting the further investigate the role of TREM2 in the deposition and the potential pathophysiological implications of modified Aβ species in the vasculature.

The analysis of human cases with rare TREM2^{R62H} or TREM2^{R62C} variants showed significantly increased accumulation of phosphorylated Aβ species inside of neurons and alterations in plaque size, load and number, further indicating that impairment of TREM2 function mediates the formation and composition of AD characteristic lesions.

Thus, in addition to the previously described effects of TREM2 on plaque morphology, our data provide evidence for a critical role of TREM2 in restriction of intraneuronal Aβ deposits that are highly correlated with clinical presentation and disease progression [2, 7, 14, 15, 27, 63, 77]. Further, we show here that TREM2 also modulates the composition of these lesions. This is interesting, because changes in the composition of extracellular plaques and CAA, in particular the occurrence of phosphorylated Aβ, are associated with clinical manifestation and progression of AD [11, 46, 54, 64].

Although TREM2 loss of function mutations could also contribute to neurodegeneration independently of Aβ by impairment of brain energy metabolism [33], synapse dynamics [26, 48], and formation of neurofibrillary tangles [45], a recent study suggests an important role of Aβ pathology in the TREM2 dependent formation of tau pathology and brain atrophy [43]. Thus, the differential interaction of TREM2 with modified Aβ species might not only be important for the deposition and composition of different Aβ lesions, but also contribute to the development of tau pathology that together determine onset and progression of AD.

Abbreviations

AD: Alzheimer's disease; ADAM: A disintegrin and metalloproteinases; ApoE4: Apolipoprotein E4 allele; APP: Amyloid precursor protein; Aβ: Amyloid-β; CAA : Cerebral amyloid angiopathy; CV: Common variant; DAB: 3,3′-Diaminobenzidine; DAPI: 4′,6-Diamidino-2-phenylindole; DG: Dentate gyrus; EDTA: Ethylenediaminetetraacetic acid; EGTA: Ethylene glycol-bis(β-aminoethyl ether)-N,N,N′,N′-tetraacetic acid; EtOH: Ethanol; FAD: Familial Alzheimer's disease; FTD: Frontotemporal dementia; GWAS: Genome-wide association studies; IF: Immunofluorescence; IHC: Immunohistochemistry; IntDen: Integrated density; KI: Knock-In; NaDOC: Sodium Deoxycholate; N3pE-Aβ: N-terminal pyroglutamate-modified Amyloid-β; NaOH: Sodium hydroxide; NFTs: Neurofibrillary tangles; NHD: Nasu–Hakola disease; nmAβ: Non-modified Amyloid-β; PBS: Phosphate buffer saline; pSer8-Aβ: Phosphorylation at serine 8 of Amyloid-β; RIPA: Radioimmunoprecipitation assay; ROI: Region of interest; RSC: Retrosplenial cortex; RT: Room temperature; SDS: Sodium dodecyl sulphate; PAGE: Polyacrylamide gel electrophoresis; SSC: Somatosensory cortex; sTREM2: Soluble variants of Triggering receptor expressed on myeloid cells 2; TREM2: Triggering receptor expressed on myeloid cells 2; Tris: Tris(hydroxymethyl)aminomethane; TBS: Tris-buffered saline; WT: Wild type.

Supplementary Information

The online version contains supplementary material available at https://doi.org/10.1186/s40478-021-01263-x.

Additional file 1: Supplementary figures.

Additional file 2: Source data.

Acknowledgements

This work was supported by the Deutsche Forschungsgemeinschaft, Grant WA1477/6-6 (to JW), the EU Innovative Medicines Initiative 2 Joint Undertaking (IMI2 JU), Grant/Award Number: No 115976 (PHAGO). PJ thanks the BIGS neuroscience and the University of Bonn for their support. PJ also thanks Lorenz Haase, Research department fundamental physics, Max Planck Institute for Radio Astronomy, Bonn, for his critical suggestions on the analysis done in this study. Authors thank the Microscopy Core Facility of the Medical Faculty at the University of Bonn for providing support and instrumentation funded by the Deutsche Forschungsgemeinschaft, Project Number: 388169927.

Authors' contributions
PJ and JW conceived the study. PJ performed most of the experiments and analyzed data. SK, FR, and ST contributed to biochemical and immunohistochemical experiments and interpretation. SP, CH, MC, NV, and MTH provided mouse brains. PJ, TA and JH selected and analyzed human brains. PJ and JW wrote the manuscript with help all co-authors. All of the authors read, edited and approved the final version of the manuscript.

Availability of data and materials
The data that support the findings of this study is available from the corresponding author upon reasonable request.

Declarations

Competing interests
The authors declare no competing financial interests.

Author details
[1]Department of Neurology, University of Bonn, Venusberg-Campus 1, (Formerly Sigmund-Freud-Str. 25), 53127 Bonn, Germany. [2]Department of Neurodegenerative Diseases and Gerontopsychiatry, University Hospital Bonn, Bonn, Germany. [3]Neuroinflammation Unit, German Center for Neurodegenerative Diseases e. V. (DZNE), Bonn, Germany. [4]Biomedical Center (BMC), Faculty of Medicine, Ludwig-Maximilians-Universität München, Munich, Germany. [5]Munich Cluster for Systems Neurology (SyNergy), Munich, Germany. [6]Molecular Neurodegeneration Unit, German Center for Neurodegenerative Diseases e.V. (DZNE) Munich, Munich, Germany. [7]Department of Pathology and Immunology, Washington University School of Medicine, St. Louis, USA. [8]Center for Neuropathology and Prion Research, Ludwig-Maximilians-Universität München, Munich, Germany. [9]Department of Psychiatry and Psychotherapy, Ludwig-Maximilians-Universität München, Munich, Germany.

Received: 13 September 2021 Accepted: 14 September 2021
Published online: 18 October 2021

References

1. Barykin EP, Mitkevich VA, Kozin SA, Makarov AA (2017) Amyloid beta modification: a key to the Sporadic Alzheimer's Disease? Front Genet 8:58. https://doi.org/10.3389/fgene.2017.00058
2. Bayer TA, Wirths O (2010) Intracellular accumulation of amyloid-Beta—a predictor for synaptic dysfunction and neuron loss in Alzheimer's disease. Front Aging Neurosci 2:8. https://doi.org/10.3389/fnagi.2010.00008
3. Benilova I, Karran E, De Strooper B (2012) The toxic Abeta oligomer and Alzheimer's disease: an emperor in need of clothes. Nat Neurosci 15:349–357. https://doi.org/10.1038/nn.3028
4. Bird TD, Koerker RM, Leaird BJ, Vlcek BW, Thorning DR (1983) Lipomembranous polycystic osteodysplasia (brain, bone, and fat disease): a genetic cause of presenile dementia. Neurology 33:81–86. https://doi.org/10.1212/wnl.33.1.81
5. Bis JC, Jian X, Kunkle BW, Chen Y, Hamilton-Nelson KL, Bush WS, Salerno WJ, Lancour D, Ma Y, Renton AE et al (2020) Whole exome sequencing study identifies novel rare and common Alzheimer's-Associated variants involved in immune response and transcriptional regulation. Mol Psychiatry 25:1859–1875. https://doi.org/10.1038/s41380-018-0112-7
6. Chen GF, Xu TH, Yan Y, Zhou YR, Jiang Y, Melcher K, Xu HE (2017) Amyloid beta: structure, biology and structure-based therapeutic development. Acta Pharmacol Sin 38:1205–1235. https://doi.org/10.1038/aps.2017.28
7. Condello C, Lemmin T, Stohr J, Nick M, Wu Y, Maxwell AM, Watts JC, Caro CD, Oehler A, Keene CD et al (2018) Structural heterogeneity and intersubject variability of Abeta in familial and sporadic Alzheimer's disease. Proc Natl Acad Sci USA 115:E782–E791. https://doi.org/10.1073/pnas.1714966115
8. Condello C, Yuan P, Schain A, Grutzendler J (2015) Microglia constitute a barrier that prevents neurotoxic protofibrillar Abeta42 hotspots around plaques. Nat Commun 6:6176. https://doi.org/10.1038/ncomms7176
9. Friedrich RP, Tepper K, Ronicke R, Soom M, Westermann M, Reymann K, Kaether C, Fandrich M (2010) Mechanism of amyloid plaque formation suggests an intracellular basis of Abeta pathogenicity. Proc Natl Acad Sci USA 107:1942–1947. https://doi.org/10.1073/pnas.0904532106
10. Friesen M, Meyer-Luehmann M (2019) Abeta seeding as a tool to study cerebral amyloidosis and associated pathology. Front Mol Neurosci 12:233. https://doi.org/10.3389/fnmol.2019.00233
11. Gerth J, Kumar S, Rijal Upadhaya A, Ghebremedhin E, von Arnim CAF, Thal DR, Walter J (2018) Modified amyloid variants in pathological subgroups of beta-amyloidosis. Ann Clin Transl Neurol 5:815–831. https://doi.org/10.1002/acn3.577
12. Glebov K, Wunderlich P, Karaca I, Walter J (2016) Functional involvement of gamma-secretase in signaling of the triggering receptor expressed on myeloid cells-2 (TREM2). J Neuroinflammation 13:17. https://doi.org/10.1186/s12974-016-0479-9
13. Gouras GK, Almeida CG, Takahashi RH (2005) Intraneuronal Abeta accumulation and origin of plaques in Alzheimer's disease. Neurobiol Aging 26:1235–1244. https://doi.org/10.1016/j.neurobiolaging.2005.05.022
14. Gouras GK, Tampellini D, Takahashi RH, Capetillo-Zarate E (2010) Intraneuronal beta-amyloid accumulation and synapse pathology in Alzheimer's disease. Acta Neuropathol 119:523–541. https://doi.org/10.1007/s00401-010-0679-9
15. Gouras GK, Tsai J, Naslund J, Vincent B, Edgar M, Checler F, Greenfield JP, Haroutunian V, Buxbaum JD, Xu H et al (2000) Intraneuronal Abeta42 accumulation in human brain. Am J Pathol 156:15–20. https://doi.org/10.1016/s0002-9440(10)64700-1
16. Gratuze M, Leyns CEG, Holtzman DM (2018) New insights into the role of TREM2 in Alzheimer's disease. Mol Neurodegener 13:66. https://doi.org/10.1186/s13024-018-0298-9
17. Guerreiro R, Bilgic B, Guven G, Bras J, Rohrer J, Lohmann E, Hanagasi H, Gurvit H, Emre M (2013) Novel compound heterozygous mutation in TREM2 found in a Turkish frontotemporal dementia-like family. Neurobiol Aging 34(2890):e2891-2895. https://doi.org/10.1016/j.neurobiolaging.2013.06.005
18. Guerreiro R, Wojtas A, Bras J, Carrasquillo M, Rogaeva E, Majounie E, Cruchaga C, Sassi C, Kauwe JS, Younkin S et al (2013) TREM2 variants in Alzheimer's disease. N Engl J Med 368:117–127. https://doi.org/10.1056/NEJMoa1211851
19. Guerreiro RJ, Lohmann E, Bras JM, Gibbs JR, Rohrer JD, Gurunlian N, Dursun B, Bilgic B, Hanagasi H, Gurvit H et al (2013) Using exome sequencing to reveal mutations in TREM2 presenting as a frontotemporal dementia-like syndrome without bone involvement. JAMA Neurol 70:78–84. https://doi.org/10.1001/jamaneurol.2013.579
20. Hardy J, Selkoe DJ (2002) The amyloid hypothesis of Alzheimer's disease: progress and problems on the road to therapeutics. Science 297:353–356. https://doi.org/10.1126/science.1072994
21. He Y, Wei M, Wu Y, Qin H, Li W, Ma X, Cheng J, Ren J, Shen Y, Chen Z et al (2019) Amyloid beta oligomers suppress excitatory transmitter release via presynaptic depletion of phosphatidylinositol-4,5-bisphosphate. Nat Commun 10:1193. https://doi.org/10.1038/s41467-019-09114-z
22. Heneka MT, Kummer MP, Stutz A, Delekate A, Schwartz S, Vieira-Saecker A, Griep A, Axt D, Remus A, Tzeng TC et al (2013) NLRP3 is activated in Alzheimer's disease and contributes to pathology in APP/PS1 mice. Nature 493:674–678. https://doi.org/10.1038/nature11729
23. Huang Y, Happonen KE, Burrola PG, O'Connor C, Hah N, Huang L, Nimerjahn A, Lemke G (2021) Microglia use TAM receptors to detect and engulf amyloid beta plaques. Nat Immunol. https://doi.org/10.1038/s41590-021-00913-5
24. Hyman BT, Phelps CH, Beach TG, Bigio EH, Cairns NJ, Carrillo MC, Dickson DW, Duyckaerts C, Frosch MP, Masliah E et al (2012) National Institute on Aging-Alzheimer's Association guidelines for the neuropathologic assessment of Alzheimer's disease. Alzheimers Dement 8:1–13. https://doi.org/10.1016/j.jalz.2011.10.007
25. Ibach M, Mathews M, Linnartz-Gerlach B, Theil S, Kumar S, Feederle R, Brustle O, Neumann H, Walter J (2021) A reporter cell system for the triggering receptor expressed on myeloid cells 2 reveals differential effects of disease-associated variants on receptor signaling and activation by antibodies against the stalk region. Glia 69:1126–1139. https://doi.org/10.1002/glia.23953
26. Jadhav VS, Lin PBC, Pennington T, Di Prisco GV, Jannu AJ, Xu G, Moutinho M, Zhang J, Atwood BK, Puntambekar SS et al (2020) Trem2 Y38C mutation and loss of Trem2 impairs neuronal synapses in adult mice. Mol Neurodegener 15:62. https://doi.org/10.1186/s13024-020-00409-0

27. Jawhar S, Trawicka A, Jenneckens C, Bayer TA, Wirths O (2012) Motor deficits, neuron loss, and reduced anxiety coinciding with axonal degeneration and intraneuronal Abeta aggregation in the 5XFAD mouse model of Alzheimer's disease. Neurobiol Aging 33(196):e129-140. https://doi.org/10.1016/j.neurobiolaging.2010.05.027
28. Jay TR, Miller CM, Cheng PJ, Graham LC, Bemiller S, Broihier ML, Xu G, Margevicius D, Karlo JC, Sousa GL et al (2015) TREM2 deficiency eliminates TREM2^{+} inflammatory macrophages and ameliorates pathology in Alzheimer's disease mouse models. J Exp Med 212:287–295. https://doi.org/10.1084/jem.20142322
29. Jiang T, Tan L, Zhu XC, Zhang QQ, Cao L, Tan MS, Gu LZ, Wang HF, Ding ZZ, Zhang YD et al (2014) Upregulation of TREM2 ameliorates neuropathology and rescues spatial cognitive impairment in a transgenic mouse model of Alzheimer's disease. Neuropsychopharmacology 39:2949–2962. https://doi.org/10.1038/npp.2014.164
30. Jonsson T, Stefansson H, Steinberg S, Jonsdottir I, Jonsson PV, Snaedal J, Bjornsson S, Huttenlocher J, Levey AI, Lah JJ et al (2013) Variant of TREM2 associated with the risk of Alzheimer's disease. N Engl J Med 368:107–116. https://doi.org/10.1056/NEJMoa1211103
31. Joshi P, Riffel F, Satoh K, Enomoto M, Qamar S, Scheiblich H, Villacampa N, Kumar S, Theil S, Parhizkar S et al (2021) Differential interaction with TREM2 modulates microglial uptake of modified Abeta species. Glia. https://doi.org/10.1002/glia.24077
32. Katzmarski N, Ziegler-Waldkirch S, Scheffler N, Witt C, Abou-Ajram C, Nuscher B, Prinz M, Haass C, Meyer-Luehmann M (2020) Abeta oligomers trigger and accelerate Abeta seeding. Brain Pathol 30:36–45. https://doi.org/10.1111/bpa.12734
33. Kleinberger G, Brendel M, Mracsko E, Wefers B, Groeneweg L, Xiang X, Focke C, Deussing M, Suarez-Calvet M, Mazaheri F et al (2017) The FTD-like syndrome causing TREM2 T66M mutation impairs microglia function, brain perfusion, and glucose metabolism. EMBO J 36:1837–1853. https://doi.org/10.15252/embj.201796516
34. Kleinberger G, Yamanishi Y, Suarez-Calvet M, Czirr E, Lohmann E, Cuyvers E, Struyfs H, Pettkus N, Wenninger-Weinzierl A, Mazaheri F et al (2014) TREM2 mutations implicated in neurodegeneration impair cell surface transport and phagocytosis. Sci Transl Med 6:243ra286. https://doi.org/10.1126/scitranslmed.3009093
35. Konishi H, Kiyama H (2018) Microglial TREM2/DAP12 signaling: a double-edged sword in neural diseases. Front Cell Neurosci 12:206. https://doi.org/10.3389/fncel.2018.00206
36. Kumar S, Kapadia A, Theil S, Joshi P, Riffel F, Heneka MT, Walter J (2021) Novel phosphorylation-state specific antibodies reveal differential deposition of Ser26 phosphorylated Aβ species in a mouse model of Alzheimer's disease. Front Mol Neurosci. https://doi.org/10.3389/fnmol.2020.619639
37. Kumar S, Lemere CA, Walter J (2020) Phosphorylated Abeta peptides in human Down syndrome brain and different Alzheimer's-like mouse models. Acta Neuropathol Commun 8:118. https://doi.org/10.1186/s40478-020-00959-w
38. Kumar S, Rezaei-Ghaleh N, Terwel D, Thal DR, Richard M, Hoch M, Mc Donald JM, Wullner U, Glebov K, Heneka MT et al (2011) Extracellular phosphorylation of the amyloid beta-peptide promotes formation of toxic aggregates during the pathogenesis of Alzheimer's disease. EMBO J 30:2255–2265. https://doi.org/10.1038/emboj.2011.138
39. Kumar S, Singh S, Hinze D, Josten M, Sahl HG, Siepmann M, Walter J (2012) Phosphorylation of amyloid-beta peptide at serine 8 attenuates its clearance via insulin-degrading and angiotensin-converting enzymes. J Biol Chem 287:8641–8651. https://doi.org/10.1074/jbc.M111.279133
40. Kumar S, Wirths O, Stuber K, Wunderlich P, Koch P, Theil S, Rezaei-Ghaleh N, Zweckstetter M, Bayer TA, Brustle O et al (2016) Phosphorylation of the amyloid beta-peptide at Ser26 stabilizes oligomeric assembly and increases neurotoxicity. Acta Neuropathol 131:525–537. https://doi.org/10.1007/s00401-016-1546-0
41. Kumar S, Wirths O, Theil S, Gerth J, Bayer TA, Walter J (2013) Early intraneuronal accumulation and increased aggregation of phosphorylated Abeta in a mouse model of Alzheimer's disease. Acta Neuropathol 125:699–709. https://doi.org/10.1007/s00401-013-1107-8
42. Kummer MP, Heneka MT (2014) Truncated and modified amyloid-beta species. Alzheimer's Res Therapy 6:28. https://doi.org/10.1186/alzrt258
43. Lee SH, Meilandt WJ, Xie L, Gandham VD, Ngu H, Barck KH, Rezzonico MG, Imperio J, Lalehzadeh G, Huntley MA et al (2021) Trem2 restrains the enhancement of tau accumulation and neurodegeneration by beta-amyloid pathology. Neuron 109:1283-1301 e1286. https://doi.org/10.1016/j.neuron.2021.02.010
44. Lessard CB, Malnik SL, Zhou Y, Ladd TB, Cruz PE, Ran Y, Mahan TE, Chakrabaty P, Holtzman DM, Ulrich JD et al (2018) High-affinity interactions and signal transduction between Abeta oligomers and TREM2. EMBO Mol Med. https://doi.org/10.15252/emmm.201809027
45. Leyns CEG, Ulrich JD, Finn MB, Stewart FR, Koscal LJ, Remolina Serrano J, Robinson GO, Anderson E, Colonna M, Holtzman DM (2017) TREM2 deficiency attenuates neuroinflammation and protects against neurodegeneration in a mouse model of tauopathy. Proc Natl Acad Sci USA 114:11524–11529. https://doi.org/10.1073/pnas.1710311114
46. Libard S, Walter J, Alafuzoff I (2021) In vivo characterization of biochemical variants of amyloid-beta in subjects with idiopathic normal pressure hydrocephalus and Alzheimer's disease neuropathological change. J Alzheimers Dis 80:1003–1012. https://doi.org/10.3233/JAD-201469
47. Linnartz-Gerlach B, Bodea LG, Klaus C, Ginolhac A, Halder R, Sinkkonen L, Walter J, Colonna M, Neumann H (2019) TREM2 triggers microglial density and age-related neuronal loss. Glia 67:539–550. https://doi.org/10.1002/glia.23563
48. Mazaheri F, Snaidero N, Kleinberger G, Madore C, Daria A, Werner G, Krasemann S, Capell A, Trumbach D, Wurst W et al (2017) TREM2 deficiency impairs chemotaxis and microglial responses to neuronal injury. EMBO Rep 18:1186–1198. https://doi.org/10.15252/embr.201743922
49. Paloneva J, Autti T, Raininko R, Partanen J, Salonen O, Puranen M, Hakola P, Haltia M (2001) CNS manifestations of Nasu–Hakola disease: a frontal dementia with bone cysts. Neurology 56:1552–1558. https://doi.org/10.1212/wnl.56.11.1552
50. Palop JJ, Mucke L (2010) Amyloid-beta-induced neuronal dysfunction in Alzheimer's disease: from synapses toward neural networks. Nat Neurosci 13:812–818. https://doi.org/10.1038/nn.2583
51. Parhizkar S, Arzberger T, Brendel M, Kleinberger G, Deussing M, Focke C, Nuscher B, Xiong M, Ghasemigharagoz A, Katzmarski N et al (2019) Loss of TREM2 function increases amyloid seeding but reduces plaque-associated ApoE. Nat Neurosci 22:191–204. https://doi.org/10.1038/s41593-018-0296-9
52. Portelius E, Bogdanovic N, Gustavsson MK, Volkmann I, Brinkmalm G, Zetterberg H, Winblad B, Blennow K (2010) Mass spectrometric characterization of brain amyloid beta isoform signatures in familial and sporadic Alzheimer's disease. Acta Neuropathol 120:185–193. https://doi.org/10.1007/s00401-010-0690-1
53. Rezaei-Ghaleh N, Amininasab M, Kumar S, Walter J, Zweckstetter M (2016) Phosphorylation modifies the molecular stability of beta-amyloid deposits. Nat Commun 7:11359. https://doi.org/10.1038/ncomms11359
54. Rijal Upadhaya A, Kosterin I, Kumar S, von Arnim CA, Yamaguchi H, Fandrich M, Walter J, Thal DR (2014) Biochemical stages of amyloid-beta peptide aggregation and accumulation in the human brain and their association with symptomatic and pathologically preclinical Alzheimer's disease. Brain 137:887–903. https://doi.org/10.1093/brain/awt362
55. Saido TC, Iwatsubo T, Mann DM, Shimada H, Ihara Y, Kawashima S (1995) Dominant and differential deposition of distinct beta-amyloid peptide species, A beta N3(pE), in senile plaques. Neuron 14:457–466. https://doi.org/10.1016/0896-6273(95)90301-1
56. Schutzmann MP, Hasecke F, Bachmann S, Zielinski M, Hansch S, Schroder GF, Zempel H, Hoyer W (2021) Endo-lysosomal Abeta concentration and pH trigger formation of Abeta oligomers that potently induce Tau missorting. Nat Commun 12:4634. https://doi.org/10.1038/s41467-021-24900-4
57. Sengupta U, Nilson AN, Kayed R (2016) The role of amyloid-beta oligomers in toxicity, propagation, and immunotherapy. EBioMedicine 6:42–49. https://doi.org/10.1016/j.ebiom.2016.03.035
58. Serrano-Pozo A, Mielke ML, Muzitansky A, Gomez-Isla T, Growdon JH, Backskai BJ, Betensky RA, Frosch MP, Hyman BT (2012) Stable size distribution of amyloid plaques over the course of Alzheimer disease. J Neuropathol Exp Neurol 71:694–701. https://doi.org/10.1097/NEN.0b013e31825e77de
59. Spangenberg E, Severson PL, Hohsfield LA, Crapser J, Zhang J, Burton EA, Zhang Y, Spevak W, Lin J, Phan NY et al (2019) Sustained microglial depletion with CSF1R inhibitor impairs parenchymal plaque development in an Alzheimer's disease model. Nat Commun 10:3758. https://doi.org/10.1038/s41467-019-11674-z

60. Takahashi RH, Almeida CG, Kearney PF, Yu F, Lin MT, Milner TA, Gouras GK (2004) Oligomerization of Alzheimer's beta-amyloid within processes and synapses of cultured neurons and brain. J Neurosci 24:3592–3599. https://doi.org/10.1523/JNEUROSCI.5167-03.2004
61. Tamboli IY, Barth E, Christian L, Siepmann M, Kumar S, Singh S, Tolksdorf K, Heneka MT, Lutjohann D, Wunderlich P et al (2010) Statins promote the degradation of extracellular amyloid {beta}-peptide by microglia via stimulation of exosome-associated insulin-degrading enzyme (IDE) secretion. J Biol Chem 285:37405–37414. https://doi.org/10.1074/jbc.M110.149468
62. Tanokashira D, Mamada N, Yamamoto F, Taniguchi K, Tamaoka A, Lakshmana MK, Araki W (2017) The neurotoxicity of amyloid beta-protein oligomers is reversible in a primary neuron model. Mol Brain 10:4. https://doi.org/10.1186/s13041-016-0284-5
63. Thal DR, Griffin WS, Braak H (2008) Parenchymal and vascular Abeta-deposition and its effects on the degeneration of neurons and cognition in Alzheimer's disease. J Cell Mol Med 12:1848–1862. https://doi.org/10.1111/j.1582-4934.2008.00411.x
64. Thal DR, Ronisz A, Tousseyn T, Rijal Upadhaya A, Balakrishnan K, Vandenberghe R, Vandenbulcke M, von Arnim CAF, Otto M, Beach TG et al (2019) Different aspects of Alzheimer's disease-related amyloid beta-peptide pathology and their relationship to amyloid positron emission tomography imaging and dementia. Acta Neuropathol Commun 7:178. https://doi.org/10.1186/s40478-019-0837-9
65. Thal DR, Walter J, Saido TC, Fandrich M (2015) Neuropathology and biochemistry of Abeta and its aggregates in Alzheimer's disease. Acta Neuropathol 129:167–182. https://doi.org/10.1007/s00401-014-1375-y
66. Turnbull IR, Gilfillan S, Cella M, Aoshi T, Miller M, Piccio L, Hernandez M, Colonna M (2006) Cutting edge: TREM-2 attenuates macrophage activation. J Immunol 177:3520–3524. https://doi.org/10.4049/jimmunol.177.6.3520
67. Ulland TK, Song WM, Huang SC, Ulrich JD, Sergushichev A, Beatty WL, Loboda AA, Zhou Y, Cairns NJ, Kambal A et al (2017) TREM2 maintains microglial metabolic fitness in Alzheimer's disease. Cell 170:649-663 e613. https://doi.org/10.1016/j.cell.2017.07.023
68. Ulrich JD, Finn MB, Wang Y, Shen A, Mahan TE, Jiang H, Stewart FR, Piccio L, Colonna M, Holtzman DM (2014) Altered microglial response to Abeta plaques in APPPS1-21 mice heterozygous for TREM2. Mol Neurodegener 9:20. https://doi.org/10.1186/1750-1326-9-20
69. Ulrich JD, Holtzman DM (2016) TREM2 function in Alzheimer's disease and neurodegeneration. ACS Chem Neurosci 7:420–427. https://doi.org/10.1021/acschemneuro.5b00313
70. Venegas C, Kumar S, Franklin BS, Dierkes T, Brinkschulte R, Tejera D, Vieira-Saecker A, Schwartz S, Santarelli F, Kummer MP et al (2017) Microglia-derived ASC specks cross-seed amyloid-beta in Alzheimer's disease. Nature 552:355–361. https://doi.org/10.1038/nature25158
71. Verheijen J, Sleegers K (2018) Understanding Alzheimer disease at the interface between genetics and transcriptomics. Trends Genet 34:434–447. https://doi.org/10.1016/j.tig.2018.02.007
72. Vilalta A, Zhou Y, Sevalle J, Griffin JK, Satoh K, Allendorf DH, De S, Puigdellivol M, Bruzas A, Burguillos MA et al (2021) Wild-type sTREM2 blocks Abeta aggregation and neurotoxicity, but the Alzheimer's R47H mutant increases Abeta aggregation. J Biol Chem 296:100631. https://doi.org/10.1016/j.jbc.2021.100631
73. Wahle T, Thal DR, Sastre M, Rentmeister A, Bogdanovic N, Famulok M, Heneka MT, Walter J (2006) GGA1 is expressed in the human brain and affects the generation of amyloid beta-peptide. J Neurosci 26:12838–12846. https://doi.org/10.1523/JNEUROSCI.1982-06.2006
74. Walter J (2016) The triggering receptor expressed on myeloid cells 2: a molecular link of neuroinflammation and neurodegenerative diseases. J Biol Chem 291:4334–4341. https://doi.org/10.1074/jbc.R115.704981
75. Wang Y, Cella M, Mallinson K, Ulrich JD, Young KL, Robinette ML, Gilfillan S, Krishnan GM, Sudhakar S, Zinselmeyer BH et al (2015) TREM2 lipid sensing sustains the microglial response in an Alzheimer's disease model. Cell 160:1061–1071. https://doi.org/10.1016/j.cell.2015.01.049
76. Wang Y, Ulland TK, Ulrich JD, Song W, Tzaferis JA, Hole JT, Yuan P, Mahan TE, Shi Y, Gilfillan S et al (2016) TREM2-mediated early microglial response limits diffusion and toxicity of amyloid plaques. J Exp Med 213:667–675. https://doi.org/10.1084/jem.20151948
77. Welikovitch LA, Do Carmo S, Magloczky Z, Malcolm JC, Loke J, Klein WL, Freund T, Cuello AC (2020) Early intraneuronal amyloid triggers neuron-derived inflammatory signaling in APP transgenic rats and human brain. Proc Natl Acad Sci USA 117:6844–6854. https://doi.org/10.1073/pnas.1914593117
78. Wunderlich P, Glebov K, Kemmerling N, Tien NT, Neumann H, Walter J (2013) Sequential proteolytic processing of the triggering receptor expressed on myeloid cells-2 (TREM2) protein by ectodomain shedding and gamma-secretase-dependent intramembranous cleavage. J Biol Chem 288:33027–33036. https://doi.org/10.1074/jbc.M113.517540
79. Xiang X, Piers TM, Wefers B, Zhu K, Mallach A, Brunner B, Kleinberger G, Song W, Colonna M, Herms J et al (2018) The Trem2 R47H Alzheimer's risk variant impairs splicing and reduces Trem2 mRNA and protein in mice but not in humans. Mol Neurodegener 13:49. https://doi.org/10.1186/s13024-018-0280-6
80. Yoo SJ, Son G, Bae J, Kim SY, Yoo YK, Park D, Baek SY, Chang KA, Suh YH, Lee YB et al (2020) Longitudinal profiling of oligomeric Abeta in human nasal discharge reflecting cognitive decline in probable Alzheimer's disease. Sci Rep 10:11234. https://doi.org/10.1038/s41598-020-68148-2
81. Yuan P, Condello C, Keene CD, Wang Y, Bird TD, Paul SM, Luo W, Colonna M, Baddeley D, Grutzendler J (2016) TREM2 haplodeficiency in mice and humans impairs the microglia barrier function leading to decreased amyloid compaction and severe axonal dystrophy. Neuron 90:724–739. https://doi.org/10.1016/j.neuron.2016.05.003
82. Zhao Y, Wu X, Li X, Jiang LL, Gui X, Liu Y, Sun Y, Zhu B, Pina-Crespo JC, Zhang M et al (2018) TREM2 is a receptor for beta-Amyloid that mediates microglial function. Neuron 97:1023-1031 e1027. https://doi.org/10.1016/j.neuron.2018.01.031
83. Zhong L, Chen XF, Wang T, Wang Z, Liao C, Wang Z, Huang R, Wang D, Li X, Wu L et al (2017) Soluble TREM2 induces inflammatory responses and enhances microglial survival. J Exp Med 214:597–607. https://doi.org/10.1084/jem.20160844

Publisher's Note

Springer Nature remains neutral with regard to jurisdictional claims in published maps and institutional affiliations.

Ready to submit your research? Choose BMC and benefit from:

- fast, convenient online submission
- thorough peer review by experienced researchers in your field
- rapid publication on acceptance
- support for research data, including large and complex data types
- gold Open Access which fosters wider collaboration and increased citations
- maximum visibility for your research: over 100M website views per year

At BMC, research is always in progress.

Learn more biomedcentral.com/submissions

BMC